VOLUME 75 APRIL 15, 1971 NUMBER 8

JPCHAx

THE JOURNAL OF PHYSICAL CHEMISTRY

PUBLISHED BIWEEKLY BY THE AMERICAN CHEMICAL SOCIETY

Inorganic Chemistry is the one...

that publishes both experimental and theoretical fundamental studies in *all phases of inorganic chemistry.*

These studies include synthesis and properties of new compounds, quantitative studies regarding structure, and thermodynamics and kinetics of inorganic reactions. Articles may range from the borders of organic chemistry to the borders of theoretical physics . . . giving you a broad expanse of authoritative information.

Besides the 35 or more papers presented in each monthly issue, you'll also profit from the shorter *Notes* and the *Correspondence* sections, that provide an informal medium of exchange for scientific views and ideas.

Inorganic Chemistry is the one . . . to order right now for your own professional interests. Simply complete and return the form below.

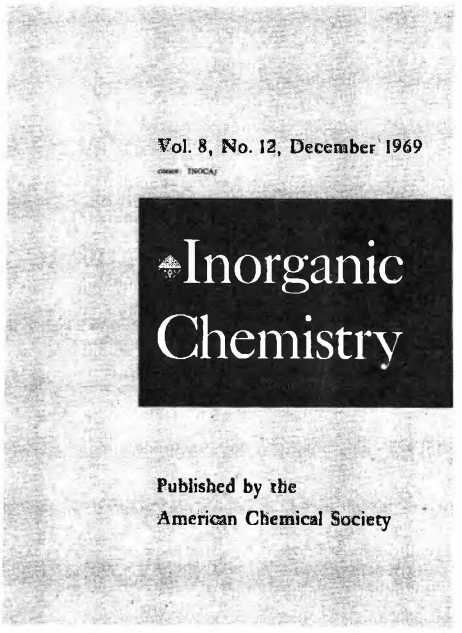

American Chemical Society / 1155 Sixteenth Street, N.W., Washington, D.C. 20036

Please enter my subscription to **Inorganic Chemistry** at the rates checked below:

ACS Members: ☐ U.S. $18 ☐ Canada, PUAS $21 ☐ Other Nations $21.50
Nonmembers: ☐ U.S. $36 ☐ Canada, PUAS $39 ☐ Other Nations $39.50

☐ Bill me ☐ Bill employer ☐ Payment enclosed (Payable to American Chemical Society)

Name _____ Title _____

Employer _____

Address: ☐ Home ☐ Business _____

City _____ State/Country _____ Zip _____

Nature of employer's business? ☐ Manufacturing or processing ☐ Academic ☐ Government ☐ Other _____ (Please indicate)

Note: Subscriptions at ACS Member Rates are for personal use only.

☐ I am an ACS member ☐ I am not an ACS member

Payment must be made in U.S. currency, by international money order, UNESCO coupons, U.S. bank draft; or order through your book dealer.

THE JOURNAL OF

PHYSICAL CHEMISTRY

AMERICAN CHEMICAL SOCIETY, *1155 Sixteenth St., N.W., Washington, D. C. 20036*
FREDERICK T. WALL, *Executive Director*

Books and Journals Division
JOHN K CRUM, *Director (Acting)*
JOSEPH H. KUNEY, *Head, Business Operations Department*
RUTH REYNARD, *Assistant to the Director*

 Published biweekly by the American Chemical Society at 20th and Northampton Sts., Easton, Pa. 18042. Second-class postage paid at Easton, Pa.

All manuscripts should be sent to *The Journal of Physical Chemistry,* Department of Chemistry, University of Minnesota, Minneapolis, Minn. 55455.

Additions and Corrections are published once yearly in the final issue. See Volume 74, Number 26 for the proper form.

Extensive or unusual alterations in an article after it has been set in type are made at the author's expense, and it is understood that by requesting such alterations the author agrees to defray the cost thereof.

The American Chemical Society and the Editor of *The Journal of Physical Chemistry* assume no responsibility for the statements and opinions advanced by contributors.

Correspondence regarding accepted copy, proofs, and reprints should be directed to Editorial Production Office, American Chemical Society, 20th and Northampton Sts., Easton, Pa. 18042. Manager: CHARLES R. BERTSCH. Assistant Editor: EDWARD A. BORGER. Editorial Assistant: EVELYN J. UHLER.

Advertising Office: Century Communications Corporation, 142 East Avenue, Norwalk, Conn. 06851.

Business and Subscription Information

Remittances and orders for subscriptions and for single copies, notices of changes of address and new professional connections, and claims for missing numbers should be sent to the Subscription Service Department, American Chemical Society, 1155 Sixteenth St., N.W., Washington, D. C. 20036. Allow 4 weeks for changes of address. Please include an old address label with the notification.

Claims for missing numbers will not be allowed (1) if received more than sixty days from date of issue, (2) if loss was due to failure of notice of change of address to be received before the date specified in the preceding paragraph, or (3) if the reason for the claim is "missing from files."

Subscription rates (1971): members of the American Chemical Society, $20.00 for 1 year; to nonmembers, $40.00 for 1 year. Those interested in becoming members should write to the Admissions Department, American Chemical Society, 1155 Sixteenth St., N.W., Washington, D. C. 20036. Postage to Canada and countries in the Pan-American Union, $4.00; all other countries, $5.00. Single copies for current year: $2.00. Rates for back issues from Volume 56 to date are available from the Special Issues Sales Department, 1155 Sixteenth St., N.W., Washington, D. C. 20036.

This publication and the other ACS periodical publications are now available on microfilm. For information write to: MICROFILM, Special Issues Sales Department, 1155 Sixteenth St., N.W., Washington, D. C. 20036.

Notice to Authors last printed in the issue of December 24, 1970

ISOTOPE EFFECTS IN CHEMICAL PROCESSES
ADVANCES IN CHEMISTRY SERIES NO. 89

Thirteen papers from a symposium by the Division of Nuclear Chemistry and Technology of the American Chemical Society, chaired by William Spindel. Includes:

- Separating isotopes by chemical exchange, distillation, gas chromatography, electromigration, and photochemical processes
- Methods for fractionating isotopes of hydrogen, lithium, boron, carbon, and nitrogen
- Thermotransport in monatomic and ionic liquids
- Statistical-mechanical theory determining isotope effects

278 pages with index | Clothbound | (1969) | $13.00

Set of L.C. cards free with library orders upon request

Other books in the ADVANCES IN CHEMISTRY SERIES in physical and colloid chemistry include:

No. 87 Interaction of Liquids at Solid Substrates. Twelve papers survey recent research on solid/liquid interaction, including work on "coupling agents," adhesion of polymers, organic/inorganic interfaces, ultrasonic impedometry. Four more papers are concerned with heparinized surfaces at the blood/material interface. 212 pages
Cloth (1968) $9.50

No. 84 Molecular Association in Biological and Related Systems. Nineteen articles survey and report new work on molecular association in fat digestion, in soap systems, in membrane constituents, and in mixed monolayers. Other topics include bile salt micelles, lipid monolayers and membranes, and a definitive review of biological membrane structure. 308 pages
Cloth (1968) $10.50

No. 82 Radiation Chemistry—II. Thirty-six papers and 17 abstracts on radiation chemistry in gases, solids, and organic liquids. Includes three plenary lectures. 558 pages
Cloth (1968) $16.00

No. 81 Radiation Chemistry—I. Forty-one papers and 17 abstracts on radiation chemistry in aqueous media, biology, and dosimetry. From the international conference at Argonne National Laboratory. 616 pages
Cloth (1968) $16.00
No. 81 and No. 82 ordered together $30.00.

No. 79 Adsorption from Aqueous Solution. Fifteen papers discuss thermodynamic and kinetic aspects of adsorption phenomena and the results of studies on a variety of adsorbate-adsorbent systems. 212 pages
Cloth (1968) $10.00

No. 68 Mössbauer Effect and its Application in Chemistry. Ten papers that will familiarize chemists with Mössbauer spectroscopy as an analytical tool, for studying chemical bonding, crystal structure, electron density, magnetism, and other properties. 178 pages
Cloth (1967) $8.00

No. 67 Equilibrium Concepts in Natural Water Systems. Sixteen papers represent the collaboration of aquatic chemists, analytical chemists, geologists, oceanographers, limnologists, and sanitary engineers, working with simplified models to produce fruitful generalizations and valuable insights into the factors that control the chemistry of natural systems. 344 pages
Cloth (1967) $11.00

No. 64 Regenerative EMF Cells. Seventeen papers survey current progress and research on regenerative systems for converting and storing electrical energy. Principal emphasis is on thermally regenerative systems, but chemical and photochemical systems are considered. 309 pages
Cloth (1967) $11.00

No. 63 Ordered Fluids and Liquid Crystals. Twenty-two studies on characterization, properties, and occurrence of these phenomena in many substances such as tristearin, p-azoxyanisole, mono-and di-hydric alcohols, phospholipids and polypeptides. 332 pages
Cloth (1967) $11.50

No. 58 Ion-Molecule Reactions in the Gas Phase. Eighteen papers survey spectrometric and other methods for producing and studying ion-molecule reactions, such as pulsed sources for studying thermal ions, reactions in flames and electrical discharges. 336 pages
Cloth (1966) $10.50

No. 54 Advanced Propellant Chemistry. Primarily directed to the search for new oxidizers; 26 papers survey oxygen-containing oxidizers, fuels and binders, fluorine systems including oxygen difluoride and difluoramines and liquid systems. 290 pages
Cloth (1966) $10.50

No. 50 Solvated Electron. Reviews of theory, structure, reactions of solvated and hydrated electrons; detailed papers on electrical transport properties, photochemistry, theory of electron transfer reactions, structure of solvated electrons, hydrated electron research. 304 pages
Cloth (1965) $10.50

No. 47 Fuel Cell Systems. Developments in theory, performance, construction, and new systems for the energy converter that is proving itself in military and space uses. 360 pages
Cloth (1965) $10.50

No. 43 Contact Angle, Wettability, and Adhesion. Twenty-six papers on theoretical and practical approaches to wettability and adhesion; with summary of the surface chemical studies of W. A. Zisman, the 1963 Kendall Award winner. 389 pages
Cloth (1964) $10.50

No. 40 Mass Spectral Correlations. By Fred W. McLafferty. Over 4000 spectra listed by mass/charge ratios of fragment ions with the most probable original structures for each. 117 pages
Paper (1963) $6.00

No. 33 Solid Surfaces and the Gas-Solid Interface. Thirty-seven papers from the Kendall Award Symposium honoring Stephen Brunauer. Theory and techniques for studying surface phenomena.
Cloth (1961) $12.00

No. 31 Critical Solution Temperatures. By Alfred W. Francis. CST answers the question, "Do two liquids mix?" and is widely used for screening solvents. Over 6000 systems are included, 70% with a hydrocarbon as one component; nearly 1100 non-hydrocarbon solvents are listed. 246 pages
Cloth (1961) $8.00

All books postpaid in U.S. and Canada; plus 30 cents in PUAS and elsewhere.

Order from: **SPECIAL ISSUES SALES**
AMERICAN CHEMICAL SOCIETY
1155 SIXTEENTH ST., N.W.
WASHINGTON, D.C. 20036

THE JOURNAL OF

PHYSICAL CHEMISTRY

Volume 75, Number 8 April 15, 1971

NOTES

COMMUNICATIONS TO THE EDITOR

AUTHOR INDEX

THE JOURNAL OF
PHYSICAL CHEMISTRY

VOLUME 75, NUMBER 8 APRIL 15, 1971

The Measurement of Photoluminescence Quantum Yields.[1] A Review[2]

by J. N. Demas[3] and G. A. Crosby*

Department of Chemistry, Washington State University, Pullman, Washington 99163 *(Received April 1, 1970)*

Publication costs assisted by the Air Force Office of Scientific Research, Directorate of Chemical Sciences

Table of Contents

I. Introduction

The use of fluorescence and phosphorescence as an experimental tool has increased immensely in the past 15 years. During this period luminescence analysis has progressed from a crude technique employed by a few spectroscopists to a sophisticated technology utilized by analytical chemists, biochemists, physical chemists, and physicists. This rise in popularity can be attributed largely to the development of relatively low cost instrumentation and a growing appreciation of the power of these methods.

The luminescence quantum yield of a compound is defined as the fraction of molecules that emit a photon after direct excitation by the source. This quantity is not the same as the total number of emitted photons which escape a bulk sample divided by the total number of absorbed photons, although in many instances the two quantities are nearly equal. The terms absolute yield, quantum yield, and yield are used interchangeably throughout this review.

Practically, absolute quantum yields are important. They allow one to assess the sensitivity of a proposed fluorimetric determination of materials and the extent of interferences.[4a,b] They are necessary for calculating thresholds for laser action[5] and for judging the suitability of materials as wavelength shifters in optical

(1) Research sponsored by AFOSR(NC)-OAR, USAF Grant 68-1342; abstracted from a dissertation by J. N. Demas submitted to the Graduate School of the University of New Mexico in partial fulfillment of the requirements for the degree Doctor of Philosophy.

(2) Editorial Note. It has been suggested that it would be useful to publish in the Journal, from time to time, a review article dealing with a specific subject of strong interest to a large number of physical chemists and of sufficient complexity that a clarifying review might be timely and helpful. The editors would seek to identify such topics and to invite appropriate colleagues to contribute such reviews. We present in this issue the first such review article; we would be grateful for comment and reactions from readers of the Journal.

(3) National Science Foundation Predoctoral Fellow, 1966–1968; American Chemical Society–Petroleum Research Fund Fellow, 1968–1969.

(4) (a) C. A. Parker, "Photoluminescence of Solutions," Elsevier Publishing Co., New York, N. Y., 1968; (b) R. M. Dagnall, S. J. Pratt, R. Smith, and T. S. West, *Analyst (London)*, 93, 638 (1968).

(5) P. P. Sorokin, J. R. Lankard, V. L. Moruzzi, and E. C. Hammond, *J. Chem. Phys.*, 48, 4726 (1968).

pumping experiments or for use as energy donors.[4a,6] Yields, coupled with luminescence data, also allow evaluation of the purity of materials.[4a]

Theoretically, absolute yields are of central importance for studies of radiationless processes in molecules,[4a,6-8] for correlation of predicted luminescence lifetimes with the observed lifetimes,[9] and for making assignments of electronic transitions.[10]

Modern instrumentation has improved the means for obtaining absolute photoluminescence quantum yields —a measurement which, 20 years ago, presented fierce obstacles. In fact, many of the quantum yields reported in the literature are wrong, for frequently measurements were made under conditions not commensurate with the underlying assumptions of the methods. In many instances errors were propagated because the researcher was unaware of corrections or subsequent modifications to the method which were made after the original papers had been published. In some cases, workers using one quantum-yield method have pointed out the necessity of applying certain correction factors; yet, workers using a similar method have remained unaware of the problem. This review is an attempt to bring together information on the various techniques for measuring quantum yields, to point out the advantages and the disadvantages of each experimental method, to explain the origins and the probable magnitudes of the numerous errors which may arise, to suggest improvements which might be made in some methods, and to point out potentially useful techniques which have been overlooked.

Reviews specifically focused on quantum-yield studies are few. In 1951 Förster[11] reviewed the subject of quantum-yield measurements, a treatment which has been the foundation for much of the subsequent work. Tregellas-Williams[12] has discussed briefly the methods for obtaining yields of inorganic phosphors. Recently, Lipsett[13] has presented an extensive review on quantum yields with particular emphasis on the secondary processes that follow optical excitation (polarization, reabsorption, reemission, and apparent lifetime changes); heavy emphasis is given to effects in powdered phosphors. Also, Parker[4a] has discussed luminescence instrumentation in detail, and his excellent book is highly recommended to anyone involved in luminescence work.

The present review is primarily concerned with quantum yields from solutions and covers the important papers through early 1969. A certain amount of overlap with previous articles has occurred, but attempts have been made to minimize this without sacrificing clarity. No attempt has been made to treat the complicated problem of quantum yields from solid substances. Readers interested in this subject are referred to the article by Lipsett[13] and to the experimental papers by Nygaard,[14] Kristianpoller,[15] and particularly Allison, *et al.*[16] The latter papers describe what is probably the most reliable procedure for measuring yields of solids. No attempt has been made here to discuss specific instrumentation.

II. Methods of Measuring Quantum Yields

A. Magnesium Oxide as a Standard. The modern era of luminescence quantum-yield measurements began in 1924 with an article by Vavilov.[17] This work described the first reliable method for measuring absolute luminescence efficiencies of solutions. Besides giving spectroscopists a powerful tool for the study of new materials, Vavilov showed for the first time that the efficiencies of luminescent materials such as dyestuffs could approach unity. His original method, in slightly modified form, was so successful that only in the past 10 years has it been supplanted.

Basically, Vavilov's technique is a substitution method employing a magnesium oxide scatterer as a standard. Since many of the problems encountered are common to other procedures, the method is described in detail here. A modern apparatus (Figure 1) of the type used by Melhuish[18,19] is assumed. Light from a medium-pressure mercury arc (A) is monochromatized by a filter (F) and focused to a small spot on element (C) by a lens (L). Either a cuvette containing the luminescent material or a plate coated with a freshly prepared layer of magnesium oxide serves as the element (C). A detector (D) views the scatterer or cuvette normal to the front surface.

The experiment consists of two measurements. First the cuvette containing the sample is placed at C, and the signal strength from the sample luminescence is recorded by the detector. The concentration of the material is normally selected so that 99% or more of the exciting light is absorbed in a few millimeters. Then the cuvette is replaced by a plate coated with MgO which scatters the exciting beam, and a second detector reading is obtained. From these data and some additional information the absolute quantum yield of the sample can be calculated.

(6) J. G. Calvert and J. N. Pitts, Jr., "Photochemistry," Wiley, New York, N. Y., 1966.

(7) B. R. Henry and M. Kasha, *Ann. Rev. Phys. Chem.*, **19**, 161 (1968).

(8) S. P. McGlynn, T. Azumi, and M. Kinoshita, "Molecular Spectroscopy of the Triplet State," Prentice-Hall, Inc., Englewood Cliffs, N. J., 1969.

(9) S. J. Strickler and R. A. Berg, *J. Chem. Phys.*, **37**, 814 (1962).

(10) F. E. Lytle and D. M. Hercules, *J. Amer. Chem. Soc.*, **91**, 253 (1969).

(11) Th. Förster, "Fluoreszenz Organisher Verbindungen," Vandenhoeck-Ruprecht, Göttingen, Germany, 1951.

(12) J. Tregellas-Williams, *J. Electrochem. Soc.*, **105**, 173 (1958).

(13) F. R. Lipsett, *Progr. Dielectrics*, **7**, 217 (1967).

(14) K. J. Nygaard, *Brit. J. Appl. Phys.*, **15**, 597 (1964).

(15) N. Kristianpoller, *J. Opt. Soc. Amer.*, **54**, 1285 (1964).

(16) R. Allison, J. Burns, and A. J. Tuzzolino, *ibid.*, **54**, 747 (1964).

(17) S. I. Vavilov, *Z. Phys.*, **22**, 266 (1924).

(18) W. H. Melhuish, *J. Opt. Soc. Amer.*, **54**, 183 (1964).

(19) W. H. Melhuish, *New Zealand J. Sci. Tech.*, **37**, 142 (1955).

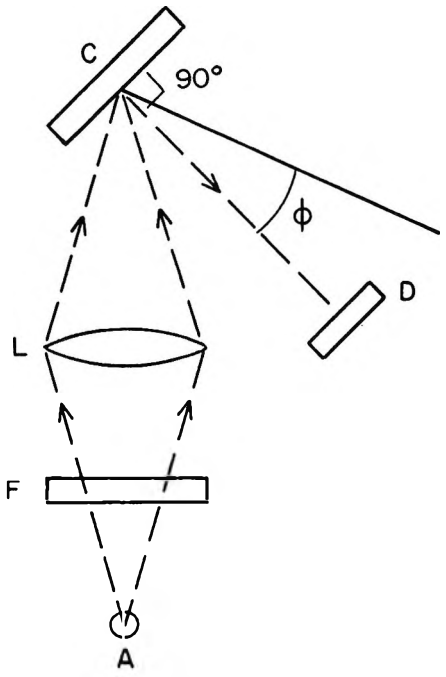

Figure 1. Quantum-yield apparatus for use with a magnesium oxide standard (after Melhuish[18,19]): A, light source; C, sample cuvette or magnesium oxide screen; D, detector; F, filters; L, focusing lens. Dashed lines represent light paths.

We proceed to derive Vavilov's equation in detail using modern terminology. The exciting image at C has an intensity, E (in units of quanta/sec). With an MgO surface in place the total number of scattered photons per second, E_s, is given by

$$E_s = ER \tag{1}$$

where R is the reflectance of the MgO surface to the exciting light. With the cuvette in place, the sample emits E_e (quanta/sec) given by

$$E_e = ET_xQ \tag{2}$$

T_x is the transmission coefficient of the cuvette window to the exciting light; Q is the absolute quantum yield of the sample.

If the sample can be treated as a point source and the emission is isotropic, the intensity of the emitted light within the cuvette is $E_e/4\pi$ (quanta/sec-steradian). For a detector subtending a small solid angle, α (steradians), and viewing a flat cuvette surface at normal incidence, the number of photons per second hitting its surface, N_e, is given by

$$N_e = T_e\alpha E_e/4\pi n^2 \tag{3}$$

where T_e is the transmission coefficient of the cuvette window to emitted photons and n^2 (n is the refractive index of the solvent at the emission wavelength) compensates for refraction at the cuvette interfaces.[20,21] Of course the emission should not be so broad that T_e and n vary significantly over the bandwidth.

To obtain the number of photons scattered by the MgO surface into the detector in terms of measurable quantities, one assumes the scatterer to be an ideal diffuse reflector obeying Lambert's cosine law. The Lambert law[17] states that the intensity of scattered light, $I(\phi)$, at an angle ϕ from the normal to the surface is represented by

$$\begin{aligned} I(\phi) &= I_0 \cos\phi \quad (0 \leq \phi \leq \pi/2) \\ I(\phi) &= 0 \quad (\pi/2 \leq \phi \leq \pi) \end{aligned} \tag{4}$$

$I_0 = I(\phi = 0)$ has units of quanta/sec-steradian. Integration over a unit sphere yields the total number of quanta per second scattered by the MgO surface.

$$E_s = \int_0^{2\pi} d\theta \int_0^{\pi/2} (I_0 \cos\phi) \sin\phi \, d\phi = \pi I_0 \tag{5}$$

For a detector subtending a small solid angle and set for normal viewing, the number of scattered photons reaching the sensitive surface per second, N_s, is αI_0. Then

$$N_s = \alpha I_0 = \alpha E_s/\pi \tag{6}$$

Because the sensitivity of most detectors (phototubes, photocells, thermopiles) is a function of wavelength, the response of the detector must be averaged over the spectral distribution of the impinging light. The detector readings for the scattered light, D_s, and for the emitted light, D_e, are given by eq 7 and 8.

$$\begin{aligned} D_s &= CK_s\alpha E_s/\pi \\ K_s &= \int S(\bar{\nu})I_s(\bar{\nu})\, d\bar{\nu} / \int I_s(\bar{\nu})\, d\bar{\nu} \end{aligned} \tag{7}$$

$$\begin{aligned} D_e &= CK_e\alpha E_e T_e/4\pi n^2 \\ K_e &= \int S(\bar{\nu})I_e(\bar{\nu})\, d\bar{\nu} / \int I_e(\bar{\nu})\, d\bar{\nu} \end{aligned} \tag{8}$$

$I(\bar{\nu})$ (quanta/sec cm^{-1}) is the spectral distribution of the light falling on the phototube; $S(\bar{\nu})$ is the relative sensitivity of the detector to light of energy $\bar{\nu}$(cm^{-1}); K is the average detector output per photon; C converts the expressions to absolute units. The subscripts s and e refer to the scattered and emitted radiation, respectively. All integrations are carried out over the entire frequency range of interest.

In principle the quantum yield, Q, can be calculated from a knowledge of the factors in eq 2 and 8. In practice some of these parameters are very difficult to obtain (especially C and α), and the scattering measurement is used to eliminate them. Combining eq 1, 2, 7, and 8 yields a working equation for Q.

$$Q = 4\left(\frac{K_s}{K_e}\right)\left(\frac{D_e}{D_s}\right)\left(\frac{R}{T_xT_e}\right)n^2 \tag{9}$$

The accuracy of quantum yields determined *via* the Vavilov method depends on several factors which

(20) J. N. Demas, Ph.D. Dissertation, University of New Mexico, Albuquerque, N. M., 1970.

(21) E. H. Gilmore, G. E. Gibson, and D. S. McClure, *J. Chem. Phys.*, **20**, 829 (1952); **23**, 399 (1955).

are difficult to measure. In particular, the reflectance of the scatterer depends significantly on its thickness, the method of preparation, the angle of incidence, and the freshness of the coating. The reflectance decreases markedly in the uv, and the coating ages rapidly.[21-23] Finally, MgO does not really satisfy eq 4.[17,21] These factors might make the uncertainty in R as large as 5–10% in some cases. Complications also arise because T'_x and T_e are composed of three terms: the reflection coefficient of the air–glass interface, the per cent transmission of the glass, and the reflection coefficient of the glass–liquid interface. Generally losses in the glass can be avoided by using high-quality windows whose reflection coefficients can be calculated from Fresnel's relations. Note that T is not just the transmission *vs.* air.[19,24] The factors T'_e and T'_x may also be wavelength dependent in the pertinent spectral region leading to more complicated equations than those presented here.

In addition to the problems discussed above which are specific to the Vavilov method, there are other factors which can contribute significantly to error in the final result. The evaluation of K_s and K_e is difficult because a detailed knowledge of the sensitivity of the detector and of the excitation and emission band shapes is required. None of these measurements is simple to carry out with high precision (see section V). Fortunately, the term K_s/K_e can be made to approach unity for a large number of compounds when a quantum counter is used as the detector (see section IV).

The explicit assumption of an isotropic emission within the cuvette can lead to serious errors. Incident light, even when completely depolarized, selectively excites molecules in particular orientations whenever the molecules absorb radiation preferentially along a molecular axis. Unless randomness of the excited molecules is achieved before luminescence occurs, the emission will not be isotropic and therefore "polarization errors" will be incurred.[21,25] Additional problems may occur from polarized emission, since some detectors have polarization-dependent sensitivities (*e.g.*, grating spectrometers[26]). Polarization effects are difficult to assess (see section VI-D).

Another common problem is reabsorption of the luminescence. If the emission and absorption spectra of the compound overlap, some of the emitted radiation will be absorbed before leaving the cuvette and will depress the measured yield. For solutions a usual way to minimize this source of error is to work at the lowest concentration possible (see section VI-B).

Still another general source of error lies in the assumption that any light not emitted in the direction of the detector is entirely lost. Light travelling back into the cuvette may be reflected internally, eventually reach the detector, and thus produce an excessively high reading. Errors of ~20% are possible.[27] Secondary emission can also cause trouble. As the primary emitted light travels through the solution, some is reabsorbed by the solute and reemitted. This secondary emission, which originated from photons that were assumed not to produce a signal, can reach the receiver and spuriously enhance the apparent yield.[22] The problem is most severe when the absorption and emission spectra overlap appreciably, the solution is concentrated, and the yield of the compound is high. In fact, impossible quantum yields of 1.25 or more have been observed under unfavorable experimental conditions.[22,28] Correcting for reemission is particularly difficult, but equations have been derived (see section VI-C).

A brief description of the actual technique used by Vavilov is of interest.[17] He used an objective spectrofluorimeter to obtain the integrated emission intensities of his compounds by comparing visually at different wavelengths the light intensity of the sample with radiation from a standard lamp. In his early optically dilute procedure he used white excitation light; this required a knowledge of the absorbance of his sample at different wavelengths. The spectral distribution of his exciting light was measured on his spectrometer. He recognized but ignored the reabsorption of any emission by his samples on the grounds of the low concentrations and foresaw errors introduced by internal reflections in his cuvettes. Vavilov measured the yields of fluorescein and a number of organic molecules. He claimed a systematic error of approximately 10–20% and a reproducibility of 10–15%, but he overlooked the refractive index correction. Such a correction, if applied to his results, gives some quantum yields greater than 1, an impossibility. It is uncertain what factors caused these discrepancies.

In 1927, Vavilov[29] measured the relative quantum yield of fluorescein as a function of excitation wavelength using an optically dense solution. This procedure obviates correcting for the relative amounts of light absorbed at different wavelengths. To minimize any errors introduced by reabsorption he presumed, correctly, that the emission spectrum was independent of excitation wavelength and viewed the emission in the long wavelength tail where the effect was negligible. He also switched from white to monochromatic exciting light. The intensity of the exciting light in the ultraviolet region was obtained by using a calibrated

(22) W. H. Melhuish, *J. Phys. Chem.*, **65**, 229 (1961).
(23) W. E. K. Middleton and C. L. Sanders, *J. Opt. Soc. Amer.*, **41**, 419 (1951).
(24) F. A. Jenkins and H. E. White, "Fundamentals of Optics," McGraw-Hill, New York, N. Y., 1957.
(25) A. H. Kalantar, *J. Chem. Phys.*, **48**, 4992 (1968).
(26) J. W. Eastman, *Photochem. Photobiol.*, **6**, 55 (1967).
(27) W. H. Melhuish, *J. Opt. Soc. Amer.*, **51**, 278 (1961).
(28) G. Weber and F. W. J. Teale, *Trans. Faraday Soc.*, **53**, 646 (1957).
(29) S. I. Vavilov, *Z. Phys.*, **42**, 311 (1927).

mercury arc and a monochromator whose dispersion was known. Since his work showed that fluorescein had a constant energy yield when excited in its first absorption band, Vavilov assumed that any material whose first absorption band spanned the near-ultraviolet would probably behave similarly. In order to check the calibration of the mercury arc he therefore selected a solution of aesculin as an energy counter for his exciting light. He felt that an additional calibration procedure was necessary because he had little faith in the mercury lamp calibration. His objective spectrometer, employing visual detection, was useless below 400 nm. Fortuitously, good agreement was found between his calibrated lamp results and his aesculin energy counter, although modern work indicates that neither fluorescein nor aesculin is a constant energy converter over any region in the visible or ultraviolet; both compounds are, in all probability, constant quantum counters.[30]

The next big advance in the Vavilov method for quantum-yield measurements was Bowen's introduction of the quantum counter in place of a spectrometer for measuring the relative intensities of the scattered and emitted light ($K_s/K_e \simeq 1$ in eq 9 for the working range of the counter).[31] Although the quantum counter, a solid uranyl nitrate screen in front of a phototube, was limited (usable range 250–436 nm), conceptually it is still the single most important improvement in the method. Bowen, as did Vavilov, missed the necessity of a refractive index correction. When this correction is applied to Bowen's values, some of the quantum yields are also greater than 1. The reasons for these discrepancies are unknown.

The need for the refractive index correction in quantum-yield measurements was recognized by Förster,[11] who gave the mathematical expressions for it (the n^2 term in eq 3 and 9). His equation also incorporates the results of Ghosh and Sengupta[32,33] by taking the reabsorption of fluorescence into account.

Further refinements of the Vavilov method were made by Gilmore, Gibson, and McClure,[21] who carried out a detailed analysis of the technique. Using a magnesium oxide standard, these authors measured the fluorescence and phosphorescence yields of a number of organic molecules in a rigid glass at 77°K. They considered the refractive index correction for 45° viewing where the simple n^2 of eq 9 is no longer valid. They provided detailed corrections for varying window characteristics. These factors become significant for handling materials which emit in the ultraviolet, a region where refractive indices and window transmission characteristics change drastically with wavelength. Reabsorption and reemission were ignored because the absorption–emission overlap of their molecules at 77°K was slight. Although sources of large systematic errors were present (Melhuish[27] has shown that their results could be off by ~20% because they used an unblackened cuvette), this elegant work is a valuable guide for any future improvements on the scattering method.

In 1955, Melhuish[19] further improved the Vavilov method and salvaged the technique from obsolescence by introducing the rhodamine B quantum counter. This device covers the range 220–600 nm which permits the study of innumerable molecules. Melhuish[22] has also presented a detailed analysis of absorption–reemission corrections applicable to such an apparatus. Correction factors are also included for the movement of the luminescing volume away from the front of the cuvette when incomplete absorption occurs. Although several simplifying assumptions are incorporated in his final expressions, the reported quantum yields are without question the best values measured by the Vavilov method and are probably some of the most accurate yields known.

In summary, the Vavilov system of measurement is one of the few truly absolute quantum-yield methods available. It is a highly tedious, exacting procedure which requires a detailed knowledge of all optical paths through the samples, of the absolute reflectance of the exciting light by the scatterer, and of the corrections required for scattered light. Since the reflection coefficient of magnesium oxide is a function of the thickness, the angle of incidence, and the sample age, the effects of these factors are difficult to assess. Since many ancillary data are necessary, and since there are difficulties in the calibrations as well as potentially large error sources in refractive index, internal reflection, reabsorption, and reemission corrections, the spread in the final quantum-yield values is substantial. A ±5% relative error in the best cases (*e.g.*, quinine sulfate) is minimal, and a ±10% uncertainty is probably more realistic for most molecules.

Regardless of the many corrections necessary, this procedure has supplied valuable data on materials such as quinine sulfate and anthracene and has led to their nearly universal adoption as standard materials for quantum-yield measurements. Nevertheless, it appears that with the advent of the Weber and Teale technique for measuring quantum yields (section II-B), the method of Vavilov will disappear and may find only limited use for determining yields of standards to be used with optically dense solutions.

B. Solution Scatterers as Standards. Such diverse substances as magnesium oxide and anthracene have been chosen for quantum-yield standards, but the most important development has been the introduction of solution scatterers by Weber and Teale.[28] For stan-

(30) G. Weber and F. W. J. Teale, *Trans. Faraday Soc.*, **54**, 640 (1958).

(31) E. J. Bowen and J. W. Sawtell, *ibid.*, **33**, 1425 (1937).

(32) I. C. Ghosh and S. B. Sengupta, *Z. Phys. Chem.* (*Leipzig*), **B41**, 117 (1938).

(33) S. B. Sengupta, *J. Indian Chem. Soc.*, **15**, 263 (1938).

dards these workers employed optically dilute colloidal solutions which behave as almost ideal dipole scatterers. These solutions attenuate, by scattering, a collimated beam of light in the same way as absorbing molecules diminish the intensity. The ideal scatterer, however, behaves as if it were a substance which reemits all the absorbed photons without changing the wavelength. Hence a dipole scatterer may be used as a quantum-yield standard of unit efficiency.

Weber and Teale[28] developed an equation for obtaining quantum yields based on a solution scatterer as the standard. Their equation, modified to correct for refractive index effects, is

$$Q = \left(\frac{(\mathrm{d}D_f/\mathrm{d}A_f)_{A_f\to 0}}{(\mathrm{d}D_s/\mathrm{d}A_s)_{A_s\to 0}}\right)\left(\frac{K_s}{K_f}\right)\left(\frac{3+p_f}{3+p_s}\right)\left(\frac{n_f^2}{n_s^2}\right) \quad (10)$$

Q is the quantum yield; D, the detector reading; A, the sample absorbance per centimeter at the exciting wavelength; K, the average detector response per incident photon (see eq 7 and 8); p, the linear polarization of the light emanating from the cuvette. Subscripts f and s refer to the luminescence and scattered light, respectively. In the region of low absorbances the plots of D_f *vs.* A_f and D_s *vs.* A_s become linear, and this limiting slope is required (see section II-C).

The above expression relates the intensity of light received by the detector from a solution of the substance under investigation to the intensity of light registered from a solution of the standard scatterer. Right-angle viewing is assumed, and identical excitation conditions for the sample and the standard are presupposed.

The first term in the equation is a direct measure of the intensity of the sample relative to the standard for equal optical densities; the second term corrects for the wavelength sensitivity of the detector ($K_s/K_f = 1$ for quantum counters). The third term corrects for anisotropy, which is obtained indirectly by measuring the linear polarization of both the emitted and scattered light. Typically, for a well-collimated exciting system p_s will be very nearly 1, whereas, for fluid solutions rotational motion reduces p_f close to zero. Therefore, under most conditions the third term will be ~0.75; Weber and Teale[28] measured values of 0.75 to 0.80 with 0.76 being the most common for excitation above 300 nm. The last term of eq 10 corrects for refractive index differences between the sample and the standard solution. This correction was not included in their original equation by Weber and Teale[28] although it is clearly necessary for comparing solutions of differing refractive indices (see section VI-A). The use of eq 10 is restricted to cases where the detector is not sensitive to the degree of polarization of the incident light, the exciting light is unpolarized, and the absorption of the samples does not change significantly over the region of excitation. For the case where the absorption spectrum is very sharp, Dawson and Kropp[34] have developed a novel method for obtaining the quantum yield of a compound excited in a single absorption line. Because of the considerable difficulties associated with calibrating phototubes, the method of Weber and Teale is primarily limited to use with quantum counters.

Several substances approximate an ideal dipole standard scatterer. Weber and Teale[28] found that their samples of horse-muscle and cat-liver glycogen obeyed the Rayleigh law reasonably well to ~250 nm, although glycogen from some sources contains absorbing impurities which render it useless for a standard. An easy check can be made. If the Rayleigh scattering law (the absorbance multiplied by λ^4 is a constant[24,26,28]) is not obeyed over the wavelength range of interest, then the solution is unsuitable as a scattering standard. The purity problem has limited the use of glycogen, but modern developments in purification techniques may make high-purity samples readily available.

An alternative scatterer introduced by Hercules and Frankel[35] is colloidal silica (Ludox produced by E. I. Du Pont) which appears to be satisfactory for a standard but does possess some unfortunate characteristics. The absorbance is not proportional to concentration (*i.e.*, a sample diluted by half with water does not exhibit half the absorbance); freshly diluted samples are not stable (the absorbance changes slowly over a period of several weeks[36]), and it absorbs below 300 nm yielding fluorescence.[26] Eastman[26] has used specially prepared Ludox, but it is not known whether his samples were any better.

The advantages of the Weber–Teale method are many. It explicitly accounts for the degree of polarization, and, since the data are obtained in dilute solutions, self-quenching as well as reabsorption and reemission can be virtually eliminated. Reabsorption can occur, however, if excitation is carried out in an absorption minimum. For instance, rhodamine B excited at 365 nm gave a yield greater than unity due to reemission effects,[28] but excitation at a wavelength where the compound absorbed the exciting light more strongly reduced the yield to a realistic value.

Equation 10 was derived assuming completely unpolarized exciting light. Obviously use of any source, such as a monochromator, which partially polarizes the exciting light could lead to large systematic errors. In fact, if the exciting beam were completely polarized, it is theoretically possible to place the detector so that no scattered light from the standard could reach it at all! Similarly, the quantum-yield expression assumes no polarization sensitivity of the detector. If a detector did exhibit sensitivity dependent upon the polariza-

(34) W. R. Dawson and J. L. Kropp, *J. Opt. Soc. Amer.*, **55**, 822 (1965).

(35) D. M. Hercules and H. Frankel, *Science*, **131**, 1611 (1960).

(36) M. W. Windsor, J. R. Novak, W. R. Dawson, J. L. Kropp, and R. S. Moore, "Liquid Laser Research, Final Report," 8657-6007-RU0000, TRW Systems, Redondo Beach, Calif. (March 20, 1963).

tion of the emission (*e.g.*, an emission monochromator or an RCA 2020 photomultiplier),[37] then large systematic errors could be introduced. This problem can be easily detected by rotating a polarizer interposed between the detector or monochromator and a luminescent sample which shows no polarized emission. Any variation in detector output with polarizer angle establishes that the detector has a polarization sensitivity.

An additional experimental difficulty is associated with the measurement of the optical density of the scattering solution. If the detector of the absorption spectrophotometer is not located at a considerable distance from the sample, or the spectrometer is not designed to tolerate appreciable scattered light, then the photomultiplier may see some of the scattered radiation; this causes the apparent optical densities to be low. For example, a Beckman DU introduces a large (~10%) systematic error,[28] whereas the Cary 14 with a 1- or 2-cm cuvette located as far from the detector as possible will give negligible error.[36] Similarly, if the fluorescent substance has a high quantum yield, sample luminescence reaching the detector might produce low absorbance readings for the test material also.[28]

The original Weber–Teale method required that the optical density of the sample at the exciting wavelength be kept quite low (preferably below 0.05). As the optical density rises the proportionality between it and the signal begins to break down, and the ratio of the slopes of the curves no longer represents accurately the relative intensities. Several improvements on the method have been developed by Dawson, *et al.* Dawson and Kropp[34] plotted D_f/A_f *vs.* A_f and D_s/A_s *vs.* A_s. The values D_f/A_f and D_s/A_s extrapolated to zero optical density were then used in place of the slopes. This procedure is superior to the original method if the signal-to-noise ratio is good and stray light is minimal, since it emphasizes the important lower optical density points and gives a better idea of the errors from reabsorption. This method also shows clearly the onset of any failure of the intensity to follow absorbance. Recently, Dawson and Windsor[38] have described a logarithmic form of the equation which allows use of higher optical densities (~0.2) and thus lessens the uncertainty due to stray light. This form is also amenable to a statistical evaluation of the data.

Another possible source of serious error arises from impure exciting light. If the exciting light is not monochromatic, an effective sample absorbance must be used. Errors from this source can easily be 100% or greater (see section II-C for details).

Several papers strongly questioning the reliability of the original Weber and Teale method have appeared. Carrying out a relative measurement with quinine as a standard, Chen[39] found that the yields for phenol, tyrosine, and tryptophan were systematically about two-thirds the values obtained by the solution scatterer method using glycogen. Dawson and Windsor[38] found yields for fluorene, naphthalene, and phenanthrene to be 25–60% higher than the values reported by Weber and Teale.[28] It is important to note that these discrepancies occur for compounds which Weber and Teale measured using 254-nm excitation. When the latter's values were determined using excitation above 300 nm, the agreement with the Dawson–Windsor data[38] is much better (5–18%). It seems probable that the discrepancies can be attributed to a failure of glycogen to behave as an ideal scatterer at 254 nm (any absorption by the glycogen would make the measured yields too high). Because the evidence to date suggests a systematic error for excitation below 300 nm, it is highly recommended that the Weber and Teale technique be used only for excitation above 300 nm and preferably with a Ludox standard.

Eastman[26] has devised an interesting, but very tedious, variation on the Weber–Teale technique. Instead of a calibrated detector he uses a spectrophotometer. His technique (as does the original method) takes into account the spacial anisotropy of the scattered light. His procedure also explicitly accounts for the polarization of the scattered light and the variable sensitivity of the detector (a grating monochromator–phototube combination) for light of different polarization at different wavelengths. He gives a logarithmic extrapolation formula to correct the data to zero absorption and zero secondary scattering. A novel spectrometer calibration technique is employed in which Ludox is used to scatter the excitation radiation from a calibrated excitation monochromator into the emission monochromator; however, some anomalous bumps in Eastman's correction curve were found that were not present when the Ludox was replaced by magnesium oxide. These unusual bumps might be traced to partial polarization of the exciting light, since the Ludox reading is very sensitive to this factor. Such anomalies cast some doubt on the validity of this calibration technique.

Eastman's method or its modifications do not appear to offer any significant advantages either in accuracy or ease of execution over other more readily implemented techniques. His work does, however, point out the meticulous concern with detail which must be taken in developing a new quantum-yield method.

If a Ludox standard and a quantum-counter detector are used, the basic Weber–Teale procedure employing the modified equations of Dawson, *et al.*,[34,38] is probably the most accurate quantum-yield method presently available. The latter researchers compared their yields on six systems with Melhuish's data (obtained by a Vavilov method);[22] the average deviation was ~6%,

(37) F. E. Shoup, III, Ph.D. Dissertation, University of New Mexico, Albuquerque, N. M., 1964.

(38) W. R. Dawson and M. W. Windsor, *J. Phys. Chem.*, **72**, 3251 (1968).

(39) R. F. Chen, *Anal. Lett.*, **1**, 35 (1967).

and the worst case was only 12%. Since Melhuish's values are among the best available, the reliability of the Dawson–Windsor modification of the Weber–Teale method seems well established. Although it is necessary to measure several solutions of both compound and standard, the procedure is still probably less tedious than any technique requiring a calibrated spectrometer. Its principal disadvantages are those inherent in any quantum-counter or calibrated-detector method. It has relatively low sensitivity which limits its use to high-yield compounds; it is sensitive to scattered light; it is virtually limited to compounds which emit entirely below 600 nm; and it does not provide the emission spectrum of the compound. Presently excitation is limited to wavelengths greater than 300 nm. In spite of these limitations the advantages of the Weber and Teale method are such that it will certainly gain in popularity both for providing reliable secondary standards and for determining yields routinely.

C. Comparison with Compounds of Known Quantum Yields. Because of the many problems associated with absolute quantum-yield measurements, several simple relative methods have been devised which substitute a compound of "known" quantum yield in place of a standard scatterer as a reference. Relative measurements fall conveniently into two classes: optically dense and optically dilute methods. In the former the light is almost completely absorbed and the luminescent spot is a near-point source, whereas in the latter most of the exciting beam emerges unattenuated. At intermediate concentrations the two types of measurements overlap and with suitable corrections yield the same results.

1. Optically Dense Measurements. For this method the Vavilov configuration (Figure 1) is adopted, but the scatterer is replaced with a cuvette containing an optically dense solution of a standard compound. The expression (easily derivable from eq 8) for the yields is

$$Q_x = Q_r\left(\frac{K_r}{K_x}\right)\left(\frac{D_x}{D_r}\right)\left(\frac{n_x^2}{n_r^2}\right) \qquad (11)$$

where Q is the quantum yield of the solution, K is the average detector output per photon over the emission spectrum (defined in eq 8), D is the detector response, and n is the refractive index of the solution. The x and r subscripts refer to the unknown and the standard reference solution, respectively. This equation is applicable provided the absorbed light produces a near-point source in both the standard and unknown sample; the detector sees the entire luminescing volume; reflection and transmission effects are the same for both samples; and the refractive index of each solution is constant over each emission band. Use of this form is restricted to a comparison of compounds which can be excited at a common wavelength. Detailed knowledge of the emission spectra of the standard and the unknown as well as the wavelength sensitivity of the detector must also be known.

To avoid numerical integrations it is customary to replace the detector by a quantum counter. With the proper quantum counter $K_r/K_x = 1$. The equation then simplifies to

$$Q_x = Q_r\left(\frac{D_x}{D_r}\right)\left(\frac{n_x^2}{n_r^2}\right) \qquad (12)$$

The quantum counter introduces simplicity and rapidity into the relative measurement. Almost no ancillary parameters are required. For estimates of yields for compounds emitting below 600 nm (the limit of present quantum counters), this technique is certainly recommended. To date it has been used with materials having yields greater than ~1%, but by introducing filters to reduce stray light[18] and switching to extended red-response photomultipliers,[40] one can improve the sensitivity considerably, especially if signal recovery techniques are employed.[41-43] (See especially ref 41 for a summary of advantages and shortcomings of the various techniques.)

In place of a quantum counter a calibrated spectrometer can be used to view the emission. The spectrometer may view the entire luminescing volume, or the emission may be collected by means of a lens or mirror and focused on the entrance slit of the spectrometer.[44] The detector responses in eq 11 are now replaced by the integrated areas of the emission spectra corrected for the spectral sensitivity of the monochromator–phototube combination. If collection optics are used, there are a number of necessary precautions:[44] a mirror or an achromatic lens must be used for collecting the light from the cuvette to eliminate changes in focal length; a geometrical correction is necessary to compensate for the changes in the amount of light collected from the cuvette as the optical density varies; and although the refractive index correction is not known with certainty, the n^2 of eq 11 should probably be assumed for normal viewing.

There are numerous other difficulties associated with the optically dense methods. The high concentrations necessary to obtain total absorption magnify the possibilities for concentration-quenching and reabsorption–reemission phenomena, although excitation at an absorption maximum reduces the required concentration level. Reabsorption–reemission is especially trouble-

(40) "RCA Phototubes and Photocells," Technical Manual PT60, Radio Corp. of America, 1963.

(41) A. T. Young, *Appl. Opt.*, **8**, 2431 (1969).

(42) S. L. Ridgway, *Princeton Applied Research Corp.—Signal Notes*, 1 (1967).

(43) M. L. Franklin, G. Horlick, and H. V. Malmstadt, *Anal. Chem.*, **41**, 2 (1969); G. A. Morton, *Appl. Opt.*, **7**, 1 (1968); R. R. Alfano and N. Ockman, *J. Opt. Soc. Amer.*, **58**, 90 (1968); J. K. Nakamura and S. E. Schwarz, *Appl. Opt.*, **7**, 1073 (1968).

(44) I. B. Berlman, "Handbook of Fluorescence Spectra of Aromatic Molecules," Academic Press, New York, N. Y., 1965.

some when the detector views the whole of the cuvette. As Budo, *et al.*,[45] point out, corrections can exceed 50%. Also as in *all* photometric quantum-yield measurements, polarization errors may arise.[25]

Melhuish[22] has given a detailed analysis of the reabsorption–reemission problem in a quantum-counter apparatus, but the equations are quite complicated and mar the attractive simplicity of the method. Berlman[44] observed that the reabsorption and reemission problems intrinsic to his spectrometer–collecting mirror apparatus were not nearly as large as predicted by Melhuish. This small reemission correction is expected because the sharp focus mirror does not view the bulk of the cuvette where most of the reemitted radiation seen by a quantum counter would appear. If the lens is focused at the entering point for the exciting beam, reabsorption corrections are also reduced but if the lens were focused on emission deep in the sample, the reabsorption corrections could become larger than those for a quantum-counter instrument.

In summary, optically dense quantum-yield measurements relative to a standard compound can be made extremely rapidly and are subject to moderate errors if the compounds are not too efficient or do not have high absorption–emission overlap (corrections, while available, greatly complicate the measurements). The accuracy is not, however, as good as with some other methods. Also only compounds of high solubility or high extinction coefficients can be measured, and if the calibration of a spectrometer is to be avoided, the technique is limited to compounds that emit below 600 nm. There appears to be very little room for improvement in the method short of adding an S-20 phototube, instituting signal-to-noise recovery techniques, and inventing a new broader band quantum counter to extend the present 600-nm long wavelength limit.

2. Optically Dilute Measurements. The determination of quantum yields using optically dilute solutions is the most common method currently employed. A spectrofluorimeter is used as the detector. The technique is relatively simple and reasonably accurate. The ready availability of high quality spectrofluorimeters and their components adds further appeal. Corrected emission spectra are also obtained. Because of the popularity of this procedure we give in this section a detailed analysis of it including underlying assumptions, useful modifications, and attainable accuracy.

The optically dilute measurement rests on Beer's law

$$I_0B = I_0(1 - 10^{-AL}) \tag{13}$$

where B is the fraction of light absorbed by the sample, I_0 (quanta/sec) is the intensity of the incident light, A is the absorbance/cm, and L (cm) is the path length. If the luminescence intensity for each compound is proportional to I_0B, then the expression for the quantum yield becomes[46,47]

$$Q_x = Q_r\left(\frac{B_r}{B_x}\right)\left(\frac{I(\lambda_r)}{I(\lambda_x)}\right)\left(\frac{n_x^2}{n_r^2}\right)\left(\frac{D_x}{D_r}\right) \tag{14}$$

A more commonly used relation is obtained by expanding the exponential of eq 13 in a power series of (AL) and truncating the result.[47]

$$B = 1 - [1 - 2.303AL + (2.303AL)^2/2 + \ldots] \simeq 2.303AL \tag{15}$$

Substitution of the approximate expression for B in eq 14 yields the working equation commonly employed by investigators using calibrated spectrometers.[46,47]

$$Q_x = Q_r\left(\frac{A_r(\lambda_r)}{A_x(\lambda_x)}\right)\left(\frac{I(\lambda_r)}{I(\lambda_x)}\right)\left(\frac{n_x^2}{n_r^2}\right)\left(\frac{D_x}{D_r}\right) \tag{16}$$

In these equations B is the fraction of incident light absorbed, $I(\lambda)$ is the relative intensity of the exciting light at wavelength λ, n is the average refractive index of the solution to the luminescence, D is the integrated area under the corrected emission spectrum, and $A(\lambda)$ is the absorbance/cm of the solution at the exciting wavelength λ. Subscripts x and r refer to the unknown and reference solutions, respectively.

Many assumptions are inherent in eq 14 and 16. For both unknown and reference it is assumed that the integrated luminescence intensity is proportional to the fraction of light absorbed, all geometrical factors are identical, the excitation beams are monochromatic, reflection losses are the same, internal reflection effects are equal, reabsorption and reemission are negligible, and all light emanating from the cuvette is isotropic. If any one of these conditions does not hold, serious error can be introduced into the final value. We proceed to give a detailed analysis of the restrictions on, and precautions necessary for, the proper use of eq 13, 14, 15, and 16.

The integrated luminescence intensity is normally proportional to the fraction of light absorbed (B) over a relatively large range (depending upon the geometry) to perhaps 30–40% absorption, but for high optical densities the luminescence may be confined to the front surface on the cuvette thereby destroying this proportionality.[4a] The applicability of eq 13 to any particular experimental setup should therefore be checked over the range of optical densities encountered by measuring the variation of luminescence intensity with concentration for a compound known to have the proper characteristics, *i.e.*, insignificant concentration quenching

(45) A. Budo, J. Dombi, and L. Szollosy, *Acta Univ. Szeged., Acta Phys. Chem.*, **2**, 18 (1956).

(46) H. V. Drushel, A. L. Sommers, and R. C. Cox, *Anal. Chem.*, **35**, 2166 (1963).

(47) C. A. Parker and W. T. Rees, *Analyst (London)*, **85**, 587 (1960).

and negligible reabsorption and reemission problems (*e.g.*, quinine sulfate).

The approximate eq 15 introduces ~5% systematic error for $AL = 0.043$ if the detector views either symmetrically around the center or the entire cuvette. If this error is unacceptable, the exact form of the equation or lower optical densities must be used. Alternatively, both the standard and the unknown can be made up to have equal absorbances at their respective exciting wavelengths and the need for any correction factor is eliminated. Even if the two experimental optical densities are not exactly the same, eq 16 may be used for relatively high optical densities if the two absorbances are comparable. For example, if $A_r(\lambda_r)L = 0.10$ and $A_x(\lambda_x)L = 0.12$, the term $A_r(\lambda_r)/A_x(\lambda_x)$ is within 2% of the value given by the exact expression.

If the exciting light is not monochromatic, eq 13 may fail. To be strictly correct it should be replaced by the expression

$$B = \frac{\int I_e(\bar{\nu})[1 - 10^{-A(\bar{\nu})L}]\,d\bar{\nu}}{\int I_e(\bar{\nu})\,d\bar{\nu}} \qquad (17)$$

where $I_e(\bar{\nu})$ is the spectral distribution of the exciting light in quanta/sec cm^{-1} and $A(\bar{\nu})L$ is the sample absorbance. The integrations are carried out over the energy range spanned by the source. If the approximate form for B is acceptable over the integration range, A in eq 16 can be replaced by an average absorbance, $\bar{A}$, given by

$$\bar{A} = \frac{\int I_e(\bar{\nu})A(\bar{\nu})\,d\bar{\nu}}{\int I_e(\bar{\nu})\,d\bar{\nu}} \qquad (18)$$

If $A(\bar{\nu})$ varies slowly enough over the excitation band, these expressions reduce to the simpler forms given above. We consider below some specific examples of this error source.

If $I_e(\bar{\nu})$ contains a small contribution of stray light which is well removed from the main excitation band and which is not specifically included in the data reduction, large errors in the yield may result. A classic example of this stray light error is given by Parker.[4a,47] Anthracene absorbs about 100 times more strongly at the 254-nm than at the 313-nm Hg line. Thus, if excitation is carried out with the 313 mercury line, but the monochromator passes 1% of the 254-nm line as stray light, the observed intensity of luminescence from anthracene will be twice the value that would be obtained if only 313-nm radiation had been incident upon it.

Even if stray light is negligible, the finite bandpass of the filters or monochromator may introduce appreciable error in the results if the sample absorbance at the wavelength of maximum excitation intensity is used as the effective absorbance. The details are too complicated to discuss here, but several examples will indicate the magnitude of the problem. Consider light selected with a monochromator having a triangular transmission curve from a source possessing a structureless continuum. Suppose this system is used to excite a dyestuff having a broad absorption band such as rhodamine B or fluorescein. If the bandwidth of excitation is 10 nm (the absorbance of the dye has fallen by ~18% at 10 nm on either side of the maximum), then the effective absorbance of the dye will be about 0.97 times the absorbance measured at the maximum.[20] If a 15-nm bandpass were used (absorbance down by ~42% of the maximum value), then the effective absorbance would be ~0.93 times the maximum absorbance.[20] On the other hand, a material such as benzene, which has very sharp bands even in solution, would need to be excited with a very narrow bandpass (less than 1 nm), if one wished to use the peak absorbance in the equation. In fact, if a 10-nm bandpass were used, the excitation range would straddle several absorption maxima and minima.[44] Thus caution must be exercised when one uses wide excitation bandwidths. Clearly, mercury arcs are to be preferred over xenon arcs if excitation can be accomplished at the mercury lines.

As pointed out in section II-B, the accurate measurement of the absorbance of a high quantum-yield compound is not always an easy task since the spectrometer detector may not be able to discriminate between the transmitted and emitted light. Errors in $A(\lambda)$ may readily exceed 5–10%.[28] The cure is to use a spectrometer with good rejection of the emitted light and to place the cuvette as far from the detector as possible.

Another difficulty may arise with molecules having long lifetimes when they are excited by intense sources. Under these conditions the concentration of ground-state molecules may become depleted, and the low-intensity absorption measurement ceases to have significance. Problems of this type are easily solved by reducing the exciting light intensity.

Equations 14 and 16 do not correct for reabsorption and reemission. Fortunately, the real beauty of the optically dilute method is that these corrections are rarely necessary—unless the material happens to be excited in an absorption minimum and there is substantial overlap between the absorption and the emission.

Several other sources of error cannot be easily avoided. A quantum yield is only as good as the certainty of the yield of the standard; hence, proper selection of the standard is paramount if the results are to be of lasting value. Also this method is particularly sensitive to errors from any polarization of the luminescence, since monochromators have reflectivities which are polarization dependent. Furthermore, isotropy was explicitly assumed in the derivations.

Equations 14 and 16 are commonly used exactly as stated. The unknown's emission spectrum is recorded, the standard is inserted and measured, the spectra are corrected, the integrations are performed, and the yield is evaluated. This specific procedure is not necessarily

reliable. Considerable time is required to scan the emission of both standard and unknown, allowing slow instrumental drift to affect the accuracy. Very long scan times with large amounts of electrical filtering in the circuitry are not uncommon, especially if structured absorption bands dictate the use of narrow monochromator slits (low-energy conditions) to define accurately the absorbance of the sample (eq 17).

To circumvent the drift problems, Parker and Rees[47] have recommended an alternative procedure. First, the ratio of the corrected emission area to the uncorrected emission intensity at some convenient wavelength is obtained by a separate experiment. For the subsequent quantum-yield measurement the emission intensity of the compound is recorded only at the selected wavelength. The product of the ratio defined above and the measured uncorrected intensity at the chosen wavelength gives the corrected area of eq 14 and 16. The advantages of this technique are numerous. Since the emission intensity for the sample (unknown or standard) is required only at a single wavelength, the data may be collected in a very short period (10–15 sec on some instruments), thus eliminating long-term instrumental drift. Even if the signals are very noisy due to weak excitation or low yields, long filter time constants can be used to reduce the noise without extending the measurement time prohibitively. A principal advantage is that the emission spectrum may be recorded at high excitation intensities where the signal-to-noise ratio is good (the assumption is made that the area to intensity ratio is not a function of excitation intensity or bandwidth, a condition normally satisfied for most pure compounds). The accuracy of the determination is substantially enhanced. Frequently also the intensity measurement may be made at a wavelength where interferences due to solvent emission and scattered light are minimized. The indirect method of Parker and Rees is highly recommended over the direct technique.

The basic optically dilute method has been modified in several ways. Quantum counters have been used for detection.[38] (In eq 14 and 16 the areas are replaced by the quantum-counter response.) Although quantum-counter detectors are less sensitive than standard calibrated spectrometers and are limited to measurements on compounds emitting below 600 nm, they compensate for these factors by introducing speed and simplicity. A calibrated detector can also be used with the method. Birks and Dyson[48] have employed a calibrated photomultiplier. They used an equation similar to 16 except that the area of the corrected emission spectrum is replaced by the average detector response per incident photon (eq 8). An independent measurement of the emission spectrum is also required, which leads to the extensive calibrations and integrations needed for any calibrated detector technique. For routine measurements it is probably not worth the trouble. Another modification makes use of an integrating sphere and a calibrated spectrometer.[49,50] This technique has a number of advantages over the conventional arrangement since polarization errors and refractive index corrections are eliminated (see section II-F).

The use of optically thin solutions *vs.* an optically thin standard compound is probably the most accurate routine method of measuring quantum yields. Results in the literature indicate that the reproducibility within a laboratory for the relative yields of two compounds is excellent, with 1–2% being claimed by some workers. Of course, relative yields for the same compounds measured in various laboratories differ substantially due, no doubt, to the problems inherent in calibrating spectrometers, in purifying materials, and in preparing samples. Nevertheless, the agreement is remarkably good between workers of good reputations with less than 5% variations being not uncommon.

D. Calorimetric Methods. A conceptually simple and somewhat overlooked method of measuring yields of compounds is calorimetry, a technique whereby absolute energy yields are obtained from temperature changes during irradiation. The temperature rise of an irradiated luminescent sample is compared with the rise in temperature of a nonluminescent material of similar optical density subjected to the same optical pumping. Since the nonluminescent sample has a zero energy yield, the ratio of the heating of the two samples gives the fraction of the absorbed energy which is lost by nonradiative processes in the luminescent sample, that is, the complement of the luminescence energy yield.

To convert energy yields to quantum yields one needs the emission spectrum of the sample and the frequency distribution in the exciting beam. The two yields are related by

$$Q_q = Q_e \frac{\int \bar{\nu} E(\bar{\nu})\, d\bar{\nu} / \int E(\bar{\nu})\, d\bar{\nu}}{\int \bar{\nu} F(\bar{\nu})\, d\bar{\nu} / \int F(\bar{\nu})\, d\bar{\nu}} \qquad (19)$$

where Q_q is the quantum yield, Q_e is the energy yield, and $E(\bar{\nu})$ and $F(\bar{\nu})$ are the unnormalized spectral distributions of the exciting and emitted light (quanta/sec cm^{-1}), respectively. The integrations are over the range of nonzero intensities. Fortunately, highly accurate spectra are not necessary, since relatively large errors in these spectra produce small errors in the quantum yield. If the exciting light extends over a wide wavelength range and the solution does not absorb all the exciting light, then the absorption spectrum of the sample is also needed (see ref 51 for details).

(48) J. B. Birks and D. J. Dyson, *Proc. Roy. Soc., Ser. A*, **275**, 135 (1963).

(49) W. R. Ware and B. A. Baldwin, *J. Chem. Phys.*, **43**, 1194 (1965).

(50) E. J. Bowen and J. Sahu, *J. Phys. Chem.*, **63**, 4 (1959).

Among the problems of the calorimetric method, reabsorption is one of the worst, for the relative insensitivity of the usual temperature sensors and the large blanks force one to choose a strongly absorbing sample. The problem is especially critical when absorption–emission overlap is pronounced. Advantages of the method are that corrections for experimental geometry, refractive index changes (the refractive index affects the measured yield indirectly by its effect on the amount of reabsorption in the cuvette—see section VI), and polarization effects are largely eliminated.

The calorimetric apparatus consists of a source and filter train to produce monochromatic radiation, a sample cuvette equipped with a temperature sensor, a readout, and an adiabatic chamber for the cuvette. The requirements for the light source and optical filter system are stringent. The lamp should be intense, stable with time, and low in infrared radiation. It should possess widely spaced spectral lines with little background continuum. No available sources satisfy all these requirements. Low-pressure mercury arcs have been used,[52] because most of their energy is concentrated in the 254-nm line. Their principal limitations are low intensities and large arc sizes which prevent easy focusing. Incandescent bulbs have been used,[51] but they have no major advantages. Carbon arcs (Gudmundsen, *et al.*,[53] used a 3-kW carbon arc) have an intense ultraviolet output and a comparatively low component in the infrared, but they are very unstable. High-pressure mercury[54] and mercury–xenon arcs do approach the ideal. They can be focused to a small area[55] (less than 0.25 cm^2 in some types) which allows small sample sizes and hence rapid sample heating. They produce high intensity, pressure-broadened line spectra in the visible and near-ultraviolet regions as well as relatively low infrared output, and they can be easily stabilized. For example, a stable 1-kW AH-6 capillary arc supplies about the same energy (300–400-nm region) as a 3-kW carbon arc.[55] For any light source it is necessary to remove infrared radiation in order to prevent undue heating. Comprehensive lists of suitable solution filters are available.[6,56]

The design of the sample chamber must assure an isolated environment to eliminate ambient thermal drift. Workers have employed concentric boxes filled with layers of cotton and wood chips,[52] concentric boxes with dead air spaces housed in a temperature-controlled room,[54] thermostated baths,[51] and even a small Pyrex dewar.[53] A thermostated environment is clearly the best arrangement, however. Low-cost thermistor controllers can regulate a chamber to $\pm 0.01°$, and, with proper insulation, thermal drift should present no problems. A design feature which may be important is the blackening (black paint or benzene soot[54]) of the chamber surrounding the sample in order to prevent spurious temperature rises from reflection of the luminescence back into the sample.

The design of the sample cell also requires care. Ideally all the sample fluorescence should escape the cell. Alentsev[54] went to great lengths to prevent radiation trapping in his cuvette. The cell was kept very thin, and its near edges were cambered and polished in order to reflect to the outside all internally reflected radiation (see section VI-A). The cell was secured in a highly polished ring for mounting the thermocouples. Even with a mirror polish the ring reduced by 10% the escaping light, which in turn dictated a 10% correction to all final values. The extent of error due to radiation trapping in a dewar is unknown, but if the compound exhibits negligible reabsorption, the error is probably not large.

Since small temperature changes occur during a calorimetric measurement, the temperature transducers must be very sensitive. Thermocouples, thermopiles, and sample expansion seem to have been the only sensors employed so far. Alentsev[54] used a 10-junction copper–constantan thermopile which gives an overall sensitivity of 500 $\mu V/°C$, whereas Gudmundsen, *et al.*,[53] were able to get by with a single iron–constantan thermocouple because of the high intensity of their source. Seybold, Gouterman, and Callis[51] have developed a very sensitive technique to monitor the temperature. When the solution is contained in a vessel which is only open to the air through a narrow bore capillary tube, the rate of expansion of the liquid up the capillary is a measure of the sample heating—the sample acts as its own thermometer. Their equipment had a capillary-rise sensitivity of 5×10^2 mm/°C. The capillary rise measures the average heating of the entire sample in contrast to thermocouples which can be unreliable because they monitor the temperature of a specific location in the cell. The capillary-rise method does have two disadvantages. The data must be recorded visually from a moving column, and water, an important solvent, cannot be used since its thermal expansion coefficient is too small.[51]

An attractive temperature sensor, which can probably surpass in sensitivity any other available device, is the thermistor. For example, a 1000-ohm 4%/°C thermistor (a common commercial item of intermediate sensitivity) operated at 0.1 mA (0.01 mW) gives a sensitivity of 4 mV/°C (equivalent to an 80-thermocouple copper–constantan thermopile). A simple sensitive differential chemical calorimeter employing thermistors has been described by Meites, *et al.*[57]

(51) P. G. Seybold, M. Gouterman, and J. Callis, *Photochem. Photobiol.*, **9**, 229 (1969).

(52) Z. Bodo, *Acta Phys. Acad. Sci. Hung.*, **3**, 23 (1953).

(53) R. A. Gudmundsen, O. J. Marsh, and E. Matovich, *J. Chem. Phys.*, **39**, 272 (1963).

(54) M. A. Alentsev, National Research Council of Canada Technical Translation TT-433, *Zh. Eksp. Teor. Fiz.*, **21**, 133 (1951).

(55) L. R. Koller, "Ultraviolet Radiation," Wiley, New York, N. Y., 1952.

(56) M. Kasha, *J. Opt. Soc. Amer.*, **38**, 929 (1948).

To calculate quantum yields from calorimetric measurements, two techniques are available for handling the raw data. Both methods are based on the differential equation below (an extension of an equation in ref 52) describing the dynamic energy balance in the system.

$$K\,dT/dt = AF(1 - Q_eS) + Af - B(T - T_0) \quad (20)$$

where K is the total heat capacity of the cuvette and its contents (energy/°C); T, the temperature of the cuvette; t, the time elapsed after start of excitation; A, the radiant energy incident on the cuvette (energy/sec); F, the fraction of incident radiant energy absorbed by sample molecules; Q_e, the energy yield of the sample; S, the fraction of luminescence which escapes the cuvette; f, the fraction of incident radiant energy absorbed by the cuvette and solvent; B, heat loss of cuvette to surroundings (energy/°C sec); and T_0, the initial temperature of cuvette which equals the temperature of the surroundings at $t = 0$.

In this expression it is explicitly assumed that the cooling rate is proportional to the first power of the temperature difference between the cuvette and the surroundings, a reasonable approximation because of the small temperature changes involved. Regardless of the data reduction procedure used, the temperature rise of the cuvette after the beginning of irradiation by the source must be registered for three separate experiments. The rise must be recorded for the cuvette filled with (1) the luminescent sample, (2) a nonluminescent material, and (3) the pure solvent. The completely nonluminescent material must exhibit no luminescence at any wavelength. Alentsev[54] showed that fluorescein quenched by potassium iodide, Aquadag, and aniline black all exhibited the same apparent energy yield; he concluded that all were probably nonfluorescent in any spectral region. Gudmundsen, *et al.*,[53] used thenoyltrifluoroacetone as an ultraviolet absorbing dye. From modern knowledge of molecular structure it is likely that this material exhibits no luminescence. Almost any molecule which displays no visible or ultraviolet luminescence and has no low-lying electronic levels would also be satisfactory. For all three measurements the total heat capacity of the cuvette and its contents must be the same value.

In one method of handling the data[51,53] the value of dT/dt is measured for each of the three systems immediately after the onset of illumination; at this time the heat loss term, $B(T - T_0)$, is insignificant in comparison with the heating terms. The experimental expression required is

$$\frac{(dT/dt)_1 - (dT/dt)_3}{(dT/dt)_2 - (dT/dt)_3} = \frac{(1 - Q_eS)F_1 + f_1 - f_3}{F_2 + f_2 - f_3} \quad (21)$$

where the subscripts correspond to the values obtained from each of the measurements enumerated above.

For the alternative data reduction procedure[54] the integrated form of eq 20 is required.[52]

$$(T - T_0) = \frac{A}{B}[F(1 - Q_eS) + f][1 - \exp(-Bt/K)] \quad (22)$$

Both experimentally and theoretically (see eq 22) the limiting temperature rises [denoted below by $(T - T_0)'$] for the three experiments are related to the parameters in eq 20 by

$$\frac{(T - T_0)_1' - (T - T_0)_3'}{(T - T_0)_2' - (T - T_0)_3'} = \frac{(1 - Q_eS)F_1 + f_1 - f_3}{F_2 + f_2 - f_3} \quad (23)$$

where the subscripts have the same meaning as above.

To obtain an energy yield from eq 21 and 23 several simplifying assumptions are made. Usually the quantities f_1, f_2, and f_3 are assumed to be equal. For measurements (1) and (2), the exciting light passes only through the entrance face and part of the solution while for measurement (3) the light passes completely through the cuvette. Thus, f_3 might be twice as large as f_1 or f_2. Fortunately, even for this worst possible case, a systematic error of no more than 5% would be expected for a value of $f_3 = 0.10$. For optically thin solutions all f's should indeed approach the same value. The quantities F_1 and F_2 are directly measurable by absorption experiments. For simplicity S is usually assumed to be unity; however, as shown experimentally,[54] this does not hold for strongly reabsorbing solutions. Alentsev[54] found that aqueous solutions with concentrations of fluorescein up to 2×10^{-4} M had constant S, but at $\sim 2 \times 10^{-3}$ M, S was down to 79% and at $\sim 10^{-3}$ M, S had decreased to 48% of its original value. He also found that his thermocouple mounting ring on the cuvette reduced S by 10%; a small thermistor could eliminate this problem. In their equipment Seybold, *et al.*,[51] calculated $S \simeq 0.65$ for 10^{-5} M fluorescein solutions.

With a well-designed apparatus the calorimetric method competes favorably with other techniques for obtaining quantum yields.[51,54] In spite of the need to know the spectral distribution of both the exciting light and the emission, it is probable that the error can be kept below 10% and perhaps below 5% for favorable cases. Its use is largely limited to compounds with energy yields greater than 0.1, however.

Because of the accuracy attainable, its applicability to red and infrared emitters, and the recent advancements in low-cost temperature sensors and controllers, the calorimetric technique for measuring yields offers considerable promise. Especially beyond 600 nm (the

(57) T. Meites, L. Meites, and J. N. Jaitly, *J. Phys. Chem.*, **73**, 3801 (1969).

limits of the rhodamine B quantum counter) it appears to be quite attractive. This method should also prove useful as a means for checking quantum-yield standards.

E. Absolute Evaluation of the Geometry. This section describes various methods of measuring quantum yields that have one feature in common—the fraction of the total luminescence reaching the detector has been evaluated from the geometry.

Of all these techniques the most interesting is the modification, by Andreeshchev and Rozman,[58] of the basic Vavilov–Bowen method for measuring quantum yields. They replaced the usual scatterer with a quantum counter. The technique is particularly well suited for measuring optically dense materials which emit below 600 nm. The geometry employed is basically the same as that used in the Vavilov method (Figure 1). A quantum counter–detector combination is suitably stopped in order to define accurately the solid angle of accepted radiation. The procedure consists of first measuring the intensity of luminescence from the sample placed at the focus of the arc. If all light entering the sample is absorbed, the quantum counter response is

$$D_x = QN_0T_xT_e\left(\frac{\alpha}{4\pi}\right)T_qS\left(\frac{1}{n^2}\right) \qquad (24)$$

D_x is the phototube current with the fluorescent sample in position; Q is the quantum yield of the phosphor; N_0 (quanta/sec) is the intensity of incident radiation; T_x is the transmission coefficient of the cuvette to the exciting light; T_e is the transmission coefficient of the cuvette to the emitted light; α is the solid angle (steradians) accepted by the quantum counter; T_q is the transmission coefficient of the quantum-counter window to the luminescence; S is the absolute sensitivity of the quantum counter in units of ampere/(photons/sec). Now instead of replacing the cuvette with a scatterer and measuring the detector response, as was done by Vavilov,[17] Andreeshchev and Rozman have placed the quantum counter–detector combination in the position of the cuvette, and the intensity of the exciting light is measured directly (the sensitive surface must be larger than the arc image). The response of the counter to the exciting light, D_s, is given by

$$D_s = N_0T_0S \qquad (25)$$

where T_0 is the transmission coefficient of the quantum-counter window to the exciting light, and the other terms are as defined in eq 24. By combining eq 24 and 25 one obtains the quantum yield in terms of measurable quantities

$$Q = \left(\frac{D_x}{D_s}\right)\left(\frac{T_0}{T_xT_eT_q}\right)\left(\frac{n^2}{(\alpha/4\pi)}\right) \qquad (26)$$

This procedure has distinct advantages over the Vavilov method; it is unnecessary to correct for deviations from Lambert's law or to know the reflectance of the scatterer. If high quality windows are used, T_0/T_x can be nearly unity. Therefore, only T_e and T_q need normally be calculated, and this may be done to sufficient accuracy from Fresnel's law.[19,24] In order to define accurately the solid angle, a small arc image is required but the size of the spot can approach 10% of the distance to the optical stops on the quantum counter without introducing more than ~1% error in the measurement.[24] If the surface of the quantum counter is not uniformly sensitive, an indeterminate factor is introduced into the final expression for Q. The problem can be avoided by using a properly designed quantum counter.[59] In the original work of Andreeshchev and Rozman[58] there may be large systematic errors, for no check for sensitivity variations over the surface of the photomultiplier was made. Their experimental arrangement, which is not generally recommended, could introduce substantial errors into yield measurements, because the results obtained from this particular geometry are very susceptible to error from small amounts of light leaking directly through the quantum counter.

Crucial to the use of eq 26 is the accurate determination of α. This angle is best defined by a hole in a thin sheet placed over the quantum counter such that the luminescence does not miss the sensitive area. When the distance from the source is large compared with the diameter of the stop, the term α in eq 26 is given by the area of the hole divided by the square of its distance from the emitting volume to the stop.

Use of a quantum counter in the manner described puts considerable demand on the detector. For $(\alpha/4\pi) \simeq 10^{-3}$ a linear range of 10^5 of the detector readout is required to measure compounds with yields ranging from 0.01 to 1.0, whereas with the Vavilov method a linear range of 400 is sufficient. Nevertheless, modern photomultipliers, coupled with highly linear picoammeters, can handle the job.[40] An alternative, but seemingly less attractive, procedure would be to attenuate the higher intensity light with very carefully calibrated neutral density filters.

Since this technique is an adaptation of the basic Vavilov method, it presents many of the same types of problems, particularly those associated with reabsorption and reemission and sensitivity to scattered light. The many difficulties notwithstanding, this absolute method recommends itself highly for future work with optically dense materials. It is free from a number of sources of error particular to the Vavilov procedure, and hence the accuracy attainable in a properly designed experiment is as good as, or better than, that obtainable by use of the standard scatterer (±10%).

Other methods based on evaluation of the geometry

(58) E. A. Andreeshchev and I. M. Rozman, *Opt. Spectrosc.*, **8**, 435 (1960).

(59) J. Yguerabide, *Rev. Sci. Instrum.*, **39**, 1048 (1968).

have been used successfully. Almy and Gillette[60] employed a method similar to that given by Andreeshchev and Rozman.[58] Instead of using an optically dense sample, an optically dilute solution was viewed at right angles. The use of a sample with low optical density introduces serious complications. The emission can no longer be treated as a simple point source, and the fraction of exciting light which is absorbed in a region seen by the detector must be estimated. This calculation is complicated by the fact that the fraction of light gathered by the detector from a volume element is strongly affected by the position of the element and the slit system–detector geometry. Almy and Gillette used an equation suitable for a sample of relatively low optical density. Henriques and Noyes[61] have given a general expression suitable for higher optical densities. In both derivations the detector was assumed to have a uniformly sensitive surface. Most detectors do not satisfy this condition,[62] and substantial deviations from the theoretical expressions could occur. A properly designed quantum counter could eliminate the problem.[59] Another source of error in the method of Almy and Gillette arises from the use of an absorption measurement for estimating the amount of light taken up by the sample. As shown by Hunt and Hill[63] the fraction of light actually absorbed in a gas sample can be 8–17% more than would be indicated by absorption data because of multiple reflections between the cell windows. Calvert and Pitts have also discussed this problem for liquids (ref 6, p 793).

Because of the considerable difficulties encountered in measuring the fraction of emitted radiation reaching the detector, absolute evaluation of the geometry using optically dilute samples has serious limitations. The technique might find use for the estimation of quantum yields of gases, although relative methods using a solution standard would probably be more reliable.

In summary, of the quantum-yield techniques that estimate the fraction of emitted light reaching the detector, only the method of Andreeshchev and Rozman[58] seems practical. Indeed the latter appears to be so reliable and simple that it should find wide use for making routine measurements on compounds emitting entirely below 600 nm.

F. Integrating Spheres. Although use of an integrating sphere does not provide a distinct new method of measuring quantum yields, such spheres are frequently used in order to eliminate the need for polarization and refractive index corrections. In this section we discuss the uses of integrating spheres, the difficulties associated with them, and the situations where they are most useful.

Typically, an integrating sphere[49] is a large globe covered on the inside with a highly reflecting coating of barium sulfate or magnesium oxide. The exciting light passes in through one window, and the detector views the emission *via* a second port. The sample is usually placed at the center of the sphere. A reflecting baffle within the sphere shields the detector from direct sample emission. The primary purpose of the integrating sphere is to average out, by multiple diffuse reflections, any spacial anisotropy of the emission. Also, refractive index and polarization errors are eliminated. Problems arise, however, because the coatings, although highly reflecting, show a slight wavelength dependence of the reflectance[23] which causes large changes in the reflectivity of the sphere. The sphere thus acts like a filter over the detector whose transmission coefficient, $T(\lambda)$, is wavelength dependent.

$$T(\lambda) = \frac{K[R(\lambda)]^2}{1 - R(\lambda)} \tag{27}$$

where K is a constant of proportionality and $R(\lambda)$ is the absolute reflectance of the sphere coating as a function of wavelength.[23] Since the shape of $R(\lambda)$ can be highly dependent on the reflecting surface and method of its preparation,[23] the emission spectrum seen by the detector may be considerably distorted.

Correcting for variable sphere transmission can be handled in several ways. If the unknown and the standard have luminescence spectra which are very similar, one might ignore the transmission curve of the sphere without introducing much error, particularly if the reflectance is relatively flat over the range of interest. If the spectra are quite different, the detector could be calibrated without the sphere, and then the observed distributions corrected for the variable transmission of the sphere.[64] A method which seems workable (although we are not aware of anyone using it) would be to calibrate the detector–sphere combination as a unit. If the detector were a monochromator, the calibration could be done easily by directing the light from a standard lamp through the excitation port. If the detector were a photocell or thermopile, monochromatic light from a calibrated monochromator–lamp combination could serve as a source. In either case it would probably be desirable to put a diffuse scatterer in place of the sample in order to duplicate the geometry as closely as possible.

Quantum-yield measurements involving integrating spheres are probably more affected by reabsorption than most other methods of measurement. Although the amount of reabsorption of emitted light on a single pass through the cuvette might be small, the sphere causes multiple passes through the cuvette and the loss is multiplied. Another problem related to multiple reflections may arise if optically dilute samples are used

(60) G. M. Almy and P. R. Gillette, *J. Chem. Phys.*, **11**, 188 (1943).
(61) F. C. Henriques, Jr., and W. A. Noyes, Jr., *J. Amer. Chem. Soc.*, **62**, 1038 (1940).
(62) J. Lee and H. H. Seliger, *Photochem. Photobiol.*, **4**, 1015 (1965).
(63) R. E. Hunt and T. L. Hill, *J. Chem. Phys.*, **15**, 111 (1947).
(64) L. S. Forster and R. Livingston, *ibid.*, **20**, 1315 (1952).

with an integrating sphere. In this case eq 13 must be used with caution, for more exciting light may be absorbed at low optical densities than expected.

It appears that integrating spheres will be most appropriate and reliable for quantum-yield measurements when the exciting light is totally absorbed, reabsorption–reemission is negligible, and polarization and refractive index problems are manifest. Since these conditions are frequently fulfilled in low-temperature emission work, and since a sphere may be evacuated to serve as a dewar, integrating spheres should find their greatest use in low-temperature studies.

G. Miscellaneous Methods. Several indirect methods, which are applicable only in very special situations, have been devised for measuring quantum yields. Procedures have been based on energy transfer from the fluorescing molecule to a standard, on the degree of quenching of fluorescence as a function of concentration, and on the change of the measured decay time of fluorescence as a function of the extent of reabsorption. None of the ingenious methods described in this section for obtaining quantum yields have general applicability. They represent, however, novel approaches for obtaining yields under difficult or unusual circumstances.

When energy transfer occurs *via* collisional transfer, Bowers and Porter[65] have devised a scheme for obtaining quantum yields of the donor. A key assumption is that every collisionally deactivated donor produces an excited acceptor that then emits with its characteristic quantum yield. Their published analysis of the experimental data is difficult to follow, but it is obvious that the yields can be calculated from the data.

A conceptually similar technique has been developed by Kellogg and Bennett.[66] The donor and acceptor are held in a rigid matrix, and energy transfer occurs by a long-range mechanism rather than by diffusion-controlled bimolecular quenching. Again it is necessary to know the yield of the acceptor and to assume that each donor molecule quenched by energy transfer produces one excited acceptor, which will then luminesce with its characteristic yield. Limitations are placed on the donor and acceptor. Certainly the donor must phosphoresce, since the phosphorescing state is responsible for the energy transfer. Because the authors worked with plastic films which are not easily standardized, the donor had to fluoresce also so that this light intensity could be used as an internal standard. To employ this procedure one must assume that the acceptor does not quench the donor fluorescence, but we note that Ermolaev and Sveshnikova[67] have shown that significant fluorescence quenching can occur in some systems. In addition, the acceptor must have a strong absorption band overlapping the donor phosphorescence and have a known quantum yield. To obtain the fluorescence (ϕ_f) or phosphorescence (ϕ_p) quantum yields of a substance, the intersystem-crossing quantum yield (ϕ_{isc}) is also needed, or it is necessary to assume, as Kellogg and Bennett[66] did, that ($\phi_{isc} + \phi_f$) is unity (*i.e.*, no direct internal conversion from the excited singlet to the ground state occurs). There is evidence that many organic molecules satisfy this condition, but some certainly do not.[6,8] Fortunately, for numerous substances ϕ_{isc} can be measured directly. Practically, the measurement of quantum yields by energy transfer must be performed with thin films in order to reduce the trivial reabsorption of the luminescence. Polarization errors for such rigid specimens may be significant, although the energy-transfer process could reduce the problem. Instrumentally the measurements are also quite difficult. No refractive index correction is required.

Two quantum-yield methods based on the reabsorption and reemission properties of the sample have been devised. Umberger and LaMer[68] made use of the bimolecular quenching constant, whereas Wright[69] used information about changes in fluorescence band shape and lifetime as a function of sample size and physical state. The method of Wright deserves comment for it represents an attempt to measure a quantum yield for a substance in the solid state. His expression for the quantum yield, Q, is

$$Q = \frac{1 - (\tau_m/\tau_e)}{1 - (\delta + K - \delta K)} \tag{28}$$

where τ_m and τ_e are the measured lifetimes of a microcrystalline powder and a macroscopic crystal of the substance. For the τ_m measurement reabsorption is assumed to be negligible, but for the τ_e determination extensive reabsorption–reemission must occur. This reabsorption–reemission revealed its presence in Wright's large crystal by a significant increase in the lifetime (τ_m = 6.4 nsec and τ_e = 18 nsec) and by the considerable attenuation of the high-energy portion of the emission in the large crystal *vs.* the powder. In eq 28, K and δ are quantities obtained from the geometry and the observed alteration of the emission spectrum as the size of the crystal increases. This equation is based on the assumption that only trivial reabsorption is responsible for the band shape alterations and the lifetime changes. The exact method of obtaining δ is unclear. Because exciton migration and nontrivial Förster energy transfer probably occur readily in such systems, it is uncertain how valid this model is and what effect the true processes involved have on the final results. Since the method is experimentally

(65) P. G. Bowers and G. B. Porter, *J. Phys. Chem.*, **68**, 2982 (1964).

(66) R. E. Kellogg and R. G. Bennett, *J. Chem. Phys.*, **41**, 3042 (1964).

(67) V. L. Ermolaev and E. B. Sveshnikova, *Opt. Spectrosc.*, **16**, 320 (1964).

(68) J. Q. Umberger and V. K. LaMer, *J. Amer. Chem. Soc.*, **67**, 1099 (1945).

(69) G. T. Wright, *Proc. Phys. Soc., Ser. B*, **68**, 241 (1955).

quite simple and might prove to be useful for the evaluation of yields for systems where other methods prove intractable (large reabsorption–reemission problems), it warrants extensive study to check the reliability. For anthracene Wright obtained a reasonable quantum yield of 0.94.

III. Quantum-Yield Standards

For relative quantum-yield measurements the selection of a reliable standard is critical. By utilizing a standard with a poorly characterized yield many authors have vitiated their results. Another common mistake is to use a reliable standard under conditions where the accepted yield is no longer appropriate (*e.g.*, at higher concentrations where reabsorption, reemission, dimerization, and concentration quenching make yields reported for dilute solutions meaningless). Some workers have even failed to specify the yield assumed for their standard. Since the established yields of standards sometimes undergo drastic revisions, such omissions prevent the updating of results. In this section the best available yields, the experimental conditions for use, and the sources of error associated with common standards are discussed.

An ideal quantum-yield standard should have no overlap between absorption and emission. It should be easily obtained and purified, be soluble in the same solvents as the compound to be studied (hence avoiding the refractive index correction), and be stable in solution. It should not be susceptible to oxygen or concentration quenching. Its yield should be independent of the exciting wavelength so that the excitation conditions are unimportant. Furthermore, the absorption and emission spectra should be similar to those of the compounds under investigation so that source- or detector-calibration errors will not greatly affect the results. Above all, the yield of the standard must be accurately known. Few compounds satisfy even the most important of these criteria.

Numerous compounds have been chosen as standards. Benzophenone,[70] naphthalene,[71] and fluorescein[72] have been used at 77°K; eosin,[73,74] 9,10-diphenylanthracene,[44,48,75] naphthalene,[76] tryptophan,[39,77] fluorescein,[51,78] and anthracene[49,50,79] have been employed at room temperature. By far the most popular has been quinine sulfate.[22,46,47,80–82]

Quinine sulfate in 0.1 or 1.0 *N* sulfuric acid appears to be a nearly perfect standard. Its emission spectrum lies completely in the sensitive region of the rhodamine B quantum counter. It is not oxygen quenched, exhibits little concentration quenching, has no significant overlap between its absorption and emission spectra, and is stable in solution. Of all compounds used as standards its yield is believed to be one of the best known. As an added benefit the absorption band at ~350 nm is broad and structureless; consequently quite broad excitation bandwidths at this wavelength can be used without introducing significant errors. These appealing factors explain its wide popularity as a standard. The most commonly assumed yield values are those given by Melhuish[22] (*vide infra*).

For optically dilute measurements the source or form of quinine seems to be unimportant. Fletcher[83] has shown that solid samples of quinine sulfate or bisulfate obtained from a number of sources have the same quantum yield ($\sim 2 \times 10^{-6}$ *M* in 0.1 *N* sulfuric acid with 313-nm excitation) after drying to constant weight at 50–60° and 60 Torr. He did not test the undried compounds, but it is reasonable to assume that drying had no effect on the yields.

In spite of the apparent reliability of quinine sulfate large errors may have crept into the literature. Most authors use 0.1 *N* sulfuric acid solutions of quinine in their measurements yet employ Melhuish's reported quantum yield for a solution of quinine in 1.0 *N* sulfuric acid. Data by Eisenbrand[84] and Dawson and Windsor[38] indicate the yield is 6–8% higher in the 1.0 *N* acid solution than in the 0.1 *N* solution. Turner[85] has, however, been unable to substantiate these claims. If the yield change with acid concentration is indeed real, a considerable number of yields reported in the literature must be recomputed. Until this question is definitively settled, quinine should be used only in 1.0 *N* sulfuric acid solutions.[86] Because of the sensitivity of quinine to halogen quenching only the highest purity acid should be employed.

Several problems are associated with the use of quinine sulfate as a standard, however. Its yield has a strong temperature dependence (−0.25%/°C),[22] which must be accounted for in accurate work, and it is photo-

(70) J. T. Dubois and F. Wilkinson, *J. Chem. Phys.*, **39**, 899 (1963).

(71) V. L. Ermolaev and K. K. Svitashev, *Opt. Spectrosc.*, **7**, 399 (1959).

(72) V. Zanker, H. Rammensee, and T. Haibach, *Z. Angew. Phys.*, **10**, 357 (1958).

(73) N. Filipescu, G. W. Mushrush, C. R. Hurt, and N. McAvoy, *Nature*, **211**, 260 (1966).

(74) A. V. Buettner, *J. Chem. Phys.*, **46**, 1398 (1967).

(75) R. Rusakowicz and A. C. Testa, *J. Phys. Chem.*, **72**, 793 (1968).

(76) J. B. Aladekomo and J. B. Birks, *Proc. Roy. Soc., Ser. A*, **284**, 551 (1965).

(77) A. Weisstuch and A. C. Testa, *J. Phys. Chem.*, **72**, 1982 (1968).

(78) L. S. Forster and D. Dudley, *ibid.*, **66**, 838 (1962).

(79) E. C. Lim, J. D. Laposa, and J. M. H. Yu, *J. Mol. Spectrosc.* **19**, 412 (1966).

(80) J. Drobnik and E. Yeargers, *ibid.*, **19**, 454 (1966).

(81) A. N. Fletcher, *ibid.*, **23**, 221 (1967).

(82) R. F. Chen, *Nature*, **209**, 69 (1966).

(83) A. N. Fletcher, *Photochem. Photobiol.*, **9**, 439 (1969).

(84) J. Eisenbrand, *Fresenius' Z. Anal. Chem.*, **179**, 170 (1961).

(85) G. K. Turner, private communication.

(86) A number of literature values of quantum yields are quoted in the remainder of this section. Wherever these yields were based on an assumed value of 0.55 for quinine in 0.1 *N* sulfuric acid, we have recomputed (rather arbitrarily in view of the present uncertainties) the yields on the basis of a value of 0.50.

chemically unstable when excited below 300 nm.[87] Careful studies[88-90] also indicate that the emission spectrum of quinine changes as the exciting wavelength is varied. The emission spectrum is independent of exciting wavelength below 350 nm but progressively red shifts for excitation at longer wavelengths. Scanning the excitation from 350 nm to 420 nm shifts the emission maximum by 15 nm.[89] Fletcher[89] has shown that this unexpected phenomenon occurs with a number of other molecules.

A question of great significance is: does a concomitant change in quantum yield accompany the shift in emission spectrum of quinine sulfate? If the yield were wavelength dependent in the 340–370-nm region, an effect which has been reported,[88] this would be most unfortunate since many authors have used Melhuish's quantum-yield value for 365-nm excitation when exciting below 350 nm. Thus, large systematic errors could be present in the published values. There have been a number of conflicting reports on the variation of the quantum yield of quinine as a function of wavelength. Turner[87] using a Turner "Spectro" 210 observed that the quantum yield was ~4% higher when exciting at 348 nm *vs.* 365 nm. More recent data by Turner[85] indicate that the yield is constant within 1% from 260 nm to 365 nm. Chen[88] found that the yield decreased ~9% as excitation changed from 366 nm to 348 nm and was approximately constant between 250 and 348 nm. Børresen[91] found that the quantum yield was 47% higher at 346 than at 250 nm. On the other hand, Eastman[26] found the quantum yield to be the same at 250 and 350 nm. Fletcher[81] using a Turner "Spectro" 210 found the quantum yield of quinine sulfate in 0.1 *N* sulfuric acid to be the same at 313 and 365 nm within 1%.

Fortunately, careful studies by both Gill and Fletcher have cleared up much of the confusion. Gill,[90] using a carefully calibrated homemade instrument, showed that the quantum yield of quinine bisulfate in 0.1 *N* sulfuric acid was constant to ±5% for excitation in the region 200–400 nm. This wavelength independence held for concentrations ranging from 10^{-2} to 10^{-6} *M*. Between 345 and 376 nm, the region of contention, no more than a 3% change in the yield occurred. Fletcher's data,[83] obtained on a Turner "Spectro" 210, show that between 345 and 390 nm the yield is constant to within ±3%. Also, from 240 to 400 nm the yield is probably constant to ±5%.

Both Gill and Fletcher analyze the possible reasons for the variations of yield found in the early work. In view of the inability of either of them to duplicate the results of Chen and Børresen, it is reasonable to assume that the early discrepancies were caused by calibration errors. We conclude that *the quantum yield of quinine sulfate in 0.1 N sulfuric acid is probably constant over the region 200–390 nm.*

There is another important paper on the wavelength variation of the quantum yield of quinine sulfate. Dawson and Windsor,[38] using a Weber and Teale method, found the yield in 1.0 *N* sulfuric acid to be constant within experimental error (~4%) at 254, 334, and 365 nm but significantly lower (~15%) at 313 nm. Purification of their quinine by recrystallization or column chromatography had no effect on the results. This apparent drop in yield at 313 nm must be viewed with some skepticism for several reasons. Melhuish[18] claimed the yield of more concentrated quinine solutions in 1.0 *N* acid to be the same at 313 and 365 nm. The data of Gill[90] and Fletcher[83] indicated no decrease in yield for 0.1 *N* solutions in this region; it seems unlikely that changing the acid concentration would cause this effect. Nevertheless, the results of Dawson and Windsor[38] withstood a number of independent checks of their experimental methods; consequently, their data cannot be lightly dismissed. The question bears further study.

Another possible anomaly associated with quinine was noted by Rusakowicz and Testa.[75] They found that the sulfate and the bisulfate were not equivalent as standards. The sulfate appeared to have a lower yield than the bisulfate for concentrations above 3×10^{-5} *M* in 0.1 *N* sulfuric acid using 365-nm excitation; at lower concentrations the yields were identical. This result seems unlikely because quinine in part-per-million concentrations in 0.1 *N* sulfuric acid should have no memory of its original chemical form. Their results could have been instrumentally induced since the deviations occurred for absorbance values where their right-angle viewing method is subject to front-surfacing errors. Even if their results are correct, however, no errors are introduced by using either salt as a standard in a typical optically dilute quantum-yield measurement (less than 10^{-5} *M*). Nevertheless, the result is disconcerting.

The critically important quantity is, of course, the value of the absolute quantum yield of quinine sulfate. For such a widely used reference there are surprisingly few data available. Melhuish's best values,[22] obtained by a Vavilov method with 365-nm excitation, are 0.508 at 5×10^{-3} *M* and 0.546 for concentrations below 10^{-4} *M*. Roberts and Hirt[92] and Eastman[26] have made measurements of relatively low accuracy which indicate that Melhuish's values are probably not grossly in error. Dawson and Windsor have carried out the only comprehensive study of the yield of quinine. They found the yield in 1.0 *N* sulfuric acid to be 0.54 ± 0.02 (90% confidence level) with 365-nm excitation, a value

(87) G. K. Turner Associates, Inc., "Notes on the Determination of Quantum Efficiency with the Model 210 'Spectro'," Feb 1966.

(88) R. F. Chen, *Anal. Biochem.*, 19, 374 (1967).

(89) A. N. Fletcher, *J. Phys. Chem.*, 72, 2742 (1968).

(90) J. E. Gill, *Photochem. Photobiol.*, 9, 313 (1969).

(91) H. C. Børresen, *Acta Chem. Scand.*, 19, 2089 (1965).

(92) B. G. Roberts and R. C. Hirt, *Ann. ISA Conf. Proc.*, 19, (III) (2.2.2.64) (1964).

in excellent agreement with 0.546 obtained by Melhuish[22] under identical conditions. At other wavelengths the yield was 0.56 ± 0.04 (334 nm), 0.48 ± 0.02 (313 nm), and 0.55 ± 0.02 (254 nm) (the latter measured relative to perylene). As discussed previously, the 313-nm value may be in error.

Drobnik and Yeargers,[80] using quinine sulfate (0.1 *N* sulfuric acid) as a standard with an assumed yield of 0.55, found the yield of 2-aminopurine to be 1.2 to 1.5 at 160°K, an impossibility. If this result is reliable, the yield of the standard could not have exceeded 46% and was probably lower; the lack of experimental detail in the report and Fletcher's[81] inability to duplicate their work both suggest systematic errors. Rusakowicz and Testa[75] found the yield of a sample of quinine bisulfate in 0.1 *N* sulfuric acid to be less than 46% that of 9,10-diphenylanthracene in deoxygenated cyclohexane, which sets the maximum yield of quinine at 0.46. The discrepancy may be traced to their use of a Beckman DU for absorption measurements (see section II-B and ref 28 for details).

In view of the available data the best quantum yield for quinine sulfate in 1.0 N sulfuric acid (less than 10^{-4} M) appears still to be Melhuish's value[22] of 0.546 for 365-nm excitation at 25°. This yield is probably good to ±5%.

If quinine sulfate is used as a standard the following are recommended. (1) Commercial quinine sulfate or bisulfate may be used. For consistency the material should be dried as described by Fletcher,[83] and its absorption spectrum should be compared with his data. (2) The temperature should be maintained at 25°. (Note large temperature dependence of yield given earlier.) (3) The compound should be made up in 1.0 *N* sulfuric acid, and Melhuish's quantum-yield values should be assumed for excitation above 330 nm.[22] If 0.1 *N* sulfuric acid solutions are used, the yield should be experimentally determined relative to quinine in 1.0 *N* sulfuric acid. (4) Use only Pyrex containers for storage of these standard solutions since quinine is adsorbed on the surface of soft glass.[85]

Fluorescein in 0.1 *N* sodium hydroxide is a good quantum-yield standard. In optically dilute solutions Weber and Teale,[30] Parker and Rees,[47] and Børresen[91] have shown that the yield is constant over the exciting range 250–530 nm. The compound is not oxygen quenched, but it decomposes slowly in solution (solutions may show significant decrease in the fluorescence intensity after 24 hr).[93] There is considerable overlap between the absorption and emission spectra which precludes the use of optically thick solutions.

A serious limitation to the use of fluorescein as a standard is its low extinction coefficient in the 340–370-nm region. For excitation in this region very high purity material must be used. Melhuish[94] has found the yield of fluorescein solutions to be ~15% lower than normal in the 340–360-nm region, presumably due to absorbing impurities. For excitation at 365 nm, Dawson and Windsor[38] claimed it was necessary to purify the dye by the chromatographic method of Lindqvist.[95] For visible excitation a good commercial grade of the dye or material purified by the method of Orndorff and Hemmer[96] is probably satisfactory.

The strongest absorption band of fluorescein is in the visible region ($\epsilon \simeq 80{,}000$)[51] and strongly overlaps the emission. Unless the concentration is kept below 10^{-6} *M*, reabsorption of the emitted light will cause problems. At such low concentrations extremely low optical densities at the exciting wavelength are encountered unless excitation is in the strong visible band. For this reason fluorescein is best employed when excitation is in the 400–500-nm region.

The quantum yield of fluorescein is a widely measured parameter. It was first studied by Vavilov. Regrettably the earlier data are of questionable accuracy, and only the more recent measurements obtained with a calibrated spectrometer or by the Weber–Teale method are considered here. Some values obtained on calibrated spectrometers are 0.77,[47] 0.85,[97] and 0.88.[92] Values by the Weber–Teale method are 0.92 (365 nm),[28] 0.93 (365 nm),[35] 0.92 (436 nm),[38] and 0.86 (313 nm).[38] An integrating sphere value of 0.91[98] and a calorimetric value of 0.90[54] have been reported. Because of the freedom from spectrometer calibration and reabsorption errors, the yields from the Weber–Teale method falling around 0.92 are probably the most accurate. We feel a compromise value of 0.90 to be accurate within 10% and probably within 5%.

If fluorescein is to be used as a quantum-yield standard, we propose the following stipulations. (1) The fluorescein should be purified by the method of Lindqvist[95] or that of Orndorff and Hemmer.[96] (2) The concentration should never exceed 10^{-6} *M*. Solutions should be prepared within 12 hr of use. (3) A yield of 0.90 should be assumed in 0.1 *N* sodium hydroxide at 25 ± 5°. (4) Excitation should be in the 400–500-nm region; its bandwidth should be held to 5 nm or less because of the sharpness of the peak.

Eosin in 0.1 *N* sodium hydroxide has properties similar to those of fluorescein, but the absolute yield of eosin is probably not as accurately known. Weber and Teale claim its quantum yield to be constant for the range 210–560 nm.[30] Values by their method are reported as 0.19[28] and 0.20;[35] those by a calibrated spectrometer, 0.17,[92] 0.18[78,97] 0.21,[47] and 0.22;[20] the most probable yield is 0.20 ± 0.03. General precautions

(93) J. N. Demas, unpublished results from this laboratory.

(94) W. H. Melhuish, *J. Opt. Soc. Amer.*, **52**, 1256 (1962).

(95) L. Lindqvist, *Ark. Kemi*, **16**, 79 (1961).

(96) W. R. Orndorff and A. J. Hemmer, *J. Amer. Chem. Soc.*, **49**, 1272 (1927).

(97) J. W. Bridges and R. T. Williams, *Nature*, **196**, 59 (1962).

(98) P. Latimer, T. T. Bannister, and E. Rabinowitch, *Science*, **124**, 585 (1956).

listed under fluorescein apply to eosin as well. It is unstable in basic solution and produces impurities which absorb in the 360-nm region;[47] hence, excitation should be restricted to the visible band. Because of its poorly defined yield and chemical instability, eosin is best used as a test substance rather than as a standard.

Anthracene in 95% ethanol is a widely used standard, but it has undesirable properties. There is considerable overlap of the absorption and emission spectra; it is strongly oxygen quenched,[44] and its relatively sharp absorption spectrum requires the use of a narrow excitation bandwidth. The yield appears to be constant from 210 to 310 nm,[30] and Fletcher[81] has found the yield to be the same at 313 and 365 nm.

Although the absolute yield of anthracene is widely reported, seldom have literature values been corrected for refractive index effects. These corrections increase the yield by ~4%. The values listed below for optically dilute solutions have been corrected for refractive index differences. Calibrated spectrometer values are 0.26,[92] 0.29,[47] 0.23,[46] 0.27,[81] 0.38;[97] values by the method of Weber and Teale are 0.27[38] and 0.31.[28,35] Melhuish[22] obtained 0.27 from optically dense measurements by correcting for reabsorption and reemission and extrapolating to infinite dilution. The best value for 95% ethanol solutions at 25° is probably 0.27 ± 0.03 for optically dilute samples.

The following points should be borne in mind when anthracene is used as a standard. (1) The material should be at least fluorescence grade and preferably recrystallized from ethanol. If excitation is to be carried out in the absorption minimum (~300 nm), then further purification may be necessary. (2) The solutions must be deoxygenated prior to use by bubbling nitrogen through them. (3) The concentrations should not exceed 10^{-5} M. (4) A yield of 0.27 should be assumed for solutions in 95% ethanol at 25 ± 5°.[49]

Rhodamine B has been used as a standard.[73] It has a constant quantum yield over a wide wavelength range and is not oxygen quenched.[30] Like fluorescein it has strong overlap between the absorption and the emission spectra, which effectively restricts its use to excitation in the visible band. The quantum yield is poorly defined with reported values of 0.66,[47] 0.71,[20] 0.76[46] (based on an assumed yield of 0.55 for quinine sulfate in water), 0.92,[92] and 0.97.[28] This spread in values is unfortunate, since the dye is one of the few standards which absorbs the mercury 546-nm line. Because of the extended red emission of rhodamine B and the poor red response of most instruments, the large range of values is probably due to calibration errors. In the absence of more reliable data, Parker's value of 0.66[47] and the value of 0.71,[20] which were run on high red-sensitivity instruments, are prefererd.

The 9,10-diphenylanthracene molecule has been used as a standard. Birks and Dyson measured the compound in benzene;[48] Berlman[44] has rather arbitrarily assigned a value of 1.00 in *cyclohexane* and refers all of his values to this. Because of the vast compilation of data dependent upon this latter value, a more reliable one is badly needed. If Melhuish's yield of 0.83[22] in *n*-hexane is appropriate, all of Berlman's values may need to be reduced by 17%.[99]

Perylene has also been used as a standard.[38,48] In deoxygenated 95% ethanol the absolute determinations of the yield agree quite well. Melhuish[22] obtained 0.89 for dilute samples, and Dawson and Windsor[38] reported 0.94 at low concentrations. An average value of 0.92 is likely to be correct within 10%. Because of reabsorption–reemission effects, the concentration should be kept below 10^{-6} M. Perylene suffers from the same disadvantages as anthracene.

The 5-dimethylaminonaphthalene-1-sulfonate molecule has been suggested as a standard. There are discrepancies among the reported yields,[28,82,100,101] but the results of ref 82 and 100 suggest that reproducibility is possible with the proper control of conditions.

From the biochemist's standpoint tryptophan is an ideal standard. Its absorption and emission properties are similar to those of proteins. Unfortunately, the widely used yield (0.20) of Weber and Teale[28] has recently come under attack. Chen[39] found an upper limit of 0.14. Weisstuch and Testa[77] found yields of some aminopyridines to be greater than 1.0 if tryptophan were used as a standard with an assumed yield of 0.09. In view of these inconsistencies tryptophan should not at this time be used as a standard. Because of bacterial attack the solution stability of the molecule is also not good, and it can be dissolved only with difficulty.[85]

Ethanol solutions of 3-aminophthalimide with an assigned value of 0.6 for an absolute yield (apparently calculated from the energy yield of Alentsev[54]) have been widely used by Russian authors. From the published literature the reliability of this standard is difficult to assess.

Because of the urgent need for quantum-yield standards, the following studies should be carried out. (1) The quantum yields of quinine, anthracene, fluorescein, eosin, rhodamine B, 9,10-diphenylanthracene, perylene, and tryptophan should be reinvestigated carefully. Of particular concern are the possible variations of the yields with excitation wavelength, the dependence of the yields on the sources of the materials, and the effects of sample handling. Particularly needed are

(99) Recent studies on potential scintillators indicate that the maximum yield of 9,10-diphenylanthracene in deoxygenated cyclohexane at room temperature is 0.85 (R. B. Lehmann, University of New Mexico, private communication).

(100) C. M. Himel and R. T. Mayer, *Anal. Chem.*, 42, 130 (1970).

(101) E. J. Bowen and D. Seaman, "Luminescence of Organic and Inorganic Materials," Proceedings of the Conference on Luminescence, New York, N. Y., H. P. Kallmann and G. M. Spruck, Ed., Wiley, New York, N. Y., 1962, p 153.

measurements using the Weber and Teale method to obtain truly absolute values. As a further check those compounds with accurately characterized yields should be compared relative to each other as a check on the internal consistency of the results. (2) New materials should be investigated as quantum-yield standards. More compounds are needed which have negligible absorption–emission overlap, negligible susceptibility to concentration and oxygen quenching, easy availability, and accurately measured yields. Visible absorbing standards which have small reabsorption and reemission overlap are lacking, and satisfactory infrared emitting standards of any kind are vitally needed.

As potential candidates for quantum-yield standards numerous molecules deserve attention for diverse reasons. Both 7-hydroxycoumarin and 4-methyl-7-hydroxycoumarin have good yields, 0.97 and 0.24, respectively, and their emission and absorption spectra are similar to quinine sulfate.[102] Methylene blue may be a suitable infrared standard.[103] Chelates of terbium[104] emit in the region covered by the rhodamine B quantum counter. Complexes of europium[104] and other rare earths emit strongly in the near-infrared region. Chromium complexes are also efficient.[105] Some of the d^6 transition metal complexes exhibiting charge-transfer or d–d transitions luminesce brightly in the red and near-infrared regions of the spectrum.[106] Some scintillators (*e.g.*, terphenyl),[44] which have small oxygen quenching and negligible absorption–emission overlap, may be satisfactory replacements for tryptophan.

IV. Quantum Counters

One of the most difficult and tedious procedures required for any quantum-yield measurement is the determination of the total relative photon output of the sample. In general, either an emission spectrum run on a calibrated monochromator or knowledge of both the corrected emission spectrum of the compound and the wavelength sensitivity curve of the detector is needed. Numerical integration is required to calculate either the total area under the corrected emission spectrum or the sensitivity of the detector averaged over the emission band. These procedures are time consuming and introduce substantial sources of error.

Detailed calibrations can be neatly avoided by using a detector which has a constant quantum sensitivity (quantum flat) over the wavelengths of interest (emission bands of reference and standard). For such a detector eq 11 would reduce to eq 12, and eq 14 and 9, to very simple forms. Unfortunately, no known simple detector is quantum flat over an extended wavelength range. The quantum sensitivities of phototubes, thermopiles, and photoconductivity cells are strongly wavelength dependent;[40] only the new photodiode detectors approach the ideal.

Numerous solid-state photocell sensors are being marketed. EG&G[107] manufactures a sensitive detector whose quantum efficiency does not change by more than 25% in the range 500–970 nm. Hewlett-Packard[108,109] produces a similar device which is flat within 25% from 500 to 850 nm. The spectral response of the silicon PIN photodiode can be extended to 1000 nm.[110] Silicon solar cells offer attractive possibilities as highly sensitive large area detectors. Although not yet in extensive use, their photometric capabilities have been explored by Witherell and Faulhaber.[111]

Although considerable sensitivity is frequently sacrificed, it is possible to level the quantum sensitivity of many common detectors over a wide range of wavelengths. An early attempt in visual photometry was made by Vavilov.[29] He used an optically dense solution of aesculin to judge visually the relative intensities of ultraviolet light of different wavelengths. The aesculin solution totally absorbed all incident ultraviolet light, and its emission spectrum and quantum yield were independent of the exciting wavelength. Therefore, the relative visual intensity of the aesculin emission was directly proportional to the incident uv light intensity (quanta/sec) independent of the wavelength. The variable sensitivity of the human eye to radiation of different wavelengths did not affect the measurement since the same emission was always viewed.

Wavelength dependences of photographic emulsions can be flattened[112] by coating a spectroscopic plate with a totally absorbing layer of a fluorescent material whose quantum efficiency and emission spectrum are wavelength independent. The sensitivity of the plate is then independent of wavelength over the region in which the material totally absorbs.

The principle used to render the eye and a photographic plate quantum flat was extended by Bowen[113]

(102) P. I. Petrovich and N. A. Borisevich, *Bull. Acad. Sci. USSR, Phys. Ser.*, **27**, 701 (1963).

(103) G. R. Seely, *J. Phys. Chem.*, **73**, 125 (1969).

(104) W. R. Dawson, J. L. Kropp, and M. W. Windsor, *J. Chem. Phys.*, **45**, 2410 (1966).

(105) K. K. Chatterjee and L. S. Forster, *Spectrochim. Acta*, 20, 1603 (1964).

(106) D. M. Klassen and G. A. Crosby, *J. Chem. Phys.*, **48**, 1853 (1968); D. H. W. Carstens and G. A. Crosby, *J. Mol. Spectrosc.*, **34**, 113 (1970); J. N. Demas and G. A. Crosby, *J. Amer. Chem. Soc.*, **92**, 7262 (1970); J. N. Demas and G. A. Crosby, *ibid.*, in press; R. J. Watts and G. A. Crosby, *ibid.*, in press.

(107) Edgerton, Germeshausen, and Grier, Inc., "Photodiode Application Notes," Boston, Mass. (Jan 1969); "SGD-040 Silicon Diffused p-i-n Photodiode" (April 1970).

(108) Hewlett-Packard, "Application Note 915" (Jan 1967).

(109) R. Fisher, *Appl. Opt.*, **7**, 1079 (1968).

(110) United Detector Technology, Inc., "Silicon Photodetector Design Manual," Santa Monica, Calif., 1970.

(111) P. G. Witherell and M. E. Faulhaber, *Appl. Opt.*, **9**, 73 (1970).

(112) G. R. Harrison and P. A. Leighton, *Phys. Rev.*, **88**, 899 (1931).

(113) E. J. Bowen, *Proc. Roy. Soc., Ser. A*, **154**, 349 (1936).

to the leveling of the sensitivity curve of a phototube. In his earliest attempts solid uranyl ammonium sulfate was placed before a phototube. This combination gave a quantum-flat detector (within 10%) over the 252–430-nm region. He also placed a fluorescent solution of aesculin before the detector for the region 252–366 nm; this combination was flat to 4% and displayed a sensitivity 250 times greater than that of his thermopile.

An apparatus consisting of an optically dense solution of a fluorescent material in conjunction with a detector has become known as a (Bowen) quantum counter. The name "quantum counter" is due to the fact that the output of such a device is proportional to the number of incident photons per second, independent of wavelength. Bowen and Sawtell[31] recognized that the quantum counter effectively evaluated the integrations involved in the usual quantum-yield measurements and exploited this feature for the determination of yields. Since Bowen's early work both the wavelength range and the sensitivity of quantum counters have been greatly increased by the introduction of new materials and modern photomultipliers.

There are two basic types of quantum counters, optically dense and optically dilute. Optically dense (Bowen) quantum counters are extensively employed for measuring quantum yields or calibrating monochromators and are discussed fully in this section. Optically dilute quantum counters find limited application for calibrating excitation monochromators and are discussed in more detail elsewhere (section V-A-2).

Quantum counters do have disadvantages for yield measurements. Their uniform sensitivity over a large wavelength range increases the susceptibility to scattered light errors. In contrast, a monochromator–detector combination discriminates at least partially between the emitted and the scattered photons. Thus quantum-yield apparatus incorporating quantum counters must be carefully designed in order to reduce scattered light, and blanks must be run.[18,19,22] Of course the sensitivity to scattered light can be reduced by interposing filters between the sample and the fluorescent screen, but this procedure limits the range of, or distorts the quantum-flat response of, the detector.

Since phototubes are usually very sensitive to short wavelength radiation, the quantum counter itself must be designed to prevent any scattered or sample light from directly reaching the photomultiplier. Any light reaching the phototube directly without being converted in the quantum counter could produce large spurious signals (see ref 18, 19, 38, 59).

For use in optically dense quantum counters, solutions of rhodamine B, introduced by Melhuish,[19] have proved to be the most popular. The principal reason is the wide wavelength range (220–600 nm) over which rhodamine B operates satisfactorily; it has the most extended red response of any available quantum counter. Melhuish originally used a 4 g/l. solution in glycerol and found the quantum yield to be constant within ±5% in the range 350–540 nm. Weber and Teale[28] confirmed his report and extended the range to approximately 340–580 nm. Later Melhuish,[94] by comparing rhodamine B (3 g/l. in ethylene glycol) with a thermopile, found the yield to be invariant within approximately ±2% from 350–600 nm and probably nearly this constant down to 220 nm. Melhuish[22] has also employed rhodamine B (4 g/l.) plus acriflavine (1 g/l.) in 90% glycerol and 10% ethanol as a quantum counter, a system possessing no clear superiority.

When a high viscosity quantum counter solution is used (*e.g.*, glycerol or ethylene glycol), serious polarization errors (section VI-D) might arise. Since the detector response depends upon the geometry, the signal could then be a function of both the intensity and the degree of polarization of the incident beam. For the rhodamine B quantum counter concentration depolarization due to energy transfer certainly reduces or eliminates polarization errors. In new quantum counters, however, this source of error may not be insignificant, and its possible presence should be recognized. Polarization errors could be minimized or eliminated by using low viscosity solvents, high solute concentrations, and a straight-through viewing arrangement.

Recent tests of the constancy of the quantum yield of rhodamine B have been performed by Yguerabide,[59] who used 8 g/l. of the dye in ethylene glycol and found the yield to be constant to within ±4% from 250 nm to 600 nm. Newer measurements on this solution indicate that the efficiency does not vary by more than 11% in the range 280–600 nm.[114] Demas[20] has shown the yield to be constant to within ±1.5% for the limited range 400–600 nm.

Associated with the major advantage of using rhodamine B, the extended red response, there is one principal drawback. The red emission of the quantum-counter solution falls in a spectral region where the usual photomultipliers are relatively insensitive.[40] Consequently to use rhodamine B for many low-light-level applications it is necessary to have extended red-response phototubes (S-10 response for intermediate sensitivities or the very expensive S-20 response for high sensitivities). When the red sensitivity of rhodamine B is not required, a quantum-counter solution which emits at shorter wavelengths and more closely matches the detector's sensitivity curve is preferable. For high-light-level applications (*e.g.*, calibration of monochromators) the common S-11 response of photomultipliers is satisfactory even with rhodamine B.[115]

For detecting light below ~360 nm, sodium 1-dimethylaminonaphthalene-5-sulfonate (0.02 *M* in sodium

(114) R. W. Harrigan, unpublished results from this laboratory.

(115) For example, a rugged relatively inexpensive RCA 2020 photomultiplier has been used quite successfully in our laboratory.

hydroxide) is well suited for optically dense quantum counting.[28,116] Fluorescein[94,117] and quinine sulfate[90,94] have been used as Bowen quantum counters, but they are not ideal substances. Fluorescein has an extremely low extinction coefficient in the 340–360-nm region which allows trace impurities to alter the counting efficiency in this region.[94] Quinine sulfate is probably satisfactory for the range 200–350 nm,[83,90] but at longer wavelengths the emission spectrum shifts[83,89,90] with the possible introduction of error. Furthermore, it is sensitive to absorbing impurities at ~270 nm, where an absorption valley occurs.

Thin films of sodium salicylate have also found use in the range 60–360 nm where they exhibit a constant quantum yield (see ref 16 and references therein). Outside of the vacuum ultraviolet, however, the more easily prepared and conveniently used solution quantum counters are probably preferable.

In summary, rhodamine B (8 g/l. in ethylene glycol) makes a nearly ideal detector for the region 250–600 nm; the efficiency certainly does not change by more than 8% over this range. For quantum counting below 360 nm, 1-dimethylaminonaphthalene-5-sulfonate (0.02 M) in dilute sodium hydroxide may be desired over rhodamine B because its blue emission better matches the usual photomultiplier response curve. Fluorescein is satisfactory for the region 380–500 nm and, if properly purified, it is probably good to 250 nm. Unfortunately, no optically dense quantum counters have been verified as quantum flat for the region beyond 600 nm, although methylene blue in ethylene glycol (8×10^{-3} M) has been used for the region 500–700 nm.[103] Thus, for compounds which emit beyond 600 nm it is necessary to resort to calibrated detectors or spectrometers to obtain quantum yields. There is a great need for new, broad range quantum counters which extend into the infrared coupled with new infrared detectors to give increased sensitivity. Such devices would fill an exceedingly important gap in the instrumentation available for this rapidly expanding area of luminescence measurements.

V. Spectrometer and Detector Calibration

Unless a quantum counter is used, knowledge concerning the emission spectra of the samples (knowns and unknowns), the wavelength sensitivity of the detector, and, in some cases, the output of the excitation monochromator as a function of wavelength is essential to any quantum-yield measurement. Whatever the necessary information—general or highly detailed—the success or failure of the quantum-yield measurement rests on the reliability of these data. The procedures for calibrating emission and excitation monochromators and detectors are conceptually simple, but the simplicity is more apparent than real. Indeed, reliable calibrations can be difficult to achieve, as may be surmised from a perusal of the diverse emission spectra reported by different authors for the same compound.

We present in this section a survey of methods for calibrating spectrometers and detectors, including brief descriptions of procedures and pertinent references. Some advantages, disadvantages, and pitfalls associated with the various methods will be discussed. A comprehensive critical review, although badly needed, is not within our purview, however.

A. Excitation Monochromator Calibration. To obtain corrected excitation spectra (relative quantum yields as a function of excitation wavelength) or to measure a quantum yield using different wavelengths to excite the standard and unknown, the relative output of the excitation monochromator as a function of wavelength must be known, or held constant. The calibration procedure used for a chosen monochromator depends on the detector, which can be a thermopile, quantum counter, actinometer, or calibrated emission monochromator.

1. Thermopiles. The principal advantage of thermopiles is that they are energy-flat detectors (equal output for equal amounts of energy) over an enormous range of wavelength. A thermopile may have a constant sensitivity extending from below 200 nm well into the infrared (2.5 μ with a quartz window or beyond with other window materials).[62] In comparison, quantum counters are in general only useful from 200 to 600 nm and under certain conditions to 700 nm.

The major attribute of thermopiles, the wide range of wavelength sensitivity, can be a source of error. Since they are equally sensitive to infrared and visible radiation, any admixture of infrared radiation in the light beam can produce a thermopile reading, although no sample emission is stimulated by it.[62] Attempts to reduce stray radiation in a light beam, either infrared or ultraviolet, by placing filters before the detector does not necessarily eliminate this source of error; the energy absorbed by the filter may be reemitted in the infrared region and produce a spurious thermopile signal. The infrared thermal sensitivity of thermopiles can be demonstrated in a most striking manner, *e.g.*, an Eppley Labs thermopile (12-junction bismuth–silver linear thermopile with a quartz window) can detect a man at a distance of 10 ft or a warm cup of coffee over 1 yard away.

Since thermopiles measure relative energy instead of the desired units of relative quanta per second emanating from the monochromator at a given wavelength, a conversion from energy to quanta is required, a minor disadvantage. A more serious problem is the low sensitivity. Relatively high light fluxes and expensive readouts are generally necessary.[4a,6] Even with a highly sensitive meter, there may be inadequate signal, par-

(116) R. F. Chen, *Anal. Biochem.*, **20**, 339 (1967).
(117) C. A. Parker, *Anal. Chem.*, **34**, 502 (1962).

ticularly if narrow slits are used and calibration is required in the ultraviolet where lamp output is low. For example, when all the light from a Hitachi MPF-2A spectrofluorimeter (150-W xenon arc source) with a 5-nm bandpass on the excitation monochromator was focused on the Eppley thermopile detector (see above), signal levels were 2.34 μV at 250 nm, 24.5 μV at 300 nm, and 76.6 μV at 470 nm.

Thermopiles are designed to measure energy per unit area in a uniform collimated field which completely covers the sensitive area.[62] Normally, for a spectrometer calibration the excitation beam is not uniform and in some cases is not large enough to cover the sensitive area completely. The assumption is usually made, however, that the total energy in the excitation beam is directly proportional to the thermopile output and that the proportionality constant is wavelength independent. For cases where the sensitive surface is more than filled, these conditions are probably satisfied as long as the size of the excitation beam does not depend on wavelength—the usual experimental situation when no lenses are included in the optical paths (most lenses have a focal length and hence a beam area which is wavelength dependent). When the source image is smaller than the sensitive area of the device, the proportionality is also probably satisfied as long as the image is completely on the sensitive surface. The sensitivity of a thermopile surface does exhibit a marked dependence on position,[62] but since the image will usually cover much of the same portion of the surface, errors should be small. For cases where nonachromatic optics are used and the image size exceeds the detector's sensitive area, reliable calibration with a thermopile would be difficult or impossible.

2. Quantum Counters. The most popular method developed for calibrating excitation monochromators employs quantum counters. The counters can be optically dense (absorb 99%+ of the incident light) or optically dilute (absorb less than ~10% of the radiation). The optically dense method, which is by far the simplest, fastest, and most reliable, has been almost universally adopted. Calibration with optically dilute counters is tedious, not too reliable, and rarely used. Both methods require a minimum of ancillary equipment.

Calibration of a source–excitation monochromator combination with an optically dense quantum counter normally consists of placing the counter at the exit slits of the monochromator and monitoring the fluorescence intensity of the spot on the counter with a second monochromator set at a fixed wavelength. The signal from the second monochromator gives the relative intensity in quanta per second of the exciting light. Thus, in a single scan it is possible to obtain the wavelength dependence of the output intensity of the source–excitation monochromator combination over the entire range of the quantum counter. Melhuish[94] used this technique successfully and described an appropriate attachment for an Aminco spectrofluorimeter which is now available from the manufacturer. As early as 1927 Vavilov used a conceptually similar method for calibrating monochromators.[29]

A limitation of the Melhuish method is its restricted wavelength span (220–600 nm with the rhodamine B quantum counter). Problems can also arise if an emission monochromator which is sensitive to the exact experimental geometry is used to view the fluorescent spot. Changes in geometry during a scan can occur due to shifts in the position and size of the fluorescent spot as a function of wavelength (from the wavelength dependences of the refractive indices of any lenses in the excitation path, from the movement of the fluorescent spot into the quantum counter as the absorbance changes with wavelength, or from shift in grating or prism projection with angle).[59]

Replacing the emission monochromator with a photomultiplier improves the Melhuish method.[4a,59] Insertion of the phototube behind the quantum counter slightly off axis so that no transmitted light can reach it assures a system which is insensitive to alignment. In addition, a filter over the detector limiting the wavelengths viewed to the long wavelength tail of the emission minimizes spurious intensity variations due to changing reabsorption and shifts in the position of the emission spot. Yguerabide[59] has described in detail such a quantum counter.

Spectrometer calibration with an optically dilute quantum counter was suggested indirectly by Weber and Teale.[30] They presented the equation

$$O(\lambda) = KQ(\lambda)I(\lambda)B(\lambda) \tag{29}$$

to relate the response of a phototube or of an emission monochromator (at fixed wavelength) which views a luminescent solution at right angles. $O(\lambda)$ is the output of the detector at wavelength λ; K is a geometric and sensitivity constant; $Q(\lambda)$ is the quantum yield as a function of excitation wavelength; $I(\lambda)$ is the excitation intensity; and $B(\lambda)$ is the fraction of incident light absorbed in the cuvette (given by Beer's law, eq 13). If $Q(\lambda)$ is wavelength independent and K is constant (*i.e.*, the emission spectrum and the fraction of emitted light reaching the detector are not wavelength dependent) then

$$O(\lambda) = K'I(\lambda)B(\lambda) \tag{30}$$

As shown in section II-C, if the sample absorbance per centimeter, $A(\lambda)$, is less than about 0.02 in a 1-cm cuvette, then $B(\lambda)$ is nearly proportional to $A(\lambda)$ and the following working equation is obtained.

$$O(\lambda) = K''I(\lambda)A(\lambda) \tag{31}$$

Hence, from knowledge of the absorption spectrum of the sample and the uncorrected detector response, it is

possible to determine the relative intensity of the source, $K''I(\lambda)$, as a function of wavelength.

The optically dilute quantum-counter method has the advantage that the same cuvette and identical geometry can be used for the calibration and for a normal quantum-yield measurement. Since numerous compounds exhibit quantum yields independent of wavelength (see ref 30, 38, 90), checks of the calibration can be made. The long wavelength limit is 690 nm attainable with chlorophyll solutions.[30]

The optically dilute quantum-counter method has major disadvantages. Since the absorption spectrum of the compound must be accurately known as a function of wavelength, appreciable error can be introduced whenever the absorption spectrum goes through deep minima. Furthermore, if the excitation monochromator slits are not narrow enough to ensure that the sample absorbance is essentially constant over the bandwidth of excitation, distortions of the excitation spectrum will occur and calibration errors will result.

Argauer and White[118] appear to be the only authors who have employed the optically dilute method for excitation monochromator calibration. They used the aluminum salt of pontiochrome blue-black R. The calibration curve obtained by this method agreed well in the range 250–550 nm with the results from a calibrated phototube or a thermopile.

The tedium associated with the optically dilute quantum-counter procedure essentially precludes its use for routine measurements; however, in a slightly modified form it is very useful for checking calibrations obtained by other methods. If $I(\lambda)$ of eq 13 is known by some other method, and $O(\lambda)$ is measured, then $A(\lambda)$ may be calculated. The agreement between $A(\lambda)$ obtained from the absorption spectrum and the excitation measurement is a measure of the quality of $I(\lambda)$. K'', which is not measurable, is chosen to give the best fit between the absorption spectrum and the calculated excitation spectrum.

3. Actinometers. One of the classical methods of measuring light intensity is chemical actinometry. A chemical actinometer is a substance which undergoes a reaction upon absorbing light. From the extent of the chemical reaction the total amount of incident light can be measured.

Uranyl oxalate was one of the earliest actinometers.[6] After absorption of radiation the substance decomposes; by monitoring the loss of oxalate after a specified radiation time by differential titration, one can determine the intensity of the incident beam. This actinometer is popular with photochemists, since it has a well-known yield which is almost independent of wavelength. It is not completely satisfactory for excitation monochromator calibration because of its low sensitivity.[4a,119]

Parker[120] and Hatchard and Parker[121] have developed the reliable potassium ferrioxalate actinometer which is satisfactory for monochromator calibration. Absorbed light reduces ferric to ferrous ion. After irradiation the virtually nonabsorbing ferrous species is determined spectrophotometrically by conversion to the highly colored tris(1,10-phenanthroline)iron(II) complex which has an extremely intense absorption band in the visible region well removed from the ferrioxalate absorption. The lower limit of detectability is about 5×10^{-10} einstein of light. Not only is the ferrioxalate actinometer hundreds of times more sensitive and much easier to use than the uranyl system, but it has a broader wavelength range, and since the absolute quantum yield of the photochemical reaction has been measured accurately,[120-122] it is possible to measure absolute excitation intensities. The combination of high sensitivity, accurately known yield, convenience, and broad spectral range account for its deserved popularity.

The ferrioxalate actinometer has a few disadvantages. Although it is the fastest actinometer available, it is still too slow for routine calibrations; exposure times on the order of minutes to hours are required, and the chemical development is time consuming. Stable light sources are also necessary or their instabilities will be reflected in the calibration curve.

The capability to measure absolute intensities is the principal advantage of an actinometer. With the possible exception of the thermopile no other apparatus allows simple measurement of absolute quantum doses. Thermopiles, however, are limited to use with large beams of light of uniform cross section; no such restrictions are imposed on actinometers. The photosensitive solution may be poured into a cuvette of any shape, including containers which completely surround a source, and the operation is not disturbed by any inhomogeneities of the light beam.

Two extended red-response actinometers are also available. Wegner and Adamson[122] have developed the convenient, sensitive *trans*-$[Cr(NH_3)_2(NSC)_4]^-$ complex for the range 316–650 nm and the less convenient $[Cr(urea)_6]^{3+}$ complex for the range 450–735 nm. Other types of actinometers and details of the use of the ferrioxalate system are discussed by Calvert and Pitts[6] and Parker.[4a]

4. Calibrated Emission Monochromators. By using a grating emission monochromator calibrated over the 250–600-nm range, Drushel, Sommers, and Cox[46] calibrated their grating excitation monochromator over the same region. They replaced the cuvette with a reflector or scatterer, set the emission and excitation monochromators at the same wavelength, and recorded the apparent emission intensity. By correcting for the

(118) R. J. Argauer and C. E. White, *Anol. Chem.*, **36**, 368 (1964).
(119) C. E. White, M. Ho, and E. Q. Weimer, *ibid.*, **32**, 438 (1960).
(120) C. A. Parker, *Proc. Roy. Soc., Ser. A*, **220**, 104 (1953).
(121) C. G. Hatchard and C. A. Parker, *ibid.*, **235**, 518 (1956).
(122) E. E. Wegner and A. W. Adamson, *J. Amer. Chem. Soc.*, **88**, 394 (1966).

known emission monochromator sensitivity, they obtained the relative number of quanta/sec falling on the scatterer. The measurement was repeated at a series of wavelengths yielding the relative output of the excitation monochromator as a function of wavelength.

As outlined here, the method is only applicable to a case involving two grating monochromators. If either monochromator has a bandpass which is a function of wavelength, the fraction of exciting light reaching the detector will be wavelength dependent and a bandpass correction will be necessary.[123] Also, the emission monochromator bandpass should be much larger than that of the excitation monochromator. Since other calibration procedures (*e.g.*, optically dense quantum counters) are more reliable, and since this technique has a number of sources of error (see section V-B-3 for details), the method of Drushel, *et al.*,[46] for calibrating excitation monochromators is not generally recommended. For wavelengths beyond 700 nm where no quantum counters are sensitive, the procedure might be worth the effort, however.

B. Emission Monochromator Calibration. Emission spectra obtained directly from a spectrometer are not true emission spectra. They are distorted by the wavelength dependence of the spectrometer transmission characteristics, the variations in the bandwidth, and, above all, the wavelength dependence of the detector sensitivity.[4a] An observed emission spectrum can be so distorted that it no longer even remotely resembles the actual emission spectrum. In order to obtain faithful representations of the spectra it is necessary to determine a series of correction factors for the spectrometer defined by the equation

$$I(\bar{\nu}) = C(\bar{\nu})O(\bar{\nu}) \qquad (32)$$

$I(\bar{\nu})$ is the corrected relative emission intensity; $C(\bar{\nu})$ is the correction factor; $O(\bar{\nu})$ is the observed spectrometer output. Correction factors are usually obtained by reference to standard lamps, to compounds with known spectral distributions of their emissions, or to calibrated monochromator–light source combinations.

1. Standard Lamps. Standard lamps are widely used for calibration. A lamp can be operated at a known color temperature or it can be a spectral-irradiance or a spectral-radiance lamp (for a discussion of these types of lamps see ref 62). All three types are commercially available (National Bureau of Standards, Washington, D. C.), although many workers prepare their own standard color temperature lamps. In any case the relative output of the lamp at different energies ($I(\bar{\nu})$ in eq 32) is known. Light from a standard lamp is passed through the emission monochromator–detector combination, the apparent spectrum, $O(\bar{\nu})$, is recorded, and the wavelength-dependent correction factors for the spectrometer are calculated from eq 32.

The desired units for plotting emission spectra are relative quanta/sec cm^{-1} of bandwidth on a linear wavenumber scale, but the usual standard lamp calibration is supplied in units of relative ergs/sec nm of bandwidth. The standard lamp data are converted to units of quanta/sec cm^{-1} by multiplying each tabulated point by λ^3. To obtain correction factors for relative quanta/sec nm (units suitable for plotting on a scale linear in wavelength) the lamp data are multiplied by λ.[4a,46,47]

Procedures using standard lamps are the fastest and usually the most reliable methods available for calibrating detector–monochromator combinations in the visible and near-infrared regions. The lamps must be run under very closely controlled conditions of voltage or current so that the intensity reproduces the curve given by the manufacturer. The standard glass envelope lamp is usable only down to ~350 nm due to window absorption, although the quartz iodine lamp is useful down to 250 nm.[124] For the latter, great care must be taken near the lower limit because of very rapid falloff of intensity. A low relative intensity magnifies the errors from stray light emanating from the intense visible portion of the lamp's spectrum.

In addition to the standard tungsten lamps which are stock items, commercial firms will produce calibration curves for xenon or mercury arcs which can then be used for calibration in the uv. Calibration for just a few points is expensive and changes with lamp age, especially below 300 nm.

2. Compounds of Known Spectral Distribution. A number of compounds have been suggested as spectral emission standards. They are used in place of standard lamps over a limited wavelength range. Lippert, *et al.*,[125] have listed the corrected emission spectra of several substances which cover the region 10–30 kK. The apparent emission spectrum of the compound, $O(\bar{\nu})$ of eq 32, is obtained on the spectrometer, and its corrected emission spectrum is substituted for $I(\bar{\nu})$. From these data the correction factors are calculated.

Of the compounds which have been suggested as spectral emission standards, only quinine sulfate has been checked by a number of authors.[91,119,125–127] Unfortunately, there is considerable disagreement over the corrected emission spectrum. The explanation of these discrepancies is not certain, but at least some of them could be due to the observation that the emission spectrum of quinine sulfate depends on exciting wavelength.[88–90] If quinine sulfate is used as an emission standard, the work of Fletcher[89] suggests that the spec-

(123) J. G. Becsey and K. Scheller, *Rev. Sci. Instrum.*, **38**, 1793 (1967).

(124) R. Stair, W. E. Schneider, and J. K. Jackson, *Appl. Opt.*, **2**, 1151 (1963).

(125) E. Lippert, W. Nagële, I. Seibold-Blankenstein, U. Staiger, and W. Voss, *Fresenius' Z. Anal. Chem.*, **170**, 1 (1959).

(126) P. Rosen and G. M. Edelman, *Rev. Sci. Instrum.*, **36**, 809 (1965).

(127) W. H. Melhuish, *J. Phys. Chem.*, **64**, 762 (1960).

trum given by Lippert, *et al.*,[125] is probably accurate for excitation below 350 nm, whereas Melhuish's spectrum[127] is reasonable for 365-nm excitation.

3. Calibrated Xenon Lamp and Monochromator. The early lack of reliable standard lamps for the calibration of ultraviolet spectrometers prompted workers to calibrate, by quantum-counter methods, a combination of a monochromator and a xenon lamp as a standard source to be used for the calibration of emission monochromators. This method appears to have been developed independently by Melhuish[94] and Parker.[117] The arc–monochromator combination is used to produce spectral lines whose bandwidths are narrower than the bandwidth of the emission monochromator. The relative intensity of this nearly monochromatic beam is measured as a function of wavelength by a quantum counter. This light is then allowed to enter the emission monochromator either by reflection from a front-surface mirror or by scattering from a magnesium oxide film, and a phototube reading is obtained. The data reduction method then depends on the nature of the emission monochromator. Melhuish's technique[94] is suitable for calibrating a pair of grating monochromators where the bandwidth is independent of wavelength. Parker's[117] method is based on a more general analysis of the monochromator–detector combination and is suitable for calibrating both grating and prism instruments, although, as originally proposed by Parker, the procedure is only usable for calibrating monochromators with independently adjustable entrance and exit slits. This instrumental flexibility is necessary so that the exit slits may be made large enough to pass the entire range of wavelengths present in the exciting beam. An alternative is to remove the exit slits entirely.[123] Becsey and Scheller have presented a rigorous, but terse, analysis of this method.[123]

Since this calibration method is relatively rapid, easy, and reliable, it has achieved wide acceptance for calibration of spectrometers in the ultraviolet region. Some precautions are necessary, however, or large errors can occur. Close attention must be paid to transmission and reflection properties of all optical surfaces, especially in the uv. The transmission of the quantum-counter window must be taken into account,[94] since some quartz samples will absorb below 300 nm. The reflection coefficient of any mirror must be considered.[94] Silvered mirrors, even front-surfaced ones, reflect poorly in the uv, and aluminized mirrors, particularly those with protective coatings, have a marked wavelength dependence of the reflection coefficient. The reflectance of the best scatterers is wavelength dependent.[4a,23] A quartz beam splitter for reflecting energy into the emission monochromator introduces problems, since the reflection coefficient of quartz for light of various wavelengths and polarizations is not constant.[90,128]

The same fraction of light from the excitation monochromator must enter the emission monochromator for each exciting wavelength. For a grating monochromator with no transmission lenses this condition is readily satisfied for low-grating angles, but insertion of a lens in the excitation path must be done with care, since the image size is wavelength dependent. A changing image size means that the emission monochromator may see varying amounts of light. Originally overlooked by Parker,[117] this source of error was shown by Børresen and Parker[129] to affect the correction factors significantly (~20%). Also the reflected or scattered light might not fill the grating and mirrors within the emission monochromator uniformly. If these components have variable transmission and reflection characteristics across their surfaces (as would be expected in the ultraviolet) the correction factors determined by this method would not necessarily apply to a different radiation distribution.[129]

Calibration curves obtained by an arc–monochromator combination have been compared with curves obtained by means of standard lamps in the region of overlap (400–600 nm).[94,116,117] The agreement is quite satisfactory, although the xenon lamp is somewhat limited in usefulness between 450 and 500 nm due to the presence of a series of intrinsic strong, narrow lines.

C. Detector Calibration. A comprehensive article on absolute detector calibration has been published by Lee and Seliger.[62] Although the procedures are more tedious and difficult than relative calibration methods, most of the same problems arise. Basically any detector calibration procedure is a substitution method. A reference detector of known spectral sensitivity is required. Usually a thermopile (an energy-flat detector) is used, but a quantum counter could often be substituted to great advantage. Typically a monochromatic, uniform light beam is established whose area is larger than the sensitive areas of both the reference and the uncalibrated detectors. The intensity is measured first with the reference detector and then with the uncalibrated one in position, and the ratio of the two signals gives the relative sensitivities. Repetition of this procedure at a number of wavelengths establishes the relative or absolute wavelength sensitivity for the uncalibrated device.

The biggest problem in these calibration procedures stems from the fact that light intense enough to activate a thermopile is usually orders of magnitude too bright for photomultipliers. Thus the source must be attenuated either by moving it to a greater distance or by interposing neutral density filters (which are only an approximation of neutral density and are often wavelength dependent). Operation of a thermopile is not trivial and for wavelengths shorter than 600 nm, a

(128) B. Witholt and L. Brand, *Rev. Sci. Instrum.*, 39, 1271 (1968).
(129) H. C. Børresen and C. A. Parker, *Anal. Chem.*, 38, 1073 (1966).

rhodamine B quantum counter would be more convenient; the absolute sensitivity could be obtained by reference to a calibrated thermopile[59] or an actinometer.

Any detector should be calibrated in a radiation field having the same spacial distribution as the fields in which it will be used. The sensitivities of all detectors, phototubes in particular, are far from uniform over the sensitive surface.[62] These inhomogeneities could introduce large systematic errors in the measurements. Phototubes also have the nasty feature that both the effective photocathode area and its spectral sensitivity are functions of the applied voltage.[37,85] As a result, varying the tube gain by changing the applied potential can significantly change the calibration. If the tube gain is to be varied, this source of error can be alleviated by holding constant the potentials between the cathode and dynode 1 and dynode 1 and dynode 2, while the voltages across the remaining stages are varied. To discriminate against stray light (section V-A-1) by placing filters before a thermopile is a risky business. Infrared radiation generated by the filter can produce spurious results. Almy and Gillette[60] encountered these problems in their detector calibration methods, and their measured quantum yields were affected by a factor of 5.

D. Self-Correcting Instruments. Manual correction of observed emission and excitation spectra is tedious and time consuming. To avoid this step a number of instruments have been constructed which produce corrected spectra automatically. Of the many self-correcting instruments described in the literature, we discuss a few briefly to show their range and variety.

Several instruments use versatile programmable analog signal generators in conjunction with analog multipliers or dividers to correct the emission spectra,[126,130,131] whereas others use mechanical cam-generated correction factors. The latter are more difficult to modify, but they require simpler equipment.[132] Some have mechanical attenuators between the sample and the phototube.[133,134]

Excitation spectra have been corrected to constant energy by thermopiles[135] and bolometers[136,137] and to constant quanta by quantum counters.[91,128,131,138,139] One very versatile instrument[128] uses digital circuitry for computing purposes. Two[128,131] are capable of providing polarized emission spectra in addition to corrected emission and excitation spectra.

Two self-correcting instruments are commercially available. The Turner "Spectro" 210[137] uses a bolometer to measure the relative amounts of energy falling on the sample at different wavelengths and then corrects the excitation spectrum to constant energy. A unique optical, cam, ratio-recording system is used for correcting an emission spectrum. The standard spectrofluorimeter of American Instrument Co.[140] is made self-correcting by a special attachment. A thermopile is used to correct all excitation spectra to constant energy. The instrument also automatically compensates for lamp fluctuations. With the help of this calibrated energy source the correction factors for the emission monochromator are obtained. These are programmed manually into an analog signal generator which approximates the true correction curve by a series of 25 straight-line segments. Once these factors are set in the machine all subsequently observed emissions are automatically corrected. The multiplication is performed by a small analog computer.

VI. Corrections for Quantum-Yield Measurements

A. Refractive Index Corrections. Although the first quantum-yield measurement was made in 1924 the possible errors introduced by refraction effects were not considered until 1950 by Förster.[11] At about the same time the need for similar corrections in scattering experiments was recognized.[141] Refraction corrections can be substantial, modifying quantum-yield results by a factor of 2 or more. When applied to the early results, yields greater than unity are sometimes obtained. There are no obvious explanations for such values.

A major source of error arises from refraction of light away from the normal. As radiation passes from a material of high to one of low refractive index, a change in intensity occurs at the interface. A second, usually smaller, source of error arises from internal reflection of the emitted light within the cuvette at all interfaces between zones of different refractive indices.

To derive the correction factor needed to compensate for an intensity change between media, consider a point source, S, emitting within a medium of refractive index, n_i (Figure 2). The emission passes at near normal incidence through a plane interface into a medium of refractive index, n_0, which contains a detector ($n_i > n_0$). The geometry for normal viewing is shown in the figure; the small angles θ_i and θ_0 are exaggerated. Reflection effects are ignored. If I photons/sec are being emitted into the cone defined by the full angle,

(130) T. D. S. Hamilton, *J. Sci. Instrum.*, **43**, 49 (1966).

(131) S. Ainsworth and E. Winter, *Appl. Opt.*, **3**, 371 (1964).

(132) F. R. Lipsett, *J. Opt. Soc. Amer.*, **49**, 673 (1959).

(133) F. J. Studer, *ibid.*, **38**, 467 (1948).

(134) S. L. Parsons, A. E. Martin, and S. N. Roberto, *J. Electrochem. Soc.*, **97**, 41 (1950).

(135) W. Slavin, R. W. Mooney, and D. T. Palumbo, *J. Opt. Soc. Amer.*, **51**, 93 (1961).

(136) S. Cravitt and B. L. Van Duren, *Chem. Instrum.*, **1**, 71 (1968).

(137) G. K. Turner, *Science*, **146**, 183 (1964).

(138) W. H. Melhuish and R. H. Murashige, *Rev. Sci. Instrum.*, **33**, 1213 (1962).

(139) C. A. Parker, *Nature*, **182**, 1002 (1958).

(140) H. K. Howerton, presented at the Symposium on Fluorescence, 153rd National Meeting of the American Chemical Society, Miami Beach, Fla., April 1967; Reprint 311, American Instrument Co., Inc., Silver Spring, Md.

(141) J. J. Hermans and S. Levinson, *J. Opt. Soc. Amer.*, **41**, 460 (1951).

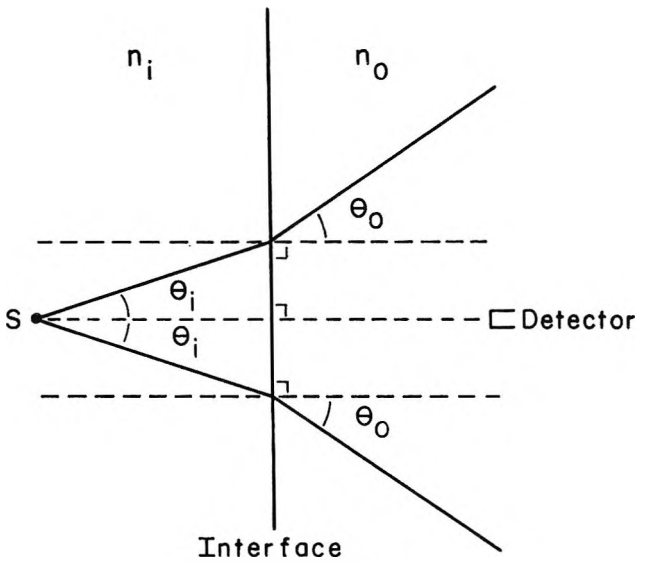

Figure 2. Refractive index effects in quantum-yield measurements. The point source, S, is in a medium of refractive index n_i; the detector, in a medium of refractive index n_0. $n_0 < n_i$.

$2\theta_i$, then the intensity of light within the source medium, I_i (quanta/sec-steradian), is given by

$$I_i \simeq \frac{4I}{\theta_i^2} \tag{33}$$

for $\sin\theta \simeq \theta$. In the second medium the same number of photons per second is enclosed in a larger solid angle; hence the intensity in the medium of low refractive index is decreased. The intensity in the detector medium, I_0, is given by

$$I_0 \text{ (quanta/sec-steradian)} \simeq \frac{4I}{\theta_0^2} \tag{34}$$

Application of Snell's law at the interface leads to the expression

$$I_i = I_0\left(\frac{\theta_0^2}{\theta_i^2}\right) = I_0\left(\frac{n_i^2}{n_0^2}\right) \qquad (n_0 = 1 \text{ for air}) \tag{35}$$

for the measured intensity.

In practice refractive effects may or may not be important depending on the particular method used for measuring quantum yields. In the Vavilov scatterer method, there is no refraction problem associated with the standard, but if the unknown is measured in a medium with a refractive index significantly greater than 1, the effect is appreciable. For a relative measurement, when a standard and unknown are compared in the same solvent, no correction is necessary. Where standard and unknown are in media of widely different refractive indices, a substantial correction is required.

In the general case where the viewing angle is ϕ from the normal, the observed intensity in air, I_0, is related to the intensity in the cuvette, I_i, by the equation

$$I_0 = \frac{I_i \cos\phi}{n_i(n_i^2 - \sin^2\phi)^{1/2}} \tag{36}$$

This relation ignores the internal reflection coefficient which is dependent upon the angle of incidence within the cuvette. Errors from reflection can equal 100% since the internal reflection coefficient approaches unity as ϕ nears the critical angle.

Equation 36 must be applied with great care. As discussed by Shepp,[142] internally reflected light escaping and reaching the detector can greatly modify the results. Shepp has suggested that angular intensities predicted by this equation will be too low except for 90° viewing, but he also predicted that observed readings will be too high as the detector approaches the cuvette. Shepp recommends normal viewing. Melhuish[27] confirmed these predictions qualitatively by examining the spacial and angular distributions of the luminescence of a fluorescent solution in a disk-shaped cuvette. As the detector approached the cuvette, the intensity increased too rapidly *when the back and sides of the cuvette were unblackened.* Melhuish found that the angular distribution (corrected for internal reflection) for an *unblackened* cuvette does not closely follow eq 36. In fact, viewed at 45° the intensity was approximately 10% higher than predicted, whereas viewed at 15° from the normal it became 15% too high. On the other hand, he found that painting the back and sides of the cuvette with a flat black paint produced an experimental distribution which followed eq 36 much more closely. This indicates that the correction factor should be applicable in all cases where the cuvette is blackened and is not too close to the detector. Unfortunately, very few authors have reported whether these conditions were satisfied during their measurements.

Equation 35 applies only for the case where the detector views the sample at a distance which is large compared to the depth of the emitting point within the cuvette. For quantum counters as employed by Melhuish this condition is not always met, but he has given an equation to compensate for the movement of the fluorescence away from the front of the cuvette.[22] Errors from this source can be substantial; for Melhuish's apparatus they amounted, at times, to 10%.

The previous discussion has applied to point or near-point sources. In a typical case where the exciting light enters a square cuvette containing an optically dilute sample and the analyzing monochromator views the emission at right angles, the source is extended. The geometry then controls the fraction of emitted light emanating from the luminescing volume which reaches the detector through the slit system. Hermans and Levinson[141] have presented a detailed analysis of the refractive index problems encountered with ex-

(142) A. Shepp, *J. Chem. Phys.*, **25**, 579 (1956).

tended sources. They have considered different viewing geometries, including viewing from other than right angles, systems with lenses, and cylindrical cuvettes. For right-angle viewing on a square cuvette and with exclusion of reflection and absorption effects, their equations confirm that the $1/n^2$ correction applies as long as the detector cannot see beyond the region of uniform luminescence. Thus the wide application of the $1/n^2$ correction is indeed warranted. For cases where the viewing condition is not satisfied, these authors also give geometrical correction formulas. For spectrometers this latter correction is negligible, but for a calibrated detector the factor may vary from 1 to $1/n^2$.

A rather startling result of Hermans and Levinson's work pertains to a cylindrical cuvette with incident exciting light falling on the curved side. Some authors had felt that a $1/n$ correction was in order here, but the $1/n^2$ factor still applies as long as the solution is optically thin, the excitation beam is uniform, and the detector does not see past the region of uniform emission.[141] For a narrow beam of light travelling down the middle of a cylindrical cuvette, the correct factor is $1/n$.

Internal reflections can cause refractive index-dependent errors in any of the integrating methods which require that some definite fraction of light emitted in a cuvette escapes (*e.g.*, integrating spheres). As shown by Shurcliff and Jones[143] a large fraction of the luminescence can, in principle, be trapped by internal reflection, even in the commonly used square cuvette. Similar results apply to cylindrical cells.[144] The trapping fraction (the fraction of emitted light permanently trapped in the cuvette) is dependent upon the refractive index of the phosphor. It increases with increasing refractive index. For an ideal rectangular parallelepiped this fraction amounts to ~24% at a refractive index of 1.5 and ~60% at a refractive index of 2.0.[143] Practically the experimental results differ markedly from the predictions. Overlap of the absorption and the emission bands causes light, which should escape, to be absorbed, thus increasing the trapping fraction. On the other hand, absorbed light can be reemitted, escape from the cuvette, and reduce the trapping fraction (particularly in high-yield compounds). Scattering, strains, and surface imperfections also reduce the trapping fraction. Nevertheless, although large departures from the ideal are to be expected, the trend is clear: radiation trapping should become more pronounced as the refractive index increases.

Trapping can be minimized by using small cuvettes of low symmetry containing imperfections to break multiple reflection paths.[54] Sandblasting at critical points, a new procedure introduced by Gordon and Curtis,[144] increases photon escape from scintillation vials by breaking the high symmetry. Further improvements in cuvette design are no doubt possible.

B. Reabsorption Corrections. During any luminescence experiment a certain amount of the emitted radiation is reabsorbed by the compound. The reduced number of photons escaping from the cuvette produces measured yields which are artificially low. For quantum-yield measurements this "reabsorption error" can be significant.

The magnitudes of reabsorption errors are affected by a number of factors: the geometry of the apparatus, the amount of overlap between absorption and emission spectra, and the relative absorbance of the sample at the exciting and the emitting frequencies. Qualitatively, reabsorption will be smallest if the detector views the emission on the excitation side instead of the back side. The differences between the front- and back-viewing cases will become more pronounced as the absorbance increases. For front-surface viewing the sample should certainly be excited at an absorption maximum to minimize the penetration of the exciting light into the cuvette. This reduces the length of solution between the emission and the detector and reduces reabsorption. For right-angle viewing, decreasing L (Figure 3) reduces reabsorption.

Reabsorption corrections may be quantitatively assessed for a variety of important experimental situations. To demonstrate how such corrections are handled, consider the simple case of right-angle viewing (Figure 3). This situation corresponds to the normal spectrometer or Weber–Teale geometry. We assume that the width of the exciting beam is small compared to the width of the cuvette, the solution is optically dilute at the exciting wavelength, and the detector views only a small volume of the luminescence (for accurate definition of L). Because of distortion of the spectrum due to reabsorption along path L, the spectrometer measures an apparent corrected emission spectrum of the sample, $I_a(\bar{\nu})$ (relative quanta/sec cm^{-1}),

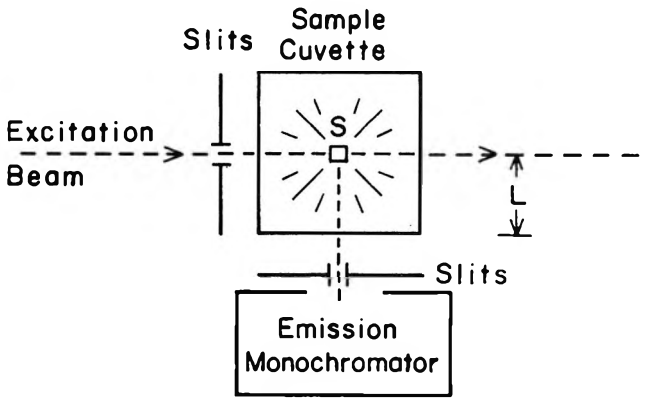

Figure 3. Right-angle viewing of a luminescent sample. The effective path length for reabsorption is assumed to be L.

(143) W. A. Shurcliff and R. C. Jones, *J. Opt. Soc. Amer.*, **39**, 912 (1949).

(144) B. E. Gordon and R. M. Curtis, *Anal. Chem.*, **40**, 1486 (1968).

which is not the same as the molecular emission spectrum, $I(\bar{\nu})$ (relative quanta/sec cm^{-1}). From Beer's law $I(\bar{\nu})$ and $I_a(\bar{\nu})$ are related by

$$I_a(\bar{\nu}) = I(\bar{\nu})10^{-A(\bar{\nu})L} = I(\bar{\nu})e^{-2.303A(\bar{\nu})L} \quad (37)$$

where $A(\bar{\nu})$ is the absorbance/cm at energy $\bar{\nu}$. In eq 15, used for the calculation of quantum yields by Parker's method, the area under the corrected apparent spectrum was employed, but, in fact, the area under the true spectrum should have been computed. By eq 37 the correct form for D in terms of observables is

$$D = \int I(\bar{\nu})\, d\bar{\nu} = \int I_a(\bar{\nu})e^{+2.303A(\bar{\nu})L}\, d\bar{\nu} \quad (38)$$

The integration is carried out over the entire emission band. For low optical densities, of course, this correction for reabsorption becomes insignificant, since $I_a(\bar{\nu})$ and $I(\bar{\nu})$ become indistinguishable.

The reabsorption correction was first studied quantitatively by Ghosh and Sengupta[32,33] who considered three cases: front-surface viewing, rear viewing, and right-angle viewing. They presented expressions similar to eq 38 for correcting the apparent quantum yield measured under such circumstances in terms of the observed emission spectrum and the sample absorbance. Their results, however, are more general than eq 38 because they take into account solutions of any optical density at the exciting wavelength. Assumptions inherent in their treatment were that no reemission occurred and that the exciting beam had a large area and a uniform intensity. The work of Ghosh and Sengupta laid the foundation for Förster's classic treatment of quantum-yield measurements.[11] Readers interested in reabsorption corrections of this type should consult the detailed discussions by Lipsett.[13]

Melhuish[22] has given reabsorption corrections to be applied to a quantum-counter quantum-yield apparatus. His equations also account for reemission corrections.

For spectrometer measurements of quantum yields, a simple, reliable procedure for minimizing reabsorption errors has been discussed by Parker.[4a] The method makes use of the fact that the integrated emission intensity can be inferred from the emission intensity at a single wavelength. The emission spectrum of the compound is first run under conditions where reabsorption is insignificant (low concentrations but usually wide excitation slits): an emission wavelength is selected which will not be attenuated by reabsorption during the yield measurement (*e.g.*, in a structured emission such as that of anthracene, the second vibrational band; in a structureless emission with a large Franck–Condon shift such as exhibited by aniline, the emission maximum; in a dye with large reabsorption effects, on the long wavelength emission tail). The ratio of the corrected emission area to the uncorrected emission intensity at this wavelength is then calculated. When the quantum yield is measured (narrow slits), the emission intensity is measured at the chosen wavelength; the integrated emission area (corrected for reabsorption) is then just the product of the measured intensity and the previously obtained ratio. It is assumed that the molecular emission spectra are the same in both cases (normally true for pure compounds) and that reemission is not significant.

In general any of the correction procedures for reabsorption will be most accurate whenever the reemission correction is small (*i.e.*, the product of the fraction of the luminescence reabsorbed and the sample quantum yield is much less than one). The calculation of the reabsorbed fraction has been outlined in some detail by Melhuish.[22] As with most corrections in quantum-yield measurements, reabsorption corrections are only approximate, and the best way to handle errors of this type is to select favorable experimental conditions. Reduction of the reabsorption correction is best accomplished by using dilute solutions and cuvettes with small path lengths. If optically dense solutions are measured, exciting at the wavelength of maximum absorbance while viewing the front surface is the best arrangement.

C. Reemission Corrections. In any quantum-yield measurement a certain amount of the sample luminescence is reabsorbed by the substance and some of these reabsorbed photons may produce secondary emission which is subsequently recorded by the detector. This excess intensity seen by the detector is the so-called "reemission error." The reemitted radiation may be reabsorbed and reemitted, etc.

Reemission errors are most significant when overlap between the absorption and emission spectra is large, the quantum yield is high, and the solution is concentrated. The effects are very clearly demonstrated by the work of Budo, *et al.*,[45] who compared the "apparent" quantum yield of fluorescein (corrected for reabsorption) and the "actual" yield (corrected for reabsorption and reemission) as a function of concentration. Even at 10^{-5} M in a 1-mm thick cuvette, the apparent yield was ~5% higher than the actual yield of ~0.86. As the concentration and, concomitantly, the reabsorption increased, the error increased to 34% at 2.5×10^{-4} M and 45% at 5×10^{-4} M. A maximum error of 52% high was measured at 1×10^{-3} M (actual yield ~0.81). In fact, impossible apparent yields greater than unity were measured for concentrations between 2.5×10^{-4} and 2×10^{-3} M. As the fluorescein concentration increased further, the error decreased. Although the amount of reabsorption continually increased, the absolute yield diminished, thus reducing the importance of reemitted fluorescence. At 1.6×10^{-2} M the actual yield was 0.16, and the error from reemission had fallen to only ~7%.

Melhuish[22] has observed reemission phenomena with aromatics. He found the apparent yield of 9,10-diphenylanthracene to be unity at concentrations

above 10^{-3} M. Below this concentration the apparent yield decreased and reached a lower limit of 0.83 at 3×10^{-5} M. Yet, when corrected for reabsorption and reemission, the yield was ~0.83 in the concentration range, 10^{-5} to 10^{-2} M, a more reasonable result.

No satisfactory general analysis of the reemission correction is presently available, although there are several papers on the subject. Budo, *et al.*,[45] in a difficult paper, have presented a mathematical analysis of the reabsorption–reemission problem in a disk-shaped cuvette. Their equations, restated in ref 145, are proposed for correcting observed quantum yields and emission spectra for the effects both of reabsorption and of reemission.

Melhuish[22] has presented a simplified modification of the equations of Budo, *et al.* He outlines in detail the general method used for calculating these corrections and applies his method to a disk-shaped cuvette viewed by a quantum-counter detector. Two limiting cases are considered: solutions which are strongly absorbing and solutions which are weakly absorbing at the excitation wavelength. Although only approximate, his data indicate that the correction factors are reasonable. As mentioned earlier, without any corrections 9,10-diphenylanthracene shows an increase in quantum yield with increasing concentration, an unexpected result. Yet, if the corrections are applied, the yield becomes independent of concentration in the range 10^{-5} to 10^{-2} M. Perylene, without any corrections, has a yield which increases and finally decreases as the concentration is raised. If Melhuish's corrections are applied, a linear Stern–Volmer quenching plot is obtained. Anthracene also shows a good Stern–Volmer plot only if the corrections are applied. The equations can probably be used with confidence. Although Melhuish's corrections apply specifically to a quantum-counter detector, they should be valid whenever any detector views the entire volume of solution. When the detector views only a portion of the cuvette, his treatment is no longer valid.

There is a simple intuitive method for estimating whether reemission errors are significant. Calculate the observed quantum yield. Estimate the fraction of directly excited sample luminescence which is reabsorbed in the region of the cuvette viewed by the detector. The product of the fraction absorbed and the observed quantum yield is approximately equal to the fractional error due to reemission.

Because of the uncertainties in correcting for reemission, every attempt should be made to minimize or eliminate the problem experimentally. This is best done by using small cuvettes and the lowest concentrations possible. If concentrated solutions are measured, however, reducing the cuvette thickness reduces the amount of reabsorbed radiation and thus increases the accuracy of the determination. The use of optical stops to limit the detector viewing field to only the directly excited region is also helpful to discriminate against reemitted radiation.

D. Polarization Corrections. Polarization factors introduce subtle sources of error which may affect (by a factor of 2) measured quantum yields. These errors arise when the sample emission is not isotropic as is generally assumed. Light falling on a solution preferentially excites those molecules whose absorbing axes are oriented parallel to the electric vector of the incident radiation. If not subsequently randomized before emitting, the resultant inhomogeneous distribution of excited molecules produces anisotropic radiation. Along with the anisotropy the emission is also polarized which leads to the term polarization errors, although it is usually not polarization but anisotropy which causes the problem. Randomization of the excited molecules is usually accomplished by molecular rotation. Thus polarization errors will typically occur under conditions where the molecules are not freely rotating (high viscosity or macromolecular solutes). The magnitude of the necessary correction is determined by a number of factors: the cuvette design, the angle between the absorbing and emitting molecular axes, the number of absorbing and emitting axes, the degree and orientation of the polarization of the exciting beam, and any polarization sensitivity of the detector.

Weber and Teale[28] have given an equation which corrects for polarization effects for right-angle viewing. The exciting light must be unpolarized (or completely polarized at 45° from the vertical if excitation and viewing is in the horizontal plane), and the emission must be electric dipole allowed. The formula uses the experimentally measured polarization ratio for the emission, rather than any theoretical analysis of the molecular structure. Their equation presupposes no depolarization of the emitted light during its passage through the cuvette and solution. It also assumes no polarization sensitivity of the detector. Fluid solutions and high quality cuvettes produce minimal depolarization, but strained rigid glasses will depolarize the emission and produce conditions under which the formula does not apply. Most optical detectors or quantum counters are not sensitive to the degree of polarization of the emission, although monochromators are a notable exception (see below).

Kalantar[25] gives general equations describing polarization effects in any randomly oriented solution. Any viewing angle, any degree of polarization of the exciting light, and the fractional transition probabilities for absorption and emission along the molecular axes are considered. Both the absorption and emission must be dipole allowed. Basing his discussion on the general equations, Kalantar takes up, in detail, three experimental situations: right-angle (90°) viewing, viewing at 45° to the excitation, and rear-surface (180°) view-

(145) A. Budo and I. Ketskemety, *J. Chem. Phys.*, 25, 595 (1956).

ing. A comprehensive table showing the maximum relative errors in intensity measurements encountered for different molecular characteristics and for varying degrees of polarization of the exciting light is given.[25] For a typical quantum-yield measurement carried out with unpolarized exciting light, the observed intensity at 90° viewing may range from 10% lower than the value for isotropic emission to 5% above it (depending on the orientations of the absorbing and emitting axes). For 180° viewing the errors range from −10% to +20%, whereas for 45° viewing they are only −2.5% to 5%. If the exciting light is polarized, far greater deviations can occur. For totally polarized exciting light the errors for 90° viewing (the worst case) may range from −40% to +20%.

For measurements relative to a standard substance both the unknown and the standard can emit anisotropically and compound the error. For unpolarized exciting light the error in the yield can be as great as 33% (180° viewing), 17% (90° viewing), and 8% (45° viewing). For polarized exciting light far greater errors might be incurred (up to a factor of 2). Only *standards exhibiting isotropic emission* should be employed in relative quantum-yield measurements (dyes in glasses are particularly undesirable from this standpoint).

Fortunately, many experimental factors tend to reduce polarization errors, and substantial difficulties are only encountered under special conditions. Molecular rotation of the excited species usually reduces the anisotropy to negligible significance for low-viscosity solvents; however, solute macromolecules (*e.g.*, proteins or polymers) can still exhibit significant anisotropy of emission even in low-viscosity solvents. High-viscosity solvents (*e.g.*, glycerol and ethylene glycol) and especially plastics and rigid glasses which prevent rotation introduce the greatest errors. Even in rigid media, however, strains and energy transfer can depolarize the emission significantly. In addition, the error extremes indicated above apply only if absorption and emission are allowed along just *one* molecular axis. Many molecules have absorption and emission bands which contain components allowed along several molecular axes. Excitation in such absorption bands can help reduce the errors substantially. If it is possible to excite the substance in a region of overlapping bands having different polarizations, isotropy is also promoted. Computation of the actual error in a particular case is difficult and is seldom done.

Sensitivity of a detector to the degree of polarization of the incident light can introduce error in a yield measurement. Monochromators, particularly grating instruments, transmit differently for light polarized parallel and perpendicular to the slits.[26] Some detectors (*e.g.*, the RCA 2020 photomultiplier)[37] also exhibit a polarization-dependent sensitivity. Therefore a detector system calibrated with unpolarized light may respond differently when it views partially polarized radiation. Since anisotropic emissions are usually partially polarized,[25] the problem is a general one. The exception is 180° viewing with unpolarized exciting light, where the detector does see an unpolarized emission. In principle, error correction factors can be obtained from the measured degree of polarization of the emission and the polarization sensitivity of the detector. In practice, this refinement greatly complicates the measurement, and it is usually ignored without justification.

Kalantar[25] and Almgren[146] have described experimental methods which, in principle, eliminate polarization errors. With an unpolarized excitation beam and a viewing port at 54.7° from the excitation path (ignoring refraction at the cuvette face), the detector monitors an intensity which equals the isotropic value. This technique does not, however, correct for the polarization sensitivity of the detector. Alternately, by suitably selecting a viewing angle, choosing the degree of polarization of the exciting light, and properly analyzing the emission with a polarizer, an investigator can eliminate polarization errors (see ref 25 and 146 for details). This method has advantages. Not only is the anisotropy of the emission accounted for, but the detector always sees light of the same polarization, thus eliminating one source of trouble (the detector must be calibrated with the polarizer in place). Although not employed at present, these techniques may prove useful where low intensity is not a problem.

Reliable correction factors for polarization errors are difficult to obtain. For fluid solutions the technique of Weber and Teale,[28] which infers the spacial anisotropy from the measured polarization ratio, is a satisfactory method, but for rigid glasses it is less useful. Some of the experimental tricks of Almgren[146] and Kalantar[25] might prove valuable for measurements both in fluid solutions and in glasses. For relative measurements it is important to use a standard which does not exhibit polarization effects, or else substantial errors may result. Integrating spheres, in spite of their disadvantages, are probably a good way to eliminate polarization errors, especially for compounds exhibiting small emission–absorption overlap. Calibration could be trying, however.

VII. Recommendations for Data Presentation

Unfortunately, a great many of the published quantum-yield studies have not included enough experimental detail to permit a critical evaluation of the results. Many workers give no estimate of errors and present little or no experimental information—indeed, some authors using relative methods have even failed to identify their standard compound. Data presented in this way are frequently useless. In view of the great

(146) M. Almgren, *Photochem. Photobiol.*, **8**, 231 (1968).

difficulties involved in making quantum-yield measurements, such practices do a disservice to both the authors and the readers.

To standardize luminescence data an international panel of experts has proposed a minimum information set which should be included in any quantitative luminescence study.[147] Enlarging upon their suggestions, we propose that authors in their reports answer as many of the questions listed below as are applicable. Inclusion of such information will permit readers to make a critical evaluation of the published quantum-yield values.

1. What basic quantum-yield measurement technique was employed? What was the method of data reduction? Were there any novel mathematical techniques and corrections used in the data reduction procedures?

2. If a relative quantum-yield method was used, what standard was employed? What yield was assumed for it? What excitation wavelengths were used?

3. If a standard-solution scatterer was used, over what wavelength range did the absorbance follow the Rayleigh scattering law?

4. What type of instrument was used for the absorption measurements? What precautions were taken to avoid absorbance errors due to sample luminescence or, in the solution-scatterer method, errors introduced from scattered light reaching the detector?

5. What was the emission instrumentation used (light sources, filters, monochromators, detector, dewar, and sample cuvette)? Was the cuvette blackened on all sides not involved directly with the transmission of light? What was the experimental geometry employed? What kind of lenses and stops were in the optical paths?

6. What was the bandpass of the emission monochromator? Were the spectra appreciably distorted by this bandpass?

7. What technique was used to calibrate the emission spectrometer, detector, and/or excitation source? Were tests made for stray light in the calibrated instrument? Only corrected emission spectra (in units of relative quanta per unit frequency interval versus a linear energy scale) should be presented. An emission spectrometer calibration curve or an indication of the magnitudes of the correction factors at various wavelengths should be given.

8. What was the spectrum of the exciting light? Usually a description of the excitation source, the monochromator bandpass (if applicable), and the characteristics of the blocking filters is adequate. For quantitative optically dilute measurements (where spectral purity is of central importance) a complete spectrum of the source or the actual transmission curve of the filter combination may be necessary. Did the excitation bandpass or stray light introduce uncertainty in the effective absorbance value assumed for the sample?

9. Were blanks or background spectra taken for pure solvents? Were background signals significant compared with the sample signals? If the blank signals were appreciable, they should be reported along with the emission.

10. What refractive index correction was applied? Did the detector see beyond the region of uniform luminescence?

11. Were reabsorption, reemission, and polarization errors significant? What corrections were applied?

12. What were the sources of the compounds, standards, and solvents? What purification methods and handling procedures were followed?

13. What were the sample concentrations and the temperatures of the solutions?

14. Were aerated or deaerated solvents used? Did oxygen appreciably quench the emissions?

15. Were there any indications of unusual behavior such as photolysis or dissociation of the compounds? Was concentration quenching observed?

16. What are the computed standard deviations and the subjective estimations of the reliability of the results?

17. What values were obtained for compounds of known quantum yield on the apparatus? Failure to present evidence of satisfactory performance casts doubt on all subsequent data.

Acknowledgments. The authors wish to thank Susan Demas and Jane Crosby for carrying out the literature survey and for their unflagging efforts to improve the quality of the manuscript.

(147) J. H. Chapman, Th. Förster, G. Kortüm, E. Lippert, W. H. Melhuish, G. Nebbia, and C. A. Parker, *Z. Anal. Chem.*, 197, 431 (1963); J. H. Chapman, Th. Förster, G. Kortüm, C. A. Parker, E. Lippert, W. H. Melhuish, and G. Nebbia, *Appl. Spectrosc.*, 17, 171 (1963).

Intersystem Crossing in the Charge-Transfer Quenching of Molecular Fluorescence

by C. R. Goldschmidt, R. Potashnik, and M. Ottolenghi*

Department of Physical Chemistry, The Hebrew University, Jerusalem, Israel *(Received September 3, 1970)*

Publication costs borne completely by The Journal of Physical Chemistry

A pulsed nitrogen laser is applied to the nanosecond flash photolysis of anthracene, 9-methylanthracene, 9,10-diphenylanthracene, and pyrene in the presence of diethylaniline as a fluorescence quencher. Independently of solvent polarity, the quenching process is found to be associated with the population of the lowest triplet state of the quenched molecule. A similar effect is observed with O_2 and dicyanobenzene as quenchers of pyrene fluorescence but not with CCl_4 in the quenching of excited anthracene. A general mechanism for the formation of triplet states in the charge-transfer quenching of aromatic molecules is discussed. The more general process of fluorescence quenching by oxygen is considered in terms of the new data.

Introduction

The detailed mechanism of intermolecular quenching of fluorescence is of major importance in the study of primary photophysical and photochemical processes of aromatic molecules in solution. Several mechanisms appear to operate in the case of aromatic systems: (a) quenching due to chemical reactions (*e.g.*, the quenching of anthracene fluorescence by carbon tetrachloride); (b) quenching involving electronic energy transfer;[1] (c) quenching by heavy atom[2] or paramagnetic molecules, due to intersystem crossing enhanced by spin-orbit coupling; (d) quenching processes proceeding *via* charge-transfer interactions.[3]

The charge-transfer mechanism, extensively investigated by Weller and coworkers,[4] shows features which are very sensitive to solvent polarity. In nonpolar solvents the original fluorescence of, *e.g.*, an electron acceptor $^1A^*$, is replaced by a new band, attributed to an excited charge-transfer complex formed between the excited acceptor and the quencher (a donor D). In polar solvents no new fluorescence band appears, and the proposed mechanism proceeds *via* ion-pair formation.[4,5] The separated ionization products (A^- and D^+) have actually been observed in flash experiments in polar solutions, together with the triplet states, *e.g.*, $^3A^*$, of the quenched molecules.[4,6a] To account for triplet formation in quenched polar solutions, a charge recombination process ($D^+ + A^- \rightarrow D + {}^3A^*$) has been postulated.[6]

Very recently we have noticed that high triplet yields are also observed following the charge-transfer quenching of fluorescence in nonpolar solutions of anthracene and pyrene. Such observations were unexpected since no ionization products can be detected in nonpolar solvents which could account for triplet formation. We have thus carried out flash photolysis experiments, with the purpose of elucidating the general mechanism of triplet-state formation associated with charge-transfer quenching. The study also bears on the more common problem of fluorescence quenching by molecular oxygen.

Experimental Section

The nanosecond flash photolysis technique using an AVCO-Everett pulsed nitrogen laser emitting at 3371 Å has been previously described.[7a] Fluorescence lifetimes shorter than the 10-nsec laser pulse were estimated by the "method of moments."[7b]

Materials employed were anthracene (Fluka, puriss.), *N,N*-diethylaniline (DEA) (BDH, redistilled under nitrogen), pyrene (Fluka, zone refined), ethanol (Fluka spectrograde). Dicyanobenzene (DCB), zone refined, was obtained from Dr. A. Watkins (Max-Planck Institute of Spectroscopy, Göttingen); 9-methylanthracene and 9,10-diphenylanthracene were obtained from Dr. M. Cohen (Weizmann Institute of Science, Rehovoth).

Results

Anthracene and Derivatives. Characteristic oscillograms in the laser photolysis of mixed anthracene–DEA solutions in toluene are shown in Figure 1. All traces were recorded at the 430-nm maximum of the anthracene triplet-state absorption. Obviously, considerable

(1) T. Förster, *Z. Elektrochem.*, **56**, 716 (1952); *Discuss. Faraday Soc.*, **27**, 7 (1959).

(2) M. Kasha, *J. Chem. Phys.*, **20**, 71 (1952).

(3) H. Leonhardt and A. Weller, *Z. Phys. Chem.*, **29**, 278 (1961); *Ber. Bunsenges. Phys. Chem.*, **67**, 791 (1963).

(4) H. Knibbe, D. Rehm, and A. Weller, *ibid.*, **72**, 257 (1968).

(5) H. Knibbe, K. Röllig, F. P. Schäfer, and A. Weller, *J. Chem. Phys.*, **47**, 1184 (1967).

(6) (a) K. H. Grellmann, A. R. Watkins, and A. Weller, *J. Luminescence*, **1,2**, 678 (1970); (b) D. Rehm and A. Weller, *Israel J. Chem.*, **8**, 259 (1970).

(7) (a) C. R. Goldschmidt, M. Ottolenghi, and G. Stein, *ibid.*, **8**, 29 (1970); (b) S. S. Brody, *Rev. Sci. Instrum.*, **28**, 1021 (1957).

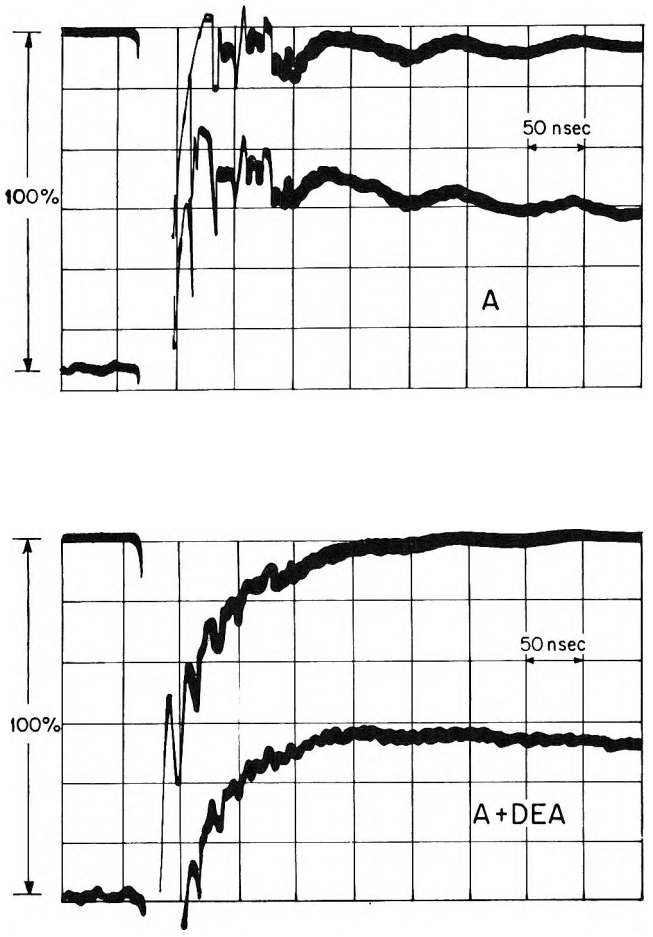

Figure 1. Oscillograms, at λ 430 nm, in the laser photolysis of anthracene (A) in the presence (lower figure) and absence (upper figure) of diethylaniline (DEA) as quencher. Experiments are in toluene at room temperatures. Concentrations: [A] = 1.1×10^{-2} *M*, [DEA] = 0.5 *M*. Upper trace in each figure is taken without the monitoring light pulse and represents the separate contribution of fluorescence to the lower trace. Lower traces are in presence of the monitoring light.

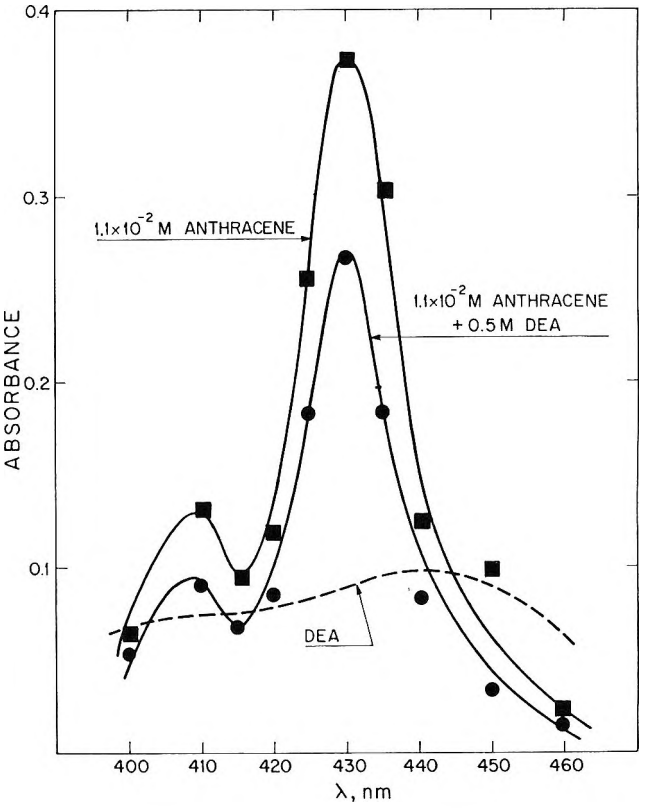

Figure 2. Spectra of the long-lived transient, attributed to the anthracene triplet, in the laser photolysis of anthracene–toluene solutions in the presence and absence of DEA. Dashed line is a transient absorbance detected in a 0.5 *M* DEA solution in toluene, probably due to the DEA triplet. Data were taken 250 nsec after firing the laser.

absorbance changes induced by the laser pulse are observed not only in quencher-free anthracene solutions, but also in the presence of 0.5 *M* DEA which reduces the original anthracene fluorescence to less than 3% of its value in the unquenched systems. The detailed transient spectra in Figure 2 indicate that the absorption of the flash intermediate (measured ~250 nsec after pulsing) in the presence of DEA, is practically identical with that of the anthracene triplet recorded in the absence of DEA. The effect of direct light absorption by DEA, leading to the triplet state of the molecule (Figure 2), could be neglected in the mixed anthracene–DEA solutions, where more than 90% of the 3371-Å exciting laser beam was absorbed by anthracene. The only significant new feature observed at 430 nm in the quenched solutions is the strong (~80 nsec) emission due to the excited anthracene–DEA complex (see Figure 1). Experiments similar to the above have also been carried out in acetonitrile as solvent, where the quenching of the anthracene fluorescence by electron donors such as DEA is not accompanied by an exciplex emission. The laser flash patterns in such a polar solvent were, however, found to be very similar to those observed in the toluene systems. Namely, the amount of anthracene triplets formed in the quenched solutions is practically identical with that observed for pure anthracene in acetonitrile (see Table I). As far as time scales are concerned, no growing-in stages for the triplet absorbance in acetonitrile (or toluene, see Discussion below) could be observed, leading to the conclusion that in quenched as well as in unquenched systems the triplet state is populated within less than ~20 nsec.

These observations, showing very small and solvent-independent effects of charge-transfer quenching in the yields of intersystem crossing, can formally be interpreted in two alternative ways: one, by assuming that intersystem crossing to the triplet state in an isolated anthracene molecule in solution does not exclusively occur from the lowest thermalized singlet state in competition with fluorescence. If a fast population of the triplet ($^3A^*$) takes place prior to the formation of the thermalized singlet ($^1A^*$), then the yields of $^3A^*$ are not expected to be altered even under total quench-

Table I: Fluorescence and Triplet-State Yields in Quenched Solutions of Anthracene and Pyrene, Relative to the Corresponding Values Observed without Quenchers

Fluorescent molecule and concentration	Quencher and concentration	Solvent	Relative fluorescence yield[a-c]	Relative yield of triplet[a,c]
Anthracene, 1.1×10^{-2} *M*	DEA, 0.5 *M*	Toluene	<0.03	0.75
Anthracene, 1.1×10^{-2} *M*	DEA, 0.5 *M*	Acetonitrile	0.02	1.0
Anthracene, 5.6×10^{-3} *M*	Bromobenzene, 0.5 *M*	Toluene	0.65	1.2
Anthracene, 5.6×10^{-3} *M*	Carbon tetrachloride, 0.5 *M*	Toluene	0.70	0.72
Anthracene, 4.0×10^{-4} *M*	Carbon tetrachloride, 0.3 *M*	Ethanol	0.32	0.35
9-Methylanthracene, 10^{-2} *M*	DEA, 0.5 *M*	Toluene	0.05	1.0
9,10-Diphenylanthracene, 10^{-2} *M*	DEA, 0.5 *M*	Toluene	0.1	(See text)
Pyrene, 2×10^{-5} *M*	DEA, 2.5×10^{-2} *M*	Toluene	<0.03	2.0
Pyrene, 2×10^{-5} *M*	DEA, 2.5×10^{-2} *M*	Acetonitrile	<0.03	1.25
Pyrene, 2×10^{-5} *M*	DCB, 6×10^{-2} *M*	Toluene	0.02	2.0
Pyrene, 2×10^{-5} *M*	O_2, $\sim 10^{-3}$ *M*	Toluene	0.04	3.0

[a] Measured at the maxima of the corresponding triplet absorption and fluorescence emission bands. Note that fluorescence is of originally excited molecule (not of exciplexes). [b] Estimated from the areas under intensity *vs.* time emission traces. These were obtained in laser flash experiments under conditions identical with those employed for determination of triplet absorptions. [c] Experimental accuracy is ~10%.

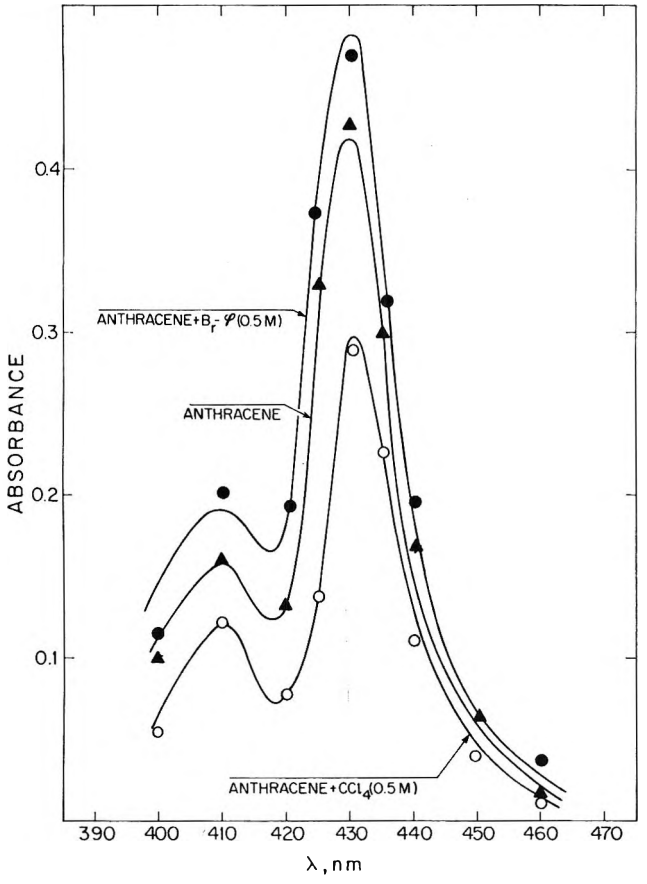

Figure 3. Anthracene triplet spectra in the laser photolysis of anthracene (5.6×10^{-3} *M*) solutions in toluene, in the presence (and absence) of fluorescence quenchers.

ing of $^1A^*$.[8-12] An alternative mechanism, which adopts the conventional scheme of intersystem crossing competing with fluorescence in the isolated molecule, implies that a singlet–triplet transition is induced by the very act of quenching by DEA. Phenomenologically, this will resemble the case of a heavy atom quencher such as bromobenzene (Figure 3 and ref 13). To discriminate between the two mechanisms we have carried out laser-excitation experiments in which carbon tetrachloride replaced DEA as a quencher of anthracene's fluorescence. The results presented in Figure 3 and Table I clearly favor the second alternative. Thus, in both toluene or ethanol solutions, the drops in the fluorescence yields due to quenching by CCl_4 are accompanied by a matching drop in the anthracene triplet yields. Such a behavior is obviously inconsistent with paths leading to triplet population, in quencher-free solutions, which do not involve the thermalized fluorescent state $^1A^*$. It should finally be mentioned that lifetime measurements (see Experimental Section)

(8) The usual assumption, that the singlet → triplet intersystem crossing in an excited aromatic molecule in solution occurs from the thermalized lowest excited singlet state S_1(th) in competition with fluorescence, still awaits a general direct experimental verification. In a few cases a growing-in of the triplet absorption occurring at the same rate as the decay of the fluorescent state, was actually observed.[9-12] Such observations, although yielding direct evidence for the process S_1(th) → T_1, do not rule out alternative (faster) paths for the population of T_1 following excitations which are not essentially within the weak $S_0 \rightarrow T_1$ band. In the cases of naphthalene and 1,2-benzanthracene submitted to fast laser excitation, the spectrum at the end of the pulse—when only a small fraction of S_1 has decayed—is very similar to that of T_1.[12] This phenomenon can be explained either by a coincidental identity between the spectra of T_1 and S_1,[12] or by assuming that a fraction of the observed triplets were present at the end of the pulse prior to any substantial decay of S_1. A final discrimination between these two alternatives still awaits further experimental work.

(9) J. R. Novak and R. W. Windsor, *J. Chem. Phys.*, **47**, 3075 (1967).

(10) R. Bensasson, R. Bonneau, J. Joussot-Dubien, and J. Faure, *J. Chim. Phys.*, **66**, 125 (1969).

(11) G. Porter and M. R. Topp, *Proc. Roy. Soc., Ser. A*, **315**, 163 (1970).

(12) R. McNeil, J. T. Richards, and J. K. Thomas, *J. Phys. Chem.*, **74**, 2290 (1970).

(13) T. Medinger and F. Wilkinson, *Trans. Faraday Soc.*, **61**, 620 (1965).

confirmed, in all cases, that the quenching process was associated with corresponding drops in the anthracene fluorescence decay rate. This rules out possible complications due to the operation of static quenching mechanisms.

Experiments similar to the above were also carried out with 9-methylanthracene and 9,10-diphenylanthracene. The behavior in the first case, where high triplet yields are already observed for the isolated molecule in solution, is very similar to that of unsubstituted anthracene. In the case of 9,10-diphenylanthracene, characterized by a low-efficiency intersystem crossing,[13] no transient absorption attributable to the triplet could be detected in the absence of quenchers. However, in the presence of 0.5 *M* DEA, a broad transient absorption band ($\lambda_{max} \simeq 460$ nm), most probably due to the triplet state of the molecule,[13] was detected.

Pyrene Systems. Pyrene solutions in toluene were submitted to laser flash experiments in the presence of DEA, DCB, and O_2 as quenchers of the lowest excited singlet state. In the cases of DEA (donor) and DCB (acceptor) the quenching process is associated with the formation of a fluorescent charge-transfer exciplex. As in the case of anthracene–DEA,[14] short-lived intermediates are observed immediately after pulsing whose lifetimes are identical with those of the corresponding exciplex emission.[15] After the decay of these fast absorptions, assigned to singlet–singlet transitions of the excited complexes, a long-lived transient is observed in both pyrene–DEA and pyrene–DCB systems whose spectrum is practically identical with that of the pyrene triplet (Figure 4). The same figure includes a transient spectrum observed in an air-saturated solution of pyrene where, as in the cases of DEA and DCB, practically total (~96%) quenching fluorescence by molecular oxygen takes place. The spectral similarity with the T → T absorption observed in pure pyrene solutions agrees with the data first reported by Thomas and coworkers,[16] who suggested that the quenching of $^1P^*$ by O_2 is associated with the formation of the pyrene triplet, $^3P^*$. (Since the rate of reaction between $^1P^*$ and O_2 exceeds that of $^3P^*$ and O_2 by a factor of ~10, the pyrene triplet could still be detected even under conditions of total quenching of $^1P^*$.) Similar observations have been previously reported by Porter and coworkers.[11]

The pyrene–DEA system has also been tested in acetonitrile as solvent. As in the case of anthracene–DEA, a substantial yield of pyrene triplet is observed even under conditions of total quenching of the pyrene fluorescence (Table I). The triplet-state generation follows the laser profile, taking place within less than ~15 nsec.

Discussion

Charge-Transfer Quenching. The detailed mechanism leading to the triplet states of excited aromatic molecules quenched *via* charge-transfer interactions should now be considered.

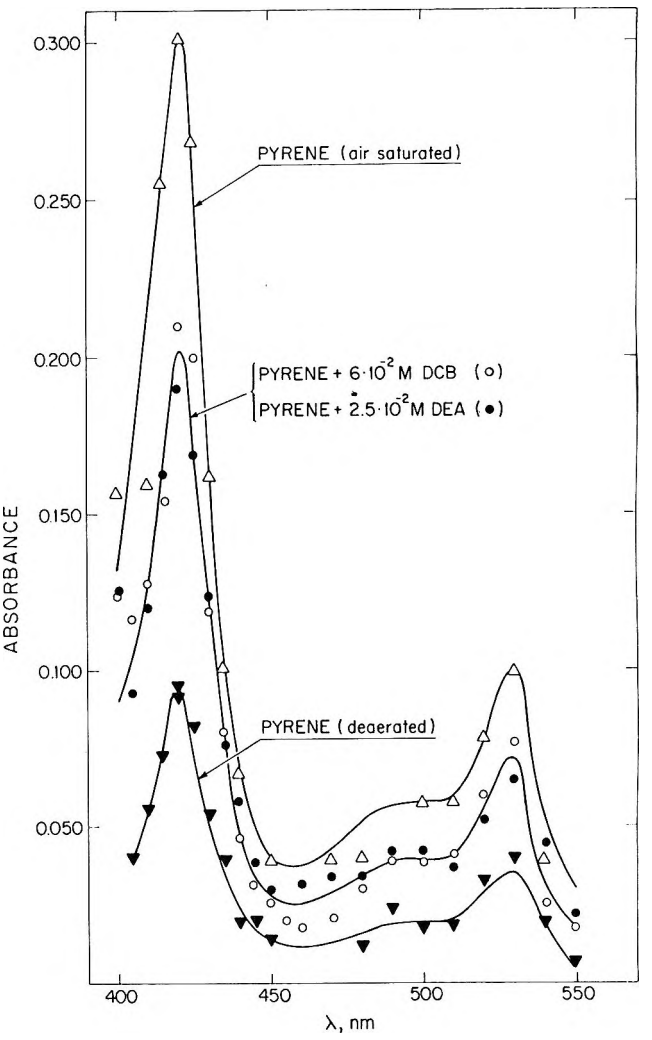

Figure 4. Spectra of long-lived transients, attributed to the pyrene triplet, in the pulsed laser photolysis of pyrene solutions in toluene. Data are extrapolated to the end of the laser pulse, 15 nsec after triggering.

To account for triplet states formation in polar solutions, Weller and coworkers proposed the scheme

$$^1A^* + D \longrightarrow {}^1A^* \ldots D \longrightarrow$$
$$(^2A_S^- \ldots {}^2D_S^+) \longrightarrow {}^2A_S^- + {}^2D_S^+ \longrightarrow {}^3A^* + D$$
$$\longrightarrow A + D \longleftarrow$$

where $(^2A_S^- \ldots {}^2D_S^+)$ is a solvent-shared ion pair which may undergo dissociation to the separated $^2A_S^-$ and $^2D_S^+$ ions. Triplet states of the originally excited molecule ($^3A^*$) will then be obtained *via* charge recombination in the bulk of the solutions (see scheme) but not,

(14) C. R. Goldschmidt and M. Ottolenghi, *Chem. Phys. Lett.*, 4, 570 (1970).

(15) Unpublished data in this laboratory.

(16) J. K. Thomas, presented at the Bat-Sheva Summer School on Fast Reactions, Rehovot-Jerusalem, Israel, July–Aug, 1970.

as previously suggested,[6a] within the geminate ($^2A_S^-$... $^2D_S^+$) ion pair. This was postulated by Rehm and Weller[6b] since triplet generation from the geminate pair (with total spin quantum number 0) implies spin-lattice relaxation which is slower by several orders of magnitude than the rate of the diffusional separation of the ion pair. However, such a reaction scheme does not seem to play an important role in the systems of the present work. This conclusion is based on the following arguments. (a) The need for a time interval of the order of 10^{-6} to 10^{-7} sec to allow for spin relaxation prior to the formation of $^3A^*$ is inconsistent with the fast (<20 nsec) appearance of the triplet state of both anthracene and pyrene in acetonitrile solutions quenched by DEA. The same applies to nonpolar solutions of the same donor–acceptor pairs (see below). (b) The amounts of triplets formed according to the above scheme are determined by the yields of formation of the geminate ion pair ($^2A_S^-$...$^2D_S^+$) which determine those of the separated ions in the bulk of the solution. The triplet yields should therefore exhibit a very strong sensitivity to the solvent polarity, becoming practically negligible in nonpolar solvents where quenching leads to the fluorescent $(A^-D^+)^*$ complex.[4-6] Such predictions are in variance with the relatively small effect (see Table I) of solvent polarity in anthracene and pyrene solutions quenched by DEA. The same applies to the pyrene–DCB system for which triplet yields, considerably higher than those measured in the corresponding unquenched solutions, are observed in both polar[17] and nonpolar (Table I and Figure 4) solutions.

An alternative approach may be that of attributing the triplet formation to intersystem crossing from the thermalized fluorescent state of the charge-transfer exciplex. Such a mechanism, which may proceed *via* locally excited triplet states of the complex, is however inconsistent with two observations. (a) A process such as $(A^-D^+)^* \rightarrow {}^3A^* + D$ implies a relatively slow growing-in of $^3A^*$, matching the fluorescence of $(A^-D^+)^*$. The analysis (presented in Figure 5) for anthracene–DEA, as well as similar ones carried out for pyrene–DEA and pyrene–DCB, indicate that the formation of the corresponding triplets ($^3A^*$ or $^3P^*$) follows the flash profile and not the relatively slow decay of the complex fluorescence. It is possible to argue of course that the process $(A^-D^+)^* \rightarrow {}^3A^* + D$ does actually take place but cannot be observed in the form of a distinct growing-in of $^3A^*$, due to a coincidental mutual cancellation of the absorbances of $^3A^*$ and $(A^-D^+)^*$. This seems, however, extremely unlikely in view of the characteristic sharp absorption bands of $^3A^*$ and $^3P^*$ at 430 and 420 nm, correspondingly. (b) Again, as in the case of the previous scheme, this second mechanism implies a strong dependence of the triplet yields on the solvent polarity. This is due to the fact that both lifetime and yields of $(A^-D^+)^*$ are sensitive to polarity.[5,18] As mentioned above, this prediction is in variance with the experimental observations.

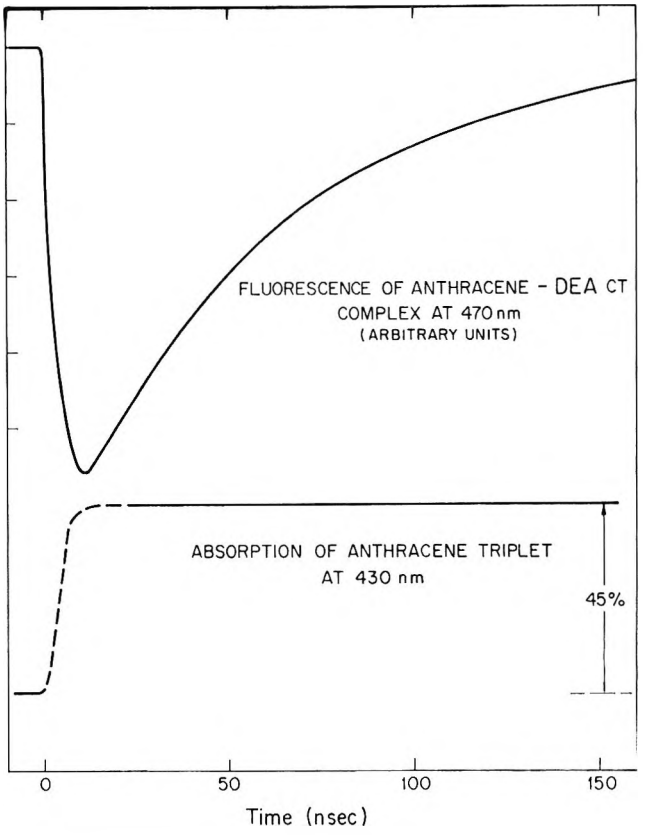

Figure 5. Profile of the anthracene–diethylaniline exciplex fluorescence decay in toluene, compared to that of the (triplet) absorbance growth at 430 nm.

A qualitative description of the formation of triplet states, which does not involve either charge recombination or intersystem crossing from the relaxed fluorescent (charge-transfer) state of the exciplex, is suggested (for a nonpolar solvent) in Figure 6. The encounter between the excited molecule (*e.g.*, $^1A^*$) and the quencher (D) leads to a state ("encounter complex") which is essentially a predominantly locally excited singlet state ($^1A^*D$). From such a state radiationless transitions will take place to the charge-transfer state $(A^-D^+)^*$ or to a dissociative locally excited triplet ($^3A^*D$) which will finally yield $^3A^*$. If there is only little mixing between the zero-order states corresponding to ($^1A^*D$) and $(A^-D^+)^*$, the probability of the internal conversion $(^1A^*D) \rightarrow (A^-D^+)^*$ may be small and comparable to that of the intersystem crossing $(^1A^*D) \rightarrow (^3A^*D)$. Alternatively, a fast population of the $(A^-D^+)^*$ state from ($^1A^*D$) may be followed by intersystem crossing competing with thermal relaxation. The latter assumption is necessary to explain the failure to observe a slow generation of $^3A^*$ (or $^3P^*$) from the (thermalized) fluorescent $(A^-D^+)^*$ state. The fact that the triplet

(17) A. Watkins, private communication.

(18) N. Mataga, T. Okada, and N. Yamamoto, *Chem. Phys. Lett.*, **1**, 119 (1967).

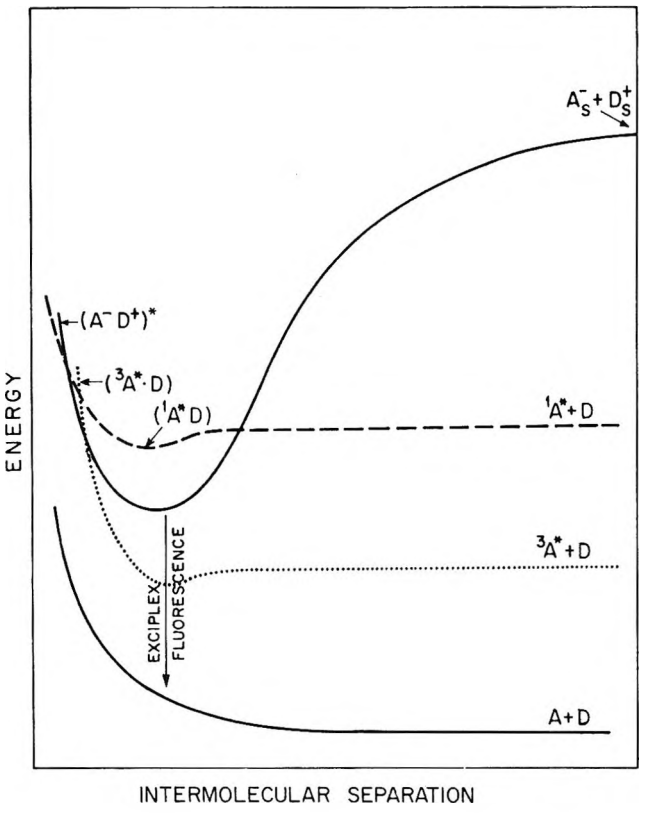

Figure 6. Postulated potential energy curves explaining the formation of triplets ($^3A^*$) and exciplexes ($(A^-D^+)^*$), following the interaction between an excited acceptor ($^1A^*$) and a ground-state donor (D) in a nonpolar solvent.

spectra observed in the presence of quenchers are practically identical with the T → T absorptions recorded in quencher-free systems suggests that the triplets observed in the quenched systems are the free monomer species, *e.g.*, $^3A^*$, rather than locally excited complexes, *e.g.*, ($^3A^*D$). The absorption spectra of locally excited triplets were in fact found to be significantly different from those of the free monomers.[19] At present the above picture should be still considered as a qualitative approach, incapable of accounting quantitatively for effects such as those of solvent polarity. At high dielectric constants (*e.g.*, acetonitrile) the $A_S^- + D_S^+$ level lies below that of $^1A^* + D$,[20] and it is difficult to predict how intersystem crossing will be affected relative to that observed in a nonpolar solvent such as toluene (see Table I).

Quenching by Molecular Oxygen. The detailed mechanism of the reversible quenching of aromatic hydrocarbon fluorescence by oxygen can still be considered as an unresolved problem. Extensive work has been carried out to discriminate between various alternatives concerning the nature of the reaction products. The products combination $S_0 + O_2(^3\Sigma_g^-)$, in which both hydrocarbon and oxygen molecules are left in their respective ground electronic states, has been ruled out in several systems by the photochemical experiments of Snelling[21] as well as by those of Stevens and Algar.[22] The formation of the products pair $T + O_2(^1\Sigma_g^+$ or $^1\Delta_g)$, where T denotes the hydrocarbon triplet state, has been examined and rejected by Parmenter and Rau[23] in the case of several aromatic molecules. The photoperoxidation experiments of Stevens and Algar yield strong, though indirect, evidence eliminating the alternative: $S_0 + O_2(^1\Sigma_g^+$ or $^1\Delta_g)$, as a possible combination of products in the quenching process. It has therefore been concluded by Parmenter and Rau[23] that

$$S_1 + O_2(^3\Sigma_g^-) \longrightarrow T + O_2(^3\Sigma_g^-)$$

represents the common process of aromatic fluorescence quenching by molecular oxygen. As mentioned previously, direct evidence from laser photolysis work is now available confirming the appearance of the hydrocarbon triplet as a quenching reaction product. As far as the states of O_2 are concerned only the $^1\Sigma_g^+$ state can be ruled out in the pyrene–O_2 system of the present work (the energy sum of $^1\Sigma_g^+$ oxygen and triplet pyrene exceeds that of S_1 by ~1 eV). The involvement of the $^1\Delta_g$ state seems unlikely in view of the recent work of Berlman, *et al.*,[24] which strictly applies, however, only to the excimer of pyrene.

The fact that the quenching of pyrene fluorescence by molecular oxygen is associated with triplet-state population as in the case of characteristic charge-transfer quenchers such as DEA (donor) and DCB (acceptor) is relevant to the general mechanism of quenching by O_2. (The effect may actually occur with other molecules but can hardly be detected if the rate constants of singlet and triplet quenching by oxygen are comparable, as is frequently the case.[25]) It is interesting to note that triplet-state population appears to be the major path in the quenching of excited pyrene by O_2. This conclusion is derived from the factor of ~3 between the triplet yields measured in the presence and in the absence of O_2 (Table I and Figure 4). Taking a value of 0.34 ± 0.05 for the yield of intersystem crossing in the free pyrene monomer in solution,[26] one obtains a value close to unity for the absolute yield of triplet formation in the quenching of $^1P^*$ by

(19) G. Briegleb, H. Schuster, and W. Herre, *Chem. Phys. Lett.*, **4**, 53 (1970); Z. Teitelbaum, R. Potashnik, and M. Ottolenghi, to be published.

(20) H. Knibbe, Ph.D. Thesis, Vrije Universiteit, Amsterdam, 1969.

(21) D. R. Snelling, *Chem. Phys. Lett.*, **2**, 346 (1968).

(22) B. Stevens and B. E. Algar, *ibid.*, **1**, 58, 219 (1967).

(23) C. S. Parmenter and J. D. Rau, *J. Chem. Phys.*, **51**, 2242 (1969).

(24) I. B. Berlman, C. R. Goldschmidt, G. Stein, Y. Tomkiewicz, and A. Weinreb, *Chem. Phys. Lett.*, **4**, 338 (1969).

(25) R. Livingston and V. S. Rao, *J. Phys. Chem.*, **63**, 794 (1959).

(26) A value of 0.38 ± 0.02 for the yields of pyrene triplet in dilute ethanol solutions has been reported by Harrocks and Wilkinson [*Proc. Roy. Soc., Ser. A*, **306**, 257 (1968)] and by Medinger and Wilkinson [*Trans. Faraday Soc.*, **62**, 1785 (1966)]. A somewhat lower value (0.27) has been reported by Parker and Joyce [*ibid.*, **62**, 2785 (1966)].

O_2. The relatively small rate constant of the reaction between $^3P^*$ and O_2 ($\sim 3 \times 10^9\ M^{-1}\ sec^{-1}$) will explain why the triplet quenching process, due to recombination within the geminate pair ($^3P^* + O_2$), does not efficiently compete with separation to yield $^3P^*$ and O_2, homogeneously distributed in the bulk of the solution.

The question now arises as to the nature of the interaction between S_1 and $O_2(^3\Sigma_g^-)$ leading to $T + O_2(^3\Sigma_g^-)$. The data of the present work cannot discriminate between such possibilities as enhanced $S_1 \rightarrow T$ intersystem crossing *via* a direct intermolecular exchange interaction,[27,28] indirect S_1–T mixing *via* charge-transfer intermediates,[28,29] or enhanced intersystem crossing due to the inhomogeneous magnetic field of $O_2(^3\Sigma_g^-)$.[30] However, the fact that fluorescence quenching by O_2 shows features analogous to those involved in typical charge-transfer quenching processes may be considered as an additional support to the charge-transfer mechanism in the case of O_2. If such a mechanism is adopted for the quenching of $^1P^*$ by O_2, it will be plausible to look for a CT emission similar to that observed in typical CT systems such as $^1P^*$ quenched by DEA or DCB. In the case of pyrene, where the yield of intersystem crossing associated with oxygen quenching is close to unity, the failure to observe a new fluorescence band may be due to the small yields of exciplex formation. In other systems, it may be due to very efficient processes of internal conversion to the complex ground state. Further experimental work, possibly involving a detailed study of the effects of solvent polarity, may help in establishing the role of charge-transfer interactions in the O_2 quenching process.

(27) G. J. Hoijtink, *Mol. Phys.*, 3, 67 (1960).

(28) K. Kawaoka, A. U. Khan, and D. R. Kearns, *J. Chem. Phys.*, 46, 1842 (1967).

(29) H. Tsubomura and R. S. Mulliken, *J. Amer. Chem. Soc.*, 82, 5966 (1960); H. Linschitz and L. Pekkarinen, *ibid.*, 82, 2411 (1960).

(30) D. F. Evans, *J. Chem. Soc.*, 1351 (1957); 3885 (1957); 2753 (1959); C. Reid, *Quart. Rev. Chem.*, 205 (1958).

Recoil Tritium Reactions with Propene in the Gas Phase[1]

by Kent I. Mahan*

Department of Chemistry, Southern Colorado State College, Pueblo, Colorado 81005

and John K. Garland

Department of Chemistry, Washington State University, Pullman, Washington 99163 *(Received July 20, 1970)*

Publication costs assisted by Washington State University

The recoil tritium–gas phase propene system was studied over a total pressure range from 79 to 511 Torr. A decreasing HT/C_3H_5T ratio was observed with increasing pressure from both unscavenged and O_2 scavenged samples. This effect was attributed to decreasing recoil loss with increasing pressure lowering HT production at the wall. The yield of C_3H_5T from different sources was estimated to be 28% *via* the hot T for H substitution reaction, 56% from excited propyl-*t* radical decomposition, and 16% *via* thermal radical routes in the unscavenged system. The radical environment indicated that the formation of dimeric products from the combination of radicals produced by radiation damage and labeled radicals in thermal equilibrium with their surroundings could be important. However, the absence of any of the unsaturated hexene-*t*'s in the gas phase indicated that most of the excited radicals produced by the addition of T to the double bond were removed from the system by decomposition or reaction with propene molecules before reaching thermal equilibrium.

Introduction

Gas phase data obtained in connection with the study of recoil tritium reactions with propene in the liquid phase[2] showed some discrepancies compared with earlier data.[3] Lower HT/C_3H_5T ratios and higher C_6-*t* yields were obtained, and there was some indication of variation in the HT/C_3H_5T ratio with pressure. No definite trend was established because the data were obtained over a narrow pressure range.

(1) A portion of the material submitted by K. I. M. in partial fulfillment of the degree of Doctor of Philosophy at the University of Missouri, Columbia, Mo.

(2) K. I. Mahan and J. K. Garland, *J. Phys. Chem.*, 73, 1247 (1969).

(3) J. K. Lee, B. Musgrave, and F. S. Rowland, *J. Amer. Chem. Soc.*, 82, 3455 (1960).

This work extends the range of investigation of gas phase recoil tritium reactions with propene and examines any trend in HT/C_3H_5T ratio and its source.

Experimental Section

Ampoules of 15–20 cc volume constructed of 1720 Pyrex glass were evacuated to about 1 μ and filled with the desired amounts of C_3H_6 (Matheson Co., 99% purity), ^3He (Monsanto Mound Laboratory, Miamisburg, Ohio), and O_2 scavenger gas, if used (Matheson Co., Reagent grade).

After sealing, the samples were irradiated in the MURR reactor, Columbia, Missouri, at the desired neutron flux to produce tritium *via* the $^3He(n,p)T$ nuclear reaction. Radiation damage ranging from 0.8 to 1.2% in scavenged samples and from 1.0 to 4.9% in unscavenged samples was calculated from an estimate of the amount of energy absorbed from radiation by heavy recoil particles (T and p) and from reactor γ.[4] Information on neutron flux and irradiation times is given in the data tables. The measured γ flux in the reactor was about 4×10^7 rads/hr for the 1.4×10^{12} n/cm^2 sec flux position.[5] Total tritium activity obtained in the samples ranged from 10^5 to 10^6 dpm. The ^3He used in this work was assayed by Monsanto to contain 99.9 mol % ^3He, 0.1 mol % ^4He, and 1.28×10^{-11} mol % tritium. In a typical gas sample (20 cc and 10 Torr of ^3He) the mole percentage of tritium corresponds to about 10^8 atoms and an activity of 10–11 dpm. This level of activity was entirely negligible compared to the total activity obtained.

Analysis of the volatile products by dual column radio-gas chromatography and polymers by liquid trapping and extraction techniques was identical with the techniques used in the analysis of the samples in the liquid phase propene system.[2,6] Tailing of the mass (propene) peak was not as great a problem as in the liquid phase work,[2,4] so more precise data were obtained.

Results and Discussion

The yields of products relative to the yield of the labeled parent (C_3H_5T) = 100 are given in Table I for representative samples containing no scavenger and in Table II for samples scavenged by O_2. The tables give the yields of all products observed except CH_3T, isobutane-*t*, and butane-*t*. The relative yields of those products were determined by analyses separate from the dual column setup and found to be (in terms of the relative units given in the tables) CH_3T = 3, isobutane-*t* = 2, and butane-*t* = 1 with no apparent pressure dependence.

Figures 1 and 2 give the $(HT + CH_3T)/C_3H_5T$ ratios of all samples analyzed plotted as a function of pressure and recoil loss as obtained from the Argersinger calculation on recoil losses to the irradiation vessel wall.[4,7] The assumptions made in the calculation of the molecular stopping power and recoil ranges in C_3H_6 were not the same as those used by Root and Rowland[8] in a recent paper, but instead were based on the atomic stopping power of C and H as calculated from the molecular stopping power of two hydrocarbons on which experimental data were available, *i.e.*, methane and acetylene.[9] Solving for the atomic stopping powers of H and C using a set of simultaneous equations, *i.e.*, if S = the atomic or molecular stopping power in eV-cm^2/molecule or atom, then

$$S_{C_2H_2} = 2S_C + 2S_H$$

$$S_{CH_4} = S_C + 4S_H$$

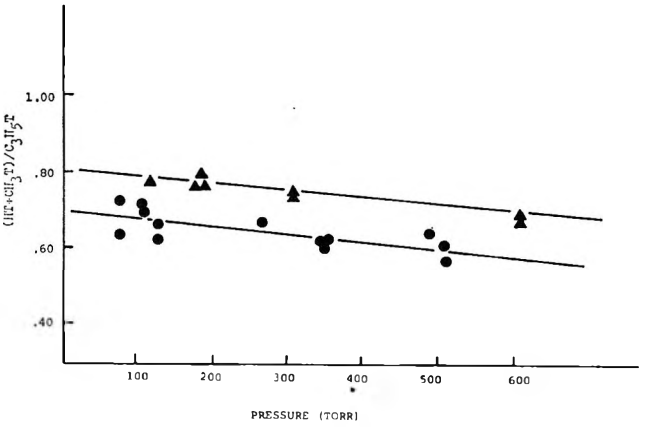

Figure 1. $(HT + CH_3T)/C_3H_5T$ ratios *vs.* total pressure: ▲, oxygen-scavenged samples; ●, unscavenged samples.

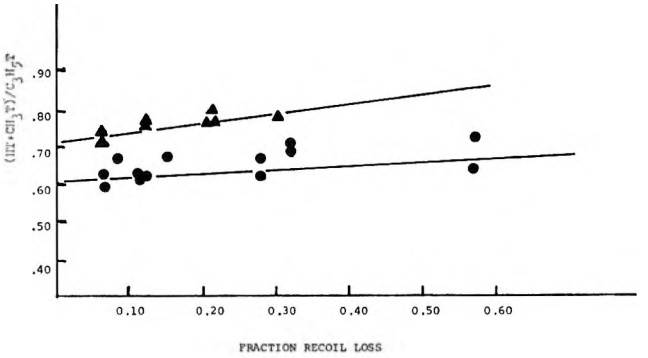

Figure 2. $(HT + CH_3T)/C_3H_5T$ ratios *vs.* recoil loss: ▲, oxygen-scavenged samples; ●, unscavenged samples. Least-squares fits: O_2 scavenged samples, slope 0.26 ± 0.08, intercept 0.72 ± 0.02; unscavenged samples, slope 0.14 ± 0.06, intercept 0.61 ± 0.02.

(4) K. I. Mahan, Ph.D. Thesis, University of Missouri, Columbia, 1969, No. 70-6607, University Microfilms, Ann Arbor, Mich.

(5) R. W. Weeks, Jr., Ph.D. Thesis, University of Missouri, Columbia, 1969.

(6) K. I. Mahan, R. W. Weeks, D. Fee, and J. K. Garland, *Anal. Lett.*, 1, 933 (1968).

(7) W. J. Argersinger, Jr., *J. Phys. Chem.*, 67, 976 (1963).

(8) J. Root and F. S. Rowland, *Radiochim. Acta*, 10, 104 (1968).

(9) W. Whaling, "Handbuch der Physik," Vol. 34, Springer-Verlag, Berlin, 1958, pp 206, 212.

Table I: Relative Yields in Unscavenged Gas Phase Propene

Pressures, Torr		Tot. act. recovered ×	Relative yields of products (C_3H_6T = 100)							
C_3H_6	^3He	10^{-3} dpm	HT + CH_3T	C_2H_3T	C_2HT	C_3H_7T	Branched $C_6H_{13}T$'s	*n*-Hexane-*t*	Light[a]	Heavy[a]
58[b]	21	273.1	64	36[g]			23	17		
58[b]	21	215.7	72	33	3.8	13	27	12	6	5
93[c]	15	809.3	71	32	3.3	16	32[h]		0.3	8
93[c]	15	646.5	70	32	2.6	10	20	13	5	5
116[b]	8	308.4	62	26	3.7	12	18	12	8	4
116[b]	8	251.2	66	25	3.4	14	19	11	9	6
258[b]	10	359.2	67	35	2.4	9	17	11	11	6
337[a]	14	956.9	61	25		14	18	9		
337[d]	14	3118.0	61	31	2.1	10	16	11		
345[b]	8	544.0	63	24	4.0	9	14	10	10	6
478[b]	10	584.3	65	29	1.8	12	16	13	9	8
497[d]	14	2498.9	58	35	2.5	10	12		9	5
497[d]	14	2382.1	62	29	2.3	11	18	10	5	5
521[e]	12		79	33	1	11	15			
109[f]	13		74	33	3	9	10	6		

[a] Rough polymer groupings as in ref 2. [b] 5-min irradiation at a flux of 1.4×10^{12} n/cm² sec. [c] 5-min irradiation at a flux of 3.0×10^{12} n/cm² sec. [d] 20-min irradiation at a flux of 1.4×10^{12} n/cm² sec. [e] Data taken from reference 3: 1–40 hr irradiation at 2×10^9 n/cm² sec. [f] Reference 3: 2–6 day irradiation at 3×10^9 n/cm² sec. [g] Sum of C_2H_3T and C_2HT. [h] Sum of all $C_6H_{13}T$'s.

Table II: Relative Yields in Oxygen Scavenged Gas Phase Propene[a]

Pressures, Torr			Tot. act. recovered ×	Relative yields of products (C_3H_6T = 100)				
C_3H_6	^3He	O_2	10^{-3} dpm	HT + CH_3T	C_2H_3T	C_2HT	C_3H_7T	$C_6H_{13}T$'s
99	9	10	1002.0	77	34	2.0[b]		
162	10	5	560.0	77	36	2.7[b]		
162	10	5	437.3	77	32	7.0	1.5	2.8
162	10	5	280.7	80	32			
296	8	8	378.7	75	35	2.5[b]		
296	8	8	1005.0	76	34	6.9[b]		
592	8	12	22.8	70	40[c]			
592	8	12	117.0	74	32			

[a] All samples irradiated 5 min at 1.4×10^{12} n/cm² sec. [b] Sum of C_2HT and C_3H_7T. [c] Sum of C_2H_3T, C_2HT, and C_3H_7T.

The values for ϵ_C and ϵ_H were obtained by solving the above equations simultaneously. As the number of carbon atoms per molecule increases, the values obtained for the stopping power by this method become consistently higher than experimental values while those of Root and Rowland are consistently lower. Our method (based on CH_4 and C_2H_2) is chosen for use with C_3H_6 because it gives closer agreement to the experimental values available for the lightest hydrocarbons[10] (Table III).

Table III

Molecule	$S_{(exptl)}$	$S_{(this\ work)}$	$S_{(ref\ 8)}$
CH_4	0.063	0.063	0.0600
C_2H_2	0.077	0.077	0.0604
C_2H_4	0.088	0.093	0.0726
C_6H_6	0.203	0.23	0.171
C_3H_6	None available	0.138	0.107

The plots in Figure 2 approximate straight lines within the limits of error (1 standard deviation) given for the slope and intercept by least-squares analysis. The scatter about the lines gives a reasonable estimate of the precision with which the values were obtained, about ±5% for the (HT + CH_3T)/C_3H_5T ratios. The precision with which the values of the other major products were obtained was about the same (±10%) as obtained for the liquid phase system.[2]

Wall Reactions. One of the most interesting things observed in this system was a slight but definite decrease in the (HT + CH_3T)/C_3H_5T ratio from the decrease in propene-*t* production due to stabilization of propyl-*t* radicals with respect to decomposition *via* the C–H bond breaking. This process has already been shown to be important in the production of labeled propene

(10) A comparison of values obtained for molecular stopping powers from interpolation of the experimental data given in reference 9; those obtained for use in determining recoil losses in this work and those obtained by Root and Rowland[8] are given in Table III.

in the liquid phase system.[2] The trend was observed (as can be seen in Figure 1) in both the unscavenged and oxygen scavenged systems. Therefore, it is not believed that the trend is a result of homogeneous gas phase reactions of thermalized atoms or radicals as a function of pressure.

The variation of the HT/C_3H_5T ratio, after correction for CH_3T, appears to be related to the fractions of recoiling tritons that reach the walls of the 1720 Pyrex irradiation vessels. This suggests wall reactions are an important source of HT in these systems. This is consistent with the observation of Miller and Rowland[11] in their work on the CD_4 system using 1720 Pyrex irradiation vessels. Analysis of the labeled hydrogen produced in the system showed that as much as 25% of the total labeled hydrogen was HT produced in a system where the only source of ^1H was the wall of the irradiation vessel. Obtaining H from the walls is consistent with the work of Thomas[12] in which he reported the production of H_2 by the action of Li on the surface of very clean and well flamed-out glass under very high vacuum.

The HT produced independently of the wall in the gas phase could be estimated by extrapolation to zero recoil loss as in Figure 2. In the liquid phase, however, where the irradiation capillary and solid LiF geometry were not so well controlled the recoil losses to the vessel wall could not be determined. The recoil losses in supposedly identical samples may, therefore, vary widely. This could add to the scatter in the HT/C_3H_5T ratios.

The yields obtained in our laboratories for HT (by reaction 1) relative to C_3H_5T were roughly 10–15% lower in the

$$T + C_3H_6 \longrightarrow HT + C_3H_5 \qquad (1)$$

unscavenged system than the yields obtained by Lee, *et al.*,[3] in their work on propene in the gas phase. This may have been due to the radiation dose effect on the production and steady-state concentration of radicals leading to differences in the yields of C_3H_5T by thermal routes. CH_3T and some C_2H_3T can be formed by the hot displacement reactions 2 and 2a

$$T + H_3C\text{–}CH_2\text{–}CH_3 \longrightarrow CH_3T + C_2H_3 \qquad (2)$$

$$T + H_3C\text{–}CH_2\text{–}CH_3 \longrightarrow CH_3\cdot + C_2H_3T \qquad (2a)$$

The production of CH_3T is favored over C_2H_3T in this mechanism by rotational inertia considerations.[13]

The two other hot reactions are direct substitution (3) and addition (4) reactions.

$$T + C_3H_6 \longrightarrow C_3H_5T + H\cdot \qquad (3)$$

$$T + C_3H_6 \longrightarrow C_3H_6T\cdot \qquad (4)$$

The importance of these two reactions will be discussed together, since C_3H_5T is the product of the decomposition of propyl-*t* radicals, as well as direct substitution.

As pointed out in the liquid phase paper,[2] energetic tritium can add to either end of the double bond in propene to produce both isopropyl-*t* and *n*-propyl-*t* radicals in nearly equal yields.

$$T + C_3H_6 \longrightarrow \begin{matrix} & H & H & \\ TC\text{–}&C\text{–}&CH_3 & \\ & H & & \end{matrix} \qquad (4a)$$

$$\longrightarrow \begin{matrix} & H & H & \\ H_3C\text{–}&C\text{–}&C\cdot & \\ & T & H & \end{matrix} \qquad (4b)$$

These radicals are quite highly excited and tend to decompose at a very fast rate, with *n*-propyl-*t* radicals showing a preference toward decomposition by C–C bond breaking to form C_2H_3T and $CH_3\cdot$ (5), and isopropyl-*t* a preference toward C–H bond split (6) to form the labeled parent.

$$n\text{-}C_3H_6T\cdot \longrightarrow C_2H_3T + CH_3\cdot \qquad (5)$$

$$i\text{-}C_3H_6T\cdot \longrightarrow C_3H_5T + H\cdot \qquad (6)$$

Isopropyl and *n*-propyl radicals exhibit the same decomposition tendencies in other systems.[14]

The importance of the decomposition of *n*-propyl-*t* radicals in this system is reflected in the high yield of C_2H_3T. The relative yields of 25–36 are more or less pressure independent over the entire pressure range studied. Drastic lowering of the yield of C_2H_3T was observed in the liquid phase,[2] consistent with the general observation in all gas–liquid recoil tritium studies of radical decomposition in olefin systems.[15,16]

The yield of C_3H_5T *via* radical decomposition could not be determined directly, since there was, of course, always C_3H_5T produced by the hot substitution reaction. Other mechanisms involving thermalized radicals can lead to propene-*t* as well. The bond energy correlations developed by Rowland and his coworkers[17–22] were used as described in ref 23 and as previously outlined[2,4] to calculate the fractions of propene-*t* produced

(11) G. Miller and F. S. Rowland, 157th National Meeting of the American Chemical Society, Minneapolis, Minn., April 1969.

(12) L. Thomas, Chemistry Section, Missouri Academy of Science, Kansas City, Mo., 1967.

(13) R. Wolfgang, *Progr. React. Kinet.*, **3**, 137 (1965).

(14) R. Cvetanovic, *Advan. Photochem.*, **1**, 155 (1963).

(15) E. K. C. Lee and F. S. Rowland, *J. Amer. Chem. Soc.*, **84**, 3085 (1962).

(16) E. K. C. Lee and F. S. Rowland, *J. Chem. Phys.*, **36**, 554 (1962).

(17) W. Breckenridge, J. Root, and F. S. Rowland, *ibid.*, **39**, 2374 (1963).

(18) J. Root, W. Breckenridge, and F. S. Rowland, *ibid.*, **43**, 3694 (1965).

(19) E. Tachikawa and F. S. Rowland, *J. Amer. Chem. Soc.*, **90**, 4767 (1968).

(20) E. Tachikawa, Y. N. Tang, and F. S. Rowland, *ibid.*, **90**, 3584 (1968).

(21) E. Tachikawa, Ph.D. Thesis, University of California, Irvine, Calif., 1967.

(22) T. Smail and F. S. Rowland, *J. Phys. Chem.*, **72**, 1845 (1968).

by hot substitution and radical routes. The calculation assumes that all thermalized T is removed from the system by scavenging by either O_2 or addition to the double bond in propene or both. Thus the assumption is that all of the HT formed in the limiting case (zero recoil loss) is *via* the hot abstraction reaction. Table IV gives the values for the HT/RT ratios after correction for CH_3T in the gas and liquid phase systems along with the calculated percentages of the total C_3H_5T by substitution and thermal radicals routes. The extent of C_3H_5T production *via* thermal radical routes was estimated from the reciprocals of the zero recoil loss HT/RT ratio values for the scavenged and unscavenged systems. The results indicate that in the recoil tritium–propene unscavenged system about 28% of the total propene-*t* was produced *via* the hot substitution reaction while about 56% was produced from excited propyl-*t* radical decomposition and 16% was produced *via* thermal radical routes. The standard deviations placed on the values in Table IV are based solely on the standard deviations obtained from the least-squares intercept values obtained in Figure 2 and do not represent the absolute limits of error[23,24] (Tables V and VI). The liquid phase numbers have been rounded off to the nearest absolute 10% in Table III since it has become obvious that wall reactions must have an effect on the production of HT in the liquid phase as well as the gas, thus affecting the accuracy of the calculations as they were made for the liquid phase system.

Formation of Heavier Products. The yields of the saturated C_6 products (measured as *n*-hexane-*t* and the sum of 2-methylpentane-*t* and 2,3-dimethylbutane-*t*) were of the same order of magnitude as obtained in the liquid phase system. However, the liquid phase trend of larger yields of *n*-hexane-*t* than the sum of the two labeled branched hexanes was reversed in the gas phase. The *n*-hexane-*t* yields were reduced (at 30°) by as much as 40–50% while the branched hexane-*t* yield was increased by as much as a factor of 2. The decrease in the yield of *n*-hexane-*t* in the gas phase is reflected in the higher C_2H_3T yield produced by in-

Table IV: Sources of Labeled Propene

	HT/C_3H_5T	C_3H_5T *via* subs, %	C_3H_5T *via* radicals, %
Gas	58 ± 2[a]	28 ± 1[b]	72 ± 2[b]
Gas (O_2 scav)	69 ± 2[a]	33 ± 1[b]	67 ± 1[b]
Liquid (30°)	74 ± 4	40	60
Liquid (−98°)	65 ± 6	30	70

[a] Corrected for CH_3T yield. [b] See ref 23.

Table V: Bond Energy Correlations for Hot Abstraction Relative to Primary C–H Bond in Propene = 1.0[21]

Bond type	Bond diss. energy, eV	Liquid	Gas
n-C_3H_7-H	4.23 ± 0.04	1.0	1.0
sec-C_3H_7-H	4.10 ± 0.02	1.7	1.7
Vinyl C-H	4.42 ± 0.09	0.55	0.53
Allyl C-H	3.42 ± 0.08 (thermal value)		
	4.09 ± 0.02 (value obtained in recoil work)	2.0	1.9

(23) Table V gives values of the cross section of the abstraction reaction per C–H bond taken from the correlation curves of Tachikawa[21] relative to the primary position in propane equal to 1.0. The shapes of the curves in the gas and liquid phases are somewhat different, leading to slightly different values. If we make the assumption (consistent with reference 24) that the yield of RT per C–H bond type is the same regardless of the bond dissociation energy, it would be expected that under identical conditions the relative amount of parent formed in the two different compounds would be in proportion to the number of C–H bonds available. Using propane as the saturated analog of propene, it is expected that on a molecular basis, under the same conditions, the relative amount of substitution in propene as compared to propane would be (C_3H_5T/C_3H_7T) subs = 6/8, since there are 6 C–H bonds on propene and 8 C–H bonds on propane. The overall relative cross sections of the formation of HT in propane and propene were calculated as shown in Table VI. The values in Table VI for propene and propane were divided giving the relative amounts of HT produced in propene and propane *via* direct substitution. Liquid phase: ($HT_{propane}/HT_{propene}$) = 9.4/7.6 = 1.24. Gas phase: ($HT_{propane}/HT_{propene}$) = 9.4/7.3 = 1.28. The results for the RT and HT yields for the two molecules were combined, and a value for HT/RT (subs only) was obtained for propane relative to propene: (propene-*t*/propane-*t*) × ($HT_{propane}/HT_{propene}$) = $(HT/RT)_{propane}/(HT/RT)_{propene}$ [(6/8)(1.28) = 0.96 (gas); (6/8)(1.24) = 0.93 (liquid)]. The yield ratio of HT to RT in propane has been reported as 1.97 in the gas phase. Therefore, the calculated yield for propene will equal 197/0.96 in the gas phase and 197/0.93 in the liquid phase.[17] No liquid phase data were available; therefore, the value above was applied to both the gas and liquid phase, since there has been only a small effect on these ratios observed for phase change in saturated compounds.[22] Inherent in the assumptions made is that all of the HT is formed by the hot abstraction reaction. In the liquid phase the results seen in Table IV are at best an estimate, since the thermal formation of HT at the wall has not been taken into account. However, the gas phase calculations are on a sound basis, since the intercept values of the lines in Figure 2 have been used to give the HT/RT ratio at zero recoil loss, the point at which wall reactions would presumably cease to be important. The values of RT from direct substitution and RT from radicals were calculated from the relationship given below using the gas phase unscavenged values corrected for CH_3T. For example, $(HT/RT_{tot})/(HT/RT_{subs})$ = 58 ± 2/205(±?) = 0.28 or 28 (±1%) which is equal to RT_{subs}/RT_{tot}, since the absolute yield of HT cancels out; for the unscavenged samples at zero recoil loss, RT_{subs}/RT_{tot} = 69 ± 2/205 ± (?) = 33 (±1). The error limits given above and in Table IV arise from the statistical analysis of our data and do not include any errors that might be incurred in the assumptions used in the calculations of recoil losses (which affects the zero recoil loss for the HT/C_3H_5T ratio in the gas phase) and in the calculations of the expected HT/C_3H_5T yield from direct substitution. For example, if recoil losses are calculated from the molecular stopping powers given by Root and Rowland[8] zero recoil values obtained in the gas phase are lowered by about 1%. More serious errors might be incurred in the choice of a reference molecule upon which to base the calculation the substitution yield of the relative HT/C_3H_5T. If methane is used rather than propane as a reference a value of 31% and 37% C_3H_5T *via* direct substitution is obtained for the unscavenged and scavenged system, respectively. If ethane is used values of 25% and 30% are obtained. Comparing the results obtained from using different reference molecules, and the other factors involved in the calculations of recoil losses, indicates that the estimates made for the fraction of C_3H_5T produced by direct substitution are good to about ±10 to 20% the values reported in Table IV.

(24) A. Odell, A. Rosenberg, R. Fink, and R. Wolfgang, *J. Chem. Phys.*, **40**, 3730 (1964).

Table VI: Bond Energy Correlations for Hot Abstraction Relative to Primary C–H Bond in Propene = 1.0[21]

Propane	Propene
Liquid	
6 (n-C_3H_7-H bonds) × 1.0/bond = 6.0	3 (vinyl C-H bonds) × 0.55/bond = 1.6
2 (sec-C_3H_7-H bonds) × 1.7/bond = 3.4	3 (allyl C-H bonds) × 2.0/bond = 6.0
Total = 9.4	Total = 7.6
Gas	
6 (n-C_3H_7-H bonds) × 1.0/bond = 6.0	3 (vinyl C-H bonds) × 0.53/bond = 1.6
3 (sec-C_3H_7-H bonds) × 1.7/bond = 1.6	3 (allyl C-H bonds) × 1.9 = 5.7
Total = 9.4	Total = 7.3

creased decomposition of n-propyl-t radicals in the gas phase. The polymer yields obtained in the gas phase were consistently lower compared to the liquid phase while the overall dimer yield was higher. The absence of any unsaturated C_6 (hexene-t's) in the gas phase was a most interesting result. The dimer yields obtained in this work were 2–3 times higher than obtained by Lee, *et al.*[3] All dimeric products as well as propane-t were almost completely removed from the system by the addition of O_2 as scavenger in moderate amounts. There appears to be a slight pressure effect on the yields of branched hexane with pressure (see Table I); however, the data are somewhat scattered and the authors are not convinced this trend is significant.

Since the dimeric and polymeric products can be formed by either radical–radical or radical–molecule routes it was important to know something about the radical environment (labeled and unlabeled) in the system. The absence of any hexene-t from the products argues against important radical-t–radical reactions in the system since the predominate radicals produced by radiation damage are allyl (~50%) in the propene system.[25]

The observation of a slightly higher yield of HT in the liquid phase is consistent with the results of Lee and Rowland[3] in the *trans*-hexene-2, *trans*-butene-2, and *cis*-butene-2 systems and with other results in our laboratory.

Acknowledgments. Fellowship support from Gulf Oil Corporation, Proctor and Gamble, and the Shell Companies Research Foundation is gratefully acknowledged.

(25) R. Holroyd and G. Klein, *J. Phys. Chem.*, **69**, 195 (1965).

Photocatalytic Reactions on Semiconductor Surfaces. I. Decomposition of Nitrous Oxide on Zinc Oxide

by Ken-ichi Tanaka[1] and George Blyholder*

Department of Chemistry, University of Arkansas, Fayetteville, Arkansas 72701 *(Received June 11, 1970)*

Publication costs borne completely by The Journal of Physical Chemistry

The steady-state photocatalytic decomposition of nitrous oxide was studied on zinc oxide. The reaction was carried out over the temperature range 371 to ~431°. At these temperatures, both thermal catalytic and photocatalytic decomposition occur. The thermal catalytic reaction obeys a first-order rate equation, *i.e.*, $r = kP_{N_2O}$; however, the photocatalytic reaction obeys a completely different rate equation $r = kP_{N_2O}/(1 + k_1P_{N_2O} + k_2P_{O_2}^{1/2})$. The kinetic equation for the photocatalytic decomposition of nitrous oxide is reasonably explained by considering the electron concentration at the surface during photocatalysis. Overall reaction rate under illumination is given by the sum of the photo- and thermal reactions. It was concluded that the photocatalytic decomposition occurs by way of N_2O^- intermediate but that thermal catalytic decomposition probably occurs without an electron transfer process.

Introduction

The catalytic decomposition of nitrous oxide has been used as a test reaction to investigate the catalytic action of oxide surfaces. Since Dell, Stone, and Tiley[2] pointed out a relation between the catalytic activities of oxides and their electronic properties, the importance of an electron transfer process in the catalytic decomposition of nitrous oxide has been emphasized.[3] It has been extensively reported that the adsorption of oxygen on semiconductor-type oxides changes the conductivity of the oxides, indicating thereby electron transfer from the oxide to adsorbed oxygen. Since the photoeffect on the conductivity of zinc oxide was shown by Myasnikov and Pshezhetskii,[4] the photoeffect on adsorption and/or desorption of oxygen has received much attention. Fujita and Kwan[5] and Barry and Stone[6] found both photoadsorption and photodesorption of oxygen for zinc oxide depended on the immediate pretreatment of the oxide. A comparison of their results indicates that the nature of the photoresponse also depends to a considerable extent on the history of the sample and its long-term pretreatment. Both groups found that the photoeffect decreased with increasing temperature and was not detectable at the temperatures above 200[5] or above 305.[6]

It has been inferred that the oxygen adsorbed on highly evacuated oxides is not necessarily the same as that which is adsorbed as an intermediate during catalytic decomposition of N_2O.[7] Accordingly, it is desirable to better define the behavior of intermediates and the roles of electrons and holes during catalysis at dark and at illumination. Morrison and Freund[8] have recently made progress in this direction for steady-state electrode reactions under illumination, but their technique is difficult to apply to other than to liquid phase reactions. However, the framework they are establishing to consider reactions at semiconductor surfaces is most useful.

The aim of this work is to study the kinetics of the steady-state photocatalytic decomposition of nitrous oxide on zinc oxide and to show the roles of electrons and holes in photocatalysis and thermal catalysis. For this purpose, the photocatalytic decomposition was carried out in the same temperature range in which the thermal catalytic reaction was observed.

Experimental Section

As shown in Figure 1, the apparatus used in this work is a closed circulating system with a total volume of 141 ml (V_1 = 112 ml and V_2 = 29 ml). The light source, a 500-W super pressure mercury lamp (OSRAM HBO-500), and a flowing water filter (55 mm length with 3 mm thick Pyrex windows) were set as shown in Figure 1. The reactor was constructed from an optically flat Pyrex glass window (63-mm diameter and

(1) On leave from Tokyo Institute of Technology.

(2) R. M. Dell, F. S. Stone, and P. F. Tiley, *Trans. Faraday Soc.*, **49**, 201 (1953).

(3) E. R. S. Winter, *Discuss. Faraday Soc.*, **28**, 183 (1959); *J. Catal.*, **15**, 144 (1969); K. Hauffe, R. Glang, and H. J. Engell, *Z. Phys. Chem. (Leipzig)*, **201**, 223 (1952); G. M. Schwab and J. Block, *Z. Phys. Chem. (Frankfurt am Main)*, **1**, 42 (1954); H. J. Engell and K. Hauffe, *Z. Elektrochem.*, **57**, 776 (1953).

(4) I. A. Myasnikov and S. Ya. Pshezhetskii, *Dokl. Akad. Nauk SSSR*, **99**, 125 (1954).

(5) Y. Fujita and T. Kwan, *Bull. Chem. Soc. Jap.*, **31**, 379 (1958).

(6) T. I. Barry and F. S. Stone, *Proc. Roy. Soc., Ser. A*, **255**, 124 (1960).

(7) K. Tanaka and A. Ozaki, *J. Catal.*, **8**, 307 (1967); K. Tanaka and A. Ozaki, *Bull. Chem. Soc. Jap.*, **40**, 420 (1967).

(8) S. R. Morrison and T. Freund, *J. Chem. Phys.*, **47**, 1543 (1967); T. Freund and S. R. Morrison, *Surface Sci.*, **9**, 119 (1968); S. R. Morrison, *ibid.*, **10**, 459 (1968); T. Freund and S. R. Morrison, *Electrochim. Acta*, **13**, 1343 (1968); S. R. Morrison, *Surface Sci.*, **15**, 363 (1969).

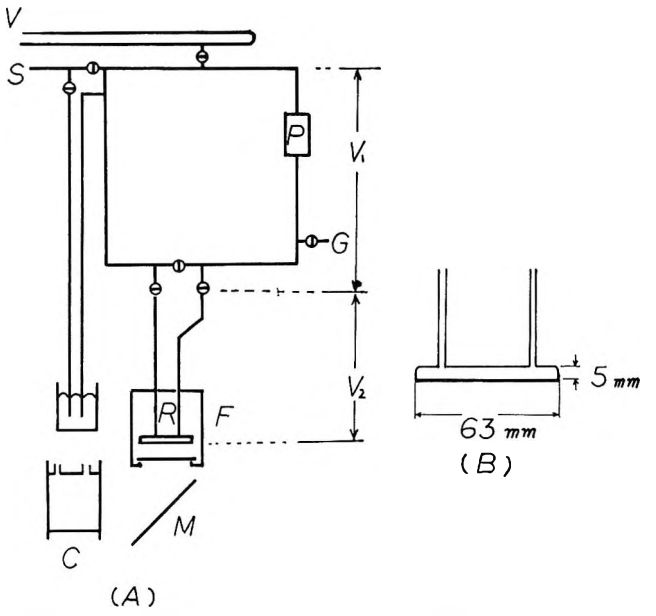

Figure 1. (A) Schematic drawing of the apparatus: C, flowing water filter; M, front surface mirror; F, furnace; R, reactor; G, to gas chromatograph; P, circulation pump; V, vacuum line; S, sample supply. (B) Details of reactor.

3-mm thickness). It was mounted in a furnace with a Pyrex window at the bottom. Illuminating light was applied to the reactor by reflection at a front surface mirror as shown in Figure 1. A blank test of the reaction under illumination without catalyst was carried out to be sure that no detectable reaction occurred at 390° either in the gas phase or on the cell walls.

The oxide used in the present experiment was a powdered sample of Kadox-25 obtained from New Jersey Zinc Co. A 2.38-g sample of zinc oxide was placed in the reaction cell and was activated by more than five treatments of overnight oxidation and several hours' evacuation at about 410° to remove carbonate impurities. The oxide was pretreated by contacting with nitrous oxide at the reaction conditions (in photocatalytic experiments the pretreatment was carried out under illumination) for more than 30 min, followed by about a 10-min evacuation. Such a pretreatment was carried out before each experimental run and gave a stable and reproducible surface in the present experiments on zinc oxide for both dark and photoreactions. Similar pretreatment schemes have been used on other oxides[7,9] to obtain reproducible surfaces for nitrous oxide decomposition. Before each experimental run the zinc oxide powder was checked for uniform spreading over the reactor window.

Nitrous oxide from a commercial cylinder was purified by freezing at liquid air temperature and subliming at Dry Ice–methanol temperature. Oxygen from a commercial cylinder was purified by passage through a liquid air trap. The effect of oxygen pressure on the reaction rate was studied by mixing a certain amount of oxygen with the nitrous oxide flowing

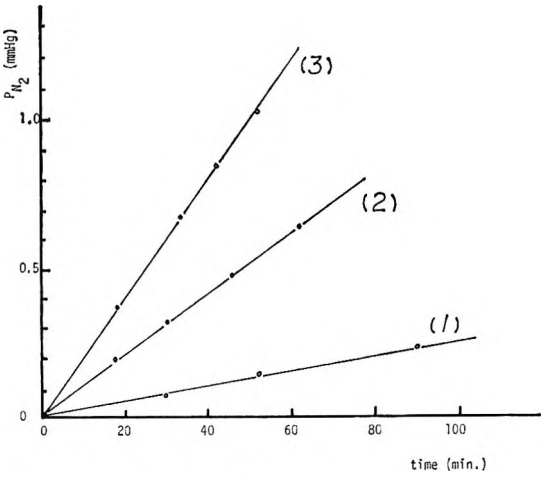

Figure 2. Time course of nitrogen evolution in the thermal catalytic reaction. The temperatures and the initial pressures of nitrous oxide are (1) 371°, 45.7 mm; (2) 405°, 46.9 mm; and (3) 426°, 45.7 mm.

through the reactor. The product mixtures, oxygen and nitrogen, were analyzed in an on-line gas chromatograph using a molecular sieve 5A column. The reaction rates were obtained from plots of the nitrogen evolution time course determined by gas chromatographic analysis.

Results

1. Thermal Catalytic Decomposition of Nitrous Oxide. The thermal catalytic decomposition of nitrous oxide was studied over the temperature range 371–426°. Figure 2 shows typical time courses of nitrogen evolution obtained at 371, 405, and 426°. The oxygen evolved is not shown in this figure; however, it is stoichiometric within experimental error. Similar time courses of the reaction were obtained with various initial pressures of nitrous oxide. Figure 3A shows the relation between the initial pressures and the reaction rates obtained from the slopes of the time courses at 424°. The effect of oxygen on the reaction rate was studied at the initial oxygen pressures of 0, 1.83, and 2.93 Torr with an initial pressure of 6.3 Torr of nitrous oxide at 424°. The result shown in Figure 3B indicates that the addition of oxygen does not change the reaction rate.

These results indicate that the kinetics of the thermal catalytic decomposition of nitrous oxide on zinc oxide are first order in nitrous oxide pressure and zero order in oxygen pressure, that is, $r = kP_{N_2O}$, over the range studied. The logarithms of the rate constants at various temperatures are plotted against the reciprocal of the temperatures in Figure 4. The apparent activation energy of the thermal catalytic decomposition of nitrous oxide is calculated as 35 kcal/mol.

2. Photocatalytic Decomposition of Nitrous Oxide.

(9) L. Rheaume and G. Parravano, *J. Phys. Chem.*, **63**, 264 (1958).

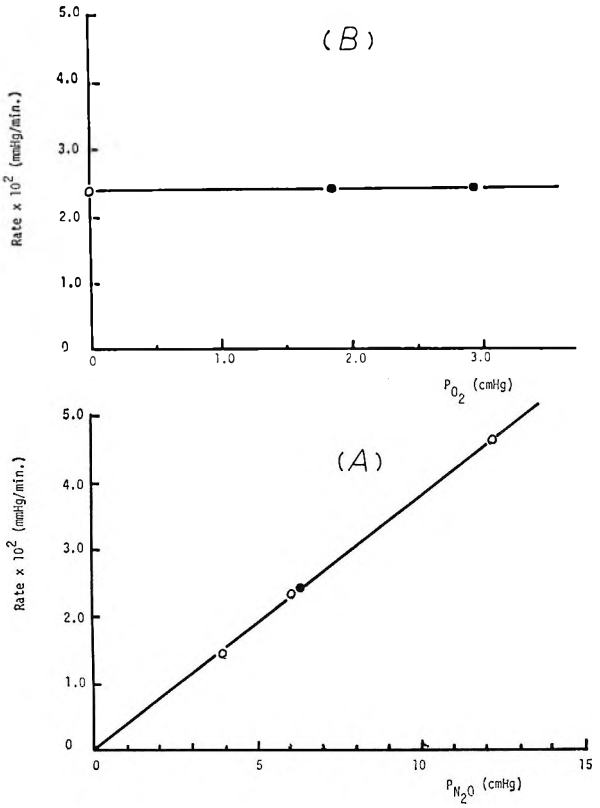

Figure 3. (A) Nitrous oxide pressure dependence of thermal catalytic reaction rate at 424°. Solid circle shows the value with oxygen added. (B) Effect of oxygen pressure on thermal catalytic reaction rate. P_{N_2O} = 6.3 cm and 424°.

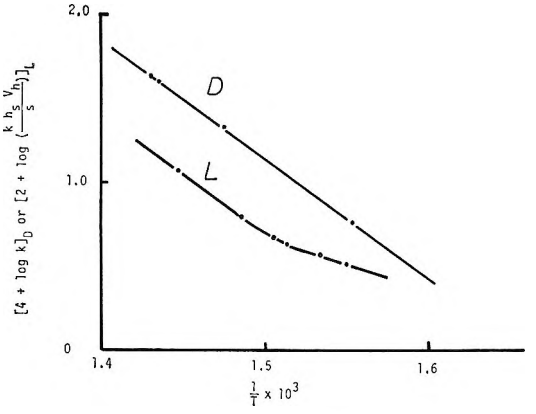

Figure 4. Arrhenius plot of rate constants: L, photocatalytic reaction; D, thermal catalytic reaction.

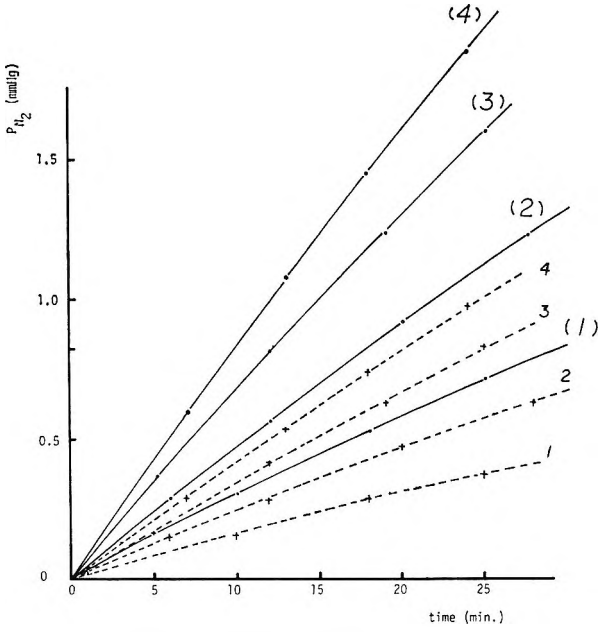

Figure 5. Time course of the photocatalytic reaction at 400°. The initial pressures of nitrous oxide are: (1) 19.0 mm; (2) 46.8 mm; (3) 107.8 mm; and (4) 158.6 mm. Solid lines indicate nitrogen pressures and dotted lines indicate oxygen pressures.

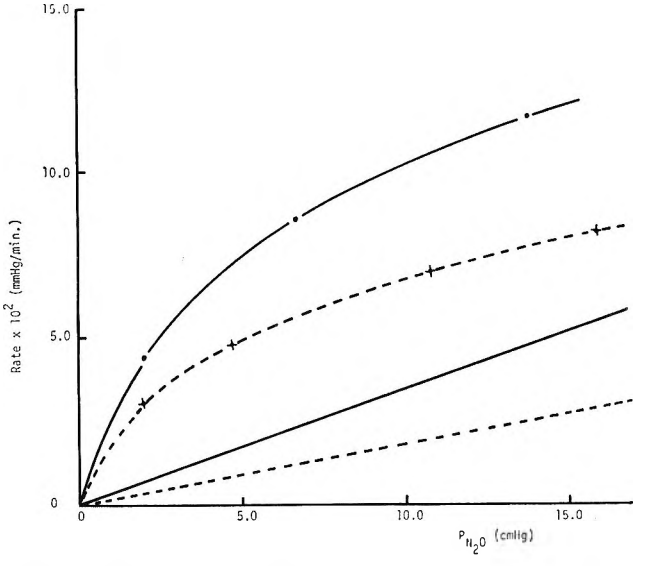

Figure 6. Nitrous oxide pressure dependence of the reaction rate under illumination: solid line, 418; dotted line, 400°. Straight lines show the expected thermal catalytic reaction rates.

The photocatalytic decomposition of nitrous oxide was carried out over the temperature range of 371–431°. Figure 5 shows typical results of the photocatalytic decomposition of nitrous oxide at 400° with various initial pressures of nitrous oxide. It is characteristic of the photocatalytic reaction that the slope of the time course gradually decreases as the reaction proceeds. Figure 6 shows a typical pressure dependence of the reaction rate obtained from the initial slope of the time course curve under illumination at 400 and 418°. The straight lines in the figure show the expected thermal catalytic reaction rates at the given temperatures. It is found that the pressure dependence of the reaction rate is markedly different from that of the thermal catalytic reaction. This figure shows that the reaction rate under illumination does not increase in direct proportion to the nitrous oxide pressure but that the slope decreases with increasing nitrous oxide pressure, and

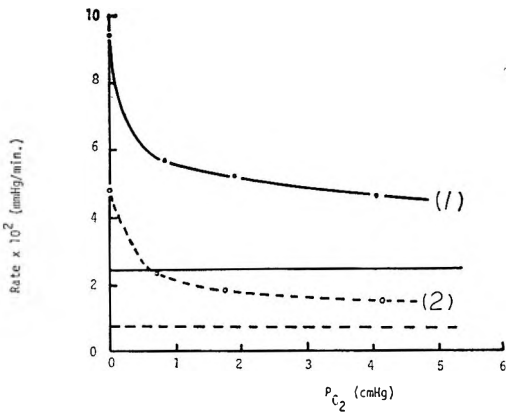

Figure 7. Effect of oxygen pressure on the reaction rate under illumination. P_{N_2O} = 4.6 cm: (1) 431°; (2) 399°. Straight lines show the expected thermal catalytic rate.

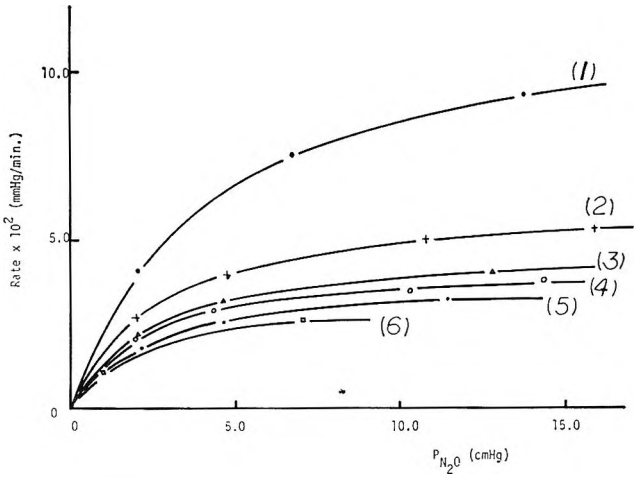

Figure 8. Pressure dependence of the photocatalytic reaction rate at various temperatures: (1) 418°; (2) 400°; (3) 391°; (4) 387°; (5) 378°; (6) 371°.

that at higher pressures the slope appears to approach that of the thermal catalytic reaction. This behavior of the reaction under illumination was also found at 371, 378, 387, 391, 400, and 418°.

The effect of the added oxygen on the reaction rate under illumination was studied at 371, 399, and 431°. While the oxygen pressure has no effect on the thermal catalytic decomposition of nitrous oxide, it was found that the reaction under illumination is markedly retarded by oxygen. Figure 7 shows the results of the oxygen effect on the reaction rate under illumination at 399 and 431°. The result at 371° is similar. The straight lines in the figure show the expected thermal catalytic reaction rates upon which oxygen has no effect. This figure shows that the reaction rate under illumination is markedly reduced in the presence of a small amount of oxygen.

The results shown in Figures 6 and 7 reveal that the reaction under illumination consists of a photocatalytic reaction plus a thermal catalytic reaction. The photocatalytic reaction may be obtained by subtracting the thermal catalytic reaction rate from the overall reaction rate obtained under illumination. Figure 8 shows this photocatalytic reaction rate at various temperatures as a function of nitrous oxide pressure. It is seen from this figure that the photocatalytic reaction approaches zero-order kinetics at higher nitrous oxide pressures. By the same procedure, the oxygen effect on the photocatalytic reaction rate may be obtained for the reactions at 371, 399, and 431°.

Discussion

The most remarkable result in this work is that the thermal catalytic and photocatalytic reactions obey completely different kinetics, and these two reactions appear to be simultaneously occurring on the zinc oxide under illumination.

The zinc oxide used in the present experiment is well oxidized in the reaction cell and is sufficiently acclimatized to the reaction condition by the pretreatment scheme to give reproducible results. Cunningham, *et al.*,[10] recently reported that zinc oxide, evacuated at 400° for 16 hr, decomposed nitrous oxide very rapidly at room temperature, but in this case 95% or more of the product was nitrogen and the reaction did not proceed catalytically. They proposed that the very low concentration of holes in zinc oxide greatly reduced the rate of neutralization of product oxygen ions at room temperature so that the desorption of this oxygen would be the slow step in the catalytic decomposition of nitrous oxide at higher temperatures. It is, however, highly doubtful that the oxygen strongly held on the evacuated zinc oxide is the same type of oxygen as that adsorbed as an intermediate in the catalytic reaction at higher temperatures because the chemisorption of oxygen on highly evacuated zinc oxide is particularly strong and the form of the adsorbed oxygen is expected to change as the temperature and coverage changes.

The heterogeneous character of the surface is readily shown by a comparison of the work done by various investigators. For example, the isotopic equilibration between $^{18}O_2$ and $^{16}O_2$ occurs rapidly on zinc oxide even at low temperatures.[6,11] This fact indicates that dissociative adsorption and desorption of oxygen occurs rapidly at temperatures at which strongly held oxygen such as produced by the decomposition of N_2O on a highly evacuated surface at room temperature does not desorb. Furthermore, the rate of adsorption and desorption of oxygen at pressures around 10^{-3} Torr obey the Elovich equation,[6] but the rate of evolution of oxygen during catalysis increases with nitrous oxide pressure according to first-order kinetics (Figure 3). The added oxygen has no effect on the reaction rate and the time courses of the thermal catalytic reaction do

(10) J. Cunningham, J. J. Kelly, and A. L. Penny, *J. Phys. Chem.*, **74**, 1992 (1970).

(11) E. R. S. Winter, *J. Chem. Soc.*, 1522 (1954).

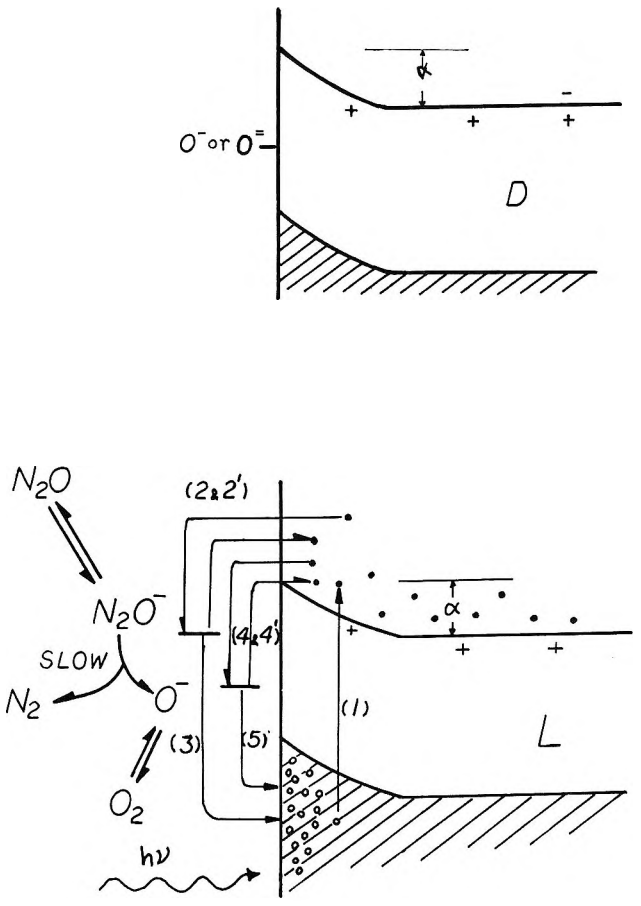

Figure 9. Model for setting up the rate equations: D, dark state; L, illuminated state.

not bend (Figure 2). These facts imply that the oxygen adsorbed on the surface as an intermediate of the thermal catalytic decomposition of N_2O is highly labile and weakly held oxygen like an intermediate of the equilibration reaction. Accordingly, the low catalytic activity at lower temperatures may not be due to a low concentration of holes, *i.e.*, slow oxygen desorption, but rather to a slow decomposition of adsorbed N_2O. The detail reaction mechanism will be discussed later.

While the electronic structure of the actual surface is presumably complicated by nonuniformities, we propose to describe that part of the surface on which the reaction proceeds catalytically in terms of the band model shown in Figure 9. Electrons in the conduction band are probably very few at our dark experimental conditions for the following reasons. (1) Most of the donor defects have been destroyed by thermal oxidation.[12] (2) The majority of the electrons in the conduction band are trapped by adsorbed oxygen whose ions are presumably different from an intermediate of the decomposition reaction as discussed above. When the oxide is exposed to light of energy corresponding to the energy gap between the conduction band and the valence band, *i.e.*, 385 mμ or shorter wavelengths, electrons in the valence band are excited into the conduction band as shown by process 1 in Figure 9. Electrons excited into the conduction band are repelled from the surface by the potential barrier (α) at the surface. Thus, the number of electrons per unit volume at the surface, e_s, is given by

$$e_s = \frac{e_T}{V} e^{-q\alpha/kT} \tag{1}$$

where e_T is the total number of conduction band electrons in the solid particle of volume V, q is the electronic charge, and α is the potential barrier at the surface. Since most of the holes produced by illumination are attracted to the surface by the surface potential,[8] the number of holes per unit volume at the surface, h_s, is given by

$$h_s \approx \frac{h_T}{V_h} \tag{2}$$

where h_T is the total number of holes and V_h is that volume next to the surface in which the holes are distributed.

When the only surface acceptor is nitrous oxide, which is known to be an efficient electron scavenger, electron transfer between zinc oxide and N_2O and/or N_2O^- will be established.

Assuming that direct electron transfer from the valence band to nitrous oxide molecules rarely occurs at the experimental conditions, the electron transfer processes established on the surface are described as follows (these processes correspond to 2 and 3 in Figure 9). The electron transfer rate of each process is

$$N_2O(g) + e_s \underset{k_2'}{\overset{k_2}{\rightleftharpoons}} N_2O^-(a)$$

$$N_2O^-(a) + h_s \xrightarrow{k_3} N_2O(g)$$

expressed as

$$\vec{V}_2 = k_2 e_s P_{N_2O} - k_2'(N_2O^-)_s \tag{3}$$

$$\vec{V}_3 = k_3 h_s (N_2O^-)_s \tag{4}$$

If N_2O^- is the only charged molecule being considered in a total charge balance, then the following charge balance is required

$$h_T = e_T + (N_2O^-)_T \tag{5}$$

where $(N_2O^-)_T$ designates the total number of N_2O^- ions on the surface. Combining eq 1, 2, and 5 with the notation that the number of N_2O^- ions per unit surface area, $(N_2O^-)_s$, is equal to $(N_2O^-)_T/S$, where S is the surface area, gives the value of e_s as

$$e_s = \frac{[h_s V_h - (N_2O^-)_s S] e^{-q\alpha/kT}}{V} \tag{6}$$

At a steady state under illumination, the rate of elec-

(12) K. M. Sancier, *J. Catal.*, 5, 314 (1966).

tron capture equals the rate of hole capture; *i.e.*, $\vec{V}_2 = \vec{V}_3$.

Accordingly, at the initial stage of the reaction, that is, the only surface acceptor is nitrous oxide, the following relation is established

$$k_2 P_{N_2O} e_s - k_2'(N_2O^-)_s = k_3 h_s (N_2O^-)_s \quad (7)$$

Substituting e_s from eq 6 into eq 7 and solving for $(N_2O^-)_s$ gives

$$(N_2O^-)_s = \frac{k_2 V_h h_s P_{N_2O}}{(k_2' + k_3 h_s) V e^{q\alpha/kT} + k_2 S P_{N_2O}} \quad (8)$$

Assuming that the slow step of the photocatalytic reaction is the decomposition of nitrous oxide ion, the initial rate of the reaction, proceeding on the surface on which nitrous oxide is the only molecule capturing electron, is described by

$$r = k(N_2O^-)_s = \frac{k k_2 V_h h_s P_{N_2O}}{(k_2' + k_3 h_s) V e^{q\alpha/kT} + k_2 S P_{N_2O}} \quad (9)$$

This equation implies that the reciprocal of the reaction rate *vs.* $1/P_{N_2O}$ will be a straight line if the variation of α, which in general is a function of P_{N_2O}, is negligible. Figure 10 shows the expected linear relation at various temperatures. It may be noted that the term $\exp(q\alpha/kT)$ plays a role in the kinetics in the low nitrous oxide pressure range.

When two kinds of surface acceptors are on the surface, oxygen and nitrous oxide, we derive similar equations for the electron transfer processes corresponding to (4) and (5) shown in Figure 9 as follows

$$\vec{V}_4 = k_4 P_{O_2}^{1/2} e_s - k_4'(O^-)_s \quad (10)$$

$$\vec{V}_5 = k_5 h_s (O^-)_s \quad (11)$$

In this equation, O^- is assumed to be an important adsorbed state of oxygen during the photocatalytic reaction at around 400°.

At a steady state under illumination, $\vec{V}_2 = \vec{V}_3$, $\vec{V}_4 = \vec{V}_5$, and $h_T = e_T + (N_2O^-)_T + O^-_T$. Then, the electron concentration at the surface e_s is given by

$$e_s = \frac{h_s V_h}{V e^{q\alpha/kT} + \frac{k_2 S}{k_2' + k_3 h_t} P_{N_2O} + \frac{k_4 S}{k_4' + k_5 h_s} P_{O_2}^{1/2}} \quad (12)$$

and the concentration of N_2O^- is given by

$$(N_2O^-)_s = \frac{k_2 e_s}{k_2' + k_3 h_s} P_{N_2O} \quad (13)$$

Accordingly, the reaction rate, r, is given by

$$r = k(N_2O^-)_s = \frac{\frac{k k_2 h_s V_h}{k_2' + k_3 h_s} P_{N_2O}}{V e^{q\alpha/kT} + \frac{k_2 S P_{N_2O}}{k_2' + k_3 h_s} + \frac{k_4 S (P_{O_2})^{1/2}}{k_4' + k_5 h_s}} \quad (14)$$

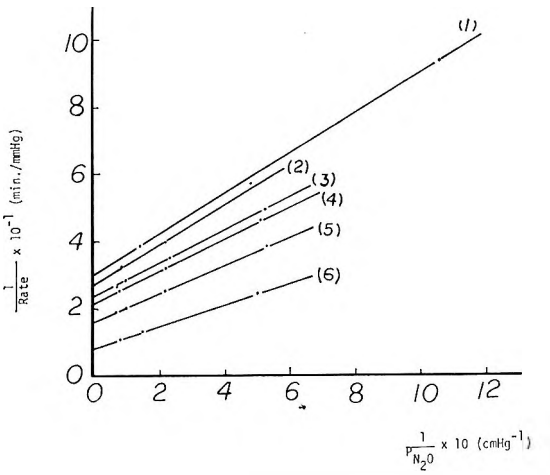

Figure 10. Plot of 1/rate *vs.* $1/P_{N_2O}$ at various temperatures: (1) 371°; (2) 378°; (3) 387°; (4) 391°; (5) 400°; (6) 418°.

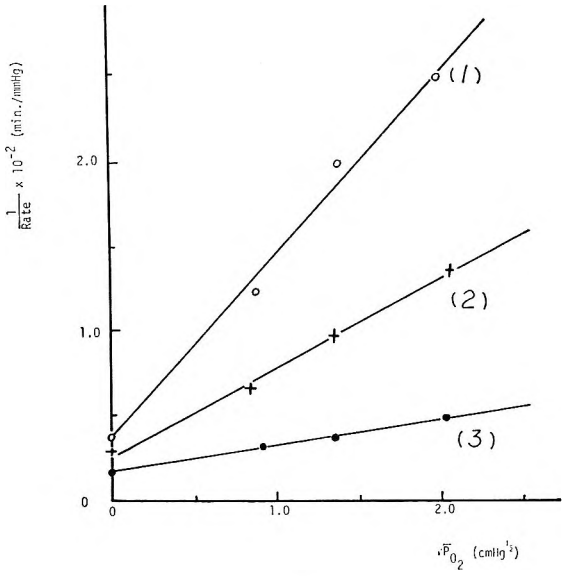

Figure 11. Plot of 1/rate *vs.* $\sqrt{P_{O_2}}$ at various temperatures; P_{N_2O} = 4.6 cm; (1) 371°; (2) 399°; (3) 431°.

This equation is just like eq 8 with the oxygen term added. This equation predicts that at a constant value of P_{N_2O} the reciprocal of the reaction rate will change linearly with the square root of oxygen pressure. Figure 11 shows the results obtained at various temperatures at a constant nitrous oxide pressure, P_{N_2O} = 4.6 cm, are indeed in accord with this expectation. Thus both the effect of added oxygen and the bending of the time course of the photocatalytic reaction (Figure 5) are reasonably explained by the competitive electron scavenge effect of oxygen.

In deriving expressions to fit the somewhat complex kinetics observed, it was convenient to assume that the decomposition of N_2O^- was the rate-controlling step. Further support for this assumption is found in evidence which suggests that desorption of oxygen should not be the rate-controlling step. Several workers have dem-

onstrated that the photoeffect on the rate of oxygen desorption from ZnO decreased with increasing temperature and was not detectable above 200°[5] or above 305°.[6] However, we find a large photoeffect on the decomposition of N_2O and hence conclude oxygen desorption is not rate determining.

The results obtained in this paper imply that the thermal catalytic and photocatalytic reaction occur simultaneously over the illuminated zinc oxide. If we consider the difficulty of homogeneous illumination of powder samples, we cannot say for certain whether the thermal catalytic reaction occurs on an illuminated part of the surface or not. Since Dell, *et al.*,[2] pointed out the importance of electronic properties of oxides in the catalytic activity of nitrous oxide decomposition, the reaction mechanism of the thermal reaction has been explained by an electron transfer mechanism. However, the completely different kinetics of the thermal catalytic reaction and the photocatalytic reaction strongly suggest different mechanisms in these reactions. Just being a photochemical reaction and having an effect by the electron scavenger oxygen fairly definitely leads to an electron transfer mechanism for the photodecomposition. However, it seems clear that the thermal catalytic reaction does not pass through an intermediate such as N_2O^- which is common to the photocatalytic process. Accordingly, it is suggested that the thermal reaction proceeds *via* an atomic and molecular mechanism as

$$N_2O(g) \rightleftharpoons N_2O(s)$$
$$N_2O(s) \longrightarrow N_2(g) + O(s) \qquad \text{(slow)}$$
$$O(s) \rightleftharpoons {}^1/_2O_2(g)$$

If the desorption of oxygen were rate controlling, the active surface sites would be covered with oxygen and the reaction would be less than first order in N_2O pressure. Since the reaction is observed to be first order in N_2O pressure, the desorption step is not rate controlling.

The activation energy of the photocatalytic decomposition of nitrous oxide, which was obtained from the temperature variation of kh_sV_h/S, was 33 kcal/mol at temperatures higher than 390° and 13 kcal/mol at temperatures lower than that. Winter[11] found in his isotopic exchange reaction that the exchange between adsorbed oxygen and lattice oxide ions is faster than the surface migration of adsorbed oxygen at temperatures higher than 415°. It seems reasonable that these two critical temperatures are related to each other. Below 400° it seems likely that the nature of the surface remains unchanged as the temperature varies so the activation energy of 13 kcal/mol reflects the temperature coefficient of k in the term kh_sV_h/S. Above 400° Winter's work indicates the lattice becomes mobile so that the active sites at the surface can change with temperature. This will result in the term h_sV_h/S exhibiting a temperature coefficient above 400° as observed. It may be noted, however, that the basic mechanism, as reflected in the dependence of the reaction on N_2O and O_2 pressures, is not changed.

In our interpretation the activation energy of 35 kcal/mol for the dark reaction represents the barrier to dissociation of a neutral N_2O molecule minus the heat of adsorption, while the 13 kcal/mol activation energy for the photocatalytic reaction represents the barrier to dissociation of N_2O^-. The difference in activation energies is then the result of putting an electron into an antibonding molecular orbital of N_2O.

Acknowledgment. This investigation was supported in part by PHS Research Grant No. 00818-01 from the National Air Pollution Control Administration.

Structural, Magnetic, and Optical Properties of Nickel Oxide Supported on η- and γ-Aluminas

by M. Lo Jacono, M. Schiavello, and A. Cimino*

Istituto di Chimica Generale ed Inorganica, Università di Roma, and Centro di Studio sulla Struttura ed Attività Catalitica di Sistemi di Ossidi, del Consiglio Nazionale delle Richerche, Rome, Italy
(Received November 4, 1970)

Publication costs assisted by SNAM-Progetti, S. Donato (Italy)

X-Ray analysis, reflectance spectroscopy, and magnetic measurements have been employed to investigate the interaction which takes place when nickel oxide is supported on η- and γ-aluminas. It was found that a "surface spinel," $NiAl_2O_4$, is formed. The degree of inversion, *i.e.*, the relative occupancy of tetrahedral and octahedral sites, of the surface spinel is affected by the atmosphere of firing, by the nickel content, and by the nature of the supports. Taking into account the different structures of η- and γ-Al_2O_3, it was possible to explain the nickel ion distribution between octahedral and tetrahedral sites in the surface spinel. The effect of the firing treatment has been related to the surface unsaturation, which is favored by a dry ambient atmosphere. The results presented here are used to account for earlier observations by several authors.

1. Introduction

The study reported in this paper aims to elucidate the structural properties of catalysts consisting of nickel oxide supported on η- or γ-aluminas. A subsequent paper will report the catalytic activity of the same solids for N_2O decomposition, with the aim of correlating structural and catalytic properties.

The system Ni^{2+}/Al_2O_3 has received much attention from many workers since the pioneering work by Hill and Selwood[1] in 1949. While it is clear that the role of the support is not merely that of dispersing the nickel oxide, the nature and extent of their interaction and the different properties of various supports still need clarification. Some divergences, in fact, can still be found in the literature regarding the interpretation of the results. By the use of aluminas of different structure (η and γ) and of preparations in different atmospheres, some new light will be thrown on the nature of the interaction between nickel ions and the support.

2. Experimental Section

2.1. Catalysts Preparation. Two η-Al_2O_3 and two γ-Al_2O_3 specimens have been used as starting materials. One γ-Al_2O_3 and one η-Al_2O_3 were prepared according to the method described by MacIver, Tobin, and Barth.[2] The other γ-Al_2O_3 and η-Al_2O_3, used for comparison, were samples obtained by firing boehmite (Peter Spence and Sons, specimen R.D. 10537 A) and an alumina hydroxide made of 95% bayerite (Peter Spence and Sons, specimen R.D. 6808), both materials kindly supplied by Peter Spence and Sons and made available to us by Dr. F. S. Stone. The catalysts prepared using these aluminas will be distinguished by the symbol P.S. The η-Al_2O_3 P.S. sample contained small quantities of γ-Al_2O_3. The two P.S. samples have been analyzed spectrophotometrically and were found to have an iron impurity not larger than 20 ppm.

The nickel-containing catalysts were prepared by impregnation of the aluminas with a titrated solution of $Ni(NO_3)_2$ (reagent grade, Carlo Erba). The soaked mass was dried at 110° and then ground. Portions of the samples were fired at 350° for 1 hr and then at 600° for 24 hr, in one of the following atmospheres: (a) air (with natural humidity content); (b) dry air, (c) dry nitrogen; (d) damp nitrogen, *i.e.*, nitrogen saturated with H_2O at 25°. (Some of these specimens have been prepared in order to test their catalytic activity (see subsequent paper), and will not be further discussed in this paper.) One sample was fired in air at 450° for 24 hr. The color of the Ni^{2+}/γ-Al_2O_3 catalysts fired in air was green, while that of the nickel Ni^{2+}/η-Al_2O_3 catalysts was pale blue. The η catalysts prepared in dry nitrogen and in dry air exhibited a more intense blue color. The corresponding γ specimens, green when prepared in damp air, changed their color and turned to blue when treated in dry nitrogen. The 450° fired sample had a greyish green color.

Table I lists the catalysts prepared with the features of their preparation and the nickel content. The analyses of the nickel content were made gravimetrically (dimethylglyoxime). The dissolution of the specimens was performed as follows: (a) concentrated H_2SO_4 was added (5–10 cc for 200–300 mg of catalyst)

(1) F. N. Hill and P. W. Selwood, *J. Amer. Chem. Soc.*, 71, 2522 (1949).

(2) D. S. MacIver, H. H. Tobin, and R. T. Barth, *J. Catal.*, 2, 485 (1963).

as well as a few drops of water; (b) the mixture was left to digest for 1 hr on a water bath and then was boiled; (c) after cooling, more water was added and the solution was boiled until it became clear. The γ-alumina–nickel oxide and the η-alumina–nickel oxide catalysts are designated as AγNx and AηNx, respectively, where the x indicates the nominal nickel content, expressed as the number of nickel atoms for 100 aluminum atoms. When required, the atmosphere in which the catalyst was fired is indicated in parenthesis after the letter x. Thus for instance, the specimen AηN6 P.S.–dry nitrogen is a catalyst containing six atoms of nickel for 100 atoms of aluminum and it was fired in an atmosphere of dry nitrogen. The η-Al_2O_3 used was prepared from the Spence bayerite.

Table I: Specimens and Their Properties

Sample	Atmosphere of firing	Ni concentration (% by weight)[b]	C[d]	θ,[d] °K	Ni_{tet}, %
AγN1	Air[c]	1.54	1.20	+4	10
AγN3 P.S.	Air	3.32	1.12	+5	2
AγN4	Air	5.0	1.10	−5	0
AγN6 P.S.	Air	6.72	1.11	0	1
AγN6	Air	6.27	1.12	−10	2
AγN1	Dry nitrogen	1.54	1.21	−3	11
AγN2 P.S.	Dry nitrogen	2.40	1.21	+10	11
AγN4	Dry nitrogen	5.0	1.31	−3	21
AγN6 P.S.	Dry nitrogen	6.81	1.20	+5	10
AηN1	Air[c]	1.67	1.23	0	13
AηN2 P.S.	Air	1.95	1.12	−10	2
AηN3 P.S.	Air	3.40	1.17	+10	7
AηN4	Air	4.54	1.25	+2	15
AηN6	Air	6.56	1.23	−12	13
AηN6	Damp nitrogen	6.58	1.23	−10	13
AηN2 P.S.	Dry nitrogen	2.48	1.31	0	21
AηN4	Dry nitrogen	4.54	1.31	−5	21
AηN6 P.S.	Dry nitrogen	7.36	1.32	−8	22
AηN6	Dry air	6.60	1.33	−8	23
AηN4[a]	Air[c]	4.54	1.21	−4	11
AηN2 P.S.	Air → dry nitrogen	1.95	1.13	−11	3
AηN6 P.S.	Dry nitrogen → air	7.36	1.31	+5	21

[a] Sample fired at 450°. [b] Analytical, see text. [c] With natural humidity content. [d] C and θ are the Curie constant and the Weiss temperature, from the Curie–Weiss law, $\chi = C/(T - \theta)$.

2.2. Reflectance Measurements. Diffuse reflectance spectra were obtained with a Beckman DK 1 spectrophotometer, using η- or γ-Al_2O_3 as reference specimen. The measurements were made in the wavelength range 2600 to 230 mμ at room temperature.

2.3. Magnetic and X-Ray Measurements. Magnetic susceptibility determinations were carried out in dry N_2 in the range of temperature 150–295°K using the Gouy method. It was difficult to make measurements below 150°K because of the large N_2 adsorption on the catalysts due to their large surface area. Some measurements, however, were carried out down to 80°K using a closed tube. The values of the Curie constant obtained in the more extended temperature interval agreed very well with those obtained in the range limited to 150°K. X-Ray analysis was carried out using a Debye–Scherrer camera with Cu Kα (Ni filtered) radiation at room temperature, (exposure time 8 hr). Further details of the apparatus used for magnetic and X-ray analysis have been described elsewhere.[3]

3. Experimental Results

3.1. Reflectance Spectra. Figures 1a and b report the reflectance spectra of certain Ni^{2+}/η-Al_2O_3 and Ni^{2+}/γ-Al_2O_3 specimens, fired in air or in dry nitrogen. For a comparison, a reflectance spectrum of $Mg_{0.9}Ni_{0.1}Al_2O_4$[4] is also reported. The abscissa values are limited to 700–300 mμ since in this interval of wavelengths the differences between tetrahedral and octahedral bands are observed more easily; the ordinates are optical densities. Table II lists the bands (expressed in cm^{-1}) for our nickel-containing aluminas, for $Mg_{0.9}Ni_{0.1}Al_2O_4$,[4] and for $Ni_{0.01}Zn_{0.99}O$.[4] From an inspection of Figure 1a and b and Table II the following points can be assessed

Table II: Reflectance Spectra of Ni^{2+} in Different Environments. Energies of Optical Transitions (in cm^{-1})

NiO/Al_2O_3[a]	$Mg_{0.9}Ni_{0.1}Al_2O_4$[b]	$Ni_{0.01}Zn_{0.99}$[b]	Transitions
4,400	4,400	4,500	$^3T_1 \rightarrow {}^3T_2$[c]
4,750	(5,000)	4,800	
8,400	8,900	8,400	$^3T_1 \rightarrow {}^3A_2$[c]
9,700	9,800		$^3A_{2g} \rightarrow {}^3T_{2g}$[d]
	12,900	12,600	$^3T_1 \rightarrow {}^1T_2$[c]
13,350	14,000	13,450	$^3T_1 \rightarrow {}^1E$[c] and/or $^3A_{2g} \rightarrow {}^1E_g$[d]
16,000	15,800	15,400	$^3T_1 \rightarrow {}^3T_1$[c] and/or
17,000	16,800	16,200	$^3A_{2g} \rightarrow {}^3T_{1g}$[d]
23,250	22,800		$^3A_{2g} \rightarrow {}^1T_{2g}$[d]
27,000	26,900		$^3A_{2g} \rightarrow {}^3T_{1g}$[d]

[a] This work. [b] Reference 4. [c] Ni^{2+} ion in tetrahedral symmetry. [d] Ni^{2+} ion in octahedral symmetry.

(i) The spectrum of the nickel-containing aluminas has qualitatively the same pattern as the spinel spectrum. This result points to the formation of a spinel-

(3) A. Cimino, M. Lo Jacono, P. Porta, and M. Valigi, *Z. Phys. Chem.*, **51**, 301 (1966).

(4) D. Schmitz Du Mont, A. Lule, and D. Reinen, *Ber. Bunsenges. Phys. Chem.*, **69**, 76 (1965).

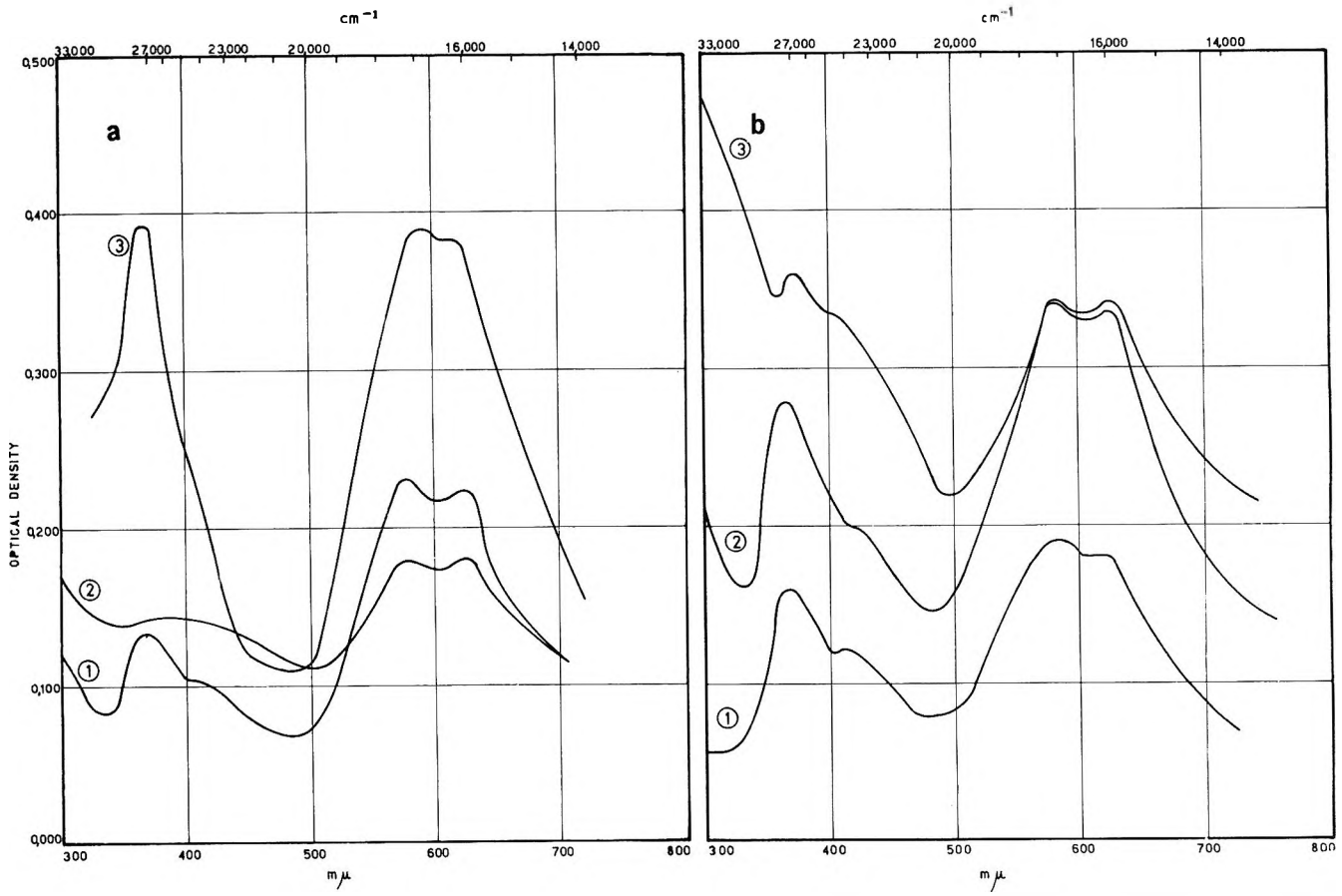

Figure 1. (a) Reflectance spectra. Samples: (1) AηN6 P.S.–dry N_2; (2) AηN3 P.S.–air; and (3) Ni($Mg_{1-x}Al_2O_4$ (x = 0.1) (ref = 4). (b) Reflectance spectra. Samples: (1) AγN2P.S.–dry N_2; (2) AγN6P.S.–dry N_2; and (3) AγN6P.S.–air.

like phase on the surface of the nickel-containing aluminas. Also the sample prepared at 450° in air shows the same behavior. Swift, Lutinski, and Tobin[5] have reported reflectance spectra of NiO supported on γ- and η-Al_2O_3, but they did not discuss the spectra as arising from a surface spinel.

(ii) The spectra of the Ni^{2+}/Al_2O_3 in air are rather different from that of Ni^{2+}/Al_2O_3 in dry nitrogen, with the same nickel content. For instance, for the specimen AγN6 P.S.–air the ratio between the intensities of the bands at 27.000 and 16.000–17.000 cm^{-1} is about unity (0.360/0.340), whereas for the sample AγN6 P.S.–dry nitrogen this ratio is less than unity (0.280/0.340). Recalling that the more intense band for the purely octahedral nickel is at 27.000,[6] while for the tetrahedral nickel it is at 16.000–17.000 cm^{-1},[4] this indicates that in the AγN6 P.S.–dry nitrogen specimen the tetrahedral Ni^{2+} concentration is higher than in the corresponding air-fired specimen. Similar variations of the relative intensities of the octahedral band with respect to the tetrahedral band are found in all air specimens (either γ or η) if compared to dry nitrogen specimens. The general conclusion is that the Ni^{2+}/Al_2O_3–dry nitrogen catalysts have a tetrahedral Ni^{2+} concentration higher than the concentration present in the Ni^{2+}/Al_2O_3–air specimens.

(iii) The same reasoning as used in (ii) can be used for the comparison between AγNx–dry nitrogen and AηNx–dry nitrogen. It can be qualitatively deduced that the amount of tetrahedral Ni^{2+} is larger in AηNx–dry nitrogen than in AγNx–dry nitrogen.

(iv) For the specimen AγN6 P.S.–air a strong absorption is present above 30.000 cm^{-1}. Absorption in this region will arise if small amounts of free NiO are present. No other specimens showed this strong absorption increase. A suspicion of the presence of NiO in AγN6 P.S.–air is supported by X-ray (see below).

In conclusion, the reflectance spectra show the presence of nickel ions in tetrahedral and in octahedral sites, like in a spinel structure. The degree of occupancy of tetrahedral sites (degree of inversion) of the spinel structure formed on the alumina surface depends on the atmosphere of firing (air or dry nitrogen), and can also depend on the nature of the support (η- or γ-Al_2O_3).

3.2. X-Ray Measurements. The X-ray diffraction spectra observed for γ- and η-Al_2O_3 were readily distinguishable and in excellent agreement with those re-

(5) H. B. Swift, F. E. Lutinski, and H. H. Tobin, *J. Catal.*, **5**, 285 (1966).

(6) W. Low, *Phys. Rev.*, **109**, 256 (1958).

ported in the literature.[7-9] The results for γ-Al_2O_3 from both sources were the same: this was essentially so also for the two specimens of η-Al_2O_3, except that η-Al_2O_3 P.S. appeared to contain small quantities of γ-Al_2O_3. X-Ray patterns were taken for two specimens of η- and γ-Al_2O_3 fired at 600° in dry nitrogen. The difference in the spectra of these two samples was identical with that of η- and γ-Al_2O_3 air-fired specimens although for the dry nitrogen-fired samples the lines were more intense. In the dry nitrogen-fired η-Al_2O_3 two additional very weak lines were developed at d = 2.11 and 1.21 Å. The line at d = 2.11 Å has been reported[7] with intensity 10 (*i.e.*, very weak) for γ-Al_2O_3 specimen, while the line at d = 1.21 Å is reported[7] for η-Al_2O_3 specimen with intensity 10.

The X-ray spectra for the nickel-containing samples were approximately identical with those of η- and γ-aluminas as far as the position of the lines are concerned. Only the specimen AγN6 P.S.–air showed a suspicion of NiO. It should be recalled that both η- and γ-Al_2O_3 have a pseudospinel structure. The lattice parameter of the pseudospinel cell is very close to that of $NiAl_2O_4$, because it is essentially determined by the packing of the anions. If, however, attention is focussed on the intensity of the lines of pure aluminas and of nickel-containing specimens as compared to those of $NiAl_2O_4$, the following characteristic behavior of the intensity of some diffraction lines is found (Table III).

Table III

d, Å	$NiAl_2O_4$	γ-Al_2O_3	η-Al_2O_3	AγN6–air	AγN6–dry nitrogen	AηN6–dry nitrogen
4.5	m (or ms)[a]	vw	mw	mw	m	m
2.4	vs	mw	m	s	s	s
2.28		m	mw	mw	mw	w

[a] m = medium; ms = medium strong; vs = very strong; vw = very weak; mw = medium weak; s = strong.

It can be seen that the intensity of the line at d = 2.4 A increases in the nickel-containing catalysts as compared with the pure η- or γ-Al_2O_3. This line is very strong in the spectrum of $NiAl_2O_4$. The result points to the incipient formation of $NiAl_2O_4$ in the Ni^{2+}/Al_2O_3 specimens. It was also noted that the lines of the nickel–alumina specimens fired in dry nitrogen were sharper than those of specimens fired in air.

3.3 Magnetic Measurements. Table I reports the values of the Curie constant, C, and of the Weiss temperature, θ [from the Curie–Weiss law $\chi = C/(T - \theta)$], for all the samples studied. The specific susceptibilities for air-and dry nitrogen-fired η- and γ-Al_2O_3 were also measured. The values were 0.35×10^{-6} erg gauss^{-2} g^{-1} for both aluminas. As can be seen from the results in Table I the values of C for the samples AηNx–dry nitrogen are around 1.31, whereas for the AηNx–air specimens the C values are lower, and vary from 1.12 to 1.25. The C values for the AγNx–dry nitrogen catalysts are also higher than the C values of the AγNx–air samples. In Table I the results are also reported for two specimens AηN2 P.S.–air and AηN6 P.S.–dry nitrogen which were refired for 24 hr in dry nitrogen and in air, respectively. No variation of C was observed.

Estimate of the Degree of Inversion from Magnetic Data. From the experimental value of the Curie constant, C_{exp}, and assuming that all the nickel is present in a "surface spinel" phase, it is possible to estimate the degree of inversion of the spinel by the following reasoning.

The additivity law can be applied to C

$$C_{exp} = x_{oct}^{Ni} \cdot C_{oct} + x_{tet}^{Ni} \cdot C_{tet} \quad (1)$$

(C_{oct}, C_{tet} are Curie constants pertaining to nickel ions in octahedral or in tetrahedral symmetry, respectively, and x_{oct}^{Ni}, x_{tet}^{Ni} are molar fractions of nickel ions in octahedral or in tetrahedral symmetry.) The values of x_{oct} and x_{tet} can then be deduced if C_{oct} and C_{tet} are known.

C_{tet} has been calculated for Ni^{2+} in ZnO, following Figgis[10] (second-order approximation), and a value of 2.10 obtained (Dq = 415 cm^{-1}, B = 800 cm^{-1}, λ = −270 cm^{-1}).[4] This value, which was confirmed by experimental measurements on the NiO–ZnO system, actually holds for room temperature since the magnetic behavior of the NiO–ZnO system does not closely obey the Curie–Weiss law.[11] The value of 2.10 will also be adopted for nickel ions in tetrahedral symmetry in the spinel structure, since the crystal field parameters for spinel do not differ much from those of the ZnO structure.[12] Furthermore, the relative weight of the x_{tet}, C_{tet} term is small, and a small deviation of C_{tet} is not strongly felt. The same criterion cannot be applied to C_{oct}. Both theoretically (second-order approximation[13,14]) and experimentally,[15] a C_{oct} value of 1.31 is calculated, for example, for Ni^{2+} in MgO. However, the experimental value of C, obtained for the

(7) A. S. Russel, W. H. Gitzen, J. W. Newsome, R. W. Richer, V. W. Stowe, H. C. Stumpf, J. R. Well, and P. Wallace, "Alumina Properties," Tech. Paper No. 10 (Revised), Alcoa, Pittsburgh, Pa., 1956.

(8) B. C. Lippens, Thesis, University of Delft, 1961.

(9) H. Krischner, Thesis, Graz, 1964.

(10) B. N. Figgis, "Introduction to Ligand Fields," Interscience, 1967, p 271.

(11) M. Lo Jacono, P. Porta, and A. Cimino, unpublished work.

(12) P. Porta, F. S. Stone, and R. G. Turner, unpublished work.

(13) J. S. Griffith, "The Theory of Transition Metal Ions," Cambridge University Press, London, 1961, p 280.

(14) See ref 10, p 265.

(15) A. Cimino, M. Lo Jacono, P. Porta, and M. Valigi, *Z. Phys. Chem.*, **55**, 1/2, 14 (1967).

spinel $Ni_xMg_{1-x}Al_2O_4$[12] was 1.31 or even lower, varying with the nickel content, even though both octahedral and tetrahedral nickel are present. Allowing for the contribution of tetrahedral Ni^{2+} (high C), it follows that the value of C for octahedral Ni^{2+} in spinels must be lower than 1.31. This is not surprising since spinel is a more compact structure than periclase. To calculate C_{oct} for Ni^{2+} in octahedral sites in the spinel phase, one may make use of the data obtained by Porta, Stone, and Turner[12] for $Ni_xMg_{1-x}Al_2O_4$ in which C values were measured for systems of known x_{tet}^{Ni} and x_{oct}^{Ni}. Taking $C_{tet} = 2.10$, for the reason indicated, their data enable one to derive C_{oct} in spinel from eq 1 as shown in Table IV.

Table IV

x[a]	Firing temp, °C	x_{tet}^{Ni} [a]	C_{exp}	C_{oct}
0.07	1000	0.22	1.23	0.98 ± 0.10
0.07	1400	0.24	1.23	0.96 ± 0.05
1.00	1000	0.22	1.31	1.09 ± 0.03
1.00	1400	0.21	1.33	1.12 ± 0.04

[a] x indicates the mole fraction in the solid solution; x_{tet}^{Ni} indicates the fraction of the nickel ions in tetrahedral sites.

The C value for nickel in octahedral sites in the spinel lattice is therefore around $C_{oct} = 1.10$. Equation 1 can now be applied with $C_{oct} = 1.10$ and $C_{tet} = 2.10$ and the values x_{tet} and x_{oct} can be estimated.

The percentage of nickel as Ni^{2+} in tetrahedral spinel sites is reported in Table I and in Figure 2 for all the catalysts as a function of the total nickel content. In Figure 2 only the specimens made from our η-Al_2O_3 are reported, since a comparison with Ni^{2+}/η-Al_2O_3 P.S. specimens cannot be justified on account of the difference in the preparation, reflected in the presence of γ-Al_2O_3 and in a much larger surface area value (see subsequent paper).

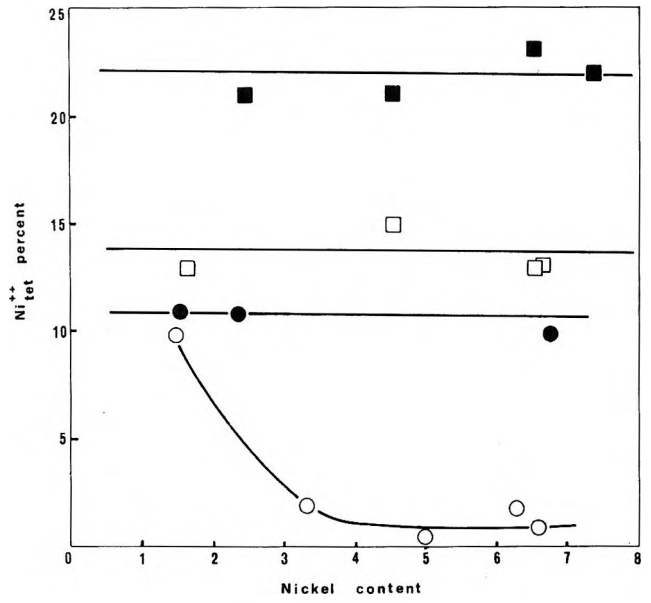

Figure 2. Per cent of Ni^{2+}_{tet} *vs.* total nickel content by weight: ○, Ni^{2+}/γ-Al_2O_3–damp atmosphere; ●, Ni^{2+}/γ-Al_2O_3–dry atmosphere; □, Ni^{2+}/η-Al_2O_3–damp atmosphere; ■, Ni^{2+}/η-Al_2O_3–dry atmosphere.

It is necessary to emphasize that the values given for x_{tet}^{Ni} are only indicative ones, because of the error in the magnetic susceptibility measurements and of the assumptions made. However, even if the values of C for tetrahedral and octahedral Ni^{2+} are slightly changed, only the absolute x_{tet}^{Ni} values are affected; the sequence would still remain in the same order and with about the same relative values. It can be seen that the qualitative conclusions drawn from the reflectance spectra measurements are fully confirmed by the magnetic data.

The following scheme summarizes the behavior so far as the quantity $[Ni^{2+}]_{tet}$ in the different specimens is concerned

$$A\eta Nx\text{–dry nitrogen} > A\eta Nx\text{–air}$$

$$A\gamma Nx\text{–dry nitrogen} > A\gamma Nx\text{–air}$$

$$A\eta Nx\text{–dry nitrogen} > A\gamma Nx\text{–dry nitrogen}$$

$$A\eta Nx\text{–air} \geqslant A\gamma Nx\text{–air}$$

$$A\gamma Nx\text{–dry nitrogen} \geqslant A\eta Nx\text{–air}$$

4. Discussion

The reflectance spectra have indicated the formation of nickel aluminate ($NiAl_2O_4$) on the surface of the aluminas. The X-ray measurements have given further support to this finding. It should be pointed out that evidence for the presence of $NiAl_2O_4$ on the surface of the aluminas is not easily offered by the X-ray technique alone. In fact, calculation of the thickness of the $NiAl_2O_4$ layer on the aluminas shows that the average thickness would vary from 1 to 4 Å. Even though the distribution will not be uniform, only a small variation of the intensity of some reflections can be observed. This fact can explain why some authors[16] failed to have direct evidence of a spinel formation at temperature of 600° or below by X-rays, even though others[17,18] reported X-ray evidence for spinel formation. If the evidence of the X-ray measurements and of the reflectance spectra are taken together, one can see that the nickel ions are interacting with the support yielding what we have called a "surface spinel." This surface spinel will accommodate nickel ions in octahedral and in tetrahedral sites, but not necessarily in the same ratio as in a bulk spinel phase. The magnetic results and

(16) J. T. Richardson and W. D. Milligan, *J. Phys. Chem.*, **60**, 1223 (1956).

(17) A. M. Rubinshtein, *Kinet. Catal.*, **8**, 936 (1967).

(18) J. L. Bousquet, P. C. Gravelle, and S. J. Turner, *Bull. Soc. Chim. Fr.*, **7**, 2229 (1969).

the reflectance spectra give evidence that the degree of inversion for the surface spinel phase depends on the atmosphere in which the catalysts were fired and for the high nickel content (6% atomic) specimens on the nature of the aluminas (η or γ). η-Al_2O_3 and/or dry nitrogen favor the formation of a more normal spinel, *i.e.*, higher Ni^{2+} concentration in tetrahedral sites (A-sites). It will be shown in a subsequent paper that the different tetrahedral and octahedral concentration will also explain the different catalytic properties of Ni^{2+}/η-Al_2O_3 and Ni^{2+}/γ-Al_2O_3.

Influence of the Support on the Nickel Symmetry. In order to explain the influence of the supports on the degree of inversion of the spinel it is necessary to recall briefly the structure of the surface of η- and γ-Al_2O_3 as well as the factors determining the cation distribution.

According to Krischner, *et al.*,[9,19] η- and γ-Al_2O_3 differ from each other primarily in the occupation of the tetrahedral and octahedral sites by Al^{+3} ions (and thereby in the ordering of the bound OH^- groups). η-Al_2O_3 shows a larger occupation of tetrahedral sites, which by contrast are largely unoccupied in γ-Al_2O_3.

It is interesting to note that preferential exposure of tetrahedral Al^{3+} ion also follows from the model offered by Lippens.[8] According to Lippens, η- and γ-Al_2O_3 differ in the exposure of different planes on the surfaces, in addition to other distinct features (such as water content, pore size distribution etc.). The γ-Al_2O_3 exhibits on the surface mainly the planes (100) and (110), whereas η-Al_2O_3 exhibits mainly the planes (111). The plane (110) exposes a layer containing anions and aluminum ions in octahedral and tetrahedral sites or a layer containing anions and aluminum in octahedral sites. The plane (100) exposes anionic sites and cationic octahedral sites, while cationic tetrahedral sites are below the plane. The (111) surface of η-alumina exposes, in the order, layers of anions (which are more likely to terminate the solid surface on account of their larger polarizability) with tetrahedral sites just below, and then octahedral sites below that. The cationic sites closer to the surface, and more likely to interact with the gas, are therefore tetrahedral ones in the case of η-Al_2O_3. Even though this reasoning is limited to the outer layer, it shows that η-Al_2O_3 is characterized by a larger number of surface Al^{3+} ions in tetrahedral positions as compared to γ-Al_2O_3, thus obtaining an agreement with the results of Krischner.[9,19]

It is now appropriate to recall that among the factors controlling the cation distribution in a spinel structure, anion polarization favors a normal distribution.[20,21] We have elsewhere emphasized that the larger polarization experienced by ions in the outermost layer will therefore assist in shifting the distribution of Ni^{2+} ions in the surface region of the spinel $NiAl_2O_4$ toward a normal one.[22] It is a logical consequence, if polarization is thought to have an appreciable weight, to deduce what one might expect for the present systems and compare with the results. For both aluminas, the initial additions of Ni^{2+} ions will result in a higher concentration of Ni^{2+} in tetrahedral sites, because of the surface effect just mentioned. However, due to the particular plane exposed, η-Al_2O_3 will experience a larger surface polarization effect, which favors a higher degree of occupancy of tetrahedral sites. Thus, η-Al_2O_3 will tend to form a "surface spinel" with a more normal distribution than the surface spinel formed by γ-Al_2O_3. The polarization effect just mentioned, however, is not the only factor to be considered. It must be remembered that γ-Al_2O_3 has more numerous vacant tetrahedral sites than η-Al_2O_3. The nickel ions will therefore be easily directed into the tetrahedral sites in γ-Al_2O_3, even though the polarization factor is not assisting the process. This effect, arising from probability reasons, will be more strongly felt for the first additions of nickel ions (low percentage specimens) and could explain the high tetrahedral content of the sample AγN1–air (see Figure 2).

Influence of the Atmosphere of Firing on the Nickel Symmetry. In order to explain the influence of the firing atmosphere on the degree of inversion of the spinel it is recalled that a dry atmosphere favors the dehydration of the surface, whereas a damp atmosphere provokes the formation of OH^- groups. In the first case (dry atmosphere) a surface unsaturation occurs while in the second case the presence of the OH^- groups allows the metal ions of the surface to be fully coordinated. A dry atmosphere has the consequence of removing a large fraction of the anion ligands, and the nickel ions will tend to shift to tetrahedral sites, thus achieving a stable configuration with strong metal–oxygen bonds. Accordingly, specimens fired in dry nitrogen have a higher concentration of tetrahedral Ni^{2+}.

The above interpretation regarding the differences between η- and γ-Al_2O_3 and the role of water vapor not only accounts for the results presented in this paper, but it is also in agreement with earlier observations by different authors, as briefly reported below.

Among other studies, one of particular relevance to our problem is the work by Swift, Lutinski, and Tobin,[5] who studied η- and γ-Al_2O_3 as a support for NiO. By reduction experiments (at 500° for 2 hr) and subsequent chemisorption of hydrogen or by removal of nickel by CO, they showed that specimens with 2% of nickel, either on η- or γ-Al_2O_3, are not reduced, and that a specimen having 6% of nickel on η-Al_2O_3 was markedly less reducible than the corresponding specimen supported on γ-Al_2O_3. These data show that some speci-

(19) H. Krischner, K. Torkar, and D. Donnert, *Ber. Deut. Keram. Ges.*, **46**, 240 (1969).

(20) J. Smit, F. K. Lotgering, and R. P. Van Stapele, *J. Phys. Soc. Jap.*, **17**, 268 (1962).

(21) G. Blasse, *Philips Res., Rep. Suppl.*, **3** (1964).

(22) A. Cimino and M. Schiavello, *J. Catal.*, in press.

mens (low nickel content, and/or η-Al_2O_3 based) have nickel ions more difficult to attack. These nickel ions are those in tetrahedral sites. There is then an agreement with our findings which show that a large concentration of tetrahedral nickel ions can be maintained in specimens supported on η-Al_2O_3 even at fairly elevated nickel contents. As the subsequent paper will show, the catalytic behavior of these supported nickel oxides can also be rationalized on the basis of the variable $[Ni^{2+}]_{oct}/[Ni^{2+}]_{tet}$ ratio.

A comment is also due regarding the much invoked "induced valency effect," which is held to result in the formation of Ni^{3+}. This hypothesis, initially proposed by Hill and Selwood[1] has been later revised by Selwood,[23] following comments by Richardson and Milligan.[16] Recent literature on supported nickel oxide however still invokes the Ni^{3+} formation, as in the review by Rubinshtein,[17] Nowak and Koros,[24] and Swift, Lutinski, and Tobin.[5] From esr measurements[25-27] and from optical spectra[28] it has been shown that the electronic configuration of Ni^{3+} in an octahedral symmetry in an oxide matrix is spin-paired ($t_{2g}^6 \cdot e_g^1$), *i.e.* the fundamental term is ^2E. The effect of such a configuration is to reduce the magnetic moments. The values of the experimental magnetic moments given by the quoted authors[1,16,17] and also found in the present work, are greater at low nickel content, when the relative Ni^{3+} content should be higher. The high magnetic moments can instead be explained by the presence of Ni^{2+} in tetrahedral configuration,[11,16] its relative concentration being higher at low nickel content.

It is important to note that the relative concentration of tetrahedral nickel is affected, as shown before, not only by the total nickel concentration, but also by the atmosphere, and by the impregnation technique. The early observations of Hill and Selwood[1] on differences of catalytic activity between singly and multiply impregnated catalysts can thus be attributed to different concentrations of tetrahedral ions. It can then be understood why the magnetic moments of nickel ions measured by Richardson and Milligan[29] for specimens prepared in dry nitrogen are higher than those found by Hill and Selwood.[1] The magnetic susceptibilities of nickel oxide supported on γ-Al_2O_3 (with small percentage of η-Al_2O_3) were interpreted[30] in terms of two nickel oxide phases. The two phases were designated as a magnetically dilute δ phase associated with the support structure and a magnetically concentrated β phase similar to the bulk NiO phase. We propose that the δ phase can be identified as our "surface spinel." Specimens containing a large fraction of nickel in tetrahedral sites are not easily reduced.[1,31,32] The low reducibility (and ensuing low catalytic properties) of multiply impregnated catalysts[1,31] can be accounted for by a more homogeneous dispersion of nickel ions within the support, resulting in a larger fraction of ions in tetrahedral sites.

Acknowledgments. The authors wish to thank Dr. F. S. Stone for valuable discussions and for critically reading the manuscript and Mr. G. Minelli for the help given in performing some of the experiments described in the paper. The financial support of SNAM-PROGETTI is also gratefully acknowledged.

(23) P. W. Selwood, "Magnetochemistry," 2nd ed, Interscience, New York, London, 1956, p 384.

(24) B. J. Nowak and R. M. Koros, *J. Catal.*, **7**, 50 (1967).

(25) P. Wysling, U. Höchli, and K. A. Muller, *Helv. Phys. Acta*, **37**, 629 (1964).

(26) U. Höchli, K. A. Muller, and P. Wysling, *Phys. Lett.*, **15**, 5 (1965).

(27) A. Cimino, D. Cordischi, P. Porta, and M. Valigi, *Ric. Sci. Parte 2: Sez A*, **35**, 1153 (1965).

(28) M. Lo Jacono, A. Sgamellotti, and A. Cimino, *Z. Phys. Chem.*, **70**, 179 (1970).

(29) W. O. Milligan and J. T. Richardson, *J. Phys. Chem.*, **59**, 831 (1955).

(30) G. T. Rymer, J. M. Bridges, and J. R. Tomlison, *ibid.*, **65**, 2152 (1961).

(31) D. Reinen and P. W. Selwood, *J. Catal.*, **2**, 109 (1963).

(32) J. L. Carter and J. H. Sinfelt, *J. Phys. Chem.*, **70**, 3003 (1966).

Catalytic Activities of Nickel Oxide Supported on γ- and η-Aluminas for the Nitrous Oxide Decomposition

by M. Schiavello, M. Lo Jacono, and A. Cimino*

Istituto di Chimica Generale ed Inorganica, Università di Roma, and Centro di Studio sulla Struttura ed Attività Catalitica di Sistemi di Ossidi, del Consiglio Nazionale delle Ricerche, Rome, Italy
(Received November 4, 1970)

Publication costs assisted by SNAM-Progetti S. Donato (Italy)

The catalytic properties of samples of Ni^{2+}/γ-Al_2O_3 and Ni^{2+}/η-Al_2O_3, prepared in damp and in dry atmospheres, were tested for the N_2O decomposition. The activity of pure γ-Al_2O_3 and η-Al_2O_3 was also tested for the same reaction. The results have shown that the damp atmosphere-fired samples are more active than the dry atmosphere ones. All the latter have almost the same activity and the same activation energy. The effect of the support on the catalytic activity is noticeable in the air-fired specimens with high nickel content (6% atomic). The results are interpreted in terms of the different $[Ni^{2+}]_{oct}/[Ni^{2+}]_{tet}$ ratio present in the various types of catalysts. It is shown that nickel ions exposed from octahedral sites ($Ni^{2+}{}_{oct}$) are more active than those exposed from tetrahedral ones ($Ni^{2+}{}_{tet}$); hence a high catalytic activity parallels a high $[Ni^{2+}]_{oct}/[Ni^{2+}]_{tet}$ ratio.

1. Introduction

A previous paper[1] has described the results of an investigation concerning the structural properties of solids made by supporting nickel oxide on γ- and η-aluminas. It was shown that the interaction between the nickel ions and the support led to the formation of a "surface spinel." This surface spinel was characterized by a distribution of nickel ions among tetrahedral and octahedral sites which was influenced by the gaseous atomosphere used in the preparation: the presence of water vapor tended to increase the concentration of nickel ions in octahedral sites at nickel concentrations higher than 1%. If the nickel concentration was 4–6% (atoms per 100 Al atoms), the distribution was also influenced by the type of support: specimens made by impregnation of γ-Al_2O_3 had a higher concentration of octahedral nickel. These findings offered an explanation[1] of the results of Swift, *et al.*,[2] who found a marked difference in the reducibility of nickel oxide supported on η-Al_2O_3 and nickel oxide supported on γ-Al_2O_3 (6% nickel ions in both cases). Consequently, catalytic reactions involving metallic nickel should also show a lower activity for Ni^{2+}/η-Al_2O_3 than for Ni^{2+}/γ-Al_2O_3, as is in fact found.[2] Tetrahedral and octahedral nickel ions also behave differently in catalytic reactions involving a cation–oxygen bond: a study of the catalytic activity of $Ni_xMg_{1-x}Al_2O_4$ solid solutions for the N_2O decomposition has shown[3] that nickel ions exposed from tetrahedral sites are far less active than ions exposed from octahedral sites. The same result emerged from a comparative study of NiO–MgO solid solutions[4,5] and of NiO–ZnO solid solutions.[6] It was therefore of interest to investigate the N_2O decomposition on Ni^{2+}/η-Al_2O_3 and on Ni^{2+}/γ-Al_2O_3 in order to check whether there were different activities which could be ascribed to the relative concentrations of tetrahedral and octahedral nickel ions.

2. Experimental Section

2.1. Catalysts. The samples used in the present work were from the same batches as those used and described in Table I of the preceding paper.[1] Tables I–III of the present paper list the catalysts, their surface area (BET), the apparent activation energy for N_2O decomposition, and also report the fraction of tetrahedral nickel ions from Table I of ref 1. AηNx and AγNx refer to nickel oxide supported on η- or γ-Al_2O_3, respectively, with a concentration of x Ni atoms per 100 Al atoms.

2.2 Catalysis Experiments. The N_2O decomposition was studied in the temperature range 250–400° in a circulating system (405 cm^3) with a vertically positioned silica reactor. The gas was passed at about 120 cm^3/min through the catalyst (~60 mg), which was spread over silica wool. Further details are reported elsewhere.[7] The following conditioning procedure was adopted before the catalysis and before the

(1) M. Lo Jacono, M. Schiavello, and A. Cimino, *J. Phys. Chem.*, **75**, 1044 (1971).

(2) H. B. Swift, F. S. Lutinski, and H. H. Tobin, *J. Catal.*, **5**, 285 (1966).

(3) A. Cimino and M. Schiavello, *ibid.*, in press.

(4) A. Cimino, R. Bosco, V. Indovina, and M. Schiavello, *ibid.*, **5**, 271 (1966).

(5) A. Cimino, V. Indovina, F. Pepe, and M. Schiavello, *ibid.*, **14**, 49 (1969).

(6) M. Schiavello, A. Cimino, and J. M. Criado, *Gazz. Chim. Ital.*, in press.

(7) A. Cimino and V. Indovina, *J. Catal.*, **17**, 54 (1970).

Table I: γ- and η-Al_2O_3 Catalysts and Their Properties

Catalyst	Atmosphere of firing	Surface area, m^2/g	E_a, kcal/mol
γ-Al_2O_3 P.S.	Air	125	29
γ-Al_2O_3	Air	154	28
γ-Al_2O_3 P.S.	Dry nitrogen	114	33
η-Al_2O_3 P.S.	Air	166	30
η-Al_2O_3	Air	176	30
η-Al_2O_3	Damp nitrogen	160	29
η-Al_2O_3 P.S.	Dry nitrogen	147	32

Table II: NiO/γ-Al_2O_3 Catalysts and Their Properties

Catalyst	Atmosphere of firing	Surface area, m^2/g	Ni^{2+}_{tet}, %	E_a, kcal/mol
AγN1	Air	163	10	27
AγN3 P.S.	Air	131	2	20
AγN6 P.S.	Air	130	1	17
AγN6	Air	136	2	18
AγN2 P.S.	Dry nitrogen	113	11	27
AγN6 P.S.	Dry nitrogen	121	10	27

Table III: NiO/η-Al_2O_3 Catalysts and Their Properties

Catalyst	Atmosphere of firing	Surface area, m^2/g	Ni^{2+}_{tet}, %	E_a, kcal/mol
AηN2 P.S.	Air	196	2	26
AηN3 P.S.	Air	219	7	20, 20[a]
AηN6	Air	183	13	23
AηN6	Damp nitrogen	173	13	22
AηN2 P.S.	Dry nitrogen	171	21	26
AηN6 P.S.	Dry nitrogen	164	22	27, 29[a]
AηN6	Dry air	168	23	25
AηN2 P.S.	Air → dry N_2	151	3	26
AηN6 P.S.	Dry N_2 → air	140	21	25

[a] The two values refer to determinations on two different specimens of the same batch.

surface area measurements. The samples were outgassed for 4 hr at a pressure of $\sim 10^{-6}$ Torr and at 480°. Between runs, the sample was evacuated at 480° for 30 min. The initial pressure of N_2O was about 60 Torr and the total N_2O decomposition was not larger than 1%. A small sample (5.3 cm^3) of the gaseous mixture was withdrawn at definite intervals of time; this was condensed in liquid nitrogen and the residual pressure was read by means of a Pirani gauge. The kinetic data are reported as absolute velocity constants expressed in cm min^{-1}.

2.3 Reduction Experiments. Hydrogen reduction experiments were performed on three specimens in a flow system. The sample (~0.400 g) was placed in a Pyrex reduction cell, whose small volume (about 5 cm^3) was limited by two fritted disks (the superior G2, and the inferior G3). The cylinder hydrogen used was of high purity and it was further purified by passing it through a "Deoxo" unit, a magnesium perchlorate trap, and a liquid nitrogen trap. The procedure adopted for determining the amount of H_2 adsorbed at 20° by the reduced specimens was as follows. The specimen was reduced at 100, 200, 300, 400, 450, and 520°, in a flow of hydrogen (110 cm^3/min for 12 hr). After each reduction the sample was outgassed at the same reduction temperature and then cooled under dynamic vacuum. At 20° the amount of adsorbed H_2 was determined at a pressure of about 0.8 Torr. This measurement was complete in about 30 min. After the adsorption the next reduction step was performed at the next higher temperature.

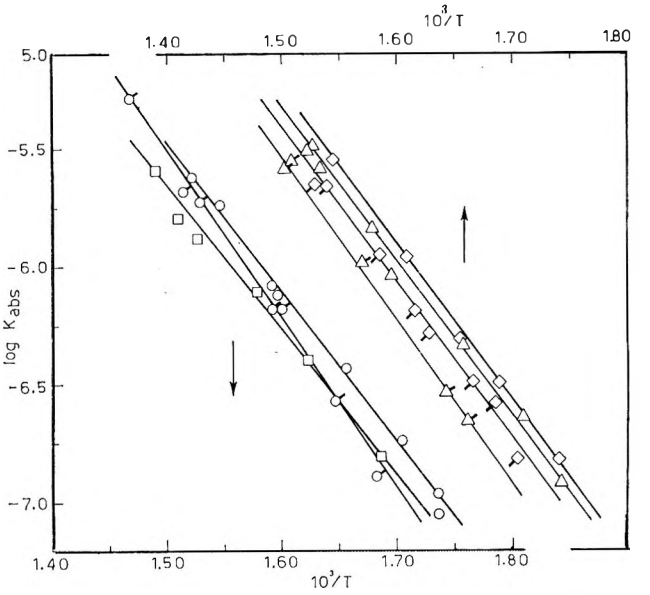

Figure 1. Arrhenius plots for γ- and η-Al_2O_3 catalysts: ○, γ-Al_2O_3 P.S.–air; □, γ-Al_2O_3–air; ⊙, γ-Al_2O_3–dry nitrogen; △, η-Al_2O_3 P.S.–air; ◇, η-Al_2O_3–air; ⊿, η-Al_2O_3 P.S.–dry nitrogen; ◇, η-Al_2O_3–damp-nitrogen.

3. Experimental Results

3.1. Catalytic Activity of η- and γ-Al_2O_3. The results for the pure aluminas, in the form of Arrhenius plots, are shown in Figure 1. The scale of the abscissas for the η-aluminas is shifted to avoid crowding of points. The two γ-Al_2O_3–air specimens have a slightly different activity, but about the same E_a value (28 and 29 kcal/mol). The γ-Al_2O_3 P.S.–dry nitrogen has a slightly lower activity and a higher E_a value (33 kcal/mol), compared to the γ-Al_2O_3 P.S.–air. The two η-Al_2O_3–air specimens have the same activity and the same E_a value (30 kcal/mol). The specimen η-Al_2O_3 P.S.–dry nitrogen is less active than the η-Al_2O_3 P.S.–air, and its E_a value is slightly higher (32 kcal/mol). The specimen η-Al_2O_3–damp nitrogen shows a catalytic activity and an E_a value (29 kcal/mol) close to that of the air-fired specimens. Several kinetic experiments had to

be performed before the catalysts gave reproducible results. The number of runs necessary to reach reproducibility was about 2 or 3 for specimens fired in damp air, while for those fired in dry nitrogen the number was larger (6–7 runs). It should be noted that in the case of dry nitrogen-treated specimens it can be deduced that practically all the oxygen produced in the initial runs was completely chemisorbed. This effect can be checked by an apparent increase of the first-order velocity constant in passing from the initial to later runs. If it is assumed that in the initial runs all the oxygen is chemisorbed (thus giving N_2 only in the gas phase) while in later runs all the oxygen is freed (thus giving $N_2 + {}^1/_2O_2$ in the gas phase), the k_{abs} value of the last runs should be 1.5 times that of the initial k_{abs} value. This, indeed, was found to be the case. For example, for the specimen γ-Al_2O_3 P.S.–dry nitrogen, the value of k_{abs} for the second run at $t = 353°$ was 3.96×10^{-7} cm min^{-1}, while, for the seventh and eleventh run at the same temperature, k_{abs} were 6.57×10^{-7} and 6.68×10^{-7} cm min^{-1}, respectively, both values being not far from $1.5 \times 3.96 \times 10^{-7} = 5.94 \times 10^{-7}$ cm min^{-1}.

3.2. Catalytic Activity of AγNx Specimens. In Table II the catalysts of this series are listed together with their main features. The Arrhenius plots of the catalytic results of AγNx specimens are shown in Figure 2 and the results for the air-fired γ-Al_2O_3 P.S. and γ-Al_2O_3 specimens are also reported for reference as dotted and dashed lines, respectively.

The activity of the samples AγNx–air increases as the nickel content increases from AγN1 to AγN6, while E_a decreases from 27 to 18 kcal/mol. The catalyst AγN1 has an activity and an E_a value lower than the pure γ-Al_2O_3. The specimen AγN6 P.S.–air contains a small fraction of unreacted NiO which is just detectable by X-ray diffraction analysis, and whose presence is consistent with the onset of absorption in the reflectance spectra, below 330 mμ.[1] Both samples fired in dry nitrogen (AγN2 P.S. and AγN6 P.S.) have a catalytic activity lower than the activity of corresponding specimens fired in damp air, and also lower than the activity of γ-Al_2O_3.

3.3. Catalytic Activity of AηNx Specimens. The catalytic results for AηNx specimens (Table III) are reported in Figure 3, where the results of η-Al_2O_3 P.S.–air and η-Al_2O_3 P.S.–dry nitrogen are also shown (dashed and dotted lines, respectively) for comparison. It can be seen that the activity of the air-fired AηNx specimens is not far from that of pure η-Al_2O_3. Furthermore, the activity does not vary with varying nickel content as much as the activity of the AγNx specimens.

The specimens AηN2 P.S. and AηN6 P.S., fired in dry nitrogen, are considerably less active than pure η-Al_2O_3 and their E_a values are the highest in this series of catalysts.

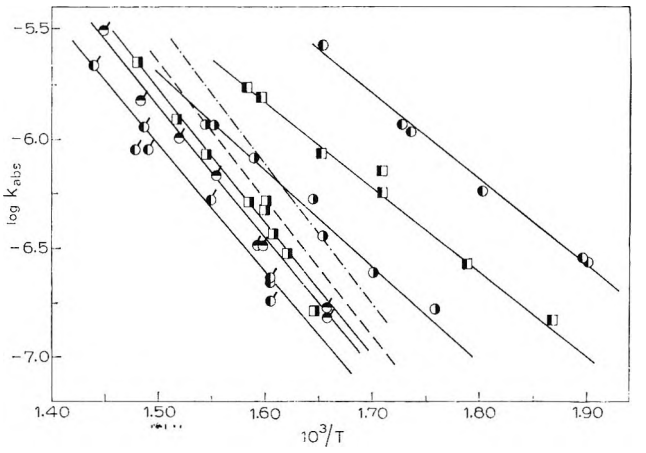

Figure 2. Arrhenius plots for NiO/γ-Al_2O_3 catalysts: ◨, AγN1-air; ◑, AγN3 P.S.-air; ◐, AγN6 P.S.-air; ◧, AγN6-air; ◒, AγN2 P.S.-dry nitrogen; ◐, AγN6 P.S.-dry nitrogen; – – – –, γ-Al_2O_3-air; –·–·–·–, γ-Al_2O_3 P.S.-air).

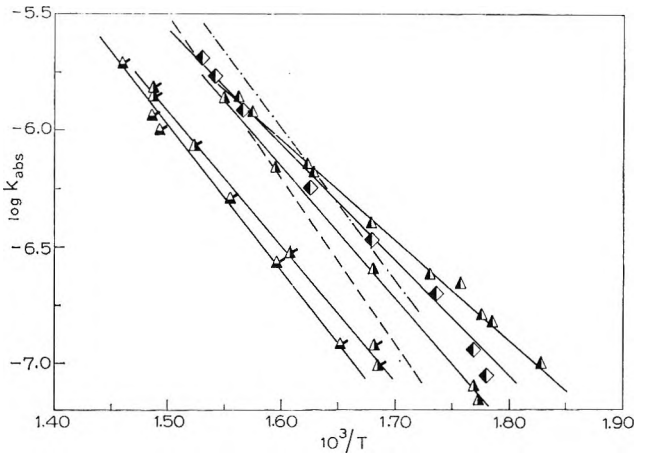

Figure 3. Arrhenius plots for NiO/η-Al_2O_3 catalysts: ◭, AηN2 P.S.-air; ◭, AηN3 P.S.-air; ◐, AηN6-air; –·–·–·–, η-Al_2O_3 P.S.-air; ◭, AηN2 P.S.-dry nitrogen; ◭, AηN6 P.S.-dry nitrogen; – – – –, η-Al_2O_3 P.S.-dry nitrogen.

3.4. Effect of Water Vapor on the Catalytic Activity. The difference in activity between air and dry nitrogen specimens prompted some experiments on the effect of the water vapor. The catalysts used for these experiments are included in Table III. One AηN6 specimen was fired in a flow of dry air: its activity and E_a value are close to that of the corresponding dry nitrogen specimens (Figure 4). However, a specimen of AηN6–damp nitrogen is similar in activity and in E_a value to AηN6–air (Figure 4). One damp air specimen (AηN2 P.S. damp air) was refired for 24 hr at 600° in dry nitrogen and its activity became significantly lower (Figure 5). Finally, one dry nitrogen sample (AηN6 P.S. –dry nitrogen) was refired in damp air and its activity increased (Figure 5).

The beneficial effect of water vapor was not found if the specimen was allowed to come into contact with

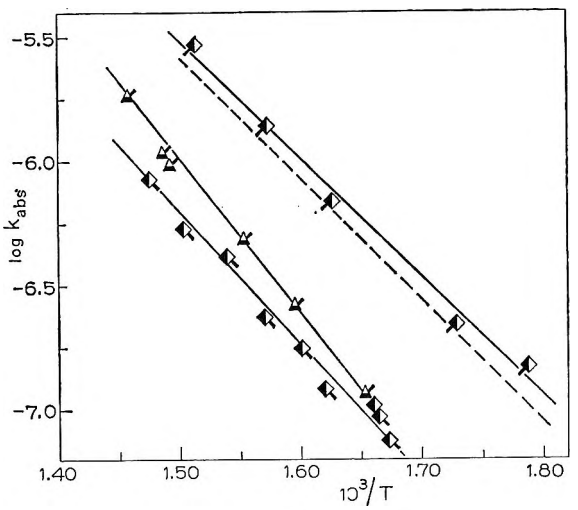

Figure 4. Arrhenius plots for NiO/η-Al_2O_3 catalysts submitted to special firing treatment: ◭, AηN6-dry air; ◬, AηN6 P.S. dry nitrogen; ----, AηN6-air; ◮, AηN6-damp nitrogen.

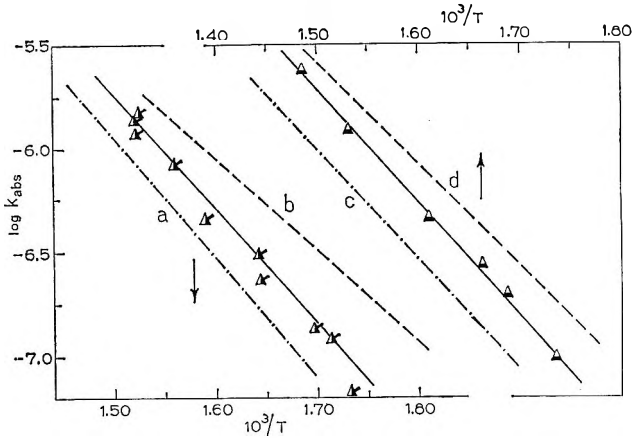

Figure 5. Arrhenius plots for NiO/η-Al_2O_3 catalysts submitted to refiring treatment: ◬, AηN2 P.S.-air → dry nitrogen; ▲, AηN6 P.S. (dry nitrogen) → air; (a) AηN2 P.S.-dry N_2; (b) AηN2 P.S.-air; (c) AηN6 P.S.-dry N_2; (d) AηN6 P.S.-air.

water after outgassing. This is illustrated by an experiment performed on a AηN6 P.S.-dry nitrogen sample. After the tenth run, when the activity was reproducible, the vapor of distilled and outgassed water at a pressure of about 20 Torr was brought into contact for 15 min with the specimen kept in the reactor at 400°. After this treatment, the specimen was outgassed at 480° for 15 min and the activity tested at 350°. The specimen was completely inactive. The catalyst was again outgassed for 2 hr at 480°: after this prolonged outgassing, the activity was restored and remained constant for many runs.

3.5. Comparison between AηNx and AγNx Specimens. From the results shown in Figure 2 and 3, it can be deduced that at high nickel content (6% atomic) a specimen based on γ-Al_2O_3 is more active than the corresponding specimen based on η-Al_2O_3. For example, at $T = 308°$ there is a factor of 2 in the catalytic

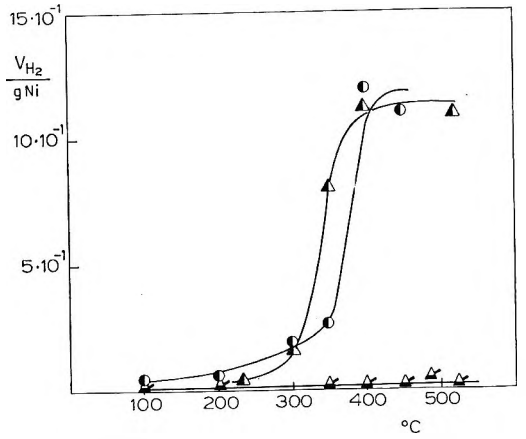

Figure 6. H_2 uptake due to the reduction treatment. ◐, AγN6 P.S.-air; ◬, AηN6 P.S.-dry nitrogen; ▲, AηN3 P.S.-air.

activity. The AγN6 specimen also has a lower E_a value. As for specimens with a low nickel content, differences are less significant, and Ni^{2+}/γ-Al_2O_3 and Ni^{2+}/η-Al_2O_3 do not differ in a clear manner. Specimens treated in a dry atmosphere, which are always less active than specimens treated in a damp atmosphere, also do not show any appreciable difference between Ni^{2+}/γ-Al_2O_3 and Ni^{2+}/η-Al_2O_3.

3.6. Reduction Experiments. For these measurements three specimens different in the content of tetrahedral nickel were selected, namely AγN6 P.S.-air, AηN3 P.S.-air, and AηN6 P.S.-dry nitrogen, with $(Ni^{2+})_{tet}$ = 1, 7 and 22%, respectively. The results are shown in Figure 6, where the volume (cc at STP) of H_2 adsorbed per gram of Ni (V_{H_2}/g of Ni) is reported as a function of the reduction temperature. It is apparent that a marked difference exists between the catalysts in their resistance to the reduction treatment. The sample AηN6 P.S.-dry nitrogen was not reducible, even at 520°, while for AγN6 P.S.-air and AηN3 P.S.-air the reduction began above 200°. The strong influence of the atmosphere on the reducibility is thus brought out by the experiments.

4. Discussion

The results obtained in the catalysis and reduction experiments will be discussed on the basis of the structural data presented in the preceding paper,[1] which showed that on the surface of alumina-supported nickel oxide nickel ions are distributed in tetrahedral and in octahedral sites left in the interstices of the oxygen anions in a manner similar to a spinel structure. In the surface spinel the relative amount of nickel ions in tetrahedral (Ni^{2+}_{tet}) and in octahedral (Ni^{2+}_{oct}) sites depends on the atmosphere in which the supported oxide has been heated, and for the high nickel concentration specimens it depends on the type of alumina used. Previous work[3] has shown that Ni^{2+}_{tet} is only slightly active for the N_2O decomposition. It is believed that the catalytic properties of these nickel–alumina solids for the N_2O decomposition also depend

to a large extent on the relative amounts of Ni^{2+}_{tet} and Ni^{2+}_{oct} concentrations exposed in the surface. The surface arrangements of nickel ions will now be discussed, after a comment on the activity of pure aluminas.

Activity of Pure Aluminas. Pure aluminas exhibit a substantial activity, which cannot simply be ascribed to impurities, since the level of impurities is not higher than that present in MgO[4] or in the spinel $MgAl_2O_4$,[3] which are much less active. The particular surface structure present in these aluminas must accordingly be responsible for the activity. Upon heating, elimination of water by combination of two OH^- groups leaves an oxide ion O^{2-} and a vacant coordinating position at the surface of the catalyst. Al^{3+} cations, coordinately unsaturated, might well be responsible for the catalytic activity of both aluminas. The active centers would be essentially the same on γ- and η-alumina and consequently the observed result that the activity is comparable for both aluminas is to be expected. The decrease of activity upon dry nitrogen treatment then reflects a rearrangement of the surface as hydroxyl groups disappear, during the heating. After this rearrangement, exposure to a damp atmosphere at room temperature cannot restore the same structural pattern of hydroxyls which was present before the oxide had been directly heated in a damp atmosphere. Hence, the removal of water prior to the catalysis experiments (conditioning at 480° *in vacuo*) fails to create the catalytically active situation.

The Influence of Nickel Ion Addition. Addition of nickel ions results in a variation of the surface configuration, due to the formation of the "surface spinel," without significantly affecting the surface hydroxyl concentrations.[2] Arrangements of hydroxyl groups and cations are critical in the sense that sites more or less favorable to the catalytic process can be created by the removal of a large fraction of the OH^- groups.

During the dehydration of Ni^{2+}/γ-Al_2O_3 and Ni^{2+}/η-Al_2O_3 surfaces, adjacent hydroxyl groups combine to form water molecules, leaving anion vacancies, which can be within the coordination spheres of cations in octahedral or tetrahedral sites. The following scheme outlines the geometrical arrangement of the anion vacancy, designated by □

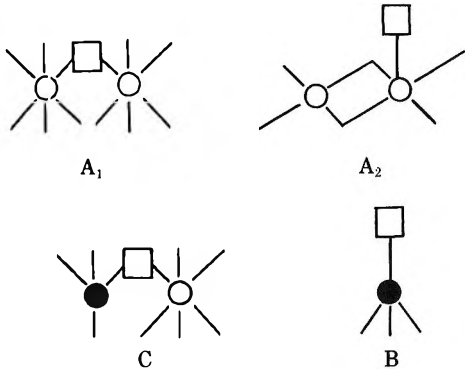

These schemes do not attempt to show a detailed description of the local configurations, but only how the vacant coordinating position can be found around cations placed in sites of different symmetry. The local configuration will depend on the type of plane exposed. For instance, the tetrahedral type B is exposed for the planes (111), (110), and (100), respectively

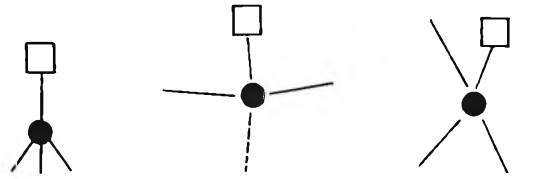

It is thought that the sites A_1 and A_2 (hereafter called the octahedral centers) and to a lesser extent C are the active ones for N_2O decomposition. Here nickel ions with incomplete octahedral configurations are exposed which could constitute sites for adsorption and decomposition of N_2O. If this were so, the catalytic activity of Ni^{2+}/Al_2O_3 specimens would be expected to be higher than that of pure Al_2O_3 and to be strongly dependent on the octahedral nickel concentration on the catalyst surface. If the centers left by the removal of water were the tetrahedral centers B the catalytic activity of Ni^{2+}/Al_2O_3 specimens would be expected to be comparable or lower than that of pure Al_2O_3 because the activity of tetrahedral nickel ions is very small.[3,6]

On the basis of the above assumptions and of structural data reported in the preceding paper, we now discuss the catalytic results in more detail.

The Activity of AγNx and AηNx in Air. Since the percentage of tetrahedral nickel decreases from 10% (AγN1) to 1–2% (AγN6) as the nickel content increases, the main population of surface centers formed by dehydration changes from the tetrahedral group of models (AγN1) toward the octahedral group of models (AγN6). Consequently, we expected that the catalytic activity should increase and this was observed (Figure 2).

With the Ni^{2+}/η-Al_2O_3 catalysts, the percentage of $[Ni^{2+}]_{tet}$ does not vary with the total nickel content; thus it is to be expected that the surface dehydration centers are not affected by the nickel content. Furthermore, for Ni^{2+}/η-Al_2O_3 specimens the ratio tetrahedral group/octahedral group is higher compared to that on Ni^{2+}/γ-Al_2O_3. This explains why the activity of the Ni^{2+}/η-Al_2O_3 specimens does not change much with the nickel content and why it is lower than that of Ni^{2+}/γ-Al_2O_3.

The Influence of the Firing Atmosphere. Preparation of a supported catalyst in the absence of water (*i.e.*, in dry nitrogen or dry air) results in a higher concentration of tetrahedral nickel than when H_2O is present. Furthermore the outer layer is more markedly affected by the atmosphere than the bulk. The quan-

tity $[Ni^{2+}]_{tet}$ determined from the magnetic susceptibility, which is a bulk property, is thus only an approximate criterion for determining the number of tetrahedral centers left at the surface after dehydration and hence the catalytic activity. If the preparation atmosphere of two specimens is the same, the relative surface properties will be accurately reflected by the relative bulk properties. However, if the preparation atmosphere is different for two specimens, their relative outer layer configurations will not depend in the same way on their bulk configurations. In fact, if magnetically the same bulk configuration is deduced for a dry N_2 and an air specimen, the dry N_2 specimen will have, in the outer layer, a higher $[Ni^{2+}]_{tet}$ value than the air specimen because the dry atmospheref avors the formation of tetrahedrally coordinated cations. Accordingly, the catalytic activity of the former will be smaller, because it will have a larger amount of tetrahedral centers. In particular, specimen AηN6 P.S.–dry N_2 was subsequently treated in damp air. Its $[Ni^{2+}]_{tet}$ value (bulk property) is practically unchanged (22 and 21%, respectively), but its catalytic activity rises (Figure 5), because a decrease in the number of $(Ni^{2+})_{tet}$ has taken place in the external layer. This explains why AηN6–air ($[Ni^{2+}]_{tet}$ = 13%) is less active than AγN6–air ($[Ni^{2+}]_{tet}$ = 2%), but more active than AγN6–dry N_2 ($[Ni^{2+}]_{tet}$ = 10%).

Centers formed by dehydration of dry atmosphere-fired samples, either γ- or η-Al_2O_3 based, must be predominantly of the tetrahedral group because of the high tetrahedral nickel content on the surface. Moreover a refiring treatment will have the effect of changing the relative amount of the two groups of models according to the variation of the surface tetrahedral nickel. To summarize, there is a correlation between the surface centers left by dehydration, as determined by the amount of tetrahedral nickel, and the catalytic activity. This correlation is illustrated in Figure 7a and 7b where the variation of E_a *vs.* $[Ni^{2+}]_{tet}$ and log k_{abs} (at T = 352°) *vs.* $[Ni^{2+}]_{tet}$ are reported.

Surface Unsaturation and Catalytic Activity. From the above consideration we conclude that the peculiar properties of the Ni^{2+}/γ-Al_2O_3 or Ni^{2+}/η-Al_2O_3 depend on the high surface area of these materials on account of the possibility of the large coverage of the surface by OH^- groups and of the particular configurations of the OH^- groups. It is only by removal of a large fraction of these groups that arrangements more or less favorable to the catalytic process can be created. If the original supported nickel catalyst did not contain OH^- groups, or contained them in a way which was determined by exposure to damp air at room temperature, its surface could be compared to a low-area, well-crystallized material, such as $NiAl_2O_4$ specimens prepared at high temperature (1400°). A comparison between the catalytic activity of AηN6–dry nitrogen with $[Ni^{2+}]_{tet}$ = 22%, and of a well crystallized spinel

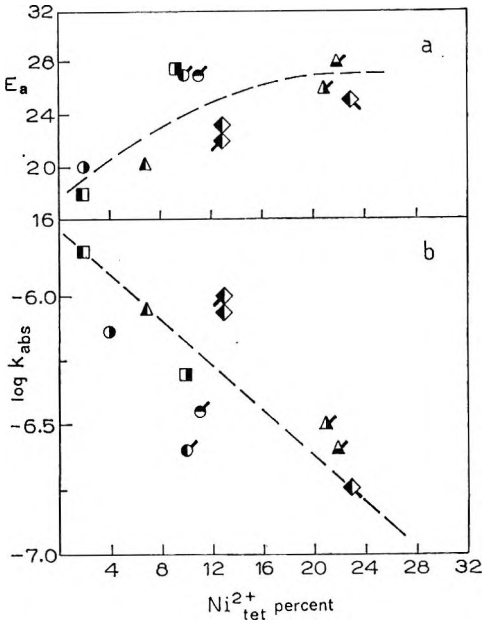

Figure 7. (a) Apparent activation energy *vs.* $[Ni^{2+}]_{tet}$: (b) log k_{abs} at $1/T \cdot 10^3$ = 1.6 *vs.* $[Ni^{2+}]_{tet}$: ■, AγN6-air; ◑, AγN3 P.S.-air; ▲, AηN3 P.S.-air; ◒, AγN2 P.S.-dry N_2; ◐, AγN6 P.S.-dry N_2; ◨, AγN1-air; ◆, AηN6 air; ◈, AηN6-damp N_2; ◭, AηN2 P.S.-dry N_2; ◮, AηN6 P.S.-dry N_2; ◈, AηN6-dry air.

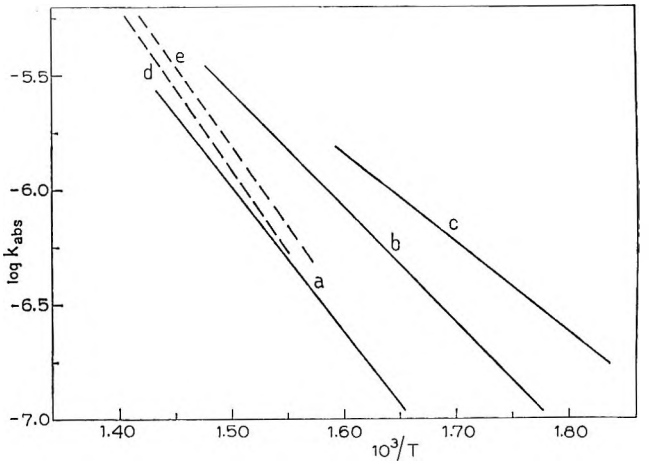

Figure 8. Comparison of activity between well crystallized spinel[3] and some NiO/Al_2O_3 specimens: (a) AηN6 P.S.-dry N_2; (b) AηN6-air; (c) AγN6-air; (d) $NiAl_2O_4$-(1400); (e) $NiAl_2O_4$-(1000).

$NiAl_2O_4$, prepared at 1400° and quenched from that temperature,[3] is shown in Figure 8. The matching of their *absolute* activity, a factor of over 100 in surface area values, is certainly striking and very significant. The above conclusions on the importance of hydroxyl ions as precursors to the formation of active centers are also in agreement with the observed rise in the activity of well crystallized nickel spinels upon treatment with water vapor at 450°.[3]

Acknowledgments. The authors wish to thank Dr. F. S. Stone for valuable discussions and for critically reading the manuscript and Dr. L. Piselli for the help given in performing the reduction experiments. The financial support of SNAM-PROGETTI is also gratefully acknowledged.

Vapor Phase Charge-Transfer Complexes. V. The Blue-Shifted Iodine Band

by Milton Tamres* and S. N. Bhat

Chemistry Department, University of Michigan, Ann Arbor, Michigan 48104 *(Received August 10, 1970)*

Publication costs assisted by the National Science Foundation

A search for the blue-shifted iodine band in the vapor phase was made on the system diethyl sulfide–iodine using more favorable conditions to observe complexation than those previously attempted. There is found a pronounced enhancement in absorbance of the iodine visible band toward the blue region, and the absorbance is markedly temperature dependent. The first characterization of a blue-shifted iodine band in the vapor phase is given.

Introduction

Charge-transfer (CT) complexes of iodine in solution show a characteristic blue shift of the iodine visible band. This shifted band often has been used to determine the thermodynamic properties of the complexes, *e.g.*, with ethers[1] and with sulfides.[2] In Mulliken's view,[3] because the antibonding orbital in iodine has a larger effective size than the ground-state orbital, the blue shift is attributed to the larger exchange repulsion between the iodine molecule in the excited state and the adjacent donor. On this basis, one would expect to see the blue shift in the vapor phase as well as in solution.

In vapor studies to date, evidence for the presence of the blue-shifted iodine band has been mostly negative or not conclusive. For mixtures of ether–iodine, an effect has been reported on the long wavelength portion of the iodine band where there is band structure[4] (*i.e.*, above ~500 mμ), but not in the continuum part of the spectrum.[5,6] For the stronger sulfide–iodine complexes, there is indication of a small effect but the existence of a blue-shifted band has not been definitely established.[7–9] A slight, rather uniform enhancement in absorbance at wavelengths shorter than 480 mμ has been noted for thiacyclopentane–iodine.[8] In a brief, more recent report, some enhancement in absorbance has been stated for iodine in the presence of several donors (diethyl sulfide, diethyl ether, triethylamine, and ammonia), with a comment that the shifted band must be quite broad.[9]

Several explanations have been offered for the lack of confirmation and identification of the blue-shifted band in the vapor phase: (1) the extinction coefficient of the complexed band (ϵ_{I_2-comp}) in solution compared to vapor may be greatly enhanced[8] by a cage effect of solvent molecules[5,7] which would decrease the intermolecular distance between donor and acceptor,[10,11] and hence increase orbital overlap; (2) freer rotation in the vapor phase allows for less favorable donor–acceptor orientation with smaller ϵ_{I_2-comp}, thereby diminishing the average value of ϵ_{I_2-comp};[12] (3) the geometry of the complexes may be different in the two phases;[8,13] and (4) complexes with electronically excited iodine should not be observed in the vapor.[14]

This problem has been reexamined for the system diethyl sulfide–iodine by going to more favorable conditions to observe complexation. In this paper, positive evidence is presented for the existence of the blue-

(1) M. Brandon, M. Tamres, and S. Searles, *J. Amer. Chem. Soc.*, **82**, 2129 (1960).

(2) M. Tamres and S. Searles, *J. Phys. Chem.*, **66**, 1099 (1962).

(3) R. S. Mulliken, *Recl. Trav. Chim. Pays-Bas*, **75**, 845 (1956).

(4) C. A. Goy and H. O. Pritchard, *J. Mol. Spectrosc.*, **12**, 38 (1964).

(5) F. T. Lang and R. L. Strong, *J. Amer. Chem. Soc.*, **87**, 2345 (1965).

(6) E. I. Ginns and R. L. Strong, *J. Phys. Chem.*, **71**, 3059 (1967).

(7) M. Tamres and J. M. Goodenow, *ibid.*, **71**, 1982 (1967).

(8) M. Kroll, *J. Amer. Chem. Soc.*, **90**, 1097 (1968).

(9) C. N. R. Rao, G. C. Chaturvedi, and S. N. Bhat, *J. Mol. Spectrosc.*, **33**, 554 (1970).

(10) J. Prochorow and A. Tramer, *J. Chem. Phys.*, **44**, 4545 (1966).

(11) P. J. Trotter, *J. Amer. Chem. Soc.*, **88**, 5721 (1966).

(12) O. K. Rice, *Int. J. Quantum Chem., Symp.*, **2**, 219 (1968).

(13) R. S. Mulliken and W. B. Person, "Molecular Complexes," Wiley-Interscience, New York, N. Y., 1969, p 161.

(14) E. M. Voigt, *J. Phys. Chem.*, **72**, 3300 (1968).

shifted band and the first characterization of such a band is given.

Experimental Section

Procedure. The experimental procedure for filling the gas cell with weighed amounts of reagent sealed in break-seal tubes has been described previously.[8,15] The concentration of iodine was determined from its absorption in the visible region (at 480 mμ, $\epsilon = 350 \pm 2$ l. mol^{-1} cm^{-1}). This determination agreed with that calculated from the known volume of the cell and the weighed sample of iodine. The weight of iodine used was 12.3 ± 0.1 mg. The volume of the cell was ~900 ml, varying only slightly from one run to another because of the small differences in the sizes of the break-seal tubes. The cell path was 50.0 cm, determined with a Wild cathetometer.

Materials. The source and purification of iodine and of *n*-heptane has been described previously.[1] The diethyl sulfide (Eastman Organic) was distilled and the middle cut was taken. Vapor phase chromatography showed the sample to be better than 99.9% pure.

Results and Discussion

In Figure 1 there are shown the spectra of iodine vapor alone (curve 1: $[I_2] = 5.33 \times 10^{-5}$ *M* at 85°) and of the same iodine in the presence of *n*-heptane ($[n\text{-}C_7H_{16}] = 3.93 \times 10^{-2}$ *M*; curve 2 at 120°, and curve 3 at 135°). The variation of absorbance at the higher temperatures is attributable to a temperature broadening and is not due to an effect of the *n*-heptane. Broadening of the iodine band over a wide temperature range has been reported by Sulzer and Wieland.[16] It was studied in this work in order to determine the extinction coefficient of free iodine, ϵ_{I_2}, over a limited temperature range. The region near 480 mμ is fairly insensitive to temperature variation over this limited range[15] or to the presence of foreign gases at this and shorter wavelengths.[4,5,15] Therefore, this region is useful in determining iodine concentrations.[5,15]

Spectra of iodine vapor alone and in the presence of varying concentrations of diethyl sulfide (6.55×10^{-3} *M*, 1.91×10^{-2} *M*, and 3.88×10^{-2} *M*) are shown in Figure 2. The conditions are much more favorable for observation of complex formation than had been tried previously. The iodine concentration is ~3 times as large and the sulfide concentration ~23 times as large as used by Kroll,[8] although his path cell was about twice as long. The concentrations are closer to those of Tamres and Goodenow,[7] but the path cell in the present study was five times as long.

The enhancement in absorbance (Figure 2) on the low wavelength side of the iodine band in the presence of diethyl sulfide is quite pronounced and increases with increasing sulfide concentration. Considering that *n*-heptane at these pressures does not affect the iodine band in this region, it is apparent that the enhancement is due to complexed iodine. No maximum is observed in the absorbance curves for the mixtures, but inspection of the difference in absorbance of the iodine band in the presence and absence of diethyl sulfide reveals that the difference passes through a maximum. Taking the difference between curve 4 (run at 115°) and curve 1 (after correction for temperature broadening from 85° to 115°) results in the dashed curve with a maximum at ~445–450 mμ.

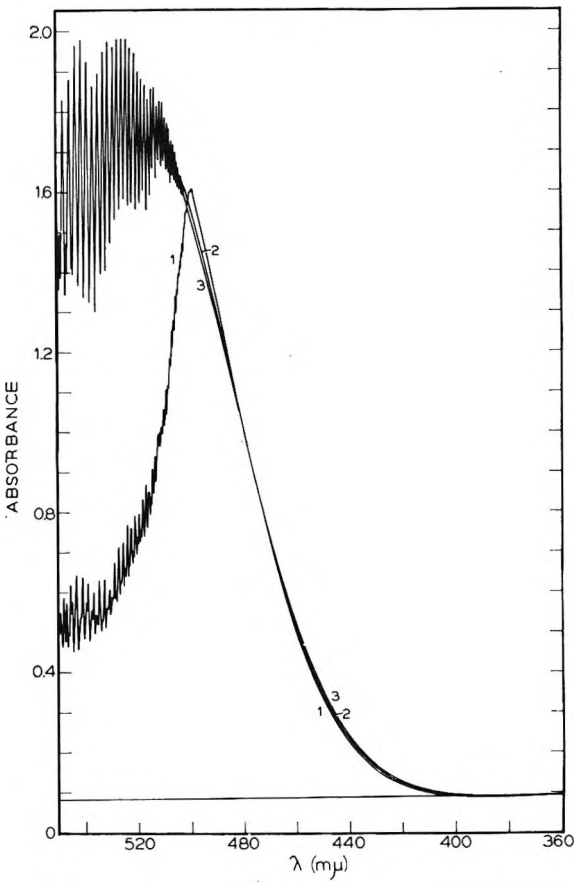

Figure 1. Absorption spectra of iodine (5.33×10^{-5} *M*) and *n*-heptane (3.93×10^{-2} *M*) mixtures: (1) iodine alone at 85°; (2) iodine + *n*-heptane at 120°; (3) iodine + *n*-heptane at 135°; 50.0-cm cell.

Further evidence that the blue-shifted enhancement is due to complexation comes from the temperature dependence study shown in Figure 3. The decrease in absorbance with increase in temperature is opposite in trend to that of temperature broadening, but is in accord with having an equilibrium between complexed and free iodine.

In solution, increasing the concentration of diethyl sulfide for a fixed concentration of iodine gives a series of curves that go through an isosbestic point at 493 mμ.[17] An increase in absorbance of the complexed

(15) M. Tamres and J. Grundnes, *J. Amer. Chem. Soc.*, 93, 801 (1971).

(16) P. Sulzer and K. Wieland, *Helv. Phys. Acta*, 25, 653 (1952).

(17) J. M. Goodenow, Ph.D. Thesis, University of Michigan, Dec 1965.

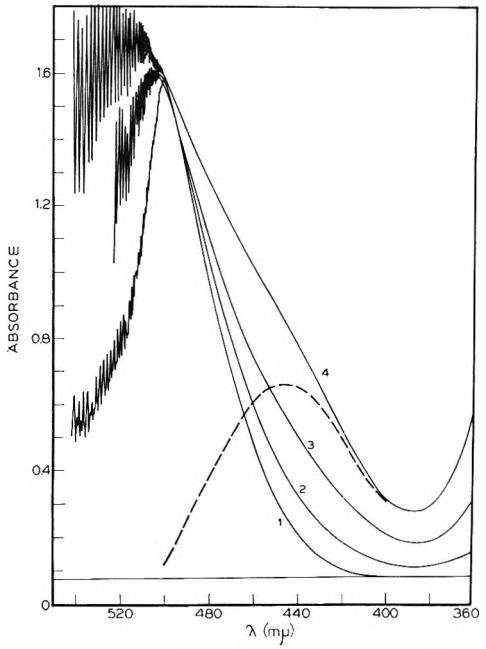

Figure 2. Donor concentration dependence of absorbance for diethyl sulfide–iodine (5.33×10^{-5} M) at 115°: (1) iodine alone (at 85°); (2) iodine + sulfide (6.55×10^{-3} M); (3) iodine + sulfide (1.91×10^{-2} M); (4) iodine + sulfide (3.88×10^{-2} M); 50.0-cm cell. Dashed curve is the difference between curve 4 and curve 1 (corrected for temperature broadening to 115°).

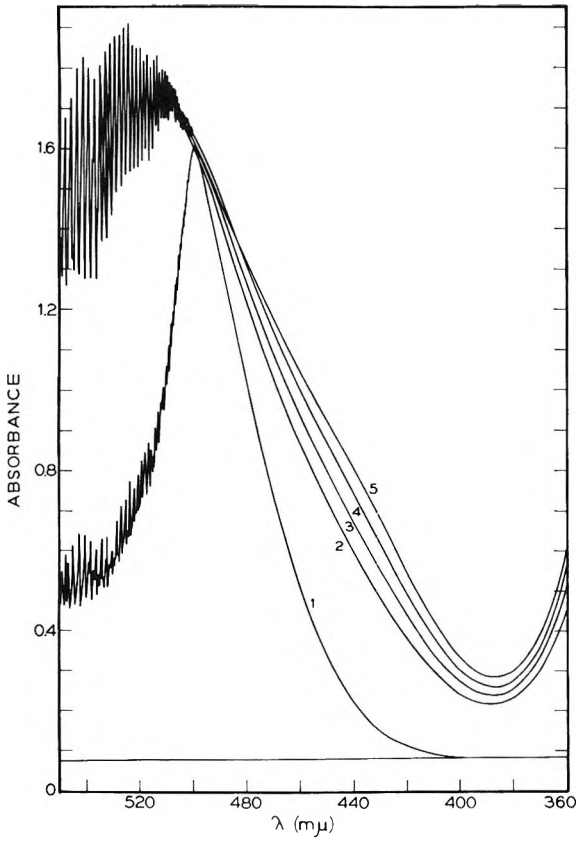

Figure 3. Temperature dependence of absorbance for diethyl sulfide (3.88×10^{-2} M)-iodine (5.33×10^{-5} M): (5) 115°; (4) 120°; (3) 127°; (2) 135°; (1) iodine alone at 85°, 50.0-cm cell.

band is accompanied by a decrease in the free iodine band. This is not observed in the present vapor phase data, as is seen in Figure 2, and therefore does not lead to an identifiable isosbestic point. There is very little change in absorbance near the band maximum of iodine when sulfide is added, and at the highest sulfide concentration the absorbance of the mixture appears to be very slightly greater than that of the original iodine vapor at all wavelengths including the band maximum, in spite of the fact that part of the iodine now is complexed.

Resolution of the total absorbance into the component bands of free and complexed iodine depends on a knowledge of the equilibrium constant for complex formation, K, and of ϵ_{I_2}. The latter is readily calculated from the data such as those in Figure 1. Values at three temperatures are listed in Table I. They are slightly lower around the maximum compared to the data of Sulzer and Wieland.[16]

Table I: Extinction Coefficient[a,b] of Iodine in the Vapor Phase in the Visible Region at Several Temperatures

λ, mμ	$\epsilon_{60°}$, l. mol^{-1} cm^{-1}	$\epsilon_{90°}$, l. mol^{-1} cm^{-1}	$\epsilon_{120°}$, l. mol^{-1} cm^{-1}
400		1	1
405		2	3
410	(1)	2	3
415	4	6	7
420	7	9	12
425	13	16	20
430	22	24	28
435	32	36	42
440	48	52	57
445	66	71	76
450	90	95	101
455	118	125	131
460	151	158	164
465	192	199	204
470	238	247	253
475	290	298	304
480	349	351	352
485	406	405	404
490	470	464	461
495	531	522	516
500	570	563	555

[a] ϵ is the average value of several determinations for iodine in the concentration range 5.08–8.85 $\times 10^{-5}$ mol l.$^{-1}$. [b] Error limit is ±2 l. mol^{-1} cm^{-1}.

It is more difficult to establish a reliable value for K. Generally in the study of CT complexes, it is the $K\epsilon$ product that is well determined, but error in the separation of the terms can be appreciable.[18,19] For the

(18) W. B. Person, *J. Amer. Chem. Soc.*, **87**, 167 (1965).

(19) R. A. LaBudde and M. Tamres, *J. Phys. Chem.*, **74**, 4009 (1970).

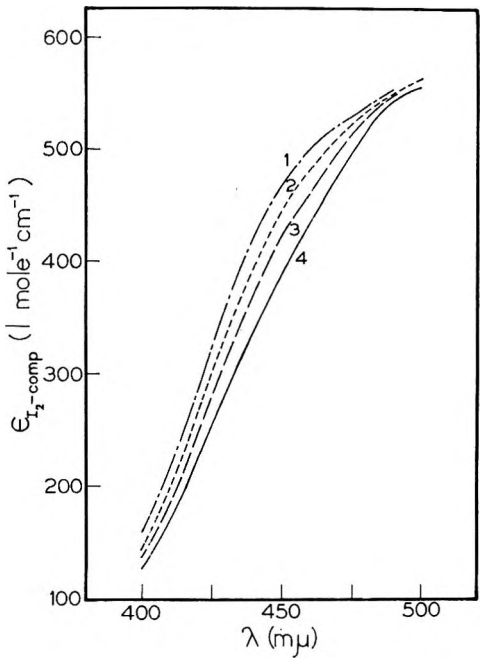

Figure 4. Resolved blue-shifted iodine band based on data of Kroll.[8]

two vapor phase studies on the diethyl sulfide–iodine complex that have been reported by Kroll[8] and by Tamres and Goodenow,[7] there is agreement within the limits of error in the values for the $K\epsilon$ product, and these results lead to agreement also in the determination of the change in internal energy on complexation, $\Delta E°$ (−7.6 and −7.5 kcal mol^{-1}, respectively). However, the values reported for the separate K and ϵ terms differ by a factor of ~3.5 (Kroll,[8] K_{373} = 58 l. mol^{-1}; and Tamres and Goodenow,[7] K_{373} = 16.5 l. mol^{-1}).

This difference in K has a pronounced effect in characterizing the blue-shifted iodine band. From the data of Kroll,[8] resolution of the total absorbance curves in Figure 3 produces the curves for the blue-shifted iodine shown in Figure 4. It is assumed in resolving the bands that ϵ_{I_2} is independent of the presence of added gases at the pressures used because no effect was observed in the presence of *n*-heptane. The curves in Figure 4 show no apparent band maximum, and extrapolation would give a maximum at a longer wavelength than for free iodine. This is not a normal characteristic of a blue-shifted band. Thus, if Kroll's data were valid, a modification in theory would be required.

Similar analysis at two temperatures based on the data of Tamres and Goodenow[7] produces the B set of curves in Figure 5. The difference from Figure 4 is quite marked and shows how dependent the shapes of the curves are on the value of K. Probably the best thermodynamic data presently available[20] are $K_{373} \simeq$ 11.5 l. mol^{-1} and $\Delta E° \simeq -8.3$ kcal mol^{-1}. These data support the earlier study of Tamres and Goodenow[7] which employed a quite different experimental procedure. Their use gives the set of curves marked A in Figure 5. This set will be discussed in characterizing the blue-shifted iodine band. The general conclusions would apply also to the B set, however, because the features of the two sets of curves are similar.

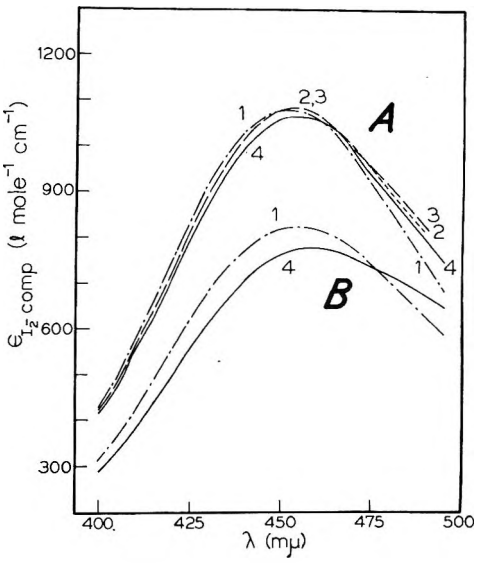

Figure 5. Resolved blue-shifted iodine band: set A, based on data of Tamres and Bhat;[20] set B, based on data of Tamres and Goodenow.[7]

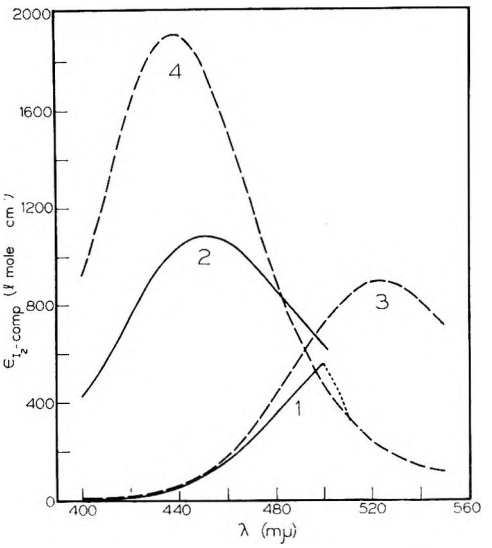

Figure 6. Extinction coefficients in the visible region for the system diethyl sulfide–iodine: vapor phase (solid line), (1) free iodine, (2) complexed iodine; *n*-heptane solution (dashed line), (3) free iodine, (4) complexed iodine.

The blue-shifted iodine in Figure 5 is more in line with theoretical expectation. There is a maximum at ~450–455 mμ, which is close to that of the difference curve in Figure 2. Only the region between 400 and 500

(20) This laboratory, study in progress on several sulfide–iodine complexes; to be published.

mμ was taken. At wavelengths longer than 500 mμ band structure appears. At wavelengths shorter than 400 mμ the absorbance rises again as a result of the contribution from the intense CT band with its maximum at 290 mμ.[7,8] The tail of the CT band probably contributes a little to the absorbance near 400 mμ, but not at 450 mμ. The variation of ϵ_{I_2-comp} with temperature is too small to be considered outside the range of experimental error.

The curves in Figure 5 have some interesting features. The band maximum is at a longer wavelength than that observed for the complex in *n*-heptane solution (λ_{max} 437 mμ).[2] This would seem reasonable. A solvent cage which reduces the intermolecular distance between donor and acceptor[10,11] should give an additional blue shift as a result of the greater interaction between the repulsive excited state of iodine and the ground state of the adjacent donor. In addition, at their respective vapor phase maxima, $\epsilon_{I_2-comp} > \epsilon_{I_2}$, which also is observed in solution. In fact the ratio $\epsilon_{I_2-comp}/\epsilon_{I_2}$ is not much different in the two phases, *i.e.*, ~1.9 in the vapor phase at 115° and ~2.1 in *n*-heptane solution at 25°. This may be seen in Figure 6, which gives the extinction coefficients as a function of wavelength for free and complexed iodine in both phases.

Figure 6 also makes clear why the isosbestic point is prominent in solution but is not observed in the vapor phase. Although the solvent enhances the intensity of both the free and complexed iodine bands, it affects their absorbance maxima in different ways. The band maximum of free iodine in the vapor phase is *red-shifted* in solution, whereas the band maximum of complexed iodine in the vapor phase is *blue-shifted* in solution. The greater overlap of the bands in the vapor phase, coupled with the increase in intensity of the complexed iodine relative to the free iodine, results in the extinction coefficient of the complexed iodine being larger than that of free iodine over the entire continuum range of the spectrum for free iodine, including the band maximum ($\lambda_{max} \simeq 500$ mμ). In solution, the free and complexed bands are separated to a sufficient extent to result in a crossing of the bands.

Acknowledgment. This research was supported by the National Science Foundation in part through Grant GP-9216, and in part through Grant GP-10367 to this department for the purchase of the Cary-14 spectrophotometer used in this study.

Nuclear Magnetic Resonance Spectra of Carbanions. II. Carbanions Produced from α-Methylstyrene and Cumyl Methyl Ether[1]

by Kensuke Takahashi,* Mikio Takaki, and Ryuzo Asami

Department of Synthetic Chemistry, Nagoya Institute of Technology, Gokiso-cho, Showa-ku, Nagoya, Japan
(Received January 30, 1970)

Publication costs borne completely by The Journal of Physical Chemistry

The pmr spectra of the title carbanions have been observed in a well separated shape suitable for first-order analysis. The excess charge of the carbanions, localized in the phenyl rings, is estimated from their chemical shifts and compared with that of 1,1-diphenylethylene dimer dianion. It was found that the spectrum of α-methylstyrene dimer dianion shows signals attributable to two different ortho protons at room temperature.

It was reported before that the aromatic proton spectrum of the 1,1-diphenylethylene dimer dianion can be observed in a well separated form suitable for first-order analysis.[2] Similar experiments have been extended to the carbanions produced from α-methylstyrene and cumyl methyl ether by following reactions 1 and 2.

$$2CH_3-\underset{\displaystyle C_6H_5}{\overset{}{C}}=CH_2 \xrightarrow[\text{in THF}]{\text{K-Na}} CH_3-\underset{\displaystyle C_6H_5}{\overset{}{\bar{C}}}-CH_2-CH_2-\underset{\displaystyle C_6H_5}{\overset{}{\bar{C}}}-CH_3 + 2K^+ \quad (1)$$

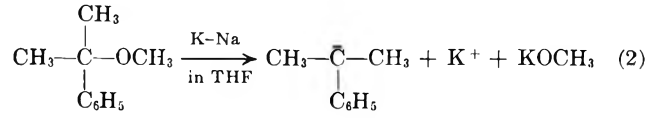

$$CH_3-\underset{\displaystyle C_6H_5}{\overset{\displaystyle CH_3}{C}}-OCH_3 \xrightarrow[\text{in THF}]{\text{K-Na}} CH_3-\underset{\displaystyle C_6H_5}{\overset{}{\bar{C}}}-CH_3 + K^+ + KOCH_3 \quad (2)$$

Experimental Section

α-Methylstyrene or cumyl methyl ether dissolved in THF was placed in contact with excess potassium–sodium alloy in a vacuum at room temperature for about 24 hr. The dark red solutions obtained were filtered, concentrated as far as possible, and then sealed into a 5-mm nmr sample tube. The concentration of the sealed solution was about 0.3 mol/l. or more. Pmr spectra were observed at 60 MHz with a Varian A-60A or a Hitachi H-60 spectrometer at room temperature. The chemical shifts were evaluated from the higher field peak of THF, used as an internal reference. This peak of THF was taken as 1.79 ppm from TMS.

Results and Discussion

A. Spectra of the Carbanions. Typical spectra and their chemical shifts are shown in Figure 1 and Table I, respectively. The well-separated signals allowed easy assignment. For example, the spectrum of the aromatic proton region of α-methylstyrene dimer dianion shown in Figure 1a consists of four parts. A triplet signal at the highest is easily assigned to the *para* protons, similar to that observed in 1,1-diphenylethylene dimer dianion.[2] The multiplet structure and intensity indicate that the two broad doublets at 4.80 and 5.38 ppm are due to the ortho protons, which are therefore nonequivalent in α-methylstyrene dimer dianion. The shape of the doublet at 4.80 ppm is a little different from that at 5.38 ppm because of overlapping of the carbon-13 satellite signal of the solvent at 4.83 ppm, as is shown in Figure 1c. The meta proton signals of α-methylstyrene dimer dianion seem to have two slightly different chemical shifts. An impurity signal near 7.15 ppm in Figure 1a is attributable to diphenylhexane, which is produced from the carbanion in contact with moisture. α-Methylstyrene dimer dianion treated with water gave 2,5-diphenylhexane, which shows pmr signals at 1.16 (doublet, J = 6.5 Hz), 1.44 (triplet-like multiplet), 2.56 (broad, probably multiplet), and 7.07 ppm in a carbon tetrachloride solution. The carbanion gives a singlet signal at 1.32 ppm, attributable to the methyl group, but 2,5-diphenylhexane gives a doublet (J = 6.5 Hz) at 1.21 ppm. The signal of the methyl protons in the carbanion therefore appears at lower field than those in the corresponding hydrocarbon. A similar observation has been made previously with methylene protons in 1,1-diphenylethylene dimer dianion.[2] This tendency may be ascribed to the change of hybridization in the carbon atom adjacent to the phenyl ring from sp^3 in hydrocarbons to near sp^2 in the carbanions. Cumyl carbanion produced from cumyl methyl ether shows a rather simple spectrum in the aromatic proton region, as shown in Figure 1b, except for two impurity peaks at 7.12 and 7.20 ppm. The methyl proton signal of the cumyl carbanion appears at 1.47 ppm as a singlet which changes to a doublet (J = 6.5 Hz) at 1.29 ppm in THF on treatment with a small amount of H_2O. The cumyl carbanion treated with

(1) Presented partly before the 20th Annual Meeting of the Chemical Society of Japan, Tokyo, April 1967, Abstract Vol. 1, p 160.

(2) K. Takahashi and R. Asami, *Bull. Chem. Soc. Jap.*, **41**, 231 (1968).

Table I: The Proton Chemical Shifts of the Carbanions Produced from 1,1-Diphenylethylene, Cumyl Methyl Ether, and α-Methylstyrene in Contact with Excess Alkali Metals in THF, in Ppm at 60 MHz

Starting material	Metal used	Assignment: Phenyl: Ortho	Meta	Para	Others
1,1-Diphenyl-ethylene	Potassium	7.01	6.55	5.67	2.48 (CH_2)
	Sodium	7.18	6.61	5.75	2.45 (CH_2)
	Lithium	7.03	6.49	5.66	2.51 (CH_2)
α-Methylstyrene	Potassium	4.80	5.89	4.20	1.32 (CH_3)
		5.38	6.01		
Cumyl methyl ether	Potassium	5.16	6.115	4.39	1.47 (CH_3)

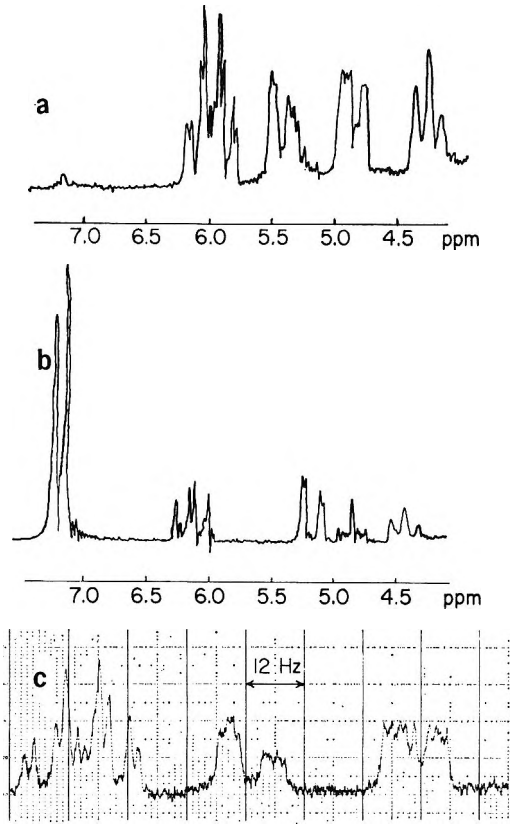

Figure 1. The spectra in the region of aromatic protons of the carbanions produced from α-methylstyrene (a) and cumyl methyl ether (b) in contact with excess potassium sodium alloy in THF. (c) An expanded spectrum of a part of (a). Applied radiofrequency increases from right to left near 60 MHz at a constant magnetic field.

D_2O also shows the methyl signal at 1.29 ppm (triplet, J = 1 Hz). The methyl signal of cumyl carbanion appears at a lower field than that of the corresponding hydrocarbon, similar to the case of α-methylstyrene. The extracts obtained from the solution of the cumyl carbanion treated with H_2O give impurity signals at 1.63 and 7.04 ppm in addition to the signals of cumene, in a carbon tetrachloride solution. These peaks are assigned to the methyl and the phenyl protons. The singlet structure of the methyl signal shows the absence of a proton at the adjacent carbon atom. The substance giving the signals at 1.63 and 7.04 ppm is therefore suggested to be 2,3-dimethyl-2,3-diphenylbutane. This compound may be obtained by the dimerization of cumyl radical, which is estimated to be present as an intermediate in reaction 2.

These experimental results are summarized as follows. (1) The aromatic proton shifts of the carbanions produced from α-methylstyrene and cumyl methyl ether are in the order of meta, ortho, and para positions from low to high field; these are different from those of the carbanions produced from 1,1-diphenylethylene, which are in the order of ortho, meta, and para positions. (2) α-Methylstyrene dimer dianion shows two nonequivalent ortho phenyl proton chemical shifts but 1,1-diphenylethylene dimer dianion does not at room temperature, even though the phenyl group seems to be bulkier than the methyl group. These two points will be discussed in the two following sections.

B. Comparison of the Extra Charges in the Carbanions. Since the carbanions studied here have extra charges coming from alkali metals, the charge distribution in the molecules is interesting from a theoretical point of view. If we assume that the chemical shift of an aromatic proton of the carbanions corresponds to the charge density of the adjacent carbon atom, we can

Table II: The Proton Chemical Shifts of the Hydrocarbons Produced from the Corresponding Carbanions in Contact with Water in THF, in Ppm at 60 MHz

Compd	Solvent	Assignment: C_6H_5	CH	CH_2	CH_3
1,1,4,4-Tetraphenyl-butane	THF	7.20	[a]		
	CCl_4	7.14	3.88	2.00	
2,5-Diphenylhexane	THF	7.15		1.50	1.21
	CCl_4	7.07	2.56	1.44	1.16
Cumene	THF	7.20			1.29
	CCl_4	7.14	2.865		1.24
2,3-Dimethyl-2,3-di-phenylbutane (estimated)	THF	7.12			
	CCl_4	7.04			1.63

[a] The chemical shift in the blank space is not available because of overlapping of the large solvent peaks.

Table III: Charge Distribution in the Carbanions Produced from 1,1-Diphenylethylene, Cumyl Methyl Ether, and α-Methylstyrene in Contact with Excess Alkali Metals in THF, in Units of the Absolute Value of the Charge of an Electron

Starting material	Metal used	Position			Sum for a phenyl ring
		Ortho	Meta	Para	
1,1-Diphenylethylene[a]	Potassium	−0.02	−0.065	−0.155	−0.325
	Sodium	−0.00	−0.06	−0.145	−0.265
	Lithium	−0.015	−0.07	−0.155	−0.325
α-Methylstyrene	Potassium	−0.205[b]	−0.12[b]	−0.295	−0.945
Cumyl methyl ether	Potassium	−0.205	−0.105	−0.28	−0.90

[a] Corrected for ring current effect using the mean values obtained for model I in Table IV. [b] These are average values since the two ortho and meta positions in each ring are not equivalent.

estimate the charge density on the carbon atom from the observed shifts. On treatment with H_2O, the carbanions form corresponding hydrocarbons, whose chemical shifts are given in Table II. When we want to estimate the charge distribution in the carbanions, a suitable reference compound must be chosen, for example the starting materials, the corresponding hydrocarbons produced from the carbanions, or another such as benzene. In this article we prefer to take the hydrocarbons produced from the carbanions as reference compounds. The chemical shifts of the hydrocarbons produced from the corresponding carbanions in contact with water are given in Table II. The aromatic proton signals of the carbanions shift to higher field than those of the reference compounds, due to the delocalization of the excess charge, as estimated in Table III. This estimation of the charge delocalization is not exact because effects other than those due to charge and ring current are neglected. At the early stage of this study we neglected the ring current effect in estimating the charge distribution in 1,1-diphenylethylene dimer dianion, because phenyl protons show almost the same chemical shifts in cumene, 2,5-diphenylhexane, and 1,1,4,4-tetraphenylbutane, the products of the reaction between the carbanions and water (see Table II). However, the configuration of the carbon atom adjacent to the phenyl ring in these hydrocarbons is sp^3 hybridized. A problem lies in the configuration of the carbon atom adjacent to the phenyl ring in the carbanions. A referee of this journal suggested that the ring current effect cannot be neglected in the estimation of the charge density distribution in these carbanions because the ortho protons give an abnormal lower-field shift in 1,1-diphenylethylene dimer dianions than those of the carbanions prepared from α-methylstyrene and cumyl methyl ether. We agreed with his comment and estimated this ring current effect, which is dependent upon the angles of twist θ_1 and θ_2 in Figure 2. Three typical models, I, II, and III, are taken for the estimation of the ring current effect. The angles of twist, θ_1 and θ_2, are measured from a standard position in the molecular plane. Both θ_1 and θ_2 in I are taken as the same magnitude, 30°, and

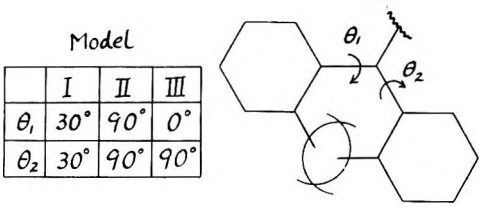

Figure 2. Models for estimating the ring current effects in 1,1-diphenylethylene dimer dianion.

in II, 90°, but θ_1 and θ_2 in III are 0° and 90°, respectively. Geometric arrangement of the atoms in 1,1-diphenylethylene dimer dianion is estimated with the assumption that the carbon atom adjacent to the phenyl ring is sp^2 hybridized. The C–C and C–H bond lengths are taken as 1.39 and 1.08 Å, respectively, in the phenyl ring, and the C–C bond length between the phenyl ring and the adjacent carbon is 1.51 Å. The twist angles of 30° in I are determined by taking the distance of two nearest ortho protons in two different twisted phenyl rings as 2.4 Å, which is equal to twice the van der Waals radius of hydrogen. This twist angle in I is approximately coincident with the equilibrium angle estimated from the extended Hückel calculation.[3] With these assumptions, the ring current effects are estimated for the three models, based upon Johnson–Bovey's calculations.[4] The results in Table IV show that model III gives a shielding effect at the ortho and meta positions and therefore this model cannot explain the experimental results shown in Table I. The ring current effects at the ortho protons in model I are negligibly small as a mean, consistent with Sandel and Freedman's statement in the case of diphenylmethylcarbanion.[5] If we assume a shorter distance of 2 Å between the two nearest ortho protons in the two phenyl rings and a smaller twist angle of 24°, the ring current effect at the ortho protons amounts to 0.13 ppm as a

(3) R. Hoffman, R. Bissell, and D. G. Farnum, *J. Phys. Chem.*, **73**, 1789 (1969).

(4) C. E. Johnson and F. A. Bovey, *J. Chem. Phys.*, **29**, 1012 (1958).

(5) V. R. Sandel and H. H. Freedman, *J. Amer. Chem. Soc.*, **85**, 2328 (1963).

Table IV: An Evaluation of the Ring Current Effects on Chemical Shift for the Aromatic Protons in the 1,1-Diphenylethylene Dimer Dianion in Ppm. Positive or Negative Sign Shows the Shift to Lower or Higher Field, Respectively

	Model			
			III	
Position	I	II	$\phi_\perp$	$\phi_\parallel$
Ortho (near)	−0.158	0.206	0.098	−0.900
Ortho (far)	0.160			0.153
Meta (near)	−0.007	−0.006	<0.08[a]	−0.168
Meta (far)	<0.15[a]			<0.05[a]
Para	<0.07[a]	−0.017	<0.10[a]	−0.017

[a] These values cannot be evaluated from the Johnson–Bovey table because of the large distances involved and these values were neglected in correcting the charge densities given in Table III.

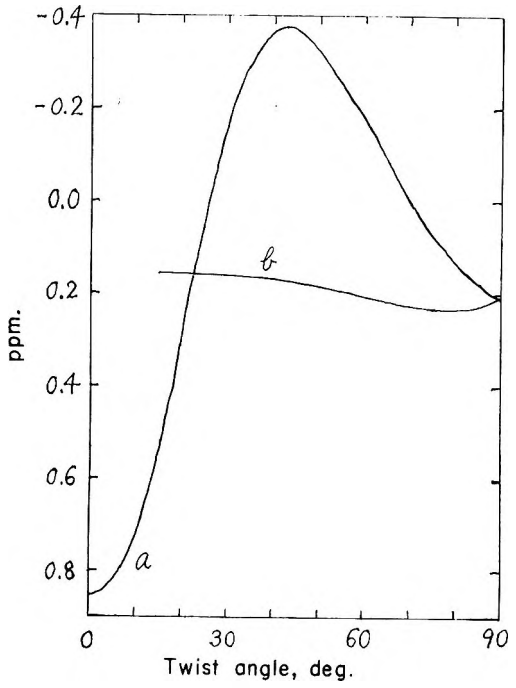

Figure 3. Dependence of the ring current effects (ordinate) at the ortho protons in the 1,1-diphenylethylene dimer dianion on the twist angle (abscissa). Curves a and b are referred to the near and far ortho protons, respectively, from the adjacent phenyl ring. Negative sign shows the shift toward higher field.

mean value. Since the magnitude of twist angle is important in estimating ring current effects, the calculation was extended to all possible twist angles between 0 and 90°. The resulting correlation (Figure 3) shows that twist angles between 30 and 60° give a shielding effect at the ortho protons as a mean value and that the ring current effect is most sensitive to the twist angle between 20 and 30°. Exact twist angles in the carbanions studied here are not known. We prefer to take 30° at this moment, as shown in the model I, but much caution is necessary since these estimations of the ring current effects were made with the assumption that the carbon atom adjacent to the phenyl ring is sp^2 hybridized. Another example of an sp^2 hybridized hydrocarbon in this study is 1,1-diphenylethylene itself, which gives chemical shifts for the phenyl protons at 7.33 ppm in THF and 7.24 ppm in CCl_4. The signal of its phenyl ring protons shows almost a singlet structure. This can be ascribed to the fact that the chemical shifts of these phenyl protons are comparable in magnitude to the coupling constants of 8 ∼ 9 Hz. Therefore the ring current effects estimated in model I seem to be of the correct order. This discussion may be applicable to the phenyl proton shifts in the sp^3 hybridized hydrocarbons as shown in Table II.

It is established that in simple aromatic systems the proton chemical shift is directly proportional to the excess π electron density on the carbon atom to which the proton is bonded.[6] The proportionality constant for the estimation of the charge density is taken to be 10 ppm/electron. Estimated charges on the phenyl ring carbons of the α-methylstyrene dimer dianion are very close to those of the cumyl carbanion and different from those of the 1,1-diphenylethylene dimer dianion. This difference may be accounted for by the number of phenyl groups available to a unit of excess charge. The α-methylstyrene dimer dianion and the cumyl carbanion have one phenyl ring for a unit of excess charge. In these cases, the localization of the charge on the phenyl ring is more than 90% of a unit, as shown in the last column in Table III. This seems too large. The magnitude of the localized charge in the α-methylstyrene dimer dianion and the cumyl carbanion decreases in the order of para, ortho, and meta positions. The 1,1-diphenylethylene dimer dianion has two phenyl rings for a unit of excess charge, and the magnitude of the localized charge decreased in the order of para, meta, and ortho positions. Their sum for one phenyl ring is about 30% of a unit. The location of the remaining 40% cannot be estimated at present. Carbon-13 resonances of these carbanions may give a more direct answer to this problem. The estimated charges in the cumyl carbanion and the α-methylstyrene dimer dianion show higher localization at the ortho and para positions than those in benzyllithium obtained by Sandel and Freedman, but are consistent with their results for the meta position.[5] The estimated charges in the 1,1-diphenylethylene dimer dianion are consistent with those of diphenylmethyllithium in the meta and para positions but show lower localization in the ortho position.[5] A comparison of these experimental results with calculations was done by Sandel and Freedman.[5] The simple Hückel LCAOMO predicts a nonbonding orbital in these odd alter-

(6) (a) G. Fraenkel, R. E. Carter, A. McLachlan, and J. H. Richard, *J. Amer. Chem. Soc.*, 82, 5846 (1960); (b) T. Schaefer and W. G. Schneider, *Tetrahedron Lett.*, No. 14, 468 (1961).

nate hydrocarbons, whose calculated charge densities are inconsistent with the experimentally evaluated values, especially at the meta positions.

Another point of interest is a comparison of the observed charge distributions of the carbanions and the corresponding carbonium ions as was done in the case of perinaphthene negative and positive ions.[7] The spectra of the perinaphthenyl carbanion and carbonium ions are mirror images of each other. The observed data for the cumyl carbanion in this study are compared with those of the cumyl cation studied by Olah and Farnum.[8] Farnum's assignment shows that the chemical shifts of the aromatic protons of the cumyl cation are in the order of ortho, para, and meta positions from the lower- to the higher-field side, *i.e.*, not a mirror image relationship to the cumyl carbanion spectrum. A similar nonmirror image relationship has been also reported for triphenylmethyl anion and cation.[5]

C. Nonequivalent Ortho Positions in the α-Methylstyrene Dimer Dianion. As Table I shows, the difference between the two ortho phenyl proton shifts in the α-methylstyrene dimer dianion is about 0.58 ppm. Although this nonequivalence has not been observed in the spectrum of 1,1-diphenylethylene dimer dianion at room temperature,[2] it has recently been observed in 3,5-dideuteriophenylallyllithium at −58° by Sandel, McKinley, and Freedman.[9] They attributed this nonequivalency to the inhibition of rotation around the bond between the phenyl ring and its adjacent carbon. The phenyl ring, the α-methyl group, and the α-carbon atom in the α-methylstyrene dimer dianion seem to prefer to take their positions in a plane because of resonance stabilization, but the two phenyl rings connected to the α-carbon in the 1,1-diphenylethylene dimer dianion cannot be coplanar due to the increased steric hindrance of the phenyl ring relative to the methyl group. From a comparison of experimental results, nonequivalency of two ortho phenyl protons seems to require coplanarity of the phenyl ring with its adjacent conjugated part of the molecule such as the ethylenyl or allyl group. The nonequivalency of the ortho phenyl protons is then caused by the absence of symmetry perpendicular to the phenyl ring through the α-carbon and the para carbon. This nonequivalency will be lost in the presence of free rotation around the bond between the phenyl ring and the α-carbon. The difference between the two ortho phenyl proton shifts in the α-methylstyrene dimer dianion is almost the same as that observed in 3,5-dideuteriophenylallyllithium.[9] The cause of this chemical shift difference may be magnetic anisotropy of neighboring groups or a different charge localization. The difference of about 0.6 ppm accidentally fits the charge densities in diphenylmethyl carbonium ion calculated by SCFMO.[10] The experimental results are not enough to establish this point, however, and studies of various carbanions produced from phenyl-substituted ethylenes are being undertaken.

In conclusion two things must be noted. First, a necessary condition for the nonequivalency of two ortho phenyl protons seems to be coplanarity between the phenyl ring and its conjugated side-chain group. Second, the ortho phenyl protons in 1,1-diphenylethylene dimer dianion show abnormal low field shifts as compared with those of the cumyl carbanion and of the α-methylstyrene dimer dianion. This low-field shift of the ortho phenyl protons cannot be explained by the ring current effect of the adjacent phenyl ring. Another interpretation is necessary. This kind of low-field shift is also observed in triphenylmethyl carbanion but not in benzyl carbanion.[5] It must be noted, therefore, that this abnormal low-field shift is observed in compounds which have two or more phenyl rings at the α carbon. The ortho phenyl protons in the di- and triphenylcarbonium ions show abnormal shifts in opposite directions. The high-field shifts in the carbonium ions are ascribed to the ring current effect of the neighboring phenyl group.[11] If these shifts are explained only by the ring current effects, the ring current effects in the carbonium ions must be opposite in direction to those in the carbanions. This is quite interesting. An increase of the twist angle seems to cause high-field shifts in these compounds, as shown in Figure 3. If this interpretation is operative, carbonium ions and carbanions must be appreciably different in configuration. Larger twist angles in carbonium ions than those in carbanions could account for reversed ring current effects. An extended Hückel calculation has shown that the twist angles in the di- and triphenylmethyl carbanions are smaller than the corresponding cations in equilibrium,[3] but only by some 5 degrees. Therefore the magnitude of the observed abnormal shifts at the ortho protons in the carbanions and the carbonium ions cannot be explained by the ring current effect of the adjacent phenyl rings only. Another interpretation is the "charge redistribution" effect. If two like charges at the ortho positions in two phenyl rings are allowed to stabilize by dispersal to the meta or para positions, the abnormal low-field shifts of the ortho protons in the diphenyl or triphenylmethyl carbanions and the abnormal high-field shifts of those in the corresponding cations can be explained. This effect has been pointed out before by Sandel and Freedman as an inter-electron repulsion term.[4] Further

(7) W. G. Schneider, "Nuclear Magnetic Resonance in Chemistry," B. Pesce, Ed., Academic Press, New York, N. Y., 1965, p 63.

(8) (a) G. A. Olah, *J. Amer. Chem. Soc.*, **86**, 932 (1964); (b) D. G. Farnum, *ibid.*, **86**, 934 (1964); **89**, 2970 (1967).

(9) V. R. Sandel, S. V. McKinley, H. H. Freedman, *ibid.*, **90**, 495 (1968).

(10) A. Brickstock and J. A. Pople, *Trans. Faraday Soc.*, **50**, 901 (1954).

(11) G. Fraenkel and D. G. Farnum, "Carbonium Ions," G. A. Olah and P. v. R. Schleyer, Interscience, New York, N. Y., 1968, p 241.

studies are necessary before any quantitative treatment can be given.

Acknowledgments. The authors wish to thank Professor A. Tatematsu (Meijo University, Nagoya) and Y. Sasaki (Osaka University, Osaka) for their kindness in giving opportunities to use the nmr facilities, and the reviewer of this journal for giving some invaluable comments.

Hindered Rotation about the S_2C-NR_2 Bond in *N,N,N′,N′*-Tetraalkylthiuram Disulfides and Monosulfides

by Nancy K. Wilson

National Institute of Environmental Health Sciences, Research Triangle Park, North Carolina 27709 *(Received October 26, 1970)*

Publication costs assisted by the National Institute of Environmental Health Sciences

Hindered rotation about the S_2C-NR_2 bond in several tetraalkylthiuram disulfides and monosulfides was studied by variable temperature proton magnetic resonance. For mono- and disulfides having the same alkyl substituents, the barrier to rotation was higher for the monosulfides. The higher barrier for the monosulfides is attributed to both increased double-bond character of the C–N bond and greater steric hindrance to rotation about this bond.

Introduction

The existence of a barrier to rotation about the carbonyl carbon–nitrogen bond, due to the partial double-bond character of this bond, in systems having the configuration

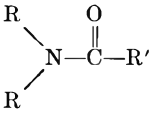

is well known. An early study of the barriers to internal rotation in these systems, using nmr techniques, was of *N,N*-dimethylformamide, carried out by Gutowsky and Holm.[1] Since then, numerous studies of amides by nuclear magnetic resonance have been reported. These are summarized in a review by Stewart and Siddall.[2] Recently, Drakenberg, Dahlqvist, and Forsén,[3] have measured the rotational barrier in *N,N*-dimethyltrichloroacetamide, employing nmr. These authors have compared their results with previous work and pointed out several sources of error inherent in approximate techniques for analysis of nmr data of this type.

The partial double-bond character of the carbon–nitrogen bond and thus restricted rotation in the analogous thiocarbonyl compounds is to be expected. Richards, Tarbell, and Hoffmeister[4] have reported nmr evidence of such hindered rotation in dithiocarbamoyl compounds. Recently, van der Werf and Engberts[5] studied a large number of alkyl-*N*-[(arylsulfonyl)-methyl]-carbamates, -thiolcarbamates, -thionocarbamates, and -dithiocarbamates by nmr and obtained evidence of restricted rotation for many of these. An nmr study of the *N,N,N′,N′*-tetraalkylthiuram disulfides and their Zn, Cd, and Hg complexes was carried out by Brinkhoff, Grotens, and Steggerda.[6] They reported evidence of hindered rotation about the partially double-bonded S_2C-NR_2 bond in tetramethyl-, tetraethyl-, and tetrabutylthiuram disulfide and their complexes, but did not give any values for the activation parameters.

In this study, the barriers to rotation about this bond were determined for tetramethylthiuram disulfide (I), tetraethylthiuram disulfide, and dicyclopentamethylenethiuram disulfide (III), and for tetramethylthiuram monosulfide (II) and dicyclopentamethylenethiuram monosulfide.

(1) H. S. Gutowsky and C. H. Holm, *J. Chem. Phys.*, **25**, 1228 (1956).

(2) W. E. Stewart and T. H. Siddall, III, *Chem. Rev.*, **70**, 517 (1970).

(3) T. Drakenberg, K. Dahlqvist, and S. Forsén, *Acta Chem. Scand.*, **24**, 694 (1970).

(4) J. L. Richards, D. S. Tarbell, and E. H. Hoffmeister, *Tetrahedron*, **24**, 6485 (1968).

(5) S. van der Werf and J. B. F. N. Engberts, *Recl. Trav. Chim. Pays-Bas*, **89**, 423 (1970).

(6) H. C. Brinkhoff, A. M. Grotens, and J. J. Steggerda, *ibid.*, **89**, 11 (1970).

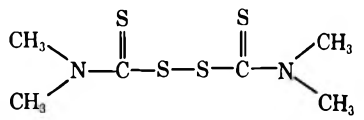

I

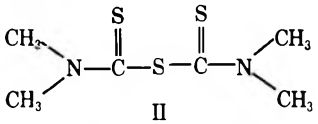

II

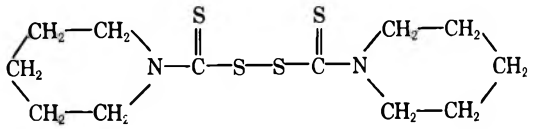

III

Experimental Section

The thiuram disulfides and monosulfides used were commercial reagent grade. Sharp melting points, when decomposition did not occur, and absence of extraneous peaks in the nmr spectra were taken as evidence of purity. Dicyclopentamethylenethiuram monosulfide was recrystallized from ethanol. Samples were 0.7 *M* solutions in deuterochloroform, with 1% v/v tetramethylsilane as an internal reference. A small amount of toluene was added to serve as a resolution standard. Spectra were run on a Varian HA-100 nmr spectrometer with the Varian temperature controller. Operation was in the internal lock mode, with tetramethylsilane as the lock signal. Temperature measurements were made before and after each spectrum was run, using a methanol sample to which a trace of hydrochloric acid had been added, and whose methyl–hydroxyl chemical shift difference as a function of temperature had been determined with a copper–constantan thermocouple. The temperature could be measured to $\pm 0.5°$ and was controlled to $\pm 1°$.

Infrared spectra were obtained on a Perkin-Elmer 621 grating infrared spectrophotometer.

Results

For tetramethylthiuram disulfide and monosulfide, the experimentally determined nmr line shapes were used to find values of τ, the lifetime of methyl protons in a particular site, as a function of temperature. Since at low temperatures, well below the slow rotation limit, only two methyl resonances were observed which then coalesced to a single peak when the temperature was increased, it can be assumed that both S_2C–NR_2 bonds in the molecule are equivalent. Thus the problem can be treated as an exchange of methyl protons between two sites: where the methyl group is cis to the thiocarbonyl group and where it is trans to the thiocarbonyl group across the C–N partial double bond.

A computer program was used to calculate the best

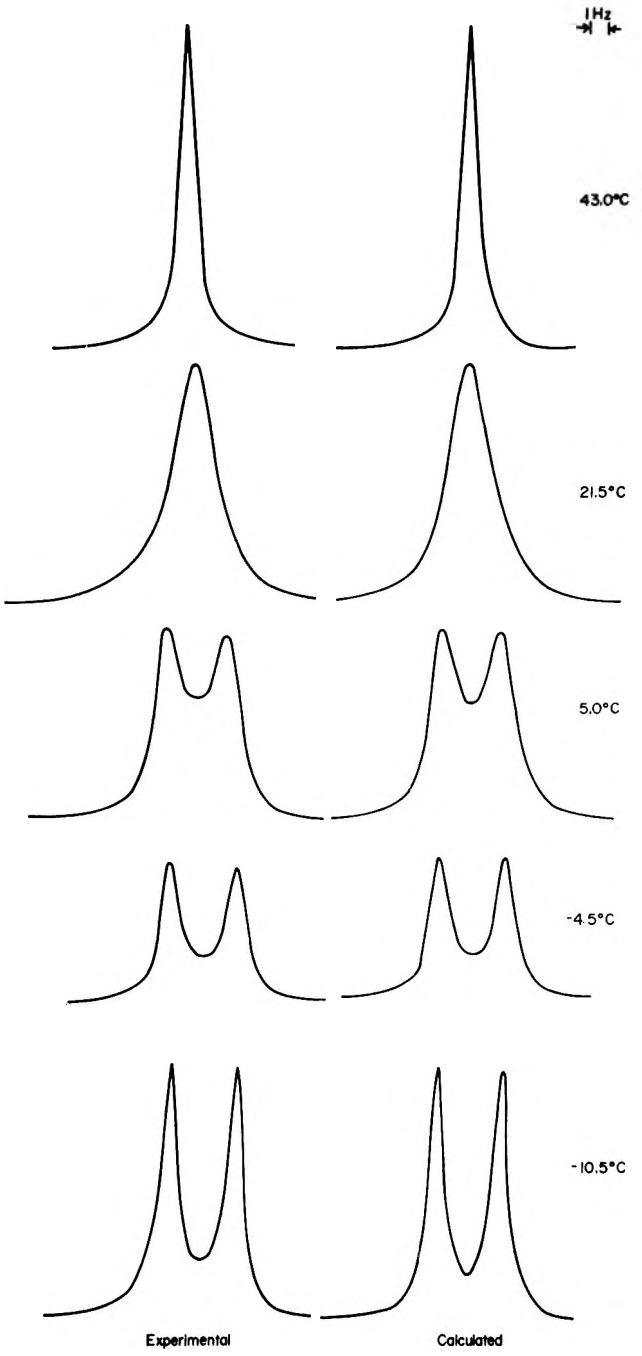

Figure 1. Some typical calculated and experimental line shapes for tetramethylthiuram disulfide.

value of τ at each temperature, from the least-squares fit of the experimental line shape. This program was based on the equation for the nmr line shape as a function of exchange lifetime developed by Gutowsky, McCall and Slichter,[7,8] as simplified by McConnell.[9] The effective value of T_2, due to both the natural line

(7) H. S. Gutowsky, D. W. McCall, and C. P. Slichter, *J. Chem. Phys.*, **21**, 279 (1953).

(8) J. A. Pople, W. G. Schneider, and H. J. Bernstein, "High Resolution Nuclear Magnetic Resonance," McGraw-Hill, New York, N. Y., 1959.

(9) H. M. McConnell, *J. Chem. Phys.*, **28**, 430 (1958).

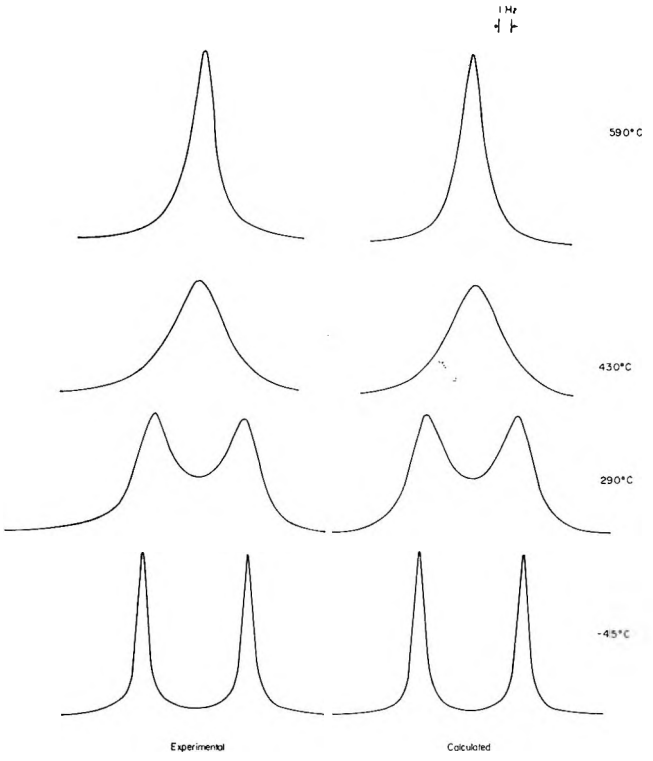

Figure 2. Some typical calculated and experimental line shapes for tetramethylthiuram monosulfide.

width and inhomogeneity broadening, was found to be the same at both the fast and slow rotation limits, and equal to 0.354 and 0.346 sec for tetramethylthiuram monosulfide and disulfide, respectively. The chemical shift difference between the two sites in the absence of exchange, $\delta\nu$, was found to show a small linear temperature dependence (about +0.01 Hz/deg) in the temperature region below the slow rotation limit. Therefore, the value of $\delta\nu$ at each temperature, in the range where τ was evaluated from the nmr line shape, was obtained from extrapolation of a plot of $\delta\nu$ *vs.* temperature at temperatures below the slow rotation limit. Figure 1 shows some typical calculated and experimental line shapes for tetramethylthiuram disulfide. Figure 2 shows line shapes for the monosulfide.

The rate constant for exchange of the methyls between the two sites is $k = 1/\tau$. A plot of the logarithm of this rate constant *vs.* $1/T$, where T is the absolute temperature, is linear. The slope gives the activation energy, E_a, for rotation about the partial double bond, from the Arrhenius equation

$$k = A \exp(-E_a/RT) \quad (1)$$

A is the frequency factor obtained from the intercept of the Arrhenius plot, and R is the gas constant. These plots are shown in Figures 3 and 4. The straight lines shown are the least-squares fits of the experimental data. The value of the enthalpy of activation, $\Delta H^{\ddagger}$, was obtained from the relation

$$\Delta H^{\ddagger} = E_a - RT \quad (2)$$

which holds true for liquids and solids.

The values of $\Delta F^{\ddagger}$ and $\Delta S^{\ddagger}$, the free energy and entropy of activation, were obtained from the Eyring equation

$$k = \frac{1}{\tau} = \kappa\frac{k_B T}{h} \exp(-\Delta F^{\ddagger}/RT) = \kappa\frac{k_B T}{h} \exp(-\Delta H^{\ddagger}/RT + \Delta S^{\ddagger}/R) \quad (3)$$

where κ is the transmission coefficient, assumed equal to 1, k_B is the Boltzmann constant, and h is Planck's constant.

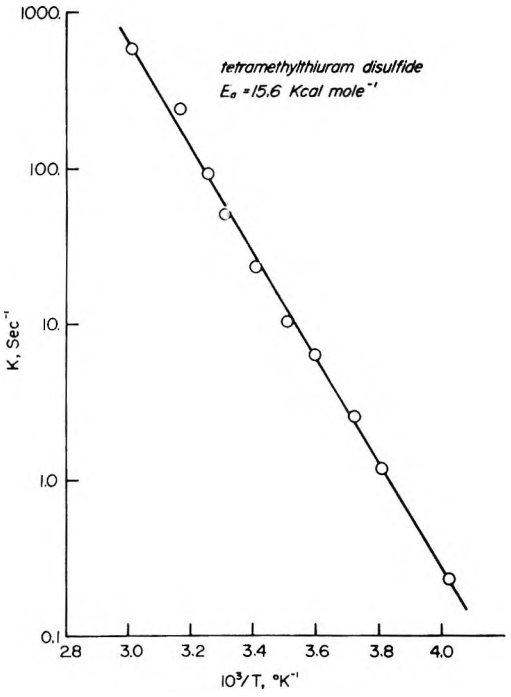

Figure 3. Arrhenius plot of the logarithm of the rate constant *vs.* the reciprocal of the absolute temperature for tetramethylthiuram disulfide.

For tetraethylthiuram disulfide and dicyclopentamethylene disulfide and monosulfide, the absence of resonances at low temperatures for alkyl groups on nitrogen singly bonded to the $-CS_2-$ again implies that both S_2C-NR_2 bonds are equivalent in these molecules. Thus these problems may be treated as exchanges of methylene protons attached to nitrogen in sites cis and trans to the thiocarbonyl group. The temperatures at which coalescence of the peaks corresponding to protons in the two sites occurs were determined. The value of the lifetime was then calculated from the relationship between τ at coalescence and the chemical shifts of protons in the two sites, ν_A and ν_B in Hz, for equal populations and lifetimes and signals whose

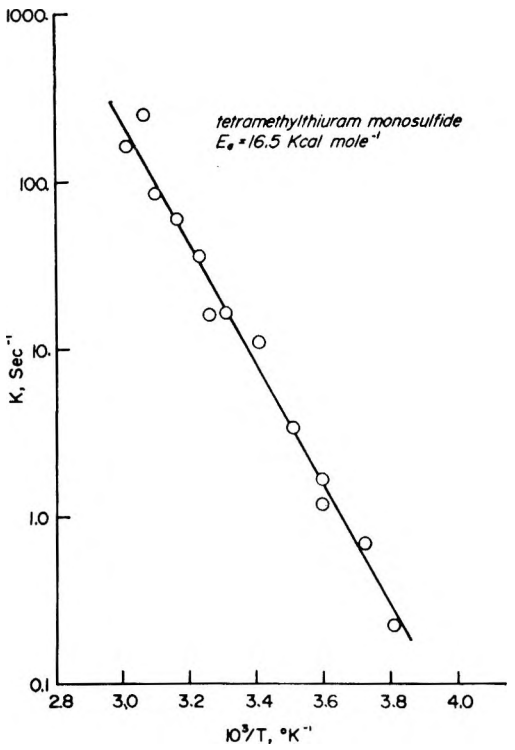

Figure 4. Arrhenius plot of the logarithm of the rate constant *vs.* the reciprocal of the absolute temperature for tetramethylthiuram monosulfide.

width in the absence of exchange is small compared to their separation.[8]

$$\tau_{\text{coalescence}} = \frac{\sqrt{2}}{2\pi(\nu_A - \nu_B)} \qquad (4)$$

Use of this equation, which is strictly valid only for two equally intense singlets having $1/T_2 = 0$, is expected to result in a value of τ slightly lower than the true value. The error thus introduced in the value of $\Delta F^{\ddagger}$ would make this value about 0.2 kcal/mol lower than the correct one at 25°.[10] From the lifetime calculated from this equation (4), activation parameters were then obtained from the Eyring equation (3). Typical spectra for these three compounds are shown in Figures 5–7.

For all the compounds, equal intensities of peaks corresponding to protons in the two sites were observed throughout the temperature range studied.

The results of the nmr experiments are summarized in Table I.

The degree of double-bond character of the S_2C-NR_2 bond should also affect the C⋯N stretching frequency in the infrared spectrum, with this vibration frequency increasing with increased bond order. Values of $\nu_{C\cdots N}$ are listed in Table II.

Discussion

The infrared C⋯N stretching frequencies are all shifted considerably toward higher frequency from the normal C–N region[11] of 900–1300 cm^{-1}, indicating a

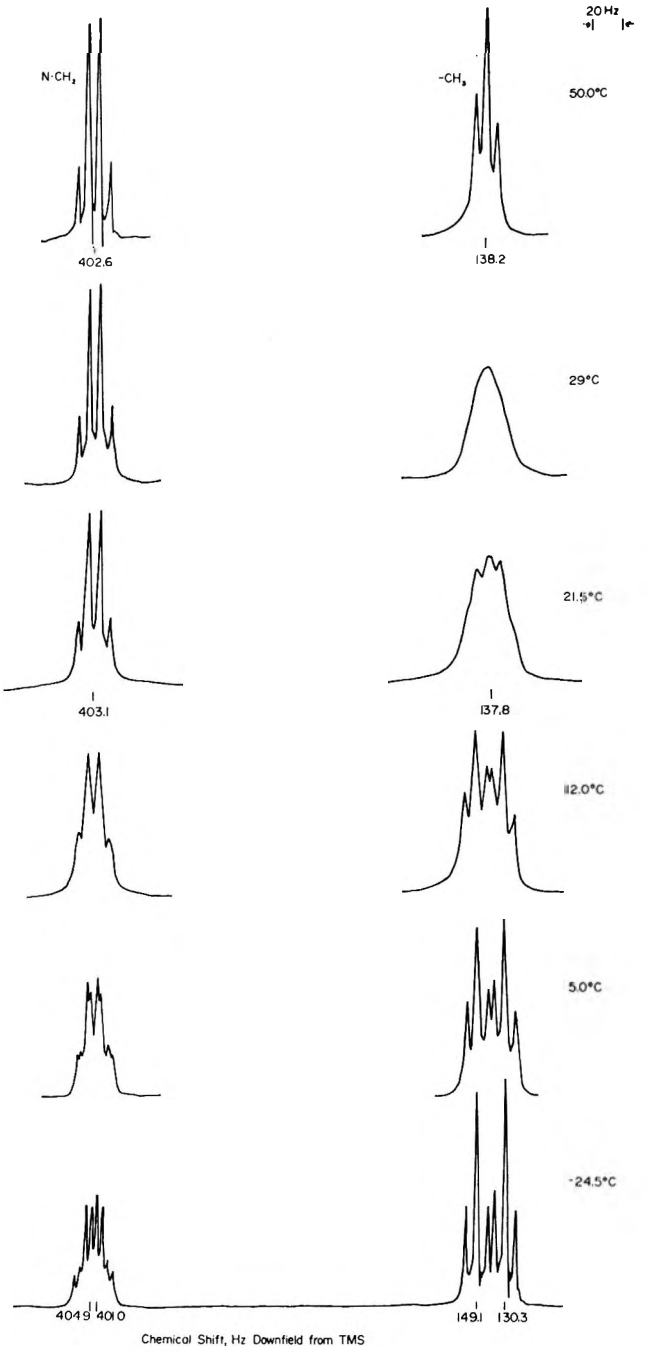

Figure 5. Typical experimental nmr spectra at 100 MHz for tetraethylthiuram disulfide.

bond order considerably greater than one. However, no correlation is apparent, within the limitations of the experiment, between $\nu_{C\cdots N}$ and degree of sulfur substitution.

The nmr results, however, show a significant difference between mono- and disulfides having the same alkyl groups on the nitrogen. In the pair tetramethylthiuram disulfide and monosulfide, the rotational

(10) K. Dahlqvist and S. Forsén, *Acta Chem. Scand.*, **24**, 651 (1970).
(11) K. Nakanishi, "Infrared Absorption Spectroscopy—Practical," Holden-Day, San Francisco, Calif., 1962.

Table I: Nmr Parameters and Activation Parameters for Restricted Rotation about the S_2C-NR_2 Bond in Thiuram Disulfides and Monosulfides

Compd	Proton chemical shifts in absence of exchange, δ, ppm				Coalescence temperature, °C		Log A	E_a, kcal/mol	$\Delta F^{\ddagger}$, kcal/mol	$\Delta H^{\ddagger}$, kcal/mol	$\Delta S^{\ddagger}$, eu
	$N-CH_2$ I	$N-CH_2$ II	CH_2 I	CH_2 II	$N-CH_2$	CH_3					
Tetramethylthiuram disulfide			3.662	3.627		[b]	12.8[a]	15.6 ± 0.4[a]	15.3 ± 0.1[c]	15.0 ± 0.4[c]	−0.9 ± 2.0
Tetramethylthiuram monosulfide			3.550	3.469		[b]	12.9[a]	16.5 ± 0.4[a]	16.0 ± 0.1[c]	15.9 ± 0.4[c]	−0.4 ± 2.0
Dicyclopentamethylene-thiuram disulfide	4.336	4.202			−4.5		[b]	[b]	13.9 ± 0.3[d]	[b]	[b]
Dicyclopentamethylene-thiuram monosulfide	4.279	3.886			34		[b]	[b]	15.3 ± 0.3[e]	[b]	[b]
Tetraethylthiuram disulfide	4.052	4.011	1.497	1.310	12	29	[b]	15.3 ± 1.2[h]	15.0 ± 0.2[f,g]	14.7 ± 1.2[e]	−0.8 ± 3.3

[a] From Arrhenius plot. [b] Not obtained. [c] 29°. [d] −4.5°. [e] 34°. [f] From CH_3 coalescence, 29°. [g] From CH_2 coalescence, 12°. [h] Estimated from τ values at 29° and 12° obtained from CH_3 and CH_2 coalescence, respectively.

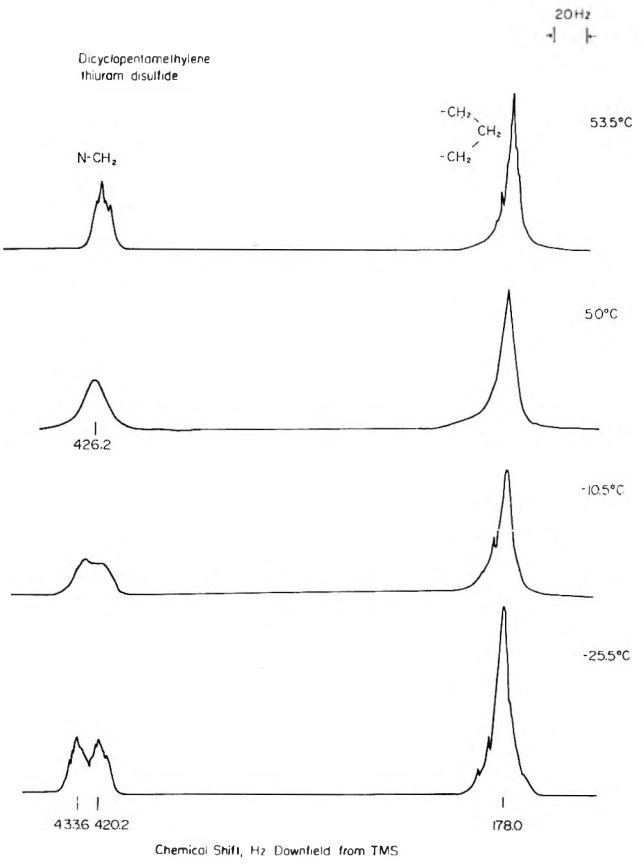

Figure 6. Typical experimental nmr spectra at 100 MHz for dicyclopentamethylenethiuram disulfide.

Table II: The C⋯N Stretching Frequencies of Thiuram Disulfides and Monosulfides in $CHCl_3$, Solution in a 0.1-mm Cell

Compd	$\nu C\cdots N$, cm^{-1}
Tetramethylthiuram disulfide	1495
Tetramethylthiuram monosulfide	1497
Tetraethylthiuram disulfide	1487
Dicyclopentamethylenethiuram monosulfide	1473
Dicyclopentamethylenethiuram disulfide	1476
Dicyclopentamethylenethiuram hexasulfide (KBr pellet)	1473

barrier is 0.9 kcal/mol greater in the monosulfide. The dicyclopentamethylene mono- and disulfides show a barrier (assuming $\Delta S^{\ddagger}$ is of the order of −1 eu) greater by about 1.4 kcal/mol in the monosulfide. This points to a much greater degree of double-bond character in the monosulfides, and the greater importance of structures such as IV in their ground state.

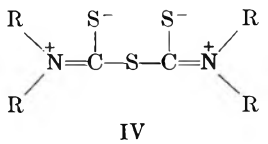

IV

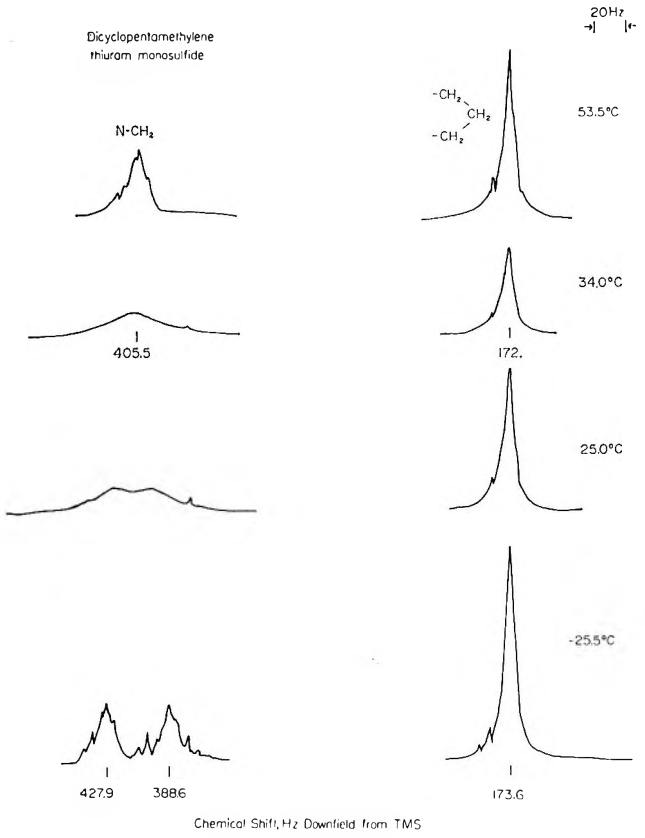

Figure 7. Typical experimental nmr spectra at 100 MHz for dicyclopentamethylenethiuram monosulfide.

Donation of lone pair electrons from the sulfide sulfur into the S–C bond, giving that bond some double bond character, should not be of importance in the monosulfides, due to the electron withdrawal by the other $\rangle C{=}S$ group. In the disulfides, however, it may well be significant in lowering the rotational barrier about the carbon–nitrogen bond, since it would place the partial positive charge on the sulfur, rather than on the more electronegative nitrogen.

An additional factor which must be considered in these molecules is the possibility of steric hindrance to rotation about the C⋯N bond due to the bulky sulfur substituents. In order to minimize repulsion between the lone pair electrons on the adjacent sulfur atoms in the disulfide, an angle between these of about 90° is expected. This angle (the dihedral angle in the $C\diagdown\!\diagup\!S{-}S\!\diagdown\!\diagup\!C$ group) has been measured in an X-ray study of the molecular structure of crystalline tetraethylthiuram disulfide[12] as 96° 25′. The X-ray study also indicates that small rotations about the C⋯N bonds, of the order of 4°, are possible. This is consistent with the high rotational barrier found. Assuming a very similar molecular structure for tetramethylthiuram disulfide, sketched in Figure 8, a molecular model shows only minor steric hindrance to rotation of the $-N(CH_3)_2$ group due to repulsion between the *N*-methyls and the adjacent thiocarbonyl sulfur.

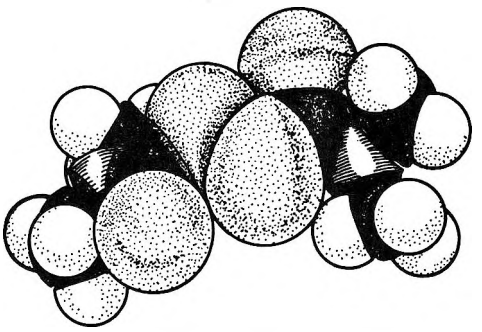

Figure 8. Sketch of the lowest energy configuration of tetramethylthiuram disulfide based on X-ray data[11] for tetraethylthiuram disulfide.

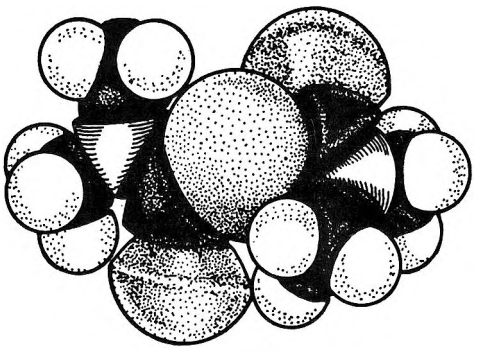

Figure 9. Sketch of the most likely configuration of tetramethylthiuram monosulfide, based on X-ray data[11] for tetraethylthiuram disulfide and construction of molecular models.

When only a single sulfur joins the two thiocarbonyl groups, as in tetramethylthiuram monosulfide, the rotational possibilities are greatly reduced. To minimize repulsion between unbonded electrons on the neighboring C=S groups, a dihedral angle slightly larger than 90° can be assumed. Rotation about the C⋯N bond brings the *N*-methyls quite close to the nonadjacent thiocarbonyl sulfur. This steric hindrance undoubtedly raises the barrier to rotation about the $S_2C{-}NR_2$ bond somewhat. A model of this molecule is sketched in Figure 9.

The very small entropy of activation for the rotation is to be expected, since the transition state must differ only slightly (by rotation about one bond) from the configuration in the ground state.

Conclusions

The barrier to restricted rotation about the $S_2C{-}NR_2$ bond in tetraalkylthiuram mono- and disulfides is higher for the monosulfides than the disulfides. This is attributed to both increased double-bond character of the C⋯N bond and additional steric hindrance by the thiocarbonyl sulfur atoms in the monosulfides.

(12) I. L. Karle, J. A. Estlin, and K. Britts, *Acta Crystallogr.*, **22**, 273 (1967).

Absolute Entropies, Conformation, and Debye Temperatures of Bicyclo[2.2.2]octane- and of Bicyclo[3.2.2]nonane-Type Molecules

by L. M. Amzel,* Martha C. M. Cucarella, and L. N. Becka

Escuela de Química, Universidad Central de Venezuela and Department of Biophysics, The Johns Hopkins University, Baltimore, Maryland 21205 *(Received September 16, 1970)*

Publication costs borne completely by The Journal of Physical Chemistry

The spectroscopic entropies of bicyclo[2.2.2]octane (BCO), 1-azabicyclo[2.2.2]octane (ABCO), 1,4-diazabicyclo-[2.2.2]octane (DABCO), 3-oxabicyclo[3.2.2]nonane (OXBN), and 3-azabicyclo[3.2.2]nonane (AZBN) were calculated. For AZBN the ir spectra between 200 and 4000 cm^{-1} are reported, together with a calculation of frequencies of the skeletal normal modes and the unit cell dimensions and space group of the high- and low-temperature crystalline phases (at 20°, orthorhombic, *Aba*2 with $a = 21.3$, $b = 11.3$, and $c = 6.15$ Å, $Z = 8$; at 50°, face-centered cubic, $a = 9.47$ Å, $Z = 4$) obtained by X-ray diffraction. The conclusions reached from the comparison between calculated and experimental third-law entropies are that there is residual entropy in the low-temperature phase of ABCO and OXBN but not in BCO and AZBN, and that the calculated frequency for the torsional mode of these compounds, ~60 cm^{-1}, should be at least 15% higher for the bicyclooctanes and at least 15% smaller for the bicyclononanes. Furthermore, an analysis of the previous information in conjunction with the published values and the interpretation of the solid–solid phase transition entropy increments of these compounds leads us to propose the following symmetries for the molecular conformations: D_{3h} for BCO, C_3 for ABCO, and C_s for OXBN (with the two twisted forms coexisting at all temperatures), and C_1 for AZBN. Finally, the experimental entropy *vs.* temperature curves are analyzed in terms of temperature-dependent Debye temperatures. The resulting curves, having a pronounced downward slope before the transition temperature, are regarded as characteristic of plastic crystals and as evidence of the onset of molecular disorder before the transition.

Introduction

This paper deals with the interpretation of recently measured thermodynamic data of the following compounds of the bicyclo[2.2.2]octane type

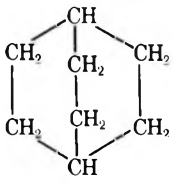

Bicyclo[2.2.2]octane (BCO)

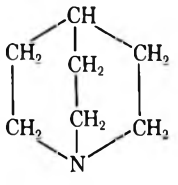

1-Azabicyclo[2.2.2]octane or quinuclidine (ABCO)

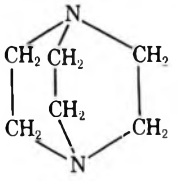

1,4-Diazabicyclo[2.2.2] octane or triethylenediamine (DABCO)

and the following of the bicyclo[3.2.2]nonane type

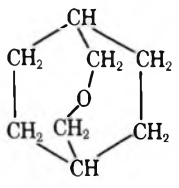

3-Oxabicyclo[3.2.2]nonane (OXBN)

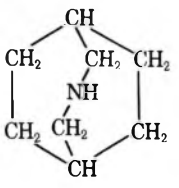

3-Azabicyclo[3.3.3]nonane (AZBN)

We are interested in these globular molecules because they are among the most studied of those that have a crystalline phase of the plastic (or embefic) type. In what follows we shall present: (a) values for the spectroscopic entropies and the corresponding experimental third-law entropies at 298.15°K; (b) a discussion of these results in terms of molecular conformation; (c) comments on the validity of the force field used to calculate the intramolecular vibration frequencies; (d) an analysis of the entropies of the solids in terms of temperature-dependent Debye temperatures, θ_D's.

Spectroscopic and Experimental Third-Law Entropies. The experimental third-law entropies for the five compounds mentioned above are given in Table I. The absolute entropies of the solids are those reported in the literature[1-4] (obtained by integration of specific heat measurements performed in Professor Westrum's laboratory). The sublimation data for BCO, ABCO, OXBN, and AZBN were recently reported by Westrum, Wong, and Morawetz,[4] who measured pressures and enthalpies of sublimation directly, so that the largest error in the resulting third-law entropies for these

(1) S. S. Chang and E. F. Westrum, Jr., *J. Phys. Chem.*, **64**, 1551 (1960).

(2) J. C. Trowbridge and E. F. Westrum, Jr., *ibid.*, **67**, 281 (1963).

(3) C. M. Barber and E. F. Westrum, Jr., *ibid.*, **67**, 2373 (1963); C. A. Wolff and E. F. Westrum, Jr., *ibid.*, **68**, 430 (1964).

(4) E. F. Westrum, Jr., W.-K. Wong, and E. Morawetz, *ibid.*, **74**, 2542 (1970).

Table I: Experimental Third-Law Entropies (in eu) at 298.15°K

Compd	DABCO	ABCO	BCO	AZBN	OXBN
$S°$ crystal	37.7[a]	49.5[b]	50.2[c]	56.1[d]	56.5[b]
S vaporization, $\Delta Hv/T$	40.9[e]	40.7[f]	38.5[f]	46.3[f]	42.7[f]
S compression, R ln (p/760)	−15.0[e]	−13.3[f]	−11.2[f]	−15.8[f]	−14.7[f]
$S°$ (298.15)	73.1	76.9	77.5	86.6	84.5

[a] Reference 2. [b] Reference 4. [c] Reference 1. [d] Reference 3. [e] Reference 5. [f] Reference 4.

four compounds is due to the error in the vapor pressure values. This error is of about 40%, which gives an error in the third-law entropy of about 0.5 eu. For DABCO the only sublimation data available are those published by Wada, *et al.*,[5] in the form of a Clausius–Clapeyron equilibrium pressure equation. Large errors in the heat of sublimation derived from this equation and in the value of the vapor pressure at a given temperature must be expected. Thus, there will be an error of several entropic units in the value presented here for the experimental entropy of DABCO. We have nevertheless included this compound in our discussion since it completes the series of bicyclooctanes and some of the results obtained for the other compounds could be extended to it. The vibrational contribution to the spectroscopic entropies for ABCO, BCO, and DABCO were calculated using the vibrational frequencies given by Bruesch.[6] We calculated the rotational contribution for these three compounds using the molecular dimensions reported for DABCO[7] to obtain moments of inertia, taking a value of 6 for the symmetry number (σ) of BCO and DABCO (they have symmetry D_{3h} or D_3) and 3 for ABCO (with symmetry C_{3v} or C_3). For AZBN and OXBN we calculated the skeleton frequencies using the force constants given by Bruesch.[6] The definition of the internal coordinates is given in Table V. The same skeleton frequencies were used for both compounds. The assignment of frequencies was completed in each case by taking the values given for CH_2, CH, and NH groups in characteristic group frequencies tables.[8] These frequencies for AZBN and OXBN are given in Table IV, together with the experimental values of the frequencies of AZBN observed in the ir spectra taken in the region 200–4,000 cm^{-1}. In order to obtain approximate molecular dimensions to calculate moments of inertia, and in order to decide on the most likely symmetry for OXBN and AZBN, we built molecular models. From these we concluded that OXBN would probably have C_s symmetry, and therefore $\sigma = 1$ and AZBN would have no symmetry with $\sigma = 1$. The spectroscopic entropies and the differences from the corresponding experimental values are given in Table II. The largest difference is that for DABCO, but since the experimental sublimation entropy is affected by the above mentioned errors for this compound, we shall not discuss the difference any further except to remark that if there is residual entropy in the solid the difference would become smaller, as would also be the case if the calculated frequencies for the low-frequency modes are too small. ABCO and BCO have calculated values that are too large also, but for BCO the difference is within the experimental error, while for ABCO it would be within experimental error if a residual disorder of a magnitude of R ln 2 = 1.4 eu is added to the third-law entropy. For OXBN, considering the maximum possible molecular symmetry as C_s a residual entropy of R ln 2 is obtained. This can be interpreted as being due to the presence

Table II: Spectroscopic Entropies (in eu) at 298.15°K

Compd	DABCO	ABCO	BCO	AZBN	OXBN
$S°$ translational	40.0	40.0	40.0	40.3	40.3
$S°$ rotational	23.9	25.3	23.9	28.1	28.1
$S°$ vibrational	13.9[a]	14.0[a]	14.1[a]	17.5[b]	17.3[c]
$S°$ calcd	77.8	79.3	78.0	85.9	85.7
$S°_{obsd} - S°_{spectr}$	−4.7	−2.4	−0.5	0.7	−1.2

[a] The vibrational frequencies used were those calculated by Bruesch in ref 6. [b] The vibrational frequencies used were those given in Table IV. [c] The same values for AZBN were used, subtracting the contribution of the two NH bending modes.

Table III: Crystal Data for the Two Solid Phases of AZBN

(a) Low-temperature phase (at 20°)

System: orthorhombic, space group: $Aba2$ or $A2_1/c2/a2/m$ compatible with extinction conditions. $Aba2$ chosen from intensity statistics; cell dimensions: a = 21.3, b = 11.3, c = 6.15 Å, D measured = 1.12 g/cm³

D calculated (for eight molecules in unit cell) = 1.12 g/cm³

(b) High-temperature phase

At 50°: face-centered cubic, with a = 9.47 Å; supercooled at 20°; face-centered cubic, with d = 9.41 Å

(5) T. Wada, E. Kishida, Y. Tomiie, and H. Suyd, S. Seki, and I. Nitta, *Bull. Chem. Soc. Jap.*, **33**, 1317 (1960).

(6) P. Bruesch, *Spectrochim. Acta*, **22**, 867 (1966).

(7) G. S. Weiss, A. S. Parkes, E. R. Nixon, and R. E. Hughes, *J. Chem. Phys.*, **41**, 3759 (1964).

(8) A. Weissberger, Ed., *Tech. Org. Chem.*, **9**, 564 (1956).

Table IV: Observed and Calculated Vibrational Frequencies for AZBN

(a) Skeletal vibrations, below 700 cm^{-1}

Calculated (used for entropy calculation): 59, 229, 274, 365, 385, 465, 498, 505, 585, 590, 660

Observed: 240, 270, 340, 390, 410, 450, 500, 610, 660

(b) Skeletal vibrations, above 700 cm^{-1}

Calculated (used for entropy calculations): 752, 757, 819, 880, 904, 1045, 1103, 1165, 1189, 1193

Observed: 755, 815, 865, 890, 1040, 1080, 1160, 1210

(c) Group frequencies

Observed	Assigned	Oscillator frequencies used for entropy calculation
710, 775	CH_2, CH rocking	8 modes at 750 cm^{-1}
835	NH "rocking"	1 mode of 835 cm^{-1}
940, 1040, 1060, 1070	CH_2 twisting	6 modes of 1000 cm^{-1}
1240, 1250, 1290, 1320, 1350, 1360	CH_2, CH wagging	8 modes of 1300 cm^{-1}
1440, 1460	CH_2 deformation	6 modes of 1450 cm^{-1}
1630	NH deformation	1 mode of 1600 cm^{-1}
2660, 2720, broad band from 2800 to 3000	CH_2, CH stretching	14 modes of 2800 cm^{-1}
Broad sound at 3300	NH stretching	1 mode of 3300 cm^{-1}

of molecules with the oxygen atom pointing in the two possible directions on crystallographically equivalent positions. This will give the molecule a crystallographic C_{2v} symmetry compatible with the interpretation of the transition entropy.[4,9] The difference in AZBN is within experimental error.

Molecular Conformation and Transition Entropies. Various studies have been published on the molecular conformation of BCO to determine whether it has D_{3h} or the twisted D_3 structure.[10] Recently, Dunitz and Ermer[11] reported a calculation of energy eigenfunctions and eigenvalues for the twisting of BCO and concluded that it had effective D_{3h} symmetry as far as diffraction methods are concerned. The third-law calculation presented here indicates that there is no residual entropy, thus excluding the possibility of a diffraction D_{3h} symmetry being due to the coexistence of the two twisted D_3 forms at low temperatures. Furthermore, it agrees with the model proposed for the description of the mechanism of the solid-state transition, namely, that above the transition temperature the BCO molecules take the 20 possible distinguishable orientations generated when aligning its D_{3h} symmetry elements with those of the O_h space group of the face-centered cubic (fcc) phase.[4,9] For ABCO the possible conformations are of symmetry C_{3v} or C_3. Bruesch and Gunthard[12] have measured the vibrational spectra of both solid phases of BCO, concluding that the molecule could have effective C_{3v} symmetry at high temperature, whereas at low temperature the site symmetry could not have a threefold axis. Bruesch also obtained X-ray powder diagrams for the low-temperature phase of ABCO and indexed it using an hexagonal unit cell, requiring two molecules per cell.[13] In the hexagonal space group the only sites with twofold multiplicity have at least threefold symmetry. If Bruesch's interpretation is correct, one would have to envisage a low-temperature phase in which the ABCO molecules have their threefold symmetry axis not coincident with the crystallographic threefold axis and taking different orientations about the latter. This would mean there would be a contribution of R ln 3 eu to the entropy due to residual disorder, but this hypothesis becomes untenable if the transition entropies are to be interpreted in a simple way, as has been successfully accomplished for a number of plastic crystals.[11,14,15] In the simple model[15] the energetically favorable orientations are those in which elements of symmetry of the molecules are aligned with equivalent symmetry elements of the cell. In that case, the number of possible orientations of ABCO, considered as having C_{3v} symmetry, in the site with O_h symmetry of the fcc phase will give a transition entropy of R ln 16 = 5.54 eu in good agreement with the observed value[4] 6.34 eu. On the other hand, if the molecules had C_3 symmetry they could take both the clockwise and the anticlockwise twisted conformations in the low-temperature phase, leading to a residual entropy of R ln 2 eu and would keep that disorder at high temperature in addition to the previously mentioned 16 orientations of the molecule. Thus, we con-

(9) W.-K. Wong, Ph.D. Dissertation, University of Michigan, 1966; *Diss. Abstr. B*, 28 (3), 874 (1967).

(10) J. D. Dunitz and O. Ermer, *Chem. Commun.*, 567 (1968), and references therein.

(11) J. D. Dunitz and O. Ermer, Collected Abstracts, VIII International Congress of Crystallography, 1969, p S-126 *Actr Crystallogr., Sect. A*, 25, S3 (1969).

(12) P. Bruesch and Hs. H. Gunthard, *Spectrochim. Acta*, 22, 877 (1966).

(13) P. Bruesch, *ibid.*, 22, 861 (1966).

(14) L. M. Amzel and L. Becka, *J. Phys. Chem. Solids*, 30, 529 (1969).

(15) G. B. Guthrie and J. P. McCullough, *ibid.*, 16, 53 (1961).

clude that the ABCO crystal has molecules with C_3 symmetry, that there is a residual entropy of R ln 2 due to the coexistence of both twisted forms, and that the crystal symmetry at low temperatures is lower than hexagonal.

One of us (L.M.A.) has studied both phases of AZBN by X-ray diffraction, obtaining the crystal data shown in Table III. The number of molecules in the low-temperature phase unit cell is equal to the multiplicity of a general position of the space group, so that the X-ray crystal data are compatible with the assumption of C_1 symmetry for AZBN. The model used to calculate the transition entropy of AZBN[14] is also compatible with the C_1 conformation which in the models we built seemed to be less strained than the conformation of symmetry C_s. The latter is also compatible with the ir, X-ray, and thermodynamic data presented above. We have no data on OXBN other than thermodynamic functions. The calculation of the spectroscopic entropy and of the transition entropy were done assuming C_s symmetry and residual disorder with C_{2v} apparent symmetry. The agreement between the calculated and experimental values supports this choice of conformation for OXBN.

Entropy Contribution from Torsions. The calculated vibrational frequencies for ABCO, DABCO, and BCO agree quite well with the frequencies observed above 300 cm^{-1} and this agreement extends to the region of 200 cm^{-1} for AZBN. Differences up to 50 cm^{-1} as found between some of the observed and the calculated values in the 300-cm^{-1} region would not seriously affect the entropy contribution of these modes at temperatures of up to 400°K. On the other hand, differences of the order of 10 cm^{-1} in the lowest calculated frequency ($\sim$60 cm^{-1}) would lead to differences of about 0.3 eu in the 300°K region. None of the measured vibration spectra extended to values in the neighborhood of 60 cm^{-1}, which is the calculated frequency for the skeletal torsional modes if the value of 0.024×10^{-5} dyn/cm[6] is used for the corresponding force constant (H_τ). This constant is the most important individual force constant for this calculation. So far there are no spectroscopic data that allow a unique choice of torsional force constant in these bicyclic molecules. The value 0.024×10^{-5} dyn/cm used by Bruesch[6] is the value proposed by Schachtshneider and Snyder[16] based on an analysis of noncyclic hydrocarbons and therefore not necessarily transferable to the bicyclic molecules. Our choice of force constant for AZBN (Table V) was made in order to follow closely the calculations reported by Bruesch for BCO, ABCO, and DABCO since we felt that in any case there was no better choice on the basis of what is known so far. If H_τ is changed by 30% the frequency of the torsional mode will change by about 15% in the same sense and the calculated vibrational entropy at 298°K would change by 0.3 eu in the opposite sense, thus making it possible to attribute part of the discrepancies between calculated and observed third-law entropies to errors in the H_τ values. Thus if the value of H_τ is taken as 0.037×10^{-5} dyn/cm for bicyclooctanes and 0.017×10^{-5} dyn/cm for the bicyclononanes the differences $S_{exp} - S_{spectr}$ would now be: BCO, −0.2 eu; ABCO (including residual entropy), −0.7 eu; OXBN (including residual entropy), −0.1 eu; AZBN, +0.4 eu. These changes in the torsional force constant (H_τ) will affect other low-frequency modes. However, since the torsional coordinate contributes mostly to the torsional mode and little to the other modes,[6] revised values for the frequencies above 200 cm^{-1} will not greatly change their calculated

Table V: Internal Coordinates for AZBN

Force constant type[a]	Atoms[b] (one internal coordinate per line)
K_R (CH_2–CH_2-stretching)	C (2′), C (3′)
	C (2″), C (3″)
$K_{R'}$ (–CH_2–CH-stretching)	C (1), C (2)
	C (1), C (2′)
	C (1), C (2″)
	C (4), C (3)
	C (4), C (3′)
	C (4), C (3″)
K_{RN} (–CH_2–N-stretching)	N, C (2)
	N, C (3)
$H_{\omega N}$ (NCC-bending CH_2)	N, C (2), C (1)
	N, C (3), C (4)
H_ω (CCC-bending CH_2)	C (1), C (2′), C (3′)
	C (1), C (2″), C (3″)
	C (4), C (3′), C (2′)
	C (4), C (3″), C (2″)
H_φ (CCC-bending CH)	C (2), C (1), C (2′)
	C (2), C (1), C (2″)
	C (2′), C (1), C (2″)
	C (3), C (4), C (3′)
	C (3), C (4), C (3″)
	C (3′), C (4), C (3″)
H_ω (CNC-bending NH)	C (2), N, C (3)
H_τ (NCCC-torsion)	C (1), C (2′), C (3′), C (4)
	C (1), C (2″), C (3″), C (4)
	C (1), C (2), N, C (3)
	C (2), N, C (3), C (4)

[a] The force constant types corresponds to those used by Bruesch.[6] For each individual force constant the atoms listed in *one* line define *one* internal coordinate. The interaction force constants were used as defined by Bruesch.[6] [b] The labels of the atoms are defined as follows: (i) N–H nitrogen is labeled as N; (ii) C–H carbons are labeled as C (1) and C (4); (iii) CH_2 carbon bound to N and C (1) is labeled as C (2); (iv) CH_2 carbon bound to N and C (4) is labeled as C (3); (v) CH_2 carbons bound to C (1) but not to N are labeled as C (2′) and C (2″); (vi) CH_2 carbon bound to C (2′) and C (4) is labeled as C (3′); (vii) CH_2 bound to C (2″) and C (4) is labeled as C (3″).

(16) J. H. Schachtschneider and R. G. Snyder, *Spectrochim. Acta*, 21, 169 (1965).

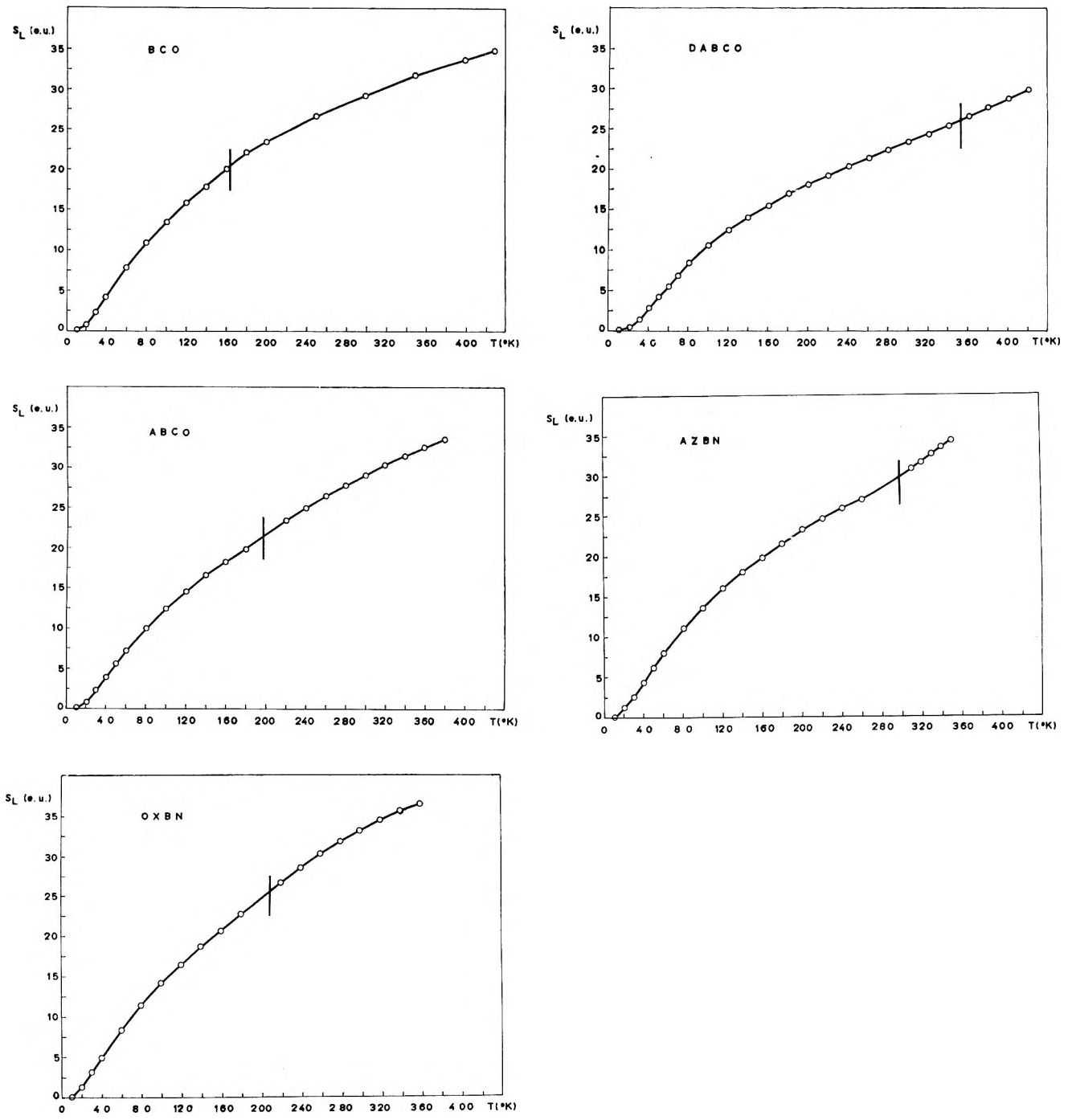

Figure 1. Lattice entropies in cal mol^{-1} $°K^{-1}$, eu for bicyclooctanes and bicyclononanes. Vertical lines crossing the curves indicate transition temperatures.

contributions to the entropy in the temperature range in which we are interested (20–400°K).

Debye Temperatures. It seemed interesting to analyze the temperature dependence of the experimental entropies in some convenient way in order to establish whether these crystals show some characteristic behavior in their entropies, apart from the changes in entropy at the transition temperatures. With crystals of more rigid molecules, such as hexamethylenetetramine (HMT), it was possible to reproduce the experimental entropy curve by assuming the following frequency distribution for the solid: Einstein-type branches for the intramolecular vibrations and a temperature-dependent Debye distribution plus a temperature-dependent Einstein distribution for the intermolecular vibrations.[17] Even though the experimentally determined dispersion curves and frequency distribution

(17) L. N. Becka and D. W. J. Cruickshank, *Proc. Roy. Soc., Ser. A*, **273**, 455 (1963).

for HMT does not follow these simple models, the calculated entropies were in agreement with their observed values. This is probably a consequence of the fact that the entropies are a result of the integration of specific heat curves, which in turn are the result of integrals involving the frequency distribution, and therefore the calculated entropies are not very sensitive to the detail of the frequency distribution and less to the detail of the dispersion curves. Thus, there is some justification in using Debye temperatures and/or Einstein temperatures to give some simple numerical measure of the overall thermodynamic behavior of solids, even though for some monoatomic solids the measured dispersion curves do not correspond to a Debye distribution. In the case of flexible molecules, such as those studied here, it is almost certain that the lowest frequency internal mode will be mixed with the intermolecular vibrations, leading to an even more complex dispersion curve. Even though a very simple model will be an unrealistic description of the dispersion curves, we think it can allow an analysis of systematic features in the experimental entropies by reducing the measured entropy curves to a form more suitable for that analysis. Thus, we decided to use the model employed for the more rigid HMT molecules. That is, we assumed that all the internal modes of vibrations follow an Einstein type distribution including the problematic torsional mode. The difference between the experimental entropies and the contribution of the internal modes we shall call "lattice entropy." In order to have comparable results for the different compounds we have subtracted the transition entropy from the values of the high-temperature phase. The resulting "lattice entropy" *vs.* temperature curves are plotted in Figure 1. The model used previously for HMT[17] was applied to these "lattice entropies." This model was tested trying to obtain the best set of "θ°" and "a" values in the expressions $\theta_{D,E} = \theta_{D,E}^{\circ} - a_{D,E}T$ that would give calculated values (S_L^{calcd} in agreement with "lattice entropies" in the region 20–200°K using

$$S_L^{calcd}{}_{(T)} = 3S_{\theta_D(T)} + 3S_{\theta_E(T)}$$

and fitting the low- and high-temperature phases separately. As we were unable to obtain a reasonable fit with this model, we proceeded to analyze these entropies in terms of a sixfold degenerate temperature dependent Debye distribution. The Debye temperature (θ_D) at each temperature was chosen to give exactly the "lattice entropy" at that temperature. The curves resulting from plotting these θ_D's *vs.* temperature are shown in Figure 2, where we have included another globular compound with plastic phase adamantane, and the geometrically analogous but nonplastic HMT. The most striking feature that emerges from this way of looking at the solid-state entropies is the marked sloping trend of the θ_D's curves shown by all the plastic crystals

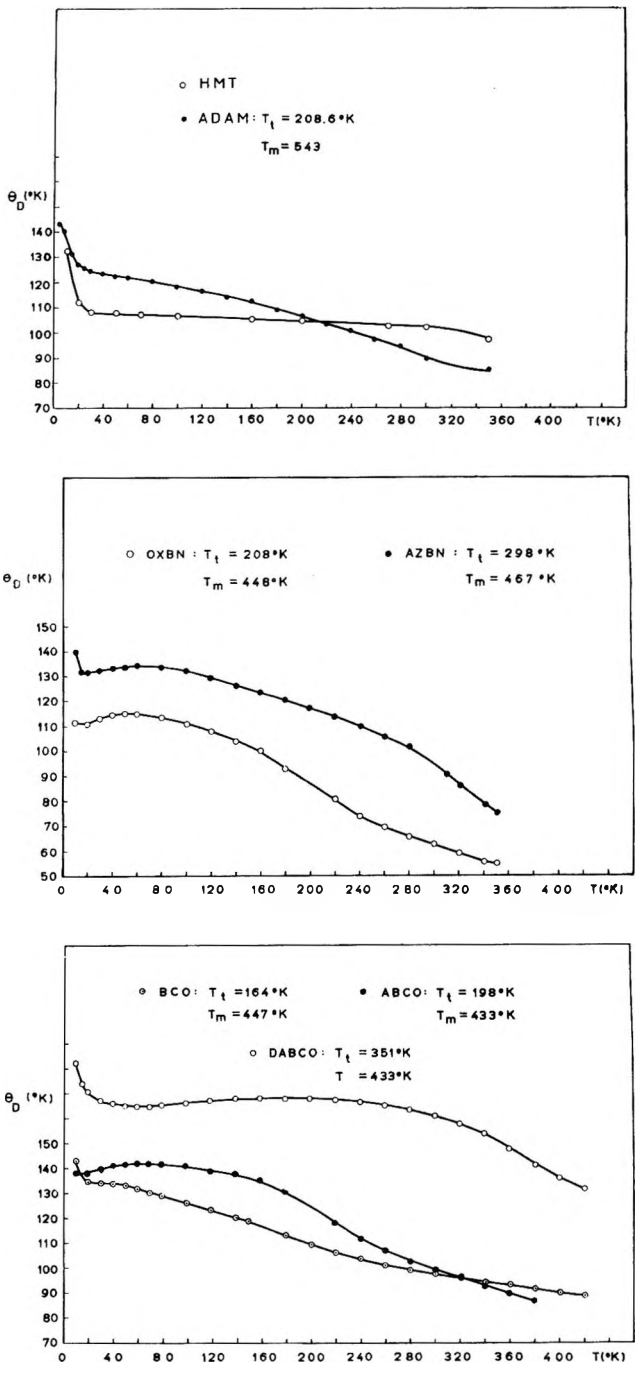

Figure 2. Debye temperature for bicyclooctanes, bicyclononanes, hexamethylenetetramine, and adamantane. $\theta_{D(T)}$ is defined so that $S_{L(T)} = 6S\theta_{D(T)}$. Transition and melting temperatures are indicated.

analyzed here, as opposed to the practically constant θ_D obtained for HMT. This could be interpreted as a "softening" of the lattice, an increase in orientational positional disorder, etc. starting at temperatures of the order of 100°K below the transition. The magnitude of the decrease of θ_D with temperature seems larger than would be expected from just lattice expansion since the volume expansion at the transition is only about 6% for BCO,[13] 2.3% for adamantane[18]

with the largest measured so far being that of DABCO with 11.5%.

The idea that the reduction in θ_D's is due to an increase in entropy produced by the onset of orientational and positional disorder would be in qualitative agreement with the model and results given in a previous paper dealing with the interpretation of the thermodynamic properties of these crystals at the transition temperature.[14] An independent indication of the qualitative meaningfulness of the θ_D's defined above is that the lattice dimension of the fcc phases of DABCO, ABCO, BCO, and AZBN increase in that order, whereas the θ_D's are smaller in that order, as would be reasonable if the θ_D and the cell dimensions reflect the magnitudes of the intermolecular forces in molecules of roughly the same shape.

Acknowledgment. One of us (L. M. A.) was supported by a Damon Runyon Memorial Fund for Cancer Research postdoctoral fellowship during the completion stages of this work.

(18) K. V. Mirskaya, *Sov. Phys. Crystallogr.*, **8**, 167 (1963).

Deexcitation of Molecular Vibration on Collision: Vibration-to-Rotation Energy Transfer in Hydrogen Halides

by Hyung Kyu Shin

Department of Chemistry,[1] University of Nevada, Reno, Nevada 89507 *(Received October 22, 1970)*

Publication costs assisted by the Air Force Office of Scientific Research

Vibrational relaxation of hydrogen halides has been investigated on the basis of the vibration-to-rotation energy transfer mechanism, with rigorous consideration of the participation of the translational motion. The collision model consists of a rotation-averaged oscillator and a rigid rotator, in which two hydrogen atoms interact strongly at close-in collisions. An expression for the probability of vibration–rotation energy transfer has been formulated by solving Hamilton's equations of motion. Calculated values of the vibrational relaxation times at 1 atm for HCl, DCl, HBr, and HI agree satisfactorily with experiment over the temperature range from 800 to 2000°K. The present treatment also explains the observed isotope effect between HCl and DCl; *i.e.*, the deuterated molecule relaxes more slowly than the normal molecule in spite of the fact that its vibrational frequency is significantly smaller than that of the normal molecule. The effect of the translational motion on vibrational relaxation is found to be most important in the hydrogen chloride molecules, the deuterated chloride being more significantly affected by the translational motion than the normal molecules, while in the hydrogen iodide molecules the effect is least important.

Introduction

Vibrationally excited deuterated molecules are known to relax more slowly than normal molecules.[2-4] According to the predictions of conventional vibration-to-translation (V–T) energy transfer theories,[5,6] we would expect the opposite result because of an increase in their masses and a decrease in vibrational frequencies. The vibrational relaxation times of CD_4 and SiD_4 have been found by Cottrell and Matheson[2b] to be longer than those of CH_4 and SiH_4, respectively; they then suggested that this might be due to vibration-to-rotation (V–R) energy transfer. From sound absorption and velocity measurements, Shields and Burks[3a] found that D_2O is from $1/3$ to $1/5$ as efficient as H_2O in deexciting the bending-mode vibration of CO_2 in the temperature range from 300 to 500°K. Recently, Breshears and Bird[3b] showed that HCl molecules relax more rapidly than DCl molecules in the range from 700 to 2100°K. Although in these molecules vibrational relaxation times become longer on deuteration,

(1) Theoretical Chemistry Group Contribution No. S-1030.

(2) T. L. Cottrell and A. J. Matheson, (a) *Proc. Chem. Soc.*, 114 (1061); (b) *Trans. Faraday Soc.*, **58**, 2336 (1962); (c) *ibid.*, **59**, 824 (1963). Also see T. L. Cottrell, R. C. Dobbie, J. McLain, and A. W. Read, *ibid.*, **60**, 241 (1964).

(3) (a) F. D. Shields and J. A. Burks, *J. Acoust. Soc. Amer.*, **43**, 510 (1968); (b) W. D. Breshears and P. F. Bird, *J. Chem. Phys.*, **50**, 333 (1969); *ibid.*, **51**, 3660 (1969).

(4) R. C. Millikan and L. A. Osburg, *ibid.*, **41**, 2196 (1964).

(5) T. L. Cottrell and J. C. McCoubrey, "Molecular Energy Transfer in Gases," Butterworths, Washington, D. C., and London, 1961, Chapter 6.

(6) D. Rapp and T. Kassal, *Chem. Rev.*, **69**, 61 (1969); an excellent review article on the problems of V–T energy transfer.

they are far shorter than those calculated by the V–T energy transfer theory (see ref 7–9 for related work).

On the basis of the energy transfer mechanism proposed by Cottrell and Matheson,[2b] Moore[10] derived an expression for the probability of V–R energy transfer directly from the conventional V–T energy transfer theory replacing the translational velocity by the relative peripheral velocity of rotation $v_r = \dot{\theta}d$ and the reduced mass of the colliding molecules by the reduced mass of the peripheral atom for the encounter, where $\dot{\theta}$ is the angular velocity of rotation and d is the bond length of the molecule. This model appears intuitively to be very reasonable, although the idea of V–R energy transfer has been questioned.[11] However, for the V–R energy transfer mechanism, we should formulate the corresponding transition probability directly from the collision model of rotating molecules rather than from the V–T energy transfer probability. Furthermore, in the molecules such as those considered by Moore for V–R energy transfer calculation, the translational motion is not completely negligible compared to the rotation so that it should be necessary to include the effect of the translational motion on V–R energy transfer.

In this paper we consider the problem of V–R energy transfer between hydrogen halide molecules and present a direct and complete formulation of probability of V–R energy transfer from solutions of the classical equations of motion.[12] We also explicitly consider the effect of the translational motion of the colliding molecules on the V–R energy transfer process. In the collision between two hydrogen halide molecules (HX–HX or DX–DX) two hydrogen atoms can interact strongly when they are "squeezed" into close proximity by two heavy halogen atoms.[13] Such an interaction will cause a strong perturbation of the colliding molecules and in turn lead to an efficient energy transfer. Fortunately, in recent years experimental data became available for these molecules[3b,7,14] so that the applicability of the V–R energy transfer model can be tested. We specifically consider the $1 \rightarrow 0$ vibrational relaxation process in HCl, DCl, HBr, and HI molecules.

Collision Model and Interaction Potential

The collision model consists of two hydrogen halide molecules (HX) in which one is a rotating oscillator (H_vX_v) and the other is a rigid rotator (H_rX_r) under the influence of the interaction potential $U(r,x,\theta_1,\theta_2,\phi)$, where r is the distance between the centers of mass of the two molecules, x is the vibrational coordinate, and θ,ϕ specify molecular orientations; see Figure 1. We consider the vibrational excitation (or de-excitation) of only one molecule. To facilitate this investigation, we approximate the collision problem by the interaction of the vibrational motion of H_vX_v with the rotational motion of H_rX_r and with the relative translational motion. We assume that the rotational motion of H_vX_v does not directly participate in the V–R energy transfer process. Although the colliding molecules H_vX_v and H_rX_r are identical, in the present model we can treat the rotation of H_vX_v separately from the rest of the system in two extreme ways, depending on whether the rotational times are assumed to be very small or very large compared to the collision time. If rotation is fast the potential can be averaged over all possible orientations of H_vX_v to obtain a θ_1 averaged form of $U(r,x,\theta_1,\theta_2,\phi)$. For slow rotation, on the other hand, the angle θ_1 is assumed to remain constant during the course of a collision, and the final expression is obtained as a function of θ_1. However, in the mechanism of V–R energy transfer we assume the peripheral velocity to be greater than the translational velocity so that the approaching collision partners "see" each other as rapidly rotating molecules. Therefore, the θ_1 average of the interaction potential should be a reasonable approximation in the present study. It is important to point out that if we adopted the latter extreme case, we were equally assuming the rotation of H_rX_r to be slow. Then, for such slow rotation the removal of the vibrational energy of H_vX_v by H_rX_r through the V–R process can be very inefficient.

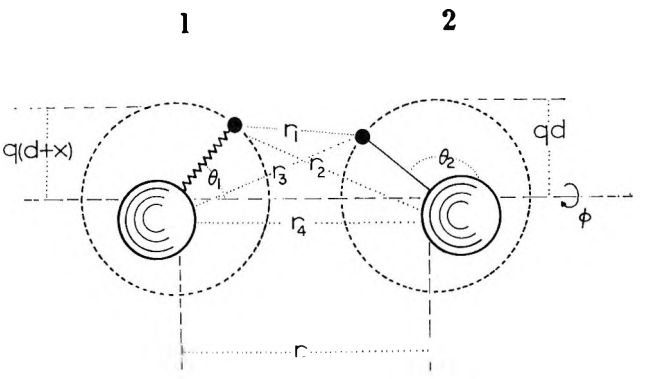

Figure 1. Collision model: the small closed and large open circles represent H (or D) and X atoms, respectively. The model assumes molecule 1 is a rotating oscillator (H_vX_v) and molecule 2 is a rigid rotator (H_rX_r).

With the θ_1 average we therefore replace the effect of the rotational motion of the oscillator on its own vibrational excitation or deexcitation by an average effect in the interaction potential. A rapidly rotating H_vX_v molecule forms "the spheres of influence," in which the

(7) C. C. Chow and E. F. Greene, *J. Chem. Phys.*, **43**, 324 (1965).

(8) P. Borrell, "Molecular Relaxation Processes," The Chemical Society, London, 1966, p 263.

(9) M. G. Ferguson and A. W. Read, *Trans. Faraday Soc.*, **63**, 61 (1967).

(10) C. B. Moore, *J. Chem. Phys.*, **43**, 2979 (1965).

(11) A. B. Callear and J. D. Lambert, "Comprehensive Chemical Kinetics," Vol. 2, C. H. Bamford and C. F. H. Tipper, Ed., Elsevier, Amsterdam, 1969, p 235.

(12) H. Shin, *Chem. Phys. Lett.*, **6**, 494 (1970); a preliminary report on V–R energy transfer.

(13) H. Shin, *J. Chem. Phys.*, **49**, 3964 (1968).

(14) J. H. Kiefer, W. D. Breshears, and P. F. Bird, *ibid.*, **50**, 3641 (1969).

outer sphere is formed by the hydrogen atom; this molecule may be then viewed as a breathing sphere. The collision system then involves the interaction of the rapidly rotating H_r atom with the sphere formed by the atom H_v of the oscillator. As the atom H_r approaches the portion of the surface formed at the neighborhood of $\theta_1 = 0$, a strong interaction will result, and in this region the V–R energy transfer can take place efficiently.

The interaction potential is assumed by the sum of exponential interaction of the type of a Morse potential between the atoms belonging to the different molecules

$$U = \sum_{i=1}^{4} U_i(r_i) \tag{1}$$

with

$$U_i(r_i) = D\left[\exp\left(l - \frac{r_i}{a}\right) - 2\exp\left(\frac{l}{2} - \frac{r_i}{2a}\right)\right] \tag{1a}$$

where l, a, and D are the potential parameters for the H_vX_v–H_rX_r interaction. The parameters l and a can be determined by fitting the exponential potential to an empirical form, *e.g.*, the Lennard-Jones potential. Fortunately, as will be seen below, l does not appear in the final expression. For r sufficiently larger than q_1d or q_2d, where $q_1 = m_H/(m_H + m_X)$ and $q_2 = m_X/(m_H + m_X)$, the interatomic distances can be approximated as[15]

$$\begin{aligned} r_1 &= r - q_2(d + x)\cos\theta_1 + q_2 d\cos\theta_2 \\ r_2 &= r - q_1(d + x)\cos\theta_1 - q_2 d\cos\theta_2 \\ r_3 &= r + q_2(d + x)\cos\theta_1 + q_1 d\cos\theta_2 \\ r_4 &= r + q_1(d + x)\cos\theta_1 - q_1 d\cos\theta_2 \end{aligned} \tag{2}$$

The θ_1 averaged potential can be then derived as

$$\begin{aligned} U(r,x,\theta_2) &= \frac{1}{2}\int_0^{\pi} U(r,x,\theta_1,\theta_2)\sin\theta_1 d\theta_1 = \\ & D\exp\left(l - \frac{r}{a}\right)\left\{\frac{a}{q_2(d+x)}\sinh\left[\frac{q_2(d+x)}{a}\right]\times\right. \\ & \left[\exp\left(-\frac{q_2 d}{a}\cos\theta_2\right) + \exp\left(-\frac{q_1 d}{a}\cos\theta_2\right)\right] + \\ & \frac{a}{q_1(d+x)}\sinh\left[\frac{q_1(d+x)}{a}\right]\left[\exp\left(-\frac{q_2 d}{a}\cos\theta_2\right) + \right. \\ & \left.\left.\exp\left(-\frac{q_1 d}{a}\cos\theta_2\right)\right]\right\} - 2D\exp\left(\frac{l}{2} - \frac{r}{2a}\right)\times \\ & \left\{\frac{2a}{q_2(d+x)}\sinh\left[\frac{q_2(d+x)}{2a}\right]\left[\exp\left(-\frac{q_2 d}{2a}\cos\theta_2\right) + \right.\right. \\ & \left.\exp\left(-\frac{q_1 d}{2a}\cos\theta_2\right)\right] + \frac{2a}{q_1(d+x)}\sinh\left[\frac{q_1(d+x)}{2a}\right]\times \\ & \left.\left[\exp\left(\frac{q_2 d}{2a}\cos\theta_2\right) + \exp\left(\frac{q_1 d}{2a}\cos\theta_2\right)\right]\right\} \end{aligned} \tag{3}$$

We now consider the relative importance of the terms in this expression in the region of strong interaction. The V–R energy transfer is most efficient through the interaction of the two hydrogen atoms.[13] Since we have already averaged the interaction over all possible values of the rotation angle θ_1, we need to specify the values of θ_2 falling in such a region. The interaction will be strong when the rotating H_r atom enters in the second and third quadrants of the angle θ_2; it is strongest at $\theta_2 = \pi$. Because the ratio d/a takes values of about 6 for the hydrogen halide molecules, we would therefore expect the overall magnitude of the interaction potential to be dominated by the first terms in both the repulsive and the attractive parts in eq 3. That is

$$\begin{aligned} U(r,x,\theta_2) = {} & D\exp\left(l - \frac{r}{a}\right)\frac{a}{q_2(d+x)}\times \\ & \sinh\left[\frac{q_2(d+x)}{a}\right]\exp\left(-\frac{q_2 d}{a}\cos\theta_2\right) - \\ & 2D\exp\left(\frac{l}{2} - \frac{r}{2a}\right)\frac{2a}{q_2(d+x)}\times \\ & \sinh\left[\frac{q_2(d+x)}{2a}\right]\exp\left(-\frac{q_2 d}{2a}\cos\theta_2\right) \end{aligned} \tag{4}$$

which will be used in the following derivation. For simplicity, we shall express θ_2 by θ and q_2 by q in the below.

Classical Equations of Motion

The rotational kinetic energy of H_r is $(1/2)m(qd)^2\dot{\theta}^2$, where m is the mass of the hydrogen atom. This energy can also be written as $(1/2)qI\dot{\theta}^2$, where I is the moment of inertia of the rotator. Then, with the potential energy given by eq 4, we obtain the Hamiltonian function for the H_v–H_r interaction by

$$\mathcal{H} = (1/2)m\dot{r}^2 + (1/2)qI\dot{\theta}^2 + U(r,0,\theta) \tag{5}$$

with, from eq 4

$$\begin{aligned} U(r,0,\theta) = {} & A\exp\left(l - \frac{r}{a}\right)\exp\left(-\frac{qd}{a}\cos\theta\right) - \\ & B\exp\left(\frac{l}{2} - \frac{r}{2a}\right)\exp\left(-\frac{qd}{2a}\cos\theta\right) \end{aligned}$$

$$A = \frac{Da}{qd}\sinh\left(\frac{qd}{a}\right)$$

$$B = \frac{4Da}{qd}\sinh\left(\frac{qd}{2a}\right)$$

where the x motion of the oscillator has been neglected. Hamilton's equations of motion needed to describe the present problem are

(15) The exact expression is, for example, $r_1^2 = r^2 - 2q_2(d + x)r\cos\theta_1 + 2q_2dr\cos\theta_2 + 2q_2^2d(d + x)(1 - \cos\theta_1\cos\theta_2 - \sin\theta_1\sin\theta_2\cos\phi)$, where the last term may be neglected for r sufficiently larger than q_2d.

$$\dot{p}_r = -\frac{\partial \mathcal{H}}{\partial r} \quad \text{and} \quad \dot{p}_\theta = -\frac{\partial \mathcal{H}}{\partial \theta} \tag{6}$$

where p's are momenta. For the peripheral atom H_r under the influence of the θ_1 averaged potential, these relations give

$$m\ddot{r} = \frac{1}{a}\left[A \exp\left(l - \frac{r}{a}\right) \exp\left(-\frac{qd}{a}\cos\theta\right) - \frac{1}{2} B \exp\left(\frac{l}{2} - \frac{r}{2a}\right) \exp\left(-\frac{qd}{2a}\cos\theta\right)\right] \tag{7a}$$

$$qI\ddot{\theta} = -\frac{qd}{a}\left[A \exp\left(l - \frac{r}{a}\right) \exp\left(-\frac{qd}{a}\cos\theta\right) - \frac{1}{2} B \exp\left(\frac{l}{2} - \frac{r}{2a}\right) \exp\left(-\frac{qd}{2a}\cos\theta\right)\right] \tag{7b}$$

The solution of eq 7b is necessary in determining the rotational trajectory $\theta(t)$ which will in turn be used in the calculation of V–R energy transfer probabilities. However, this equation also shows the effect of varying relative separation r on the rotational motion. In heteronuclear diatomic molecules such as hydrogen halides the translational motion may play a secondary role in causing vibrational transitions, the rotational motion being primary, while in homonuclear diatomic molecules the situation may be reversed; *i.e.*, the translational motion may dominate the rotational motion in controlling vibrational energy transfer. Even in HX, however, the rotation may not be much faster than the translation, particularly since the collisions involved are hard collisions. Therefore, for a rigorous description of the energy transfer problem in hydrogen halides, it should be important to include the effect of the translational motion by recognizing in eq 7b that both θ and r are time dependent.

Before solving eq 7b for $\theta(t)$, we thus need to obtain the r–t relation of the collision. Once we have this relation, the exponential part containing r in eq 7b can then be replaced by the corresponding θ-dependent factors. The function $r(t)$ determines the change of the distance between the centers of mass of H_vX_v and H_rX_r with the time. The potential energy for this relative motion is taken as

$$U(r) = D\left[\exp\left(l - \frac{r}{a}\right) - 2\exp\left(\frac{l}{2} - \frac{r}{2a}\right)\right] \tag{8}$$

which is in accordance with the form for the overall potential given above. The equation of motion subject to this energy is

$$\frac{dr}{dt} = \left\{\frac{2}{\mu}[E_0 - U(r)]\right\}^{1/2} \tag{9}$$

where μ is the reduced mass of the collision system and E_0 is the relative translational energy. The solution of this equation is well known[5]

$$t = a\left(\frac{2\mu}{E_0}\right)^{1/2} \cosh^{-1}\left\{\frac{\exp\left(\frac{r}{2a} - \frac{l}{2}\right) + \frac{D}{E_0}}{\left[\frac{D}{E_0} + \left(\frac{D}{E_0}\right)^2\right]^{1/2}}\right\} \tag{10}$$

In the region of strong interaction, however, the trajectory is affected little by the attractive energy, so we can approximate the potential by the repulsive form as[16] $U(r) = E_0 \exp(l - r/a)$. For this potential eq 10 reduces to

$$t = a\left(\frac{2\mu}{E_0}\right)^{1/2} \cosh^{-1}\left[\exp\left(\frac{r}{2a} - \frac{l}{2}\right)\right] \tag{11}$$

Upon substituting this expression into eq 7b, we find

$$qI\ddot{\theta} = -\frac{qd}{a}\left[A \operatorname{sech}^2\left(\frac{t}{a}\sqrt{\frac{E_0}{2\mu}}\right) \exp\left(-\frac{qd}{a}\cos\theta\right) - \frac{1}{2} B \operatorname{sech}\left(\frac{t}{a}\sqrt{\frac{E_0}{2\mu}}\right) \exp\left(-\frac{qd}{2a}\cos\theta\right)\right] \tag{12}$$

To be consistent with the approximation made in obtaining eq 11 from eq 10, we take the repulsive part of eq 12 in obtaining the rotational trajectory. It will be shown below that the molecular attraction term in eq 12 only affects the preexponential part of vibrational transition probabilities. However, the molecular attraction can contribute significantly to vibrational transitions, but this contribution results from the effect of molecular attraction on the collision time which will be derived below by use of the complete form of the rotational potential energy

$$U(\theta) = \frac{Da}{qd} \sinh\left(\frac{qd}{a}\right) \exp\left(-\frac{qd}{a}\cos\theta\right) - \frac{4Da}{qd} \sinh\left(\frac{qd}{2a}\right) \exp\left(-\frac{qd}{2a}\cos\theta\right) \tag{13}$$

The second term on the right-hand side represents the molecular attraction. Using the identity $\ddot{\theta} = \dot{\theta}(d\dot{\theta}/d\theta)$, we can integrate eq 12 from $\dot{\theta} = 0$ at $\theta = \theta_0$ to $\dot{\theta}$ at θ to find the following expression for the angular velocity produced by the collision

$$\dot{\theta} = \operatorname{sech}\left(\frac{t}{a}\sqrt{\frac{E_0}{2\mu}}\right)\left\{\frac{2A}{qI}\left[\exp\left(-\frac{qd}{a}\cos\theta_0\right) - \exp\left(-\frac{qd}{a}\cos\theta\right)\right]\right\}^{1/2}$$
$$\equiv \operatorname{sech}\left(\frac{t}{a}\sqrt{\frac{E_0}{2\mu}}\right)\left\{\frac{2}{qI}[E_r - U(\theta)]\right\}^{1/2} \tag{14}$$

which furnishes the angular velocity of the rotator if θ is known. The lower θ integration limit gave the rotational energy $A \exp[-(qd/a)\cos\theta_0]$, where we took $\theta_0 = 0$ at which the interaction potential between H_r and the oscillator is minimal; it takes the maximum

(16) D. Rapp, *J. Chem. Phys.*, **32**, 735 (1960).

value at $\theta = \pi$. The energy is then in the form of the relative rotational energy E_r at the lower limit, and in the second relation of eq 14 the limiting value was replaced by E_r.

Equation 14 can further be integrated from $\theta = \theta^*$ at $t = 0$ to θ at t to obtain the trajectory $\theta(t)$. The result is

$$a\left(\frac{2\mu}{E_0}\right)^{1/2} \tan^{-1}\left[\sinh\left(\frac{t}{a}\sqrt{\frac{E_0}{2\mu}}\right)\right] = \left(\frac{qI}{2}\right)^{1/2}\int_{\theta^*}^{\theta}\frac{d\theta}{[E_r - U(\theta)]^{1/2}} \quad (15)$$

where θ^* is the largest root of $U(\theta) = E_r$. The E_0 dependence of the left-hand side in eq 15 resulted from the translational motion of the colliding molecules. Of course, if we assumed that the translational motion is stationary during the rotational interaction (*i.e.*, the translational motion is "frozen"), then the left-hand side would simply reduce to t. We can show explicitly how the translational motion can affect the V–R energy transfer process. For the collision between two HX molecules, the translational motion bringing them together may be slow compared to the rotational motion (but not at all negligible). Then, in eq 15 we would expect $(t/a)(E_0/2\mu)^{1/2}$ to be smaller than unity, so that we can write

$$\sinh\left(\frac{t}{a}\sqrt{\frac{E_0}{2\mu}}\right) = \frac{t}{a}\sqrt{\frac{E_0}{2\mu}}\left[1 + \frac{E_0}{12\mu}\left(\frac{t}{a}\right)^2 + \dots\right]$$

and, in turn

$$\tan^{-1}\left[\sinh\left(\frac{t}{a}\sqrt{\frac{E_0}{2\mu}}\right)\right] = \frac{t}{a}\sqrt{\frac{E_0}{2\mu}}\left[1 - \frac{E_0}{12\mu}\left(\frac{t}{a}\right)^2 + \dots\right]$$

Hence, eq 15 becomes approximately

$$t\left[1 - \frac{E_0}{12\mu}\left(\frac{t}{a}\right)^2\right] = \left(\frac{qI}{2}\right)^{1/2}\int_{\theta^*}^{\theta}\frac{d\theta}{[E_r - U(\theta)]^{1/2}} \quad (16)$$

Although this relation will not be used in the following formulation of the vibrational transition probability, we find it useful in understanding the effect of the translational motion on the V–R energy transfer; the second term in the left-hand side stands for this effect.

An explicit evaluation of the integral in eq 15 for the rotational trajectory $\theta(t)$ does not appear to be possible because of the exponential dependence of U on θ. Although numerical solutions are possible, such solutions would make the present problem of deriving V–R energy transfer probabilities untractable because numerical integrations have to be carried out for all subsequent calculations. We can avoid these difficulties, however, by writing the integral in the form

$$-i\int\frac{\theta'(U)dU}{[U(\theta) - E_r]^{1/2}}$$

in which the inverse derivative, in the region of strong interaction, can be expressed in the general form

$$\theta'(U) = \frac{d\theta}{dU} = \frac{1}{U}\sum_{i=0}^{\infty}\frac{\alpha_i^*}{U^i} \quad i = 0, 1/2, 1, 3/2, 2, \dots \quad (17)$$

The region of strong interaction is the neighborhood of $\theta_2 = \pi$. Therefore, as θ_2 approaches this angle through clockwise rotation the derivative $\theta'(U)$ is negative while it is positive for counterclockwise rotation. On the other hand, when θ_2 move away from π the derivative takes a positive value for clockwise rotation and a negative value for counterclockwise rotation. However, in the following determination of the trajectory, we find that the derivative has to be a negative function. In eq 23 and 26 given below for the θ–t relation and the collision time, respectively, we shall take this aspect into consideration.

From the potential energy $U(\theta)$ given in eq 13 we obtain the inverse function as

$$\theta(U) = \cos^{-1}\left\{-\frac{2a}{qd}\log\left[\frac{B + (B^2 + 4AU)^{1/2}}{2A}\right]\right\} \quad (18)$$

and its derivative as

$$\theta'(U) = \frac{4aA}{qd} \times \frac{1}{(B^2 + 4AU)^{1/2}[B + (B^2 + 4AU)^{1/2}] \times \left\{1 - \left(\frac{2a}{qd}\right)^2 \log^2\left[\frac{B + (B^2 + 4AU)^{1/2}}{2A}\right]\right\}^{1/2}}$$

Since $(2a/qd)^2 \ll 1$ and $U \gg B^2/4A$ (but not necessarily $U \gg A$), we can perform lengthy but elementary expansions of the parts in the denominator of the above expression for the derivative including the logarithmic function to obtain eq 17 with the coefficients

$$\alpha_0^* = \frac{(1 + \alpha)a}{qd}$$

$$\alpha_{1/2}^* = -\frac{\alpha_0^*}{2A^{1/2}}\left(B + \frac{\beta}{1 + \alpha}\right)$$

$$\alpha_1^* = \frac{\alpha_0^*(2\beta B + \gamma)}{4A(1 + \alpha)}$$

$$\alpha_{3/2}^* = \frac{\alpha_0^*}{16A^{3/2}}\left(B^3 - \frac{3\beta B^2 + 2\gamma B + 4\beta\gamma}{1 + \alpha}\right)$$

$$\alpha_2^* = \frac{\alpha_0^*(2\beta\gamma B + B^2\gamma + \beta^2\gamma)}{16A^2(1 + \alpha)}$$

where

$$\alpha = \frac{9}{2}\left(\frac{a}{qd}\right)^2\left[1 + \frac{4}{3}\left(\frac{a}{qd}\right)^2\right]$$

$$\beta = 26\left(\frac{a}{qd}\right)^2\left[1 + \frac{24}{13}\left(\frac{a}{qd}\right)^2\right]A$$

$$\gamma = 50\left(\frac{a}{qd}\right)^2\left[1 + \frac{72}{25}\left(\frac{a}{qd}\right)^2\right]A^2$$

In the sum, the $i = 1$ and $i = 2$ terms are very small compared to the others. Furthermore, in the $i = {}^1/_2$ term $B \gg \beta/(1 + \alpha)$ and in the $i = {}^3/_2$ term $B^3 \gg (3\beta B^2 + 2\alpha B + 4\beta\gamma)/(1 + \alpha)$. Therefore, for practical purposes we can approximate the inverse derivative by

$$\theta'(U) = \frac{\alpha_0^*}{U}\left[1 - \frac{B}{2(AU)^{1/2}} + \frac{B^3}{16(AU)^{3/2}} + \cdots\right] \equiv \frac{1}{U}\sum_{i=0}^{\infty}\frac{\alpha_i}{U^i} \quad (19)$$

which will be used in the following derivation of the θ–t relation and the rotational collision time. By comparing eq 19 with eq 17, we note that $\alpha_i \neq \alpha_i^*$ except $i = 0$. We also note that the leading term of the derivative, which is α_0^*/U, is the most important factor for the present collision problem.

Amount of Vibrational Energy Transfer and Transition Probability

The amount of the vibrational energy transferred to an oscillator, which has no initial vibrational energy, is given by[16-18]

$$\Delta E = \frac{1}{2M}\left|\int_{-\infty}^{\infty} F(t)\exp(i\omega t)\mathrm{d}t\right|^2 \quad (20)$$

where M, ω are the reduced mass and angular frequency of the oscillator, respectively, and $F(t)$ is the time-dependent perturbing force, which is obtained from the overall interaction by linearizing eq 4 in the vibrational coordinate x. The resulting form of $F(t)$ is

$$F(t) = -\frac{Da}{qd^2}\exp\left(l - \frac{r}{a}\right)\sinh\left(\frac{qd}{a}\right)\times \exp\left(-\frac{qd}{a}\cos\theta\right)\left[1 - \frac{qd}{a}\coth\left(\frac{qd}{a}\right)\right] + \frac{4Da}{qd^2}\exp\left(\frac{l}{2} - \frac{r}{2a}\right)\sinh\left(\frac{qd}{2a}\right)\times \exp\left(-\frac{qd}{2a}\cos\theta\right)\left[1 - \frac{qd}{2a}\coth\left(\frac{qd}{2a}\right)\right] \quad (21)$$

where the t dependence on the right-hand side is implicitly given through the trajectories $\theta(t)$ and $r(t)$ derived above. We need the result of eq 15 in eq 20; with the inverse derivative given in eq 19 we can make an explicit evaluation of the right-hand side in eq 15. However, the resulting form is difficult to use in the evaluation of eq 20. To facilitate the evaluation,[19] we replace integration along the real axis by integration along a contour, which extends from $+i\infty$, encircles the singular point of the integrand, and from this point follows a cut in the plane of the complex variable t. Recognizing that $U(\theta) \gg E_r$ in the region of strong interaction, we can write[20]

$$a\left(\frac{2\mu}{E_0}\right)^{1/2}\tan^{-1}\left[\sinh\left(\frac{t}{a}\sqrt{\frac{E_0}{2\mu}}\right)\right] = i\left(\frac{qI}{2}\right)^{1/2}\int_{\theta^{\pm}}^{\theta^*}\frac{\mathrm{d}\theta}{[U(\theta) - E_r]^{1/2}} - i\left(\frac{qI}{2}\right)^{1/2}\times \int_{\theta^{\pm}}^{\theta}\frac{\mathrm{d}\theta}{[U(\theta) - E_r]^{1/2}} \equiv it_r - i\left(\frac{qI}{2}\right)^{1/2}\int_{\theta^{\pm}}^{\theta}\frac{\mathrm{d}\theta}{[U(\theta) - E_r]^{1/2}} \quad (22)$$

where t_r will be defined as "the collision time" for the V–R energy transfer process. The integration limit $\theta^{\pm}$ represents the rotational angle at which the interaction potential is most repulsive. Physically, the rotator will have difficulty in aligning itself with H_vX_v at $\theta = \pi$ because of strong repulsion at close-in collisions. Therefore, the most favorable angle for V–R energy transfer would be close to but not equal to π; *i.e.*, $\theta^{\pm} \simeq \pi$ satisfying the condition $U(\theta^{\pm}) \gg E_r$. The solution of eq 22 will then be used to transform $U(\theta)$ to $U(t)$.

To obtain the rotational trajectory, we need to solve the second integral of eq 22 in the region of strong interaction, where the derivative can be approximated by the leading term, $\theta'(U) = (1 + \alpha)a/qdU$. The effect of the higher order terms of $\theta'(U)$ on the collision process will be explicitly considered in the formulation of the collision time. Then, the integration leads to the θ–t relation in the form

$$A^{1/2}\exp\left(-\frac{qd}{2a}\cos\theta\right) = \frac{(2qI)^{1/2}\alpha_0}{i\left\{a\sqrt{\frac{2\mu}{E_0}}\tan^{-1}\left[\sinh\left(\frac{t}{a}\sqrt{\frac{E_0}{2\mu}}\right)\right] - it_r\right\}} \quad (23)$$

from which the time-dependent force $F(t)$ can be explicitly obtained.

With eq 21 and 23, we find two integrals of the type

$$\int_{-\infty}^{\infty}\frac{\mathrm{sech}^2\left(\frac{t}{a}\sqrt{\frac{E_0}{2\mu}}\right)\exp(i\omega t)\mathrm{d}t}{\left\{a\sqrt{\frac{2\mu}{E_0}}\tan^{-1}\left[\sinh\left(\frac{t}{a}\sqrt{\frac{E_0}{2\mu}}\right)\right] - it_r\right\}^n}$$

in eq 20, where $n = 2$ and 1 representing, respectively, the parts due to the repulsive and the attractive interactions. The integrand has a simple pole at

$$t = a\sqrt{\frac{2\mu}{E_0}}\sinh^{-1}\left[i\tanh\left(\frac{t_r}{a}\sqrt{\frac{E_0}{2\mu}}\right)\right]$$

(17) K. Takayanagi, *Progr. Theoret. Phys. Suppl. (Japan)*, **25**, 1 (1963).

(18) H. Shin, *Chem. Phys. Lett.*, **5**, 137 (1970).

(19) E. E. Nikitin, *Opt. Spectrosk.*, **6**, 141 (1959); *Opt. Spectry. (USSR) (English Transl.)*, **6**, 93 (1959). Also see, L. Landau and E. Teller, *Phys. Z. Sowjetunion*, **10**, 34 (1936).

(20) H. Shin, *J. Phys. Chem.*, **73**, 4321 (1969).

and straightforward contour integration gives the result of eq 20 as

$$\Delta E = \frac{8}{M}\left(\frac{\pi\omega I a}{d^2}\right)^2\left(\frac{a}{qd}\right)^2(1+\alpha)^4 \times \left[1-\frac{qd}{a}\coth\left(\frac{qd}{a}\right)\right]^2\left[1-\frac{1}{\omega a}\sqrt{\frac{2E_0}{\mu}}\sinh\left(\frac{t_r}{a}\sqrt{\frac{E_0}{2\mu}}\right)\right]^2 \times \left\{1-\frac{4\sinh\left(\frac{qd}{2a}\right)\left[1-\frac{qd}{2a}\coth\left(\frac{qd}{2a}\right)\right]}{\left[\sinh\left(\frac{qd}{a}\right)\right]^{1/2}\left[1-\frac{qd}{a}\coth\left(\frac{qd}{a}\right)\right]}\right\}^2 \times \sqrt{\frac{Dd}{2Ia}}\frac{1}{(1+\alpha)\omega}\frac{1}{\left[1-\tanh^2\left(\frac{t_r}{a}\sqrt{\frac{E_0}{2\mu}}\right)\right]^{1/2}} \times \frac{1}{\left[1-\frac{1}{a\omega}\sqrt{\frac{2E_0}{\mu}}\sinh\left(\frac{t_r}{a}\sqrt{\frac{E_0}{2\mu}}\right)\right]^{1/2}} \times \exp\left\{2i\omega a\sqrt{\frac{2\mu}{E_0}}\sinh^{-1}\left[i\tanh\left(\frac{t_r}{a}\sqrt{\frac{E_0}{2\mu}}\right)\right]\right\} \quad (24)$$

In the preexponential part, the D-dependent term resulted from the molecular attraction, but its contribution to the overall magnitude of ΔE is not large.

The completion of the formulation of ΔE requires the evaluation of the collision time, which in the region of strong interaction can be written as

$$t_r = \left(\frac{qI}{2}\right)^{1/2}\lim_{U^{\pm}\to\infty}\int_{U^{\pm}}^{E_r}\frac{\theta'(U)\mathrm{d}U}{[U(\theta)-E_r]^{1/2}} \quad (25)$$

which, with eq 19, becomes

$$t_r = \left(\frac{qI}{2}\right)^{1/2}\sum_{i=0}^{\infty}\alpha_i\lim_{U^{\pm}\to\infty}\int_{E_r}^{U^{\pm}}\frac{\mathrm{d}U}{U^{1+i}(U-E_r)^{1/2}} \quad (26)$$

In this expression the integral can be readily reduced to the β function. The result is then

$$t_r = \left(\frac{\pi qI}{2E_r}\right)^{1/2}\sum_{i=0}^{\infty}\frac{\Gamma(1/2+i)}{\Gamma(1+i)}\frac{\alpha_i}{E_r{}^i} \quad (27)$$

The final expression for the amount of energy transfer can then be derived from eq 24 and 27. For practical purposes, we would need to include only a few early terms of the i sum in eq 27 for the collision time. Here the second- and higher-order terms are responsible for the effect of molecular attraction.

In the classical model, the probability of vibrational excitation ($0 \to 1$) per collision can be expressed as

$$\mathbf{P}_{01}(E_r,E_0) = \frac{\Delta E}{\hbar\omega} \quad (28)$$

To investigate the relaxation process of vibrationally excited molecules ($1 \to 0$), we need to derive the thermal-average transition probability from eq 24 and 28. Assuming a Boltzmann distribution of the rotational and translational energies, this probability may be defined by

$$\mathbf{P}_{01}(\mathrm{T}) = \frac{1}{(kT)^2}\int_0^{\infty}\int_0^{\infty}\mathbf{P}_{01}(E_r,E_0) \times \exp[-(E_r+E_0)/kT]\mathrm{d}E_r\mathrm{d}E_0 \quad (29)$$

We first evaluate the E_r integral by writing eq 29 as

$$\mathbf{P}_{01}(\mathrm{T}) = \frac{1}{(kT)^2}\int_0^{\infty}\int_0^{\infty}Q(E_r,E_0)\exp\left\{2i\omega a\sqrt{\frac{2\mu}{E_0}} \times \sinh^{-1}\left[i\tanh\left(\frac{t_r}{a}\sqrt{\frac{E_0}{2\mu}}\right)\right]-\frac{E_r}{kT}\right\} \times \exp\left(-\frac{E_0}{kT}\right)\mathrm{d}E_r\mathrm{d}E_0$$

$$= \frac{1}{(kT)^2}\int_0^{\infty}\exp\left(-\frac{E_0}{kT}\right)\mathrm{d}E_0 \times \int_0^{\infty}\exp[\mathfrak{F}(E_r,E_0)]\mathrm{d}E_r \quad (30)$$

in which t_r is given by eq 27. Here $Q(E_r,E_0)$ is the preexponential part of ΔE divided by $\hbar\omega$ and is weakly dependent on E_r. In $Q(E_r,E_0)$, the E_r dependence appears in the hyperbolic function of $(t_r/a)(E_0/2\mu)^{1/2} = t_r v_0/2a$, where v_0 is the relative velocity. The last quantity may be identified as $t_r/2t_t$, where t_t ($= a/v_0$) is defined as the translational collision time. The present study is based on the model in which H_rX_r is making rapid rotational motion, while the relative translational motion varies slowly in the region of strong interaction. Therefore, we have the situation that $t_r/t_t \ll 1$ or $(t_r/a)(E_0/2\mu)^{1/2} \ll 1$. Hence, $\sinh[(t_r/a)(E_0/2\mu)^{1/2}] \simeq \tanh[(t_r/a)(E_0/2\mu)^{1/2}] \simeq (t_r/a)\cdot(E_0/2\mu)^{1/2}$, so that in the preexponential part of eq 24

$$\left[1-\frac{1}{\omega a}\sqrt{\frac{2E_0}{\mu}}\sinh\left(\frac{t_r}{a}\sqrt{\frac{E_0}{2\mu}}\right)\right]^2 \simeq \left[1-\frac{t_r E_0}{\omega\mu a^2}\right]^2 \quad (31)$$

If we further define $1/\omega$ as the vibration period t_v, then this last quantity can be written as

$$\left[1-\frac{1}{2}\left(\frac{t_r}{t_t}\right)\left(\frac{t_v}{t_t}\right)\right]^2$$

Unless the collision energy is very high, we normally have the relation $t_v/t_t \ll 1$; therefore this quantity is not significantly different from unity. A similar simplification can be made to the hyperbolic tangent term in the attractive part. While such a simplification can be made in the preexponential part, we must not apply it to the exponential part which is strongly dependent on E_r and E_0.

In the evaluation of the E_r integral in eq 30 we can therefore replace the slowly varying preexponential part by its value at $E_r{}^*$ and use the Laplace integration method,[21] where $E_r{}^*$ is the largest root of

$$\frac{\partial \mathfrak{F}(E_r,E_0)}{\partial E_r} = 0 \tag{32}$$

i.e., from eq 30

$$2\omega \operatorname{sech}\left(\frac{t_r}{a}\sqrt{\frac{E_0}{2\mu}}\right)\frac{\partial t_r}{\partial E_r} = -\frac{1}{kT} \tag{33}$$

where

$$\frac{\partial t_r}{\partial E_r} = -\left(\frac{\pi qI}{2}\right)^{1/2}\sum_{i=0}^{\infty}\frac{\Gamma(3/2+i)}{\Gamma(1+i)}\frac{\alpha_i}{E_r^{3/2+i}}$$

The energy E_r^*, which may be called "the most probable rotational energy" for vibrational energy transfer, is found to be

$$E_r^* = \chi + \frac{8}{3\pi}\left(\frac{\alpha_{1/2}}{\alpha_0}\right)\chi^{1/2} - \left[\frac{16}{3\pi^2}\left(\frac{\alpha_{1/2}}{\alpha_0}\right)^2 + \frac{\pi^2(1+\alpha)^2}{12}\frac{m}{\mu}E_0\right] \tag{34}$$

where

$$\chi = \left[\left(\frac{qI}{2}\right)^{1/2}\frac{\pi(1+\alpha)a\omega kT}{qd}\right]^{2/3}$$

After a lengthy calculation by use of the Laplace method, we obtain the expression

$$\mathbf{P}_{01}(\mathrm{T}) = \left(\frac{4\pi\chi}{3kT}\right)^{1/2}\exp\left\{-\frac{3\chi}{kT} + \frac{8}{\pi}\left(\frac{a}{qd}\right)^{1/2}\frac{\sinh\left(\frac{qd}{2a}\right)}{\left[\sinh\left(\frac{qd}{a}\right)\right]^{1/2}}\times \frac{(D\chi)^{1/2}}{kT} + \frac{64}{3\pi^2}\frac{a}{qd}\frac{\sinh^2\left(\frac{qd}{2a}\right)}{\sinh\left(\frac{qd}{a}\right)}\frac{D}{kT} - \frac{\hbar\omega}{2kT}\right\}\times \int_0^\infty Q(E_r^*,E_0)\exp\left[\frac{\pi^2}{12}(1+\alpha)^2\times\left(\frac{m}{\mu}\right)\frac{E_0}{kT} - \frac{E_0}{kT}\right]\frac{dE_0}{kT} \tag{35}$$

Since E_r is the relative rotational energy before excitation of the oscillator, the final rotational energy is $E_r - \hbar\omega$, so that we can write the symmetrized energy as $E_{sym} = E_r - (1/2)\hbar\omega$. The last term in the exponent of eq 35 is due to this symmetrization. To obtain the thermal-average transition probability appropriate to deexcitation of the oscillator, *i.e.*, $\mathbf{P}_{10}(\mathrm{T})$, rather than to an excitation, we have merely to replace this last term by $+\hbar\omega/2kT$.

Before carrying out the E_0 integration in eq 35, we make the following observation to simplify the preexponential part of $\mathbf{P}_{01}(E_r,E_0)$. As shown in eq 24 the E_0 dependence appears in both the repulsive and the attractive contributions in the preexponential part. However, in this type of problem, the second term in the preexponential part, which is due to molecular attraction, is very small compared to the first term (the former being normally less than 5% of the latter). Furthermore, the E_0 dependence appears in the preexponential part as higher order corrections in both the first and second terms. Therefore, for all practical purposes, we can ignore the E_0 dependence of the second term but not that of the first. Hence, the preexponential part can be written as

$$Q(E_r^*,E_0) = \frac{8\omega}{\hbar M}\left(\frac{\pi Ia}{d^2}\right)^2\left(\frac{a}{qd}\right)^2(1+\alpha)^4\times \left[1-\frac{qd}{a}\coth\left(\frac{qd}{a}\right)\right]^2\left[1-\frac{t_r^*E_0}{\omega\mu a^2}\right]^2\times \left\{1-\frac{4\sinh\left(\frac{qd}{2a}\right)\left[1-\frac{qd}{2a}\coth\left(\frac{qd}{2a}\right)\right]}{\left[\sinh\left(\frac{qd}{a}\right)\right]^{1/2}\left[1-\frac{qd}{a}\coth\left(\frac{qd}{a}\right)\right]}\times \left(\frac{Dd}{2Ia}\right)^{1/2}\frac{1}{(1+\alpha)\omega}\right\}^2 \equiv Q\left[1-\frac{t_r^*E_0}{\omega\mu a^2}\right]^2 \tag{36}$$

where the relation given in eq 31 has been used. Here t_r^* is the collision time given by eq 27 evaluated $E_r = E_r^*$, and we will take the leading term only. With eq 36, the E_0 integration has been carried out with the result

$$\mathbf{P}_{01}(\mathrm{T}) = Qf_{vt}(\mathrm{T})\left(\frac{4\pi\chi}{3kT}\right)^{1/2}\times \exp\left\{-\frac{3\chi}{kT} + \frac{8}{\pi}\left(\frac{a}{qd}\right)^{1/2}\frac{\sinh\left(\frac{qd}{2a}\right)}{\left[\sinh\left(\frac{qd}{a}\right)\right]^{1/2}}\frac{(D\chi)^{1/2}}{kT} + \frac{64}{3\pi^2}\frac{a}{qd}\frac{\sinh^2\left(\frac{qd}{2a}\right)}{\sinh\left(\frac{qd}{a}\right)}\frac{D}{kT} - \frac{\hbar\omega}{2kT}\right\} \tag{37}$$

where

$$f_{vt}(\mathrm{T}) = \left[1-\frac{\pi^2}{12}(1+\alpha)^2\left(\frac{m}{\mu}\right)\right]^{-1}\times \left[1-\frac{2}{\left[1-\frac{\pi^2}{12}(1+\alpha)^2\left(\frac{m}{\mu}\right)\right]^2}\left(\frac{t_r^*kT}{\omega\mu a^2}\right)^2\times \left[1-\frac{\pi^2}{12}(1+\alpha)^2\left(\frac{m}{\mu}\right)\right]\frac{\omega\mu a^2}{t_r^*kT} - 1\right] \tag{38}$$

(21) N. G. de Bruijn, "Asymptotic Methods in Analysis," North-Holland Publishing Co., Amsterdam, 1961, 2nd ed, Chapter 4.

This last factor represents the effect of the translational motion on the vibrational excitation of H_vX_v. The remaining portion of eq 37, which we shall denote $\mathbf{P}_{vr}(T)$, is of course due to the rotational motion of H_rX_r under the interaction energy $U(r,x,\theta)$ given by eq 4. If we completely neglected the effect of the translational motion, then $f_{vt}(T) = 1$. The transition probability can also be expressed as

$$\mathbf{P}_{01}(T) = f_{vt}\mathbf{P}_{vr}(T) \tag{39}$$

In eq 37 the second and third terms in the exponent are due to molecular attraction which is represented by the second term of $U(\theta)$. The molecular attraction normally makes a substantial contribution to the overall value of $\mathbf{P}_{01}(T)$. We also note that the molecular attraction tends to increase the magnitude of the exponential part but decreases that of the preexponential part; the former effect is *always* much greater than the latter.

Calculation of Vibrational Relaxation Times and Discussion

In this section we will apply the above formulation to calculate vibrational relaxation times of HCl and DCl for the temperature range from 800 to 2000°K. The real test of the formulation comes in finding relaxation times of the proper magnitude and, at the same time, the proper temperature dependence of the isotope effect. After establishing the applicability of the present formulation to these collision systems and investigating the isotope effect, we shall calculate relaxation times of HBr and HI molecules for the same temperature region. The vibration relaxation time is expressed by

$$\tau_v = \frac{1}{Z\mathbf{P}_{10}(T)[1 - \exp(-\hbar\omega/kT)]} \tag{40}$$

Here Z is the number of collisions per molecule and per second, which is conveniently based on the kinetic theory expression $Z = 4N\rho^2(\pi kT/m^*)^{1/2}$, where N is the number of molecules per cubic centimeter, ρ is the collision diameter to be defined, and m^* is the molecular mass. For the collision systems, we have used the molecular and potential constants listed in Table I. The quantity a which appeared in the formulation is a range parameter for the interaction potential, and it should be uniquely determined for the collision system under consideration. This parameter can be determined by equating $\mathbf{P}_{01}(T)$ for the present potential with that for Lennard-Jones (12–6) potential. Since the dominating part of $\mathbf{P}_{01}(T)$ is the exponential part $\exp(-3\chi/kT)$, we may determine it by equating this factor with the corresponding value for the Lennard-Jones potential. In the present formulation, instead of the exponential potential, if we used the Lennard-Jones potential, we obtain[22]

$$\exp\left\{-\frac{19}{7kT}\left[\frac{\Gamma\left(\frac{19}{12}\right)(2\pi qI)^{1/2}(4D)^{1/12}\sigma\omega kT}{\Gamma\left(\frac{1}{12}\right)d}\right]^{12/19}\right\}$$

as the corresponding factor, where σ is the Lennard-Jones potential parameter, *i.e.*, $U_{LJ}(\sigma) = 0$. The calculated values of a, which change very little with the temperature, are listed in Table II.

Table I: Potential and Molecular Constants

	HCl	DCl	HBr	HI
D/k, °K[a]	360	360	417	324
σ, Å[a]	3.305	3.305	3.41	4.123
ν, cm^{-1} [b]	2886	2090	2560	2230
$\tilde{\mu}$, D[a]	1.08	1.08	0.8	0.42

[a] J. O. Hirschfelder, C. F. Curtiss, and R. B. Bird, "Molecular Theory of Gases and Liquids," Wiley, New York, N. Y., 1964, pp 1112, 1200. [b] G. Herzberg, "Spectra of Diatomic Molecules," D. Van Nostrand Co., Princeton, N. J., 1950, Table 39. For the $1 \rightarrow 0$ transition of the normal molecules, we employ $\nu \simeq \omega_e - 2\omega_e\chi_e$; see p 95.

Table II: Calculated Values of a and r^* (in Å)

		T, °K					
		800	1000	1200	1500	1800	2000
HCl	a	0.227	0.225	0.222	0.219	0.217	0.216
	r^*	2.72	2.73	2.74	2.75	2.76	2.77
DCl	a	0.227	0.225	0.222	0.219	0.217	0.216
	r^*	2.83	2.84	2.85	2.86	2.87	2.88
HBr	a	0.238	0.235	0.233	0.230	0.228	0.226
	r^*	2.79	2.80	2.81	2.83	2.84	2.85
HI	a	0.281	0.278	0.275	0.272	0.269	0.268
	r^*	3.14	3.15	3.16	3.18	3.19	3.20

In making the calculation of relaxation times, it should be necessary to introduce a physical argument to define the collision diameter so that the expression Z can properly represent characteristic of close-in collisions. In the present system, molecules exchange their energies at small separations, and we consider only those collisions with the separation r^* to be effective for energy transfer; *i.e.*, we define $\rho = r^*$ in the expression for Z. This distance should then represent "the most probable distance" for the colliding molecules to exchange their energies. The distance has been derived in an earlier paper by an independent procedure;[23] the derivation for the present interaction model gives

$$r^* = \left[\frac{14\sigma^6}{\omega}\left(\frac{2A'}{\mu}\right)^{1/2}\right]^{1/7} \tag{41}$$

(22) H. Shin, *J. Chem. Phys.*, **41**, 2864 (1964).
(23) H. Shin, *ibid.*, **46**, 744 (1967).

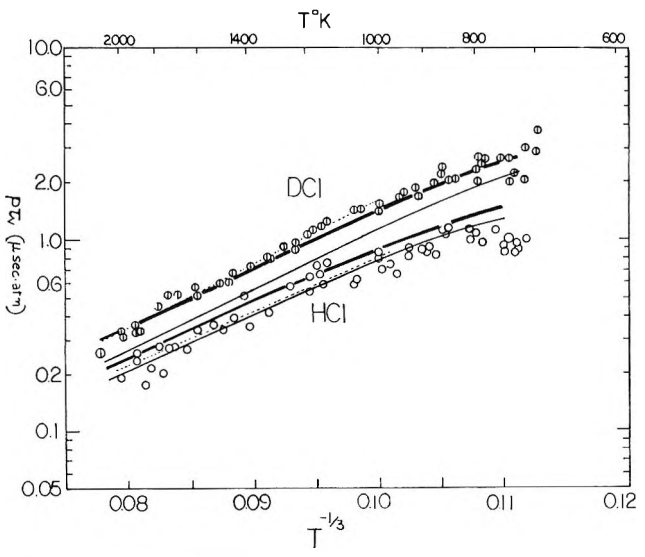

Figure 2. Plot of log $p\tau_v$ *vs.* $T^{-1/3}$ for HCl and DCl. The solid curves represent the present calculation; the heavy curves with $\mathbf{P}_{10}(T) = \mathbf{P}_{vr}(T)f_{vt}(T)$ and the light curves with $\mathbf{P}_{10}(T) = \mathbf{P}_{vr}(T)$. Experimental points and their least-squares fits are reproduced from Figure 3 of ref 3b (O, HCl; ⊕, DCl). The dotted lines represent least-squares fits.

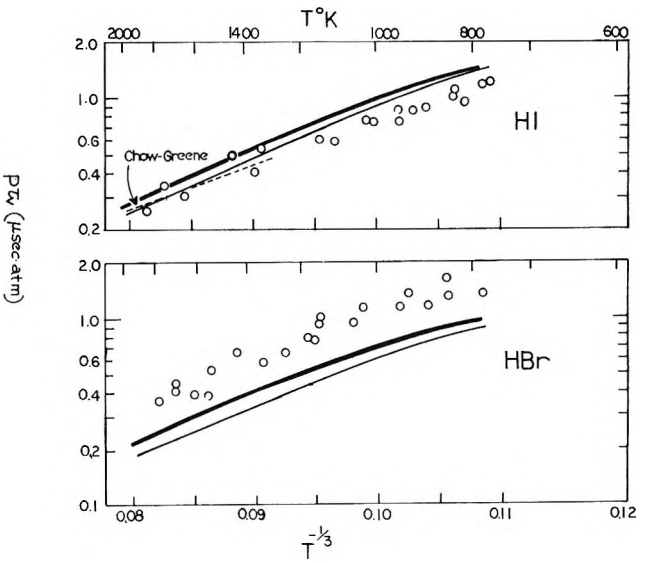

Figure 3. Plot of log $p\tau_v$ *vs.* $T^{-1/3}$ plot for HBr and HI; the heavy curves with $\mathbf{P}_{10}(T) = \mathbf{P}_{vr}(T)f_{vt}(T)$ and the light curves with $\mathbf{P}_{10}(T) = \mathbf{P}_{vr}(T)$. Experimental data (O) are reproduced from Figure 1 of ref 14. The dotted line for HI is reproduced from Figure 8 of ref 7.

where $A' = (aD/2qd)\exp(qd/a)$. The calculated values of r^* are also shown in Table II; they are nearly constant over the temperature range considered. Both r^* and a are now explicitly known.

We shall calculate vibrational relaxation times (actually $p\tau_v$, the relaxation time at 1 atm) for HCl and DCl and plot the results in Figure 2 as a function of $T^{-1/3}$ for the temperature range from 800 to 2000°K. In this figure, as well as in Figure 3 below, the *heavy* solid curves represent the values of $p\tau_v$ obtained from $\mathbf{P}_{01}(T) = f_{vt}(T)\mathbf{P}_{vr}(T)$ which includes the effect of the translational motion, while the *light* solid curves represent the $p\tau_v$ values obtained based on the purely V–R mechanism, *i.e.*, $\mathbf{P}_{01}(T)$ with $f_{vt}(T) = 1$. Experimental values of $p\tau_v$ shown in this figure were obtained by Breshears and Bird by means of shock-wave measurements;[3b] the broken lines represent least-squares fits of their data above 1000°K to the Landau–Teller form. The agreement between this calculation (heavy solid curve) and the experimental data for HCl is in general good, although the calculation gives somewhat larger values. For DCl, the present theory is excellent over the entire temperature range considered. If we do not consider the translational motion at all, the calculation gives the values of $p\tau_v$ smaller than the experimental result by a factor of about 1.6 (see light solid curve). In both HCl and DCl, the calculated temperature dependence (*i.e.*, slope) also agrees with experiment. Another important result is that the calculated effect of isotopic substitution is in line with experiment. The ratio $p\tau_v(DCl)/p\tau_v(HCl)$ takes the values 1.89, 1.51, 1.43, 1.35, 1.29, and 1.25 at 800, 1000, 1200, 1500, 1800, and 2000°K, respectively.

It is seen that because of the dominating role of the leading term $-3\chi/kT$ in the exponent of $\mathbf{P}_{10}(T)$, the calculation shows an essentially linear relationship between log $p\tau_v$ and $T^{-1/3}$ especially at higher temperatures. For example, for HCl the values of $3\chi/kT$, $8(D\chi)^{1/2}G/\pi kT$, $64DG^2/3\pi^2kT$, and $\hbar\omega/2kT$ are 16.2, 1.21, 0.091, and 2.59, respectively, at 800°K, where $G = \sinh(dq/2a)/[(qd/a)\sinh(qd/a)]^{1/2}$. Here the second and third terms are due to molecular attraction, and make a substantial contribution to the magnitude and temperature dependence of the relaxation time.

The molecular collision has been treated as one dimensional. Since we have started the formulation of the probability with the interaction potential which specifically considers the role of the orientation angles θ_1 and θ_2 of the colliding molecules, the introduction of a steric factor, less than unity, is not needed. In V–T energy transfer treated by assuming the molecules to collide collinearly, such a factor must be multiplied to obtain an average over all initial collision orientations. However, to make a full three-dimensional analysis of the present collision problem it should be necessary to introduce the impact parameter in the solution of the equation of motion. Another aspect we need to mention is the possibility of multiple rotational collision during a single molecular encounter. Such a possibility arises since the molecular collision time is long compared to both the rotational time and the vibrational period. In V–T energy, with the assumption of hard-sphere interaction, we can make quantitative analyses of the effect of impact multiplicity on energy transfer.[24–26] However, for soft interaction potentials such as one we used above it is not so clear exactly

what constitutes a collision, and in turn it is nearly impossible to calculate the number of impacts in a single encounter and the amount of energy transfer at each impact. As in V–T energy transfer, we should be able to analyze the problem of multiple-impact rotational collision for the hard-sphere interaction, however.

An important difference between the magnitude of V–R energy transfer probability in HCl and that in DCl comes from the difference in their vibrational quanta which appear in the exponent of $\mathbf{P}_{10}(T)$ as $\hbar\omega/2kT$ and from the translational effect which appears in the preexponential part (see Table III). Other terms in both the exponential and preexponential parts changed little, if any, by the isotopic substitution; *e.g.*, at 800°K the four terms in the exponent of $\mathbf{P}_{10}(T)$ for HCl are 16.2, 1.21, 0.091, and 2.59, while the corresponding values for DCl are 16.7, 1.23, 0.091, and 1.88. The isotopic substitution changes χ through ω and I. The deuteration results in an increase in the mass and a decrease in the vibrational frequency, but these two quantities enter in χ as $I^{1/3}\omega^{2/3}$ such that the two opposing effects largely cancel out each other. The preexponential part of $\mathbf{P}_{10}(T)$ for DCl is larger than that of HCl by a factor of about 1.5.

Table III: Calculated Values of $f_{vt}(T)$

T, °K	HCl	DCl	HBr	HI
800	0.891	0.812	0.939	0.966
1000	0.868	0.775	0.926	0.956
1200	0.844	0.744	0.914	0.948
1500	0.814	0.706	0.897	0.937
1800	0.788	0.676	0.881	0.927
2000	0.771	0.661	0.871	0.921

By comparing the above expression for $\mathbf{P}_{10}(T)$ with the conventional V–T energy transfer probability, we find a close similarity between their forms. An important relation is that the reduced mass μ occurs in the V–T expression instead of the quantity I/d^2 as shown in eq 37. In the well-known SSH theory[27] for V–T energy transfer, the same form of χ appears in $\mathbf{P}_{10}(T)$ containing μ instead of I/d^2. Also, the WKB evaluation of $\mathbf{P}_{10}(T)$ in the method of distorted waves for V–T energy transfer shows[28] a close resemblance with the present V–R result. With the mass μ, then the leading term $3\chi/kT$ becomes very large and furthermore, the value of $(3\chi/kT)_{HCl}$ greatly exceeds that of $(3\chi/kT)_{DCl}$; *e.g.*, at 1000°K, $(3\chi/kT)_{HCl} = 33.6$ and $(3\chi/kT)_{DCl} = 27.7$, which lead to the ratio

$$\frac{\exp(-3\chi/kT)_{DCl}}{\exp(-3\chi/kT)_{HCl}} = 365$$

Although other factors and terms appeared in $\mathbf{P}_{10}(T)$ for V–T energy transfer may contribute to change this large difference, we will still find that $\tau_v(HCl) \gg \tau_v(DCl)$, the result which disagrees with the present calculation based on the V–R energy transfer mechanism and with the experimental evidence (see Figure 4 of ref 3b). Note that for V–R energy transfer process, $3\chi/kT$ at 1000°K is 15.0 for HCl and 15.3 for DCl. In addition to this disagreement we must point out that the V–T energy transfer probability increases much more rapidly than does the V–R probability with the temperature. Therefore, in this type of heteronuclear diatomic molecules, the *pure* V–T process would result the energy transfer rates so slow as to have negligible effect compared to the rate of *pure* V–R energy transfer. The actual energy transfer process should therefore be an intermediate between these two extreme situations.

We now extend the above calculation to HBr–HBr and HI–HI collisions. The calculated values of $p\tau_v$ are plotted in Figure 3. The values for HBr are somewhat low compared to experiment, but the temperature dependence agrees with experiment. For HI molecules, the calculated relaxation times are in general agreement with those found by Kiefer, Breshears, and Bird[14] and Chow and Greene,[7] except at lower temperatures where the calculated values tend to be somewhat high.

In Table III we present the calculated values of the factor $f_{vt}(T)$ which represent the effect of the translational motion on the vibrational relaxation of hydrogen halides. The values are not greatly different from unity, but they are significant enough to make an important influence on both the magnitudes and slopes of the relaxation times; compare the heavy and light solid curves in Figures 2 and 3. As the temperature increases, the values of $f_{vt}(T)$ deviate from unity by larger extent as expected, because of the increasing role of the translational motion, which is far less efficient than the rotational motion in exciting or deexciting the vibrational motion, at higher temperatures in controlling the molecular collision. We also find that the effect in DCl–DCl is larger than that in HCl–HCl reflecting the situation that the translational motion plays a more important role in the former system. With eq 39 we may therefore find that as the temperature increases the relative importance of the translational motion with respect to the rotational motion increases so that the rate of increase of the value of $\mathbf{P}_{10}(T)$, *i.e.*, decrease of the value of $p\tau_v$, slows down. It is interesting to note that relaxation times of HCl and DCl are decreased by factors of about 5 and 7, respectively, from 800 to 2000°K. These numbers

(24) B. Widom, *J. Chem. Phys.*, **30**, 238 (1959).
(25) H. Shin, *J. Phys. Chem.*, **68**, 3410 (1964).
(26) D. Secrest, *J. Chem. Phys.*, **51**, 421 (1969).
(27) R. N. Schwartz, Z. I. Slawsky, and K. F. Herzfeld, *ibid.*, **20**, 1591 (1952).
(28) H. Shin, *ibid.*, **42**, 59 (1965).

include factors of 1.15 and 1.23, respectively, resulted from the effect of the translational motion (see Table III). As shown in this table, we also note, for example, that the pure V–R energy transfer probability is reduced by a factor of 0.77 for HCl at 2000°K; the corresponding value for DCl is 0.66. These reduction factors at 800°K are 0.89 and 0.81, respectively.

As the mass of the halogen atom increases, the translational effect becomes less important. For heavy HI molecules, the translational motion bringing the molecules together may change very little in the region of strong interaction where the rotational motion is rapid, so that the energy transfer would essentially take place through the V–R mechanism; this may be particularly so at lower temperatures. The translational factor $f_{vt}(T)$ for HI is very close to unity (0.996) at 800°K. Even at 2000°K, the factor is still not significantly different from unity (0.921). At the latter temperature $f_{vt}(T) = 0.661$ for DCl.

In the present study we did not consider the effect of the dipole–dipole interaction on the relaxation process. The most favorable interaction (strongest attraction) between two dipoles occurs at the collinear alignment "←←," *i.e.*, $\theta_1 = \theta_2 = \pi$ or $\theta_1 = \theta_2 = 0$, and the corresponding dipole–dipole interaction energy is $U_{dd} = -2\tilde{\mu}^2/r^3$, where $\tilde{\mu}$ is the dipole moment; values of $\tilde{\mu}$ are given in Table I. The V–R energy transfer is most efficient when the two hydrogen atoms are interacting at close proximity where the two dipoles would take orientations equal to or close to "→ ←" with $U_{dd} = +2\tilde{\mu}^2/r^3$, the strongest repulsive interaction. In the present study, the collision model is based on the interaction of a rotation-averaged oscillator and a rotator, so that the overall effect of the dipole interaction on the V–R energy transfer process is not expected to be important. As the temperature decreases, however, the dipoles tend to align themselves about the most favorable orientation so that the inclusion of this effect may become necessary. This would mean that the relaxation times decrease after reaching the maximum value at an intermediate temperature as the temperature decreases from the region we considered above. Indeed, Breshears and Bird[3b] have shown the appearance of a possible maximum in the experimental $p\tau_v$ at least for HCl around 800°K.

Concluding Remarks

As can be seen from Figures 2 and 3, the agreement between the calculated and experimental values of $p\tau_v$ for HCl, DCl, HBr, and HI is good over a rather wide range of temperature. In all cases, better agreements both in the absolute magnitudes and temperature dependence of $p\tau_v$ are found when the effect of the translational motion is explicitly taken into consideration. Although a series of approximations have been made in obtaining the final result, it is apparent that the vibrational relaxation of hydrogen halide molecules can be satisfactorily explained in terms of the mechanism of vibration-to-rotation energy transfer with specific consideration of the participation of the translational motion. The participation is most important with the chlorides, the deuterated chloride being affected more by the translational motion than the normal, and is least with the iodide. The model has the advantage of conceptual and mathematical simplicity and leads to results that are quantitatively correct. These satisfactory agreements with the cases considered indicate that the theory is consistent for all gases.

For all four collision systems, vibrational relaxation times are close to each other in spite of large differences in their masses, vibrational frequencies, and potential parameters. This is due to the fact that the energy term χ is proportional to $(I/d^2)^{1/3}(\omega a)^{2/3}$, whose values for these halide molecules differ only slightly from each other.

Of more than passing interest are the values of the range parameter a which we have uniquely determined for each collision system. This is not an adjustable parameter, and the probability sensitively depends on its magnitude; $\chi \propto a^{2/3}$.

Finally, we note that the formulation of the potential functions appears to be reasonable. Any substantial alteration in the forms would give the result which is seriously different from the above. For example, instead of the H_v–H_r interaction, if we considered the H_r–X_v, H_v–X_r, or X_v–X_r interaction to be the dominating part of the overall potential energy for vibrational energy transfer, the resulting expression would give a very long relaxation time and too steep temperature dependence.

Acknowledgment. This work was supported by the Directorate of Chemical Sciences, the U. S. Air Force Office of Scientific Research under Grant No. AFOSR-68-1354.

Low-Frequency Dielectric Dispersion in Suspensions of Ion-Exchange Resins[1]

by Charles W. Einolf, Jr.,*[2] and Edwin L. Carstensen

Department of Electrical Engineering, The University of Rochester, Rochester, New York *(Received September 21, 1970)*

Publication costs assisted by The University of Rochester

A model is proposed to explain the dielectric properties of suspensions of porous particles with uniformly distributed fixed charge sites. The theory predicts a relaxation with very large, effective, dielectric constants at low frequencies. The magnitude of the low-frequency dielectric constant is proportional to the size of the particle and the square root of the fixed charge concentration in the porous material. The relaxation frequency depends directly on counterion mobility and is inversely proportional to the square of particle size. Experimental tests with suspensions of ion-exchange resins have provided quantitative as well as qualitative confirmation of the theoretical model. The effective dielectric constants of micron sized ion-exchange resin particles are as high as 10^6.

Introduction

It has been shown that certain bacteria have effective dielectric constants in excess of 10^4 at frequencies below 1 kHz.[3] Schwarz[4] proposed a mechanism to explain the low-frequency dispersion in solid colloidal particles which involves movement of ions along the charged surface of the particles. The Schwarz mechanism relates the magnitude of the low-frequency dielectric constant to the surface charge density of the particle. Studies with bacteria and their protoplasts have demonstrated that the low-frequency dispersion of bacteria is related to the properties of the porous cell wall.[5] Furthermore, the low-frequency dielectric constant of bacteria appears to be correlated with the cell wall conductivity (or the volume charge density within the wall) rather than the surface charge density of the cell.[6]

This paper describes an extension of the Schwarz theory to cover the case of a porous particle with a uniform volume distribution of fixed charges. Ion-exchange resins have provided a nearly ideal model system for an experimental test of the theory. The results of this study are a significant step in the understanding of the low-frequency dielectric properties of bacteria.

Theory

This section is devoted to the development of a model for the low-frequency dielectric properties of homogeneous porous spheres containing a uniform volume density of fixed charge.[7] The formulation of the model is composed of two parts. The first part contains the solution of the electric potential, the electric field intensity, the ion concentrations, and the charge distribution at equilibrium with no externally applied electric field (static case). The second part considers the effects of an applied electric field. In particular, the equation of continuity for positive and negative mobile ions is studied.

In the region where the static electric field intensity is greater than the applied electric field intensity (*i.e.*, at the surface of the particle), the equation of continuity takes on the form of a boundary condition. This boundary is not discontinuous but must be considered to include a region extending distances of the order of a Debye length on either side of the geometrical boundary of the sphere. The boundary region is characterized by the presence of a very large, radially directed, static field with a corresponding radial variation in the distribution of mobile ions. Maintaining this distribution has the effect of requiring the ions in the boundary layer to move in a path tangent to the surface of the particle. This situation is very similar to the case of solid charged spheres treated by Schwarz. In fact, the only difference in the two cases is that, whereas Schwarz needed to consider only those mobile ions external to the solid particle, in the case of a porous charged particle, mobile ions just inside the boundary of the sphere as well as those external ions are subject to the large radial static field. It is not surprising to find, therefore, that porous charged particles like solid colloidal particles are characterized by a low-frequency dielectric relaxation leading to large static dielectric constants. The final result is a polarization of the ionic atmosphere at the surface of the particle caused by the external electric field. This effect can be expressed by an additional "apparent" dielectric constant of the particle, exceeding the actual dielectric

(1) This work was supported in part by U. S. Public Health Service Grant No. GM 09933. Dr. Einolf was a N.I.H. Fellow under U. S. Public Health Service Grant No. 2TIGM540.

(2) Dr. Einolf's present address is Westinghouse Electric Corporation, Research Laboratories, Churchill Borough, Pittsburgh, Pa. 15235.

(3) C. W. Einolf, Jr., and E. L. Carstensen, *Biochem. Biophys. Acta*, **148**, 506 (1967).

(4) G. Schwarz, *J. Phys. Chem.*, **66**, 2636 (1962).

(5) C. W. Einolf, Jr., and E. L. Carstensen, *Biophys. J.*, 9 (1969).

(6) E. L. Carstensen, H. A. Cox, Jr., W. B. Mercer, and L. A. Natale, *ibid.*, **5**, 289 (1965).

(7) It will be shown that a particle containing a uniform surface density of fixed charge can be treated as a special case of this model.

constant by several orders of magnitude at low frequencies.

Static Case. Consider a spherical particle of radius R containing a uniform, net fixed volume ion density N (ions/m^3). The particle is suspended in an electrolyte containing single species of univalent positive and negative mobile ions. At large distances from the particle the mobile positive and negative ions have concentrations p_0 and n_0 (ions/m^3), respectively. In order to satisfy charge neutrality, $p_0 = n_0$. The distributions p and n (ions/m^3) for the positive and negative mobile ions, respectively, may be determined from the Poisson and Maxwell–Boltzmann equations. To avoid the complexities of obtaining a solution in spherical coordinates, a solution for the distribution in one dimension will be used. This approach is justified because all changes in mobile ion concentrations occur over very short distances compared with the particle radius R.

Mauro[8] has obtained a one-dimensional solution for the mobile ion concentrations at equilibrium. He considers the following system. The fixed charge medium extends for all negative x and the electrolyte extends for all positive x. In his solution the dielectric constant is assumed to be uniform. In the present discussion, Mauro's solution is generalized to include the case in which the fixed charge medium has a dielectric constant κ_i while the electrolyte has a dielectric constant κ_1.

The static ion distributions result from opposing currents caused by the concentration gradient and the electric field. At equilibrium the net current density will be zero. The current density J_p (C/m^2 sec) carried by the positive mobile ions is given by

$$J_p = -e_0kTu_p \text{ grad } p - e_0^2pu_p \text{ grad } \psi \qquad (1)$$

where e_0 is the electronic charge, k is the Boltzmann constant, T is the absolute temperature, u_p is the mobility of positive mobile ions (velocity per unit force), and ψ is the static electric potential (no external field). For the one-dimensional case

$$p = p_0e^{-e_0\psi/kT} \qquad (2)$$

Likewise the current density J_n carried by the negative mobile ions is given by

$$J_n = +e_0kTu_n \text{ grad } n - e_0^2nu_n \text{ grad } \psi \qquad (3)$$

where u_n is the mobility of the mobile negative ions. Again, at equilibrium where $J_n = 0$, eq 3 becomes

$$n = n_0e^{+e_0\psi/kT} \qquad (4)$$

Equations 2 and 4 describe the Maxwell–Boltzmann distribution of ions at equilibrium with no applied electric field. The net volume charge density ρ is given by

$$\rho = (p - n + N_+ - N_-)e_0$$

If the fixed charge is distributed uniformly throughout the region $x < 0$, we need consider only the net fixed ion density $N = N_+ - N_-$. Following the procedure used by Mauro, the following relations were obtained for $\psi(x)$

$$-x = L_i\int_{y_0}^{y} \frac{dy}{\sqrt{2\cosh y - \frac{N}{n_0}\cdot y + c}} \text{ for } x \leq 0 \qquad (5)$$

and

$$x = L_1\left\{\ln\frac{e^{y_0/2}-1}{e^{y_0/2}+1} - \ln\frac{e^{y/2}-1}{e^{y/2}+1}\right\} \text{ for } x > 0 \qquad (6)$$

where $y = e_0\psi/kT$ and the Debye length

$$L_{1(i)} = \left\{\frac{\kappa_{1(i)}\epsilon_0kT}{2n_0e_0^2}\right\}^{1/2} \qquad (7)$$

The constant c is given by[9]

$$c = -\frac{2\kappa_1}{\kappa_i} + \frac{N}{n_0}\cdot y_0 + 2\left[\frac{\kappa_1}{\kappa_i} - 1\right]\cosh y_0 \qquad (8)$$

The value of y_0 (or ψ at $x = 0$) is given by

$$\frac{N}{n_0}\cdot y_0 + 2\left[\frac{\kappa_1}{\kappa_i} - 1\right]\cosh y_0 = -2\cosh y_{\infty-} + \frac{N}{n_0}\cdot y_{\infty-} + 2\frac{\kappa_1}{\kappa_i} \qquad (9)$$

where

$$\sinh y_{\infty-} = \frac{N}{2n_0} \qquad (10)$$

An electric double layer exists about $x = 0$. To satisfy charge neutrality the charge on one side of $x = 0$ must be equal in magnitude and opposite in sign to that on the other side. The net charge $e_0\Sigma_0$ per unit area of surface (C/m^2) for $x > 0$ can be calculated with the integral

$$e_0\Sigma_0 = \int_0^\infty \rho\, dx = -4e_0n_0L_1 \sinh y_0/2 \qquad (11)$$

Mauro has shown that the previous equations can be simplified if $|N|/n_0 \gg 1$. In particular, the net charge $e_0\Sigma_0$ on one side of the electric double layer (eq 11) becomes

$$e_0\Sigma_0 \simeq -2e_0n_0L_1\left[\frac{N}{en_0}\right]^{1/2} \qquad \text{(for } N > 0\text{)} \qquad (12)$$

The solution obtained for ψ when $x > 0$ will hold if the particle containing the uniform, fixed volume ion density N is replaced by a particle with $N = 0$ and

(8) A. Mauro, *Biophys. J.*, **2**, 179 (1962).

(9) With Mauro's assumption that $\kappa_i = \kappa_1$, c becomes

$$c = \frac{N}{n_0}\cdot y_0 - 2$$

containing a uniform, fixed surface ion density Σ_0 given in eq 11. This can be seen by noting that the boundary condition

$$-\epsilon_0\kappa_1 \left.\frac{d\psi}{dx}\right|_{x=0} = e_0\Sigma_0 \tag{13}$$

is satisfied by eq 11. In this sense, the case of a surface charged particle can be considered a special case of the volume charged particle.

The results obtained may be applied to a spherical particle of radius R if R is much greater than the Debye length L. Therefore, the results can be used to describe all changes in the electric potential and ion concentrations as they occur in the vicinity of $r = R$. Furthermore, the static electric field, the static electric currents, and the static diffusion currents are directed radially from the particle and are independent of any angular orientation of the particle.

Perturbation of the Static Solution. The effects of an external electric field perturbing the static solution have been tested in detail.[10] The starting point is the consideration of the equation for the continuity of charge. Again consider the same spherical particle of radius R. Let ϕ be the applied electric potential and require that $|d\psi/dr| \gg |\partial\phi/\partial r|$ at the surface of the particle. Let $\bar{p}$, $\bar{n}$, and $\bar{\rho}$ be the perturbations of p, n, and ρ, respectively, which result from application of the external field ϕ, since $|d\psi/dr| \gg |\partial\phi/\partial r|$, $\bar{p} \ll p$, and $\bar{n} \ll n$. Also, the quantities ϕ, $\bar{p}$, and $\bar{n}$ depend upon r, θ, and t while ψ, p, and n depend only upon r. Conservation of charge requires that

$$\frac{\partial(\rho + \bar{\rho})}{\partial t} = -\text{div}\,(J_p + J_n) \tag{14}$$

where $\bar{\rho} = e_0(\bar{p} - \bar{n})$ and J_p and J_n are given by eq 1 and 3, respectively, with p replaced by $(p + \bar{p})$, n by $(n + \bar{n})$, and ψ by $(\psi + \phi)$. Following the procedure outlined by Schwarz[4] but considering both radial and tangential components of J (instead of tangential components only as the Schwarz treatment), it can be shown that to a good approximation eq 14 can be written as

$$e_0\frac{\partial\bar{\delta}}{\partial t} = \sigma_1\left.\frac{\partial\phi_1}{\partial r}\right|_R - \sigma_i\left.\frac{\partial\phi_i}{\partial r}\right|_R + \text{div}_\theta\left(\frac{e_0^2u\delta_0}{R}\cdot\frac{\partial\phi_s}{\partial\theta} + \frac{e_0ukT}{R}\frac{\partial\bar{\delta}}{\partial\theta}\right) \tag{15}$$

where $u = u_p = u_n$ and $\phi_s = \phi_1(R) = \phi_i(R)$. The quantity δ_0 is the summation of all mobile ions located in the fixed charge region and the electrolyte where the condition $|d\psi/dr| \gg |\partial\phi/\partial r|$ exists. $\bar{\delta}$ is the perturbation of δ_0. Equation 15 is similar to Schwarz's continuity equation except for the first two terms on the right which relate to radial currents. Schurr[11] observed the absence of a dc surface conductance in Schwarz's development for colloidal particles and saw that it resulted from the elimination of radial currents in the continuity equation.

Schurr's correction for this omission involved two "continuity equations". It is now apparent that the continuity equation contains all the information needed to solve the problem when both radial and tangential currents are considered. Furthermore, all objections raised by Schurr concerning the Schwarz development are satisfied.

Following similar procedures used by Schwarz, it can be shown that the effective, homogeneous complex conductivity $\sigma_2^+ = \sigma_2 + i\omega\epsilon_0\kappa_2$ of the particle is given by

$$\sigma_2^+ = \sigma_i^+ + i\omega\epsilon_0\frac{\Delta\kappa_2}{1 + i\omega\tau} + h \tag{16}$$

where $\sigma_i^+ = \sigma_i + i\omega\epsilon_0\kappa_i$ σ_i and κ_i are the bulk conductivity and dielectric constant, respectively, of the particle, and where

$$\Delta\kappa_2 = \frac{e_0^2R\delta_0}{\epsilon_0kT} \tag{17}$$

$$\tau = \frac{R^2}{2ukT} \tag{18}$$

$$h = \frac{\sigma_1\kappa_i - \sigma\kappa_1 + \sigma_1\left(\dfrac{\Delta\kappa_2}{1 + i\omega\tau}\right)}{\kappa_1 - \dfrac{\sigma_1\tau}{\epsilon_0} + i\omega\tau\kappa_1} \tag{19}$$

and σ_1 and κ_1 are the conductivity and dielectric constant, respectively, of the electrolyte.

The value of δ_0 is determined by the summation of all mobile ions both in the electrolyte and in the fixed charge region where the condition $|\partial\psi/\partial r| \gg |\partial\phi/\partial r|$ holds. Thus if $N/n_0 \gg 1$, $\delta_0 = \Delta R_i|N|$. If we assume a value of ΔR_i corresponding to the point where $|\partial\psi/\partial r| = |\partial\phi/\partial r|$ (see Discussion), ΔR_i is given by

$$\Delta R_i = -\left(\frac{\epsilon_0\kappa_ikT}{|N|e_0^2}\right)^{1/2}\ln\left(\frac{3\sigma_1E_0}{2\sigma_1 + \sigma_2}\left(\frac{\epsilon_0\kappa_i}{|N|kT}\right)^{1/2}\right) \tag{20}$$

where E_0 is the applied electric field at a large distance from the particle. If the field in the particle, $3\sigma_1E_0/(2\sigma_1 + \sigma_2) \approx 1$ V/m and $\kappa_i \approx \kappa_1$, as for the case of ion-exchange particles

$$\delta_0 \simeq \frac{(|N|\epsilon_0\kappa_ikT)^{1/2}}{2e_0}\ln\left(\frac{|N|kT}{\epsilon_0\kappa_i}\right) \tag{21}$$

Therefore, δ_0 is approximately proportional to the square root of N and independent of n_0. Likewise, $\Delta\kappa_2$ in eq 17 will be proportional to $\sqrt{|N|}$ and R but independent of u and n_0.

(10) C. W. Einolf, Jr., "The Low Frequency Dielectric Dispersion of Microorganisms," Ph.D. Thesis, The University of Rochester, Rochester, N. Y., 1968. Available from University Microfilms, Ann Arbor, Michigan, Order No. 68-15,852.

(11) J. M. Schurr, *J. Phys. Chem.*, **68**, 2407 (1964).

If $h = 0$, the result shown in eq 16 is exactly that of Schwarz. However, the term h is not zero and can be very important under certain conditions. For the case of the charged polystyrene sphere where $\Delta\kappa_2 \gg \kappa_1 > \kappa_i$ and $\sigma_i \simeq 0$, the term h at $\omega = 0$ becomes

$$h_{\omega=0} = \frac{\epsilon_0 \Delta\kappa_2}{\tau} = \frac{2\lambda}{R} \qquad (22)$$

where $\lambda = e_0^2 u \delta_0$ is the surface conductance. Therefore, even though the charged particle has a zero conductivity ($\sigma_i = 0$), its effective, homogeneous conductivity is nonzero because of the factor h which contains the surface conductance λ. The data of Schwan[12] show that the charged polystyrene sphere does indeed have a nonzero surface conductance at $\omega = 0$.

Experimental Procedure

Ion-Exchange Resin Preparation. The preceding section outlines a theory for the dielectric properties of porous particles with a uniform volume distribution of fixed charge. As a test of the theory, a complete study of the low-frequency dielectric properties of finely ground particles of the ion-exchange resin Bio-Rex 70 (Bio-Rad Laboratories, Richmond, Calif.) was carried out. Bio-Rex 70 is an acrylic lattice with a large, effective pore size containing weakly acidic carboxylic groups. The resin is supplied in the sodium form and was used in that form unless otherwise indicated. Two different size ranges were obtained from the manufacturer. One was 0.1–2.0 μ in diameter (designated as BR-70S) and the other was 1–10 μ in diameter (BR-70M).

In order to determine the effect of a change in the counterion mobility on the low-frequency dielectric properties, glucose was added to the suspending medium to increase the viscosity. Because of the small size of the glucose molecule, it could safely be assumed that the glucose freely permeates the resin particle. Particles of BR-70S were washed first in a 0.1 M NaCl solution. Then the resin pellet was resuspended in a 0.1 M NaCl plus glucose solution to give the desired volume fraction and glucose concentration.

BR-70S was also prepared in the hydrogen form (BR-70SH) so that samples could be titrated to determine the fixed volume charge density of the resin. The preparation of BR-70SH was carried out as rapidly as possible to avoid damage to the resin. The resin was washed twice in 0.1 M HCl and four times in demineralized water. The resin was then ready for use as BR-70SH.

Samples of BR-70SH can be partially titrated with NaOH to produce Bio-Rex 70 in the part-hydrogen–part-sodium form (BR-70SPH). It was found that Bio-Rex 70 binds hydrogen ions so tightly that the hydrogen ion mobility is greatly reduced in comparison with sodium ions. The reduction is so pronounced that the low-frequency dielectric dispersion for the hydrogen form is shifted to frequencies far below the dispersion for the sodium form (see Figure 5). Thus in the part-hydrogen–part-sodium form, only the sites with sodium are effective. This fact permitted a study of the effect of fixed charge concentration N on the low-frequency dielectric dispersion. The preparation of BR-70SPH is identical with the preparation of BR-70SH except that the final wash included a known amount of NaOH. The BR-70SPH pellets were resuspended in aqueous NaCl solutions to give the desired volume fraction and NaCl concentration. In order to maintain the sodium–hydrogen ion balance in the resin, the measurements were made without delay.

The effective, fixed, volume ion density N represents those sites out of the total exchange capacity N_0 of the resin which have sodium ions as counterions. The value of N was determined by a base titration. The determination of N_0 was also done by this technique. The value of N_0 was 3.4 equiv/l. for both BR-70S and BR-70M.

Particle Size. The size of BR-70S has been determined using a light microscope and a Vickers AEI image splitting eyepiece. The average radius was 0.6 μ for BR-70S. The BR-70S particle radius ranged from 0.4 to 1.0 μ with a standard deviation of the mean = 0.3 μ. Since the resin particles have a distribution in size, only a qualitative comparison of the effect of particle size (BR-70S *vs.* BR-70M) on the dielectric properties was made in this investigation. It is possible that there may be particles too small to see with the light microscope. Such small particles would not have a significant effect upon the dispersion in the dielectric constant. However, these small particles could increase the relaxation frequency for the conductivity dispersion (see Discussion).

Volume Fraction Determination. In order to calculate the effective, homogeneous, complex conductivity of the resin particle, it was necessary to determine the volume fraction that the particles occupy in a suspension. The volume fraction was taken to be that part of the suspension which is not available to dilute a large tracer molecule.[6] The tracer molecule in this case was a dextran with molecular weight of 150,000. Dextran concentrations were determined colorimetrically by the phenol–H_2SO_4 method.[13]

Electric Conductivity and Dielectric Constant. If p is the volume concentration of the suspended particles with an effective, homogeneous complex conductivity σ_2^+ and form factor x, suspended in material of complex conductivity σ_1^+, the complex conductivity σ^+ of the suspension is given by the equation[14]

(12) H. P. Schwan, G. Schwarz, J. Maczuk, and H. Pauly, *J. Phys. Chem.*, **66**, 2626 (1962).

(13) M. Dubois, K. A. Gilles, J. K. Hamilton, P. A. Rebers, and F. Smith, *Anal. Chem.*, **28**, 350 (1956).

(14) H. Fricke, *J. Phys. Chem.*, **59**, 168 (1955).

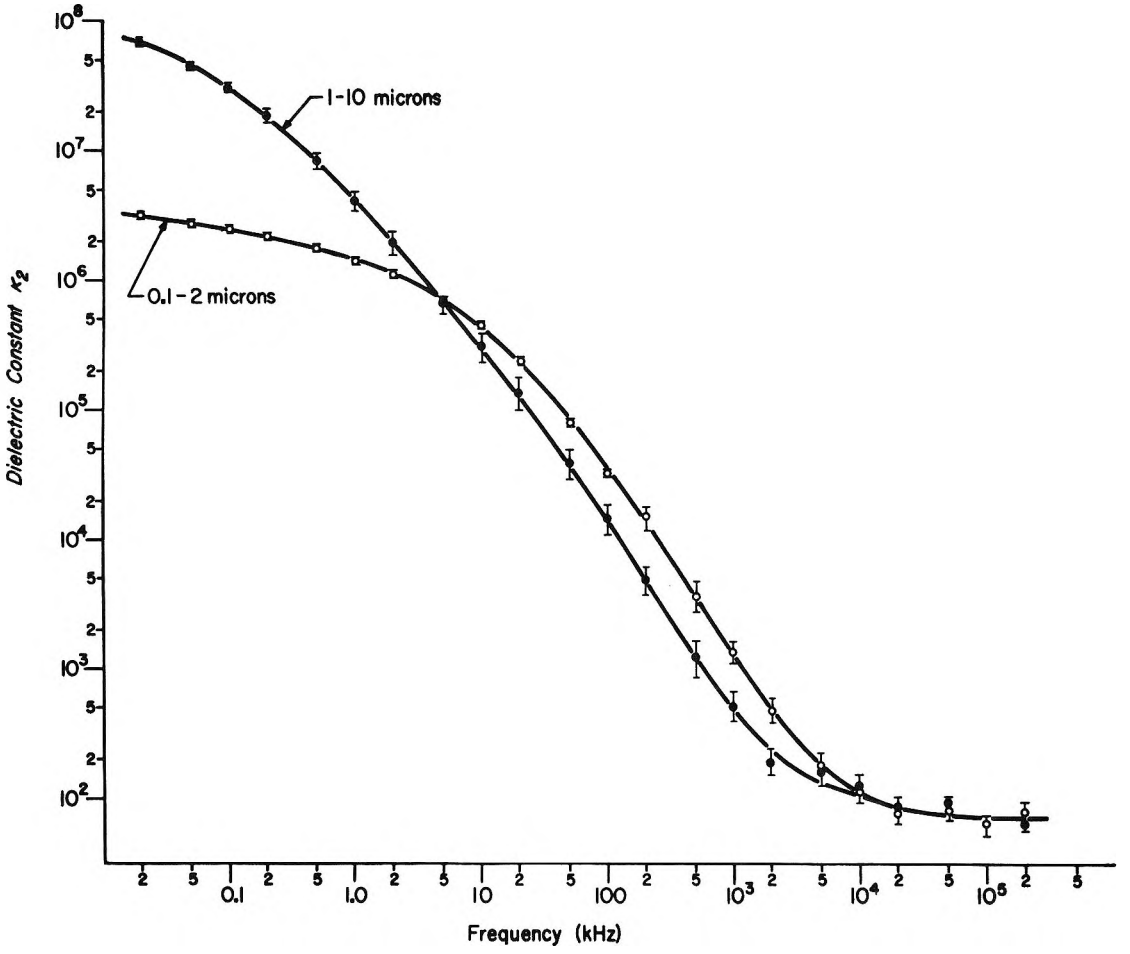

Figure 1. The effective, homogeneous dielectric constant κ_2 of Bio-Rex 70 as a function of frequency for two size distributions in 0.05 M NaCl, $T = 25°$.

$$\frac{\sigma^+ - \sigma_1^+}{\sigma_1^+ + x\sigma_1^+} = p\frac{\sigma_2^+ - \sigma_1^+}{\sigma_2^+ + x\sigma_1^+} \tag{23}$$

Here the complex conductivity is given by

$$\sigma^+ = \sigma + i\omega\epsilon_0\kappa \tag{24}$$

where σ is the conductivity, ω is the angular frequency, κ is the relative dielectric constant, and $\epsilon_0 = 8.854 \times 10^{-12}$ F/m is the permittivity of free space. Whenever possible the value of p was kept close to 0.5 to ensure accurate determinations of σ_2^+.[3] For spherical particles, the form factor x is 2.[15] For nonspherical particles, such as the ion-exchange particles, the form factor may depart significantly from $x = 2$. However, as long as σ_2/σ_1 is less than 3, eq 23 with a form factor $x = 2$ should work reasonably well for all particles regardless of shape. In order that the form factor $x = 2$ could be used, σ_1 was kept as near to σ_2 as possible.

For dispersion measurements over the frequency range from 20 Hz to 200 kHz, a low-frequency admittance bridge was used. A more complete description can be found in earlier papers.[3,10] All measurements were made at 25°.

Conductivity measurements were made at a frequency of 1592 Hz with a Wayne Kerr Universal Bridge (Wayne Kerr Lab., Ltd., Chessington, Surrey, England). The bridge and conductivity cells have been previously described by Carstensen.[6] All measurements were made at 25°.

A Boonton Radio Corporation RX meter was used to measure complex conductivities over the frequency range from 0.5 to 200 MHz. The sample holder and calibration procedures were similar to those described by Pauly and Schwan.[16]

Results and Discussion

Equations 16–21 describe a low-frequency dielectric dispersion that is expected for a particle containing a net fixed volume charge density e_0N. These equations predict that the change in the effective, homogeneous dielectric constant $\Delta\kappa_2$ is proportional to $\sqrt{N}$ (assuming that $N/n_0 \gg 1$). The value of $\Delta\kappa_2$ is also proportional to the radius R and independent of the environmental salt concentration n_0 and the ion mobility u. The relaxation frequency $f_0 = 1/2\pi\tau$ is proportional to the

(15) H. Fricke, *Phys. Rev., Ser. 2*, **24**, 575 (1924).
(16) H. Pauly and H. P. Schwan, *Biophys. J.*, **6**, 621 (1966).

inverse square of the radius ($1/R^2$) and directly related to the mobility u. The relaxation frequency is independent of the concentrations N and n_0.

In order to test the theory, the effects of each parameter (R, n_0, u, N) on the dielectric dispersion ($\Delta\kappa_2$, f_0) were observed. As shown in Figure 1, BR-70M and BR-70S have a low-frequency dielectric dispersion between the frequencies of 20 Hz and 10 MHz. The limits of error shown are the standard errors of the means. The two curves illustrate the effect of particle size on the dielectric constant κ_2. Because of the size distribution, it would be difficult to make a quantitative comparison of these two curves. However, qualitatively the results show that as the particle size increases, the change in the effective, homogeneous dielectric constant $\Delta\kappa_2$ also increases ($\Delta\kappa_2 = 3.3 \times 10^6$ for BR-70S in 0.05 M NaCl; $\Delta\kappa_2 = 8 \times 10^7$ for BR-70M in 0.05 M NaCl). The results also illustrate that the relaxation frequency decreases as the particle size increases.

The change in the effective, homogeneous dielectric constant $\Delta\kappa_2$ is determined by means of Cole–Cole circle plots. By plotting the real conductivity σ_2 on the abscissa and the imaginary conductivity $\sigma_2'' = \omega\epsilon_0\kappa_2$ on the ordinate, a circle plot is obtained. A typical example is shown in Figure 2 for BR-70S in 0.05 M NaCl. The zero frequency value of the effective, homogeneous conductivity $\sigma_2(0)$ is obtained from the intersection of the circle with the abscissa. The value of $\sigma_2(0)$ is then used to calculate the imaginary dielectric constant, $\kappa_2'' = \{\sigma_2 - \sigma_2(0)\}/\epsilon_0\omega$. By plotting the real dielectric constant on the abscissa and the imaginary dielectric constant on the ordinate, a second circle plot is obtained. Figure 3 illustrates such a circle plot using the value of $\sigma_2(0)$ determined in Figure 2. The value of $\Delta\kappa_2$ is determined by the distance between the two intersections of the circle with the abscissa. In Figure 3 $\Delta\kappa_2 = 3.3 \times 10^6$ for BR-70S in 0.05 M NaCl.

The theory also predicts that if $N/n_0 \gg 1$, the value of $\Delta\kappa_2$ should remain independent of n_0. Figure 4 illustrates the change in the effective, homogeneous

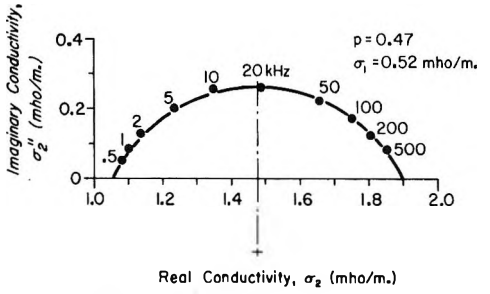

Figure 2. Cole–Cole circle plot of the real and imaginary, effective, homogeneous conductivities (σ_2 and σ_2'', respectively) for BR-70S in 0.05 M NaCl, $T = 25°$. This circle plot determines the value of $\sigma_2(0) = 1.06$ mhos/m.

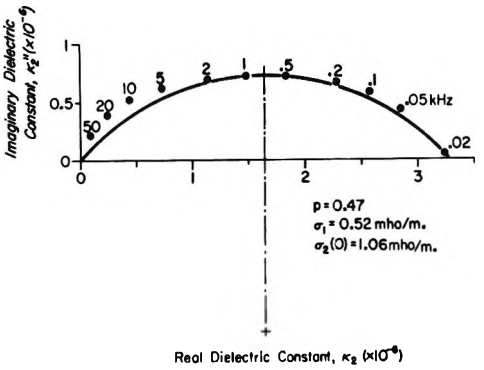

Figure 3. Cole–Cole circle plot of the real and imaginary, effective, homogeneous dielectric constant (κ_2 and κ_2'', respectively) for BR-70S in 0.05 M NaCl, $T = 25°$. This circle plot uses the value of $\sigma_2(0) = 1.06$ mhos/m from Figure 2 and determines the value of $\Delta\kappa_2 = 3.3 \times 10^6$.

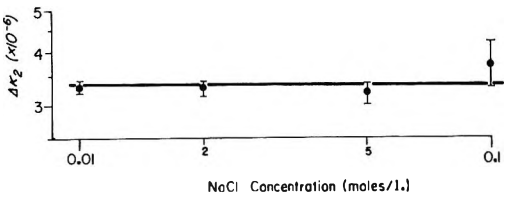

Figure 4. Effective, homogeneous dielectric constant $\Delta\kappa_2$ for BR-70S as a function of the NaCl concentration, $T = 25°$.

dielectric constant $\Delta\kappa_2$ as a function of the environmental salt concentration n_0. As predicted, $\Delta\kappa_2$ remains nearly independent of n_0 even though n_0 has been varied by a factor of 10. The range of n_0 possible for this investigation was limited. For values of n_0 less than 0.01 M, the condition $\sigma_2/\sigma_1 < 3$ is no longer satisfied. The form factor $x = 2$ can no longer be used to calculate σ_2^+ with eq 23. For values of n_0 greater than 0.1 M, the condition $N/n_0 \gg 1$ is no longer satisfied.

The ion mobility u also affects the low-frequency dielectric dispersion. According to the theory, the value of f_0 is proportional to u, whereas $\Delta\kappa_2$ is independent of u. Table I illustrates the effects of adding glucose to lower the ion mobility. The zero frequency, effective, homogeneous conductivity $\sigma_2(0)$ is related directly to u by the equation

$$\sigma_2(0) = e_0^2 u(p_i + n_i) + \frac{2e_0^2 u\delta_0}{R} \qquad (25)$$

As shown in Table I, the value of u [indicated by $\sigma_2(0)$] is reduced by 45% by the addition of 2.4 m glucose to BR-70S in 0.1 M NaCl. The relaxation frequency f_σ (obtained from the peak of a conductivity circle plot similar to Figure 2) is also reduced in direct proportion to u. The value of $\Delta\kappa_2$ which should remain constant does so within the limits of accuracy.

Finally, the net, fixed volume ion density N was varied to determine its influence on the change in the effective, homogeneous dielectric constant $\Delta\kappa_2$. Figure

Table I: The Effect of a Change in Ion Mobility by the Addition of Glucose

	$\Delta\kappa_2$	$\sigma_2(0)$, mho/m	f_σ, kHz
0.1 *M* NaCl environment	3.8×10^6	1.30	13.5
0.1 *M* NaCl + 2.4 *m* glucose environment	3.7×10^6	0.58	6.3
Change produced by addition of glucose	0	−45%	−47%

5 shows how κ_2 (as a function of frequency) is affected as the sodium ions in BR-70S are replaced by hydrogen ions. When BR-70S is in the complete hydrogen form, the lowest curve in Figure 5 is obtained. Three examples of BR-70S in the part-hydrogen–part-sodium form (BR-70SPH) are also illustrated. Note that the relaxation frequency for BR-70S in the complete hydrogen form (BR-70SH) is much lower than any other sample containing sodium ions. Therefore, the dielectric dispersion above 20 Hz is dominated by the presence of sodium ions in the resin. This fact permits the determination of the relationship between the fixed ion concentration N and the change in the effective, homogeneous dielectric constant $\Delta\kappa_2$. Figure 6 illustrates this relationship. Again as the theory predicts, for $N/n_0 \gg 1$, $\Delta\kappa_2$ is proportional to the square root of N.

As shown in Figure 7, the relationship between fixed charge concentration and conductivity is more complex than for the dielectric constant. From eq 25, it appears that to a first approximation the low-frequency effective conductivity $\sigma_2(0)$ should be directly proportional to N for $N/n_0 \gg 1$. Even though the term involving δ_0 is proportional to $\sqrt{N}$, it accounts for only a few per cent of the total conductivity at high values of N. Furthermore, when $N/n_0 \gg 1$, the counterion concentration (p_i in this case) greatly exceeds the co-ion concentration and is roughly equal to the fixed charge concentration N. In Figure 7, the value of $\sigma_2(0)$ is plotted against the relative fixed ion concentration N/N_0. The horizontal limits of error are the same as those of Figure 6. Numbers in parentheses indicate the value of the ratio σ_2/σ_1. From the data at $N/N_0 = 1$, it is apparent that $\sigma_2(0)$ varies considerably with σ_1 and hence the assumption that $p_i \gg n_i$ is not valid. However, by keeping the σ_2/σ_1 ratio constant, the contribution of n_i to $\sigma_2(0)$ should also be roughly proportional to N. Comparing values of $\sigma_2(0)$ *vs.* N/N_0 while holding the ratio σ_2/σ_1 constant, we see in Figure 7

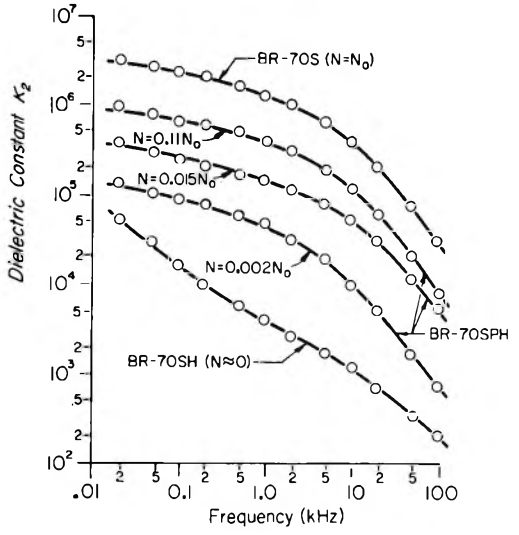

Figure 5. The effective, homogeneous dielectric constant κ_2 of Bio-Rex 70S as a function of frequency for various concentrations of effective, fixed, volume charge N within the ion-exchange resin, $T = 25°$.

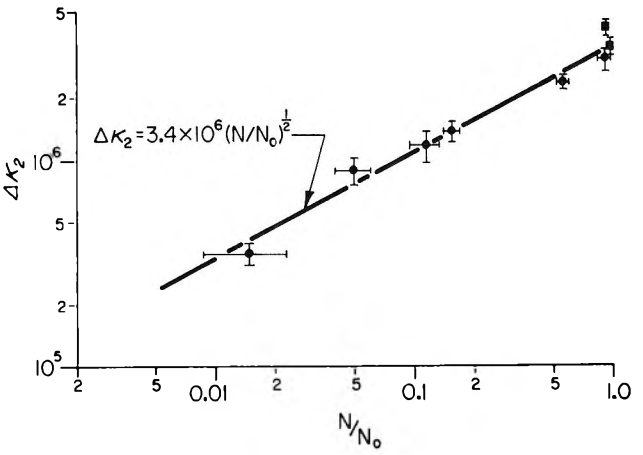

Figure 6. The change in the effective, homogeneous dielectric constant $\Delta\kappa_2$ as a function of the relative, fixed, volume ion density N/N_0 for BR-70SPH; $N_0 = 3.4$ equiv/l.; $N/n_0 \gg 1$; $T = 25°$.

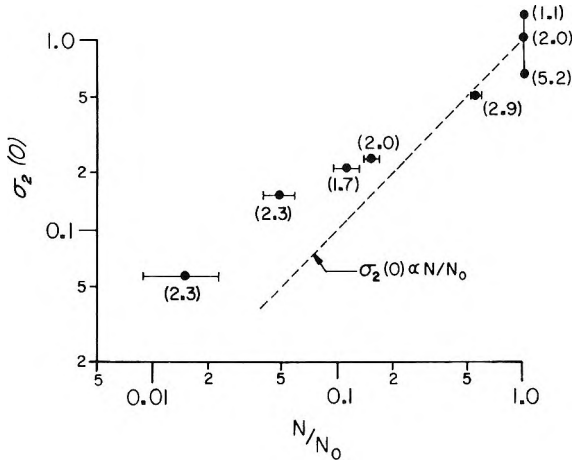

Figure 7. The zero frequency, effective, homogeneous conductivity $\sigma_2(0)$ as a function of the relative, fixed, volume ion density N/N_0 for BR-70SPH: $N_0 = 3.4$ equiv/l.; $N/n_0 \gg 1$; $T = 25°$. The numbers in parentheses correspond to the ratio σ_2/σ_1.

that the conductivity is proportional to N only for large N.

While interpreting eq 25, at least two phenomena should be considered. First of all, the hydrogen ions in the BR-70SPH are not completely immobile. The resin in the complete hydrogen form (BR-70SH) has a conductivity of 0.02 mho/m. More important, however, is the fact that the mobility of the counterions may be expected to be somewhat smaller than the values found for the same ions in free solution. As discussed by Schwarz,[4] the mobility of the counterion will decrease as it comes closer to the fixed charge site. Thus one would expect the mobility of the counterions to be smallest at high ion concentrations. No detailed investigations of the mobility of counterions has been undertaken. Therefore, for the present, the low-frequency dielectric constant is a more accurate indicator of fixed volume charge concentration than the conductivity.

From these studies it is apparent that the dielectric properties of the ion-exchange resins have the correct functional dependence upon size, ion mobility, and fixed charge concentration as proposed by the theory. It now remains to be determined whether the theory predicts the correct absolute magnitudes of the dielectric constant and relaxation time. For the ion-exchange particle it must be shown that eq 17, 18, and 21 describe the values of $\Delta\kappa_2$, τ, and δ_0, respectively. Using the values $N = 3.4$ equiv/l., $\kappa_i = 60$, $(1/R)\partial\phi_s/\partial\theta \simeq 1$ V/m, and $R = 0.6 \times 10^{-6}$ m which correspond to BR-70S, the value of δ_0 from eq 21 is 0.78×10^{19} ions/m^2. Therefore, from eq 17 the value of $\Delta\kappa_2$ is 3.2×10^6. The average measured value of $\Delta\kappa_2$ was 3.4×10^6. Furthermore, the choice of

$$\left|\frac{d\psi}{dr}\right| = \left|\frac{\partial\phi}{\partial r}\right|$$

as the boundary of ΔR_i is not critical. This boundary may be changed to

$$\left|\frac{d\psi}{dr}\right| = 10\left|\frac{\partial\phi}{\partial r}\right|$$

or even

$$\left|\frac{d\psi}{dr}\right| = 0.1\left|\frac{\partial\phi}{\partial r}\right|$$

with the result that $\Delta\kappa_2$ is affected by less than 7%. Therefore, the assumption

$$\left|\frac{d\psi}{dr}\right| = \left|\frac{\partial\phi}{\partial r}\right|$$

seems to be a reasonable one. The assumption $\Delta R_i \ll R$ is also satisfied since $\Delta R_i \simeq 38$ Å $\ll R = 6000$ Å.

Using $u = 3.4 \times 10^{11}$ m^2/(C V sec), the mobility for the sodium ion in free solution, the predicted value of f_0 is 1.3 kHz. This theoretical value for f_0 then should

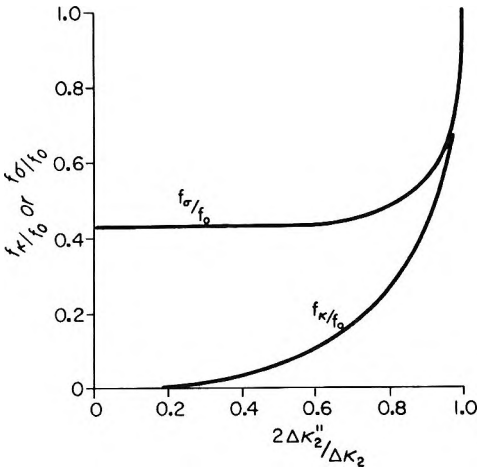

Figure 8. The relative relaxation frequencies f_κ/f_0 and f_σ/f_0 as a function of the degree of depression of the circle plot ($2\Delta\kappa_2''/\Delta\kappa_2$).

be compared with the values of $f_\kappa = 580$ Hz (from the peak of the dielectric constant circle plot; *e.g.*, Figure 3) and $f_\sigma = 13$–20 kHz (from the peak of the conductivity circle plot; *e.g.*, Figure 2). This apparent discrepancy in the relaxation frequencies has been explained by Schwarz[4] in terms of the counterion activation energy. The activation energy and effective mobility of a counterion will depend upon its proximity to the fixed charge site. Therefore, a broad distribution in activation energies may be anticipated. As the distribution broadens, the dielectric constant circle plot becomes depressed. The ratio $2\Delta\kappa_2''/\Delta\kappa_2$ indicates the degree of depression. When the ratio is unity, the circle plot is a full semicircle. The value of $\Delta\kappa_2''$ is the height of the circle from the abscissa, and $\Delta\kappa_2$ is the distance between the two intersections of the circle with the abscissa. As the distribution broadens ($2\Delta\kappa_2''/\Delta\kappa_2$ decreases), the value of f_κ decreases rapidly towards zero as shown in Figure 8. The value of f_σ, on the other hand, approaches a constant value of $0.428f_0$ as the distribution broadens. Therefore, $f_\kappa < f_\sigma < f_0$, for the case of a particle with a distribution only in the activation energy of the ion mobility. However, for the ion-exchange resin particle f_σ is greater than f_0. A distribution in particle size will tend to increase the value of f_σ as the distribution broadens. (It is possible that BR-70S contained particles which were too small to see in the light microscope but still influenced f_σ.) The value of f_κ, however, is decreased slightly as the distribution in size broadens. Therefore, it appears that the decrease in f_κ from f_0 is mainly the result of a distribution in the activation energy. The increase in f_σ from f_0, on the other hand, is due to a distribution in the particle size.

The reason for choosing f_σ and not f_κ to show the effects of the ion mobility in Table I now becomes apparent. With a constant particle size distribution f_σ will reflect, with more accuracy than f_κ, the effect

of the ion mobility on f_0. The value of f_0, calculated from f_κ, depends very strongly upon the depression of the dielectric constant circle plot (see Figure 8). Since the circle plot cannot be drawn with sufficient accuracy to indirectly determine f_0, f_σ was used as a direct indicator of f_0.

Summary

A theory has been proposed to explain the low-frequency dielectric properties of porous particles with uniform volume distribution of fixed charge N. It predicts a relaxation in which the change $\Delta\kappa_2$ in the effective, homogeneous dielectric constant is proportional to $\sqrt{N}$ and to the radius R of the particle and in which $\Delta\kappa_2$ is independent of the environmental salt concentration n_0 and counterion mobility u. The relaxation frequency is proportional to u/R^2. Experimental tests with colloidal suspensions of ion-exchange resins were found to agree both qualitatively and quantitatively with the theoretical predictions. The mechanism is very similar to that proposed by Schwarz for solid colloidal particles with a fixed surface charge. However, in the present case, all counterions in the region of the high static radial electric field (those counterions just inside the porous particle as well as those outside the surface of the particle) are part of the ion cloud which flows about the surface of the particle under the influence of the electric field.

Acknowledgment. The authors are indebted to Mrs. Sally Child for her technical assistance and to Drs. R. E. Marquis, L. P. Hunter, and W. Striefer for helpful discussions.

Electrical Conductances and Ionization Behavior of Sodium Chloride in Dioxane–Water Solutions at 100° and Pressures to 4000 Bars[1a]

by LeRoy B. Yeatts,* Lawrence A. Dunn,*[1b] and William L. Marshall*

Reactor Chemistry Division, Oak Ridge National Laboratory, Oak Ridge, Tennessee 37830 *(Received August 3, 1970)*

Publication costs assisted by the Oak Ridge National Laboratory, U. S. Atomic Energy Commission

The ionization behavior of NaCl in dioxane–water at 100° to pressures of 4000 bars was determined from electrical conductance measurements of dilute solutions (0.001–0.02 *m*). The conductance equation of Shedlovsky was used to calculate the limiting equivalent conductances (Λ_0) and conventional ionization constants (K_d) for NaCl in solvent mixtures whose compositions ranged from 30 to 70 wt % dioxane. For these calculations, estimates of dielectric constants, densities, and viscosities were made and are presented. The complete ionization constant (K^0), which includes the polar solvent water as a reactant species, has a value of $10^{-12.7}$; the net change in the number of solvating water molecules (k) is equal to 7.8. These values are identical with those established earlier for NaCl in dioxane–water at 100° and at saturation vapor pressure. Hence, this study supports the earlier proposal that the complete constant is independent of both pressure and dioxane–water solvent composition and is only temperature dependent.

Introduction

The concept of a complete isothermal equilibrium constant (K^0) proposed earlier[2,3] has been applied successfully to numerous electrolytes in aqueous, polar organic, or mixed aqueous–nonpolar organic solvents. The basic tenet of this principle is that the polar solvent molecules are undergoing a change in concentration during an ionization reaction involving ions, ion pairs, and the solvent. Therefore, polar solvent molecules must be considered participants in the reaction and included in the equilibrium constant expression. Both solubility and ionization equilibria,[2-4] including the ionization of water,[5] are described accurately by this principle under such widely varying conditions as temperatures to 800° and pressures to 4000 bars. Generally, data at higher temperatures or pressures than these are not available to test this hypothesis.

(1) (a) Research sponsored by the U. S. Atomic Energy Commission under contract with the Union Carbide Corporation. Presented before the Division of Physical Chemistry at the 160th National Meeting of the American Chemical Society, Chicago, Ill., Sept 13–18, 1970. (b) Department of Chemistry, University of Tasmania, Hobart, Tasmania 7001, Australia.

(2) W. L. Marshall and A. S. Quist, *Proc. Nat. Acad. Sci. U. S.*, **58**, 901 (1967).

(3) A. S. Quist and W. L. Marshall, *J. Phys. Chem.*, **72**, 1536 (1968).

However, the molar ionization constant of ammonia in water at 45° has been determined by Hamann and Strauss[6] at pressures up to 12,000 bars and the complete constant principle continues to be applicable.[7] Recently, this approach was further generalized by extending it to include the rates of reactions,[7] such as the hydrolysis of methyl and isopropyl bromides.[8]

The concentration of the polar solvent can be changed significantly at the lower temperatures only by using a solvent containing both a polar and a nonpolar component while at higher temperatures, or lower densities, pressure can be used also to produce this effect. Dunn and Marshall[9] have used essentially nonpolar dioxane to reduce the water concentration in order to study the ionization of sodium chloride, by conductance measurements, at 100° and *saturation vapor pressure*. From these measurements they were able to obtain values for K^0, the complete ionization constant, and k, the net change in the number of waters of solvation for the ionization equilibrium. Their value of 7.8 at 100° for k was close to that predicted elsewhere[10] from the values of this constant at 25° and saturation vapor pressure for NaCl in dioxane–water and from 400 to 800° for NaCl in pure water at various densities.

The purpose of this present study was to make conductance measurements of NaCl in dioxane–water at 100° while varying the pressure on this system from 1 to 4000 bars to establish whether these values for K^0 and k are independent of pressure, as one would predict from the original complete constant concept. Since values for density, dielectric constant, and viscosity as a function of pressure needed for calculating conventional ionization constants (K_d) are not available, estimates of these properties were made for the various compositions of the dioxane–water solvent. With these estimates the agreement with the earlier results[9] at 100° and saturation vapor pressure is remarkably good.

Experimental Section

The preparation of the sodium chloride–dioxane–water solutions,[9] as well as a description of the experimental procedures and the conductivity apparatus,[4a] were presented earlier. Two inner electrodes with cell constants at 100° of 0.501 and 2.103 cm^{-1}, determined from 0.01 and 0.1 demal potassium chloride, were used to make the conductance measurements in this study at a signal frequency of 2 kHz. The smoothed experimental specific conductances (κ) at 100° for the various compositions of dioxane–water solvent are listed in Table I. In general, five sodium chloride solutions in the range of 0.001–0.02 m were studied for each of five solvent compositions. The solution resistances were usually in the range of 10^3 to 10^4 ohms. Values for the density (d), dielectric constant (D), and viscosity (η) of these dilute solutions are assumed to be the same as those of the two-component solvent alone. At saturation vapor pressure, approximately 1 bar, the values of these properties given elsewhere[9] were used in this paper. Estimates of the three physical properties for higher pressures were made by the methods discussed below.

Densities. The specific volume of pure dioxane at 100° as a function of pressure up to 500 bars was calculated by the method of Lydersen, Greenkorn, and Hougen[11a] as discussed by Reid and Sherwood.[11b] This method relates the specific volume of a liquid to its reduced temperature, reduced pressure, and critical compressibility. (Reduced properties are fractions of liquid–vapor critical properties; for example, $P_r = P/P_c$ where P_r, P, and P_c are the reduced pressure, the pressure on the given system, and the critical pressure, respectively.) The values reported by Højendahl[12] for the critical temperature (312°), critical pressure (~50 bars), and critical density (0.36 g/cm^3) of pure dioxane were used for the calculations. A reliable experimental specific volume or density value, at a temperature as close as possible to the temperature for which the calculations are to be made, is required also. The experimental value of 0.965 g/cm^3 for the density of dioxane at 80° and saturation vapor pressure was used since both Geddes[13] and Hovorka, *et al.*,[14] report this value from independent determinations. Presumably, this method of calculating densities is reliable in this case up to pressures of 1500 bars but the calculated densities indicated that dioxane was a little less compressible than water above 500 bars. This did not appear to be reasonable; hence, above 500 bars pressure it was assumed that dioxane had the same absolute increase in density per unit increase in pressure as that of water. The densities of water which were used are those compiled by Sharp[15] from the published[16] and

(4) (a) A. S. Quist and W. L. Marshall, *J. Phys. Chem.*, **72**, 684 (1968); (b) A. S. Quist and W. L. Marshall, *ibid.*, **72**, 1545 (1968); (c) A. S. Quist and W. L. Marshall, *ibid.*, **72**, 2100 (1968); (d) A. S. Quist and W. L. Marshall, *ibid.*, **72**, 3122 (1968); (e) L. A. Dunn and W. L. Marshall, *ibid.*, **73**, 723 (1969); (f) E. U. Franck, *Z. Phys. Chem. (Frankfurt am Main)*, **8**, 107, 192 (1956).

(5) W. L. Marshall, *Rec. Chem. Progr.*, **30**, 61 (1969); A. S. Quist, *J. Phys. Chem.*, **74**, 3396 (1970).

(6) S. D. Hamann and W. Strauss, *Trans. Faraday Soc.*, **51**, 1684 (1955).

(7) W. L. Marshall, *J. Phys. Chem.*, **74**, 346 (1970).

(8) B. T. Baliga and E. Whalley, *ibid.*, **73**, 654 (1969).

(9) L. A. Dunn and W. L. Marshall, *ibid.*, **73**, 2619 (1969).

(10) W. L. Marshall, *Rev. Pure Appl. Chem.*, **18**, 167 (1968).

(11) (a) A. L. Lydersen, R. A. Greenkorn, and O. A. Hougen, "Generalized Thermodynamic Properties of Pure Fluids," Vol. 4, College of Engineering, University of Wisconsin, Engineering Experiment Station Report, Madison, Wisc., Oct 1955; (b) R. C. Reid and T. K. Sherwood, "Properties of Gases and Liquids," McGraw-Hill, New York, N. Y., 1958, pp 60–65.

(12) K. Højendahl, *Kgl. Danske Vidensk. Selsk., Mat.-Fys. Medd.*, **24** (2), 1 (1946).

(13) J. A. Geddes, *J. Amer. Chem. Soc.*, **55**, 4832 (1933).

(14) F. Hovorka, R. A. Schaefer, and D. Dreisbach, *ibid.*, **58**, 2264 (1936).

(15) W. E. Sharp, "The Thermodynamic Functions for Water in the Range −10 to 1000° and 1 to 250,000 Bars," University of California Radiation Laboratory Report, UCRL-7118, 1962.

Table I: Properties of Dioxane–Water Solvent Compositions at 100° from 1 to 4000 Bars

Dioxane, wt %	Satn V.P.[a]	Pressure, bars: 500	1000	1500	2000	2500	3000	3500	4000
				Densities,[b] g/cm³					
29.7	0.970	0.984	1.004	1.021	1.037	1.051	1.064	1.078	1.090
40.3	0.970	0.986	1.006	1.023	1.039	1.053	1.066	1.079	1.091
50.8	0.968	0.987	1.007	1.024	1.040	1.054	1.067	1.080	1.092
60.5	0.964	0.988	1.008	1.025	1.041	1.055	1.068	1.081	1.093
70.5	0.960	0.989	1.009	1.026	1.042	1.056	1.069	1.082	1.094
				Dielectric Constants[b]					
29.7	35.3	36.2	37.1	37.9	38.7	39.4	40.0	40.7	41.3
40.3	28.6	29.4	30.1	30.8	31.4	32.0	32.5	33.0	33.4
50.8	22.6	23.0	23.5	24.1	24.5	25.0	25.4	25.8	26.1
60.5	16.8	17.4	17.9	18.2	18.6	18.9	19.2	19.5	19.8
70.5	11.8	12.2	12.5	12.7	13.0	13.2	13.4	13.6	13.8
				Viscosities,[b] cP					
29.7	0.42	0.43	0.45	0.48	0.50	0.52	0.55	0.58	0.61
40.3	0.45	0.47	0.49	0.51	0.54	0.57	0.60	0.64	0.68
50.8	0.48	0.50	0.53	0.56	0.59	0.62	0.66	0.70	0.74
60.5	0.50	0.53	0.56	0.59	0.62	0.66	0.70	0.74	0.79
70.5	0.51	0.54	0.57	0.60	0.64	0.68	0.72	0.77	0.82
				Specific Conductances of Solvent,[c] $ohm^{-1}cm^{-1}$, $\times 10^6$					
29.7	4.1	4.4	4.6	5.0	5.3	5.7	6.0	6.3	6.7
40.3	1.6	1.8	2.0	2.3	2.5	2.8	3.1	3.4	3.7
50.8	0.8	1.0	1.1	1.2	1.4	1.6	1.7	1.9	2.1
60.5	0.5	0.6	0.7	0.8	0.8	0.9	1.0	1.1	1.1
70.5	0.2	0.2	0.2	0.2	0.3	0.3	0.3	0.3	0.3

[a] Saturation vapor pressure is approximately 1 bar for all these solutions. Data are from Dunn and Marshall, ref 9. [b] Calculated values (see Experimental Section of text). [c] Values derived from experimental measurements.

unpublished work of Kennedy, *et al.* To estimate the densities of the solutions at different dioxane–water compositions and a given pressure, it was assumed that ideal solutions were formed at 100°: solvent density = density of pure water × volume fraction of water + density of pure dioxane × volume fraction of dioxane. These solution densities are given in Table I.

Dielectric Constants. When the dielectric constants (D) of Åkerlöf and Short[17] for dioxane–water solutions at 1 bar and at both 20 and 80° were plotted as log ($D - 1$) *vs.* log C_{H_2O}(mol/l.), straight lines resulted in both cases at solvent compositions less than 90 wt % dioxane. Since our solutions do not contain more than 71 wt % dioxane, the dielectric constants assigned by Dunn and Marshall[9] to several compositions of dioxane–water at 100° and saturation pressure were treated by a method of nonlinear least squares[18] to calculate the slope and intercept of the best straight line which describes them. The equation for this line is

$$\log (D - 1) = -0.56055 + 1.32965 \log C_{H_2O} \quad (1)$$

By using the densities estimated previously to calculate the molar concentration of water, and with the assumption that eq 1 applies at high pressures, the dielectric constants were estimated with eq 1 for each experimental solvent composition at various pressures to 4000 bars. Table I contains these estimated dielectric constants; again, it should be emphasized that these values are based on the assumed validity of eq 1 to high pressures.

Viscosities. The viscosities (η) of water at 100° and pressures to 4000 bars which were used are those determined by Bett and Cappi.[19] To estimate the viscosities of pure dioxane as a function of pressure, it was assumed that the fluidities ($1/\eta$) of dioxane decrease in absolute value with increasing pressure to the same extent as do the fluidities of water. The viscosities for various dioxane–water compositions at 100° and 1 bar given elsewhere[9] were plotted against wt % dioxane; curves for the higher pressures were drawn symmetrical to this one through the previously fixed data points for pure water and pure dioxane. The solution viscosities estimated in this manner are recorded in Table I.

(16) G. C. Kennedy, W. L. Knight, and W. T. Holser, *Amer. J. Sci.*, 256, 590 (1958).

(17) G. Åkerlöf and O. A. Short, *J. Amer. Chem. Soc.*, 58, 1241 (1936).

(18) M. H. Lietzke, U. S. Atomic Energy Commission Report ORNL-3259, Oak Ridge National Laboratory, Oak Ridge, Tenn., April 1962.

(19) K. E. Bett and J. B. Cappi, *Nature*, 207, 620 (1965).

Table II: Specific Conductances (ohm^{-1} cm^{-1}) × 10^5 of NaCl in Dioxane–Water Solutions at 100° from 1 to 4000 Bars

Dioxane, wt %	NaCl ($m \times 10^3$)	Pressure, bars: Satn V.P.[a]	500	1000	1500	2000	2500	3000	3500	4000
29.7	3.146	72.2	70.2	68.5	66.8	65.3	63.8	62.4	61.1	59.8
	6.923	150.5	147.2	144.1	141.1	138.1	135.2	132.5	129.8	127.3
	17.18	356.5	349.7	343.1	336.5	330.1	323.8	317.8	312.0	306.4
40.3	0.9510	21.01	20.28	19.62	18.99	18.41	17.85	17.34	16.86	16.39
	2.889	61.2	58.9	57.0	55.3	53.8	52.4	51.1	49.8	48.7
	7.313	146.8	142.2	138.2	134.3	130.8	127.4	124.4	121.5	118.7
	13.24	254.2	248.3	242.0	236.1	230.3	224.8	219.2	213.9	208.5
	21.79	398.0	387.6	376.4	367.4	357.8	348.6	340.0	332.0	324.4
50.8	1.015	21.16	20.44	19.75	19.08	18.46	17.88	17.32	16.74	16.20
	1.931	36.64	35.16	33.82	32.52	31.30	30.20	29.14	28.12	27.16
	3.047	54.2	52.0	49.8	47.8	46.1	44.6	43.3	42.0	40.6
	7.086	116.4	112.3	108.5	104.6	101.2	98.0	95.0	92.1	89.3
	16.28	244.4	237.5	230.7	223.7	217.2	210.5	205.1	199.1	193.2
60.5	1.015	18.20	17.32	16.49	15.70	14.95	14.25	13.61	12.99	12.40
	1.654	27.76	26.22	24.80	23.50	22.34	21.30	20.36	19.50	18.68
	3.278	49.1	46.6	44.3	42.2	40.3	38.57	36.95	35.40	34.05
	6.948	91.3	87.6	83.9	80.5	77.2	74.2	71.4	68.7	66.1
	16.43	179.2	173.4	167.5	161.9	156.5	151.4	146.7	142.4	138.2
70.5	0.9515	10.92	10.27	9.69	9.18	8.73	8.32	7.93	7.56	7.20
	1.527	15.12	14.43	13.78	13.19	12.64	12.11	11.60	11.10	10.62
	2.940	24.72	23.70	22.74	21.86	21.06	20.28	19.56	18.82	18.08
	7.367	48.6	46.7	45.0	43.2	41.6	40.1	38.60	37.25	36.00
	15.85	87.8	84.7	81.6	78.5	75.5	72.7	70.0	67.4	64.6

[a] See footnote *a*, Table I.

Results and Discussion

Results. The conductance readings were converted to resistances and a correction made for the resistance of electrical leads between the bridge and electrodes. These values in turn were corrected to resistances at infinite signal frequency, since the conductances showed a slight (1–3%) frequency dependence. By using the appropriate cell constant, specific conductances were calculated and corrections for solvent conductance were made. (See ref 4a for detailed description.) Figure 1 shows the typical form of the curve produced when the corrected specific conductances (κ) of NaCl in various compositions of dioxane–water are plotted against pressure at 100°. The gradual decrease in the specific conductance with increasing pressure at this temperature was found also for NaCl in aqueous solutions[4a] as well as for aqueous solutions of other 1–1 salts.[4c,4e,20] This behavior can be explained qualitatively on the basis of the effect of pressure upon density and viscosity. The values for these two physical properties increase with an increase in pressure (see Table I). However, increased densities (or water concentrations) promote ionization and thereby increased conductivity, while increased viscosities decrease ionic mobilities resulting in lowered conductivity. Therefore, at 100° and pressures to 4000 bars, the viscosity effect must be the dominant one in these cases. The decrease in specific conductance of NaCl, at isothermal and isobaric conditions, as the fraction of dioxane in the solvent rises is due to decreased water concentrations along with increased viscosities.

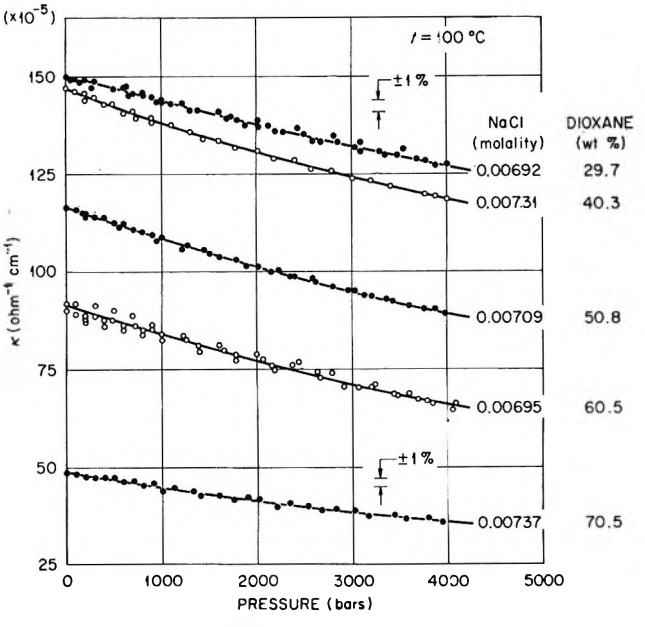

Figure 1. Specific conductances of some NaCl solutions as a function of pressure in several dioxane–water solvent compositions at 100°.

From graphs similar to Figure 1 for all NaCl solutions in the five dioxane–water solvent compositions, smoothed

(20) A. S. Quist and W. L. Marshall, *J. Phys. Chem.*, **73**, 978 (1969).

specific conductances were read at 500-bar intervals. These values to 4000 bars are presented in Table II.

Equivalent conductances (Λ) were calculated from the smoothed specific conductances, the molalities of NaCl, and the estimated densities of the solvents, which were assumed to be the densities of these dilute solutions. The effect of pressure on the equivalent conductances of approximately 0.0071 m NaCl in different solvent compositions is illustrated in Figure 2. The equivalent conductances are seen to decrease by 30 ± 5% as the pressure rises from 1 to 4000 bars.

Figure 3 shows the effect of solvent composition upon the equivalent conductances for exactly 0.00710 m NaCl at several different pressures. A solution with this exact molality was not measured in the various dioxane–water compositions (see Figure 2); hence, the equivalent conductances were interpolated from plots of Λ *vs.* $m^{1/2}$ for each solvent composition. Equivalent conductances for NaCl in pure water as solvent were interpolated from values of an earlier study.[4a] The dashed portions of the curves in Figure 3 are not included in the range of experimental measurements. However, this general shape for the curves is substantiated by the curve calculated for 1 bar from simple conductance theory (see inset, Figure 3). As an approximation, it was assumed that the activities of the species in solution were equal to one so that the conventional ionization or dissociation constant for NaCl was defined by

$$K_d = \frac{m\theta^2}{1 - \theta} \qquad (2)$$

where m is NaCl molality and θ is the fraction ionized. Equation 2 was solved for values of θ after substituting 0.00710 for m and the published values of K_d at 1 bar.[9] The values of Λ plotted against wt % dioxane, which form the curve in the inset figure, are equal to $\theta\Lambda_0$, where Λ_0 is the limiting equivalent conductance at 1 bar for the corresponding solvent composition.[9]

Limiting Equivalent Conductances. In dioxane–water solvent compositions, considerable association or ion-pair formation of Na^+ and Cl^- may be expected on the basis of similar studies at 25° and saturation vapor pressure.[21] Therefore, the conductance equation used to calculate limiting equivalent conductances (Λ_0) from our data should include a conventional ionization constant for the dissociation of NaCl

$$NaCl(aq) \overset{K_d}{\rightleftharpoons} Na(aq)^+ + Cl(aq)^- \qquad (3)$$

For this reason the equations of Fuoss and Kraus,[22] Shedlovsky,[23] and Fuoss, Onsager, and Skinner[24] for a weak or incompletely dissociated electrolyte were considered. The last equation was not used because our data are not precise enough for such an extensive treatment. Shedlovsky's equation was then chosen

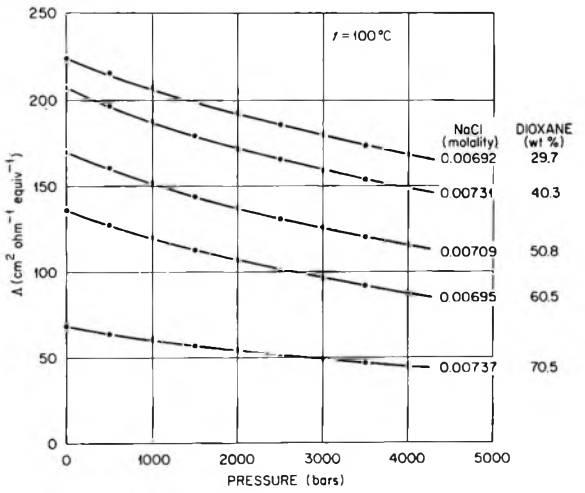

Figure 2. Representative behavior of equivalent conductances of NaCl solutions as a function of pressure in several dioxane-water solvent compositions at 100°.

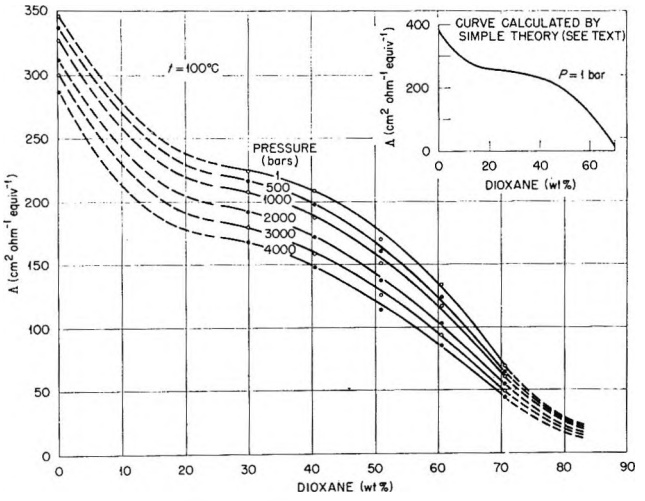

Figure 3. Variation of equivalent conductances of 0.0071 m NaCl with dioxane-water solvent composition for pressures from 1 to 4000 bars.

since it reproduces conductance data to significantly higher concentrations (~0.01 M) than does the Fuoss–Kraus equation for electrolytes whose $K_d \geq 10^{-4}$. The Shedlovsky conductance equation in the form

$$\frac{1}{\Lambda S(z)} = \frac{1}{\Lambda_0} + \frac{C\Lambda S(z) f_\pm^2}{K_d \Lambda_0^2} \qquad (4)$$

where C is the stoichiometric normality, $f_\pm$ is the mean molar activity coefficient of the ions, and $S(z)$ is defined in terms of C, Λ, Λ_0, and the Onsager limiting slope, was solved simultaneously for Λ_0 and K_d by the

(21) R. W. Kunze and R. M. Fuoss, *J. Phys. Chem.*, **67**, 911 (1963).

(22) R. M. Fuoss and C. A. Kraus, *J. Amer. Chem. Soc.*, **55**, 476 (1933); R. M. Fuoss, *ibid.*, **57**, 488 (1935).

(23) T. Shedlovsky, *J. Franklin Inst.*, **225**, 739 (1938); R. M. Fuoss and T. Shedlovsky, *J. Amer. Chem. Soc.*, **71**, 1496 (1949).

(24) R. M. Fuoss, L. Onsager, and J. F. Skinner, *J. Phys. Chem.*, **69**, 2581 (1965).

Table III: Limiting Equivalent Conductances and Conventional Ionization Constants for NaCl in Dioxane–Water Solutions from 1 to 4000 Bars at 100°

Dioxane, wt %	Satn V.P.[a]	Pressure, bars: 500	1000	1500	2000	2500	3000	3500	4000
				Limiting Equivalent Conductances, $cm^2\ ohm^{-1}\ equiv^{-1}$					
29.7	252	243	232	223	214	205	198	191	185
40.3	239	226	214	204	195	186	178	171	165
50.8	226	213	199	187	176	166	158	150	144
60.5	216	202	186	173	160	150	141	133	125
70.5	209	191	173	159	144	133	124	114	106
				Negative Logarithms of Conventional Ionization Constants					
29.7	0.43	0.41	0.26	0.26	0.08				
40.3	0.82	0.63	0.50	0.38	0.33	0.06			
50.8	1.72	1.67	1.60	1.54	1.46	1.39	1.34	1.28	1.29
60.5	2.32	2.30	2.24	2.19	2.12	2.08	2.03	2.00	1.95
70.5	3.37	3.31	3.25	3.20	3.13	3.09	3.05	3.00	2.96

[a] See footnote *a*, Table I.

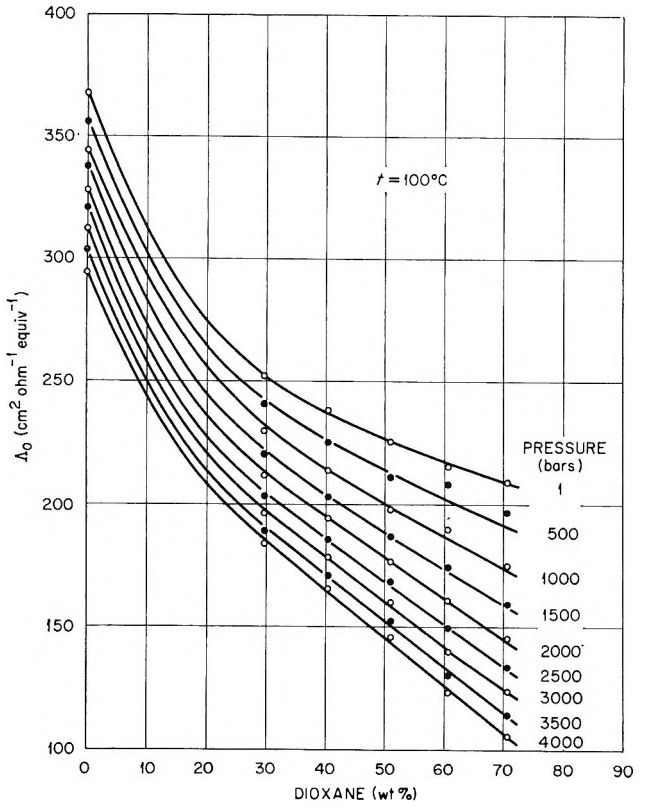

Figure 4. Limiting equivalent conductances of NaCl in dioxane-water solutions as a function of solvent composition and pressure at 100°.

method discussed previously.[4a] The pronounced dependence of limiting equivalent conductances for NaCl at 100° upon solvent composition is depicted in Figure 4 for pressures at 500-bar intervals from 1 to 4000 bars. (Values for the aqueous NaCl solutions are from data given elsewhere.[4a]) Smoothed limiting equivalent conductances were read from these curves for presentation in Table III.

Earlier conductance studies with such diverse electrolytes as $KHSO_4$,[25] NaCl,[4a] NaBr,[4c] NaI,[4e] HBr,[4b] and NH_4OH[4d] have shown a linear relationship between limiting equivalent conductance and density (or concentration) of the solvent water at constant temperature over a range as great as 0.4–1.0 g/cm³. In those investigations, applied pressure determined the densities so that this wide range of densities was attainable only at temperatures of 400° or greater, whereas at 100° the range was only 0.96–1.09 g/cm³. For the present study at 100°, however, concentrations (or densities) of water in dioxane–water solutions were varied largely by the addition of dioxane to the solutions; hence, the range is from <0.3 to nearly 1.1 g/cm³ of water. That the linear relationship of Λ_0 *vs.* density or concentration of H_2O continues to hold is apparent from Figure 5, where the lines are those resulting from a least-squares fit of the data. The concentration of water is equal to wt % water times the density of the solvent. It is of interest to note that all of these systems have a Λ_0 value of 884 ± 90 $cm^2\ ohm^{-1}\ equiv^{-1}$ at a water concentration of zero.

Dissociation (Ionization) Constant of NaCl. Since dioxane in the presence of water gives no evidence of solvating ions,[26,27] the ionization equilibrium of NaCl in dioxane–water[2,9] is considered to be

$$NaCl(aq) + kH_2O \overset{K^0}{\rightleftharpoons} Na(aq)^+ + Cl(aq)^- \quad (5)$$

where k is the net change in the number of solvating water molecules when one hydrated NaCl ion pair forms hydrated ions. Therefore, the complete equilibrium constant is

(25) A. S. Quist and W. L. Marshall, *J. Phys. Chem.*, **70**, 3714 (1966).

(26) T. W. Davis, J. E. Ricci, and C. G. Sauter, *J. Amer. Chem. Soc.*, **61**, 3274 (1939).

(27) A. Fratiello and D. C. Douglass, *J. Chem. Phys.*, **39**, 2017 (1963).

$$K^0 = K_d/C_{H_2O}{}^k \quad (6a)$$

or

$$\log K_d = \log K^0 + k \log C_{H_2O} \quad (6b)$$

where K_d is the conventional equilibrium constant (see eq 3) and C_{H_2O} is the molar concentration of water. The standard state for the solute species in a given solvent composition is the hypothetical 1 M solution, which has the same thermodynamic properties as a solution at infinite dilution at the particular pressure on the system. The activity of water is defined[7] as equivalent to its analytical molarity (C_{H_2O}) in the mixed solvent.

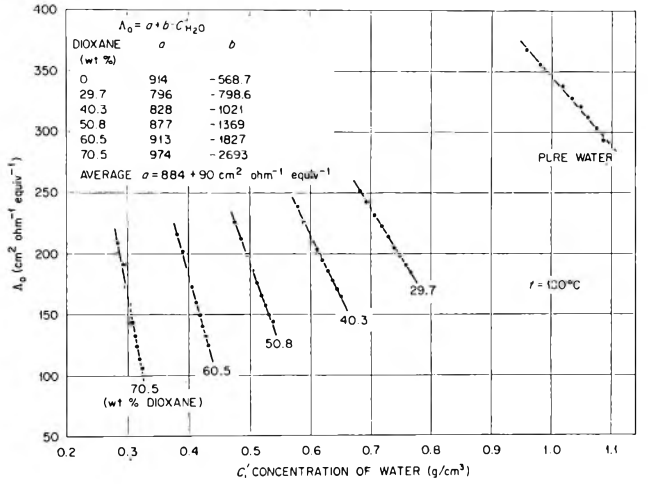

Figure 5. Dependence of the limiting equivalent conductances of NaCl on the concentration of water in several dioxane–water compositions at 100° from 1 to 4000 bars.

The smoothed limiting equivalent conductances from Table III were used with the Shedlovsky equation (eq 4) to calculate conventional ionization constants (K_d) whose negative logarithms to base 10 are reported in Table III also. According to eq 6b a plot of log K_d *vs.* log C_{H_2O} should produce a straight line of intercept log K^0 and slope k. Figure 6 shows that our values adhere to this relationship with k, the net change in the water molecules of hydration, equal to 7.8 and log K^0 equal to -12.7, in agreement with the earlier results for this system at 1 bar.[9] As also indicated in the previous paper, this value of k for sodium chloride at 100° offers a smooth transition from 6.4 at 25° in dioxane–water at saturation vapor pressure[2,3] to 10.2 at 400–800° in water under pressure.[4a]

Since values for the density, dielectric constant, and viscosity of the solvent are estimated ones, the question of the dependence of limiting equivalent conductance and the conventional dissociation constant upon these properties arises naturally. The density is first used to convert the specific conductance (κ) for a solution of given molality to the corresponding equivalent conductance (Λ) of NaCl by

$$\Lambda = 1000\kappa/md \quad (7)$$

Hence, a given percentage error in density results in the same percentage error for equivalent conductance but in the opposite direction. The normality, or molarity, for a 1–1 electrolyte is directly proportional to the density, of course. The limiting equivalent conductance, to a first approximation, is related to the equivalent conductance and to the square root of the molar concentration (C) by

$$\Lambda = \Lambda_0 - A\sqrt{C} \quad (8)$$

where A is a constant. With the dilute solutions used here, the effect of concentration errors upon the limiting equivalent conductance is negligible so that this quantity is very nearly inversely proportional to density, or directly proportional to equivalent conductance. The relationship between density and the conventional ionization constant, using eq 7 and eq 4, is not readily apparent since

$$S(z) \equiv (z/2 + [1 + (z/2)^2]^{1/2})^2 \quad (9)$$

$$z = [8.21 \times 10^5 \Lambda_0/(DT)^{3/2} + 82.5/\eta(DT)^{1/2}]C^{1/2}\Lambda^{1/2}/\Lambda_0{}^{3/2} \quad (10)$$

$$\log f_\pm = -\frac{(\text{D.H.S.})C^{1/2}\theta^{1/2}}{1 + C^{1/2}\theta^{1/2}} \quad (11)$$

where D.H.S. is the Debye–Hückel limiting slope for a 1–1 electrolyte and

$$\theta = S(z)\Lambda/\Lambda_0 \quad (12)$$

However, with the use of a computer and by varying only the density, it was found that as the density increases the conventional ionization constant increases slowly at first, then rapidly goes to plus infinity, minus infinity, and slowly becomes less negative in value but

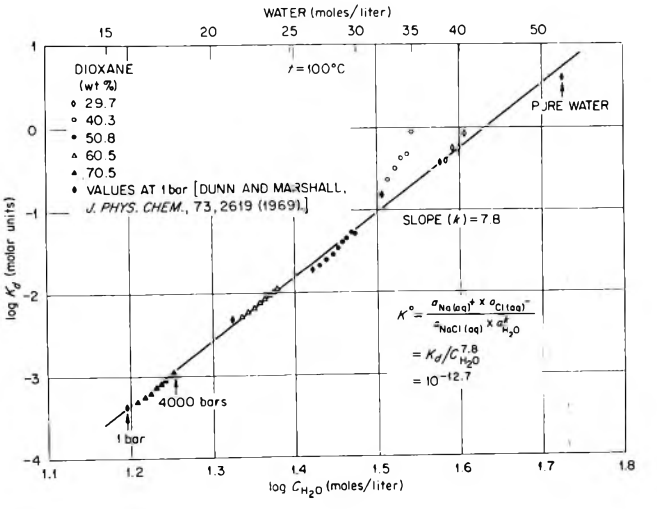

Figure 6. Variation of the logarithm of the conventional ionization constant for NaCl with the logarithm of the molar concentration of water in various dioxane–water solvent compositions at 100° from 1 to 4000 bars.

asymptotically so. The change to plus infinity from about 0.1 for K_d occurs within a narrow range of density; for the 29.7 and 40.3 wt % dioxane solutions, this transition is close to the actual densities because the ratio of Λ/Λ_0 is nearly unity. Negative values for K_d result from θ, the degree of ionization, being greater than one, while positive but infinite values of K_d are produced when θ is only slightly less than one. This becomes apparent upon writing the conventional equilibrium constant expression in the form

$$K_d = \frac{C\theta^2 f_\pm^2}{1 - \theta} \qquad (13)$$

In addition to this density effect, the molar concentration of water used in eq 6 and, subsequently, in Figure 6 is fairly sensitive to the value assigned to the solvent density. From this discussion it can be seen that both k and K^0 are strongly dependent upon the solvent densities.

Likewise, the relationships of dielectric constant and viscosity to limiting equivalent conductance and the conventional ionization constant are complex. The degree of ionization (θ) of a weak electrolyte, according to Shedlovsky,[23] can be expressed by

$$\theta = \frac{\Lambda}{\Lambda_0}(1 + z + z^2/2 + z^3/8 \ldots \text{etc.}) \qquad (14)$$

Therefore, when θ, C, and Λ are held constant, the limiting equivalent conductance increases as either or both dielectric constant and viscosity of the solvent decrease. A variation of $\pm 20\%$ in the assigned dielectric constant for one case caused only $\pm 0.6\%$ change in the opposite direction in the Λ_0 value. As expected from eq 10 and 14, the effect of viscosity upon Λ_0 is still less. Upon increasing the value for viscosity by 40–75%, the Λ_0 value was decreased merely by 1–2%. The conventional ionization constant (K_d), however, is much more sensitive to changes in these two properties, particularly when K_d is greater than about 0.1, that is, for NaCl solutions in the solvent composition range of 30–40 wt % dioxane at 100°. As the dielectric constant or viscosity is increased, the values for K_d go from slightly negative to negative infinity, to plus infinity, and finally approach asymptotically a small positive value. Again, the infinite values for K_d occur for the NaCl in 30 to 40 wt % dioxane solutions within a narrow range of D or η and close to the actual values because the calculated degree of ionization (θ) is slightly greater than or less than unity. The missing values of K_d in Table III for NaCl in solvents of 29.7 and 40.3 wt % dioxane in water were calculated and found to be either negative or high positive ones which are inconsistent with those listed here and plotted in Figure 6. This means that either the experimental data or the estimates of any one or all three of the physical properties are not accurate enough, with the latter much more probable, to enable a reliable determination of values for K_d near unity. On the other hand, a reduction of viscosity to 60% of the assigned value increased K_d only by 50 to 15% as the dioxane composition increased from 50.8 to 70.5%, respectively, or as K_d steadily decreased from about 0.1.

This discussion of the effect of errors in the values assigned to the physical properties of dioxane–water (see Table I) indicates clearly the need for measured values, especially of density, to completely justify acceptance of the calculated values for K_d, K^0, and k and the pressure independence of the latter two.

Kinetic Studies of Permanganate Oxidation Reactions. III. Reaction with Tris(1,10-phenanthroline)iron(II)

by Kenneth W. Hicks[1] and John R. Sutter*

Department of Chemistry, Howard University, Washington, D. C. 20011 *(Received March 2, 1970)*

Publication costs borne completely by The Journal of Physical Chemistry

The kinetics of the reaction between tris(1,10-phenanthroline)iron(II) and permanganate

$$5Fe(phen)_3^{2+} + MnO_4^- + 8H^+ \longrightarrow 5Fe(phen)_3^{3+} + Mn(II) + 4H_2O$$

has been studied in acidic medium. The progress of the reaction was followed spectrophotometrically at 510 and 590 nm with a Beckman DU spectrophotometer using both a rapid mixing device and a stopped flow device. The empirical rate law

$$-\frac{(1/5)d[Fe(phen)_3^{2+}]}{dt} = \frac{k_{obsd}k_{III}[MnO_4^-][Fe(phen)_3^{2+}]^2}{k_{II}[Fe(phen)_3^{3+}] + k_{III}[Fe(phen)_3^{2+}]}$$

where $k_{obsd} = 9.28 \times 10^4\ M^{-1}\ sec^{-1}$ and $k_{III}/k_{II} = 0.55$ at 25.0° describes the results to greater than 87% completion at a hydrogen ion concentration of 0.115 M. The results obtained at various hydrogen ion concentrations indicate that the protonated forms of both permanganate ion and the intermediate manganate ion play a role in the kinetics. The enthalpy and entropy of activation were evaluated for k_{obsd} using the transition state equation. The value for $\Delta H^{\pm}$ is 15.5 ± 0.7 kcal/mol, while the value for $\Delta S^{\pm}$ is 16.3 ± 2.3 eu.

Introduction

Tris(1,10-phenanthroline)iron(II), hereafter Fe(phen)$_3^{2+}$, and the permanganate ion are inert complexes[2] in that neither complex readily exchanges its ligands with the solvent.[3,4]

The oxidation of Fe(phen)$_3^{2+}$ has been examined using a variety of oxidizing agents: Cr(VI),[5] $P_2O_8^{4-}$,[6] $S_2O_8^{2-}$,[7] H_2O_2,[8] chlorine oxidants,[9] and Mn(III).[10] In the cases where there was no dissociation of the tris complex prior to oxidation, the general rate expression

$$\text{rate} = k_{obsd}[Fe(phen)_3^{2+}][ox]$$

was found to be valid. Because of these observations it was felt that Fe(phen)$_3^{2+}$ might be useful in the attempt to elucidate the mechanism of permanganate oxidations. The overall equation for the reaction involved in this study is

$$5Fe(phen)_3^{2+} + MnO_4^- + 8H^+ \longrightarrow 5Fe(phen)_3^{3+} + Mn(II) + 4H_2O$$

This reaction is also of interest since it represents a reaction in the overall Fe(II)–MnO_4^- oxidation system in which the 1-equiv reduction of permanganate ion to

$$Fe(phen)_3^{2+} \longrightarrow Fe(phen)_3^{3+} + e^- \qquad \mathcal{E}_f^0 = -1.06\ V^{11}$$

$$MnO_4^{2-} \longrightarrow MnO_4^- + e^- \qquad \mathcal{E}^0 = -0.56\ V^{12}$$

MnO_4^{2-} is thermodynamically unfavorable, so that these ions may react *via* a path other than the second-order scheme generally encountered.[13,14]

The present reaction system is amenable to theoretical calculations using the theory of Marcus, since both reactants are inert complexes. Reactions of labile complexes are more difficult to predict from theory because of the formation and breaking of bonds during the electron transfer process and also because of difficulties in calculating the "electron conductivities" of the bridging groups.[15]

Experimental Section

Baker Analyzed reagent grade potassium perman-

(1) This paper is based on a dissertation submitted by K. W. Hicks to the faculty of Howard University in partial fulfillment of the requirements for the Ph.D. degree.

(2) H. Taube, *Advan. Inorg. Chem. Radiochem.*, 1, 1 (1959).

(3) M. C. R. Symons, *J. Chem. Soc.*, 3676 (1954).

(4) E. Eichler and A. C. Wahl, *J. Amer. Chem. Soc.*, 80, 4145 (1958).

(5) J. H. Espenson and E. L. King, *ibid.*, 85, 3328 (1963).

(6) A. A. Green, J. O. Edwards, and P. Jones, *Inorg. Chem.*, 5, 1858 (1966).

(7) J. Burgess and R. H. Prince, *J. Chem. Soc.*, 1772 (1966).

(8) J. Burgess and R. H. Prince, *ibid.*, 6061 (1965).

(9) B. Z. Shakhashiri, Doctoral Thesis, University of Maryland, College Park, Md, 1967.

(10) H. Diebler and N. Sutin, *J. Phys. Chem.*, 68, 174 (1964).

(11) G. F. Smith and F. P. Richter, *Ind. Eng. Chem., Anal. Ed.*, 16, 580 (1944).

(12) W. Latimer, "Oxidation Potentials," 2nd ed, Prentice-Hall, Englewood Cliffs, N. J., 1952, p 241.

(13) M. A. Rawoof and J. R. Sutter, *J. Phys. Chem.*, 71, 2767 (1967).

(14) B. M. Gordon and N. Sutin, *J. Amer. Chem. Soc.*, 83, 70 (1961).

(15) N. Sutin, *Annu. Rev. Phys. Chem.*, 17, 119 (1963).

ganate was used, and the solutions were handled as previously described.[13,16]

Optical density–concentration plots for permanganate showed that Beer's law is obeyed at 510, 520, and 590 nm, and the extinction coefficients were determined to be 1768 ± 15, 2248 ± 32, and 273 ± 5 M^{-1} cm^{-1}, respectively. The stock solution was diluted before each run to reaction concentration, and the concentration was checked spectrophotometrically.

A stock solution of 0.020 M $Fe(phen)_3^{2+}$ was prepared by weighing a known amount of ferrous ammonium sulfate, $Fe(NH_4)_2(SO_4)_2 \cdot 6H_2O$, Primary Standard, Thorn Smith, Royal Oak, Mich., and dissolving it in distilled water. A weighed amount of 1,10-phenanthroline, G. F. Smith Co., Columbus, Ohio, in slight excess (3%) to that needed for complete complexation, based on a 1:3 M ratio of iron to ligand, was added. The concentrations of total iron(II) and complexed iron(II) under reaction conditions of hydrogen ion concentration and ionic strength were checked potentiometrically using the millivolt scale of a Metrohm E-200 pH meter equipped with a saturated calomel–platinum electrode system. The phenanthroline complex was titrated with standard permanganate. The results showed that all of the iron(II) was present as $Fe(phen)_3^{2+}$ over extended periods of time at most H^+ concentrations.

The extinction coefficient of $Fe(phen)_3^{2+}$ was found to be 1.100 ± 0.011 × 10^4 and 316 ± 8 M^{-1} cm^{-1} at 510 and 590 nm, respectively. The values for $Fe(phen)_3^{3+}$ were 318 ± 5 and 818 ± 11 M^{-1} cm^{-1} at the given wavelengths. These values were determined by oxidizing known concentrations of $Fe(phen)_3^{2+}$ to $Fe(phen)_3^{3+}$ with a slight excess of either Ce(IV) or permanganate solutions in 0.5 M sulfuric acid. The sulfate complexes of Ce(IV) or Ce(III) do not absorb at 590 nm, and the contribution to the total optical density due to the residual permanganate was negligible at the concentrations used.

Sodium sulfate, Na_2SO_4, was used to control the ionic strength of the solutions. A solution was prepared by weighing a given amount of anhydrous sodium sulfate (Baker Analyzed reagent), used without further purification, together with a stock sulfuric acid solution (Baker Analyzed reagent), the mixture being diluted to final volume. The hydrogen ion concentrations for these solutions and the overall ionic strength were calculated by an iterative procedure using Kerker's values for K_2', the dissociation constant for HSO_4^-.[17] For example, a solution consisting of the stoichiometric concentration of H_2SO_4 and Na_2SO_4 of 0.1784 and 0.0742 M, respectively, will have a hydrogen ion concentration of 0.204 M, a sulfate ion concentration of 0.102 M, and a bisulfate ion concentration of 0.151 M. The ionic strength is 0.456. In this calculation the value of K_2', the ionization constant for HSO_4^- at 25° from Kerker's table, used is 0.142. Three iterations were made; the value used for K_2' was changed each time the ionic strength was calculated, until successive values of the concentration agreed. Thus, when H_2SO_4 concentration was changed to a new value, the sodium sulfate concentration was also changed in order to fix the ionic strength. The hydrogen ion concentration then was calculated as before. In these calculations the concentrations of permanganate ion and $Fe(phen)_3^{2+}$, being low, were neglected.

The progress of all the rapid mixing kinetic experiments was measured using the Beckman DU as a monochromator. The phototube compartment was altered in such a manner that a second nine-stage RCA IP28 photomultiplier, operating from its own power supply (Calibration Standard 120-B), which replaced the red sensitive phototube of the Beckman DU, could be positioned in the light path with the existing sliding rod. This modification allowed the DU to be used as a monochromator when making kinetic runs, and as a spectrophotometer when making optical density measurements. The separate power supplies increased the signal to noise ratio and improved stability enormously. A rapid mixing syringe, designed by Thompson and Gordon,[18] was used to bring the two reactants together rapidly.

A constant temperature bath (Forma-Temp Jr., 2095) was used to thermostat the reactant stock solutions in volumetric flasks and the water-jacketed observation compartment of the kinetic equipment at the desired temperature. The equilibration was done for at least 1 hr prior to further dilution of the stock solutions for experiments. The present investigators designed a constant temperature observation compartment to fit into the normal Beckman long-path sliding observation cell for use with the rapid mixing device. The water within this compartment completely surrounded both reaction and reference cells.

It was found possible to use the same reaction stock solutions for several kinetic runs when working at moderate acid concentrations. However, at high acid concentrations (approximately 0.5 M), fresh solutions of $Fe(phen)_3^{2+}$ were prepared from the thermostated stock prior to each run to prevent decomposition.

A Durrum-Gibson stopped-flow apparatus (Durrum Instrument Corp., Palo Alto, Calif.) was used to investigate the reaction under conditions where the 50-msec mixing time of the Thompson and Gordon rapid mixer could not be tolerated. The monochromator used in conjunction with the mixing chamber was a Beckman Model DU, and the associated power supplies were the same as those used in the rapid mixing experiments. For experiments using the Durrum

(16) L. J. Kirschenbaum and J. R. Sutter, *J. Phys. Chem.*, **70**, 3863 (1966).

(17) M. Kerker, *J. Amer. Chem. Soc.*, **79**, 3664 (1957).

(18) R. C. Thompson and G. Gordon, *J. Sci. Instrum.*, **41**, 480 (1964).

when large hydrogen ion concentrations were used, the acid was added to the permanganate solution while the sodium sulfate was added to the $Fe(phen)_3^{2+}$. This procedure gave identical results as when acid was contained in both solutions, but was used to prevent decomposition of the complex, so that the stock solution of the complex could be used over a longer period of time.

In both types of experiment, the output from the photomultiplier (filtered) was fed into a Tektronix storage oscilloscope, and the resultant kinetic trace was then photographed. The analysis of the curve was handled using computer techniques.

Edwards[6] reported that two discrete peaks were observed at 345 and 360 nm in the reaction of $Fe(phen)_3^{2+}$ with peroxydiphosphate, $P_2O_8^{4-}$, while Shakhashiri[9] reported a shoulder at 355 nm in the reaction of $Fe(phen)_3^{2+}$ with chlorine gas. In the former case, no blue $Fe(phen)_3^{3+}$ is formed, while in the latter both the blue complex and another species appear to be formed.

A brown solution is known to form when the $Fe(phen)_3^{3+}$ complex is allowed to stand in dilute acid, the spectrum being similar to that obtained from solutions which contain Fe(III) and 1,10-phenanthroline in a 1:3 molar ratio. This brown color is reported to be that of the dimer[19,20] and has an absorbance maximum at 360 nm.

Both Edwards and Shakhashiri attributed this shoulder to the presence of the iron(III) dimer $[(phen)_2Fe(OH)_2Fe(phen)_2]^{4+}$ or $[(phen)_2Fe{-}O{-}Fe(phen)_2]^{4+}$.

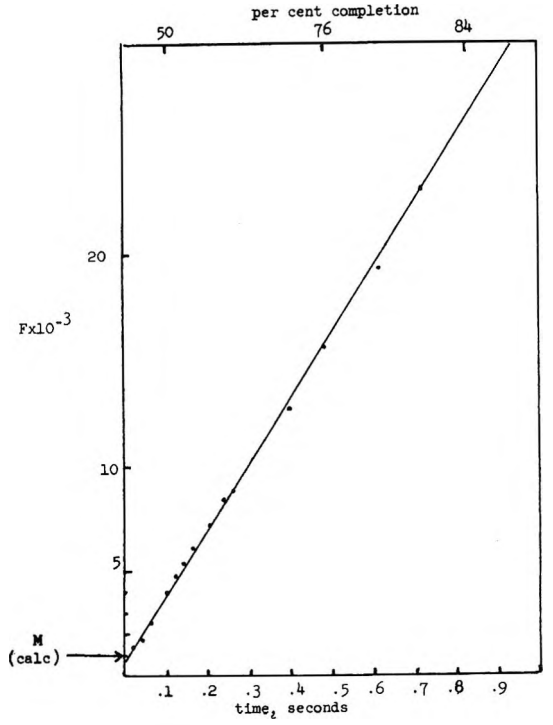

Figure 1. Reaction plot: $[MnO_4^-]_0 = 16.17 \times 10^{-5}$ M; $[Fe(II)]_0 = 83.03 \times 10^{-5}$ M; $[H^+] = 0.043$ M; $t = 25.0°$; $I = 0.45$; $k_{obsd} = 3.263 \times 10^4$ M^{-1} sec^{-1}; $k' = 0.586$.

It was therefore of interest to determine if any dimer was being formed in the oxidation of $Fe(phen)_3^{2+}$ by permanganate.

Several scans of the spectral region between 330 and 650 nm were made for a given experiment using a 2-cm path reaction cell in the Cary 14 spectrophotometer. All reactions were performed at room temperature with a hydrogen ion concentration of 0.52 M. As a spectral reference, solutions of $Fe(phen)_3^{2+}$ were oxidized with either Ce(IV) or chlorine water using similar reaction conditions. The spectra of the resulting reaction solutions showed evidence of a shoulder only with the reaction involving the saturated chlorine water. The spectrum of the reaction products of the complex with permanganate was identical with that obtained from the products of the $Fe(phen)_3^{2+}$–Ce(IV) reaction. Neither spectrum showed any detectable shoulder and the stoichiometric amount of the complex could be accounted for in each case. No detectable amount of dimer was formed in the reaction between permanganate and $Fe(phen)_3^{2+}$.

The overall stoichiometry of the reaction between permanganate and $Fe(phen)_3^{2+}$ in acid was verified to be a ratio of 1:5 and can be represented by the equation

$$5Fe(phen)_3^{2+} + MnO_4^- + 8H^+ \longrightarrow 5Fe(phen)_3^{3+} + Mn(II) + 4H_2O$$

Varying amounts of permanganate and the complex were allowed to react. The optical densities of these solutions were measured at 590 nm, the absorbance maximum of $Fe(phen)_3^{3+}$, to obtain the amount of $Fe(phen)_3^{3+}$ produced. The permanganate concentrations ranged from 0.415×10^{-5} to 6.805×10^{-5} M, while the $Fe(phen)_3^{2+}$ was varied from 0.244×10^{-4} to 4.505×10^{-4} M. The hydrogen ion concentration was 0.52 M, the temperature was 25.0°, and the ratio $Fe(phen)_3^{3+}/MnO_4^-$ was 4.94 ± 0.09.

The dependence of the rate of reaction on the concentration of permanganate, $Fe(phen)_3^{2+}$, and the reaction products was determined using rapid mixing and stopped-flow techniques, using the method of initial rates. The concentration of $Fe(phen)_3^{2+}$ was plotted against time, and the rate of the reaction at $t = 0$ was determined using a glass prism. The results indicated that the rate law was of the form

$$-\frac{1}{5}\left(\frac{d[Fe(phen)_3^{2+}]}{dt}\right)_0 = k'_{obsd}[MnO_4^-]_0[Fe(phen)_3^{2+}]_0$$

This relation, when integrated, however does not represent the reaction progress for more than 45%

(19) G. Anderegg, *Helv. Chem. Acta*, **45**, 1643 (1962).

(20) A. E. Harvey, Jr., and D. L. Manning, *J. Amer. Chem. Soc.*, **74**, 4744 (1952).

Table I: Dependence of Rate Constants on the Concentration of Permanganate Ion and $Fe(phen)_3^{2+}$; $t = 25.0°$, $I = 0.45$

$[H^+]$, M	$[MnO_4^-]$, $M \times 10^5$	$[Fe(phen)_3^{2+}]$, $M \times 10^5$	$[Fe(phen)_3^{3+}]$, $M \times 10^5$	$k_{obsd} \times 10^{-4}$, M^{-1} sec^{-1}	k'
0.043	16.17	83.14		3.21	0.58
0.043	8.355	44.29		3.41	0.58
0.043	7.272	37.39		2.75	0.58
0.043	5.033	26.67		2.94	0.58
				Av 3.08 ± 0.25	0.58[a]
0.043	3.072	17.90	14.0 ± 1	3.98 ± 0.5	0.59
0.104	2.115	5.00		9.11	0.59
0.104	2.115	3.75		8.76	0.57
0.104	2.115	2.50		8.26	0.57
0.104	1.269	2.00		9.68	0.55
				Av 8.95 ± 0.44	0.57[b]
0.104	2.115	3.75[c]		8.42	0.56[b]

[a] λ 590 nm. [b] λ 510 nm. [c] 10^{-3} M $MnSO_4$ added. k_{obsd} value obtained only when Mn(II) concentration omitted from the calculation.

completion, the rate falling off as products accumulate, and a more useful expression of the rate law

$$-\frac{d[MnO_4^-]}{dt} = -{}^1/_5\left(\frac{d[Fe(phen)_3^{2+}]}{dt}\right) = \frac{k_{obsd}k_{III}[MnO_4^-][Fe(phen)_3^{2+}]^2}{k_{III}[Fe(phen)_3^{2+}] + k_{II}[Fe(phen)_3^{3+}]} \quad (1)$$

was found to represent the data for more than 87% of the reaction when a suitable value for the ratio k_{III}/k_{II}, termed k', was chosen. The temperature was 25.0°, the hydrogen ion concentrations were 0.043 and 0.104 M, and the ionic strength was 0.45.

Integration of eq 1 gives the expression

$$k_{obsd}k'\gamma t = \ln\left(\frac{B+\gamma}{B}\right)\left[\frac{B_0 + C_0}{\gamma} + 1 - k'\right] + \left[(B_0 + C_0)\frac{1}{B}\right] + M \quad (2)$$

where $A = [MnO_4^-]$, $B = [Fe(II)]$, $C = [Fe(III)]$, $\gamma = 5A_0 - B_0$, $k' = k_{III}/k_{II}$, and the subscript 0 refers to conditions at time = 0. The concentration of permanganate ion may be calculated from the equation

$$[MnO_4^-] = \frac{D_\infty - D_t}{5\epsilon'}$$

where D_t = absorbance at any time, D_∞ = absorbance at infinite time, $\epsilon' = (\epsilon_{Fe(III)} - \epsilon_{Fe(II)} - {}^1/_5\epsilon_{MnO_4^-})l$, where ϵ is the extinction coefficient and l is the path length.

That value of k' was selected for each experiment which gave the best linear plot for over three half-lives and whose intercept agreed closest with the constant of integration, M, calculated from the initial concentration of reactants. The value of the rate constant, k_{obsd}, was determined by a linear least-squares program using the values determined by eq 2, and their corresponding time values. The progress of a reaction is shown in Figure 1. The ordinate, F, is the right-hand side of eq 2, excluding M. The intercept obtained by extrapolation to a somewhat arbitrary zero time is seen to be 0.66×10^3, where the value calculated from the best k' and initial conditions is 1.02×10^3. This is excellent agreement, for it represents an error of about 8 msec in the "choice" of the start of the reaction (zero time) from the original oscilloscope trace.

The inverse dependence of the rate expression on $Fe(phen)_3^{3+}$ was verified by performing the reaction using the rapid mixing device, with known quantities of $Fe(phen)_3^{3+}$ present initially. Known amounts of $Fe(phen)_3^{2+}$, in excess of that of the permanganate present, were allowed to react. This produced solutions which contained known amounts of $Fe(phen)_3^{2+}$, $Fe(phen)_3^{3+}$, and Mn(II). More permanganate was then added rapidly, and the subsequent reaction was recorded. The results of all concentration studies are given in Table I, and all entries are the average of at least three determinations. Experiments with added $MnSO_4$ (Table I) showed that added Mn(II) had no effect on the rate constant.

The dependence of the rate constant on the hydrogen ion concentration was determined using the stopped-flow apparatus with the hydrogen ion concentrations varying over a range of 0.043 to 0.398 M. The temperature was held constant at 25.0°, while the ionic strength was maintained at 0.45 with sodium sulfate. The rate constants are presented in Table II.

The temperature dependence of the reaction rate constants was measured at a constant hydrogen ion concentration and ionic strength of 0.115 and 0.45, respectively. The results are presented in Table III.

Discussion

The hydrogen ion dependence of k_{obsd} in the empirical rate law (eq 1) was investigated and k_{obsd} was found to be linearly related to the hydrogen ion concentration. A least-squares fit of the data in Table II to an equation

Table II: Dependence of the Rate Constants on Hydrogen Ion Concentration; $t = 25.0°$, $I = 0.45$, $[MnO_4^-]_0 = 2.115 \times 10^{-5}\ M$, $[Fe(phen)_3^{2+}]_0 = 5.000 \times 10^{-5}\ M$

$[H^+]$, M	$k_{obsd} \times 10^{-4}$, M^{-1} sec^{-1}	$k_{III}/k_{II} = k'$
0.043	3.08	0.58
0.074	6.21	0.54
0.104	8.95	0.57
0.115	9.28	0.55
0.204	15.7	0.48
0.398	30.0	0.31
		Av 0.50 ± 0.08

$k_{obsd} = (7.4 \pm 0.1) \times 10^5[H^+] + (6.1 \pm 2.2) \times 10^3$

Table III: Dependence of the Rate Constants on Temperature; $[H^+] = 0.115\ M$, $I = 0.45$, $[MnO_4^-]_0 = 2.115 \times 10^{-5}\ M$, $[Fe(phen)_3^{2+}]_0 = 5.000 \times 10^{-5}\ M$

t, °C	$k_{obsd} \times 10^{-4}$, M^{-1} sec^{-1}	k'
18.00	5.11	0.55
25.00	9.28	0.55
28.10	13.82	0.48
32.75	19.02	0.45

$\Delta H^{\pm}_{obsd} = 15.5 \pm 0.7$ kcal/mol
$\Delta S^{\pm}_{obsd} = 16.3 \pm 2.3$ eu

of that form yields $k_{obsd} = (7.42 \pm 0.11) \times 10^5[H^+] + (6.1 \pm 2.2) \times 10^3$ with the errors cited being the probable errors.

The empirical rate law, eq 1, and the hydrogen ion dependence of k_{obsd} indicate that two paths are available

$$Fe(II) + Mn(VII) + H^+ \rightleftharpoons [\ ]^{\pm} \qquad (A)$$

$$Fe(II) + Mn(VII) \rightleftharpoons [\ ]^{\pm} \qquad (B)$$

for the reduction process with path A being the major one. In view of the quite obvious importance of the proton in overcoming a thermodynamically forbidden reaction between $Fe(phen)_3^{2+}$ and permanganate ion, and of the reported permanganic acid species $HMnO_4$,[21] we shall interpret the experimental results by considering the following reaction sequence. The thermodynamic standard values for the protonation equilibrium constants at infinite dilution have been corrected to our ionic strength of 0.45, using the Davies equation.[23] Making the usual steady-state approximations on Mn(VI) one obtains

$$MnO_4^- + Fe(II) \underset{2}{\overset{1}{\rightleftharpoons}} MnO_4^{2-} + Fe(III) \qquad (I)$$

$$HMnO_4 + Fe(II) \underset{2'}{\overset{1'}{\rightleftharpoons}} HMnO_4^- + Fe(III) \qquad (II)$$

$$MnO_4^{2-} + Fe(II) \xrightarrow{3} MnO_4^{3-} + Fe(III) \qquad (III)$$

$$HMnO_4^- + Fe(II) \xrightarrow{3'} HMnO_4^{2-} + Fe(III) \qquad (IV)$$

$HMnO_4 = K_1[H^+][MnO_4^-]$ $\quad K_1 = 2.99 \times 10^{-3}$ [21]

$HMnO_4^- = K_2[H^+][MnO_4^{2-}]$ $\quad K_2 = 4.0 \times 10^{9}$ [22]

$$\text{rate} = \frac{[MnO_4^-][Fe(II)]^2\{k_1k_3 + k_1k_3'K_2[H^+] + k_1'k_3K_1[H^+] + k_1'k_3'K_1K_2[H^+]^2\}}{[Fe(II)](k_3 + k_3'K_2[H^+]) + [Fe(III)](k_2 + k_2'K_2[H^+])} \qquad (V)$$

One expects, according to Marcus theory, k_3 to be much, much less than k_1 since step III is even less thermodynamically favorable than step I. At 0.1 M $[H^+]$, k_2 is less than 10% of $k_2'K_2[H^+]$; at lower hydrogen ion concentration one can observe k_{obsd} falling off the linear plot. Values of k_{obsd} were not determined at lower than about 0.05 M $[H^+]$ because instability of the iron complexes made reproduction of the k's difficult. If, then, $k_3 \equiv 0$, and $k_2'K_2[H^+]$ is $\gg k_2$, an approximation that is true at all but the lowest hydrogen ion concentration, the rate law becomes

$$\text{rate} = \frac{[MnO_4^-][Fe(II)]^2k_3'\{k_1 + k_1'K_1[H^+]\}}{[Fe(II)]k_3' + [Fe(III)]k_2'} \qquad (VI)$$

where $k_{obsd} = \{k_1 + k_1'K_1[H^+]\} = 7.42 \times 10^5[H^+] + 6.1 \times 10^3$ in the empirical rate law. This value of $6 \times 10^3\ M^{-1}$ sec^{-1} for k_1 may be compared with that expected on the basis of Marcus theory, 4×10^3, suggesting that this step proceeds by an outer-sphere mechanism with a minimum of inner-sphere reorganization. A value of $1.2 \times 10^{11}\ M^{-1}$ sec^{-1} is calculated for k_2, using the experimental value of k_1 and the equilibrium constant determined from $\mathcal{E}°$ values, and compares with an experimental value for a diffusion-controlled reaction of this charge type for ion-pair formation.[24] While k_2 does seem fast for a redox reaction, Baxendale[25] has reported a value for the reaction between permanganate and Cd^+ of $2 \times 10^{10}\ M^{-1}$ sec^{-1}.

The value of k_1' calculated from the above equation and K_1 is $k_1' = 2.4 \times 10^8\ M^{-1}$ sec^{-1}. From the reported values of K_1 and K_2 and the equilibrium constant for step I, a value of 5.45×10^4 is computed for the equilibrium constant for step II, and thus $k_2' = 4.5 \times 10^3\ M^{-1}$ sec^{-1}. Alternatively, this would require the potential for the half-cell

$$HMnO_4 + e^- \longrightarrow HMnO_4^-$$

to be $\mathcal{E}_f° = 1.3$ V, a value consistent with the observed

(21) A. Carrington and M. C. R. Symons, *Chem. Rev.*, **63**, 443 (1963); N. Baily, A. Carrington, K. A. K. Lott, and M. C. R. Symons, *J. Chem. Soc.*, 290 (1960).

(22) M. W. Lister and Y. Yoshino, *Can. J. Chem.*, **38**, 2342 (1960).

(23) C. W. Davies, "Ion Association," Butterworths, Washington, D. C., 1962, p 39.

(24) A. Elder and S. Petrucci, *Inorg. Chem.*, **9**, 19 (1970).

(25) J. H. Baxendale, Symposium on Relaxation Kinetics, State University of New York at Buffalo, Summer 1965.

value of k_1'. The speed of the reaction thus stems from the rather sharp increase in the reduction potential due to protonation, making this path thermodynamically allowed. Further, using an average value of $k' = 0.5$, k_3' is equal to $2.24 \times 10^3\ M^{-1}\ \text{sec}^{-1}$ at $I = 0.45$ and 25°. This result is quite large when compared to the expected value for the nonprotonated reactants and products, *i.e.*, k_3, step III. The overall $\mathcal{E}°$ value for step III, −0.775 V,[26] leads to a calculated value of $k_3 \ll 1$. If this value of k_3' is attributed to an increase in the $\mathcal{E}°$ value of the MnO_4^{2-}–MnO_4^{3-} couple due to protonation of both species, then an estimate of the ionization constant of $HMnO_4^{2-}$ may be made. The equilibrium constant for reaction IV is calculated to be 6.9×10^{-8} using the same molecular parameters as those used in the calculation of k_1. This value of K_{IV} would require K_a, the ionization of $HMnO_4^{2-}$, to be equal to 4.6×10^{-16}. (For comparison, the K_a for HVO_4^{2-} is 4×10^{-15}.[21] This result would indicate that the blue color of MnO_4^{3-} solution was due to $HMnO_4^{2-}$ even in solutions as basic as 6 *M* and that the rapid decomposition of Mn(V) in less basic solution was due to the formation of $H_2MnO_4^-$. Thus, in 6 *M* base, $HMnO_4^{2-}$ would constitute 80% of the total Mn(V) and 70% at 10 *M*. This would be in keeping with the findings of Carrington and Symons[26] regarding the constancy of the electrode potential for the Mn(VI)–Mn(V) couple and the obedience to Beer's law for Mn(V) in 6–12 *M* base, except that $HMnO_4^{2-}$ would be the predominant species and not the minor one as they argued.

More extensive hydrolysis of Mn(VI) to yield H_2MnO_4 as an additional reactant might also be considered.

Lister and Yoshino[22] report the rate constant for the forward reaction

$$2MnO_4^{2-} \underset{k_b}{\overset{k_a}{\rightleftharpoons}} MnO_4^- + MnO_4^{3-}$$

k_a, to be $1.8\ M^{-1}\ \text{sec}^{-1}$ at 35° in 0.1 *M* base. In acid the reactants are likely to be $HMnO_4^-$, disproportionating, accompanied by an increase in the value of k_a and of the decomposition of Mn(V). No side reaction of this sort, in competition with our step IV, is observed even at the highest acid concentrations used, necessitating that $k_a < k_3'$. We intend to investigate the disproportionation of Mn(VI) in acid solution to verify this directly.

The temperature dependence of k_{obsd} was used to obtain activation parameters. A least-squares fit of $\log k_{obsd}/T$ *vs.* $1/T$ yields $\Delta H^{\ddagger} = 15.5 \pm 0.7$ kcal and $\Delta S^{\ddagger} = +16.3 \pm 2.3$ eu. The error in k_1 is rather large, *e.g.*, $(6.1 \pm 2.2) \times 10^3$ at 25°. Fortunately, k_1 contributed less than 10% to the overall k_{obsd}, at least at 25°, and it shall be assumed to contribute little to k_{obsd} at all temperatures in this study. Thus, approximately, $k_{obsd} = k_1'K_1[H^+]$ and the $\Delta H^{\ddagger}_{obsd}$ and $\Delta S^{\ddagger}_{obsd}$ may be equated to $\Delta H°_{K1} + \Delta H^{\ddagger}_{k1'}$ and $\Delta S°_{K1} + \Delta S^{\ddagger}_{K1'}$. After correction for hydrogen ion concentration, $\Delta S^{\ddagger}_{obsd} = 20.6$ eu.

Thermodynamic values for the protonation of permanganate have not been reported, however, a good estimate may be made by comparing permanganate with perchlorate.[27] After correcting for the difference in $\overline{S°}$ for these two ions, $\Delta S°_{K1} = -3.4$ eu and $\Delta H°_{K1} = 2.4$ kcal results, and hence, $\Delta S^{\ddagger}_{k1'} = 24$ eu and $\Delta H^{\ddagger}_{k1'} = 13$ kcal. This value for $\Delta S^{\ddagger}_{k1'}$ is admittedly not precise, but its positiveness deserves some comment. The reaction (II) is between a negative ion and a neutral species, and thus, formally at least, the coulombic part of the activation entropy is zero, while the inner- and outer-sphere contributions should be negligible. The largest factor in $\Delta S^{\ddagger}_{outer}$ is from the overall thermodynamic entropy change for the step, $\Delta S°_{II}$, which for this reaction would be zero or slightly negative.[28] The coulombic entropy contribution resulting from the products of the step (Fe(III) and $HMnO_4^-$ in this case) is also expected to be small, though positive, if the distance of closest approach is taken as the outer-sphere value of 9.8 Å. If the $HMnO_4$ penetrates between the planes of the phenanthrolines, sterically possible without distortion, then the collision complex will approach a situation

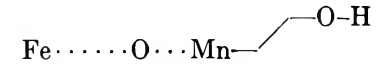

in which the Fe–O–Mn distance would be considerably less than 9.8 Å. Such a case could predictably swing the $\Delta S^{\ddagger}$ to a positive value, without greatly affecting a Marcus calculation of the rate constant, since the *k*'s are not terribly sensitive to the distance of closest approach. However, if penetration is important in the mechanism it must be done without covalency between the species. It seems necessary to invoke noncovalency in this pseudo-direct attack if the favorable results of the outer-sphere calculations are to be believed. In this sense, outer sphere does not denote simply outer-sphere contact, but allows for penetration provided no appreciable iron–oxygen overlap occurs. In this case, the penetration by the negative end of the $HMnO_4$, *i.e.*, oxygen, could partially reduce the effective charge on the collision complex from the plus two associated with the $Fe(phen)_3^{2+}$, with an accompanying release and/or loosening of water molecules resulting in a fairly sizable positive $\Delta S^{\ddagger}$. The function of the hydrogen ion at the other end would be to "tug" at the transferred electron.

In Table III the value of 0.55 for k' is there because

(26) A. Carrington and M. C. R. Symons, *J. Chem. Soc.*, 3373 (1956), report 0.285 V for the MnO_4^{2-}–MnO_4^{3-} couple in concentrated KOH solution.

(27) G. C. Hurd and C. A. Reilly, *J. Chem. Phys.*, **32**, 127 (1960).

(28) J. W. Cobble, *ibid.*, **21**, 1443, 1446, 1451 (1953).

it was the one determined at a hydrogen ion concentration of 0.115 M as were all the other k' values listed. Table II however shows that k' may be independent of hydrogen ion concentration and that at 25° a value of 0.50 would be better. In this case a plot of log k' *vs.* $1/T$ is quite linear. Little should be said about the relative activation parameters of k' in view of the small changes in k'. Finally, it should be pointed out that the k' value of 0.31 in Table II which looks out of line is not statistically reliably different from the average value of 0.50 listed (Pierce–Chauvenet criterion). However, at higher hydrogen ion concentration, both k_{obsd} and k' are difficult to reproduce, so we really cannot test to see if k' has a hydrogen ion dependence. The slight overall decrease in k' with increasing hydrogen ion concentration may be real. With the present data we ourselves are not sure if there is a functional dependence on hydrogen ion concentration or not in k'; we tend to feel there is not.

Acknowledgment. The authors wish to acknowledge partial support of this research under National Science Foundation Grant GP 8097. K. W. H. received support under a NASA Predoctoral Trainee Fellowship.

Ionic Reactions at High Ionic Strengths. Further Equilibrium and Kinetic Measurements on the Formation and Dissociation of Monochloroiron(III)

by Theophilus C. King[1] and J. Keith Rowley*

Chemistry Department, Brookhaven National Laboratory, Upton, New York 11973 *(Received December 21, 1970)*

Publication costs assisted by the U. S. Atomic Energy Commission

The equilibrium constant for the reaction $Fe^{3+} + Cl^- = FeCl^{2+}$ has been measured at 25° in several nearly isopiestic solutions containing varying amounts of $HClO_4$ and $NaClO_4$. The rate of approach to equilibrium of this reaction in 9.00 M $HClO_4$ has been measured by the stopped-flow technique. The results of the equilibrium measurements are that the equilibrium constant increases from 110 M^{-1} in 6.00 M $HClO_4$ to 168 M^{-1} in the nearly isopiestic mixture, 2.00 M $HClO_4$ + 6.16 M $NaClO_4$. These results have been used to test a simple method which has been previously proposed for calculating activity coefficients in mixed solutions of electrolytes. The possible reasons for the observed change in the equilibrium constant with changing medium at constant water activity are discussed. The observed rate constant at 25° in 9.00 M $HClO_4$ is given by $k_{obsd} = k_d + k_f[[Fe(III)] + [Cl^-]_T]$ where $k_d = 0.2$ sec^{-1} and $k_f = 2.10 \times 10^3$ M^{-1} sec^{-1}. This result indicates that the rate of dissociation of $FeCl^{2+}$ by the acid-independent path is proportional to the water activity, but is otherwise essentially medium independent in perchloric acid solutions.

Introduction

From a spectrophotometric study of the reaction

$$Fe^{3+} + Cl^- \underset{k_d}{\overset{k_f}{\rightleftharpoons}} FeCl^{2+} \qquad (1)$$

Coll, Nauman, and West[2] concluded that the water activity, a_w, is of primary importance in determining the magnitude of the molar concentration equilibrium quotient, K_c. This conclusion suggests that solvation is a very important factor in determining the activity coefficients of ions in concentrated solutions of electrolytes. Their data also indicate that the water activity is not the only determining factor since K_c is not constant when the medium is changed at constant a_w. Since an erroneous assumption about the molar absorptivity was made by Coll, *et al.*, it seemed worthwhile to repeat and extend some of their measurements in order to establish more firmly the existence of the other factor (or factors) affecting the value of K_c and also to test a simple method for calculating activity coefficients in mixtures of electrolytes which uses only single electrolyte data.[3] The new measurements were confined to perchloric acid–sodium perchlorate mixtures because excellent data are available on the water activities in this system.[4]

We have also extended the kinetic measurements on

(1) Summer student from Mississippi Valley State College.

(2) H. Coll, R. V. Nauman, and P. W. West, *J. Amer. Chem. Soc.*, **81**, 1284 (1959).

(3) V. M. Vdovenko and M. A. Ryazanov, *Radiokhimiya*, **7**, 39, 442 (1965).

(4) R. M. Rush and J. S. Johnson, *J. Phys. Chem.*, **72**, 767 (1968).

reaction 1 to a 9.00 M perchloric acid medium. Rowley and Sutin[5] found that the rate constant, k_{-1}, for the acid-independent dissociation of $FeCl^{2+}$ was essentially the same in 6.00 M perchloric acid as in 1.00 M and 3.00 M perchloric acid, but that k_{-1}/a_w was perhaps more nearly constant. Which of these two quantities is "more nearly constant" is a question which is relevant to the role of water in the dissociation reaction. In order to answer this question, it is necessary to study the kinetics in a medium in which the water activity is very low. For this reason 9.00 M perchloric acid ($a_w = 0.093$) was chosen.

Experimental Section

The preparation and standardization of stock solutions of perchloric acid and of iron(III) perchlorate was done as previously described.[5] A nearly saturated stock solution of sodium perchlorate was made using sodium perchlorate prepared from perchloric acid and sodium carbonate and recrystallized from perchloric acid. This solution was standardized by carefully evaporating aliquots to dryness, heating to constant weight at 160°, and weighing as $NaClO_4$. The concentration of a small amount of perchloric acid in the sodium perchlorate stock solution was determined by titration with standard sodium hydroxide using a glass electrode to follow the titration. A Gran plot[6] showing the disappearance of H^+ was used to determine the end point.

The spectrophotometric measurements at equilibrium were performed and the resultant data were treated in essentially the same manner as previously described.[5] The range of iron(III) concentrations used was 2.0×10^{-3} M to 5.5×10^{-2} M. The chloride concentration was 2.10×10^{-4} M in all solutions to which chloride was added. All measurements in a given series were performed at a constant molar ionic strength. The perchloric acid concentration was held constant and the concentration of sodium perchlorate was varied to maintain constant ionic strength as the iron(III) perchlorate concentration was varied. A Cary 16 spectrophotometer was used to measure absorbances at eight wavelengths between 330 and 380 nm. In choosing the perchloric acid–sodium perchlorate mixture for each series of measurements an attempt was made to choose a mixture with a water activity close to 0.459, the water activity of 6.00 M perchloric acid. Since the iron(III) perchlorate and sodium perchlorate concentrations were varied and the ionic strength was held constant in a series, the water activity varied slightly with increasing iron(III) perchlorate concentration. The water activities, densities, and sodium perchlorate concentrations listed in Table III refer to the perchloric acid–sodium perchlorate mixture corresponding to zero iron(III) perchlorate concentration in each series. Such solutions were prepared and their densities measured. Their water activities were estimated by calculating the molal concentrations of perchloric acid and sodium perchlorate using the measured densities, and then interpolating the data of Rush and Johnson.[4] The method of interpolation was such that the error in a_w due to interpolation was probably less than 0.001.

The kinetic measurements were performed and k_f and k_d were evaluated as previously described.[5] The formation of $FeCl^{2+}$ was followed at a wavelength of 352 nm. The ionic strength was maintained at a constant value of 9.00 M using perchloric acid (no sodium perchlorate was present in these kinetic measurements).

Results

Table I summarizes the results of the kinetic measurements at an ionic strength of 9.00 M. The values of k_d and k_f calculated from the relationship

$$k_{obsd} = k_d + k_f\{[Fe(III)] + [Cl^-]_T\} \qquad (2)$$

are 0.02, 0.2, and 0.6 sec^{-1} and 5.0×10^2, 21.0×10^2, and 59×10^2 M^{-1} sec^{-1} at 5.1, 25.0, and 38.7°, respectively. In Table II the present results and the activation parameters derived from them are compared with the results of previous measurements at other ionic strengths (all maintained with perchloric acid). The values for k_{-1}, the acid-independent rate constant for the dissociation of $FeCl^{2+}$, and for k_1, the acid-independent rate constant for its formation, in 9.00 M perchloric acid are based on the assumption that the con-

Table I: First-Order Rate Constants for the Reaction between Iron(III) and Chloride at Ionic Strength 9.00 M Maintained with Perchloric Acid

Temp, °C	10^3[Fe(III)], M	$10^3[Cl^-]_T$, M	k_{obsd}, sec^{-1}
5.1	0.2063	0.03941	0.146
	0.4126	0.03941	0.243
	0.8252	0.03941	0.433
	1.238	0.03941	0.68
	1.650	0.03941	0.85
25.0	0.2063	0.03941	0.75
	0.4126	0.03941	1.17
	0.5030	0.05255	1.34
	0.8252	0.03941	2.05
	1.006	0.05255	2.28
	1.238	0.03941	2.97
	1.650	0.03941	4.0
	2.012	0.05255	4.5
	4.024	0.05255	8.6
	6.036	0.05255	13.1
38.7	0.2063	0.03941	2.05
	0.4126	0.03941	3.16
	0.8252	0.03941	5.5
	1.238	0.03941	8.0
	1.650	0.03941	10.3

(5) J. K. Rowley and N. Sutin, *J. Phys. Chem.*, **74**, 2043 (1970).
(6) G. Gran, *Analyst (London)*, **77**, 661 (1952).

Table II: Summary of Rate Constants for the Reaction between Iron(III) and Chloride in Perchloric Acid Solutions at 25°

μ,[a] M	a_w	k_{-1},[b] sec^{-1}	k_1,[c] M^{-1} sec^{-1}	k_{-1}/a_w, sec^{-1}	$\Delta H_{-1}^{\ddagger}$, kcal mol^{-1}	$\Delta S_{-1}^{\ddagger}$, cal deg^{-1} mol^{-1}	$\Delta H_1^{\ddagger}$, kcal mol^{-1}	$\Delta S_1^{\ddagger}$, cal deg^{-1} mol^{-1}	Ref
1.00	0.961	1.61	8.4	1.7	15.6	−5	20[e]	12[e]	*f*
3.00	0.829	1.1	10.8	1.3					*g*
6.00	0.459	0.8	90	1.7	15.2[d]	−8[d]	15.2[d]	1 ± 3[d]	*h*
9.00	0.093	0.2[d]	2.1×10^3 [d]	2	15 ± 1.4[d]	−10 ± 5[d]	12 ± 1[d]	−3 ± 3[d]	*i*

[a] Ionic strength. [b] Rate constant for the acid-independent path for dissociation of $FeCl^{2+}$. [c] Rate constant for the acid-independent path for formation of $FeCl^{2+}$. [d] Calculated on the assumption that the acid dependent path may be neglected. [e] Calculated on the assumption that $K_c = 5.2\ M^{-1}$ and $\Delta H = 4.2$ kcal mol^{-1}. [f] H. N. Po and N. Sutin, unpublished work. [g] E. G. Moorhead and N. Sutin, *Inorg. Chem.*, **6**, 428 (1967). [h] Reference 5. [i] This work.

Table III: Summary of Equilibrium Spectrophotometric Data

Series	Temp, °C	$[HClO_4]$, M	$[NaClO_4]$, M	d^{25}_4, g ml^{-1}	$[HClO_4]$, m	$[NaClO_4]$, m	K_c, M^{-1}	a_w	K_m, m^{-1}	K_c^0,[b] M^{-1}	K_m^0,[b] m^{-1}	$\frac{K_m m_T}{K_m^0 m_T^0}$[b,c]
A[a]	25.0	6.00		1.3417[d]	8.120		110	0.459	149	110	149	1.00
B	25.0	4.950	1.550	1.3974	6.97	2.183	121	0.466	170	105	141	1.38
C	25.0	3.200	4.400	1.4995	5.006	6.88	156	0.450	245	120	163	2.17
D	25.0	2.000	6.16	1.5707	3.250	10.01	168	0.467	273	104	140	3.22
	44.1	2.000	6.16				226					
	12.3	2.000	6.16				131					

[a] Reference 5. [b] The superscript zero refers to the value of the particular quantity in a perchloric acid solution at the specified water activity. [c] m_T is defined as the total molal concentration of solute species. [d] A. Markham, *J. Amer. Chem. Soc.*, **63**, 874 (1941).

tributions of the acid-dependent paths are negligible at this acidity. The activation parameters in 9.00 M $HClO_4$ given in Table II are not based entirely on the kinetic results since there is considerable error in the values of k_d. Instead they are based on the more reliable values of the activation parameters for the formation reaction and the assumptions that $\Delta G = -5.2 \pm 0.3$ kcal mol^{-1} (*i.e.*, K_c is between 4,000 and 10,000 M^{-1}) and $\Delta H = -3 \pm 1$ kcal mol^{-1}.[7] The values obtained from the kinetic data alone without making these assumptions are $\Delta H_{-1}^{\ddagger} = 17 \pm 3$ kcal mol^{-1} kcal mol^{-1} and $\Delta S_{-1}^{\ddagger} = -5 \pm 5$ cal deg^{-1} mol^{-1}. These values are consistent with the values listed in Table II within the assigned errors.

Tables III and IV summarize the results of the equilibrium spectrophotometric measurements. For purposes of comparison the results in 6.00 M perchloric acid from ref 5 are included. The slope, S, and the intercept, I, of a plot of $[Fe(III)][Cl^-]_T/A$ *vs.* $[Fe(III)] + [Cl^-]_T$ [in which A is the absorbance per unit path length measured against a blank with the same iron(III) concentration] were evaluated by an unweighted linear least-squares analysis of the data. The values tabulated are S/I and $10^{-3}/S$ which are identified in the tables as K_c and 10^{-3} ϵ_1 [which is equal to $(\epsilon_{FeCl^{2+}} - \epsilon_{Fe^{3+}})$], respectively. The meaning of these measured quantities is discussed later. No variation of S/I with wavelength was observed. The measurements in series D at temperatures other than 25.0° were carried out at only one wavelength, 340 nm. Then the absorbance of a single solution containing chloride *vs.* its blank was measured at the listed wavelengths in order to determine the spectral band shape at these temperatures. The thermodynamic parameters for reaction 1 at 25° for series D resulting from these measurements are: $\Delta G = -3.03 \pm 0.02$ kcal mol^{-1}, $\Delta H = 3.1 \pm 0.1$ kcal mol^{-1}, and $\Delta S = 20.5 \pm 0.7$ cal deg^{-1} mol^{-1}. These values may be compared with $\Delta G = -2.79 \pm 0.01$ kcal mol^{-1}, $\Delta H = 0.0 \pm 0.8$ kcal mol^{-1}, and $\Delta S = 9 \pm 3$ cal deg^{-1} mol^{-1} for series A at 25°.[5]

Table IV: Values of 10^{-3} ϵ_1[a] as a Function of Wavelength

λ, nm	Series A	B	C	D	D 44.1°	D 12.3°
	25.0°					
330	2.45	2.44	2.54	2.52	2.41	2.64
335	2.63	2.60	2.69	2.66	2.57	2.78
340	2.71	2.67	2.75	2.72	2.65	2.82
345	2.69	2.62	2.70	2.67	2.63	2.74
350	2.57	2.51	2.57	2.53	2.52	2.58
355	2.39	2.31	2.35	2.30	2.33	2.33
365	1.83	1.75	1.78	1.73	1.81	1.71
380	1.02	0.95	0.97	0.93	1.02	0.88

[a] These are values of $10^{-3}/S$ which is usually taken to be the molar absorptivity of $FeCl^{2+}$. The units of $(1/S)$ are M^{-1} cm^{-1}.

(7) In ref 2, $K_c = 6100\ M^{-1}$ in 9.0 M $HClO_4$ and $\Delta H = -2.3$ kcal mol^{-1} in 8.5 M $HClO_4$.

A comparison at 25° of the shapes of the absorption bands of $FeCl^{2+}$ indicates that the band shifts slightly (about 2 nm for series D relative to series A) toward shorter wavelengths with increasing sodium perchlorate concentration. This shift is considerably larger than the shift occurring in perchloric acid solutions for the same change in water activity.

Discussion

Equilibrium Measurements. Before discussing the equilibrium results, it is useful to clarify as much as possible the meaning of the measured quantities. In order to accomplish this, we will assume that the outer-sphere complex formation constant, K_{out}, is negligibly small and extend a previous treatment of medium effects.[5] The extension is necessary because there are now three important molar concentration variables, the concentrations of $HClO_4$, $NaClO_4$, and $Fe(ClO_4)_3$, denoted by H, N, and F, respectively. Using an extension of the notation used previously, we may write

$$d \ln K_c = \left(\frac{\partial \ln K_c}{\partial H}\right)_{N,F} dH + \left(\frac{\partial \ln K_c}{\partial N}\right)_{H,F} dN + \left(\frac{\partial \ln K_c}{\partial F}\right)_{H,N} dF = \sigma_{N,F}\, dH + \sigma_{H,F}\, dN + \sigma_{H,N}\, dF \quad (3)$$

Two of the variables, H and N, are of considerably greater importance than the third, F, because of the much larger experimental variations in H and N. We cannot assume without additional justification that the σ values defined in eq 3 remain constant over the concentration ranges used. However, when comparing the results of the different series of measurements, it seems reasonable that the observed differences in S/I are mainly due to the changing values of H and N and to a lesser extent to the relatively much smaller changes in F (at constant ionic strength). We will therefore neglect the third term on the right-hand side of eq 3 and offer a supporting argument for this later. Under these conditions eq 3 becomes

$$d \ln K_c = \sigma_{N,F}\, dH + \sigma_{H,F}\, dN \quad (4)$$

Equation 4 applies only to comparisons between the different series of measurements. Since these measurements were made at essentially constant a_w, and since a_w is determined by the major concentration variables, H and N, eq 4 may be simplified by using a relationship which refers to isopiestic solutions of $HClO_4$ and $NaClO_4$[3,4,8]

$$\frac{H}{H^0} + \frac{N}{N^{00}} = 1 \quad (5)$$

in which H° is the concentration of a solution of the specified water activity containing only $HClO_4$ and N^{00} is the concentration of a solution at the same water activity containing only $NaClO_4$. In our experiments $H^0 = 6.0\ M$ and $N^{00} = 9.3\ M$. Equation 5 is not exact, but it is a good approximation using both the molar and molal concentration scales. Consequently, for isopiestic solutions

$$dH = -\frac{H^0}{N^{00}}\, dN \quad (6)$$

On substituting into eq 4 we obtain

$$d \ln K_c = \left[\sigma_{H,F} - \frac{H^0}{N^{00}}\sigma_{N,F}\right] dN \quad (7)$$

If $(\sigma_{H,F} - H^0\sigma_{N,F}/N^{00})$ is constant, then upon integration

$$\frac{\ln (K_c/Q_c^0)}{N} = \sigma_{H,F} - \frac{H^0}{N^{00}}\sigma_{N,F} = \text{constant} = \sigma^0_{H,F} - \frac{H^0}{N^{00}}\sigma^0_{N,F} \quad (8)$$

in which $Q_c^0 = 110\ M^{-1}$, the value of K_c when $H = 6.0\ M$ and $N = F = 0$, and the superscript zero refers to the value of the quantity when $H = 6.0\ M$ and $N = F = 0$. For series B, C, and D the calculated values of $\ln (K_c/Q_c^0)/N$ are 0.09_6, 0.06_1, and 0.07_8, respectively. In making these calculations S/I was assumed to equal K_c and the value of N used was the value for the series when $F = 0$. The average of these three values is $0.07_8\ M^{-1}$. This number is very sensitive to small errors in K_c and is constant within the errors of the measurements. Consequently, $\sigma^0_{H,F}$ may be evaluated using eq 8 and the previously measured value of $\sigma^0_{N,F} = 1.4\ M^{-1}$ at $H^0 = 6.0$ and $F = 0$. Note that the quantity $(\sigma^0_{H,F} - H^0\sigma_{N,F}/N^{00})$ is quite small and, consequently, the resulting calculated value of $\sigma^0_{H,F} = 1.0\ M^{-1}$ is not very sensitive to variations in this quantity. The quantity $\sigma^0_{H,F}$ is a measure of the change of $\ln K_c$ with N when $H = 6.0\ M$ and $F = 0$. By using $\sigma^0_{N,F}$ and $\sigma^0_{H,F}$ one can calculate K_c for $HClO_4$–$NaClO_4$ mixtures when H is close to $6.0\ M$ and N is relatively small. The quantity $\sigma_{H,F}$ cannot be evaluated using our data unless it is constant over the range of N which was investigated, in which case, $\sigma_{H,F} = \sigma^0_{H,F}$ and $\sigma_{N,F} = \sigma^0_{N,F}$.

We can now turn to the measurements made within a given series for which H and the ionic strength, μ, are both held constant. In a given series

$$\mu - H = \text{constant} = N + 6F$$

and

$$dN = -6\, dF \quad (9)$$

Remembering that $dH = 0$ for measurements within a series and substituting eq 9 into eq 3, we obtain

$$d \ln K_c = (\sigma_{H,N} - 6\sigma_{H,F})\, dF \quad (10)$$

(8) C. Perrin and F. H. Westheimer, *J. Amer. Chem. Soc.*, **85**, 2773 (1963).

The quantity in parentheses is essentially constant over the small range of F covered and, therefore, eq 10 integrates to give

$$\ln K_c = \ln K_c' + (\sigma_{H,N} - 6\sigma_{H,F})F \qquad (11)$$

in which $\ln K_c'$ is the value of $\ln K_c$ for the series when $F = 0$. Consequently, as has been shown previously,[5] the measured quantities are given by

$$(S/I) = K_c' - (\sigma_{H,N} - 6\sigma_{H,F})$$

$$1/S = \frac{\epsilon_1 K_c'}{K_c' - (\sigma_{H,N} - 6\sigma_{H,F})} \qquad (12)$$

Since neither $\sigma_{H,N}$ nor $\sigma_{H,F}$ is known, an exact interpretation of our experimental results is not possible. However it seems very likely that $(\sigma_{H,N} - 6\sigma_{H,F})$ is quite small compared to K_c'. This is certainly true if $\sigma_{H,N}$ (and, consequently, $\sigma_{H,F}$) remains essentially constant over the ranges of H and N covered by the different series. In this case, $\sigma_{H,N} = \sigma^0_{H,N} = 5\ M^{-1}$,[6] and $\sigma_{H,F} = \sigma^0_{H,F} = 1.0\ M^{-1}$. Consequently, $(\sigma_{H,N} - 6\sigma_{H,F}) = -1\ M^{-1}$ and, within the experimental error $S/I = K_c'$ and $1/S = \epsilon_1$. In order to simplify the following discussion we will henceforth use this identification of S/I and $1/S$ while bearing in mind the above uncertainties. The primed superscript will also be dropped from K_c' since the distinction is unimportant in the following discussion.

It can be seen from Tables III and IV that although ϵ_1 remains essentially constant on replacing $HClO_4$ by $NaClO_4$ at constant a_w, K_c varies considerably. The direction of this change is in agreement with the results of Coll, Nauman, and West. Clearly some factor (or factors) other than water activity is also of importance in determining K_c. Before discussing various possible reasons for the changes in K_c, it is instructive to consider first the changes in K_c predicted by a simple method of calculating activity coefficients in mixed electrolyte solutions, and to use departures from these predictions as a basis for further discussion.

The basis for this method is Zdanovskii's rule[9] which states that when isopiestic solutions are mixed, the resulting solution is isopiestic with the starting solutions. Consequently, for isopiestic aqueous solutions containing two solutes a plot of the molality of one solute *vs.* the molality of the other solute is an exact straight line. This rule is not exact but is a good approximation for electrolytes,[8-10] for nonelectrolytes,[11] and for mixtures of electrolytes and nonelectrolytes.[12-14] Vdovenko and Ryazanov investigated the consequences if solutions containing more than one electrolyte obeyed Zdanovskii's rule exactly.[3] One of the consequences is that the McKay–Perring integral[15] is equal to zero and, consequently, the mean molal activity coefficient of electrolyte i in mutually isopiestic solutions is given by

$$\gamma_i = \frac{\nu_i m_i^0 \gamma_i^0}{m_T} \qquad (13)$$

in which ν_i is the number of moles of ions formed in solution by one mole of electrolyte i, m_i^0 is the molal concentration of an isopiestic solution containing only the electrolyte i, γ_i^0 is the mean molal activity coefficient of electrolyte i in an isopiestic solution containing only electrolyte i, and $m_T = \Sigma_j \nu_j m_j$ in which m refers to molal concentrations and the sum is over all electrolytes in the solution (m_T is the total molal concentration of solute species).

In an attempt to rationalize similar behavior of mutually isopiestic solutions of nonelectrolytes, Stokes and Robinson[11] proposed a simple model and derived an expression analogous to eq 13 for the activity coefficients of nonelectrolytes (for nonelectrolytes $\nu = 1$). This model may be based on the assumptions that the only interactions are solvent–solvent and solvent–solute, that all interactions are of such a nature that they may be expressed in the form of equilibrium constants, and that the activity of any species is equal to its mole fraction in solution.[16] An analogous treatment for electrolytes using the same assumptions leads also to eq 3. This relationship enables one to calculate the molal activity coefficients in mixed electrolyte solutions using data pertaining to the aqueous solutions of the individual electrolytes alone. In a mixture of two electrolytes, 1 and 2, it is necessary to know only m_1^0 and m_2^0 at the same value of a_w as the mixed solution.

In order to test this method with our experimental data it is convenient to rewrite reaction 1 to include counterions so that mean ionic activity coefficients may be used.

$$Fe(ClO_4)_3 + HCl = FeCl(ClO_4)_2 + HClO_4 \qquad (14)$$

Then K, the thermodynamic equilibrium constant, is equal to

$$K = K_m \frac{\gamma_2^3 \gamma_H^2}{\gamma_1^2 \gamma_3^4} \qquad (15)$$

in which K_m is the molal equilibrium quotient for reaction 14, and the γ's are the mean molal activity coefficients for HCl (1), $FeCl(ClO_4)_2$ (2), $Fe(ClO_4)_3$ (3),

(9) See ref 3 for references to Zdanovskii's work.

(10) W. H. McCoy and W. E. Wallace, *J. Amer. Chem. Soc.*, **78**, 1830 (1956).

(11) R. H. Stokes and R. A. Robinson, *J. Phys. Chem.*, **70**, 2126 (1966).

(12) V. E. Bower and R. A. Robinson, *ibid.*, **67**, 1524 (1963).

(13) V. W. Bower and R. A. Robinson, *J. Res. Nat. Bur. Stand., Sect. A*, **69**, 131 (1964).

(14) H. Uedaira and H. Uedaira, *J. Phys. Chem.*, **74**, 1931 (1970).

(15) H. A. C. McKay and J. K. Perring, *Trans. Faraday Soc.*, **49**, 163 (1953). The integral referred to is their eq 6.

(16) The derivation of Stokes and Robinson is unnecessarily restricted by their assumption that the average hydration number $\bar{h}$ is equal to $a_w/(1 - a_w)$. This assumption, which is valid only for nonassociated water, is not necessary if the assumptions listed above are made.

and $HClO_4$ (H). If the appropriate expression of eq 13 is substituted in eq 15 for each γ, the result is

$$K = K_m \frac{(3)^3(m_2^0\gamma_2^0)^3(m_H^0\gamma_H^0)^2}{(4)^4(m_1^0\gamma_1^0)^2(m_3^0\gamma_3^0)^4} m_T = K_m\beta m_T \quad (16)$$

The factor defined as β in eq 16 is constant at a specified a_w. Therefore, for mutually isopiestic solutions

$$\frac{K}{\beta} = \text{constant} = K_m m_T = K_m^0 m_T^0 \quad (17)$$

in which the superscript zero again refers to a reference solution at the same water activity. In our experiments the reference solution is a solution of perchloric acid with the same water activity as the series and with $N = F = 0$. When applied to reaction 1, the model predicts that $K_m m_T$ is a function of water activity only and, consequently, that $K_m m_T/K_m^0 m_T^0$ is equal to one for all water activities. This quantity is easily calculated for each series since $m_T = 2(m_{HClO_4} + m_{NaClO_4})$ and K_m^0 and m_T^0 may be estimated from the data in ref 5 using appropriate densities.

Table III shows that $K_m m_T/K_m^0 m_T^0$ is not constant and equal to one for the solutions studied. In fact, the observed change in K_m is opposite to that predicted and K_m/m_T is more nearly constant. This means that the small experimentally observed deviations from Zdanovskii's rule are of importance in determining the activity coefficients of trace components. This test of Vdovenko and Ryazanov's method is very severe since the reaction involves ions present in small or trace concentrations. In spite of the failure of the method when applied to this reaction the model remains very useful as an approach to mixed solutions because the model leads to Zdanovskii's rule which, although approximate, is still a major feature in the behavior of solutions containing more than one solute. Since the assumptions of the model are clearly stated, they can serve as a basis for discussion of the observed deviations from the rule.

Clearly, some other explanation for the observed changes in K_c at constant a_w must be found. The explanation must be consistent with the observed changes in ΔH and ΔS for reaction 1. A comparison of series D with series A shows that the changes in K_c at constant water activity reflect changes in both ΔH and ΔS. In perchloric acid solutions without added $NaClO_4$ both ΔH and ΔS decrease as K_c increases (with a_w varying). When $HClO_4$ is replaced by $NaClO_4$ at constant a_w, both ΔH and ΔS increase as K_c increases. This is evidence that there are at least two separate effects involved. The change in ΔH at constant a_w strongly suggests that energies of interaction are changed as the medium is changed. These changes must involve solute–solute interactions since the measurements were made at constant solvent activity.

One possibility is that the values of m_T in $HClO_4$ and in $HClO_4$–$NaClO_4$ solutions used in calculating $K_m M_T/K_m^0 m_T^0$ are wrong because of ion pairing of the major constituents. The extreme situation giving the desired direction of change would be if $NaClO_4$ were completely ion paired and $HClO_4$ were completely dissociated. If this highly unlikely situation existed, then m_T for series A would still equal 16 m while m_T for series D would equal 16.5 m. Since $K_m m_T/K_m^0 m_T^0$ would still be far from constant, this possibility is ruled out, at least as the only explanation.

Perchlorate ion pairing with Fe^{3+} and $FeCl^{2+}$ would also seem to be ruled out as an explanation on the basis that the interaction of ClO_4^- with Fe^{3+} would be expected to be stronger than the interaction of ClO_4^- with $FeCl^{2+}$. As $HClO_4$ is replaced by $NaClO_4$, the ClO_4^- concentration increases, reactants in reaction 1 would be stabilized relative to products, and K_c should decrease. This is in disagreement with the experimental observations.

The interaction of Cl^- with Na^+ and H^+ is capable of explaining the results if the H^+–Cl^- interaction is sufficiently stronger than the Na^+–Cl^- interaction. In this case, the reactants in reaction 1 are stabilized by an increasing concentration of H^+, and K_c would become smaller, in agreement with experiment. A lower limit for the ion-pair formation constant for HCl may be estimated from the experimental data by ignoring the change predicted by the Vdovenko–Ryazanov method and assuming that Na^+ and Cl^- do not form ion pairs. The resulting value of 0.2 M^{-1} is about ten times as large as the value estimated by Högfeldt in 7.7 M HCl,[17] for which the water activity is the same as in the $HClO_4$–$NaClO_4$ solutions studied.

All of the other possible solute–solute coulomb interactions are repulsive. It is difficult to see how these repulsive interactions could lead to the observed changes in K_c. As the ionic strength is increased, nonspecific coulomb interactions would tend to stabilize reactants rather than products in reaction 1.

If it is assumed that there are only two factors determining the observed changes in K_c and that one of them is due to solvation, it is of interest to evaluate the relative contributions of the two factors. Since the variables determining the second factor are unknown, this cannot be done without making some additional assumptions. If the second factor is assumed to be due to ion pairing of H^+ and Cl^-, then this ion pairing would increase with increasing $HClO_4$ concentration and, consequently, would tend to decrease K_c. Since experiments show that K_c increases with increasing $HClO_4$ concentration, solvation would have to be much more important than ion pairing. A more quantitative treatment leads to the same conclusion.

Kinetic Measurements. The data in Table II indicate that k_{-1}/a_w is much more nearly constant over large medium changes than is k_{-1}. The activation pa-

(17) E. Högfeldt, *J. Inorg. Nucl. Chem.*, 17, 302 (1961).

rameters, $\Delta H_{-1}^{\ddagger}$ and $\Delta S_{-1}^{\ddagger}$, are also essentially medium independent[18] over the wide range of perchloric acid concentrations investigated. These results imply that the reactants for dissociation of $FeCl^{2+}$ lose one water molecule in going to the activated complex and that the activated complex closely resembles these reactants, at least insofar as medium effects are concerned. Since the equilibrium constant, K_c, for reaction 1 in perchloric acid medium has an approximate inverse fourth power dependence on a_w, the rate of formation of $FeCl^{2+}$ has roughly an inverse third power dependence on a_w. It is possible to interpret this behavior as the loss of three waters in going from reactants in reaction 1 to the activated complex. However, since the equilibrium measurements show the existence of an effect due to solute–solute interactions and seem to indicate that this effect involves the reactants in reaction 1 (rather than the products), such an interpretation does not seem justified. The kinetic measurements also support this view. The formation reaction, which involves oppositely charged ions, might be expected to show a more complicated medium dependence than the dissociation reaction, which involves an ion and the solvent. The formation reaction probably involves the loss of more than one water, but it is difficult to draw any conclusions about the number lost. A mechanism involving ion-pair formation of Cl^- with $Fe(H_2O)_m^{3+}$ followed by exchange of the chloride for an inner-sphere water is more consistent with the observed water activity dependence than is a mechanism involving loss of water to give $Fe(H_2O)_{m-1}^{3+}$ followed by addition of Cl^-.[19]

In conclusion we will summarize the implications of our observations on reaction 1 in solutions of high ionic strengths.

1. In perchloric acid solutions of increasing concentration the observed increase in K_c is due to an increase in the rate of formation of $FeCl^{2+}$. Over a large range of perchloric acid concentrations, k_{-1}/a_w and the activation parameters pertaining to k_{-1}/a_w are relatively constant.

2. The effect of decreasing water activity is to drive reaction 1 to the right. This happens not only because of the replacement of an inner-sphere water on Fe^{3+} by Cl^-, but also because two ions, Fe^{3+} and Cl^-, react to form one ion, $FeCl^{2+}$, which is probably less strongly hydrated than even one of the reactants, Fe^{3+}. As water gets scarce, formation of the less strongly hydrated $FeCl^{2+}$ is favored.

3. In addition to the hydration effect there is a less important effect due to ion–ion interactions. The interactions causing this effect are not known, but many possibilities seem to be ruled out.

Acknowledgment. The work was performed under the auspices of the U. S. Atomic Energy Commission. We are also deeply indebted to Dr. Norman Sutin for permitting us to use his stopped-flow apparatus and for his many helpful comments and criticisms.

(18) Since k_{-1}/a_w is more nearly constant, it is more logical to compare the activation parameters based on k_{-1}/a_w. If this is done, $S^{\ddagger}$ is increased by about 0.2 cal mol^{-1} deg^{-1} and $\Delta H^{\ddagger}$ is decreased by 1.4 kcal mol^{-1} in 9.00 M $HClO_4$. This change in $\Delta S^{\ddagger}$ is negligible and the change in $\Delta H^{\ddagger}$ is comparable to the experimental error. At lower $HClO_4$ concentrations the changes are even smaller.

(19) N. Sutin, *Annu. Rev. Phys. Chem.*, **17**, 121 (1966).

Medium Effects of Some Denaturing Agents on Volume Changes Produced by Acid–Base Reactions[1]

by Sam Katz* and Jane E. Miller

Department of Biochemistry, West Virginia University Medical Center, Morgantown, West Virginia 26506
(Received October 23, 1970)

Publication costs assisted by U. S. Public Health Service, National Institutes of Health

The effect of agents such as guanidine hydrochloride, urea, and sodium chloride on the volume changes resulting from acid–base reactions is quite disparate. The two types of reactions investigated were (i) the protonation of carboxylate, imidazole, and amine groups coupled to organic moieties and (ii) the reaction of hydroxyl ions with the protonated forms of the above compounds. The volume changes were determined dilatometrically at 30.0 ± 0.001°. Protonation caused volume changes of about 10 ml/mol for carboxylates and −3 ml/mol for both amines and imidazole in 0.1 *M* NaCl and in 0.1 *M* guanidine hydrochloride. The neutralization of protonated amines and imidazoles caused volume increases of about 22 ml/mol in 0.1 *M* NaCl and 18–20 ml/mol in 0.1 *M* guanidine hydrochloride. The use of 8 *M* urea as solvent caused a −1 to −5 ml/mol reduction of the volume changes compared to those found in 0.1 *M* NaCl. The use of 6 *M* guanidine hydrochloride caused larger reductions of volume changes than did 8 *M* urea with the largest effects being found in neutralization processes. The volume changes due to the reaction of NaOH with HCl decreased from 18.6 to 6.6 ml/mol as the concentration of guanidine hydrochloride increased from 0.05 to 2 *M*. If NaCl was used as electrolyte, the volume changes decreased from 20.4 to 16.7 ml/mol in the same concentration range.

Introduction

The effect of denaturing agents such as guanidine hydrochloride and urea on the ΔV resulting from acid–base reactions[2] has been a subject of considerable conjecture. This study was designed to compare the volume changes produced by several representative acid–base reactions in systems which contained urea, guanidine hydrochloride, and NaCl to establish the effect of these solutes. Another objective was to establish the background requisite for the dilatometric titrations[3] of proteins in denaturing media. With this information one can assess the contribution of the protein's structure to the volume effects and thus employ this technique as a predictive tool. To help clarify the mechanism of the action of guanidine hydrochloride, an electrolyte, similar studies were performed with another uni-univalent electrolyte, NaCl, to ascertain the magnitude of the electrostatic contribution.

Experimental Section

Dilatometry. The volume changes were measured with Teflon-sheathed[4] Linderstrøm-Lang–Lanz type dilatometers;[5] these incorporated 10-μl capillaries which could be read to ±0.01 μl. The experiments were performed at 30.0 ± 0.001°. After the solutions were degassed, 5.00 ml of the organic acid or base, in the appropriate solvents, was pipetted into one arm of the reaction vessel and 5.00 ml of either HCl or NaOH, in the same solvent, was introduced into the other arm. Solutions which contained alkali and urea were prepared immediately before use to minimize cyanate formation. The concentrations of the reactants were selected to produce volume changes of 3–6 μl. Purified *n*-heptane was used as the manometric fluid.[4] Each datum recorded for an individual experiment was the mean of two to three replicate dilatometer measurements. Most of the values reported are the average of two or more experiments with the range about the mean being ≤0.04 μl. When this precision was not achieved, the experiments were repeated until a standard deviation of ±0.06 μl was obtained. The uncertainty of the data reported is ±0.1 μl or 1.5%, whichever represents the smallest error, except for three values in which the error was larger; these will be indicated in the text. An analysis of certain errors associated with dilatometry has been made previously.[4]

pH values were determined with a Radiometer pH meter, Model 26, using a Radiometer semimicro combination electrode GK 2321C standardized with Harleco buffers. The pH drift due to immersion in concentrated solutions of denaturants was ≤0.02 unit between restandardization intervals. Potentiometric titrations were performed with a recalibrated 2-ml Gilmont microburet; titrations of bases were performed

(1) This research was supported in part by U. S. Public Health Service, National Heart and Lung Institute Grant HE12955. Portions of this study were presented at the 160th National Meeting of the American Chemical Society, Chicago, Ill, Sept 1970.

(2) ΔV is defined as the volume change produced by a given reaction and is expressed in terms of milliliters per mole.

(3) W. Kauzmann, A. Bodanszky, and J. Rasper, *J. Amer. Chem. Soc.*, 84, 1777 (1962).

(4) S. Katz and T. G. Ferris, *Biochemistry*, 5, 3246 (1966).

(5) K. Linderstrøm-Lang and H. Lanz, *C. R. Trav. Lab. Carlsberg*, 21, 315 (1938).

Table I: ΔV for Protonation Reactions

Reaction	Reactants	ΔV, ml/mol: NaCl (0.1 *M*)	Guanidine hydrochloride (0.1 *M*)	Guanidine hydrochloride (3 *M*)	Guanidine hydrochloride (6 *M*)	Urea (8 *M*)
1	Sodium acetate	10.3	10.2	7.0	5.3	8.7
	β-Alanine	7.1	7.0	4.76	3.46	5.6
2	Sodium glycinate	−2.79	−2.78	−3.24	−3.9[a]	−3.6[b]
	Tris(hydroxymethyl)-aminomethane	−3.64	−3.58	−3.82	−4.34	−3.7
3	Imidazole	−1.70	−1.73	−2.46	−3.28	−2.75

[a] Uncertainty of datum is 5%. [b] Uncertainty of datum is 15%.

under N_2 atmosphere. The end points were determined by ΔpH/Δmilliliter analysis, with the agreement being $\leq 0.3\%$.

Materials. Standard HCl and CO_2-free NaOH were purchased from Harleco Co. All basic solutions were prepared with CO_2-free H_2O. The standard bases were checked by titration against potassium acid phthalate and the HCl against the standard base. All of the standard reagents agreed to within 0.3% of the stated normalities except for one NaOH solution which was found to be 0.9892 instead of 1.00_0 *N*. The organic reagents were purchased from either Sigma Chemical Co. or from Calbiochem Co., and were interchanged without any detectable differences. Urea (Mallinckrodt, AR) was purified according to our standard procedure.[4] Guanidine hydrochloride, Sigma Chemical Co., was purified by treatment with carbon, Darco G-60 (3% w/v), and Celite (1% w/v).[6,7] After filtration, the solution was adjusted to pH 2.5 and refiltered. The filtrate was adjusted to pH 6 before flash evaporation. The crystals were washed with acetone at −10° before drying *in vacuo;* the temperature at no time exceeded 40°.

Results

The selection of the model compounds and experimental conditions was facilitated by reference to a definitive review of the ΔV for acid–base reactions in aqueous media.[3] The first phase of this study deals with the effect of two denaturants, guanidine hydrochloride, an electrolyte, and urea, a nonelectrolyte, on the ΔV produced by the protonation of carboxylate, imidazole, and amine-containing compounds. Parallel studies employing 0.1 *M* NaCl provided a frame of reference. The following protonation processes were studied.

$$\underset{(0.200\ M)}{RCO^-} + \underset{(0.100\ M)}{HCl} \longrightarrow RCOOH + Cl^- \quad (1)$$

$$\underset{(0.400\ M)}{RNH_2} + \underset{(0.200\ M)}{HCl} \longrightarrow RNH_3Cl \quad (2)$$

$$\underset{(0.400\ M)}{\text{imidazole}} + \underset{(0.200\ M)}{HCl} \longrightarrow \text{imidazolium Cl} \quad (3)$$

The concentrations of the reactants are given in brackets under the reaction scheme. The experiments were designed (i) to produce a sufficiently large volume change to minimize dilatometric error, (ii) to provide an excess of the organic reactant to drive the reaction to the right, and (iii) to achieve a final pH in the region of 3.5–9.5 to avoid correction for unbound protons or hydroxyl ions.

A summary of the volume changes determined for some protonation reactions in 0.1 *M* NaCl, 8 *M* urea, and 0.1–6 *M* guanidine hydrochloride is presented in Table I.

The use of different types and concentrations of organic bases results in a considerable variation of ionic strengths of the systems after mixing. For example, the mixing of HCl with sodium acetate at the concentrations indicated in eq 1 results in an equilibrium mixture of 0.05 *M* sodium acetate, 0.05 *M* NaCl, and 0.05 *M* acetic acid; ionic strength of 0.10. The corresponding β-alanine system had an ionic strength of 0.05 while the sodium glycinate system had an ionic strength of 0.02. For both tris(hydroxymethyl)aminomethane and imidazole systems the concentration of the resultant hydrochloride forms were 0.1 *M*. Therefore, there is a substantial ionic strength contribution by the reactants to those systems which used 0.1 *M* NaCl, 0.1 *M* guanidine hydrochloride, and 8 *M* urea as solvents.

All of the protonation processes studied were characterized by similar values for ΔV in 0.1 *M* NaCl and 0.1 *M* guanidine hydrochloride. In addition, these data substantiate the finding that the values for the ΔV of protonation of carboxylate groups are strongly dependent on the nature of the associated organic moiety;[3,8] compare sodium acetate with β-alanine (Table I). The ΔV values for the protonation of amines show a smaller dependency on structure; *e.g.*,

(6) Y. V. Wu and R. J. Dimler, *Arch. Biochem. Biophys.*, **108**, 490 (1964).

(7) Y. Nozaki and C. Tanford, *J. Amer. Chem. Soc.*, **89**, 736 (1967).

(8) S. D. Hamann and S. C. Lim, *Aust. J. Chem.*, **7**, 329 (1954).

Table II: ΔV for Neutralization Processes

Reaction	Reactant	ΔV, ml/mol: NaCl (0.1 *M*)	Guanidine hydrochloride (0.1 *M*)	Guanidine hydrochloride (3.0 *M*)	Guanidine hydrochloride (6.0 *M*)	Urea (8.0 *M*)
4	Glycine	21.6	18.3	7.7	5.9	18.0
	Tris(hydroxymethyl)aminomethane hydrochloride	23.2	19.9	9.0	6.9	19.8
5	Imidazolium hydrochloride	21.6	18.3	7.6	6.2	19.3[a]

[a] Uncertainty of datum is 1.7%.

the ΔV for sodium glycinate and tris(hydroxymethyl)-aminomethane were -2.79 and -3.64 ml/mol in 0.1 *M* NaCl, respectively. The ΔV for the protonation of imidazole was similar to that of the amines giving a value of -1.70 ml/mol in 0.1 *M* NaCl. The insertion of a methyl group in imidazole, 2-methylimidazole, causes a diminution of the volume change; a value of -0.6 ml/mol was determined in 0.1 *M* NaCl.

Increased guanidine hydrochloride caused the ΔV for all the protonation processes to become more negative. Compounds containing carboxylate groups exhibited the same relative decrease in ΔV as a function of guanidine hydrochloride concentration; *i.e.*, the values for ΔV in 6 *M* guanidine hydrochloride were about 50% lower than in 0.1 *M* NaCl. However, the presence of 8 *M* urea caused only a 20% reduction in ΔV values for the same systems. With respect to the protonation of amines, the decrease of ΔV with an increase of guanidine hydrochloride concentration differed for the compounds studied; in 6 *M* guanidine hydrochloride there was a 20 and 40% decrease for tris(hydroxymethyl)aminomethane and sodium glycinate, respectively. The ΔV for these compounds in 8 *M* urea were approximately the same, being about -3.6 ml/mol. The precision for determining ΔV of sodium glycinate in 6 *M* guanidine hydrochloride and in 8 *M* urea was poor, the error being 5 and 15%, respectively. We have no explanation for this. The values for ΔV of protonation of imidazole exhibited a larger dependency on guanidine hydrochloride than did the amines, *i.e.*, in 6 *M* guanidine hydrochloride ΔV was 90% more negative than the corresponding value in 0.1 *M* NaCl. In 8 *M* urea the value for ΔV was 65% more negative than in 0.1 *M* NaCl.

In agreement with previous investigations,[3,8] the volume changes for the reaction of hydroxyl ions with amines and imidazole compounds differed substantially from those produced by the protonation processes; the values were large, positive, and relatively uninfluenced by the nature of the substituents incorporated in the molecule. The systems studied are

$$\underset{\substack{(0.180\ M\ \text{acid form}\\ 0.020\ M\ \text{basic form})}}{RNH_3^+} + \underset{(0.05\ M)}{OH^-} \longrightarrow RNH_2 + H_2O \quad (4)$$

$$\underset{\substack{(0.180\ M\ \text{acid form}\\ 0.020\ M\ \text{basic form})}}{\text{imidazolium}^+} + \underset{(0.05\ M)}{OH^-} \longrightarrow \text{imidazole} + H_2O \quad (5)$$

About 10% of the nitrogenous reactants were initially in the basic state for buffering purposes. The values for ΔV for these neutralization processes exhibited a strong dependence on guanidine hydrochloride concentration. The substitution of 0.1 *M* guanidine hydrochloride for 0.1 *M* NaCl caused a 15% decrease in ΔV (see Table II). In 6 *M* guanidine hydrochloride the values for ΔV were about 30% of that found in 0.1 *M* NaCl. The use of 8 *M* urea as solvent caused only a 15–20% reduction in this parameter. Interestingly, the values for imidazolium hydrochloride were similar to glycine in both NaCl and guanidine hydrochloride, but ΔV was about 1 ml/mol more positive in 8 *M* urea.

To elucidate the effect of guanidine hydrochloride on these volume changes, the effect of varying concentrations of guanidine hydrochloride and NaCl, both electrolytes, on the ΔV for the following reactions was investigated. The sum of eq 6 and 7 yields an expression similar to eq 8 making necessary allowances for concentration differences. The relationship of ΔV for the above reactions with the concentration of guanidine hydrochloride or NaCl is summarized in Table III. The molarity stated in column 1 is the concentration of the supporting electrolyte and does not include contributions from the reactants.

$$\underset{(0.06\ M)}{\text{Tris } NH_3Cl} + \underset{(0.05\ M)}{NaOH} \longrightarrow \text{Tris } NH_2 + NaCl + H_2O \quad (6)$$

$$\underset{(0.06\ M)}{\text{Tris } NH_2} + \underset{(0.05\ M)}{HCl} \longrightarrow \text{Tris } NH_3Cl \quad (7)$$

$$\underset{(0.10\ M)}{NaOH} + \underset{(0.10\ M)}{HCl} \longrightarrow NaCl + H_2O \quad (8)$$

The ΔV for neutralization of tris(hydroxymethyl)-aminomethane hydrochloride by NaOH, eq 6, decreased from 21.8 to 9.8 ml/mol as the guanidine hydrochloride

Table III: ΔV for Neutralization Reactions as a Function of Electrolyte Type and Concentration

	ΔV, ml/mol					
	Guanidine hydrochloride				NaCl	
Molarity	Eq 6	Eq 7	Eq 6 + Eq 7	Eq 8	Eq 8 (calcd)	Eq 8 (exptl)
0.05	21.8	−3.5	18.3	18.6	20.3	20.4
0.10	20.1	−3.4	16.7	16.9	20.1	20.2
0.50	14.6	−3.4	11.2	11.6	19.3	19.4
1.00	12.0	−3.4	8.6	9.0	18.8	18.4
2.00	9.8	−3.5	6.3	6.6	18.3	16.7

concentration increased from 0.05 to 2 M (column 2, Table III). This parameter exhibited a negative linear logarithmic dependency on guanidine hydrochloride concentration. The concentration of tris(hydroxymethyl)aminomethane hydrochloride had little effect on ΔV for this reaction; *i.e.*, changing the acid concentration from 0.20 to 0.06 M caused ΔV to change from 19.9 to 20.1 ml/mol in 0.1 M guanidine hydrochloride (compare Tables II and III). The ΔV for protonation of tris(hydroxymethyl)aminomethane, eq 7, exhibited no demonstrable dependency on guanidine hydrochloride concentration in the region of 0.05–2 M with ΔV being -3.4 ± 0.1 ml/mol (column 3, Table III). The ΔV for this process exhibited a relatively small dependence on the initial concentration of reactants, *e.g.*, 0.4 M tris(hydroxymethyl)aminomethane and 0.2 M HCl gave a ΔV of -3.5_8 in 0.1 M guanidine hydrochloride; this differed by 0.1_4 ml/mol from the value of -3.4_4 ml/mol for reaction 7. However, when the guanidine hydrochloride concentration was ≥ 2 M the values for ΔV tended to become more negative (see Table I).

The value for the ΔV of water formation, $H^+ + OH^- \rightarrow H_2O$, can be calculated from the sum of eq 6 and 7 (column 4, Table III). The dependency of these values on guanidine hydrochloride concentration reflects the concentration dependency of the neutralization step in this process, eq 6. The graphical analysis of these data (Figure 1) reveals the negative linear logarithmic dependency of this parameter on guanidine hydrochloride concentration. These results were verified by determining the ΔV of water formation, by the reaction of HCl with NaOH, eq 8 (see column 5, Table III). The resultant data exhibit the same negative linear logarithmic dependence on guanidine hydrochloride concentration noted previously (Figure 1). A comparison of the two sets of values for water formation (columns 4 and 5, Table III) reveals a close agreement with the values for the direct process, eq 8, being about 0.3 ± 0.1 ml/mol larger than that obtained by the summation procedure. This difference reflects the variation introduced by salt type, concentration effects, and systematic error.

To resolve the effect of salt type and ionic strength on

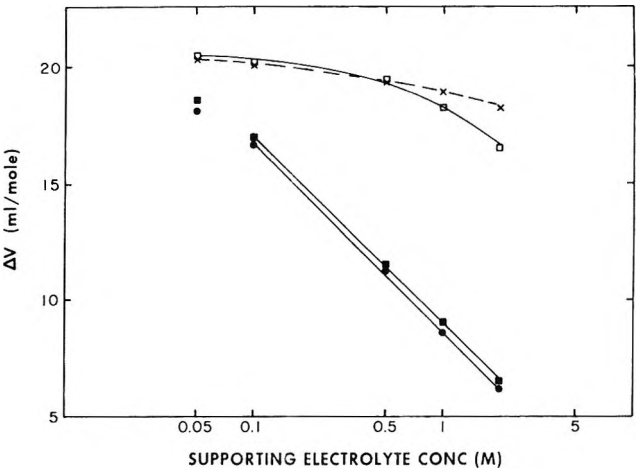

Figure 1. The volume changes resulting from the formation of water as a function of salt type and reaction type: □, NaOH + HCl → H_2O + NaCl, experimental; ×, same process, calculated values; ■, NaOH + HCl → H_2O + NaCl, in guanidine hydrochloride; ●, H_2O formation, calculated as the sum of eq 6 and 7 in guanidine hydrochloride (see Table III).

these volume changes, the study of the reaction of HCl with NaOH, eq 8, was repeated using NaCl as electrolyte. The resultant ΔV values were substantially different in NaCl than they were in guanidine hydrochloride (see Table III and Figure 1). The depressant effect of NaCl on ΔV was less than that of the corresponding guanidine hydrochloride systems; *e.g.*, in 0.05 M NaCl, ΔV was 20.4 compared to 18.6 ml/mol, in 0.05 M guanidine hydrochloride, while in 2 M NaCl, ΔV was 16.7 compared to 6.6 ml/mol in 2 M guanidine hydrochloride. Obviously, factors other than electrostatic effects are responsible for these differences.

To establish whether guanidine hydrochloride contributed any interfering agents, tris(hydroxymethyl)-aminomethane in 0.1 M NaCl and in 6 M guanidine hydrochloride was titrated with standard HCl; values of 1.00_3 and 1.00_6 compared to the calculated value of 1.00_0 M were obtained. The interfering contaminants in guanidine hydrochloride are apparently insignificant.

Discussion

Prior to discussing the effect of denaturants on the ΔV of acid–base reactions a comparison of these results with previous investigations is in order. Bodanszky and Kauzmann[9] derived the relationship

$$\Delta V = 21.28 - 2.30(M)^{1/2} + 0.40\,M \qquad (9)$$

for this reaction

$$\text{HCl}\ (M) + \text{NaOH}\ (M) \longrightarrow \text{NaCl}\ (M/2) + H_2O \qquad (10)$$

where M is the molarity. The agreement between the experimental and calculated value, correcting for the

(9) A. Bodanszky and W. Kauzmann, *J. Phys. Chem.*, **66**, 177 (1962).

NaCl produced by the reaction, is within 0.1 ml/mol at NaCl concentrations ≤ 0.5 M (Table III, columns 6 and 7). At 1 and 2 M NaCl the calculated values were 0.6 and 1.6 ml/mol higher than the experimental values. Lack of agreement at higher concentrations is not unexpected since eq 9 was derived for lower concentrations.

It is of interest to compare the values for the volume changes obtained here with the results of others. Kauzmann, *et al.*,[3] stated that the ΔV for the reaction of HCl with sodium acetate was dependent on concentration and ranged from 11.47 ml/mol at infinite dilution to 9.60 ml at 1 M concentration. The result obtained here of 10.3 ml/mol in 0.1 M NaCl (Table I) agrees with the value of 10.3 reported by Weber.[10] One can infer from Weber's report that the experimental conditions employed by both groups did not differ greatly. The datum for the protonation of imidazole of -1.70 ml/mol in 0.1 M NaCl (Table I) is in agreement with Weber's value of -1.8 ml/mol.[10] The results for the protonation of amines, glycine, and tris(hydroxymethyl)aminomethane fall within the region of -2.2 to -5.5 determined for a group of amines studied by Weber[10] and by Verrall and Conway.[11] The ΔV values for the neutralization of glycine and imidazolium hydrochloride in 0.1 M NaCl were found to be identical, 21.6 ml/mol; Weber[10] reported values of 23.6 and 23.9 ml/mol, respectively. This discrepancy reflects concentration differences and/or a systematic error. Values for the protonation of tris(hydroxymethyl)aminomethane are not available.

The introduction of a methyl group in the imidazole ring causes a relatively large decrease in ΔV for the protonation process; *e.g.*, the ΔV for the protonation of 2-methylimidazole in 0.1 M NaCl or guanidine hydrochloride was -0.5 ml/mol as compared to -1.7 ml/mol for imidazole. In 6 M guanidine hydrochloride, a ΔV of -2.5 ml/mol was obtained for 2-methylimidazole as compared to -3.3 ml/mol for the parent compound.

The effect of the solutes studied depends on the type of acid–base reaction and the nature and concentration of the solute. In protonation processes the action of NaCl or guanidine hydrochloride at 0.1 M was virtually identical. Increasing guanidine hydrochloride concentration to 6 M, caused a decrease of ΔV which ranged from -0.7 for amines to -5 ml/mol for carboxylate groups. The effect of guanidine hydrochloride on neutralization processes was substantially larger, being about -15 ml/mol for both ammonium and imidazolium residues in 6 M guanidine hydrochloride. The studies of the reaction of HCl with NaOH in both guanidine hydrochloride or NaCl (Table III) reveal that the guanidine hydrochloride effect must be due to factors other than electrostatic effects (Figure 1).

Urea (8 M) tends to depress the values for ΔV for all systems but to a lesser degree than 6 M guanidine hydrochloride. In protonation processes this ranged from 0 to -1.5 ml/mol; there was no apparent correlation with the action of guanidine hydrochloride. In neutralization reactions the decrease of ΔV due to 8 M urea ranged from -2 to -3.5 ml/mol and showed no relationship with the action of guanidine hydrochloride. Thus the mechanisms of action of urea and guanidine hydrochloride respective to acid–base reactions are dissimilar and reflect structural and electrostatic differences.

Concentrated solutions of urea or guanidine hydrochloride can conceivably alter the stoichiometry of the acid–base reaction by either (i) changing the pK values of the ionizable groups or (ii) by the introduction of competitive impurities. The literature indicates relatively minor shifts of pK values in 8 M urea or 6 M guanidine hydrochloride.[7,12] The pH of systems containing equal concentrations of acids and salts of the acids, used in this study, in 6 M guanidine hydrochloride exhibited a pH decrease of about 0.2 unit compared to that in 0.1 M NaCl. In urea, there was a small increase of pH with the maximum effect found for acetic acid, which increased from 4.63 in 0.1 M NaCl to 5.40 in 8 M urea.[13]

The action of guanidine hydrochloride and urea on the volume changes produced by acid–base reactions in aqueous system is explicable by several models. The Drude–Nernst hypothesis[3,14] considers the electrostatic polarization of the solvent produced by a spherical particle of radium, r, with an electrical charge, eZ, smeared uniformly over its surface, submerged in a medium of a given dielectric constant, D. The expression for the consequent electrostriction is

$$\Delta V = -\beta(V\mathrm{d}D/\mathrm{d}V)e^2Z^2/2rD^2 \qquad (11)$$

where β and V are the compressibility and volume of the medium. The volume change varies directly with the square of the charge, the derivative of dielectric constant with respect to volume, the compressibility and the volume of the medium, and inversely with the radius and the square of the dielectric constant of the medium. The introduction of urea or guanidine hydrochloride to an aqueous medium would influence all of these factors to some extent, but the increase of dielectric constant would dominate. Since this is a squared term, the resultant volume decrease would be in accord with our data. This does not explain the disparate action of 8 M urea and 6 M guanidine hydrochloride in certain systems and similar effects in others. In view of the qualitative nature of the

(10) H. H. Weber, *Biochem. Z.*, **218**, 1 (1930).

(11) R. E. Verrall and B. E. Conway, *J. Phys. Chem.*, **70**, 3961 (1966).

(12) E. Mihalyi, *Biochemistry*, **9**, 804 (1970).

(13) R. G. Bates in "Solute-Solvent Interactions," J. F. Coetzee and C. D. Ritchie, Ed., Marcel Dekker, New York, N. Y., 1969, p 45.

(14) P. Drude and W. Nernst, *Z. Phys. Chem.*, **15**, 80 (1894).

Drude–Nernst relationship this approach will not be pursued.[15]

An explanation for the reduction of ΔV for neutralization in guanidine hydrochloride was suggested by a referee who proposed that since guanidine hydrochloride is a weak acid, pK 13.74 in 6 M guanidine hydrochloride,[7] hydroxyl ion would react with it to form guanidine. This would lower the hydroxyl ion concentration and would in turn produce guanidine, an organic base which is a competitive proton acceptor. The equilibrium concentrations of hydroxyl ion, guanidine, and guanidine hydrochloride can be calculated from the appropriate equilibrium and conservation equations. For these calculations the following assumptions were made: the pK of water is 14, the constituents' activity coefficients were about unity, and that these parameters were not substantially altered by the different media. The following values were derived for systems with an initial hydroxyl ion concentration of 0.05 M. If we assumed a pK of 13 for guanidine hydrochloride, the percentage of hydroxyl ion would be 53, 3, and 1.6%, respectively, for systems with initial guanidine hydrochloride concentration of 0.1, 2.0, and 6.0 M, respectively. For a pK of 14 the hydroxyl ion concentrations would be 91, 34, and 16%. Inspection of the data in Tables II and III reveals a reasonable correspondence between the reduction of the ΔV values and the reduction of hydroxide ion concentration in guanidine hydrochloride as calculated for a pK of 14. Another contributing factor would be the reaction of protons with guanidine. These volume effects should be relatively minor since the volume changes associated with the protonation of nitrogenous bases are small (see Table I).

While either 8 M urea or 6 M guanidine hydrochloride can be used for protonation studies, 8 M urea should be the medium of choice for studies employing hydroxyl ions. Although urea and guanidine hydrochloride act similarly with respect to protein denaturation, this concordance of action does not hold for acid–base reactions.

Acknowledgment. The authors wish to express their appreciation to Dr. John H. Strohl, Chemistry Department, for advice relative to certain analytical problems and to a referee for suggesting the basis for the volume effects arising from the reaction of hydroxyl ion with guanidine hydrochloride.

(15) B. E. Conway, *Ann. Rev. Phys. Chem.*, 17, 481 (1966).

Heats of Mixing. II. Temperature Dependence of Aqueous Electrolytes with a Common Ion[1]

by Henry L. Anderson,* Ronald D. Wilson, and Danne E. Smith

Department of Chemistry, University of North Carolina at Greensboro, Greensboro, North Carolina 27412
(Received September 28, 1970)

Publication costs assisted by the Office of Saline Water, U. S. Department of the Interior

The heats of mixing of KCl–KF–H_2O, KCl–KBr–H_2O, KCl–$KC_2H_3O_2$–H_2O, KF–$KC_2H_3O_2$–H_2O, LiCl–CsCl–H_2O, NaCl–CsCl–H_2O, KCl–CsCl–H_2O, and HCl–KCl–H_2O at constant total ionic strength have been measured in the 40–80° temperature range. The cesium chloride mixtures show a large temperature dependence, whereas all of the other mixtures have a small or no temperature dependence. The results have been interpreted in terms of the solute–water structural properties.

Introduction

In a previous communication[2] the temperature dependence of the heats of mixing of some cations in the presence of the common chloride ion were reported. The mixtures studied involved the H^+, Li^+, Na^+, K^+, and $(CH_3)_4N^+$ ions. Except for the mixtures involving the sodium ion, the heats of mixing were remarkably temperature independent.

The lack of a strong or complicated temperature dependence in the heats of mixing allows for a simple and accurate estimation of the other excess thermody-

(1) This study was aided by a grant from the Office of Saline Water, U. S. Department of the Interior.

(2) H. L. Anderson and L. A. Petree, *J. Phys. Chem.*, 74, 1455 (1970).

Table I: Aqueous Heats of Mixing Parameters (I = 1.0)

Mixture	25° RTh_0	40° RTh_0	40° RTh_1	60° RTh_0	60° RTh_1	80° RTh_0
KF–KCl	−22.6[a]	−23.0 ± 0.3		−19.9 ± 0.5	+2.0 ± 0.7	−16.4 ± 0.8
KF–$KC_2H_3O_2$	9.5[a]	9.4 ± 0.4		10.1 ± 0.6		10 ± 1
KCl–KBr	3.2[a]	2.9 ± 0.2		3.2 ± 0.3		3.9 ± 0.3
KCl–$KC_2H_3O_2$	−34.3[a]	−38.1 ± 0.4	+2.8 ± 0.6	−37.5 ± 0.4		−31 ± 2
HCl–KCl	−15.0[b]			−13.3 ± 0.8		
LiCl–CsCl	−194.6[b]			−176.4 ± 2.7	−5.9 ± 3.8	−170 ± 5
NaCl–CsCl	−34.8[b]			−46.7 ± 0.7		−51.1 ± 0.9
KCl–CsCl	6.4[b]			1.38 ± 0.09		1.5 ± 0.8

[a] See ref 11. [b] See ref 5.

namic properties of these mixtures *via* an expression of the kind

$$\Delta_m G^E(T_2) = \Delta_m G^E(T_1) + \Delta_m C_p]_{T_1}^{T_2}\Delta T - \Delta_m S^E(T_1)\Delta T - T_2\Delta_m C_p]_{T_1}^{T_2} \ln (T_2/T_1) \quad (1)$$

where

$$\Delta_m C_p]_{T_1}^{T_2} = \frac{\Delta_m H(T_2) - \Delta_m H(T_1)}{\Delta T}$$

There are very few excess free energy of mixing data available in the literature that can be used to check the high-temperature values of $\Delta_m G^E$ as calculated from eq 1. The only data of sufficient accuracy with which to make comparison are those of Harned.[3,4] A previous comparison for the system, HCl–NaCl–H_2O, in the 25–80° temperature range[2] was not good in that Harned's data indicate that $\Delta_m G^E$ goes through a minimum at about 40°, whereas the values calculated from eq 1 indicate that $\Delta_m G^E$ decreases continuously from 25 to 80°. In the present research the mixture HCl–KCl–H_2O was investigated and compared with Harned's[4] work.

The temperature dependence of heats of mixing has been informative in studying specific ion interactions.[2] Anderson and Petree proposed that common ion heats of mixing were primarily the result of specific ion interactions at the interface of the structure-making, structure-breaking regions of the ion. For the ions studied (except for the sodium ion), they suggested that this region was thermally stable in the 25–80° temperature range. The temperature dependence of the heats of mixing of the sodium ion mixtures was interpreted as a reflection of the thermal instability of the water in that region. The present research was designed to expand the types of ions mixed in order to test the above conclusions.

Experimental Section

Calorimeters. The HCl–KCl–H_2O mixture and all mixtures involving CsCl were performed in the 250-ml dewar calorimeter described previously.[2] The anion mixings were performed in a new 700-ml dewar calorimeter. The construction was similar to that of the previous calorimeter except for the increased size. The increased size of the pipet (~40 ml) presented some difficulties in that heating the solution in the vessel from room temperature to the desired operating temperatures of 60 and 80° resulted in an extremely long equilibration time for the solution in the pipet. To compensate for this a 100-ohm heater was inserted inside the glass pipet plunger tube and the pipet was heated simultaneously with the vessel during the preliminary heating period.

The new calorimeter was checked by measuring the heat of mixing of NaCl–KCl–H_2O at 25° and in terms of the parameters of eq 2 RTh_0 was found to be −38.2 cal kg^{-1} m^{-1} as compared with values of −38.3 and −38.5 reported in the literature.[5,6]

Materials. Concentrated stock solutions of Mallinckrodt potassium chloride, potassium bromide, potassium fluoride, potassium acetate, hydrochloric acid, sodium chloride, Kawecki cesium chloride, and Research Inorganic lithium chloride were prepared and stored in polyethylene bottles. The experimental procedure has been described previously.[7]

Results and Treatment of Data. The experimental heats of mixing were fitted by the method of least squares to the equation[8]

$$\Delta_m H(\text{cal/kg of solvent}) = RTI^2y(1 - y)[h_0 + (1 + 2y)h_1] \quad (2)$$

where R is the universal gas constant, T is the temperature, I is the total ionic strength, y is the mole fraction of the salt having the largest formula weight, h_0 is the magnitude of the interaction, and h_1 is the first-order skew term from a quadratic relation in mole fraction.

The parameters of eq 1 are listed in Table I. A statistical "F" test (95% confidence level) was per-

(3) H. S. Harned, *J. Phys. Chem.*, **63**, 1299 (1959).
(4) H. S. Harned, *ibid.*, **64**, 112 (1960).
(5) Y. C. Wu, M. B. Smith, and T. F. Young, *ibid.*, **69**, 1868 (1965).
(6) J. H. Stern and C. W. Anderson, *ibid.*, **69**, 2974 (1965).
(7) R. H. Wood and R. W. Smith, *ibid.*, **69**, 2974 (1965).
(8) H. L. Friedman, *J. Chem. Phys.*, **32**, 1134 (1960).

formed on each mixture to test for the significance of h_1. In those cases where the inclusion of h_1 was not justified, it was set equal to zero and the data were refitted using only h_0.

For each mixture, from 10 to 12 experimental determinations were made between 0 to 0.2 and 0.8 to 1.0 mole fraction. It has been shown[5,7] that this is sufficient to determine the mixing parameters.

Discussion

Thermodynamics. Of the mixtures studied in this work, the only excess free energy of mixing data available in the literature are those of the HCl–KCl–H_2O mixture. From emf measurements Harned[4] determined the excess free energy of mixing for this system at 5 degree intervals between 0 and 40° and parts of those results are recorded in Table II. For comparison the heats of mixing along with the excess free energies of mixing as calculated from eq 1 are recorded in Table II. The agreement between the experimental and calculated excess free energies of mixing is quite good except at 40°.[9] However, the heat capacity data obtained from the present work should allow for a more accurate estimation of the excess free energies of mixing at higher temperatures provided the reference temperature (25°) experimental value is reliable.[2] A simple consistency test of the two methods of obtaining $\Delta_m G^E(40°)$ can be made using eq 1. The first test is made by assuming that Harned's $\Delta_m H^E(40°)$ and $\Delta_m G^E(25°)$ values and the experimental $\Delta_m H^E(25°)$ determinations are correct. This calculation gives a value of −19.2 cal/kg for $\Delta_m H(40°)$, as compared with the experimental value of −3.60 cal/kg. The probability of a 430% error in the direct heat of mixing measurement is extremely remote. The second test is made by assuming Harned's value of $\Delta_m G^E(25°)$, along with the experimental values of $\Delta_m H(40°)$ and $\Delta_m H(25°)$ are correct. This result gives a value of $\Delta_m G^E(40°)$ of 3.91 cal/kg as compared to Harned's value of 4.30 cal/kg. The difference between these two values is approximately 10%, well within the plausible experimental error of the excess free energy of mixing data. Thus, it appears that the excess free energy of mixing can be obtained more reliably *via* eq 1. In fact, if Harned's lower temperature data (0–35°) are extrapolated to 40° a value of 4.05 cal/kg for $\Delta_m G^E(40°)$ is obtained. This agrees within the experimental error of the heat of mixing value calculated from eq 1.

Table II: Excess Thermodynamic Properties of HCl–KCl–H_2O (I = 1.0, y = 0.5)

Temp, °C	$\Delta_m G^E$ (eq 1)	$\Delta_m G^E$ (exptl)[a]	$\Delta_m H$	$\Delta_m S^E$
25	3.55[a]	3.55	−3.75[b]	−0.0245
30	3.56	3.68	−3.70[c]	+0.0239[d]
35	3.79	3.81	−3.63[c]	−0.0241[d]
40	3.91	4.30	−3.60	−0.0240[d]

[a] See ref 4. [b] See ref 5. [c] Interpolated from Table I. [d] Based on $\Delta_m G^E$ (eq 1) values.

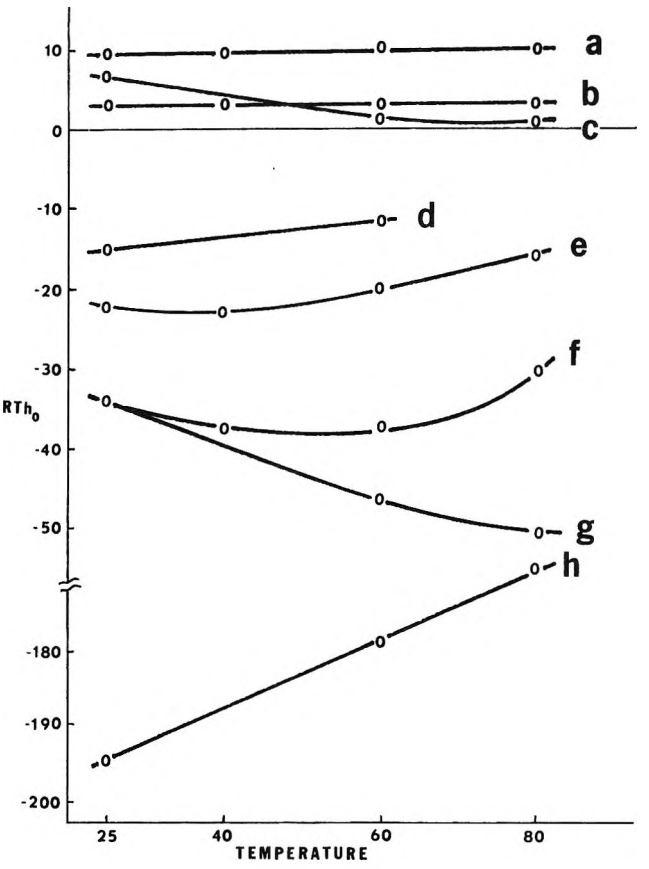

Figure 1. a, KF–$KC_2H_3O_2$; b, KCl–KBr; c, KCl–CsCl; d, HCl–KCl; e, KCl–KF; f, KCl–$KC_2H_3O_2$; g, NaCl–CsCl; h, LiCl–CsCl.

Solute–Solvent Structure. The temperature dependence of the heats of mixing can best be summarized *via* Figure 1. For two of the anion mixing, KF–$KC_2H_3O_2$–H_2O and KCl–KBr–H_2O the heat of mixing is temperature independent. For the other two anion mixings, KCl–KF–H_2O and KCl–$KC_2H_3O_2$–H_2O, there is a small temperature dependence with the heat of mixing going through an apparent maximum in the 40–50° temperature range. For all four of these systems the temperature dependence is small enough to draw the conclusion that the types of interactions observed for these anions is no different than those recorded for the bulk of the cation mixings reported previously.[2] That is, the water in the region of the structure-making, structure-breaking interface is either thermally stable or very nearly thermally stable for

(9) (a) See ref 2; (b) this is implied in the reporting of these data in H. S. Harned and R. A. Robinson, "The International Encyclopedia of Chemistry and Chemical Physics," Vol. 2, R. A. Robinson, Ed., Pergamon Press, New York, N. Y., 1968, Topic 15, p 63.

these anions. There has been considerable discussion in the literature[10] concerning the differences in the solute–H_2O interactions of cations and anions. In terms of the solute–H_2O interactions that determine heats of mixing one can say that the magnitude[11] and the temperature dependence of anion heats of mixing behave no differently than cation interactions. If this interpretation[2] as to the origin of the specific ion–H_2O interactions is correct this means that the primary hydration sphere of both cations and anions is thermally stable in the 25–80° temperature range.

The evidence for the existence of a maximum in the heat of mixing for the KF–KCl–H_2O and KCl–$KC_2H_3O_2$–H_2O systems is marginal enough that at this time no rationalization of this will be attempted.

The small temperature dependence of the HCl–KCl–H_2O mixture suggests that the hydrogen ion was not responsible for the large temperature dependence reported for HCl–NaCl–H_2O.[2] Thus, it is concluded that the hydrogen and potassium ions behave normally in the temperature range studied.

In the three mixtures involving the cesium ion a rather large temperature dependence in the heat of mixing was observed. In fact the NaCl–CsCl–H_2O mixture is the first example where the heat of mixing clearly increases in magnitude as the temperature increases. This result can be correlated with the purely empirical mixing rule governing the sign of the heat of mixing.[5,11] The sign rule states that when mixing ions of like structural classification the heat of mixing is endothermic and upon mixing ions of unlike structural classification the heat of mixing is exothermic. For the mixtures showing a strong temperature dependence in the heat of mixing the sign and structural classification is recorded in Table III. From purely empirical reasoning

Table III

Mixture	Cation structural class[a]	Sign of $\Delta_m H$	Change in $\Delta_m H$ as T increases
HCl–NaCl	SM–SM	+	Less positive
LiCl–NaCl	SM–SM	+	Less positive
KCl–NaCl	SB–SM	−	Less negative
LiCl–CsCl	SM–SB	−	Less negative
NaCl–CsCl	SM–SB	−	More negative
KCl–CsCl	SB–SB	+	Less positive

[a] SM = structure-maker, SB = structure-breaker.

if the Na^+ ion is considered to become more of a structure-breaker (less structure-making) with increasing temperature in the region sensitive to heats of mixing and the structural classification of the H^+, Li^+, and K^+ are assumed to be temperature independent then the direction of the change in the heat of mixing as recorded in the last column of Table III can be rationalized. For example, if the H^+ ion is a structure-maker and the Na^+ ion becomes more structure-breaking as temperature is increased the heat of mixing should change to a more negative, or less positive, value.

This conclusion does not follow exactly since the heat of mixing parameter, $h_{R_hR_i}{}^{X_j}$, involves terms of the type[8,12]

$$h_{R_hR_i}{}^{X_j} = -T\frac{\partial g_{R_hR_i}{}^{X_j}}{\partial T} - T\frac{\partial}{\partial T}[B^{hi} - B^{hh} - B^{ii}] \quad (3)$$

where the B's are cluster integrals involving the cations h and i. According to the present explanation, the $B^{H^+-H^+}$ term would be temperature independent and the $B^{H^+-Na^+}$ and $B^{Na^+-Na^+}$ would be temperature dependent to approximately the same degree or at least so the difference in these terms did not change sign. In fact, if this is true for every mixture involving only one ion that is sensitive to temperature one would predict the heat of mixing to decrease as is the case for every known mixture.

There is evidence that the Cs^+ ion is incompletely hydrated at 25°.[13] As temperature is increased and bulk water structure is broken down it should be easier for the Cs^+ ion to make water-structure about it. If in fact this is correct, the Na^+–Cs^+ mixture represents the first example where both cations are changing in structural properties as temperature is increased. In general, the B terms of eq 3 are of the same magnitude and $h_{R_hR_i}{}^{X_j}$, is quite sensitive to these values. If all three of these terms are temperature dependent as should be the case for the Na^+–Cs^+ mixture it is not surprising to find the heat of mixing actually increasing with temperature.

It is worth noting at this point that the authors are not proposing that these interpretations should imply that the heats of mixing in the concentration range studied can be used to determine the ultimate structure-making, structure-breaking classification of the ions involved. On the contrary, using the structural concept one can show that the signs and temperature dependences of the heats of mixing quite nicely correlate with this concept. Quite clearly the heats of mixing are due primarily to specific ion interactions which are the result of ion–H_2O structure interaction.

Acknowledgment. The authors would like to thank Dr. R. H. Wood for helpful discussions concerning this work.

(10) For a review see: J. L. Kavanau, "Water and Solute-Water Interactions," Holden-Day, San Francisco, Calif., 1964.

(11) R. H. Wood and H. L. Anderson, *J. Phys. Chem.*, **71**, 1869 (1967).

(12) R. H. Wood and H. L. Anderson, *ibid.*, **70**, 992 (1966).

(13) J. C. Rasaiah, *J. Chem. Phys.*, **52**, 704 (1970).

A Thermodynamic Study by Infrared Spectroscopy of the Association of 2-Quinolone, Some Carboxylic Acids, and the Corresponding 2-Quinolone–Acid Mixed Dimers[1]

by J. Claine Petersen

Laramie Energy Research Center, Bureau of Mines, U. S. Department of the Interior, Laramie, Wyoming 82070
(Received October 23, 1970)

Publication costs assisted by the Bureau of Mines, U. S. Department of the Interior

Self-association of 2-quinolone in carbon tetrachloride was studied by infrared spectroscopy, using the absorption bands in the amide NH and carbonyl stretching regions. 2-Quinolone forms a cyclic dimer from which the enthalpy ($\Delta H°$, kcal/mol), free energy ($\Delta G°_{22}$, kcal/mol), and entropy ($\Delta S°$, eu) of association are −8.69, −6.11, and −8.76, respectively. Dimer formation is *via* a carbonyl–hydrogen bond, although evidence exists for the formation of a small amount of dimer *via* a π–hydrogen bond. 2-Quinolone was also found to form cyclic mixed dimers with carboxylic acids. Mixed dimers of 2-quinolone with benzoic, cyclohexanecarboxylic, and 4-cyclohexylbutanoic acids gave $\Delta H°$ values of −12.2, −10.3, and −10.4; $\Delta G°_{22}$ values of −6.36, −5.94, and −5.78; and $\Delta S°$ values of −19.9, −14.8, and −15.6, respectively. Thermodynamic data on the acid dimers and spectral data on the different systems studied are also reported. The 2-quinolone–carboxylic acid interaction is of importance because of the simultaneous occurrence of quinolones and carboxylic acids in many biologically derived materials.

Introduction

Several studies[2-7] have been made in which quinolones have been characterized by their infrared spectra; however, intermolecular interactions of these compounds have not generally been recognized. The lack of information in this area probably results from the extremely low solubility of most quinolones in suitable infrared solvents, although some efforts[6] have been made to find more suitable solvents. Consequently, most infrared studies of quinolones have relied heavily on the use of suspensions of solid quinolones, either as mulls or in KBr disks, thus hindering the detection or study of molecular interactions by infrared spectroscopy. *N*-Unsubstituted 2-quinolones are lactams which are capable of forming cyclic dimers through hydrogen bonding analagous to dimers formed by carboxylic acids. Dimer equilibrium studies of the closely related pyridones have been reported.[8-10]

Quinolones are important in the study of quinoline alkaloids and have been identified in the high-boiling fractions of petroleum crude oils.[11,12] The recent discovery in our laboratory of a strong interaction between quinolones and carboxylic acids in petroleum distillation residues, and the likely existence of this interaction in other biologically derived systems, prompted the present study of this interaction. Because of the molecular complexity of petroleum residues and the difficulties attendant in the isolation of the individual compounds from their natural environment for quantitative studies, we decided to conduct a model study of the interaction of 2-quinolone with several carboxylic acids to obtain thermodynamic data. To obtain these data on the 2-quinolone–carboxylic acid interaction, however, it was first necessary to obtain similar data on the self-association of 2-quinolone and the acids individually. Results on the self-association of both pure compound types and on the association of the mixed systems are reported.

Experimental Section

Materials. Carbon tetrachloride was Baker and Adamson[13] CP grade (water content < 0.001 *M*) and was found by infrared spectroscopy in 10-cm cells to

(1) The work upon which this report is based was done under a cooperative agreement between the Bureau of Mines, U. S. Department of the Interior, and the University of Wyoming.

(2) J. A. Gibson, W. Kynaston, and A. S. Lindsay, *J. Chem. Soc.*, 4340 (1955).

(3) D. J. Cook, R. S. Yunghans, T. R. Moore, and B. E. Hoogenboom, *J. Org. Chem.*, **22**, 211 (1957).

(4) M. F. Grunden and N. J. McCorkindale, *J. Chem. Soc.*, 2177 (1957).

(5) J. R. Price and J. B. Willis, *Aust. J. Chem.*, **12**, 589 (1959).

(6) N. J. McCorkindale, *Tetrahedron*, **14**, 223 (1961).

(7) O. Buchardt, P. L. Kumler, and C. Lohse, *Acta Chem. Scand.*, **23**, 159 (1969).

(8) A. R. Katritsky and R. A. Jones, *J. Chem. Soc.*, 2947 (1960).

(9) M. H. Krackov, C. M. Lee, and H. G. Mautner, *J. Amer. Chem. Soc.*, **87**, 892 (1965).

(10) N. Kulevsky and W. Reineke, *J. Phys. Chem.*, **72**, 3339 (1968).

(11) E. C. Copelin, *Anal. Chem.*, **36**, 2274 (1964).

(12) L. R. Snyder, B. E. Buell, and H. E. Howard, *Anal. Chem.*, **40**, 1303 (1968).

be free of interfering impurities. 2-Quinolone, Eastman White Label, was found to be of greater than 96% purity by potentiometric titration with perchloric acid. Recrystallization from ethanol produced no detectable changes in the infrared spectra. Infrared spectra also showed the absence of the possible contaminants, 4-quinolone or 2,4-quinolinediol. Benzoic acid was Baker and Adamson primary standard. Cyclohexanecarboxylic and 4-cyclohexylbutanoic acid, from Eastman, gave neutralization equivalents of 131.7 and 180.5, indicating 97.4 and 94.3% purity, respectively. Reagent purities were taken into account in calculating concentrations. The negligible effect of trace water in the spectral solvent on the infrared spectra was verified by the addition of 0.002 M water to a stock quinolone solution with no measurable change in the free or bonded NH and carbonyl bands.

Methods. Stock solutions (0.00197, 0.00984, 0.00912, and 0.00886 M at 24° for 2-quinolone, benzoic acid, cyclohexanecarboxylic acid, and 4-cyclohexylbutanoic acid, respectively) were prepared by weighing into a flask exactly the required amount of sample which was then dissolved in carbon tetrachloride. 2-Quinolone–acid mixtures having the same component normalities as the single component solutions were similarly prepared. A series of concentrations were prepared for study from each of the stock solutions by 5- and 10-fold dilutions with an additional $^5/_3$-fold dilution for 2-quinolone. Infrared spectra were obtained on the solutions at 8, 22, 35.7, 48.5, and 65°, each temperature controlled to within ±0.3°. Multiple infrared traces (3–6) of each analytical band were run and averaged to improve the precision of the absorbance measurements. All solutions were prepared and diluted at 24°. Solution concentrations were corrected for volume changes by eq 1 and 2.

$$V_t = V_0(1 + 1.18384 \times 10^{-3}t + 0.89881 \times 10^{-6}t^2 + 1.35135 \times 10^{-8}t^3) \quad (1)$$

$$X_t = \frac{V_t}{V_{24}} \quad (2)$$

In these equations, t is the temperature in °C, V_t is the volume at temperature t, V_0 is the volume at 0°, and X_t is the volume correction factor for carbon tetrachloride. Solvent-compensated spectra with 4× base line expansion were recorded on a Perkin-Elmer Model 521 spectrophotometer after samples in KBr cells had attained temperature equilibrium in a Model VTC-140 Barnes variable temperature chamber. The frequency of the spectrophotometer was calibrated with standard polystyrene film. Cells of 1.06 and 5.07 cm were used while recording the OH, NH stretching regions; 0.100 and 1.06-cm cells were used for the carbonyl stretching region. Spectral slit openings were 125 μ for the OH and NH regions and 120 μ for the carbonyl region. Overlapping peaks in the spectra were resolved into their component peaks using a duPont Model 310 curve resolver.

Calculations and Results

Carboxylic acids are known to form cyclic dimers by hydrogen bonding. This study shows that 2-quinolone similarly forms a cyclic dimer, and further, forms a mixed, cyclic dimer with carboxylic acids. Therefore, the equilibria of interest are

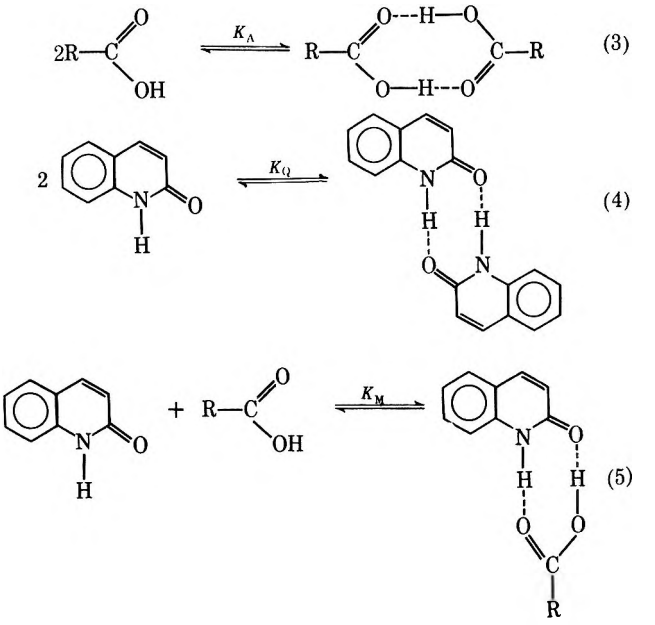

where K_A, K_Q, and K_M are the equilibrium constants for the dimerization of the carboxylic acid, 2-quinolone, and mixed dimer, respectively. The equilibrium constants K_A and K_Q are given by the equation

$$K_A \text{ or } K_Q = \frac{C_B}{2C_F^2} \quad (6)$$

where C_B and C_F are the concentrations of the bonded (dimer) and monomer (free) species, respectively, each referred to one formula weight of quinolone or acid. The total acid or 2-quinolone concentration (C) is given by

$$C = C_B + C_F \quad (7)$$

The free NH and OH stretching bands were used to calculate the concentrations of 2-quinolone and carboxylic acid monomers. Dimer concentrations were calculated using the bonded carbonyl stretching bands. Molar absorptivities for the bands representing the free and bonded species (ϵ_F and ϵ_B), which are necessary to determine C_F and C_B, were obtained by the method of Allen and coworkers.[14] In this method ϵ_F and ϵ_B are estimated by a graphical solution of eq 7 in which

(13) Mention of specific brand names or models of equipment is made for information purposes only and does not imply endorsement by the Bureau of Mines.

(14) G. Allen, J. G. Watkinson, and K. H. Webb, *Spectrochim. Acta*, 22, 807 (1966).

Table I: Spectral Data on 2-Quinolone, Some Carboxylic Acids, and Their Mixed Dimers

	Stretching frequency,[a] ν, cm^{-1} 22.0°	$\Delta\nu$, cm^{-1} 22.0°	Molar absorptivity,[b] ϵ, l./cm per mole functional group 8.0°	22.0°	35.7°	48.5°	65.0°	Estimated precision[c]
2-Quinolone								
Free NH	3408		266	266	266	266	266	±13
Free C=O	1680		[d]	[d]	[d]	[d]	[d]	
Bonded C=O	1664	16	2420	2330	2240	2160	2040	±31
Benzoic acid								
Free OH	3543		239	227	217	210	204	±5
Free C=O	1743		1070		935		980	
Bonded C=O	1696	47	1005	945	910	890	880	±15
Cyclohexanecarboxylic acid								
Free OH	3535		178	172	167	164	160	±5
Free C=O	1752		653	600	560	530	503	±20
Bonded C=O	1706	46	977	957	938	922	901	±15
4-Cyclohexylbutanoic acid								
Free OH	3538		213	185	174	171	169	±5
Free C=O	1757		525		450		470	
Bonded C=O	1711	46	916	911	907	902	896	±20
2-Quinolone–benzoic acid								
Mixed dimer								
2-Quinolone C=O	1648	32						
Acid C=O	1674	69						
2-Quinolone–cyclohexanecarboxylic acid								
Mixed dimer								
2-Quinolone C=O	1651	29						
Acid C=O	1689	63						
2-Quinolone–4-cyclohexylbutanoic acid								
Mixed dimer								
2-Quinolone C=O	1651	29						
Acid C=O	1691	66						

[a] Limit of error ±2 cm^{-1} except ±3 cm^{-1} on mixed dimers. [b] Values reported obtained from best fit of ϵ *vs.* t plot. [c] Standard deviation of average from ϵ *vs.* t plot. [d] Reliable figure not available because of band overlap, estimated at about 1600.

C_F and C_B have been replaced by their equivalent expressions derived from the Beer–Lambert law, $A = \epsilon Cl$, where A is the absorbance of the infrared band and l is the cell length. Frequencies and molar absorptivities of the analytical bands are included in Table I.

Because of band overlap in the carbonyl region of the spectra of a mixture of 2-quinolone and carboxylic acid, molar absorptivities of the bonded carbonyl bands in the mixed dimers could not be determined accurately. Therefore, mixed dimer concentration, C_M, was determined by difference, using the acid absorption band according to the equation

$$C_M = C - (C_F + C_B) \tag{8}$$

where C, C_F, and C_B refer to the initial, monomer, and dimer concentration of acid (each referred to one formula weight of acid). The value C_F was determined using the absorbance of the free OH followed by calculation of C_B from eq 6. The equilibrium constant for the mixed dimer was then calculated by the equation

$$K_M = \frac{C_M}{C_F \text{ (acid)} \times C_F \text{ (2-quinolone)}} \tag{9}$$

in which the concentration of free quinolone was determined using the absorbance of the free NH band.

The enthalpies of association ($\Delta H°$) were calculated from the log K *vs.* $1/T$ plot which has a slope of $-\Delta H°/2.303R$. These plots were found to be linear in all cases. From the values of $\Delta H°$ and log K which were obtained, values of $\Delta G°$ and $\Delta S°$ were calculated at the various temperatures.

The spectral data for 2-quinolone, the carboxylic acids, and the mixed dimers are shown in Table I. In Table II the thermodynamic data are summarized. Within experimental error, $\Delta S°$ was found to be independent of temperature over the temperature range studied. Equilibrium constants reported are least-square values taken from the log K *vs.* $1/T$ plot with

Table II: Thermodynamic Functions for the Association of 2-Quinolone, Some Carboxylic Acids, and Their Mixed Dimers

	K,[a] l./mol						
	8.0°	22.0°	35.7°	48.5°	65.0°	$-\Delta H°$,[b] kcal/mol	$-\Delta S°$,[c] eu	$-\Delta G°$, kcal/mol at 22°
2-Quinolone	69,500 (400)	33,400 (200)	17,220 (80)	9,790 (50)	5100 (40)	8.69 ± 0.03	8.76	6.11
Benzoic acid	18,600 (250)	7,015 (105)	2,925 (45)	1,390 (20)	581 (9)	11.5 ± 0.1	21.4	5.19
Cyclohexanecarboxylic acid	9,725 (215)	3,840 (80)	1,665 (35)	815 (17)	355 (7)	11.1 ± 0.2	20.9	4.84
4-Cyclohexylbutanoic acid	9,140 (350)	3,450 (130)	1,455 (55)	685 (26)	292 (12)	11.4 ± 0.2	22.6	4.78
2-Quinolone–benzoic acid mixed dimer	144,000 (18,000)	51,300 (6300)	20,300 (2500)	9,160 (1140)	3640 (450)	12.2 ± 0.8	19.9	6.36
2-Quinolone–cyclohexanecarboxylic acid mixed dimer	60,600 (4800)	25,150 (2500)	11,500 (900)	5,880 (470)	2700 (220)	10.3 ± 0.5	14.8	5.94
2-Quinolone–4-cyclohexylbutanoic acid mixed dimer	46,100 (2500)	19,200 (1030)	8,750 (500)	4,470 (250)	2040 (120)	10.4 ± 0.4	15.6	5.78

[a] Reported values from least-squares plot of log K *vs.* $1/T$. Standard deviation in parentheses. [b] Estimate of precision, ± one standard deviation. [c] Constant over temperature range.

precision of the data indicated by the standard deviation of the average shown in parentheses. Where more than one concentration was studied (see Methods section), no systematic variation of K with concentration was observed, and the K's reported are averaged values. The precision of the $\Delta H°$ values shown in Table II was calculated from the indicated precision of the K values. Accuracy of the $\Delta H°$ values is believed to be within 5% for the carboxylic acids and 10% for 2-quinolone and the mixed dimers.

Discussion

Before equilibrium data could be obtained it was necessary to determine molar absorptivities of the analytical infrared bands identified with the free and bonded species. Although the acids presented no special problems, the large equilibrium constants for the 2-quinolone system required the use of long path-length cells and very dilute solutions to obtain significant amounts of the free species. Precision of the calculated molar absorptivities for the free NH band was therefore somewhat limited by small absorbance bands in the more dilute solutions. The small intensity of this band is probably the reason this band is not reported by workers in the field. Within the limits of experimental measurements, no temperature dependence was found for the molar absorptivity of the free NH in 2-quinolone. This is consistent with the temperature independence of the free NH found by Chen and Swenson[15] for the closely related saturated lactams. The molar absorptivity of 266 l./mol cm (Table I) determined for the free 2-quinolone NH was considerably larger than the value of 109 l./mol cm reported[15] for six-membered ring saturated lactams.

A problem which made determination of the absorptivities of the 2-quinolone carbonyl bands difficult was the severe band overlap caused by the small $\Delta\nu$ (16 cm^{-1}, Table I) between the free and bonded bands. The band overlap was further complicated by nonuniform band envelopes. The free carbonyl peak in 2-quinolone, and probably most quinolones, has gone unrecognized by workers in the field who have apparently been consistently reporting the frequency of the bonded carbonyl. For example, McCorkindale,[6] although noting a small shoulder on the high-frequency side of the carbonyl band of some quinolones, includes this shoulder in calculating integrated intensities of the carbonyl band. Thus his integrated intensities include, but do not differentiate between, bonded and free species. To verify that McCorkindale reported the bonded carbonyl frequencies, we examined 2-quinolone in chloroform (the solvent used by McCorkindale) and found the bonded carbonyl frequency to be 1659 cm^{-1}, identical with the carbonyl frequency reported by McCorkindale.[6] We found the free carbonyl

(15) C. Y. S. Chen and C. A. Swenson, *J. Phys. Chem.*, **73**, 1363 (1969).

frequency in chloroform to be 1673 cm^{-1}. In this case the frequencies of bonded and free species are separated by only 14 cm^{-1}. Apparently, earlier workers have not worked with sufficiently dilute solutions and have not had sufficient band resolution to recognize the free carbonyl band.

In our work, a graphical curve resolver was used to resolve the complex carbonyl band of 2-quinolone and obtain absorptivities of the overlapping bonded and free species. Band absorptivities for the bonded band which gave consistent results in subsequent calculations were obtained by adjusting the width and height of the individual free and bonded bands so that their sum gave the best fit of both the curve maxima and the valley between the bonded and free bands, while ignoring minor fine structure on the extreme outside limits of the bands. Because of the large equilibrium constant for dimer formation, the free carbonyl band was usually small with respect to the bonded carbonyl band. As a result, the absorptivities determined for the free carbonyl were not precise. The free NH band was therefore used in the calculations to represent the amount of free 2-quinolone present. There was no significant overlap of the bonded carbonyl peak maximum by the free carbonyl band generated on the curve resolver. Therefore, errors in intensity measurements of the bonded carbonyl band were not introduced by resolving overlapping nonlinear absorption bands on the linear-responding curve resolver.

The small shift of the carbonyl band of 2-quinolone on dimer formation has already been noted. As shown in Table I it is only about $^1/_3$ as large as the $\Delta\nu$ for carboxylic acids. The $\Delta\nu$ for both carboxylic acids and 2-quinolone in the mixed dimer is considerably larger. For example, the $\Delta\nu$ for the 2-quinolone carbonyl increases from 16 cm^{-1} in the 2-quinolone dimer to 32 cm^{-1} in the mixed dimer with the aromatic acid, benzoic acid; the $\Delta\nu$ of the benzoic acid carbonyl increases from 47 cm^{-1} in the acid dimer to 69 cm^{-1} in the mixed dimer with 2-quinolone. Similar, but slightly smaller, increases are noted for the mixed dimers with the saturated acids cyclohexanecarboxylic acid and 4-cyclohexylbutanoic acid. The smaller $\Delta\nu$'s for the mixed dimers with saturated acids are probably a result of their slightly weaker hydrogen bond ($\Delta H°$, Table II).

Because of the differences in $\Delta\nu$'s between dimers and mixed dimers it was possible to observe all six carbonyl bands in the mixed system. The spectrum of the carbonyl region for the mixed system of 2-quinolone and 4-cyclohexylbutanoic acid is shown in Figure 1. The broad envelope approximates the infrared spectrum and is a summation of individual peaks under the envelope. The individual peaks were obtained using the curve resolver and represent the various carbonyl species present. As seen in Figure 1, band overlap is large. In initial attempts to calculate the enthalpies of the mixed dimers, we used the method of Baker and

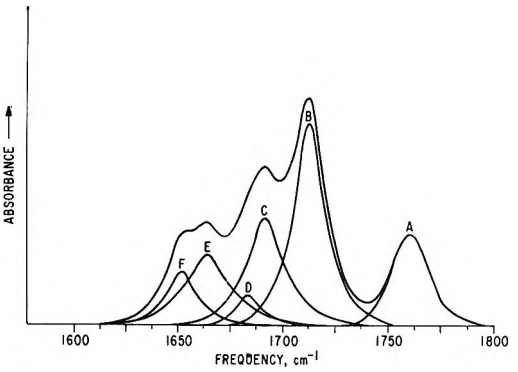

Figure 1. Resolution obtained on a curve resolver of carbonyl stretching region of a mixture of 2-quinolone (0.00186 M) and 4-cyclohexylbutanoic acid (0.0084 M) at 65° in CCl_4. Curve A, free acid C=O; B, acid dimer C=O; C, acid C=O, mixed dimer; D, free 2-quinolone C=O; E, 2-quinolone dimer C=O; F, 2-quinolone, mixed dimer.

Yeaman[16] in which enthalpies are calculated using absorption ratios after making some simplifying assumptions. This method circumvents the need to determine concentrations of the species present; however, it was not possible to resolve the intensity of the individual bands with sufficient precision to obtain good enthalpy values. In spite of the large variance in the enthalpies calculated by this method, results obtained did confirm that correct assignments had been made to the bands and that the correct equilibrium species had been assumed. That the major associated species are cyclic dimers and not linear or larger complexes is evidenced by the linearity of the log K *vs.* $1/T$ plots used to calculate enthalpies.

Although measurements of intensities of the resolved bands for the mixed dimer carbonyls lacked precision, the frequency assignments obtained at different temperatures, concentrations, and concentration ratios of acid to 2-quinolone were found to be consistent and reproducible. Thus, frequencies reported in Table I for the mixed dimer carbonyl bands are believed to be accurate to within ± 3 cm^{-1}.

Because of the difficulty in obtaining accurate absorbance values of the mixed dimer in the complex spectra, thermodynamic properties of the mixed system were obtained by first calculating the monomer and dimer concentrations of the acid, using only the free OH band for the acid which can be accurately measured. The concentration of the mixed acid–quinolone dimer could then be calculated by difference. The amount of free quinolone was determined from its free NH band. Using this procedure it was unnecessary to resolve the complex carbonyl region to calculate the equilibrium data on the mixed dimers.

Upon examination of the spectra of 2-quinolone at different temperatures, a lack of correspondence was

(16) A. W. Baker and M. D. Yeaman, *Spectrochim. Acta*, 22, 1773 (1966).

noted between the intensities of the free carbonyl and the free NH bands. This was particularly evident at low temperatures (−14°) where considerable free carbonyl band remained after the free NH band had nearly vanished. Quantitatively these results are shown in Figure 2 in which the apparent molar absorptivities of the two bands are plotted against each other as a function of temperature at two different concentrations. (The apparent molar absorptivity assumes the stoichiometric concentration in calculating absorptivity.) On the basis of the dimer shown in eq 4, this plot should pass through the origin. The possibility that the excess carbonyl at the lower temperatures could result from a carbonyl-containing impurity in the 2-quinolone sample was virtually eliminated by consideration of the following observations: (1) recrystallization of the 2-quinolone from methanol produced no changes in the infrared spectra of the sample; (2) the possible contaminants of 4-quinolone and 2,4-quinolinediol did not have carbonyl adsorption bands characteristic of those found in the 2-quinolone sample; and (3) reaction of the 2-quinolone with hexamethyldisilazane, which reacts with the enol tautomer of the carbonyl group of 2-quinolone to form a silyl ether,[17] completely removed the carbonyl infrared absorption from the sample. Only carbonyl compounds which readily form enol tautomers can undergo this reaction.

The formation of a small amount of cyclic dimer *via* a π–hydrogen bond, as illustrated below, is proposed as an explanation for the excess carbonyl. In this dimer the

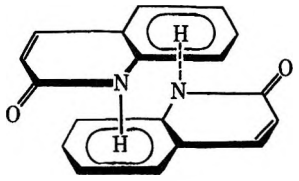

amide hydrogen is associated with the π electrons on the aromatic ring of the adjacent molecule, rather than the carbonyl group, leaving the carbonyl unassociated. The formation of some of this dimer would cause the free NH to decrease at a faster rate than the free C=O, in agreement with Figure 2. Similar associations are well known in phenolic systems[18−20] where the hydrogen of the phenolic OH forms a π–hydrogen bond with aromatics. An analogous association has been proposed for the dimerization of pyrrole through association of the NH proton of one molecule with the π electron ring system of the second.[21−23] Further indication of the presence of a π complex in 2-quinolone solutions was obtained from examination of the uv spectra of several solutions of 2-quinolone at different concentrations. When absorbance ratios of two different concentrations were plotted as a function of wavelength, an absorption band in the 2900-Å region was found to be concentration dependent, showing increased absorptivity with decreasing concentration, which is characteristic of

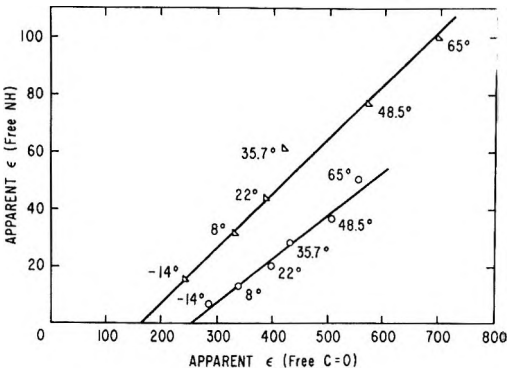

Figure 2. Relationship between apparent molar absorptivities of free NH and free C=O of 2-quinolone in CCl_4 as a function of temperature: O, 0.00197 *M* at 22°; △, 0.000394 *M* at 22°.

molecular association. This probably arises from perturbations of the electronic transitions of the π electrons. An additional attempt to confirm the presence of the NH–π bond in 2-quinolone by looking at the out-of-plane infrared bending vibrations of the aromatic hydrogens was not successful, probably because of the low absorptivities of these bands and the low concentrations used. Also, any effect seen by infrared would be only a second-order effect on the aromatic hydrogens.

If 2-quinolone dimers of both the π– and carbonyl–hydrogen bond types are present, the question arises as to what effect this would have on the thermodynamic data (Table II) which were calculated on the assumption that only the carbonyl–hydrogen bond was present. It is estimated, by comparing the apparent molar absorptivity (Figure 2) of the free carbonyl band with the calculated molar absorptivity of this band at infinite dilution (Table II), that a maximum of 10–15% of the dimer present at the lowest temperature and highest concentration studied is of the π complex type. This may cause the calculated molar absorptivity for the bonded carbonyl to be as much as 10–15% lower than the true value. However, because this calculated molar absorptivity is used in calculating the thermodynamic properties, these calculated properties (Table II) should quite accurately reflect the actual equilibria which include both dimer species. Because the π–hydrogen bond would contribute to the enthalpy, but is probably a much weaker bond[24] than the carbonyl–hydrogen bond, the actual enthalpy for the dimerization involving only the carbonyl–hydrogen bond may be

(17) J. C. Petersen, *et al.*, submitted for publication in *Anal. Chem.*

(18) Z. Yoshida and E. Osawa, *J. Amer. Chem. Soc.*, **87**, 1467 (1965).

(19) E. Osawa, T. Kato, and Z. Yoshida, *J. Org. Chem.*, **32**, 2803 (1967).

(20) K. Szczepaniak and M. Golinska, *Acta Phys. Pol.*, **34**, 421 (1968).

(21) J. A. Happe, *J. Phys. Chem.*, **65**, 74 (1961).

(22) M. Gomel and H. Lumbroso, *Bull. Soc. Chim. Fr.*, 2200 (1962).

(23) H. Lumbroso, *J. Chim. Phys. Physiochim. Biol.*, **51**, 132 (1954).

(24) J. V. Hatton and W. G. Schneider, *Can. J. Chem.*, **40**, 1285 (1962).

5–10% higher than the value reported for 2-quinolone in Table II. The negligible effect of the π complexes on the enthalpy calculation is evidenced by the fact that the same enthalpy of association was obtained from calculations at four different concentrations.

Of primary interest in this study were the thermodynamic functions of 2-quinolone and its mixed dimer with carboxylic acids (Table II). The data for 2-quinolone were found to be quite different from the data for the saturated lactams studied by Chen and Swenson.[15] For example, $\Delta H°$ (kcal/mol), $\Delta S°$ (eu), and $\Delta G°_{22}$ (kcal/mol) for 2-quinolone were found to be -8.69, -8.76, and -6.11, compared with -5.90, -11, and -2.74 for the six-membered ring saturated lactam. As indicated by the $\Delta H°$ values, the hydrogen bond strength of 2-quinolone is about 1.5 as great as that of the saturated lactam. The marked tendency for 2-quinolone to associate is indicated by the large equilibrium constants for dimerization. At 22° the equilibrium constant is over two orders of magnitude greater for 2-quinolone than for the saturated lactam (33400 l./mol compared to 108 l./mol calculated from data of Chen and Swenson[15]). As might be expected, the thermodynamic functions of 2-quinolone were found to be quite similar to those of the closely related 2-pyridone. The $\Delta H°$, $\Delta S°$, and $\Delta G°_{25}$ for 2-pyridone are reported[10] to be -8.8, -12.0, and -5.25, respectively.

Thermodynamic properties of the benzoic acid dimer were found to be essentially the same as those reported by Allen and coworkers,[14] thus offering a check on the techniques used in this study.

The mixed dimers of 2-quinolone and carboxylic acids were found to associate through relatively strong hydrogen bonds (10.3–12.2 kcal/mol) of nearly the same strength as for the dimers of the carboxylic acids (11.1–11.5 kcal/mol) and greater than for the 2-quinolone dimer. Equilibrium constants for the mixed dimers were found to be larger than for the corresponding carboxylic acid dimers. The mixed dimer of the aromatic acid, benzoic acid, shows the greatest amount of association. These data show that the formation of the mixed dimer is important in mixtures of 2-quinolone and carboxylic acids. As an example, when a 1:1 M ratio of 2-quinolone and cyclohexanecarboxylic acid is mixed in carbon tetrachloride at 22°, each at an initial concentration of only 0.00337 M, 43% of all the acid and quinolone is present as the mixed dimer. Only 5% of the 2-quinolone and 14% of the carboxylic acid exist in the free or unassociated state under these conditions, the balance being accounted for by the dimers of the individual compounds.

Enthalpies reported for the mixed dimer are the sum of two hydrogen bonds which are not equivalent. The individual contributions of the NH–carbonyl and the OH–carbonyl bonds are not known. Entropy changes for the mixed dimer were intermediate between those for the acids and 2-quinolones.

In summary, the mixed dimers formed from carboxylic acids and 2-quinolone are strongly associated, hydrogen-bonded complexes and must be considered important in systems which contain these compound types.

Acknowledgment. The author gratefully acknowledges the assistance of Dr. James Weber of the spectroscopy group at the Laramie Energy Research Center for his assistance in developing the uv data.

Heats of Association for Divalent Transition Metal Ethylene–Maleic Acid Copolymer Complexes

by Betty J. Felber and Neil Purdie*[1]

Department of Chemistry, Oklahoma State University, Stillwater, Oklahoma 74074 *(Received September 16, 1970)*

Publication costs borne completely by The Journal of Physical Chemistry

The heats of association of the 1:1 ethylene–maleic acid copolymer complexes of Mn^{2+}, Co^{2+}, Ni^{2+}, Cu^{2+}, and Zn^{2+} have been measured calorimetrically at 25°. Values are less endothermic, even to becoming exothermic for Co^{2+} and Ni^{2+}, than the corresponding monosuccinate complexes. Using the previously measured free energies of complexation, the entropy of association is seen to be very large and positive. This has been interpreted in terms of the changes in the polyion–solvent environment as the electrostatic charge on the polyanion is neutralized on forming a 1:1 complex.

Introduction

The free energy change for the equilibrium process in which a metal ion interacts with a polyelectrolyte has been measured frequently and by numerous methods.[2] Values are for the most part large and this is indicative of a very stable complex. From free energies alone it is not possible to conclude what is the nature of the interaction or the intimate structure of the complex.[3] The mechanism for binding may be[4] (1) electrostatic in character and therefore dependent upon the charge of the counterion or (2) site binding and therefore dependent upon complex formation. This distinction is analogous to the one made between ion pairs and complexes for metals with monomeric ligands. From the multistep mechanism of complex formation used in kinetic studies[5] it is suggested that ion pairs and complexes exist in equilibrium with each other and with the free aquated ions. Consequently, both mechanisms may operate, to a greater or lesser extent, depending upon the structure of the polymer and upon the identity of the anionic repeating unit. Preferential site binding can be expected to be really important when the same effect manifests itself in the low molecular weight or monomeric units of the polymer *e.g.*, in polycarboxylates and polyphosphates[6] as opposed to polysulfonates, the latter groups behaving as strong acids.[6,7] Ethylene–maleic acid copolymer might then be considered to form complexes by the site-binding mechanism, since the monomer succinic acid forms stable complexes.[8]

The relative magnitudes of ΔG of complexation cannot be used to distinguish between the two possibilities. Accompanying enthalpy and entropy changes are more profitable quantities to consider when trying to interpret the changes in the immediate solute–solvent environment.[3] Data on the heats of association for metal polymer complexes are sparse and as a rule has been obtained from the temperature dependence of the apparent formation constants.[9] No consideration was given to the possible variation in heat capacity of the process with temperature so that the resultant heat changes are subject to the limitation that the van't Hoff isochore expression is linear over the entire range. To eliminate this problem in a study of some divalent transition metal ethylene–maleic acid complexes the heats of formation were measured calorimetrically at 25°. The corresponding metal monosuccinate complexes[8] are used for comparative purposes in discussing the results.

Experimental Section

Reagents. The copolymer of molecular weight 20,000–30,000 (Monsanto Chemical Co.), supplied as the anhydride, was readily hydrolyzed to the acid by heating at 70–80° for 2 hr. Its physical characterization has been previously described.[10] Solutions in deionized water were stored in Pyrex containers at 5°. Metals were added as the perchlorates (G. Frederick Smith Chemical Co.); stock solutions were standardized by titration of the acid obtained after cation exchange with standard base.

(1) To whom communications should be directed.

(2) H. Morawetz, *High Polym.*, **21**, 369 (1965).

(3) G. H. Nancollas, "Interactions in Electrolyte Solutions," Elsevier, New York, N. Y., 1966.

(4) F. T. Wall, *J. Phys. Chem.*, **61**, 1344 (1957).

(5) M. Eigen and K. Tamm, *Z. Elektrochem.*, **66**, 93, 107 (1962).

(6) U. P. Strauss and Y. P. Leung, *J. Amer. Chem. Soc.*, **87**, 1476 (1965).

(7) M. Reddy, J. A. Marinsky, and A. Sarkar, *J. Phys. Chem.*, **74**, 3891 (1970).

(8) A. McAuley, G. H. Nancollas, and K. Torrance, *Inorg. Chem.*, **6**, 136 (1967).

(9) E. M. Loebl, L. M. Luttinger, and H. P. Gregor, *J. Phys. Chem.*, **59**, 559 (1955).

(10) S. Machi, T. Sakai, M. Gotoda, and T. Kagiya, *J. Polym. Sci. Part A-1*, **A4**, 821 (1966).

Apparatus. The basic circuitry for electrical calibration and measurement of heat changes is essentially that described in previous work.[11] A dual titration microcalorimeter system was developed incorporating many of the features of that described by Nancollas.[3] Insulated Dewar reaction vessels were enclosed in brass thermal jackets fitted with lids allowing total immersion in the thermostat maintained at 25 ± 0.05°. Both solutions were stirred by vertical agitation using a single stirring motor (Corning Model LM-2). Each reaction vessel was equipped with a heater element, a 2000-ohm thermistor (GB32-PM12 Fenwal Electronics, Inc.), and a 22-gauge Teflon delivery needle sufficiently long that an adequate volume of titrant would be kept in temperature equilibrium with the contents of the vessel before addition. With this arrangement each compartment served alternatively as the reaction and comparison vessel.

Performance of the calorimeter was checked by the measurement of the heat of protonation of 1.008×10^{-2} *M* tris(hydroxymethyl)aminomethane (THAM, NBS Standard Reference Material No. 724) with 0.5456 *M* HCl as titrant. A value of 11.39 ± 0.05 kcal/mol at 25° was obtained from a series of measurements, after correction for the heat of dilution, which agrees to within 0.1% of the literature value.[12,13]

Procedure

Solutions of the metal perchlorates, approximately 0.5 *M*, were titrated into EMA solutions, approximately 10^{-2} *M*, which were about 25% neutralized by adding the appropriate volume of 0.1037 *M* tetramethylammonium hydroxide. The quaternary ammonium cation was used because its interaction with the polyion is much less than that of the larger alkali metal ions.[14] From previous work on the stability of these complexes the appropriate *apparent* acid ionization constants and the *apparent* stability constant could be chosen to correspond with the above degree of neutralization.[14] (See later discussion.) Corrections were made to the observed heat changes for the heats of dilution of the metal perchlorates measured by titration into a KCl solution of similar ionic strength to the EMA mixture of acid and salt. The heat of protonation of HA^- was also determined by titration with 0.4884 *M* $HClO_4$. Since the total increase in volume during the titration was always less than 0.5 ml, any heat change associated with this dilution was neglected. For each run the average of two heat capacity measurements, made before and after the titration, was taken to determine the energy change of the system. pH measurements were made before and after the additions using a glass electrode–calomel electrode assembly, calibrated with a standard buffer solution of pH 4.01 on a Beckman Research pH meter Model 1019.

Results

It was shown previously that a simple 1:1 metal to ligand complex was formed according to

$$M^{2+} + A^{2-} \rightleftharpoons MA \quad (1)$$

when the concentration of the polyion was expressed in mol/l. of monomer.[14] Concentrations of species needed in the determination of the heat of this reaction were calculated from the known acid apparent ionization constants ($K_{a1,app}$ and $K_{a2,app}$), the metal complex stability constants (K_{MA}), the measured pH of the solutions, and the analytically obtained concentrations of metal (*m*), EMA (*a*), and base[14] (*b*) according to the equilibria

$$K_{a1,app} = [H^+][HA^-](f_1^2/[H_2A]) \quad (2)$$

$$K_{a2,app} = [H^+][A^{2-}](f_2/[HA^-]) \quad (3)$$

$$K_{MA} = [MA]/[M^{2+}][A^{2-}]f_2^2 \quad (4)$$

and the mass balance equations

$$m = [M^{2+}] + [MA] \quad (5)$$

$$a = [H_2A] + [HA^-] + [A^{2-}] + [MA] \quad (6)$$

$$b + [H^+] + 2[M^{2+}] = [HA^-] + 2[A^{2-}] + 2m \quad (7)$$

Comments on the acid ionization constants and the activity coefficients f_i are significant[14] and bear repetition. For polyacids the ionization "constant" varies with the degree of ionization α: the variation is frequently described by the equation[15]

$$pK_i = pH - n_i \log [\alpha/(1 - \alpha)] \quad (8)$$

where the parameter n_i has different values for first and second proton ionizations from a pair of vicinal carboxylic groups.[16] It is also possible to define apparent ionization constants by the equations

$$pK_{a1,app} = pH - \log [\alpha/(1 - \alpha)] + \log f_1 \quad (9)$$

and

$$pK_{a2,app} = pH - \log [\alpha/(1 - \alpha)] + 3 \log f_1 \quad (10)$$

(Activity coefficient terms are usually not included but have been added specifically for the present discussion.) These are related to the intrinsic thermodynamic constants through the equation

$$pK_i = pH - \log [\alpha/(1 - \alpha)] + y \log f_1 - 0.434e\psi_{el}/kT \quad (11)$$

(11) D. P. Fay and N. Purdie, *J. Phys. Chem.*, **73**, 3462 (1969).

(12) R. G. Bates and H. B. Hetzer, *ibid.*, **65**, 667 (1961).

(13) J. O. Hill, G. Ojelund, and I. Wadso, *J. Chem. Thermodyn.*, **1**, 111 (1969).

(14) B. J. Felber, E. M. Hodnett, and N. Purdie, *J. Phys. Chem.*, **72**, 2496 (1968).

(15) A. Katchalsky and P. Spitnik, *J. Polym. Sci.*, **23**, 451 (1957).

(16) J. D. Ferry, D. C. Udy, F. C. Wu, G. F. Heeder, and D. B. Fordyce, *J. Colloid Sci.*, **6**, 429 (1951).

Table I: Equilibrium Constants and Concentration Data

Ion, M^{n+}	K_{MA}	$C_M \times 10^3$, F^a	$C_A \times 10^3$, $F^{a,b}$	$\Delta[H^+] \times 10^5 F$	$\Delta[H_2A] \times 10^3 F$	$\Delta[MA] \times 10^3 F$
Mn^{2+}	6.41×10^3	2.71	9.34	8.52	2.28	1.47
		2.71	9.34	9.98	2.54	1.30
		2.71	9.34	9.96	2.54	1.31
Co^{2+}	4.29×10^3	2.70	9.63	9.35	2.45	1.11
		2.70	9.63	9.74	2.52	1.07
		2.70	9.63	8.27	2.25	1.24
Ni^{2+}	3.76×10^3	2.70	10.2	8.43	2.29	1.11
		2.70	10.2	8.62	2.36	1.06
		2.70	10.2	8.59	2.34	1.08
Cu^{2+}	4.45×10^{10}	3.39	10.2	55.93	3.06	2.47
		3.39	10.2	51.88	2.96	2.56
		3.39	10.2	62.81	3.20	2.34
Zn^{2+}	4.97×10^3	2.96	9.33	9.25	2.47	1.31
		2.96	9.33	9.25	2.47	1.31
		2.96	9.33	8.34	2.29	1.47
		2.96	9.33	9.23	2.48	1.32
H^+(1st)	1.32×10^{-5}	2.96	9.33	26.86	2.66	2.72
H^+(2nd)	2.87×10^{-10}	2.96	9.33	28.93	2.64	2.70
		2.96	9.33	30.73	2.62	2.76

[a] C_M, C_A are final analytical concentrations. [b] Final volume is 33.36 ml for metals, 32.48 for $HClO_4$.

where the last term is the Debye–Hückel limiting expression for "polyionic work" included to account for the additional electrostatic energy required to remove a proton from the vicinity of the heavily charged polyion. Haymann[17] has shown that the limiting case adequately describes the "polyionic work" if the analytical concentration of the polymer $a \leqslant 10^{-2}$ M which it is in the present case. Furthermore it has been proposed[2] that the concept of ionic strength has meaning in polymer solutions only if the product $e\psi_{el}$ is less than kT. The maximum value of $e\psi_{el}$ calculated from the last point used in the first buffer region[14] is $0.7kT$ which has given us some confidence in applying the interionic-attraction theory to the calculation of activity coefficients. These were calculated using the Davies equation[18]

$$-\log f_i = 0.509 z_i^2 \left[\frac{I^{1/2}}{1 + I^{1/2}} - 0.3I \right] \qquad (12)$$

where

$$I = b + [H^+] + 3[M^{2+}] + [A^{2-}] \qquad (13)$$

by reiteration to constant f_1 around eq 5–7, 12, and 13. By selecting the apparent ionization constant to correspond with the degree of ionization of the partially neutralized acid solution in the calorimeter vessel a correction was made for the "polyionic work" term. In spite of the obvious limitations to this approach, especially since an analogous correction could not be made at the starting pH to K_{a2}, the method was considered to be preferable to measurements in a constant ionic strength medium where uncertainties would have been introduced from competitive ion binding by the cation of the added salt.

The values given in Table I correspond to the changes in concentration which occur as a result of complexation. Energy changes in calories were calculated from $Q_E = D \times \bar{h}$ where D is the pen deflection during addition and $\bar{h}$ is the average heat capacity of the system. When thermal equilibrium of the calorimeter was not ideal, *i.e.*, $dT/dt \neq 0$, corrections to D were made using the Regnault–Pflaunder method.[19] The experimental energy change is given by the expression

$$Q_E = Q_{MA} + Q_{H_2A} + Q_{HA^-} + Q_{DIL} + Q_{H_2O} \qquad (14)$$

where $Q_{MA} = \Delta[MA] \times \Delta H_{MA}$; $Q_{H_2A} = \Delta[H_2A] \times \Delta H_{H_2A}$; $Q_{HA^-} = \Delta[HA^-] \times \Delta H_{HA^-}$; Q_{DIL} is equal to the energy change for dilution of the titrant; and Q_{H_2O} is equal to the energy change for neutralization. Under the conditions of the experiment Q_{HA^-} and Q_{H_2O} were negligible. From the experiments in which $HClO_4$ was added to the EMA solution a value of $\Delta H_{H_2A} = -0.24$ kcal/mol was obtained, in good agreement with the heats of protonation of similar monomeric dicarboxylic acids.[20] The value was substantiated by a temperature dependence study of $K_{a1,app}$ in which the plot of log $K_{a1,app}$ *vs.* $1/T$ was observed to pass through a maximum around 300°K. Energy changes are collected in Table II. Values for ΔG_{MA}, ΔH_{MA}, and ΔS_{MA}, calculated from the Gibbs free energy equation, are given in Table III, together with the literature values for the corresponding metal monosuccinates.[8]

(17) H. J. G. Haymann, *J. Chem. Phys.*, 22, 1234 (1954).

(18) C. W. Davies, "Ion Association," Butterworths, London, 1962, p 122.

(19) W. Eitel, "Thermochemical Methods in Silicate Investigation," Rutgers University Press, New Brunswick, N. J., 1952.

(20) J. J. Christensen, R. M. Izatt, and L. D. Hansen, *J. Amer. Chem. Soc.*, 89, 213 (1967).

Table II: Heats of Complexation of Metal–EMA

Ion, M^{n+}	Heat capacity, $\bar{h}$, cal/cm	Deflection, D, cm	Q_E, 10^2 cal	Q_{MA}, 10^2 cal	Q_{H_2A}, 10^2 cal	Q_{DIL}, 10^2 cal	ΔH_{MA},[a] kcal/mol
Mn^{2+}	0.032	1.48	4.73	8.48	−1.83	−1.92	1.73
	0.031	1.45	4.49	8.42	−2.01	−1.92	1.94
	0.032	0.96	3.08	7.25	−2.25	−1.92	1.61
						Mean = 1.76 ± 0.14	
Co^{2+}	0.030	2.76	8.36	−2.90	−1.94	+13.2	−0.78
	0.030	2.71	8.20	−3.00	−2.00	+13.2	−0.84
	0.034	2.11	7.09	−3.33	−1.78	+13.2	−0.81
						Mean = −0.81 ± 0.05	
Ni^{2+}	0.022	3.01	6.63	−3.44	−1.83	+11.9	−0.93
	0.024	2.88	6.91	−3.11	−1.88	+11.9	−0.88
	0.025	2.41	6.03	−4.00	−1.87	+11.9	−1.11
						Mean = −0.97 ± 0.12	
Cu^{2+}	0.026	9.00	23.1	31.3	−2.43	−5.76	3.80
	0.022	8.02	17.5	25.6	−2.34	−5.76	2.99
	0.023	10.30	23.2	31.5	−2.54	−5.76	4.03
						Mean = 3.61 ± 0.51	
Zn^{2+}	0.026	2.90	7.55	12.50	−1.94	−3.01	2.97
	0.027	1.67	4.50	9.45	−1.94	−3.01	2.17
	0.032	1.70	5.47	10.06	−1.58	−3.01	2.26
	0.034	2.13	7.17	12.13	−1.95	−3.01	2.75
						Mean = 2.54 ± 0.43	
H^+	0.033	0.83	−2.76		−2.76	0	−0.32
	0.033	0.55	−1.82		−1.82	0	−0.21
	0.028	0.56	−1.57		−1.57	0	−0.18
						Mean = −0.24 ± 0.07	

[a] Error expressed as standard deviation.

Table III: Thermodynamic Parameters for M–EMA and M–Succinate Complexes

Ion	M–EMA			M–Succinates		
	$-\Delta G$, kcal/mol	ΔH, kcal/mol	ΔS, eu	$-\Delta G$, kcal/mol	ΔH, kcal/mol	ΔS, eu
Mn	12.05	1.76	46.3	3.09	3.02	20.5
Co	11.75	−0.81	36.8	3.02	3.15	20.7
Ni	11.95	−0.97	36.8	3.20	2.46	19.0
Cu	14.53	3.61	60.9	4.42	4.56	30.1
Zn	11.88	2.54	48.4	3.36	4.39	26.0
H (1st)[a]	6.63	−0.24	21.4	5.75	−0.76	16.8
H (2nd)[a]				7.59	−0.06	25.6
				Mean	−0.41	21.2

[a] Values are for protonation rather than ionization. (See ref 20.)

Discussion

As predicted,[14] the enthalpies of complex formation defined in terms of a monomeric unit of ligand are less endothermic than the values for the monosuccinate complexes which could be considered to be the monomeric analogs. By analogy, therefore, one would conclude that the metals are bound to the polyion at specific sites and in the process substitution into the coordination sphere of the metal ion has occurred. This change in ΔH_{MA} to a more favorable value does not exclusively account for the extreme stability of the metal–EMA complexes over the monosuccinates, but rather the discussion should emphasize the much more favorable entropy contribution to the overall stability—an increase in $T\Delta S$ of the order of 4.8–9.2 kcal/mol. Consideration of the changes in ΔH_{MA} would indicate that the metal ions are more tightly bound to the polymer at the specific sites than is possible in the monomeric analog. This result would have far-reaching effects on the solvation of the metal ions when bound, perhaps accounting for a small increase in entropy. It may be concluded that this small "secondary" entropy increase is fairly constant since the variation in ΔH_{MA} from metal to metal is comparable to the monosuccinate case.

To account for the remaining, or "primary," increase in ΔS the implications of the effect of a structural or conformation change of the polyion must be considered.

It was pointed out that the heat of protonation of HA^- was not unusual when compared to values for simpler monomeric acids;[20] *e.g.*, ΔH_{HA^-} for succinic acid is −0.76 kcal/mol. The present value for EMA is perhaps best considered to be an average value. For example, it is instructive to observe that the average ΔH of protonation of citric acid,[20] for which the successive values are −1.0, −0.58, and +0.08 kcal/mol, respectively, is −0.26 kcal/mol. The comments are

equally valid for the entropies of protonation. (Table III). It is therefore proposed that the structure of the partially neutralized acid in the first ionization process is an elongated chain in which the vicinal carboxylic acid groups are linked by intramolecular hydrogen bonds. When the hydrogen bonds are opened, with the release of protons, to allow the strong metal interaction at the specific sites, the polyion may adopt a more rigid conformation in which hydrophobic contacts are produced. Any loss in entropy from additional proton solvation and the change in conformation is nevertheless exceeded by the gain in entropy realized by the liberation of ordered solvent molecules as the metal ions and the polymer are constrained.

Two specific observations are perhaps worthy of further comment. Copper could again appear to undergo a change in coordination number on complexation[8] which would account for the much more endothermic ΔH_{MA} and much more favorable entropy change. The most endothermic changes are for Zn^{2+} and Cu^{2+}, both of which have tetrahedral geometry (if the above interpretation for Cu^{2+} is valid). This may reflect the increasing strain introduced in the ligand molecule in bonding with these ions.

Finally, there is little correspondence with results from other systems, *e.g.*, copper polyacrylate,[9] ΔH_{MA} = 0.5 kcal/mol and ΔS_{MA} = 28 eu, but this may be a consequence of the experimental limitations of the temperature dependence method. It is conceivable, for example, that conformational changes with temperature substantially change the heat capacity of the process.

Acknowledgment. We wish to express our appreciation to the Research Foundation, Oklahoma State University, for the financial support given to this project, the Graduate College, Oklahoma State University, for the fellowship given to B. J. F., and Dr. John H. Johnson, Monsanto, St. Louis, Missouri, for providing us with the polymer samples.

Non-Newtonian Viscosity and Excluded Volume Effect of Dilute Solutions of Flexible High Polymers[1a]

by Noriko Yamaguchi,[1b] Yoshihiko Sugiura,* Koji Okano, and Eiich Wada

The Institute of Physical and Chemical Research, Yamato-machi, Saitama Pref. Japan *(Received March 26, 1970)*

Publication costs borne completely by The Journal of Physical Chemistry

The shear rate dependence of the intrinsic viscosity of flexible high polymers has been studied with anionically polymerized and fractionated polystyrene samples in three solvent systems: benzene, a good solvent for the polymer; butanone, a moderately good solvent; and cyclohexane, a θ solvent. The shear rate applied ranged from 0.2 to 11,800 sec^{-1}, which was attained by using four kinds of viscometers: a Zimm-type rotating coaxial viscometer; a tilting capillary viscometer; a double capillary viscometer with external hydrostatic pressure; and a conventional Ubbelohde viscometer. The data were analyzed using the following equation $[\eta]_{\dot\gamma} = [\eta]_0(1 - B\beta^2 + \ldots)$ where $[\eta]_{\dot\gamma}$ and $[\eta]_0$ are the intrinsic viscosities at given shear rates $\dot\gamma$ and zero shear rate, respectively, B is a parameter related to the non-Newtonian character of the intrinsic viscosity, and β is the reduced value of shear rate expressed by $\beta = (M[\eta]_0\eta_0/RT)\dot\gamma$. Here, M is the molecular weight of the polymer, η_0 the solvent viscosity, R the gas constant, and T the absolute temperature. It was found that the shear rate dependence or the non-Newtonian character of the intrinsic viscosity differs with the solvent systems used and becomes pronounced with increasing solvent power, *i.e.*, excluded volume effect. At the θ condition, the non-Newtonian viscosity was not actually observed in the range of β below 1, but in the range of the larger values of β a slight decrease of solution viscosity was observed. The coefficient B was shown to increase slightly with increasing molecular weight for anionically polymerized polystyrene systems. The results obtained in the present work semiquantitatively agree with recent theory of Fixman, indicating that the non-Newtonian viscosity of dilute polymer solutions is mainly caused by the excluded volume effect.

Introduction

The viscosity of polymer solutions is essentially non-Newtonian. It depends on the shear rate or shear stress. Since the viscosity of dilute solutions of polymers with medium molecular weights does not exhibit any appreciable non-Newtonian behavior, it has been treated practically as Newtonian viscosity. The recent progress in the field of polymerization, however, has made it possible to prepare polymers having very high molecular weights with sharp molecular weight distributions. With the use of these polymers some experiments have revealed that the non-Newtonian character cannot be neglected even at infinite dilution, *i.e.*, in the case of intrinsic viscosity. In addition, along with the recent development in theories of dilute polymer solutions, it has become clear that the non-Newtonian character of the intrinsic viscosity is closely connected with the excluded volume effect of the polymer chain segments. Thus, the non-Newtonian viscosity of dilute polymer solutions is now becoming a significant and attractive research area.

The non-Newtonian intrinsic viscosity of polymer solutions can generally be expressed in the form of a series expansion in even power of the shear rate, $\dot\gamma$. It is convenient to express it by using a nondimensional reduced shear rate, β.

$$[\eta]_{\dot\gamma} = [\eta]_0(1 - B\beta^2 + \ldots) \qquad (1)$$

where $[\eta]_{\dot\gamma}$ and $[\eta]_0$ are the intrinsic viscosities (ml/g) at a given shear rate $\dot\gamma$ and at zero shear rate, respectively, and the reduced shear rate is defined by the equation

$$\beta = \frac{M[\eta]_0\eta_0}{RT}\dot\gamma \qquad (2)$$

Here M is the molecular weight of the polymer, η_0 the solvent viscosity, R the gas constant, and T the absolute temperature.

The molecular theory of the non-Newtonian viscosity of dilute polymer solutions has a long history. A number of authors have presented various theories, but the origin of non-Newtonian viscosity remained obscure until recently. For example, Kuhn and Kuhn,[2] and Cerf,[3] assumed that the non-Newtonian character arises from imperfect flexibility of the polymer chain and introduced a concept of "internal viscosity." According to their theories, the value of B was calculated to be 2.00 and 0.72, respectively. In the theories of Ikeda,[4] Peterlin and Čopič,[5] and Peterlin,[6] attention

(1) (a) Presented in part at the Fifth International Congress on Rheology, Kyoto, Japan, Oct 1968; (b) based on a dissertation submitted by N. Yamaguchi in partial fulfillment of the requirements for the Ph.D. degree in chemistry. Department of Chemistry, Tokyo Kyoiku University, Tokyo.

(2) W. Kuhn and H. Kuhn, *Helv. Chim. Acta*, **28**, 1533 (1945).

(3) R. Cerf, *J. Polym. Sci.*, **23**, 125 (1957).

(4) Y. Ikeda, *J. Phys. Soc. Jap.*, **12**, 378 (1957).

(5) A. Peterlin and M. Čopič, *J. Appl. Phys.*, **27**, 434 (1956).

was focused on the hydrodynamic interaction between chain segments, and they estimated the value of B as 0.0196, 0.148, and 0.152, respectively. In all the above theories, B was independent of the solvent power, because a polymer chain was taken as a Gaussian coil. As a result, the comparison of these theories with experimental results should be confined to the θ temperature.

The recent theory of polymer solutions developed by Kurata and Stockmayer,[7] however, has revealed that most polymer chains in dilute solutions should be regarded as "non-free-draining," and the molecular weight dependence of the intrinsic viscosity at zero shear rate can well be explained by the excluded volume effect. Along with this, several refined theories of the non-Newtonian intrinsic viscosity in which the excluded volume effect is taken into account have been developed by Chikahisa,[8] Subirana,[9] Okano, *et al.*,[10] and Fixman.[11] These four theories agree well with each other in that the coefficient B depends on the excluded volume effect or the solvent power and becomes larger as the latter increases.

On the other hand, many experimental data also have been accumulated up to the present. Scharman, *et al.*,[12] pointed out that the non-Newtonian viscosity of polystyrene solutions depends not only on the molecular weight of the polymer and the temperature but also on the solvent power. Čopič,[13] and Passaglia, *et al.*,[14] also obtained similar results. In fact, the above-mentioned theories have been motivated by these experimental results. Unfortunately, from the quantitative point of view, these experiments seem unsatisfactory for elucidating the non-Newtonian viscosity of polymer solutions, because (1) the data were unsuitable to evaluate accurately the value of B, and (2) the effect of the molecular weight distribution of the fractionated samples used was not taken into account.

Recently, Kotaka, *et al.*,[15] studied the non-Newtonian viscosity of polystyrene solutions and found that the non-Newtonian viscosity was independent of the solvent power, contrary to the observations by Čopič[13] and Passaglia, *et al.*[14] In addition, Noda, *et al.*,[16] have made a similar study with poly-α-methylstyrene, indicating that the decrease of the intrinsic viscosity is pronounced at lower values of $\dot{\gamma}$ for the lower molecular weight samples. Both the experiments by Kotaka, *et al.*, and Noda, *et al.*, however, seem likely to include certain uncertainties originating from the use of two or three types of viscometers without carefully applying corrections.

Very recently, Suzuki, *et al.*, presented a report,[17] in which, contrary to their previous observations,[15] the relation between $[\eta]_{\dot{\gamma}}/[\eta]_0$ and log β is different for the systems having different solvent power: the larger the solvent power, the more marked is the non-Newtonian viscosity. The present study is aimed to elucidate experimentally the non-Newtonian viscosity of dilute solutions of flexible high polymers. Anionically polymerized and fractionated polystyrene samples were employed to eliminate the uncertainty originating from the molecular weight distribution in the samples. In benzene, butanone, and cyclohexane, the estimation of B was performed by plotting carefully $[\eta]_{\dot{\gamma}}$ against $\dot{\gamma}^2$ over a suitable range of $\dot{\gamma}$. To cover the necessary range of $\dot{\gamma}$, four types of viscometers having different ranges of shear rates were used. The results obtained were compared with the above-mentioned theories in detail.

Experimental Section

1. Sample. Four anionically polymerized polystyrene samples (L1, L2, L3, and L4) and two fractionated ones (F1 and F2) were used. The sample L1 was obtained from the Pressure Chemical Co. Ltd., and L2, L3, and L4 were obtained from Dow Chemical Co. Ltd. The fractionated samples (F1 and F2) were kindly supplied by Professor Nagasawa. The molecular weight of the samples was determined by light scattering measurements in butanone at room temperature, as shown in Table I. These values were also ascertained to be in good agreement with the ones derived from the intrinsic viscosities by published viscosity–molecular weight relationships.[18] The ratio M_w/M_n was 1.20 for L1 and it was not greater than 1.24 for L2, L3, and L4. However, the molecular weight distribution of the fractionated polystyrenes was less sharp than that of L series samples.

2. Viscosity Measurements. Viscosity measurements were made in benzene, a good solvent for polystyrene, butanone, a moderately good solvent, and cyclohexane, a θ solvent (θ temperature is 34.5°). To obtain the shear rate dependence of the intrinsic viscosity over a wide range of shear rates according to eq 1 and 2, four types of viscometers were used, as described below.

(6) A. Peterlin, *J. Chem. Phys.*, **33**, 1799 (1960); *Makromol. Chem.*, **44–46**, 338 (1961).

(7) M. Kurata and W. H. Stockmayer, *Fortschr. Hochpolym. Forsch.*, **3**, 196 (1962).

(8) Y. Chikahisa, *J. Phys. Soc. Jap.*, **19**, 2188 (1964); **21**, 2324 (1966).

(9) J. A. Subirana, *J. Chem. Phys.*, **41**, 3852 (1964).

(10) K. Okano, N. Yamaguchi, and E. Wada, *Rep. Progr. Polym. Phys. Jap.*, **9**, 89 (1966).

(11) M. Fixman, *J. Chem. Phys.*, **45**, 793 (1966).

(12) L. J. Scharman, R. H. Sones, and L. H. Cragg, *J. Appl. Phys.*, **24**, 703 (1953).

(13) M. Čopič, *J. Chim. Phys.*, **54**, 348 (1957).

(14) E. Passaglia, J. T. Yang, and N. J. Wegemer, *J. Polym. Sci.* **47**, 333 (1960).

(15) T. Kotaka, H. Suzuki, and H. Inagaki, *J. Chem. Phys.*, **45**, 2770 (1966).

(16) I. Noda, Y. Yamada, and M. Nagasawa, *J. Phys. Chem.*, **72**, 2890 (1968).

(17) H. Suzuki, T. Kotaka, and H. Inagaki, *Rep. Progr. Polym. Phys. Jap.*, **10**, 115 (1967); **11**, 75 (1968); *J. Chem. Phys.*, **51**, 1279 (1969).

(18) For example, W. Krigbaum and P. J. Flory, *J. Polym. Sci.*, **11**, 37 (1953); P. Outer, C. Carr, and B. H. Zimm, *J. Chem. Phys.*, **18**, 830 (1950).

Table I: Molecular Weights of Samples and Conditions of Viscosity Measurements

Sample	$M \times 10^{-6}$	Solvent	Temp, °C	Viscometer	$\dot{\gamma}_{max}$, sec^{-1}	β_{max}
L1	1.83	Benzene	35.0	T	9,000	1.27
L2	3.06	Benzene	35.0	Z, U	2,030	0.688
L3	3.35	Benzene	35.0	T	7,600	3.29
L4	3.50	Benzene	35.0	T	2,200	1.16
F1	7.10	Benzene	35.0	Z, T	2,460	4.08
L4	3.50	Butanone	25.0	T	4,690	0.830
F2	3.98	Butanone	35.0	T	8,850	1.68
L2	3.06	Cyclohexane	34.5	Z, U	660	0.059
L3	3.35	Cyclohexane	39.0	T	5,290	0.767
L4	3.50	Cyclohexane	39.0	T	1,520	0.289
F1	7.10	Cyclohexane	34.5	Z, T, P	11,800	5.50

i. Zimm-Type Rotating Coaxial Viscometer (Z). The viscometer was constructed according to the specifications of Zimm and Crothers.[19] The schematic representation is given in Figure 1 (1). The radius (R_2) of the stator was 1.095 cm and that of the rotor (R_1) varied from 0.806 to 0.913 cm. The range of shear rates attained in this viscometer was 0.2 to 15 sec^{-1} as calculated from

$$\dot{\gamma} = \frac{\langle S \rangle}{\eta_0} = \pi\Omega\left[\frac{R_2 + R_1}{R_2 - R_1} f(R_1, R_2)\right] \quad (3)$$

where $f(R_1, R_2)$ is a correction factor given by

$$f(R_1, R_2) = \frac{8R_1^2R_2^2}{(R_1 + R_2)^3(R_2 - R_1)} \ln\left(\frac{R_2}{R_1}\right) \quad (4)$$

$\langle S \rangle$ is the average shear stress, and Ω is the speed of the rotor in revolutions per unit time. The time per revolution, $1/\Omega$, was measured by means of a travelling microscope for both solvent and solution under the same stress. The relative viscosity at a given shear rate was calculated from the ratio of the value of $1/\Omega$ for the solution to that for the solvent. Special attention was paid to avoid the errors caused by surface films.[20a]

ii. Tilting Capillary Viscometer (T). The schematic diagram of the viscometer is shown in Figure 1 (2). Details of the dimensions of the five viscometers used are shown in Table II. The shear rate ranged from 300 to 9000 sec^{-1} and was calculated using the following equation

$$\dot{\gamma} = \frac{4V}{\pi R^3} \frac{1}{t_0} \quad (5)$$

where V is the volume of the bulb, R the radius of the capillary, and t_0 the efflux time of the solvent. The relative viscosity was calculated[20b] from

$$\eta_{rel} = \frac{4\left(\frac{t_s}{t_0}\right)}{3 + \left(\frac{t_0}{t_s}\right)\left(\frac{dt_s}{dt_0}\right)} \left\{1 + \frac{V\rho}{8\pi L\eta_0} \frac{1}{t_0}\left(1 - \frac{t_0^2}{t_s^2}\right)\right\} \quad (6)$$

Table II: Details of Tilting Capillary Viscometers

Viscometer	Radii of capillary, $R \times 10^2$, cm	Length of capillary, L, cm	Volume of bulb, V, ml	Range of shear rate for benzene, $\dot{\gamma}$, sec^{-1}
No. 1	1.45	19.95	0.69	340–1370
No. 2	2.04	20.0	0.66	420–2400
No. 3	2.27	10.05	0.67	1400–3380
No. 4	1.43	4.0	0.74	3200–9000
No. 5	1.45	4.0	3.74	2400–6500

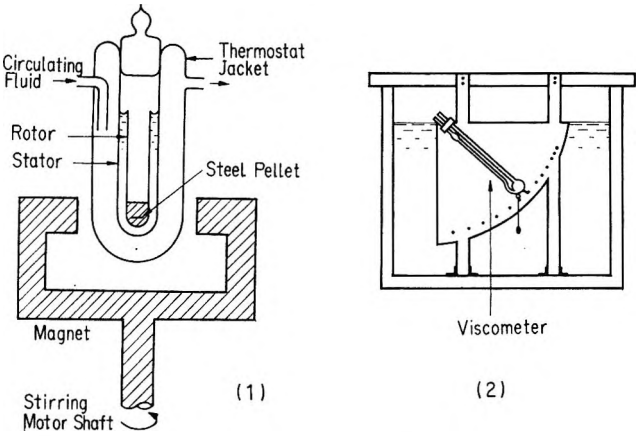

Figure 1. Schematic representations of (1) Zimm-type rotating coaxial viscometer and (2) tilting capillary viscometer.

where L is the length of the capillary, and ρ and η_0 are the density and the viscosity of the solvent, respectively. The subscripts 0 and s attached to t indicate solvent and solution, respectively.

iii. Double Capillary Viscometer with External Hydrostatic Pressure (P). The viscometer was constructed according to Čopič's description;[13] the schematic diagram is shown in Figure 2. The same pressure was

(19) B. H. Zimm and D. M. Crothers, *Proc. Nat. Acad. Sci.*, **48**, 905 (1962).

(20) (a) Y. Sugiura and N. Yamaguchi, *Rep. Inst. Phys. Chem. Res. Tokyo*, **43**, 70 (1967); (b) E. Wada, *J. Sci. Res. Inst.*, **47**, 149 (1957).

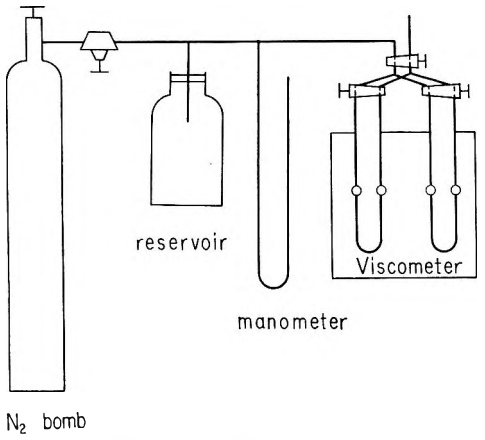

Figure 2. Schematic representation of double capillary viscometers with external hydrostatic pressure.

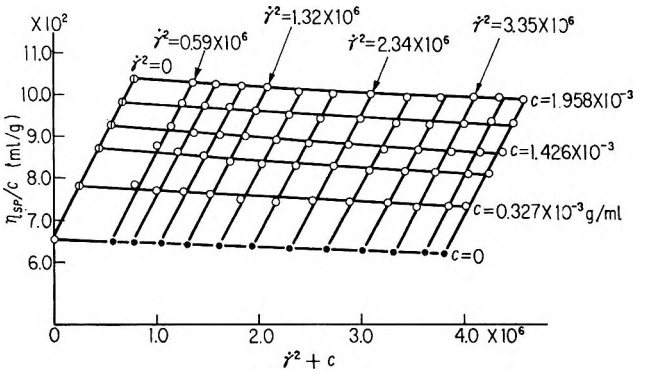

Figure 3. Reduced viscosities and their values extrapolated to zero shear rate and to infinite dilution plotted as a function of the sum of the square of the shear rate and the solution concentration (g/ml) for polystyrene L3 (M = 3.35 × 10⁶) in benzene at 35.0°.

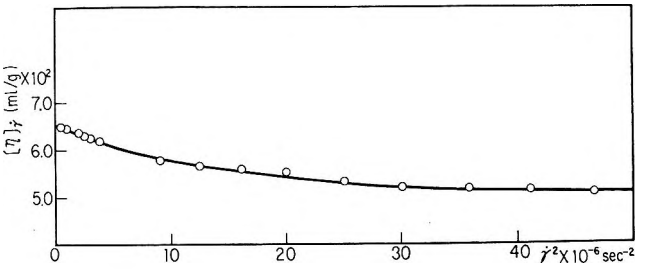

Figure 4. Plot of intrinsic viscosities at given shear rates against the square of shear rate for polystyrene L3 in benzene at 35.0°.

applied at the same time to two capillary viscometers of very nearly identical dimension, and the efflux times of solvent and solution were measured. The pressure applied to the viscometers, $\langle P \rangle$, was determined as the average of the heights of the mercury in the U-tube observed before and after the liquid flowed. The shear rate ranged from 5000 to 11,800 sec^{-1} and was calculated from the observed value of the pressure from the equation

$$\dot{\gamma} = \frac{1}{\eta_0} \frac{\langle P \rangle R}{2L} \qquad (7)$$

where R and L are the radius and the length of the capillary, respectively.

iv. Conventional Ubbelohde Viscometer (U). The shear rate was about 2000 sec^{-1}.

Experimentally, it is most important to ascertain whether all of the viscometers used give consistent results.

For this purpose, the viscosity ratios of various pairs of organic solvents such as cyclohexane–benzene or cyclohexane–toluene were measured with the four types of viscometers. These organic solvents are, of course, Newtonian liquids. The values obtained by three of the viscometers, the Zimm-type rotating coaxial, the tilting capillary and the Ubbelohde viscometers, were in good agreement with each other within an error of 0.2–0.3%, but the value obtained by the double capillary viscometer with external hydrostatic pressure was smaller by 1.5% than those obtained by the other three. This seemed to be related to the relatively low precision attainable with this viscometer which is fraught with many technical difficulties. Therefore, the use of this viscometer was confined to measurements in which high shear rates were especially needed. In most cases, the tilting capillary viscometers were used. The Zimm-type viscometer was used in the measurements at the lowest shear rates. The types of viscometers used, the maximum shear rates $\dot{\gamma}_{max}$, and the maximum reduced values β_{max} attained for each of the polymer–solvent systems are shown in Table I.

Results

An example of viscosity measurements by the tilting capillary viscometer (no. 2) is represented in Figure 3 for sample L3 in benzene at 35.0°. The reduced viscosities at a given shear rate, η_{sp}/c, are plotted against the sum of the concentration c (g/ml) and the square of the shear rate $\dot{\gamma}^2$. The open circles denote the reduced viscosities at given shear rates and the filled circles denote the intrinsic viscosities at given shear rates, $[\eta]_{\dot{\gamma}}$. The values of $[\eta]_{\dot{\gamma}}$ are obtained by extrapolating the reduced viscosities at the same shear stress[20b] to infinite dilution. The extrapolation of the reduced viscosities at the same concentration to zero shear rate, on the other hand, gives the reduced viscosities at $\dot{\gamma}$ = 0, $(\eta_{sp}/c)_0$. The extrapolation of both $[\eta]_{\dot{\gamma}}$ to zero shear rate and $(\eta_{sp}/c)_0$ to infinite dilution is shown to give a common intercept, *i.e.*, the intrinsic viscosity at $\dot{\gamma}$ = 0, $[\eta]_0$.

The intrinsic viscosity at zero shear rate, $[\eta]_0$, is generally obtained by the single extrapolation of $[\eta]_{\dot{\gamma}}$ to zero shear rate. Unfortunately, this conventional method often yields additional errors in the values of $[\eta]_0$, because of the arbitariness in drawing only a single line. In comparison with the single extrapolation, the

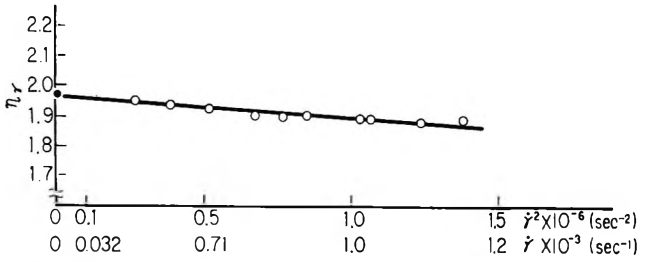

Figure 5. Relative viscosities at $c = 7.01 \times 10^{-4}$ g/ml plotted as a function of shear rate for polystyrene F1 ($M = 7.1 \times 10^6$) in benzene at 35.0°.

double extrapolation technique employed here is considered to be very adequate for the present purpose, similarly to the Zimm plot for the derivation of molecular weights by light scattering measurements.

Figure 4 shows a plot of $[\eta]_{\dot{\gamma}}$ against $\dot{\gamma}^2$ over a wide range of $\dot{\gamma}^2$ up to about 5×10^7 sec^{-2} for sample L3 in benzene. The intrinsic viscosity $[\eta]_{\dot{\gamma}}$ begins to decrease linearly with an increase in the shear rate squared, $\dot{\gamma}^2$. This is clearly shown in Figure 5.

Figure 5 shows plots of the relative viscosities measured at various shear rates for sample F1 in benzene at 35.0°. In the figure, the open circles indicate the values observed in the tilting capillary viscometer, and a filled circle, a value obtained in the Zimm-type rotating coaxial viscometer. The latter, in fact, represents four points obtained in a very narrow range of low shear rates from 0.2 to 15 sec^{-1}. The straight line through the open circles also passes through the filled circle. Thus, the linear extrapolation of the reduced viscosities measured with the tilting capillary viscometers, as shown in Figure 3, is reasonable.

Figure 6 shows a plot of the relative intrinsic viscosities against the reduced shear rates for the three systems of polystyrene solutions. The expansion factor cubed, α_η^3, shown in the figure is closely related to the excluded volume effect, the value being calculated by the equation

$$\alpha_\eta^3 = [\eta]_0/[\eta]_\theta \quad (8)$$

$$[\eta]_\theta = K_\theta M^{1/2} \quad (9)$$

where $K_\theta = 8.2 \times 10^{-2}$.[7] It is seen that the shear rate dependence of the intrinsic viscosity differs in the three systems, the extent of the non-Newtonian character increasing with increasing values of α_η^3. The figure also shows that the non-Newtonian character is hardly observed in the cyclohexane system near the θ temperature in the region of low reduced shear rates ($\beta < 1$).

Figure 7 shows the shear rate dependence of the intrinsic viscosities for sample F1 in benzene at 35.0° and in cyclohexane at 34.5° (θ temperature). In the latter case, however, the reduced viscosities at the concentration of 0.002546 g/ml were measured over a wide range of shear rates up to 11,800 sec^{-1} by using

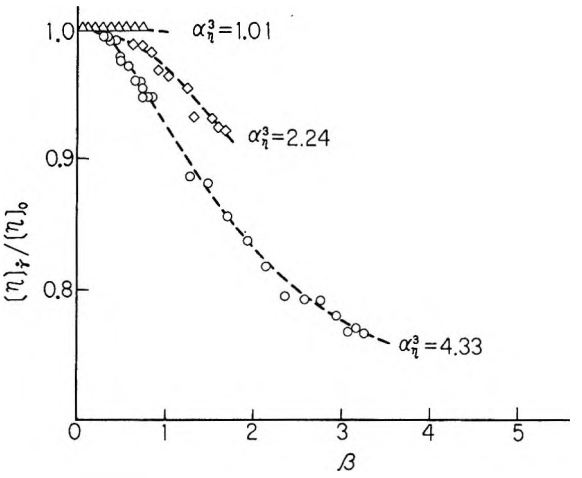

Figure 6. Relative intrinsic viscosities plotted as a function of reduced shear rate: O, polystyrene L3 ($M = 3.35 \times 10^6$) in benzene at 35.0°; Δ, L3 in cyclohexane at 39.0°; ◇, polystyrene F2 ($M = 3.98 \times 10^6$) in butanone at 35.0°. α_η^3 is the expansion factor cubed.

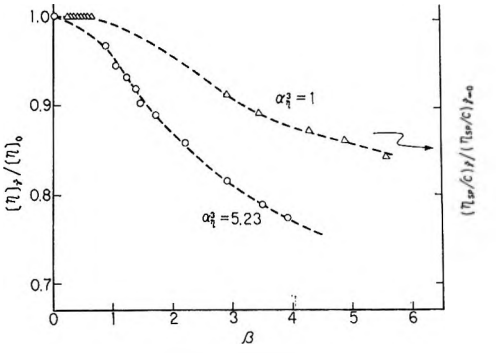

Figure 7. Relative intrinsic viscosities and relative reduced viscosities plotted as a function of reduced shear rates for polystyrene F1 ($M = 7.1 \times 10^6$) in benzene at 35.0° (O) and in cyclohexane at 34.5° (Δ), respectively. α_η^3 is the expansion factor cubed.

the double capillary viscometer with external hydrostatic pressure. The decrease in viscosity with increasing shear rate is evident at the θ temperature. In other words, the non-Newtonian character appears even at the θ condition, though its extent is far smaller than that for the benzene system.

Figure 8 shows the relative intrinsic or reduced viscosities shown in Figure 7 replotted against the square of the reduced shear rate, β^2. According to eq 1, the extent of the non-Newtonian character, *i.e.*, the value of the coefficient B, can be calculated from the initial slope of the curve shown in this figure. The value thus obtained is 0.046 for the benzene system, and that for the θ condition is estimated not to exceed 0.005.

Discussion

The experimental results have shown that the shear rate dependence of the intrinsic viscosity, *i.e.*, the non-Newtonian viscosity, depends upon the solvent power

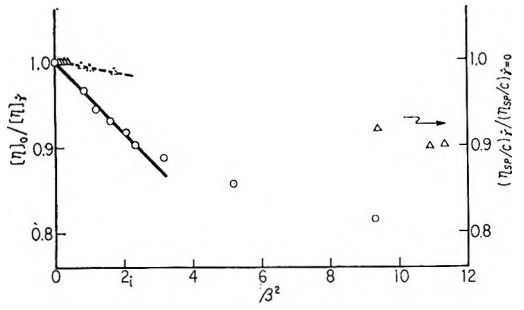

Figure 8. Plots of relative intrinsic viscosities and relative reduced viscosities as a function of the reduced shear rates squared for polystyrene F1 in benzene at 35.0° (○) and in cyclohexane at 34.5° (△), respectively. ⛬ is written according to the $(\eta_{sp}/c)_\dot{\gamma}/(\eta_{sp}/c)_{\dot{\gamma}=0}$ *vs.* β curve shown in the Figure 7.

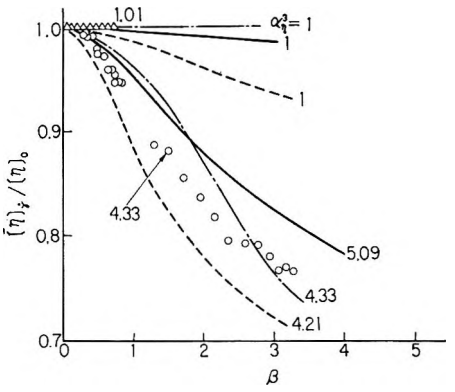

Figure 9. Comparison of the experimental and theoretical relations between the relative intrinsic viscosity and the reduced shear rate for the sample L3 and F2. The dotted lines show Chikahisa's, the chain lines Subirana's, and the solid lines Fixman's theory, respectively. The numerical parameters show the expansion factor rubed, α_η^3.

and becomes pronounced with an increase in the excluded volume effect. At the θ condition, the non-Newtonian character is not observed in the range of low shear rates, $\beta < 1$, but is actually observed for high values of β. Before advancing detailed comparisons of these results with the theories, it is reasonable to discuss the adequacy of these theories.

Chikahisa considered that the non-Newtonian viscosity is caused by the orientation of equivalent "rigid" ellipsoids whose axial ratio and volume are affected by the excluded volume effect. He considered that the use of the equivalent ellipsoid model is reasonable if the shear rate is not large, because in this case polymer molecules do not deform and are non-free-draining.

Subirana considered that the expansion of polymer molecules due to the excluded volume effect decreases with increasing shear rate, thus causing the lowering in viscosity or the non-Newtonian character of the viscosity.

Fixman has developed a general theory of polymer dynamics based upon a Boson representation technique, in which both the effect of excluded volume and hydrodynamic interaction are taken into account. He applied this formalism to non-Newtonian viscosity and calculated quantitatively the shear rate dependence of the intrinsic viscosity. According to his theory, the shear rate dependence of the intrinsic viscosity arises mainly from the decrease of the excluded volume force due to the expansion of the polymer coil with increasing shear rate.

We shall compare the theories presented by Chikahisa, Subirana, and Fixman with experimental results, because those theories are quantitative and cover the appropriate experimental range of shear rate and excluded volume effect.

The relation between the observed relative intrinsic viscosity $[\eta]_\dot{\gamma}/[\eta]_0$ and β are compared with the theoretical ones for several polystyrene solutions in Figure 9. The plotted points in the figure are reproduced from Figure 6. The dotted lines are drawn according to numerical values shown in Table II of Chikahisa's paper, which were calculated for given values of the expansion factor cubed, α_η^3, from his own theoretical equations. The chain lines represent the Subirana theory. The solid lines are drawn according to the results of Fixman's numerical calculation. From the qualitative point of view, all of the above-mentioned theories show similar behavior, and particularly Chikahisa's theory indicates more pronounced non-Newtonian character than the other two theories do. It is to be noted that the theory of Chikahisa and Fixman predicts a non-Newtonian viscosity even at $\alpha_\eta^3 = 1$, *i.e.*, for unperturbed chains.

Figure 10 shows another comparison of the theoretical and experimental relations between $[\eta]_\dot{\gamma}/[\eta]_0$ and β. The plotted points are reproduced from Figure 7. For the cyclohexane system in the range of the large reduced shear rates ($\beta > 3$) attained with the double capillary viscometer with external hydrostatic pressure, the reduced viscosity is plotted in place of the intrinsic viscosity. Detailed comparisons with the theories, therefore, could not be attempted here.

As shown in Figures 9 and 10, the above-mentioned theoretical results qualitatively agree with our experimental results, *i.e.*, the non-Newtonian viscosity must be expressed in terms of, at least, β and α_η^3. Our experimental points, observed in a good solvent, lie between two theoretical curves calculated by Chikahisa and Fixman over the whole range of β examined, while our data observed at or near the θ condition agree well with Fixman's theoretical curve at low values of β. On the other hand, the theoretical curves calculated by Subirana depend differently on β from those calculated by Chikahisa and Fixman, *i.e.*, the former for good solvent decreases steeper with an increase of β than the latter. Therefore, the agreement between Subirana's theory and our data seems to be poorest among the three theories.

Before going into more detailed comparison of the

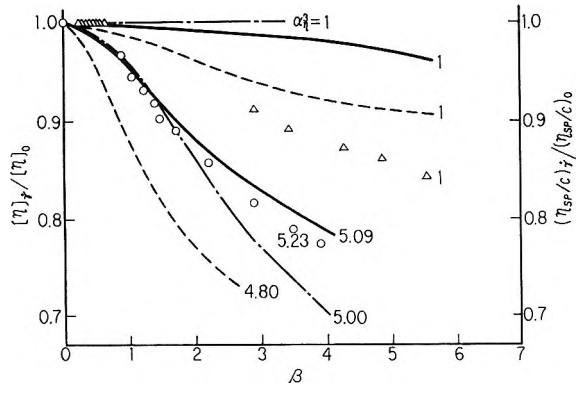

Figure 10. Comparison of the experimental and theoretical relations between the relative intrinsic or relative reduced viscosity and the reduced shear rate for the sample F1.

theories with the experiments, we wish to discuss recent experiments by other authors.

Recently, Kotaka, *et al.*,[15] investigated experimentally the non-Newtonian viscosity of solutions of fractionated polystyrene samples by making use of Zimm-type and Ubbelohde viscometers, concluding that the relation between $[\eta]_\gamma/[\eta]_0$ and log β is expressed by a universal curve for any solution system, irrespective of the solvent power and the molecular weight of the polymer. Their observation, however, does not agree with the present work and it also contradicts the experiments by Čopič[13] and Passaglia, *et al.*[14] Later on, they presented another report[17] in which, contrary to their previous observations, the relation between $[\eta]_\gamma/[\eta]_0$ and log β is different for systems having different solvent power; the larger the solvent power, the more marked is the non-Newtonian viscosity. This tendency agrees with that observed by us.

Table III shows the intrinsic viscosities at zero shear rate $[\eta]_0$, and the corresponding values of α_η^3 and the coefficient B. In this table, $[\eta]_\theta$ is the intrinsic viscosity at zero shear rate and at the θ temperature, and $[\eta]_0$ denotes that not at the θ condition. It may be pertinent here to consider the effect of molecular weight on the non-Newtonian viscosity. For this purpose, it is convenient to discuss the results obtained for one solvent. It is seen from Table III for the benzene systems that the value of B slightly increases with increasing molecular weight for polymers having sharp molecular weight distribution, *i.e.*, the L series. For one of the fractionated samples, F1, on the other hand, the value of B is smaller than expected from its molecular weight which is the highest among all the samples used. The small value of B for the F1 system may be explained by the following facts: (i) fractionated samples obtained by the conventional precipitation technique have broader molecular weight distributions than anionically polymerized polymers, such as the L series in the table;[21] and (ii) the extent of the non-Newtonian viscosity decreases as the molecular weight distribution in the sample broadens.[22]

Inspection of the value of B for the systems of the L series leads to the conclusion that the shear gradient dependence of the intrinsic viscosity is clearly affected not only by the solvent power but also by the molecular weight of the polymer, although the effect of the latter is rather small.

Very recently, Noda, *et al.*,[16] have published experimental results on the non-Newtonian viscosities of the systems: anionically polymerized poly-α-methylstyrene in toluene, and anionically polymerized polystyrene in toluene and also in decalin (at the θ temperature) by use of three types of viscometers: the Zimm-type and the Ubbelohde type with and without external hydrostatic pressure. They plotted $[\eta]_\gamma/[\eta]_0$ against log β. The curves showed that (i) the shear rate dependence of the intrinsic viscosity becomes marked as the solvent power increases, and (ii) for poly-α-methylstyrene in toluene, $[\eta]_\gamma/[\eta]_0$ of the sample having a low molecular weight drops faster than that of the polymer having a high molecular weight (Figure 4 of their paper). In order to explain the latter result, they took into account the rigidity of polymer chains in addition to the excluded volume effect as a cause for the non-Newtonian viscosity. However, the molecular weight dependence of the non-Newtonian viscosity observed in their work contradicts that of the present work. Their conclusion was derived exclusively from the data obtained with an Ubbelohde viscometer with external hydrostatic pressure.

Suzuki, *et al.*,[17] have investigated the non-Newtonian viscosities of the systems: fractionated polystyrene in four good or moderate solvent, *i.e.*, benzene, 1-chlorobutane, butanone, and Aroclor 1248 and in three poor solvents, *i.e.*, decalin, dioctyl phthalate, and cyclohexane by use of low shear capillary viscometers of the Maron-Belner type. Their work shows the same tendency as ours, but there is a little difference between both works. At and near the θ condition their experimental results show more pronounced non-Newtonian character than our experimental results do and the theory of Fixman predicts, while in good solvent their results show that the non-Newtonian viscosity does not depend so significantly on the excluded volume effect as our results show and the theory of Fixman predicts.

We shall now turn to a more detailed analysis of our experimental results. Figure 11 shows a plot of B against α_η^3, *i.e.*, the relation between the extent of the non-Newtonian viscosity and the excluded volume effect. The vertical lines attached to each circle indicate the magnitude of the experimental errors in determining the initial slope of the curve of $[\eta]_\gamma/[\eta]_0$ against β^2. The fairly large errors, which are inevitable with present day techniques of viscometry of dilute solutions,

(21) P. Flory, "Principles of Polymer Chemistry," Cornell University Press, Ithaca, N. Y., 1953, Chapter 8.

(22) S. Fujishige, *Rep. Textile Res. Inst. Jap.*, **73**, 13 (1964).

Table III: Results of Viscosity Measurements

Sample	$M \times 10^{-6}$	Solvent	$[\eta]_0$, ml/g	$[\eta]_\theta$, ml/g	α_η^3	B
L1	1.83	Benzene	372	111	3.35	0.047
L2	3.06	Benzene	540	143	3.77	0.052
L3	3.35	Benzene	656	150	4.33	0.069
L4	3.50	Benzene	735	153	4.80	0.080
F1	7.10	Benzene	1141	218	5.23	0.046
L4	3.50	Butanone	315	153	2.05	0.054
F2	3.98	Butanone	321	143[a]	2.24	0.030
L2	3.06	Cyclohexane θ			1	0
L3	3.35	Cyclohexane	151	150	1.01	0
L4	3.50	Cyclohexane	193	153	1.26	0
F1	7.10	Cyclohexane θ		218	1	0.005

[a] Observed value. From this value, the value of K_θ was calculated to be 7.2×10^{-2}, which is smaller by 12% than the value obtained by Kurata and Stockmayer, 8.2×10^{-2}. If our value is used, all the values of α_η^3 except sample F2 increase by 12%. If Figure 11 is replotted using our own value of K_θ, the experimental points will lie further near the theoretical line of Fixman.

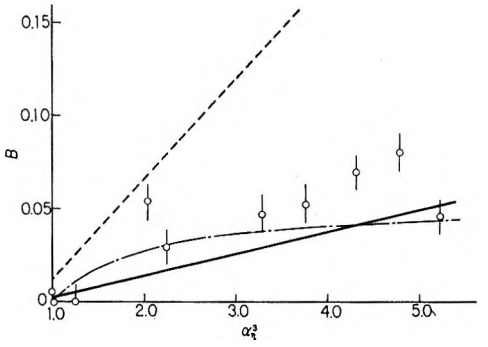

Figure 11. Comparison of the experimental and theoretical relations between the value of B and the extent of the excluded volume effect for polystyrene solutions. The dotted lines show Chikahisa's, the chain lines Subirana's, and the solid lines Fixman's theory, respectively. The vertical lines attached to each circle indicate the magnitude of experimental errors.

arise from uncertainties in determining the initial slope of the relation between $[\eta]_\dot{\gamma}/[\eta]_0$ and β^2. The solid line, dotted line, and chain line represent the Fixman, Chikahisa, and Subirana theory, respectively. Since the theoretical values of B were not given explicitly in their papers, we have calculated them by replotting their theoretical values of $[\eta]_\dot{\gamma}/[\eta]_0$ against β^2 for a given value of α_η^3. We may conclude that our experimental data are in rather better agreement with Fixman's and also with Subirana's theory than Chikahisa's one, so far as the coefficient B is concerned. We also conclude that the value of B at θ conditions is very small.

There have been some reports which describe the shear degradation of dilute solutions of polystyrene.[23] These indicate that when the solution is subjected to a large shearing force for a long time, a decrease in viscosity due to the scission of polymer chains evidently occurs, and the extent of the degradation differs depending upon the solvent, the butanone system suffering a larger effect than the benzene, toluene, or other systems. In the present work, no sign of a shear degradation in viscosity was detected for the benzene systems and also the F1-cyclohexane system for which the measurement was made at very high shear rates. A slight shear degradation occurs for the F2-butanone system measured with the tilting capillary viscometer no. 5, having a large flow time. However, this does not affect the above conclusion on the non-Newtonian viscosity.

The experimental results are qualitatively in agreement with the theories of Chikahisa, Subirana, and Fixman. The dependence of the coefficient B defined in eq 1 on the excluded volume effect, moreover, agrees semiquantitatively with Fixman's and Subirana's theory. At the θ temperature, a decrease of the intrinsic viscosity was not actually observed in the range of β below 1, but at larger values of β a slight decrease in the solution viscosity was observed. However, Subirana's theory gives no shear rate dependence of intrinsic viscosity at the θ temperature. Accordingly, it may be concluded that among these theories, Fixman's theory explains most adequately our experimental data, which were obtained using polystyrene with the limited range of the molecular weight under the limited solvent–temperature combinations. Since the non-Newtonian viscosity did not disappear at the θ condition, the non-Newtonian intrinsic viscosity cannot be attributed to the excluded volume effect alone. Therefore, it may be suitable to take into consideration the contribution of the hydrodynamic interaction to the non-Newtonian viscosity, because according to Fixman's theory at the θ temperature the non-Newtonian intrinsic viscosity is caused by the change of the hydrodynamic interaction. Although this contribution is difficult to be estimated definitely, it must be far smaller than that of the excluded volume effect.

(23) R. E. Moor and A. G. Parts, *Polymer*, 9, 52 (1968); R. E. Harrington and B. H. Zimm, *J. Phys. Chem.*, 69, 161 (1965).

The non-Newtonian viscosity of dilute solutions of flexible polymers is a very complex phenomenon which is affected by many contributing factors such as excluded volume effect, hydrodynamic interaction rigidity of polymer chains and so on. Therefore, it is difficult to assess definitely various contributing factors from our experimental results alone.

Acknowledgments. The authors wish to express their deep gratitude to Dr. S. Iwayanagi of the Institute of Physical and Chemical Research for many helpful discussions and suggestions during this work. The authors thank Professor M. Nagasawa of Nagoya University for supplying the fractionated polystyrene samples and Dr. Y. Chikahisa of Tokyo University of Agriculture and Technology for supplying the numerical results of Fixman's theory.

Infrared Spectra of Ground Graphite

by R. A. Friedel*

U. S. Bureau of Mines, Pittsburgh, Pennsylvania

and G. L. Carlson

Carnegie-Mellon University, Pittsburgh, Pennsylvania 15213 *(Received November 3, 1970)*

Publication costs assisted by the U. S. Bureau of Mines

The infrared spectrum of ground graphite has been observed. After very intense grinding two broad absorption bands appeared at 1587 and 1362 cm^{-1} and weak bands appeared at 830 and 2200 cm^{-1}; 1587 and 1362 cm^{-1} are practically the same frequencies found by Tuinstra and Koenig in Raman spectra of powdered graphite and various powdered carbons. A shift of about 20 cm^{-1} to higher frequencies was observed for the most intense infrared band as particle sizes decreased; a similar shift has been reported by Tuinstra and Koenig for Raman frequencies. Their Raman lines were obtained on crystalline graphites while the similar infrared bands were observed for noncrystalline graphite; thus both sets of bands probably originate in the "aromatic" structure of the graphite matrix, crystalline or noncrystalline.

Infrared investigations of some carbonaceous materials have not been possible in the past because of the intractability of these materials, *e.g.*, carbon blacks, coal chars, and activated carbons. Recently, Friedel and Hofer succeeded in obtaining an infrared spectrum of one of the most difficult substances, a coal-based activated carbon.[1] By the use of appropriate sample preparation and instrumental techniques a transmission spectrum of activated carbon was obtained for the first time. Extensive and efficient grinding were found to be important. Mattson, *et al.*, have published spectra of sorbates on activated carbon using the attentuated total reflectance (ATR) method.[2-4]

There are other carbonaceous materials, both more and less tractable than activated carbon; the literature contains infrared spectra of difficult carbonaceous materials such as pyrolytic chars,[5-8] carbon black,[9,10] and coal chars.[5,11,12] Coals should also be mentioned here though they are less difficult materials; it is possible to obtain good spectra of coals with absorption intensities up to 80% by the transmission method.[8,12-15] Until recently it has been difficult to obtain good spectra of coals by the ATR method. Various people over a period of years have tried; S. Polchlopek succeeded

(1) R. A. Friedel and L. J. E. Hofer, *J. Phys. Chem.*, **74**, 2921 (1970).

(2) J. S. Mattson, H. B. Mark, Jr., M. D. Malbin, W. J. Weber, and J. C. Crittenden, *J. Colloid. Interface Sci.*, **31**, 116 (1969).

(3) J. S. Mattson and H. B. Mark, Jr., *ibid.*, **31**, 131 (1969).

(4) J. S. Mattson and H. B. Mark, Jr., *Anal. Chem.*, **41**, 355 (1969).

(5) R. A. Friedel and M. G. Pelipetz, *J. Opt. Soc. Amer.*, **43**, 1051 (1953).

(6) R. A. Friedel, "Proceedings of the 4th Carbon Conference," S. Mrozowski, Ed., Pergamon Press, New York, N. Y., 1960, pp 321-336.

(7) R. A. Friedel, R. A. Durie, and Y. Shewchyk, *Carbon*, **5**, 559 (1968).

(8) J. K. Brown, *J. Chem. Soc.*, 744 (1955).

(9) V. A. Garten and D. E. Weiss, *Aust. J. Chem.*, **10**, 295 (1957).

(10) V. A. Garten and D. E. Weiss, "Proceedings of the 3rd Carbon Conference," S. Mrozowski, Ed., Pergamon Press, New York, N. Y., 1959, p 295.

(11) J. K. Brown, *J. Chem. Soc.*, 752 (1955).

(12) R. A. Friedel and J. A. Queiser, *Anal. Chem.*, **28** 22 (1956).

(13) C. G. Cannon and G. B. B. M. Sutherland, *Trans. Faraday Soc.*, **41**, 279 (1945).

(14) R. A. Friedel, *Brennst. Chem.*, **44**, 23 (1963).

(15) R. A. Friedel, "Applied Infrared Spectroscopy," D. N. Kendall, Ed., Reinhold Pub. Co., New York, N. Y., 1966, pp 319, 321.

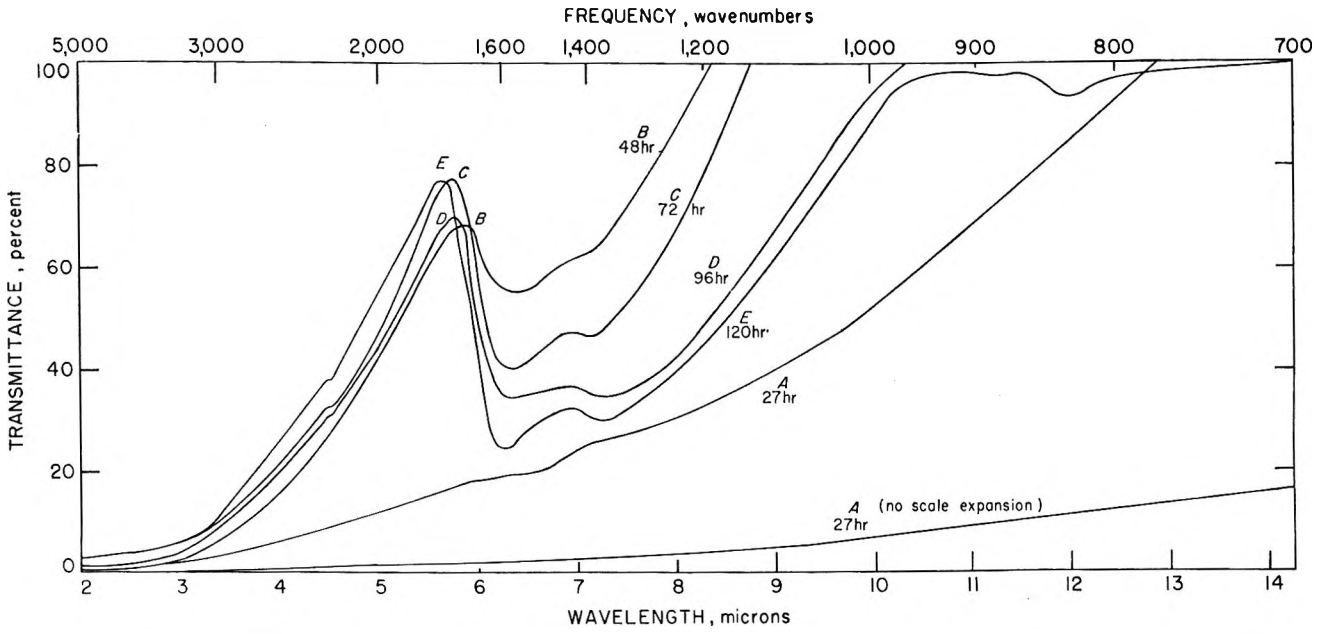

Figure 1. Spectral intensities of ground graphite increased with efficient grinding for: A, 27 hr; B, 48 hr; C, 72 hr; D, 96 hr; E, 120 hr. These spectra are on aliquots removed from the sample after grinding for the times indicated. All spectra are scale-expanded except the one indicated. KBr pellets were used.

in getting a weak ATR spectrum of a Pittsburgh bituminous coal (unpublished work), and Bent and Ladner obtained a spectrum from a solid piece of anthracite coal.[16] Of the anthracite samples investigated only the one was sufficiently flat to produce a spectrum, actually a partial spectrum. However, Mattson has demonstrated recently that a good spectrum of a Pittsburgh coal can be obtained through the use of ATR methods with modern infrared instruments having accurate scale-expansion systems (unpublished work). The ATR method is advantageous because of the simplicity of sample preparation, whereas the transmission method has the advantage of being applicable to very small samples.

Good spectra by transmission measurements on KBr pellets of various carbonaceous materials have been recorded successfully; next it seemed appropriate to attempt to obtain spectra of the most difficult carbonaceous substance, graphite. By means of exhaustive, efficient grinding it was possible to demonstrate that infrared spectra of ground graphite could be observed. The infrared absorption of graphite was first looked at by Cannon,[17] who investigated a thin mineral oil mull of graphite. He ascertained that absorption (and/or scatter) was essentially the same throughout a wide range of infrared frequencies. No spectral information was obtained from such data.

Later, attempts were made to obtain absorption spectra of graphite in the infrared (Friedel, unpublished work). Samples were prepared by rubbing powdered graphite on soft polyethylene which retained the graphite as a film; no specific infrared absorption was found. However, absorption and reflectance bands were found in the ultraviolet region on examination of powdered graphite on soft polyethylene.[18]

Infrared studies of polycrystalline graphite have been carried out by Foster and Howarth.[19] They determined refractive and absorption indices from 1 to 10 μ by the reflection method of Avery.[20] One absorption maximum of moderate intensity was observed at $\sim$1300 cm^{-1}; for reasons unknown, this frequency does not coincide with the frequencies of either of the two strong absorption bands observed in our spectra and discussed below.

Experimental Section

For the present investigation of possible absorption of graphite in the 4000–250-cm^{-1} infrared region it was decided to try the sample preparation technique that was successful with activated carbons, namely, very extensive and efficient grinding.[1] Partial spectra were obtained after grinding for 24 hr but for better development of the spectrum many more hours of grinding were required. As noted elsewhere, it was necessary to utilize a very small sample, as a large sample softens the blow of the small ball bearings used for grinding in a steel capsule.[1] It is obvious that much more extensive grinding would be required for graphite because of its good lubricating charac-

(16) R. Bent and W. R. Ladner, *Fuel*, **44**, 243 (1965).

(17) C. G. Cannon, *Nature*, **171**, 308 (1953).

(18) R. A. Friedel and H. L. Retcofsky, "Proceedings of the 5th Carbon Conference," Vol. II, S. Mrozowski, Ed., Pergamon Press, London, 1963, p 165.

(19) P. J. Foster and C. R. Howarth, *Carbon*, **6**, 719 (1968).

(20) D. G. Avery, *Proc. Roy. Soc., Ser. B*, **65** 1087 (1952).

teristics. Grinding for 72 hr developed a reasonably good infrared spectrum. Two broad bands were observed at 1565 and 1382 cm^{-1}. With continued grinding the two bands become stronger and sharper, as shown in Figure 1. Also, the frequencies shift slightly to 1587 and 1362 cm^{-1} (Table I). In addition to these two absorption bands of graphite there is a weak absorption band at 830 cm^{-1} and a combination band at 2200. The spectrum out to 250 cm^{-1} was investigated but no further absorption was observed.

Table I: Infrared and Raman Frequencies of Graphite

Raman	1575	1355		
Infrared	1587	1362	830 (w)	2200 (w)

Discussion of Results

The extensive grinding reduces the graphite sample to minute particle sizes on which useful infrared transmission measurements were obtained. The process works also for lamp black, for several activated carbons, and for carborundum.[21] The frequencies found for ground graphite are essentially the same as those found for similar carbons. By the criterion of X-ray diffraction patterns, it is apparent that the materials measured are not crystalline graphites. Under extensive grinding graphite loses many of the X-ray diffraction peaks that are characteristic of graphite.[22] However, this situation does not alter the fact that the infrared spectra obtained for ground graphite produce information concerning the molecular structures involved. Graphite is altered by the grinding but the disappearance of crystallinity does not mean that the carbon–carbon bondings in the original graphite are broken. The grinding operation does not introduce sufficient energy into the system to break many carbon–carbon bonds. Therefore it is considered that the infrared spectrum of graphite shown is indeed characteristic of the molecular structure of graphite.

These results are very similar to the laser–Raman results reported by Tuinstra and Koenig.[23] Their results indicate for ground graphite one intense scattering band at 1575 cm^{-1} and a weaker band at 1355 cm^{-1}. They assigned these frequencies to the E_{2g} and the A_{1g} modes respectively of crystalline graphite with D_{6h}^4 crystal symmetry. The two infrared bands that we find at about 1587 and 1362 cm^{-1} compare reasonably well with the Raman bands. Further, the infrared maximum of the strongest band shifts from 1565 to 1587 as particle sizes decrease with grinding. Tuinstra and Koenig found that a closely similar shift occurred in the Raman spectra with decreasing particle sizes. The infrared bands were obtained on ground graphite for which X-ray measurements indicate that the typical crystalline fine structure of graphite has disappeared. And yet, the frequencies observed are practically the same as those of the Raman bands. It would appear that the observed infrared and Raman spectra are not related to the crystallinity of graphite. Perhaps vibrations of the "aromatic" structure of graphite, crystalline or noncrystalline, are responsible for the observed spectra.

The weak infrared bands found at 830 and 2200 cm^{-1} are not reported for the Raman spectra. It is likely that the 2200 band is a combination band resulting from the 830- and 1362-cm^{-1} bands which total 2212 cm^{-1}. This value is reasonably close to the observed 2200 cm^{-1}. The 830-cm^{-1} band could be due to an aromatic impurity in graphite. If so, this would then remove the possibility of assigning the 2200-cm^{-1} band as a combination band.

(21) R. A. Friedel and L. J. E. Hofer, unpublished work.

(22) P. L. Walker, Jr., and S. B. Seeley, "Proceedings of the 3rd Carbon Conference," S. Mrozowski, Ed., Pergamon Press, New York, N. Y., 1959, p 481.

(23) F. Tuinstra and J. L. Koenig, *J. Chem. Phys.*, **53**, 1126 (1970).

A Thermodynamic Theory of Ion-Exchange Equilibria in Nonaqueous Solvents

by A. R. Gupta

Bhabha Atomic Research Centre, Chemistry Division, Trombay, Bombay -85, India *(Received November 30, 1970)*

Publication costs borne completely by The Journal of Physical Chemistry

Ion-exchange equilibria in nonaqueous and mixed solvents have been treated in a thermodynamically rigorous fashion. Using the concept of standard free energy of transfer of ions and resinate from the nonaqueous–mixed solvent to water, the thermodynamic equilibrium constants for exchange equilibria in nonaqueous–mixed solvents have been correlated with the equilibrium constants in aqueous systems. The free energies of transfer of the resinates have been formulated in terms of the free energies of swelling of resinates from dry monoionic forms of the resins to the equilibrium, a completely swollen state in the respective solvents. The equations developed for the mixed solvent systems have been applied to the available data in the literature on sodium–hydrogen exchange on Dowex 50WX-8 in methanol–water mixtures.

Ion-exchange equilibria in aqueous systems have been treated thermodynamically by considering them as reversible bimolecular reactions. In the earlier treatments on this basis, water activity terms and their variations were not included.[1,2] Later this problem was treated by Hogfeld,[3] Gaines and Thomas,[4] and Davidson and Argersinger[5] independently. A good review of these approaches has been given by Holm.[6] The treatment of Gaines and Thomas is most thermodynamically rigorous. Using this approach as a model, the problem of ion exchange in mixed solvents has been treated[7] in a semiempirical manner. In the present communication, the general problem of ion-exchange equilibria in nonaqueous solvents including mixed solvents has been considered in a thermodynamically rigorous fashion. An attempt has been made to treat all the solvent systems on the basis of a common set of standard states, so that a comparison among them is possible.

Pure Nonaqueous Solvents. The problem of ion-exchange equilibria in pure nonaqueous solvents, with reference to aqueous systems, is first considered. For simplicity, only uni-univalent exchanges have been treated.

For the ion-exchange equilibrium

$$AR + B^+ \rightleftharpoons BR + A^+ \qquad (A)$$

for every solvent, there exists an equilibrium constant

$$K_s = \frac{a_{BR}a_{A^+}}{a_{AR}a_{B^+}} \qquad (1)$$

where A and B are the univalent ions, R represents the resin matrix, a's denote the activities of the various components, and K_s is the equilibrium constant in solvent s. The activities of the ions are defined with reference to the state of infinite dilution in the particular solvent, *i.e.*, $\lim_{c\to 0} \gamma = 1$, where γ is the activity coefficient on the molal scale. The resinate activities are defined with reference to the standard state of the monoionic form of the resinate in equilibrium with an infinitely dilute solution of the corresponding salt in that solvent. In Gaines and Thomas' treatment of ion-exchange equilibria, the equilibrium constant can be written in terms of the chemical potentials as

$$RT \ln K_s = \mu^{os}_{AR} - \mu^{os}_{BR} + \mu^{os}_{B^+} - \mu^{os}_{A^+} \qquad (2)$$

A similar expression can be written for the aqueous system

$$RT \ln K_w = \mu^{ow}_{AR} - \mu^{ow}_{BR} + \mu^{ow}_{B^+} - \mu^{ow}_{A^+} \qquad (3)$$

Subtracting eq 3 from eq 2

$$RT \ln \frac{K_s}{K_w} = (\mu^{os}_{AR} - \mu^{ow}_{AR}) - (\mu^{os}_{BR} - \mu^{ow}_{BR}) + (\mu^{os}_{B^+} - \mu^{ow}_{B^+}) - (\mu^{os}_{A^+} - \mu^{ow}_{A^+}) = \Delta G_t^\circ(AR) - \Delta G_t^\circ(BR) + \Delta G_t^\circ(B^+) - \Delta G_t^\circ(A^+) \qquad (4)$$

The free energies of transfer are defined by the relation

$$\Delta G_t^\circ(i) = \mu^{os}_i - \mu^{ow}_i = RT \ln \gamma_i^*$$

The individual equilibrium constants K_s and K_w are given by the following expression for moderately cross-linked resins (more than 6% DVB resins), where the molar volume terms can be neglected[6]

(1) E. Ekedehl, E. Hogfeld, and L. G. Sillen, *Acta Chem. Scand.*, **4**, 556, 828 (1950).

(2) W. J. Argersinger, Jr., A. W. Davidson, and O. D. Bonner, *Trans. Kans. Acad. Sci.*, **53**, 404 (1950).

(3) E. Hogfeld, *Ark. Kemi*, **5**, 147 (1950).

(4) G. L. Gaines and H. C. Thomas, *J. Chem. Phys.*, **21**, 714 (1953).

(5) A. W. Davidson and W. J. Argersinger, Jr., *Ann. N. Y. Acad. Sci.*, **57**, 105 (1953).

(6) L. W. Holm, *Ark. Kemi*, **10**, 151 (1956).

(7) A. R. Gupta, *J. Phys. Chem.*, **69**, 341 (1965).

$$\ln K_w = \int_0^1 \ln K_a \, d N_{BR} + \int_{a_w(N_{BR}=0)}^{a_w(N_{BR}=1)} n_w \, d \ln a_w - \int_{a_w=1(N_{BR}=1)}^{a_w(N_{BR}=1)} n_w \, d \ln a_w + \int_{a_w=1(N_{BR}=0)}^{a_w(N_{BR}=0)} n_w \, d \ln a_w \quad (5)$$

where K_a is the selectivity coefficient (K_D) for reaction A corrected for the solution phase activity coefficients (K_D) being defined by

$$K_D = \frac{N_{BR} m_{A^+}}{N_{AR} m_{B^+}}$$

where N's are the equivalent fractions of the resin components, the m's are the molalities of the ions in the outside solution, and n_w is the number of moles of water associated with 1 eq of the exchanger. A similar expression can be written for K_s in terms of solvent activity terms a_s and n_s, the number of moles of solvent associated with 1 eq of the exchanger. The various terms in eq 5 are, in principle, accessible to experimental determination.[8,9] The left-hand side of eq 4 can, therefore, be evaluated from experimental data. The quantities ΔG_t^c for the ions are well defined and have been reported for many ions in different solvents.[10-12] The ΔG_t° terms for the resinates have not yet been defined in terms of experimentally obtainable quantities. These can be best understood in terms of the free energy changes occurring in the swelling[13,14] of the ion exchangers in the two solvents. For this purpose, the reference state of dry monoionic form of the resin is chosen for the resins. For the solvent vapor, the vapor over the pure solvent is taken as the reference state. When the resin in ionic form i is in equilibrium with pure water, the free energy of swelling is given by[13,14]

$${}^w\varphi_{sw}(iR) = -RT \int_{a_w=0}^{a_w=1} n_w \, d \ln a_w \quad (6)$$

where a_w and n_w have their usual meaning. Similarly the free energy of swelling of resin iR in the solvent s is

$${}^s\varphi_{sw}(iR) = -RT \int_{a_s=0}^{a_s=1} n_s \, d \ln a_s \quad (7)$$

As ${}^w\varphi_{sw}(iR)$ and ${}^s\varphi_{sw}(iR)$ are measured with reference to the same state of dry monoionic form of the resin, their difference gives the change in free energy in going from the equilibrium state of resin iR in solvents s to the equilibrium state of resin iR in water, *i.e.*, the free energy differences in the standard states of the resinates in the two solvents, as used in Gaines and Thomas treatment. Therefore

$${}^s\varphi_{sw}(iR) - {}^w\varphi_{sw}(iR) = \Delta G^\circ{}_t(iR) \quad (8)$$

Thus $\Delta G_t^\circ(iR)$ can be evaluated in terms of ${}^s\varphi_{sw}(iR)$ and ${}^w\varphi_{sw}(iR)$ with the help of eq 6 and 7. Substituting for these terms in eq 4, we get

$$\log K_s - \log K_w = \frac{\Delta G_t^\circ(B^+) - \Delta G_t^\circ(A^+)}{2.303RT} - \int_{a_s=0(N_{BR}=0)}^{a_s=1(N_{BR}=0)} n_s \, d \log a_s + \int_{a_w=0(N_{BR}=0)}^{a_w=1(N_{BR}=0)} n_w \, d \log a_w + \int_{a_s=0(N_{BR}=1)}^{a_s=1(N_{BR}=1)} n_s \, d \log a_s - \int_{a_w=0(N_{BR}=1)}^{a_w=1(N_{BR}=1)} n_w \, d \log a_w \quad (9)$$

Mixed Solvents. The case when one of the solvents is water, has been experimentally investigated by many workers.[15] The problem has also been treated theoretically in a semiempirical manner.[7] As the problem of ion exchange in mixed solvents is an important one it will now be treated in a more rigorous fashion.

The quantities pertaining to the mixed solvent containing an organic solvent and water will be denoted by the superscript "mix." Rewriting eq 4 for the mixed solvent

$$\log K_{mix} - \log K_w = \{\Delta^{mix}G_t^\circ(AR) - \Delta^{mix}G_t^\circ(BR) + \Delta^{mix}G_t^\circ(B^+) - \Delta^{mix}G_t^\circ(A^+)\}/2.303RT \quad (10)$$

Now K_{mix} represents the ion-exchange equilibrium constant referred to the standard states in the mixed solvent having N_{H_2O} mole fraction of water and N_s mole fraction of the nonaqueous solvent. As has been pointed out earlier,[7] Gaines and Thomas equations can be used for evaluating equilibrium constants in mixed solvents. $\Delta^{mix}G_t^\circ(i)$ terms have definite thermodynamic significance and have been determined for many ions in mixed solvents.[11] The free energy of transfer of the pure resinates from the mixed solvent to water, *i.e.*, $\Delta^{mix}G_t^\circ(iR)$, needs further analysis. Again for the resins, the reference state of the dry, monoionic form of the resin is chosen and for the component solvents, the pure solvents are taken as the reference

(8) M. R. Ghate, A. R. Gupta, and J. Shankar, *Indian J. Chem.*, **4**, 64 (1966).

(9) M. R. Ghate, A. R. Gupta, and J. Shankar, *ibid.*, **4**, 353 (1966).

(10) Roger G. Bates in "The Chemistry of Nonaqueous Solvents," J. J. Lagowski, Ed., Academic Press, New York, N. Y., 1966, pp 97-127.

(11) D. Feakins in "Physico-chemical Processes in Mixed Aqueous Solvents," F. Franks, Ed., Heinemann Educational Books Ltd., London, 1967, pp 71-89.

(12) H. Strehlow in "The Chemistry of Nonaqueous Solvents," J. J. Lagowski, Ed., Academic Press, New York, N. Y., 1966, p 152.

(13) G. E. Boyd and B. A. Soldano, *Z. Elektrochem.*, **57**, 162 (1953).

(14) G. V. Samsonov and V. A. Pasechnik, *Russ. Chem. Rev.*, **38** (7), 547 (1969).

(15) M. R. Ghate, A. R. Gupta, and J. Shankar, *Indian J. Chem.*, **3**, 286 (1965); M. R. Ghate, A. R. Gupta, and J. Shankar, *ibid.*, **5**, (1967); M. R. Ghate, A. R. Gupta, and J. Shankar, *ibid.*, **6**, 98 (1968). For other references see ref 7.

state. Let a'_s and a'_w denote the activity of solvent "s" and water in the mixture, respectively, and n_s and n_w the corresponding moles of solvent s and water absorbed by the resin iR when in equilibrium with the mixed solvent. The free energy of swelling, *i.e.*, the change in the free energy of the system when dry resin iR comes to equilibrium with the mixed solvent, can be expressed as

$$^{mix}\varphi_{sw} = -RT \int_{(a_w,a_s)=0}^{a'_w,a'_s} (n_w, n_s)\, d \ln (a_w, a_s)$$

This free energy change can be described in terms of the free energy changes in the following two steps. 1. Dry resin iR (one equivalent) absorbs n°_w moles of water at water activity $a_w = 1$, *i.e.*, pure water. 2. Organic solvent is gradually added maintaining the equilibrium between solvent and resinate, until the requisite composition of the solvent mixture (a_w, a_s) is reached. During this process resin absorbs n_s moles of the solvent and water attains its new equilibrium value of n_w moles.

As discussed earlier, the free energy in step 1 is given by $^{w}\varphi_{sw}$ (eq 6). In the second step, the free energy changes pertaining to the solvent and water can be treated separately as shown below.

In the absorption of the solvent, the free energy change is

$$-RT \int_{a_w=1,a_s=0}^{a'_w,a'_s} n_s\, d \ln a_s$$

The corresponding free energy change in the readjustment of the water content of the resinate is

$$-RT \int_{a_w=1,a_s=0}^{a'_w,a'_s} n_w\, d \ln a_w = +RT \int_{a'_w,a'_s}^{a_w=1,a_s=0} n_w\, d \ln a_w$$

The total free energy change in the second step, thus, becomes

$$\varphi(2) = -RT \int_{a_w=1,a_s=0}^{a'_w,a'_s} n_s\, d \ln a_s + RT \int_{a'_w,a'_s}^{a_w=1,a_s=0} n_w\, d \ln a_w$$

Therefore

$$^{mix}\varphi_{sw}(iR) = \varphi(1) + \varphi(2) = {}^{w}\varphi_{sw}(iR) + \varphi(2) \quad (11)$$

The free energy of transfer of resin iR from the mixed solvent to water is defined by

$$\Delta^{mix}G_t^\circ(iR) = {}^{mix}\varphi_{sw}(iR) - {}^{w}\varphi_{sw}(iR) = {}^{w}\varphi_{sw}(iR) + \varphi(2) - {}^{w}\varphi_{sw}(iR) = \varphi(2) = -RT \int_{a_w=1,a_s=0}^{a'_w,a'_s} n_s\, d \ln a_s + RT \int_{a'_w,a_s'}^{a_w=1,a_s=0} n_w\, d \ln a_w \quad (12)$$

Finally, putting the values of $\Delta^{mix}G_t^\circ(iR)$ in eq 10, we get

$$\log K_{mix} - \log K_w = \frac{\Delta^{mix}G_t^\circ(B^+) - \Delta^{mix}G_t^\circ(A^+)}{2.303RT} - \int_{a_w=1,a_s=0(N_{BR}=0)}^{a'_w,a'_s(N_{BR}=0)} n_s\, d \log a_s + \int_{a'_w,a'_s(N_{BR}=0)}^{a_w=1,a_s=0(N_{BR}=0)} n_w\, d \log a_w + \int_{a_w=1,a_s=0(N_{BR}=1)}^{a'_w,a'_s(N_{BR}=1)} n_s\, d \log a_s - \int_{a'_w,a'_s(N_{BR}=1)}^{a_w=1,a_s=0(N_{BR}=1)} n_w\, d \log a_w \quad (13)$$

A comparison of eq 9 for pure nonaqueous systems with eq 13 for mixed solvents shows that the two types of systems have different integration limits for the various integrals. This basic difference has some far reaching consequences. The integration limits in eq 9 imply that the absorption isotherms of resinates, needed for the evaluation of integrals, should be obtained by equilibrating the resinates with solutions in pure solvents, having different solvent activities. On the other hand, the absorption isotherms needed for the evaluation of various integrals in eq 13, should be obtained by equilibrating the resinates with mixed solvents, having different activities of the two components.

It is interesting to compare eq 13 with the semiempirical equation derived by the author earlier. For this purpose it is better to rearrange the equation to give $\log K_w$ in terms of $\log K_{mix}$. From the definition of free energy of transfer of an ion from solvent s to water

$$\mu^{os}_i - \mu^{ow}_i = \Delta G_t^\circ(i) = RT \ln \gamma^*_i$$

where γ^* is interpreted as an activity coefficient related to the free energy of transfer, $\Delta G_t^\circ(i)$. Writing $\Delta^{mix}G_t^\circ(i)$ in terms of γ^* in eq 13 and rearranging

$$\log K_w = \log K_{mix} + \log \frac{\gamma^*_{A^+}}{\gamma^*_{B^+}} + \text{other terms} \quad (14)$$

Here $\log K_w$ and $\log K_{mix}$ are given by expression 5 for the two solvents involved, *i.e.*, water and the mixture. In the earlier treatment γ^* values were incorporated in the first integral in the expression for $\log K_{mix}$. Therefore, the first four integrals in eq 10 of ref 7 are equivalent to $\log K_{mix} + \log (\gamma^*_{A^+}/\gamma^*_{B^+})$ of eq 14. Further comparison of these two equations reveals that the remaining two integrals of the former are the same as the two integrals involving n_w and a_w terms in the latter. Thus, eq 14 differs from the eq 10 (ref 7) in having two additional integrals involving n_s and a_s terms. In these mixed solvent systems, where the ion exchangers do not absorb one of the components (like the organic component in water–organic solvent mixtures), *i.e.*, n_s is equal to zero, eq 14 reduces to eq

10 (ref 7). Therefore, the latter equation is strictly applicable only to those systems where ion exchangers completely exclude the nonaqueous component. On the other hand, eq 14 is a general one and applicable to all mixed solvent systems. This equation can be used for computing log K_{mix} from log K_w and other parameters which can be determined by independent experiments. For this purpose, further simplification of eq 14 can be achieved for solutions of low ionic strength ($\leq 0.1\ M$). Under these conditions, as has been shown previously,[8,9] the last three integrals in the right-hand side of eq 5 defining log K_w or log K_{mix} are unimportant and log K_w or log K_{mix} is given by the simple expression

$$\log K_w \text{ (or } \log K_{mix}) = \int_0^1 \log {}^{w}K_a \text{ (or } \log {}^{mix}K_a)\, dN_{BR}$$

Using this simplification one can rewrite eq 14 for computing log K_{mix} as follows

$$\log K_{mix} = \int_0^1 \log {}^{mix}K_a\, dN_{BR} =$$

$$\int_0^1 \log {}^{mix}K_D\, dN_{BR} + 2 \log \frac{{}^{mix}\gamma_{A^+}}{{}^{mix}\gamma_{B^+}} =$$

$$\log K_w - \log \frac{\gamma^*_{A^+}}{\gamma^*_{B^+}} - \int_{\substack{a_s=0\ (N_{BR}=0)\\ a_w=1}}^{\substack{a_w=a'_w\\ a_s=a'_s(N_{BR}=0)}} n_s\, d \log a_s +$$

$$\int_{\substack{a_w=a'_w(N_{BR}=0)\\ a_s=a'_s}}^{\substack{a_s=0\\ a_w=1(N_{BR}=0)}} n_w\, d \log a_w +$$

$$\int_{\substack{a_s=0(N_{BR}=1)\\ a_w=1}}^{\substack{a_w=a'_w\\ a_s=a'_s(N_{BR}=1)}} n_s\, d \log a_s -$$

$$\int_{\substack{a_w=a'_w(N_{BR}=1)\\ a_s=a'_s}}^{\substack{a_s=0\\ a_w=1(N_{BR}=1)}} n_w\, d \log a_w \quad (15)$$

Application of Eq 15. In the numerous studies reported in the literature on ion exchange in mixed solvents, the swelling data needed for the evaluation of various integrals in eq 15 have not been recorded. However, Starobinets, Novitskaya, and Sevostyanova[16] have recently published their results on Na/H exchange on Dowex 50 WX_8 in methanol–water mixtures, which includes the swelling data on sodium and hydrogen forms of the exchanger in the various solvent mixtures. These workers used expt 12 of ref 7 (valid for ionic strength $\leq 0.1\ M$) for calculating log K_{mix}. These calculated value of log K_{mix} differed from the experimentally observed values by an order of magnitude. They had ignored the 2 log $({}^{mix}\gamma_{H^+}/{}^{mix}\gamma_{Na^+})$ term in their computation, which is not permissible as this term has significant values in methanol–water mixtures. All the same, their work emphasizes the importance of integrals involving n_s and a_s terms. Their data have been used for computing log K_{mix} by use of eq 15. As they have reported the experimental values of the integral $\int_0^1 \log {}^{mix}K_D\, dN_{BR}$, the same has been computed here, *i.e.*, log ${}^{mix}\gamma_i$ term has been taken on the right-hand side of eq 15.

The activity coefficients of NaCl and HCl in methanol–water mixtures at an ionic strength of 0.1 M (${}^{mix}\gamma_i$ terms) have been obtained from the data of Akerlof.[17] As the value of the activity coefficients of the NaCl were not reported at this molality, they were obtained by interpolation using the data at 0.05, 0.2, and 0.5 M solutions. The values of the integrals involving water activity terms have been tabulated by Starobinets, *et al.*,[16] in their paper. The values of $\gamma^*_{H^+}$ and $\gamma^*_{Na^+}$ for various methanol–water mixtures have been reported by Akerlof.[17] The same values have been used here and were apparently used by the Russian workers (this could be checked by an analysis of their data). The evaluation of integrals involving a_s and n_s poses a problem as the limits of integration are from $a_s = 0$ ($\log a_s = -\infty$) to $a_s = a'_s$. This difficulty was circumvented by extrapolating the plots of n_s *vs.* log a_s to values of $n_s = 0$. These plots were constructed using the reported values of n_s for the hydrogen and sodium form of resinates for various water–methanol mixtures. The activity of methanol in these solvent compositions was obtained from the data of Butler, *et al.*[18] The values of the two integrals involving n_s and a_s, were computed by graphical integration of the plots of n_s *vs.* log a_s within the appropriate limits for the various mixtures. The relevant data are shown in Table I. All the quantities are thus available for the computation of log K_{mix} by use of eq 15. The calculated values of log K_{mix} and the corresponding observed values[16] are also given in Table I. The agreement between the values of log K_{mix} computed on the basis of present thermodynamic approach and the observed ones, at low values of N_s, is more than satisfactory. At larger values of N_s, the computed values show larger deviations from the observed ones. Considering the uncertainties in the values of various quantities used in this computation, this is not surprising. The difficulties in the experimental determination of γ^* or ΔG_t°(i) and uncertainties involved in their reported values, have been pointed out by Strehlow[19] in a general way. The uncertainty in the value of γ^* increases with its intrinsic value. As γ^* for both HCl and NaCl increases with methanol content, the reported values of γ^* at high values of N_s are unreliable to the same extent. Thus, the larger deviations in the computed values of

(16) G. L. Starobinets, L. V. Novitskaya, and L. I. Sevostyanova, *Zh. Fiz. Khim.*, **42** (5), 1098 (1968).

(17) G. Akerlof, *J. Amer. Chem. Soc.*, **52**, 2353 (1930).

(18) J. A. V. Butler, D. V. Thomson, and W. H. Mailennan, *J. Chem. Soc.*, 674 (1933).

(19) Reference 12, pp 145, 146.

Table I: Evaluation of Methanol Activity Integrals in Eq 15 for Na/H Exchange on Dowex 50WX-8 and Computed and Observed Values of Log K_{mix}

N_s	a_s	n_s(HR)[b]	n_s(NaR)[b]	Difference[a] in the value of integral	$^{mix}\gamma_{NaCl}$	$^{mix}\gamma_{HCl}$	log K_{mix} (eq 15)	log K_{mix}[b] (obsd)
0.1	0.148	1.2	0.66	−0.093	0.735	0.768	0.46	0.36
0.2	0.282	1.8	1.10	−0.256	0.675	0.735	0.64	0.62
0.3	0.393	2.4	1.54	−0.374	0.625	0.705	0.84	0.78
0.4	0.476	2.8	1.76	−0.459	0.57	0.676	0.97	0.89
0.5	0.555	3.2	2.00	−0.532	0.518	0.653	1.30	0.98
0.6	0.636	3.4	2.07	−0.605	0.455	0.62	1.56	1.07
0.7	0.740	3.6	2.07	−0.680	0.415	0.585	1.69	1.16

[a] Values tabulated are for

$$-\int_{\substack{a_s=0(N_{NaR}=0)\\ a_w=1}}^{a_w=a'_w,\ a_s=a'_s(N_{NaR}=0)} n_s \, d \log a_s + \int_{\substack{a_s=0(N_{NaR}=1)\\ a_w=1}}^{a_w=a'_w,\ a_s=a'_s(N_{NaR}=1)} n_s \, d \log a_s$$

[b] Taken from ref 16.

log K_{mix} compared to the observed ones may arise due to these uncertainties in the values, and the data in Table I can be taken in a general way as an experimental verification of eq 15.

In conclusion, it should be emphasized that eq 9 and 13 are exact equations and have been derived thermodynamically in a rigorous fashion. Equation 9 relates the ion exchange in a pure nonaqueous solvent to ion exchange in aqueous medium. Equation 13 does the same correlation for ion exchange in mixed solvent systems, one solvent being water. Here for convenience the aqueous system has been chosen as the reference system, primarily because most of the thermodynamic data, like standard free energy of transfer of an ion from one solvent to another, are available with reference to aqueous medium. In principle, any solvent could have been chosen as the reference solvent. These equations thermodynamically describe the ion-exchange systems in any solvent, pure or mixed, in terms of the ion exchange in aqueous or any other chosen medium.

Acknowledgment. The author expresses his sincere thanks to Dr. J. Shankar for his encouragement and keen interest during the course of this investigation.

Spectroscopic Determination of Association Constants of Primary Aromatic Amines with Dimethyl Sulfoxide and Hexamethylphosphorotriamide[1]

by Christian Madec, Jacques Lauransan, and Pierre Saumagne*

Laboratoires de Thermodynamique Chimique et de Spectrochimie Moléculaire, Faculté des Sciences, 29N-Brest, France
(Received September 21, 1970)

Publication costs assisted by Université de Bretagne Occidentale, Brest

The formation constants of 1–1 complexes of substituted anilines, naphthylamines, aminopyridines, and aminopyrimidines with the proton acceptors DMSO and HMPT were determined at room temperature by infrared spectroscopy. These primary aromatic amines are classified according to their proton-donor power; the nature and position of the substituents are discussed and correlations are established between the values of the association constants and some parameters.

I. Introduction

Hydrogen-bonded complexes in which aromatic amines act as proton donors have been studied extensively in recent years.[2-6] It is well known that the infrared spectra of the stretching vibrations of the NH_2 group of primary aromatic amines with proton acceptors demonstrate the presence of 1–1 and 1–2 complexes in which one of the donor molecules is bonded to one or two acceptor molecules, respectively.

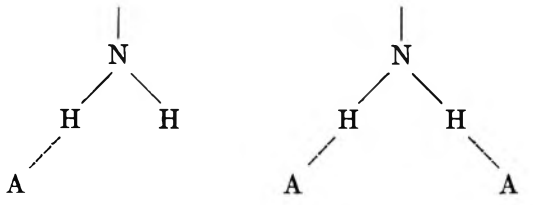

1–1 complex 1–2 complex

The work reported in this paper was undertaken in order to obtain the association constant of 1–1 complexes between various primary aromatic amines (substituted anilines, naphthylamines, aminopyridines, and aminopyrimidines) and the proton acceptors dimethyl sulfoxide (DMSO) and hexamethylphosphorotriamide (HMPT) in dilute carbon tetrachloride solutions at 25°.

The association between donor D, acceptor A, and complex C can be represented by the equilibrium A + D $\rightleftharpoons$ C, if only 1–1 complexes are present.

The association constant K, for such a system is given by

$$K = \frac{C_C}{C_D C_A} = \frac{C_C}{(C_D^\circ - C_C)(C_A^\circ - C_C)}$$

where C_D° and C_A° are the initial concentrations of donor and acceptor, and C_D, C_A, and C_C are the equilibrium concentrations (in moles per liter). (In dilute solutions, activities are replaced by the corresponding concentrations.)

Because of the various overlapping bands of donors and molecular complexes in the infrared spectrum between 3200 and 3600 cm^{-1}, equilibrium concentrations cannot be obtained directly by application of the Beer–Lambert law.

Therefore, the Kagarise method was used.[7] The absorbance per unit length is plotted as a function of C_C, the complex concentration, calculated from initial concentrations C_D° and C_A° and from an arbitrary value for K. For a constant value C_D°, when the arbitrary value of K is equal to the true equilibrium constant we obtain a linear correlation between D/l and C_C (as shown in Figure 1).[8] This method is applicable for any relative values of C_D° and C_A°. When $C_A^\circ \gg C_D^\circ$, the Basu–Chandra method was also used.[9-11]

II. Experimental Section

All spectra were obtained with a Perkin-Elmer 225 spectrophotometer. The spectral slit width was ap-

(1) Part of "Thèse de 3ème cycle" of C. Madec, Brest, 1970.

(2) K. B. Whetsel and J. H. Lady, *J. Phys. Chem.*, **69**, 1596 (1965).

(3) K. B. Whetsel and J. H. Lady, *ibid.*, **71**, 1421 (1967).

(4) J. Lauransan, P. Pineau, and J. Lascombe, *J. Chim. Phys.*, **63**, 635 (1966).

(5) J. Lauransan and P. Pineau, *ibid.*, **65**, 1937 (1968).

(6) S. Nishimura and N. C. Li, *J. Phys. Chem.*, **72**, 2908 (1968).

(7) R. E. Kagarise, *Spectrochim. Acta*, **19**, 629 (1963).

(8) $D/l = \epsilon_D(C_D^\circ - C_C) + \epsilon_C C_C$, where ϵ_D and ϵ_C are the molar absorptivities of donor D and complex C and l is the optical path length in centimeters.

(9) B. B. Bhowmik and S. Basu, *Trans. Faraday Soc.*, **58**, 48 (1962).

(10) A. K. Chandra and S. Basu, *ibid.*, **56**, 632 (1960).

(11) A. B. Sannigrahi and A. K. Chandra, *J. Phys. Chem.*, **67**, 1106 (1963).

Table I: Association Constants of Some Primary Aromatic Amines with Dimethyl Sulfoxide (DMSO) and Hexamethylphosphorotriamide (HMPT) in Carbon Tetrachloride Solution at 25°

No. of compound	Compound	DMSO K, l. mol^{-1}	DMSO $\Delta\nu_1$, cm^{-1}	HMPT K, l. mol^{-1}	HMPT $\Delta\nu_1$, cm^{-1}	$\nu_2(NH_2)$, cm^{-1}	$\nu_1(NH_2)$, cm^{-1}
1	Aniline	2.5	44	7	66	3482	3396
2	2-Nitroaniline	11	76	35	112	3523	3400
3	3-Nitroaniline	15	67	65	90	3497	3407
4	4-Nitroaniline	22.5	76	85	99	3509	3416
5	4-Bromoaniline	4.5[a]	55	14	76	3488	3401
6	2-Nitro-4-chloroaniline	30	81	130	116	3522	3400
7	2-Chloro-4-nitroaniline	35	87	140	114	3516	3414
8	2-Aminopyridine	5	61	18	88	3511	3409
9	3-Aminopyridine	8	54	27.5	76	3485	3398
10	4-Aminopyridine	20	65	65	90	3509	3415
11	2-Aminopyrimidine	2.5	110	9	130	3543	3430
12	4-Aminopyrimidine			40	117	3537	3425
13	5-Aminopyrimidine			50	88	3487	3400
14	α-Naphthylamine	5	44			3477	3395
15	β-Naphthylamine	8	49			3484	3397

[a] Calculated by Lauransan.[5]

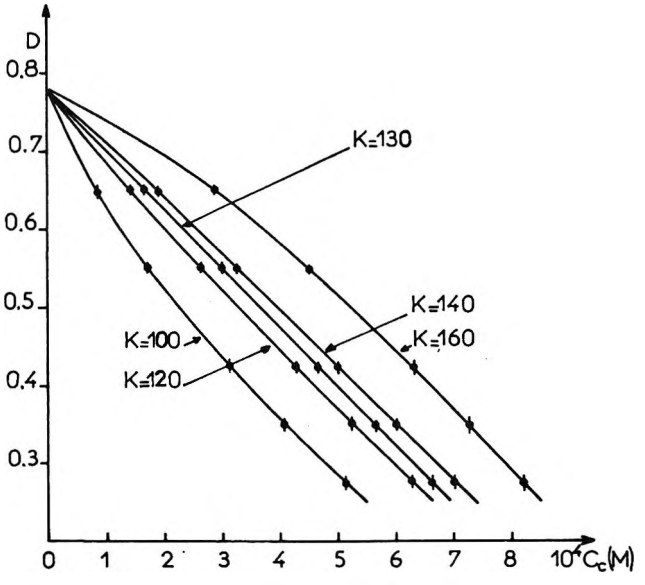

Figure 1. Evaluation by Kagarise method of the association constant of the 2-nitro-4-chloroaniline–HMPT system in carbon tetrachloride solution at 25°. D = absorbance of $\nu_1(NH_2)$ at 3400 cm^{-1}. The uncertainty in each value is represented by a vertical line. $C_D° = 7.9 \times 10^{-4}$ M; $6.5 \times 10^{-3} M < C_A° < 4 \times 10^{-2} M$; l = 5 cm; the assumed value of K is 130 ± 10 l. mol^{-1}.

proximately 1 cm^{-1}. The wave number precision was about 1 or 2 cm^{-1} depending on band shapes, while the precision of measured absorbance was about 1%.

Because of the weak solubility of amines in carbon tetrachloride, cells of 3- or 5-cm path length with CaF_2 windows were used.

The amines were commercial products from Prolabo, Aldrich, and Eastman Kodak; the aminopyrimidines were kindly provided by Mr. P. Dizabo.

DMSO was obtained from Laboratoires du Bois de Boulogne; HMPT, pyridine, and CCl_4, RP or "spectroscopic" grade, were Prolabo products. All solvents were dried by storing over Linde 4A molecular sieves and manipulated in a drybox to avoid atmospheric moisture.

III. Results

In each case a series of ternary mixtures consisting of amine, acceptor, and carbon tetrachloride, was prepared. The amine concentration was maintained at a constant low value (about 10^{-3} M). The acceptor concentration which was always larger than that of the donor, was varied between 10^{-1} and 10^{-2} M. Under these conditions self-association of the amine is not observed, while the acceptor concentrations were chosen to avoid formation of 1–2 complexes, as confirmed by the infrared spectra.

The determinations of the various constants were made by studying either the absorbances of the $\nu_1(NH_2)$ bands or those of $[\nu_1(NH_2)]_{1-1}$.[12] The precision in the determination of absorbances of donor bands is often reduced by the presence of absorptions due to the acceptors. However, in some cases it was confirmed that the constants obtained from measurements of $\nu_1(NH_2)$ or $[\nu_1(NH_2)]_{1-1}$ are equal. The Kagarise determinations are illustrated by the example of Figure 1. This graph allows the determination of uncertainty in the value of the constant K of about 10%. For any donor–acceptor mixture the equilibrium constant, calculated using the Basu–Chandra method, is in good agreement with that obtained by the Kagarise method.

(12) $\nu_1(NH_2)$ is the symmetrical stretching vibration of the free amine and $[\nu_1(NH_2)]_{1-1}$ the symmetrical stretching vibration of the 1–1 complex.

The experimental results are summarized in Table I. For each amine the frequencies of the $\nu_1(NH_2)$ and $\nu_3(NH_2)$, symmetric and antisymmetric stretching vibrations are listed as well as the value of the frequency shifts of the symmetric stretching vibration, $\Delta\nu = \nu_1(NH_2) - [\nu_1(NH_2)]_{1-1}$ for each complex. The association constants obtained with HMPT are always approximately four times larger than those obtained with DMSO. Among the various acceptors generally studied, these two are among the strongest.

IV. Discussion

The results obtained in the present work are compared with those reported for related hydrogen-bonded systems. The influence of substituents on the acidity of amines is discussed, and correlations between the values of association constants and other physicochemical quantities are established.

1. Comparison with Other Proton Donors. In Table II are reported the values of association constants, in liters per mole, between several proton donors and DMSO. The comparison between our results (Table I) and those of Table II places the ability of the NH_2 group to form hydrogen bonds with DMSO between that of chloroform and alcohols. Hence, from the values of association constants, we obtain the following order of proton donors by increasing acidity:[13-15] chloroform < aromatic amines, pyrrole and alcohols < phenols. This classification can be changed by the presence of substituents.

Table II: Association Constants between Some Proton Donors and DMSO in Carbon Tetrachloride Solution at 25°

Compound	K, l. mol^{-1}
α-Naphthol	275[a]
Phenol	188.5,[a] 230[b]
Indole	21[a]
Pyrrole	12.3,[a] 15.6[c]
Benzylic alcohol	15[a]
Heptyl alcohol	9[a]
Butyl alcohol	9[a]
Chloroform	3.2 (mol fract)$^{-1}$ [d]

[a] J. P. Leicknam, Thesis, Paris, 1966. [b] T. Gramstad, *Spectrochim. Acta*, **19**, 829 (1963). [c] F. Cruege, 3rd cycle Thesis, Bordeaux, 1963. [d] Calculated from nmr studies of binary mixtures [W.-C. Lin and S.-J. Tsay, *J. Phys. Chem.*, **74**, 1037 (1970)].

2. Effect of Substituents on the Aniline Acidity. a. Nature of Substituent. The results of Table I show that *p*-bromoaniline and *p*-nitroaniline are more acidic than aniline. Indeed these electron-withdrawing substituents discharge the nitrogen atom and increase the acidity of the NH_2 group, the charge density on the nitrogen atom varying from 1.729 for aniline to 1.694 for *p*-chloroaniline, whose acidity is equal to that of *p*-bromoaniline,[4] to 1.531 for the *p*-nitroaniline.[16] On the other hand, an electron-donating substituent decreases the acidity of the amine; this effect has been shown by Lauransan.[4]

b. Position of Substituent. The association constants of the three nitroanilines, ortho, meta, and para, with DMSO are 11, 15, and 22.5 l. mol^{-1}, respectively. This order is the same as that of the melting points (71.5, 112.5, and 147.8°) and the decrease in the solubility of these amines in carbon tetrachloride.

In *p*-nitroaniline, the contribution of the mesomeric effect +M of the amino group and −M of the nitro group decreases the charge density of the nitrogen atom the NH_2 group and increases the acidity of this amine. As this type of resonance is weaker in the meta compound, the mesomeric effect is transmitted with more difficulty and this compound is less acidic. The charge density of the nitrogen atom confirms this result, being 1.651 and 1.531 for the *m*- and *p*-nitroanilines, respectively. The same calculations give a value of 1.502 for the nitrogen charge density in *o*-nitroaniline. This results seems to be in opposition to the value of the association constant. In this compound the influence of the ortho substituent is anomalous and will now be discussed.

c. Ortho Compounds. In these compounds interaction between one hydrogen atom of the NH_2 group and the neighboring substituent have been considered. For these amines, the stretching frequencies $\nu_3(NH_2)$ are raised and the differences $\nu_3(NH_2) - \nu_1(NH_2)$ are increased, in comparison with the corresponding para-substituted anilines (see Table I). Recently Dyall[17,18] has assumed an intramolecular bond between one hydrogen atom of the NH_2 group and one oxygen atom of the NO_2 group in *o*-nitroaniline. This intramolecular bond decreases the amine acidity. It was established by studying $\nu_3(NH_2)$ and $\nu_1(NH_2)$ frequencies of nitroanilines in various proton acceptor solutions that there were 1–2 complexes for the *m*- and *p*-nitroanilines, whereas there is only formation of the 1–1 complex for *o*-nitroaniline.[19]

N-Methyl-2-nitroaniline was studied in carbon tetrachloride solution with weak DMSO concentrations ($C_A^\circ < 10^{-1}$ *M*). Under these conditions association is not observed. We assume that the intramolecular

(13) The values of the association constants of amide–DMSO systems can be compared with the result of Table II: rhodanine, K = 168 l. mol^{-1}; succinimide, K = 65 l. mol^{-1}; maleimide, K = 60 l. mol^{-1}.[14,15]

(14) L. Le Gall, J. Lauransan, and P. Saumagne, *J. Chim. Phys.*, **66**, 650 (1969).

(15) L. Le Gall, A. Le Narvor, J. Lauransan, and P. Saumagne, *C. R. Acad. Sci. Paris*, **268**, 1285 (1969).

(16) B. R. Lynch, *Tetrahedron Lett.*, **17**, 1357 (1969).

(17) L. K. Dyall, *Spectrochim. Acta*, **25**, 1423 (1969).

(18) L. K. Dyall, *ibid.*, **25**, 1727 (1969).

(19) J. Lauransan, Thesis, Bordeaux, 1967.

bond prevents association between the hydrogen atom and the oxygen atom of DMSO. Therefore, in DMSO Dyall[20] supposes that the hydrogen atom is bonded simultaneously to the substituent and the acceptor. The ortho substituent decreases the amine reactivity, which accounts for the fact that the association constant of *o*-nitroaniline with DMSO is weaker than those of the meta and para isomers. This weaker reactivity of ortho compounds has also been observed by Pineau[21] for chlorophenols.

d. Comparison of the Acidity of 2-Chloro-4-Nitro- and 2-Nitro-4-chloroanilines. Our results (Table I) show that two electron-withdrawing substituents strongly increase the acidity of NH_2 group. In these compounds an interaction between one hydrogen atom of the NH_2 group and the ortho substituent is possible. This interaction is weaker in compound A than in compound B because of the different hydrogen-acceptor

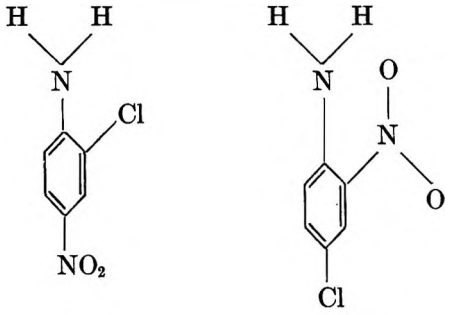

A B

center distances. This observation can explain the larger acidity of 2-chloro-4-nitroaniline.

e. Correlation between the Association Constant and the Hammett σ Parameter. It is well known that in aromatic series the Hammett σ constant characterizes the electronic effect of a substituent. The value of σ depends on the nature and position of the substituent.

Thus we have plotted log K as a function of σ (Figure 2[22]) for the substituted aniline–HMPT systems. The correlation obtained is reasonably good. Therefore the Hammett relations are suitable for describing complexation in nonionizing solvents. Similar correlations have been recently established for the substituted phenol–pyridine systems.[23,24]

3. Acidity of Naphthylamines, Aminopyridines, and Aminopyrimidines. The acidity of these amines is compared to that of aniline and the influence of the position of the NH_2 group on the acidity of aminopyridines and aminopyrimidines is discussed.

a. Naphthylamines. The acidity of these amines is somewhat larger than that of aniline (Table I). The conjugation of the lone pair of electrons of the nitrogen atom with the π electrons of the aromatic rings seems to be increased slightly.

b. Aminopyridines. The results of Table I show that the endocyclic nitrogen atom has qualitatively the same effect as an electron-withdrawing substituent

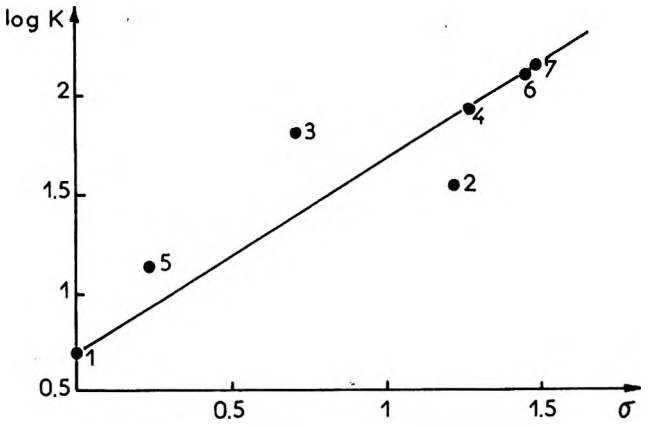

Figure 2. Plot of log K *vs.* σ (from ref 22) for substituted aniline–HMPT systems. Numbers correspond to the donors listed in Table I.

(NO_2, for instance). The order of the acidity of these amines is the same as that presented for the nitroanilines: 4-aminopyridine is more acidic than 3-aminopyridine, in good agreement with the values of the charge density of the exocyclic nitrogen atom (see Figure 3).[25] As in *o*-nitroaniline, the stretching frequency $\nu_3(NH_2)$ is raised and the difference $\nu_3(NH_2) - \nu_1(NH_2)$ is larger for 2-aminopyridine, by comparison with 4-aminopyridine (Table I). The decreasing value of the association constant of compound IV (Figure 3) can be explained by an interaction between a hydrogen atom of the NH_2 group and the lone pair of electrons of the endocyclic nitrogen atom. We note that the three isomers become more acidic as their dipole moments increase in the order 3.04, 3.12, and 3.95 D for compounds IV, III, and II, respectively (values were determined in benzene solution[26]).

c. Aminopyrimidines. The tendency for these amines to form hydrogen-bonded systems with a proton acceptor has been studied qualitatively by Jaque-Lafaix.[27] The values of the association constants with HMPT confirm her conclusion that the 4-amino- and 5-aminopyrimidines have an acidity of same magnitude, larger than those of 2-aminopyrimidine and aniline. For each aminopyrimidine the influence of the relative position of the NH_2 group is discussed by comparison with the corresponding aminopyridines.

i. 5-Aminopyrimidine (Compound VI). The presence of the two endocyclic nitrogen atoms in positions

(20) L. K. Dyall, *Spectrochim. Acta*, 22, 467 (1966).

(21) P. Pineau, Thesis, Bordeaux, 1961.

(22) R. W. Taft, Jr., "Steric Effects in Organic Chemistry," M. S. Newmann, Ed., Wiley, New York, N. Y., 1956, pp 571–619.

(23) T. Zeegers-Huyskens, Thesis, Louvain, 1969.

(24) J. Rubin, B. Z. Zenkowski, and G. S. Panson, *J. Phys. Chem.*, 68, 1601 (1964).

(25) S. F. Mason, *J. Chem. Soc.*, 3619 (1958).

(26) J. Barassin and H. Lumbroso, *Bull. Soc. Chim. Fr.*, 492 (1964).

(27) A. Jaque-Lafaix, A. Burneau, and M. L. Josien, *J. Chim. Phys.*, 65, 345 (1968).

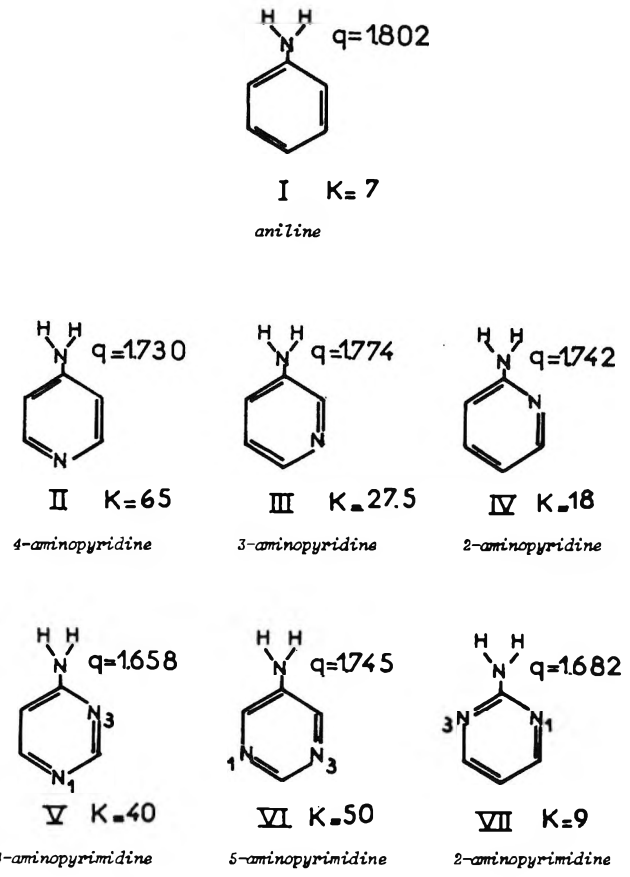

Figure 3. Values of the charge density of the exocyclic nitrogen atom of aniline, aminopyridines, and aminopyrimidines (calculated by Mason[26]) and association constants with HMPT (in l. mol^{-1}).

1 and 3 increases the acidity of this amine. The association constant with HMPT is approximatively twice that of 3-aminopyridine (compound III). This result is in good agreement with the values of charge density of the exocyclic nitrogen atoms (Figure 3).

ii. 4-Aminopyrimidine (Compound V). As in 4-aminopyridine (compound II) the presence of the 1-nitrogen atom increases the acidity of this amine by comparison with aniline, but this effect is decreased because of interaction of hydrogen atom of the NH_2 group with the lone pair of electrons of the 3-nitrogen atom as in 2-aminopyridine (compound IV). Here we can make the same comment about $\nu_3(NH_2) - \nu_1(NH_2)$ as in the case of the nitroanilines and the aminopyridines (Table I). The compound 4-aminopyrimidine is less acidic than 4-aminopyridine.

iii. 2-Aminopyrimidine (Compound VII). The reactivity of this amine is strongly decreased because of the interaction between the hydrogen atoms and the two nitrogen atoms 1 and 3. This effect is more important than in 2-aminopyridine (compound IV); the association constant with HMPT is twice as weak for 2-aminopyrimidine as for 2-aminopyridine.

As in aminopyridines, we note that the acidity of the three isomers increases with their dipole moments,

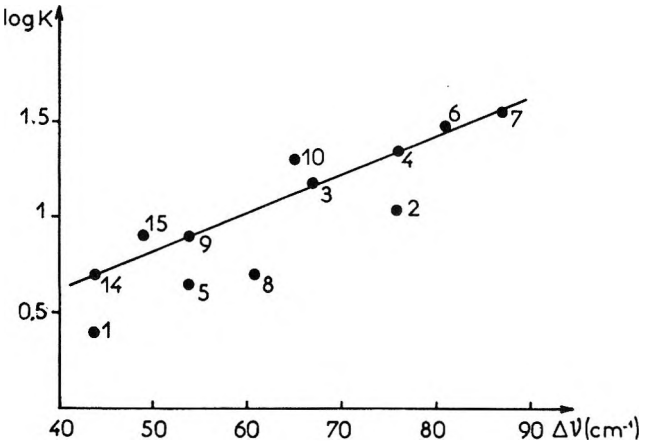

Figure 4. Plot of log K *vs.* $\Delta\nu$ for amine–DMSO systems. Numbers correspond to the donors listed in Table I.

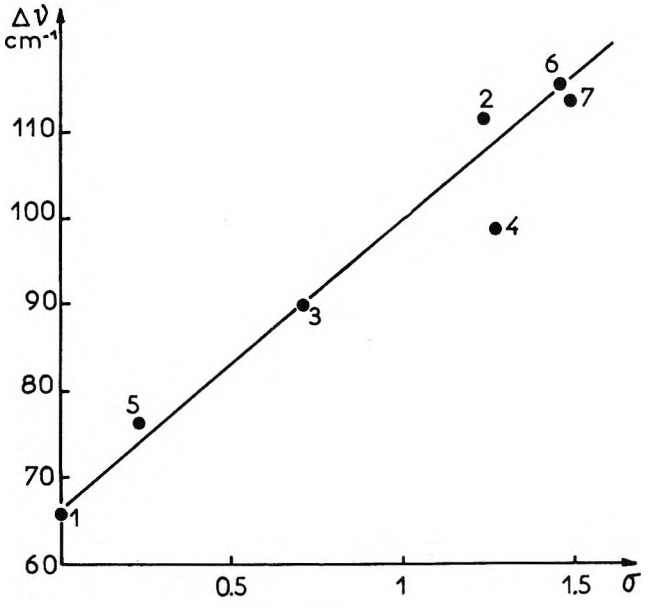

Figure 5. Plot of $\Delta\nu$ *vs.* σ for substituted aniline–HMPT systems. Numbers correspond to the donors listed in Table I.

which are 0.827, 2.623, and 2.625 D for compounds VII, V, and VI (values calculated by Kwiatkowski[28]), respectively. We can conclude that the effect of an endocyclic nitrogen atom ortho to the NH_2 group is to decrease the value of the association constant. This value is not, then, in agreement with the charge density calculated for the exocyclic nitrogen atom.

4. Correlation between Association Constants and Frequency Shifts. The frequency shifts, defined by $\Delta\nu = \nu_1(NH_2) - [\nu_1(NH_2)]_{1-1}$, of the symmetrical stretching vibrations are listed in Table I. For the same donor, the value of $\Delta\nu$ increases with the basicity of the acceptor. Larger values are found for HMPT complexes than for those of DMSO. This result is in good agreement with the fact that HMPT is more basic than DMSO, as shown previously. For the same ac-

(28) J. S. Kwiatkowski, *Acta Phys. Polon.*, **30**, 963 (1966).

ceptor the value of $\Delta\nu$ increases with the acidity of the donor, except in the case of ortho-substituted amines. In Figure 4, log K is plotted as a function of $\Delta\nu$ for amine–DMSO systems.[29] We obtain a linear relationship between these two factors. The points off of the straight line correspond to the ortho compounds. The values of $\Delta\nu$ are plotted in Figure 5 as a function of the Hammett σ parameter for the substituted aniline–HMPT systems. The correlation between these two factors is good because of the relationships previously established. Similar correlations have been found in the systems phenol–pyridine and phenol–aniline.[23]

Acknowledgments. We wish to thank Dr. G. Turrell (Bordeaux) for valuable comments on the manuscript, and Dr. P. Dizabo (Paris) for the gift of aminopyrimidines.

(29) A Fermi resonance is observed between $\nu_1(NH_2)_{1-1}$ and the first overtone of the in-plane bending vibration at about 3200 cm^{-1}. This resonance is weaker in the case of 1–1 complexes but can slightly perturb the value of the $[\nu_1(NH_2)]_{1-1}$ frequency.[19]

NOTES

The Far-Ultraviolet Spectrum of Ice

by Allen P. Minton[1]

Polymer Department, Weizmann Institute of Science, Rehovoth, Israel
(Received October 15, 1970)

Publication costs borne completely by The Journal of Physical Chemistry

During a study of the relationship between optical properties and intermolecular interactions in the water substance, the absorption spectrum of ice in the far-uv (180–190 mμ) was considered to be of interest, especially when compared to those of liquid water and water vapor. The only previous quantitatively reported measurements of uv absorption in ice[2] were limited to wavelengths shorter than 170 mμ, and it was not clear whether these data could be safely extrapolated into the region of interest.

The molar extinction coefficient ϵ of liquid water increases exponentially with decreasing wavelength throughout this region and shifts to the blue with decreasing temperature.[3,4] It was therefore assumed that the absorption of ice would be somewhat less than that of water at the same wavelength, and that correspondingly longer transmission path lengths would be required to bring the absorptivity of the sample into the region capable of accurate measurement.

Experimental Section

The sample cell illustrated in Figure 1 was constructed of copper to ensure effective thermal connection between the sample and the thermostat (a refrigerated bath of ethylene glycol solution). The length of the path was determined by the thickness of the central spacer, and several of these were prepared with thicknesses ranging from 1 to 10 mm.

The following procedure was employed to prepare the sample for measurement. The end plate not containing the quartz window was removed and a small aliquot (0.1–0.3 cc) of previously degassed double-distilled water was introduced into the prerefrigerated

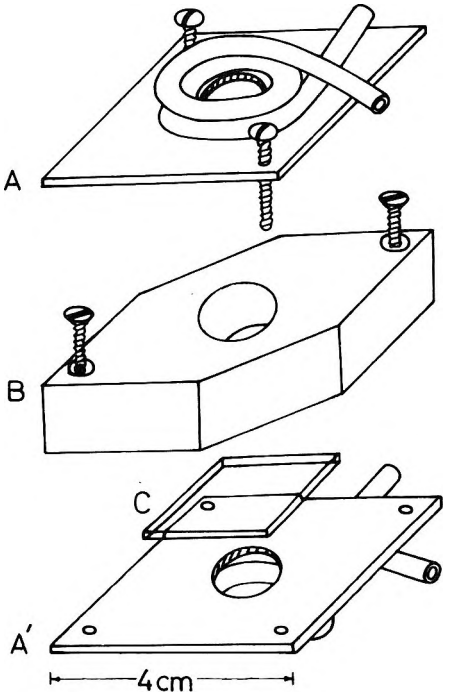

Figure 1. Sample cell for the measurement of the far-uv spectrum of ice: A,A′, end plates with cooling coils; B, central spacer; C, quartz window.

(1) Chaim Weizmann Junior Postdoctoral Fellow; present address: Laboratory of Biophysical Chemistry, National Institute of Arthritis and Metabolic Diseases, NIH, Bethesda, Md. 20014.

(2) K. Dressler and O. Schnepp, *J. Chem. Phys.*, **33**, 270 (1960).

(3) M. Halmann and I. Platzner, *J. Phys. Chem.*, **70**, 580 (1966).

(4) D. P. Stevenson, *ibid.*, **69**, 2145 (1965).

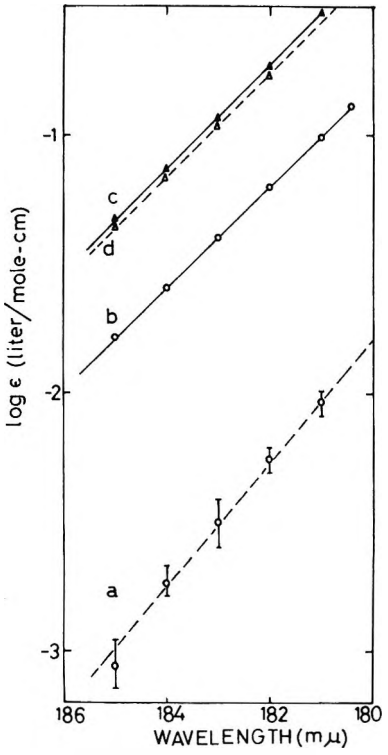

Figure 2. a, Far-uv absorption of ice; b, far-uv absorption of water, 0°; c, far-uv absorption of water, 36°; d, far-uv absorption of water, 36°, data of ref 4.

cell. Because of thermal nonuniformity the water froze unevenly leaving an uneven and cloudy ice–air interface. This interface was smoothed and polished with a clean tissue and slight application of pressure. Another aliquot was added, and the procedure was repeated until the central spacer was completely filled with ice, with a small quantity extending beyond the surface of the spacer. Subsequent polishing leveled off the interface and set it parallel to and contiguous with the surface of the spacer. In this way a clear sample of polycrystalline ice containing two parallel faces of known separation was obtained. Any residual deviations from parallelicity between the faces would serve to scatter transmitted light and increase the observed absorptivity. The same may be said of any impurities which may have gotten into the sample during the preparation procedure. Thus the measured extinction coefficients may be regarded as reliable upper limits to the true extinction coefficients.

The absorption measurements were carried out on a Cary 15 spectrophotometer purged with dry nitrogen. As a check of the reproducibility of the results, several samples were prepared and measured at each of several path lengths. As a check of the instrumentation and technique the absorption spectrum of liquid water in this wavelength region was measured in a conventional thermostated quartz cell at several temperatures in the range 1–50°. The results so obtained were found to agree, where comparable, with the results of Stevenson[4] to within 5% in ϵ.

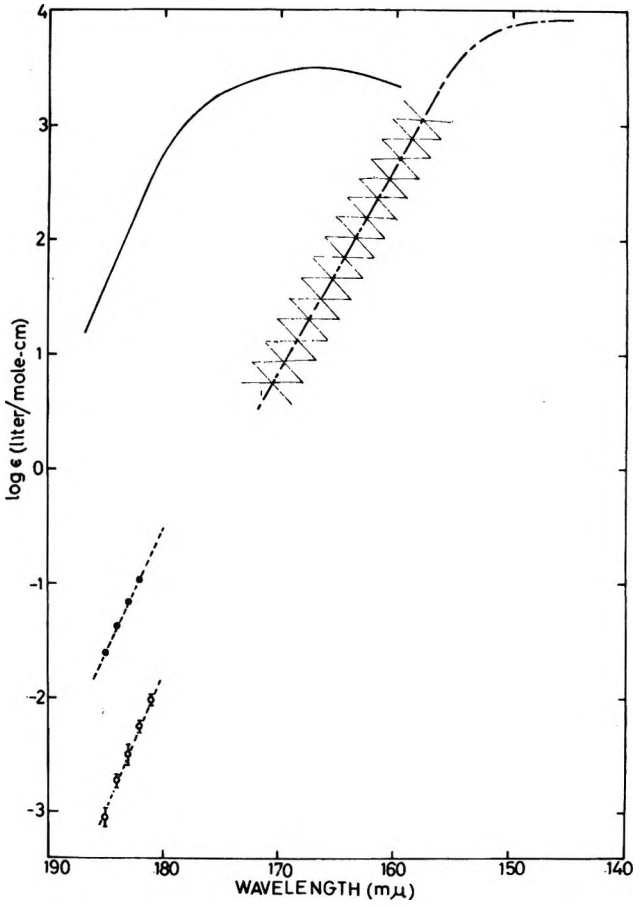

Figure 3. Comparison of data, far-uv absorption: ———, water vapor, ref 5; —●—●—●—, liquid water, 24°, ref 3; - -O- -O- -O- -, ice, this study; —·—·—·—, ice, ref 2. Crosshatched area corresponds to the estimated uncertainty.

Results

In Figure 2 the logarithm (base 10) of the extinction coefficient of ice (in units of liters/(mole-cm)) is plotted against the wavelength, showing the average values obtained and the spread of measured values. For comparison the corresponding results for water at 1 and 36° are also shown. In Figure 3 the same ice data are reproduced on a graph of smaller scale so as to include for additional comparison the results of Halmann and Platzner[3] for liquid water, Watanabe and Zelikoff[5] for water vapor, and Dressler and Schnepp[2] for ice.

The results for ice reported were obtained at a cell temperature of −10°. Test measurements yielded negligible change in the spectrum upon lowering the temperature to −40°.

Discussion

One point worth remarking upon is that the data of Dressler and Schnepp,[2] if extrapolated to the wavelengths at which the present measurements were made, would provide apparent extinction coefficients significantly greater than those reported here. The differ-

(5) K. Watanabe and M. Zelikoff, *J. Opt. Soc. Amer.*, **43**, 753 (1953).

ence in temperature at which the two studies were performed (−10° *vs.* −100° to −200°) would not seem to account for the discrepancy since in both studies variations in temperature did not significantly affect the spectrum. However, Dressler and Schnepp have pointed out that there exist large possible errors in their measurement of ϵ due to the uncertainty in the determination of path length; when this uncertainty is taken into account (see crosshatching in Figure 3) the two sets of data are easily seen to be compatible.

The results further indicate that the uv spectrum of liquid water is less like that of ice than might have previously been supposed. The spectrum of ice is presumed not to vary substantially between 0° and the temperature of measurement. If we assume that the difference between the spectra of ice and water at 0° is due primarily to a shift in frequency of the lowest energy uv continuum (maximum at ~170 mμ in the vapor[5]), then the electronic transition responsible for this continuum increases in energy by approximately 5 kcal/mol upon freezing of liquid water. A structural interpretation of this result would require knowledge of the extent to which the interactions between a molecule and its neighbors differ in the ground and excited states.

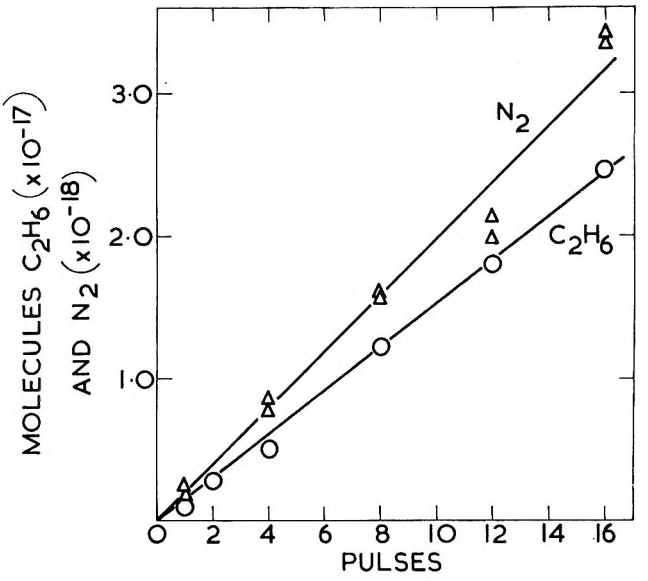

Figure 1.

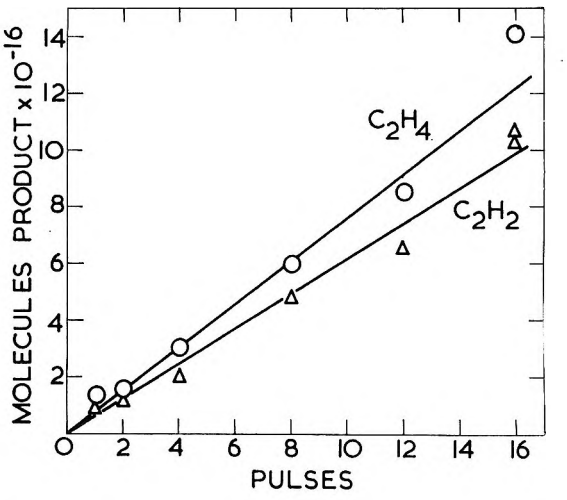

Figure 2.

The Formation of Ethane, Ethylene, and Acetylene from Methane on Radiolysis with High-Intensity Electron Pulses

by R. W. Hummel* and J. A. Hearne

U. K. Atomic Energy Authority, Wantage Research Laboratory (AERE), Wantage, Berks, England *(Received October 2, 1970)*

Publication costs assisted by the Atomic Energy Research Establishment

The radiolysis of CH_4 with electrons from a Febetron-pulsed electron generator has been reported[1] to yield significant quantities of C_2H_2 and C_2H_4 (G = 0.5 and 0.7, respectively, for a dose of 1.8 × 10^6 rads). However, the C_2H_6 yield (G = 0.7) was very low compared to that usually obtained at much lower dose rates (G = 2.1).[2-4] Because knowledge of the dose rate dependence of the yields of these three primary products assists in understanding the radiation chemistry of the system, it was considered worthwhile to confirm, or disprove, the results reported. As shown below, we can confirm the relatively high unsaturate yields but find $G(C_2H_6)$ unchanged from the low dose rate value.

Methane, purified as described previously,[4,5] was irradiated in 220-ml Pyrex vessels fitted with a 0.002-in. Al window compressed onto an indium wire to make a vacuum-tight seal. Analyses were by gas chromatography.

Nitrous oxide, purified by distillation into a continuously pumped (10^{-4} Torr) trap held at −195°, was used for dosimetry, taking $G(N_2)$ = 12.4 as reported[6] for Febetron irradiations. The dose rate in CH_4 was calculated on the basis of the ratio of electron densities (1.25). Nitrogen analyses were by gas chromatography.

(1) R. W. Cahill, A. K. Seeler, and R. A. Glass, *J. Phys. Chem.*, **71**, 4564 (1967).

(2) F. W. Lampe, *J. Amer. Chem. Soc.*, **79**, 1055 (1957).

(3) K. Yang and P. J. Manno, *ibid.*, **81**, 3507 (1959).

(4) R. W. Hummel, *Trans. Faraday Soc.*, **62**, 59 (1966).

(5) R. W. Hummel and J. A. Hearne, *Chem. Ind. (London)*, 1827 (1961).

(6) C. Willis, A. W. Boyd, and D. A. Armstrong, *Can. J. Chem.*, **47**, 3783 (1969).

Using the Febetron 706 at 0.5 MeV with the vessel window about 5 cm from the tube window the results shown in Figures 1 and 2 were obtained. From the slope of the line for N_2 in Figure 1 and the above-mentioned $G(N_2) = 12.4$, the dose in N_2O was found to be 1.61×10^{18} eV pulse^{-1}, corresponding to a dose rate of 1.33×10^{27} eV g^{-1} sec^{-1} for 3-nsec pulses given to 220 ml of gas at 76 cm, 20°. In CH_4 under the same conditions the calculated dose rate was 1.64×10^{27} eV g^{-1} sec^{-1}. The line through the experimental points for C_2H_6 in Figure 1 corresponds to $G(C_2H_6) = 2.1$. The mean, and standard deviation, of the G values calculated for each of the six experimental points is 1.93 ± 0.22. The difference between these values is caused mainly by the first experimental point.

Our results therefore show that $G(C_2H_6)$ at the given dose rate is identical with the value obtained at lower dose rates (5.6×10^{15} eV g^{-1} sec^{-1} (ref 3); 2.7×10^{19} eV g^{-1} sec^{-1} (ref 4)). The small differences in dose rate (a factor of 4) and absorbed dose between the present work and that of Cahill, *et al.*, are unlikely to be the cause of the widely different values obtained for $G(C_2H_6)$ in the two studies. This conclusion follows from the range of dose rates quoted above (from 10^{15} to 10^{27} eV g^{-1} sec^{-1}), for which $G(C_2H_6) = 2.1$ is claimed, and from recent work[7] using absorbed doses from 10^{17} to 10^{20} eV g^{-1} over which $G(C_2H_6)$ remained constant at 2.1. Nor can the discrepancy be explained by the use by Cahill, *et al.*, of $G(N_2) = 10.0$ for the N_2O dosimeter and a correction factor of 1.38 (rather than 1.25) to allow for the relative energy losses in CH_4 and N_2O; the G values for C_2H_6 still differ by a factor of 2. The presence of adventitious oxygen can cause a large reduction in $G(C_2H_6)$, but Cahill's observation of $G(C_2H_6) = 2$ for ^{60}Co irradiations appears to remove this as a possibility. The reason for the difference is therefore unresolved.

From Figure 2 calculations give $G(C_2H_4) = 1.05$ and $G(C_2H_2) = 0.85$, values not significantly different from those reported by Cahill, *et al.* (0.9 and 0.65, respectively, based on $G(N_2) = 12.4$ from N_2O).

Over the same dose range $G(C_2H_4)$ is not significantly different from a value recently determined[7] at a much lower dose rate (1.06×10^{18} eV g^{-1} sec^{-1}). It appears that the initial G value (*i.e.*, the value determined at low doses where insufficient C_2H_4 has accumulated for $H + C_2H_4 \rightarrow C_2H_5$ to compete with $H + H + CH_4 \rightarrow H_2 + CH_4$) is independent of dose rate. There are insufficient data available on $G(C_2H_2)$ from CH_4 to comment on the dose rate dependence of the initial value.

Acknowledgment. We are indebted to Dr. G. R. A. Johnson and the University of Newcastle upon Tyne for the use of the Febetron.

(7) R. W. Hummel, *Int. J. Rad. Phys. Chem.*, in press.

An Electron Paramagnetic Resonance Study of Y-Type Zeolites. III. O_2^- on AlHY, ScY, and LaY Zeolites

by Katherine M. Wang and Jack H. Lunsford*

Department of Chemistry, Texas A & M University, College Station, Texas 77843 *(Received June 26, 1970)*

Publication costs assisted by the National Science Foundation

The magnetic and crystal field interactions between an adsorbed paramagnetic species, O_2^-, and a number of different Y-type zeolites including decationated zeolite,[1] NaY,[2] BaY,[2,3] and other alkaline earth Y-type zeolites[3] have been studied by means of epr spectroscopy. It has been shown that the crystal field interaction does not significantly change as one goes up the group IIA series from BaY to MgY zeolites.[3] In addition, the study of the O_2^- ion adsorbed on decationated zeolite has furnished strong evidence that an aluminum atom is involved.

In the present investigation an attempt was made to study crystal field interactions between the adsorbed O_2^- ion and some group III cation-exchanged Y-type zeolites including AlHY, ScY, and LaY zeolites. Each of these cations is characterized by nuclei with nonzero spin. In principle, it should be possible to determine whether the cation is part of the adsorption site by observing the hyperfine interaction between the cation and the unpaired electron of the superoxide ion.

Experimental Section

The AlHY, ScY, and LaY zeolites were prepared by exchanging the sodium form of a Linde type Y zeolite with the cations from a nitrate or chloride solution of the desired cation. The acidity of the nitrate and chloride solutions, as well as the formulas of the trivalent zeolites, are shown in Table I.[4]

The above formulas were obtained by means of (1) neutron activation analysis to detect the percentage of Sc and La contained in a ScY and a LaY zeolite, respectively; (2) atomic adsorption to determine the percentage of exchangeable sodium and aluminum; and (3) a total elemental analysis of an AlHY zeolite.

The zeolite samples were broken into chips with a 1-mm maximum dimension and then placed in a Vycor sample tube which contained a quartz side arm of 18 cm length with a 3 or 1-mm inside diameter. The samples were degassed under vacuum (10^{-5} Torr) with

(1) K. M. Wang and J. H. Lunsford, *J. Phys. Chem.*, **73**, 2069 (1969).

(2) P. H. Kasai, *J. Chem. Phys.*, **43**, 3322 (1965).

(3) K. M. Wang and J. H. Lunsford, *J. Phys. Chem.*, **74**, 1512 (1970).

(4) J. A. Rabo, C. L. Angell, and V. Schomaker, 4th International Congress on Catalysis, Moscow, 1968.

Table I

	Acidity of the exchange solution (pH)	Formula of the trivalent zeolites
AlHY	1.30	$H_{39}Na_5Al_4[(AlO_2)_{56}(SiO_2)_{136}]\cdot 264H_2O$
ScY	2.50	$Na_{11}Sc_{15}[(AlO_2)_{56}(SiO_2)_{136}]\cdot 264H_2O$
LaY	2.55	$Na_{14}La_{14}[(AlO_2)_{56}(SiO_2)_{136}]\cdot 264H_2O$[a]

[a] This formula is in agreement with the chemical analysis of LaY by Rabo, Angell, and Schomaker.[4]

a heating interval of 100° per hour. The experimental details were described in previous papers.[1,3] The radiation source was a ^{60}Co γ emitter with a dose rate of 300 R/min.

A Varian spectrometer (Model 4502) with a $T.E._{102}$ mode cavity was employed. The cavity resonance frequency was about 9.5 GHz/sec (X-band). A 35-GHz/sec (Q-band) microwave bridge and cavity were also used.

Results

The X-band spectrum shown in Figure 1 was observed at 77°K after an AlHY zeolite had been degassed at 400°, γ-irradiated in the presence of oxygen, and then heated at a temperature of 150°. The spectrum, which is identical within experimental error to that of O_2^- on a decationated zeolite, can be resolved into three sets of six lines. Each set of lines represents the hyperfine interaction along one of the three principal axes (x, y, and z) which are defined by the orientation of the molecule with respect to the external magnetic field. Here, z is chosen along the internuclear axis while x and y are in the directions of the pπ functions. The six lines for the z direction are well defined, but since $g_{xx} \simeq g_{yy}$, two sets of hyperfine lines partially overlap. The O_2^- spectrum is characterized by $g_{zz} = 2.009 \pm 0.001$, $g_{yy} = 2.003 \pm 0.001$, and $g_{zz} = 2.038 \pm 0.001$, with $|a_{xx}| = 4.8 \pm 0.5$ G, $|a_{yy}| = 5.7 \pm 0.5$ G and $|a_{zz}| = 6.5 \pm 0.5$ G.

In the presence of 50 Torr of O_2, measured at 23°, the spectrum was broadened uniformly due to the spin–spin interactions between the chemisorbed superoxide ion and physically adsorbed oxygen. The spectrum shown in Figure 1 could be reproduced after a 30-min evacuation, which removed all molecular oxygen.

The spectrum of the O_2^- ion on an AlHY zeolite was also observed at a resonance frequency of 35 GHz/sec and a field of 12,500 G. The six hyperfine lines for the z direction were not well resolved, but a g_{zz} value of 2.038 was obtained. The six lines for the x direction were well resolved, and a g_{xx} value of 2.010 and $|a_{xx}|$ of 4.8 ± 0.5 G were obtained. The six lines for the y direction were hardly observed due to the presence of a sharp line with a g value of 2.0025. This line is more prominent at 35 GHz/sec because it has an isotropic g value.

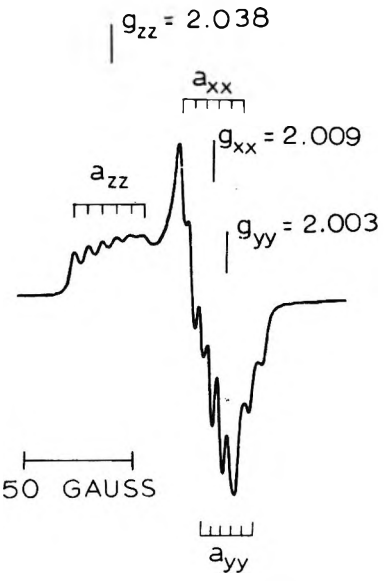

Figure 1. Epr spectrum of O_2^- on γ-irradiated AlHY zeolite.

When oxygen was not present in the sample tube, the spectrum of the γ-irradiated AlHY zeolite exhibited 11 weak hyperfine lines. The relative intensity of this 11-line spectrum is about a factor of 20 less than the spectrum shown in Figure 1. The relative intensities of the 11 lines are 1:2:3:4:5:6:5:4:3:2:1. A g value of 2.007 and an $|a|$ of 10 G were obtained. It was somewhat difficult to saturate this spectrum by increasing the microwave power of the spectrometer. In the presence of 150 Torr of O_2, the lines were broadened simultaneously. The oxygen broadening was reversible.

The X-band spectrum shown in Figure 2 was observed at 77°K when a ScY zeolite was degassed at 500°, γ-irradiated in the presence of oxygen, and then heated at 150°. Although this spectrum was somewhat more difficult to analyze because of the overlapping x and z components, it was possible to determine g_{zz} from the Q-band spectrum in which the low-field maximum is clearly resolved. This increase in resolution occurs at the higher frequency and magnetic field because the Zeeman interaction is a linear function of the magnetic field, whereas the hyperfine interaction is independent of the field. Once the value of g_{zz} had been established, it was clear from the spectrum in Figure 2 that there were four lines on the low-field side of g_{zz} and, therefore, there are eight hyperfine lines in the z direction. The spectrum of O_2^- on ScY may then be characterized by $g_{xx} = 2.009 \pm 0.001$, $g_{yy} = 2.002 \pm 0.001$, and $g_{zz} = 2.030 \pm 0.001$ with $|a_{xx}| = 4.4 \pm 0.5$ G, $|a_{yy}| = 5.1 \pm 0.5$ G, and $|a_{zz}| = 5.7 \pm 0.5$ G. The peaks of this spectrum were reduced simultaneously upon heating the sample gradually.

The X-band spectrum shown in Figure 3 was observed at 77°K when a LaY zeolite was degassed at

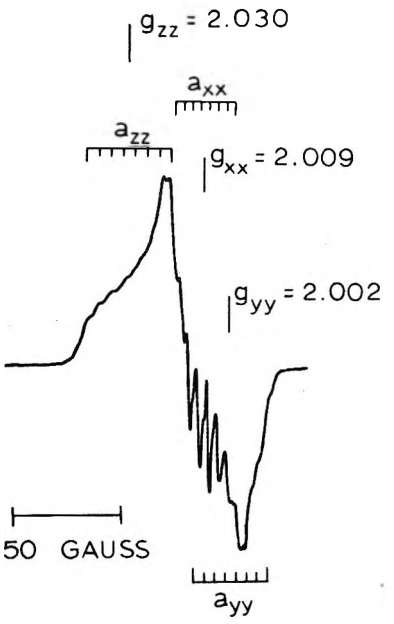

Figure 2. Epr spectrum of O_2^- on γ-irradiated ScY zeolite.

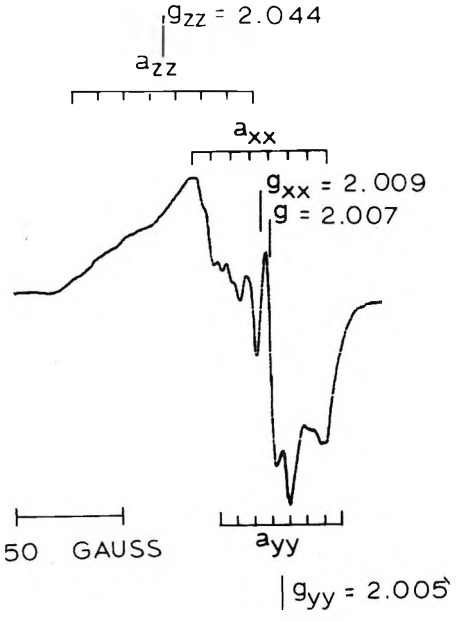

Figure 3. Epr spectrum of O_2^- on γ-irradiated LaY zeolite.

500° and γ-irradiated in the presence of oxygen. This spectrum was not well resolved even upon heating the sample. The sharp line which has a g value of 2.007 was more easily saturated than the remainder of the spectrum when the microwave power of the spectrometer was increased, and, upon addition of 20 Torr of oxygen, it was broadened more than the remainder of the spectrum.

The Q-band spectrum was also obtained, but the g_{zz} component and hyperfine lines were still not well resolved. If one assumes that the spectrum of O_2^- on LaY is basically similar to that of O_2^- on ScY, it is possible to develop a consistent set of g values and coupling constants. These are indicated in Figure 3. Values for the coupling constants are $|a_{zz}| = 9 \pm 1$ G, $|a_{yy}| = 8 \pm 1$ G, and $|a_{zz}| = 12 \pm 1$ G, where the latter constant was estimated from the shape of the curve around g_{zz}.

Discussion

It is clear from the analytical data shown in Table I that the major charge-balancing cation in this particular AlHY zeolite is the proton rather than aluminum. This form of the zeolite is not deficient in aluminum ions and, therefore, is unlike the ultrastable HY zeolite. The unit cell dimension, as determined from the powder X-ray pattern, is only slightly smaller than in the orignal NaY form. The AlHY is more stable to thermal treatment than the normal HY zeolites produced from NH_4Y.

The three sets of six hyperfine lines which appeared in the O_2^- spectrum of a γ-irradiated AlHY zeolite indicate that an interaction occurs between an ^{27}Al ($I = {}^5/_2$) and the unpaired electron of the O_2^- ion. Since the three principal g values and coupling constants are identical with those obtained for a γ-irradiated decationated Y-type zeolite, one may conclude that the adsorption site of the O_2^- ion on an AlHY zeolite is the same as on a decationated Y-type zeolite. It appears, therefore, that the aluminum which is involved in the adsorption site is a lattice aluminum and not an exchangeable aluminum. This is not surprising since the amount of exchangeable aluminum is small. The line broadening effect indicates that there is only one adsorption site for the O_2^- ion adsorbed on an AlHY zeolite.

The 11 lines, which appeared when an AlHY zeolite was irradiated in the absence of oxygen, indicate an unpaired electron (perhaps a trapped hole) between two equivalent aluminum atoms. Since the aluminum atom has a nuclear spin of ${}^5/_2$, the coupling between two equivalent aluminum atoms will induce (2)(2)(5/2) + 1 = 11 lines with the relative intensities 1:2:3:4:5:6:5:4:3:2:1. The reversible line broadening effect with molecular oxygen indicates that the lattice aluminums are exposed to the supercage of the zeolite.

The three sets of eight hyperfine lines which appeared on the γ-irradiated ScY zeolite indicate that an interaction also occurs between a ^{45}Sc ($I = {}^7/_2$) and the unpaired electron of the O_2^- ion. Since the peaks were reduced simultaneously by heating the sample, there is apparently only one adsorption site for the O_2^- ion adsorbed on an ScY zeolite.

Based on infrared data, it has been proposed that upon mild dehydration the cations in alkaline earth zeolites form M^+-O-M^+ complexes in the sodalite unit.[5] By means of X-ray[6] studies, it has also been proposed

(5) J. B. Uytterhoeven, R. Schoonheydt, B. V. Liengme, and W. K. Hall, *J. Catal.*, 13, 425 (1969).

that the La atoms locate at site I′ and site II′ positions and are joined by an oxygen atom. Since the epr lines were broadened upon addition of 150 Torr of oxygen, we proposed that the Sc atom which is involved in the adsorption site of the O_2^- ion must be located at site II′, which is available to molecules in the supercage of the zeolite.

Conclusions based on the spectrum of O_2^- on LaY are more tentative because of the poor resolution and the greater overlap of the hyperfine structure. It appears that the interactions of O_2^- on LaY are much the same as those found in ScY; that is, the O_2^- ion is experiencing coupling with ^{139}La ($I = {}^7/_2$) ions at site II′.

Acknowledgment. The authors wish to acknowledge the contributions of Drs. B. O'Brien and J. B. Natowitz in obtaining an analysis of the zeolite. This work was supported by the National Science Foundation under Grants GP-8319 and GP-19875.

(6) J. V. Smith, J. M. Bennett, and E. M. Flanigen, *Nature*, **215**, 241 (1967).

Photolysis of 1,4-Dichlorobutane Sensitized by Various Aliphatic Ketones

by Morton A. Golub[1]

Ames Research Center, National Aeronautics and Space Administration, Moffett Field, California 94035 *(Received August 12, 1970)*

Publication costs assisted by the Ames Research Center, NASA

While photosensitization by the n,π* triplet state of ketones has been known for some time,[2] only recently has the involvement of the corresponding singlet state in organic photochemistry become generally appreciated. Thus, photocycloaddition of ketones to olefins to form oxetanes,[3] ketone sensitization of biacetyl fluorescence,[4] quenching of alkyl ketone fluorescence by high concentrations of 1,3-pentadiene,[5] Norrish type II photoelimination,[2,6] and α-cleavage (or type I) reactions from cyclic[7] and acyclic[8] ketones, are all processes in which $[n,\pi^*]^1$ states of ketones have been implicated for part or all of the respective chemistry. Recently we disclosed still another process attributable to $[n,\pi^*]^1$ sensitization, *viz.*, the acetone-sensitized photolyses of several dichlorobutanes.[9,10] In view of increasing interest in the role of excited singlet states,[11] we extended the dichlorobutane photolysis by examining the relative efficiencies of a number of aliphatic ketones in photosensitizing the evolution of HCl, the main product, from 1,4-dichlorobutane (DCB) in solution.

Experimental Section

Materials. The following ketones were employed: spectroquality acetone from J. T. Baker Chemical Co.; research grade acetone-d_6, 3-pentanone, 2-hexanone, 3-hexanone, and 2,4-dimethyl-3-pentanone from Aldrich Chemicals Co.; chromatoquality 2-butanone and cyclohexanone from Matheson Coleman and Bell; chromatoquality cyclopentanone from Analabs, Inc.; and 2-pentanone, 2-heptanone, 3-heptanone, and 4-heptanone from Chem Service Inc. The last four ketones were distilled prior to use.

A purified sample of 1,4-dichlorobutane (Aldrich Chemicals Co.) comparable to that in the previous work[9,10] was used in the present study.

Acetophenone and benzophenone (from J. T. Baker photosensitizer kit) were used without further purification.

Procedure. Irradiations of degassed DCB–isooctane–ketone solutions in Pyrex tubes at 3130 Å, as well as analysis for HCl evolution, followed the procedures described in ref 9 and 10. In addition, quenching of fluorescence of acetone (0.068 *M* in isooctane) at 405 nm by DCB was measured with an Aminco-Bowman spectrofluorometer, using excitation at 313 nm.

Results and Discussion

Figure 1 presents a Stern–Volmer analysis of HCl formation from DCB (~2–8 *M* in isooctane) photosensitized by a number of aliphatic ketones (0.54–0.56 *M*).[12] From the intercept/slope ratios of the linear Φ^{-1} *vs.* $[DCB]^{-1}$ plots, relative sensitization efficiencies for various ketones were determined and presented in Table I. A common intercept (which corresponds to the reciprocal of the probability that quenching of singlet ketone by DCB leads to product, analogous to the treatment used, *e.g.*, in photocycloaddition studies[3]) is expected since there was negligible loss of ketone in any run.

(1) National Research Council–National Aeronautics and Space Administration Resident Research Associate, 1968–1970.

(2) See P. J. Wagner and G. S. Hammond, *Advan. Photochem.*, **5**, 21 (1968), for a review of ketone triplet photochemistry.

(3) J. C. Dalton, P. A. Wriede, and N. J. Turro, *J. Amer. Chem. Soc.*, **92**, 1318 (1970), and references cited therein.

(4) See F. Wilkinson, *Advan. Photochem.*, **3**, 241 (1964), for a review of this topic.

(5) F. S. Wettack, G. D. Renkes, M. G. Rockley, N. J. Turro, and J. C. Dalton, *J. Amer. Chem. Soc.*, **92**, 1793 (1970).

(6) N. C. Yang, S. P. Elliott, and B. Kim, *ibid.*, **91**, 7551 (1969), and references cited therein.

(7) J. C. Dalton, D. M. Pond, D. S. Weiss, F. D. Lewis, and N. J. Turro, *ibid.*, **92**, 2564 (1970).

(8) N. C. Yang and E. D. Feit, *ibid.*, **90**, 504 (1968).

(9) M. A. Golub, *ibid.*, **91**, 4925 (1969).

(10) M. A. Golub, *ibid.*, **92**, 2615 (1970).

(11) For examples of aromatic hydrocarbons as singlet sensitizers, see: P. S. Engel, *ibid.*, **91**, 6903 (1969); S. Murov and G. S. Hammond, *J. Phys. Chem.*, **72**, 3797 (1968).

(12) By working at a ketone concentration of ~0.54–0.56 *M*, and staying away from nearly neat DCB, we avoid the sharp upturn in the Φ–[DCB] plot observed previously[9,10] for [acetone] $\lesssim$ 0.2 *M and* [DCB] ~9 *M*.

Table I: Photosensitization Efficiencies for Different Aliphatic Ketones[a]

Ketone	Relative sensitization efficiency[b]	Relative energy transfer efficiency[c]	τ_s, nsec
CH_3–CO–C_2H_5	1.00	1.00	4.4[d]
C_2H_5–CO–C_2H_5	0.66	0.62	2.8[d]
C_2H_5–CO–C_3H_7	0.45		
C_3H_7–CO–C_3H_7	0.35		
CH_3–CO–CH_3	0.33	0.40	1.8,[d] 2.0[e]
CD_3–CO–CD_3	0.33		2.7[f]
CH_3–CO–C_3H_7	0.28		1.8,[e] 2.0[g]
$(CH_3)_2CH$–CO–$CH(CH_3)_2$	0.10		4.2[h]
C_2H_5–CO–C_4H_9	0.03		
CH_3–CO–C_5H_{11}	0.03		
CH_3–CO–C_4H_9	0		0.73[g]
	0	0.44	1.9[d,i]
	0		

[a] [Ketone] = 0.54–0.56 M in all DCB–isooctane–ketone solutions. [b] Given by intercept/slope ratio of Φ^{-1} *vs.* $[DCB]^{-1}$ plot relative to that for 2-butanone (0.092 M^{-1}). [c] Based on singlet–singlet transfer constants for the ketone-sensitized fluorescence of biacetyl (see text). [d] Reference 4; data for 2-butanone and 3-pentanone corrected for typographical errors introduced in reviewing the original work.[13] [e] Reference 5. [f] Estimated at 1.4 times that of acetone.[14,15] [g] Reference 6. [h] Reference 14. [i] Reference 7.

The straight-chain ketones, R_1R_2CO, where R_1 and/or $R_2 \leqslant C_3$, have photosensitization efficiencies which range from 0.8 to 3.0 times that of acetone (or acetone-d_6) while the branched ketone, 2,4-dimethyl-3-pentanone, has an efficiency which is only $^1/_3$ of that of acetone. On the other hand, those ketones in which R_1 or $R_2 > C_3$, and also the cyclic ketones, cyclopentanone, and cyclohexanone, have little or no efficiency at sensitizing the photolysis of DCB. Interestingly, the order of efficiency, 2-butanone > 3-pentanone > acetone, parallels the order of relative efficiency of these same ketones in sensitizing biacetyl fluorescence.[4,13] The quantities given in the third column of the table, all relative to the efficiency for 2-butanone taken as unity, were based on average values for the singlet–singlet transfer constants, K_s and K_q, for sensitization of biacetyl fluorescence and quenching of donor fluorescence, respectively, in each of the ketone–biacetyl systems examined by Dubois and Cox.[13] Since $K_s = K_q = k\tau_s$, where k is the specific rate constant for the singlet–singlet transfer process (assumed to be diffusion controlled here) and τ_s is the mean (singlet) lifetime of the excited donor, the biacetyl fluorescence work provided "kinetic" estimates for τ_s for the above three ketones and also for cyclopentanone.[4] Likewise, biacetyl quenching measurements[6] yielded τ_s data for 2-pentanone and 2-hexanone, while fluorescence decay or intensity measurements afforded τ_s data for acetone,[5]

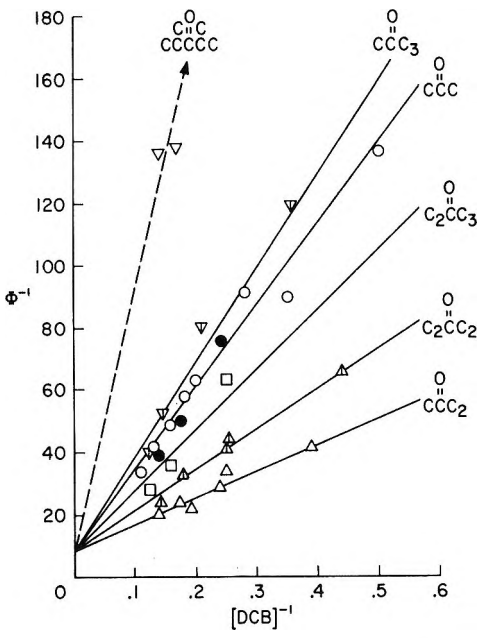

Figure 1. Concentration dependence of the photoinduced formation of hydrogen chloride from 1,4-dichlorobutane sensitized by various aliphatic ketones at 3130 Å: △, 2-butanone; ▲, 3-pentanone; □, 3-hexanone; ○, acetone; ●, acetone-d_6; ▽, 2-pentanone; ▼, 2,4-dimethyl-3-pentanone.

2-pentanone,[5] cyclopentanone,[7] acetone-d_6,[14,15] and 2,4-dimethyl-3-pentanone[14] (see Table I).

While the efficiencies for 2-butanone, 3-pentanone, acetone, and 2-pentanone in sensitizing the photolysis of DCB can be correlated with their singlet lifetimes, the efficiencies of the other ketones in Table I cannot. That τ_s is clearly not the only factor can be seen, for example, in the fact that cyclopentanone is not a sensitizer for DCB photolysis, yet it sensitizes biacetyl fluorescence with an efficiency close to that of acetone (and hence has nearly the same "kinetic" lifetime as does acetone). Again, 2,4-dimethyl-3-pentanone, with a τ_s over twice that of acetone, has only a third of the latter's efficiency; also, the efficiency of acetone-d_6 does not reflect its deuterium-enhanced τ_s. Furthermore, 2-hexanone with a τ_s about a third of that of acetone is not a sensitizer at all. Evidently, steric factors must also play an important role in singlet transfer.[16]

Since the S_1 state of DCB is some 25–35 kcal/mol

(13) J. T. Dubois and M. Cox, *J. Chem. Phys.*, **38**, 2536 (1963).

(14) M. O'Sullivan and A. C. Testa, *J. Amer. Chem. Soc.*, **92**, 5842 (1970).

(15) N. C. Yang, E. D. Feit, M. H. Hui, N. J. Turro, and J. C. Dalton, *ibid.*, **92**, 6974 (1970).

(16) This view is in line with the recent observation (F. S. Wettack, Hope College, private communication) that fluorescence quenching of aliphatic ketones by 1,3-pentadiene shows a strong structural effect. In particular, the finding that 2,4-dimethyl-3-pentanone exhibits an unexpectedly low rate constant for fluorescence quenching may provide an explanation for the relatively low photosensitization efficiency observed here for this particular ketone.

above the corresponding state of the aliphatic ketones (based on absorption spectra), singlet–singlet energy transfer from the latter to the former in the case of 3130-Å irradiation can be ruled out. The mechanism for sensitized photolysis of DCB must hence involve collisional deactivation of the ketone S_1 state (80–85 kcal/mol) by DCB whereby the energy released is used to rupture C–Cl bonds (bond strength ~80 kcal/mol) and produce the detailed chemistry described earlier.[10] Accordingly, the order of relative efficiencies for ketone sensitization of biacetyl fluorescence,[4,13] or for ketone photocycloaddition to 1,2-dicyanoethylene,[17] should not be expected to carry over exactly to the ketone-sensitized photolysis of DCB.

Quenching of acetone fluorescence at 405 nm by DCB provided further substantiation of the singlet mechanism beyond the arguments advanced originally.[9] Thus, the value of $k_q\tau_s \cong 0.04\ M^{-1}$, given by the slope of the Stern–Volmer plot for fluorescence quenching, agrees well with the $k_q\tau_s \cong 0.03\ M^{-1}$ obtained from the intercept/slope ratio of the acetone sensitization plot in Figure 1. It is noteworthy that these rather low values are of the same order of magnitude as the $k_q\tau_s \cong 0.08\ M^{-1}$ found for fluorescence quenching of 2-pentanone by 1,3-pentadiene.[5]

Finally, it should be mentioned that acetophenone and benzophenone (~0.02–0.05 M) were also found to sensitize the DCB photolysis, with Φ values in neat DCB of 0.008 and 0.010, respectively. These yields drop sharply to ~0.001 in 5 M DCB in isooctane, no doubt due to competing photoreduction of the aromatic ketones by solvent. In view of the recent report on delayed fluorescence[18] in acetophenone and benzophenone, which indicates significant concentrations of S_1 molecules (E_S = 76 and 72 kcal/mol, respectively) in equilibrium with T_1 molecules (E_T = 72 and 69 kcal/mol, respectively), the assumption is that these compounds likewise serve as singlet sensitizers of the DCB photolysis. That their maximum Φ values are about $^1/_4$ to $^1/_3$ as large as that for acetone (≃0.03 at 9 M DCB),[10] despite their reportedly very short singlet lifetimes (≃0.1 nsec),[3] could be due to an effectively longer τ_s as a result of the S_1–T_1 equilibrium in which T_1 serves to repopulate S_1.

Acknowledgment. The author wishes to thank Dr. John A. Parker for his continued support during this study.

(17) According to N. J. Turro and P. A. Wriede, *J. Org. Chem.*, **34**, 3562 (1969), cyclohexanone > acetone > cyclopentanone > 2-pentanone > 2-hexanone in order of efficiency of photocycloaddition to 1,2-dicyanoethylene. Although this reaction proceeds through the $[n,\pi^*]^1$ state of alkyl ketones,[3] the mechanism involves π complex formation and is therefore quite different from the ketone–DCB system.

(18) J. Saltiel, H. C. Curtis, L. Metts, J. W. Miley, J. Winterle, and M. Wrighton, *J. Amer. Chem. Soc.*, **92**, 410 (1970).

The Kinetics of the Unimolecular Dehydrofluorination of Methyldifluoramine

by David S. Ross* and Robert Shaw

Stanford Research Institute, Menlo Park, California 94025
(Received November 25, 1970)

Publication costs assisted by the Office of Naval Research

This work was undertaken to determine the activation energy of the process

$$R_2HCNF_2 \longrightarrow R_2CNF + HF \qquad (1)$$

By analogy with similar 4-center eliminations,[1] the Arrhenius A factor may be estimated to be $10^{13.5}$ sec^{-1}. Direct observation of the HF elimination is usually masked[2] by the competing reaction

$$R_2HCNF_2 \longrightarrow R_2HC + NF_2 \qquad (2)$$

which is a simple bond fission with an A factor of around $10^{17.5}$ sec^{-1}. However, an interesting solution to the problem is made possible by reversing the competing reaction to give a vibrationally hot molecule

$$R_2HC + NF_2 \longrightarrow R_2HCNF_2^*$$

The hot difluoroaminoalkane can redissociate, eliminate HF, or can be collisionally stabilized.

$$R_2HCNF_2^* \longrightarrow R_2HC + NF_2 \qquad (3)$$

$$R_2HCNF_2^* \longrightarrow R_2CNF + HF \qquad (4)$$

$$R_2HCNF_2^* + M \longrightarrow R_2HCNF_2 + M \qquad (5)$$

Experimental measurements of the yields of R_2CNF and R_2HCNF_2 as a function of M give the ratio of rate constants k_4/k_5. An estimate of collision frequency and stabilizing efficiency will give k_5, and from the ratio k_4/k_5, k_4 can be obtained. According to RRK theory,[3] $k_4 = A_1[(E - E_1)/E]^{s-1}$ where A_1 and E_1 are the Arrhenius parameters for the decomposition of a thermalized molecule, E is the energy of the vibrationally hot molecule, and where s is the number of "effective" oscillators. From k_4 and estimates of A_1, E, and s, E_1 can be obtained. A more sophisticated treatment, RRKM, which requires a model for the transition state, can also be used.[4]

Methyldifluoramine, the simplest R_2HCNF_2, was chosen as the model compound. Vibrationally hot methyldifluoramine was first prepared by Frazer,[5] who found both HCN and stabilized methyldifluoramine.

(1) H. E. O'Neal and S. W. Benson, *J. Phys. Chem.*, **71**, 2903 (1967).

(2) D. S. Ross, T. Mill, and M. E. Hill, to be published.

(3) S. W. Benson and G. Haugen, *J. Phys. Chem.*, **69**, 3898 (1965).

(4) S. W. Benson, "The Fundamentals of Chemistry Kinetics," McGraw-Hill, New York, N. Y., 1960, p 222.

(5) J. W. Frazer, *J. Inorg. Nucl. Chem.*, **16**, 63 (1960).

$$CH_3NF_2^* \longrightarrow HCN + 2HF \quad (6)$$

$$M + CH_3NF_2^* \longrightarrow M + CH_3NF_2 \quad (7)$$

The HCN most likely comes from the intermediate CH_2NF after loss of another HF. Bumgardner, Lawton, and Carmichael[6] (BLC) have also made vibrationally hot methyldifluoramine, with results similar to those of Frazer. The added features of the present work are a tenfold extension of the pressure range to obtain a more precise ratio of rate constants, and the RRK and RRKM treatments to derive the activation energy for HF elimination.

In each experiment, 3.5 Torr of N_2F_4 and 3.5 Torr of di-*tert*-butyl peroxide were heated for 15 min with either N_2 or CF_4 as diluent in a monel reaction vessel at 198°. At this temperature the N_2F_4 is almost completely dissociated into $2NF_2$ and methyl radicals are formed at a convenient rate from the pyrolysis of the peroxide. After quenching, an aliquot was analyzed by gas chromatography for the relative amounts of HCN and CH_3NF_2 using a Poropak Q column and a flame ionization detector. The results are plotted in Figure 1. As expected, CF_4 is more effective at stabilizing the hot methyldifluoramine. The slopes of the lines give rate constant ratios k_4/k_5 for N_2 and CF_4. The ratios are in qualitative agreement with those of BLC. No CH_3F could be detected, which places an upper limit of about 0.01 on the ratio of rate constants k_8/k_9.

$$CH_3 + NF_2 \longrightarrow CH_3F + NF \quad (8)$$

$$CH_3 + NF_2 \longrightarrow CH_3NF_2 \quad (9)$$

A value for k_5 can be calculated from $k_5 = Z\lambda$ where Z is the number of collisions per second and λ is the collision efficiency.[3] At 198° for CF_4 as M, Z is 10^7 $Torr^{-1}$ sec^{-1} and λ is ~ 1, giving k_5 (CF_4) = 10^7 $Torr^{-1}$ sec^{-1}. From Figure 1, k_5/k_4 (CF_4) = 0.4 atm^{-1}, $k_4 = 2.5 \times 760 \times 10^7 = 10^{10.3}$ sec^{-1}.

For the RRK treatment, $A_1 = 10^{13.5}$ sec^{-1} and E = 64 kcal mol^{-1} comprised of 60 kcal mol^{-1} for the CH_3–NF_2 bond strength at 25° (ref 7) and 4 kcal mol^{-1} for the thermal energy at 198° (see Figure 2). The total number of oscillators is $3n - 6$, where n is the number of atoms. For methyldifluoramine, $n = 7$, giving a total of 15 oscillators. The usual procedure[3] is to assume that $^2/_3$ of the oscillators are effective. Taking $s = 10$, we calculate $E_1 = 35$ kcal mol^{-1}. If $s = 9$, $E_1 = 38$ kcal mol^{-1}, and if $s = 11$, $E_1 = 33$ kcal mol^{-1}.

For the RRKM treatment[8] the transition state was assumed to be

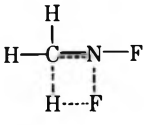

where the dotted lines are $^1/_2$ bonds. The frequencies for these partial bonds were assumed to be those estimated by O'Neal and Benson.[1] The RRKM calculation predicts the relative yield CH_3NF_2/HCN as a function of M for different values of E_1. In Figure 3, the

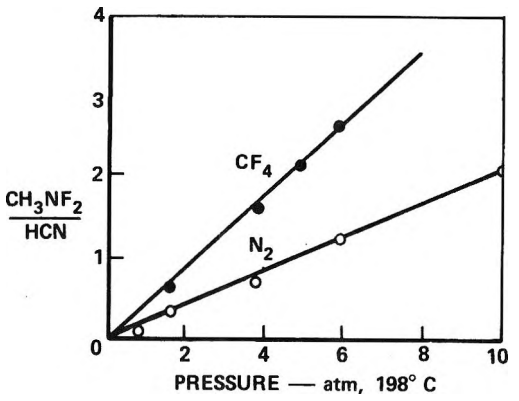

Figure 1. CH_3NF_2/HCN *vs.* pressure for $CH_3 + NF_2$ at 198° with N_2 and CF_4 as diluents.

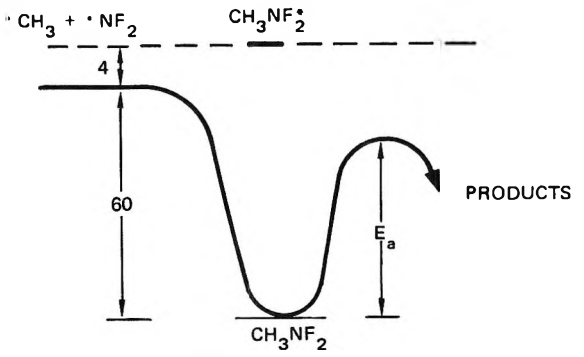

Figure 2. Reaction coordinate diagram for $CH_3 + NF_2$.

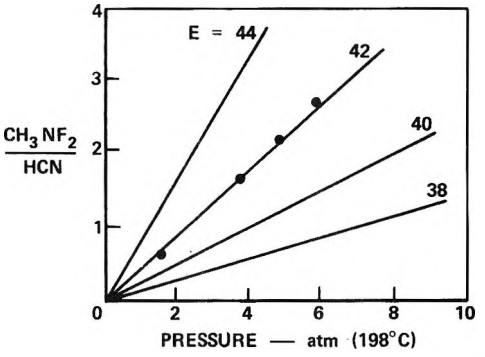

Figure 3. Comparison of theoretical and experimental data for $CH_3 + NF_2$ with CF_4 as diluent.

(6) C. L. Bumgardner, E. Lawton, and H. Carmichael, *Chem. Commun.*, 1079 (1968).

(7) This value is based on our observation (manuscript in preparation) that a tertiary C-NF_2 bond is 56 kcal/mol. We estimate about a 4 kcal/mol increase in strength in proceeding from a tertiary to a primary bond. In addition, we have calculated the heat of the reaction $CH_3NF_2 \rightarrow CH_3 + NF_2$ to be 60.4 kcal/mol (from data in S. W. Benson, "Thermochemical Kinetics," Wiley, New York, N. Y., 1968).

(8) The program was generously supplied by Dr. G. Haugen of the Institute's Thermochemistry and Kinetics Department.

experimentally observed yields are compared with yields calculated using RRKM for different values of E_1 between 38 and 44 kcal mol^{-1}. From Figure 3, we conclude that $E_1 = 42$ kcal mol^{-1}. Taking methyldifluoramine as the model compound, R_2HCNF_2, the rate parameters for HF elimination are then log (k_1/sec^{-1}) = 13.5 − 42/θ, where θ is 2.3RT kcal mol^{-1}, and those for C–N bond breaking[2] are log (k_2/sec^{-1}) = 17.5 − 60/θ. The isokinetic temperature where both rates are equal is in the region of 100°K. For other difluoraminoalkanes, R ≠ H, the C–N bond strength is significantly lower,[2] which reduces the isokinetic temperature.

Acknowledgment. This work was supported by the Office of Naval Research on Contract No. Nonr 3760 (00).

Mass Spectrometric Study of the Reaction of Nitrogen Atoms with Nitrosyl Chloride

by M. R. Dunn, C. G. Freeman, M. J. McEwan, and L. F. Phillips

Chemistry Department, University of Canterbury, Christchurch, New Zealand *(Received December 3, 1970)*

Publication costs borne completely by The Journal of Physical Chemistry

The reaction of N with ONCl might reasonably be expected to resemble that of N with NO_2. The latter[1] is a very fast reaction ($k = 1.8 \times 10^{-11}$ cm^3 molecule^{-1} sec^{-1}) which is remarkable chiefly for the variety of decomposition channels that are available to the N–NO_2 transition state. Thus 43% of primary reactions yield N_2O + O, and 33% yield NO + NO, with about 10% each of N_2 + O + O and N_2 + O_2. It is therefore of interest to determine whether the reaction of N with ONCl can take a similar variety of paths. Also, in view of the recent suggestion[2] that the reaction with ONCl could serve as a gas-phase titration for estimating N-atom concentrations, it is useful to reexamine the stoichiometry of the reaction and to establish whether the primary reaction is sufficiently rapid to give an accurate end point in the presence of wall and homogeneous recombination of N atoms.

We have studied the reaction in a fast-flow system by a combination of mass spectrometric and photometric techniques. Our conclusions concerning the stoichiometry of the reaction differ significantly from those of Biordi;[2] this difference is attributable to the differing importance of wall recombination of Cl atoms in the two systems. We find that the primary rate constant is about three orders of magnitude smaller than that of the usual NO titration reaction, so that the usefulness of the ONCl titration must be restricted to systems with large N-atom concentrations and relatively slow flow speeds, preferably with a large tube diameter or an effective wall poison to minimize heterogeneous recombination. In contrast to the reaction with NO_2, the reaction of N with ONCl does not produce detectable amounts of N_2O, and it appears that the observations can be satisfactorily accounted for by a mechanism based on a single primary step yielding NO + NCl.

Experimental Section

The apparatus, procedures (including poisoning the walls of the flow tube with phosphoric acid), and materials were as previously described.[3,4] A sample of $O^{15}NCl$ was prepared from 99% enriched ^{15}NO by reaction with an excess of chlorine at 180°K and purified by repeated fractional distillation in a LeRoy still. Photometric observations were made downstream from the mass spectrometer sampling leak using a 1P21 photomultiplier in conjunction with either a Spectrolab P-type interference filter (1.5 nm half-width at 625 nm) to detect the nitrogen afterglow, or a Corning 7-39 filter to detect the NO β bands. The consumption of ONCl could be monitored from the height of either the NO^+ peak at mass 30 or the NCl^+ peak at mass 49; the results obtained in the presence of excess N were independent of which peak was used. Both NO and NCl are products of the primary reaction and their parent peaks might therefore contribute appreciably to the peak heights measured at masses 30 and 49. However, in the presence of excess N atoms the steady-state concentration of each of these species is expected to be low enough to cause negligible error in measurements of the ONCl concentration. Also, in a previous study of the reaction of N atoms with Cl_2O,[5] where there was no interference from the mass spectrum of the reactants, we were not able to detect any peak at mass 49 from NCl radicals even though they were certainly present in the reaction system.

Results and Discussion

The products of the reaction at long times (*ca.* 300 msec) were N_2, Cl_2, and O_2. The production of N_2 could not normally be observed because of the large amount of N_2 already present, but was readily apparent in experiments with $O^{15}NCl$. From the lack of a detectable increase in the mass 45 peak due to ^{15}NNO in these experiments we conclude that the yield of N_2O in the primary reaction is less than 0.1%. A smaller value for this limit might have been obtained but for

(1) L. F. Phillips and H. I. Schiff, *J. Chem. Phys.*, **42**, 3171 (1965).
(2) J. C. Biordi, *J. Phys. Chem.*, **73**, 3163 (1969).
(3) C. G. Freeman and L. F. Phillips, *ibid.*, **72**, 3025 (1968).
(4) M. R. Dunn, M. M. Sutton, C. G. Freeman, M. J. McEwan, and L. F. Phillips, *ibid.*, in press.
(5) C. G. Freeman and L. F. Phillips, *ibid.*, **72**, 3028 (1968).

the presence of about 1% of $^{15}NO_2$ impurity in the $O^{15}NCl$.

The stoichiometry of the reaction at long reaction times was investigated in two ways, the first being to determine the number of ONCl molecules destroyed by a known concentration of N atoms with ONCl in excess, and the second to determine the number of ONCl molecules consumed by a known concentration of N atoms at the "titration end point"[2] which was indicated by the photomultiplier output signal having dropped to zero. For both methods the reaction time, from inlet to sampling leak, was 300 msec, and the N-atom pressure was in the range 4–9 $\times$ 10^{-3} Torr. Both gave stoichiometries close to 1:1, the mean ratio of N atoms to ONCl molecules destroyed being 0.94 $\pm$ 0.15 by the first method, and 1.20 $\pm$ 0.12 by the second method (16 and 12 determinations, respectively).

The elementary reaction steps which need to be considered are

$$N + ONCl \longrightarrow NO + NCl \quad (1)$$

$$N + NO \longrightarrow N_2 + O \quad (2)$$

$$N + NCl \longrightarrow N_2 + Cl \quad (3)$$

$$Cl + ONCl \longrightarrow Cl_2 + NO \quad (4)$$

$$O + ONCl \longrightarrow \text{products} \quad (5)$$

$$Cl + \text{wall} \longrightarrow {}^1/_2Cl_2 \quad (6)$$

Here reaction 1 was found in this work to have a rate constant k_1 of the order of 10^{-14} cm^3 molecule^{-1} sec^{-1}, whereas k_2 is 2 $\times$ 10^{-11},[6] k_3 is expected to be of similar magnitude to k_2, and k_4 is about 4 $\times$ 10^{-12}.[7] Hence reactions 2–4 can be expected to be important at very short reaction times relative to the time scale of reaction 1. For reaction 5, however, the rate constant is of similar magnitude to k_1,[8] so that reactions initiated by step 5 should not be significant except at long reaction times. Reaction 6 should be almost negligible in our poisoned system, but would have been important in the unpoisoned system used by Biordi.[2] Homogeneous recombination of N atoms was negligible in our system because of the low partial pressures of N that we used (typically 7 $\times$ 10^{-3} Torr).

Reactions 1–4 lead to the removal of four N atoms and two ONCl molecules each time reaction 1 occurs and result in the production of two O atoms. Our current studies of the O + ONCl reaction[8] indicate that its stoichiometry at long times is close to 1:1 in a poisoned system. Hence, provided sufficient ONCl is introduced to ensure that all N atoms are removed by reactions 1–4, the effect at long times would be to have 4N and 2ONCl removed by steps 1–4, and 2ONCl removed by step 5, thus giving the overall 1:1 stoichiometry that we observed. In an unpoisoned system reaction 4 would have to compete with reaction 6, the recombination of Cl atoms on the wall. If Cl atoms were removed entirely by 6 the result at short times would be to remove 3N for each ONCl reacting. To predict the stoichiometry at long times in an unpoisoned system it is necessary to know the stoichiometry of the O + ONCl reaction in such a system. On the basis of the simple mechanism (which is in accord with our current findings)

$$O + ONCl \longrightarrow NO + ClO \quad (7)$$

$$O + ClO \longrightarrow O_2 + Cl \quad (8)$$

together with reaction 6, it can be seen that two O atoms are required to remove one ONCl molecule, so that the effect at long times is to remove 3N and 1.5(ONCl). Thus we can account for the 2:1 stoichiometry found by Biordi. Our experimental stoichiometry was actually slightly greater than 1:1; this can be understood in terms of a competition between reactions 4 and 6.

To measure the rate of reaction 1 we monitored the disappearance of ONCl in the presence of a known excess (typically eightfold) of N atoms, the rate constant being calculated with the assumption that 4N and 2ONCl were removed each time reaction 1 occurred. Rate constants were calculated at times such that not less than 20% of the ONCl had been consumed, so that sufficient time would have elapsed for steady states to be attained with respect to NO, NCl, and Cl. The mean of 32 determinations at 295°K gave k_1 = 1.9 $\times$ 10^{-14} cm^3 molecule^{-1} sec^{-1}, with a standard deviation of 0.9 $\times$ 10^{-14}. The rather large scatter of the values, which is reflected in the standard deviation, may have been associated with variations in the effectiveness of the wall poison.

The experiments with $O^{15}NCl$ have enabled us to rule out the primary step

$$N + ONCl \longrightarrow N_2O + Cl \quad (9)$$

However, because of the speed of reactions 2 and 3 and the presence of NO^+ and NCl^+ peaks in the mass spectrum of ONCl, these experiments could give no information about whether the initial attack by N occurs preferentially on the oxygen or the chlorine atom. Attack on the chlorine atom should be favored by the weakness of the N–Cl bond relative to the N–O bond in ONCl.

Two other primary reactions which must be considered, by analogy with the NO_2 reaction, are

$$N + ONCl \longrightarrow N_2 + ClO \quad (10)$$

and

$$N + ONCl \longrightarrow N_2 + Cl + O \quad (11)$$

(6) K. Schofield, *Planet. Space Sci.*, **15**, 643 (1967).

(7) W. G. Burns and F. S. Dainton, *Trans. Faraday Soc.*, **48**, 52 (1952).

(8) M. R. Dunn, C. G. Freeman, M. J. McEwan, and L. F. Phillips, unpublished work.

which are exothermic to the extent of 100 and 47 kcal, respectively (compared with approximately 50 kcal for reaction 1 and 77 kcal for reaction 9). Reaction 10 leads to exactly the same predictions of overall stoichiometry as does reaction 1. However, although we cannot distinguish between 1 and 10 experimentally, we consider that 10 can be eliminated because it requires an improbable concerted mode of decomposition of the activated complex. Reaction 11, on the other hand, *can* be ruled out experimentally because it leads to the prediction that at long reaction times 2N and 4ONCl should be consumed.

Acknowledgments. This work was supported by the New Zealand Universities Research Committee and by Grant AF-AFOSR-1265-67 from the United States Air Force Office of Scientific Research.

COMMUNICATIONS TO THE EDITOR

Homogeneous and *Heterogeneous* Platinum-Catalyzed Isotopic Hydrogen Exchange in Polycyclic Aromatic Hydrocarbons

Publication costs borne completely by The Journal of Physical Chemistry

Sir: Exchange between aromatic compounds and heavy water is catalyzed by both *homogeneous* and *heterogeneous* platinum.[1,2] Using data essentially from the exchange of the monosubstituted benzenes, common π-complex mechanisms have been proposed for the two systems.[1-3] This type of reactivity is fundamentally significant since such relationships indicate that the chemistry of adsorbed molecules and the chemistry of inorganic coordination complexes are intimately related. An important class of compounds in mechanistic studies of these catalytic systems are the polycyclic aromatic hydrocarbons. In particular, to develop the above correlations further, studies in isotope orientation with these hydrocarbons are essential and, at present, only *homogeneous* catalysis data are available.[1] No equivalent systematic *heterogeneous* study has been performed with the polycyclics because of the difficulty of separating the exchange reaction from the competing randomization process, which only occurs heterogeneously.[2] For a direct comparison between *homogeneous* and *heterogeneous* catalytic exchange it is necessary to be able to observe initial deuteration rates and orientation in both systems. This is now possible by a recently developed epr method.[4] Nmr is not sufficiently sensitive at low deuteration incorporation for this purpose and mass spectrometry does not distinguish positional substitution (*e.g.*, naphthalene-α-d_1 *vs.* naphthalene-β-d_1).

For the first time, we now wish to report that using the above experimental techniques,[4] we have been able to observe in the deuteration of a representative number of polycyclics (i) initial *heterogeneous* exchange as distinct from competing randomization and (ii) identical deuteration patterns between *heterogeneous* platinum data and the corresponding *homogeneous* platinum(II) system. The results (Tables I and II) show that in exchange with both *homogeneous* and *heterogeneous* platinum catalysts, the polycyclic aromatic hydrocarbons fall into two groups, *e.g.*, condensed polycyclics (naphthalene) and the polyphenyls (biphenyl). With the condensed polycyclics, initial deuteration is exclusively stepwise and to the β position or its equivalent, whereas the polyphenyls exhibit multiple deuteration and exchange predominantly, one ring at a time, in the *meta* and *para* positions. Thus naphthalene gives naphthalene-β-d_1 after initial exchange with either

Table I: Homogeneous and Heterogeneous Platinum-Catalyzed Deuteration of Polycyclics[a]

Run	Compound	Phase	Wt, g × 10	Temp, °C	Time, hr	Solvent vol, ml	Cat. wt, g × 10^2	% D (theoret)	% D (exptl)
1	Naphthalene	Homogeneous	2.5	75	0.5	10.0		56.6	1.8
2	Naphthalene	Heterogeneous	4.0	150	168	5.0	8.0	95.7	17.9
3	Naphthalene	Homogeneous	4.0	75	168	16.0		56.6	44.2
4	Naphthalene	Heterogeneous	4.0	150	2 × 168[b]	2 × 5.0[b]	2 × 2.5[b]	99.8	42.3
5	Naphthalene	Heterogeneous	4.0	150	4 × 168[b]	4 × 5.0[b]	4 × 2.5[b]	100.0	98.5
6	Anthracene	Homogeneous	1.0	75	1.0	13.0		98.8	1.50
7	Pyrene	Homogeneous	0.5	75	0.7	20.0		96.2	5.2
8	Pyrene	Heterogeneous	4.0	150	4	5.0	5.0	96.8	5.6
9	Diphenyl	Homogeneous	4.0	75	39	8.0		38.6	37.6
10	*p*-Terphenyl	Homogeneous	1.0	116	3 × 2.5[b]	3 × 15.0[b]		100.0	41.2
11	*p*-Terphenyl	Heterogeneous	1.0	150	3 × 336[b]	3 × 10.0[b]	20.0	100.0	93.9
12	*m*-Terphenyl	Homogeneous	1.0	116	3 × 2.5[b]	3 × 15.0[b]		100.0	48.4
13	*m*-Terphenyl	Heterogeneous	5.0	150	336	5.0	10.0	94.4	42.8

[a] Experimental exchange procedures as in relevant references.[1,2] [b] Number of equilibrations.

(1) R. J. Hodges and J. L. Garnett, *J. Phys. Chem.*, **73**, 1525 (1969).

(2) J. L. Garnett and W. A. Sollich-Baumgartner, *Advan. Catal.*, **16**, 95 (1966).

(3) R. R. Fraser and R. N. Renaud, *J. Amer. Chem. Soc.*, **88**, 4365 (1966).

(4) K. P. Davis, J. L. Garnett, and J. H. O'Keefe, *Chem. Commun.*, in press.

Table II: Deuterium Distribution and Orientation in Compounds in Table I

Run (from Table I)	Deuterium distribution[a]														Predominant substitution position	Isotope orientation[b] species
	D_0	D_1	D_2	D_3	D_4	D_5	D_6	D_7	D_8	D_9	D_{10}	D_{11}	D_{12}	D_{13}	D_{14}		
1	87.5	10.4	2.1													2	d_1
2	40.5	25.6	13.2	8.4	5.9	1.9	1.0	1.0	2.5							2	d_1
3	0.0	0.0	3.1	20.4	58.7	15.3	2.5									2	d_4
4	4.1	12.2	19.5	22.1	20.0	8.4	3.8	3.0	6.9							2	d_4
5	0.0	0.0	0.0	0.0	0.0	0.0	0.0	15.4	84.6							1 and 2	d_8
6	89.5	6.5	3.5	0.5												2[c,d]	d_1[c,d]
7	56.0	35.6	8.4													2	d_1
8	62.1	25.1	9.4	2.0	1.4											2	d_1
9	8.0	7.2	10.8	16.1	12.9	23.2	21.2	0.6								*meta* and *para*[d]	d_6[d]
10	0.0	0.0	0.0	0.8	5.2	21.9	62.8	6.8	2.5							*meta* and *para*[d]	d_6[d]
11	0.0	0.0	0.0	0.0	0.0	0.0	0.0	0.0	0.0	0.0	0.6	4.4	15.9	34.3	44.8	*ortho*, *meta*, and *para*	d_{14}
12	0.0	0.0	0.0	0.0	1.0	6.2	26.4	55.5	7.9	2.0	0.5	0.5				*meta* and *para*	d_7
13	0.0	2.3	2.9	7.5	16.5	19.3	23.2	12.6	5.6	1.2	1.1	0.7	2.1	2.4	3.6	*meta* and *para*	d_7

[a] By low voltage mass spectrometry. [b] By epr and/or nmr. [c] Using NaCl instead of HCl, no acid exchange observed in 9,10 positions of anthracene (see ref 1). [d] Isotope orientation and deuterium distribution in homogeneously exchanged samples similar to heterogeneously exchanged compounds (heterogeneous conditions: anthracene, 6 hr; diphenyl, 24 hr; *p*-terphenyl 336 hr at 150°).

homogeneous or *heterogeneous* platinum. Prolonged deuteration with both catalysts yields predominantly naphthalene-β-d_4, although some scrambling to the α positions is observed *heterogeneously* since temperatures of 150° are required under these conditions to obtain appreciable amounts of the d_4 species within reasonable periods of exchange.

Again, in both catalytic systems, analogous stepwise, β selectivity is observed with anthracene, phenanthrene, chrysene, and tetracene. Pyrene deuterates successively and preferentially in the 2- then the 2,7- followed by the 1, 2, 3, 6, 7, 8 positions.

With *homogeneous* platinum(II), the stepwise β selectivity for the condensed polycyclics has been attributed to bond localization.[1] In naphthalene, it has been proposed[1] that the intermediate π complex is formed with the 1–2 bond, *i.e.*, the bond of highest bond order. Because of steric hindrance with the α position, exchange is confined to the β position where multiple π–σ conversions are possible, although the system exhibits an M value of unity.

Because the present *heterogeneous* results are remarkably similar to the previous *homogeneous* data,[1] it is suggested that the original π complex exchange mechanisms[2] postulated for molecules such as naphthalene under *heterogeneous* conditions can now be modified. Thus it is plausible to propose that condensed polycyclics exhibit π-bond localization on the catalyst surface and are adsorbed as π-olefin type complexes. A π-olefin type complex is consistent with the observed strong toxicity of naphthalene in *heterogeneous* exchange with heavy water.[2] Further, the β orientation, together with stepwise exchange in naphthalene and similar compounds, supports accumulating evidence[5,6] which indicates that π-dissociative, and not π-associative, processes predominate in *heterogeneous* deuteration. If a π-associative mechanism were significant, steric hindrance from the adjacent α position in naphthalene would be minimal and appreciable deuteration in both α and β positions would be expected during initial rates of exchange.

Again, with the polyphenyls (Tables I and II) initial isotope orientation under both *homogeneous* and *heterogeneous* conditions is identical. By contrast with the condensed polycyclics, the polyphenyls deuterate *via* a multiple process and exhibit strong *ortho* deactivation.

Because of the importance of the present results to catalytic theory and also to general deuteration and tritium labeling work, a final check on the isotope orientation data has been made by subjecting all of the above polycyclics to the back exchange technique[3] where gradual protonation of the fully deuterated molecule is effected. Identical exchange patterns have been observed under *homogeneous* and *heterogeneous*

(5) R. J. Harper, S. Siegel, and C. Kemball, *J. Catal.*, **6**, 72 (1966).
(6) G. E. Calf and J. L. Garnett, *Chem. Commun.*, 373 (1969).

conditions using both forward and back exchange methods. This remarkable correlation in isotope orientation and multiplicity of exchange during initial isotope incorporation suggests that analogous π-complex mechanisms operate under *homogeneous* and *heterogeneous* conditions. The data thus unequivocally support the general π-complex theory of metal catalysis.[1,2]

Acknowledgment. We thank the Australian Research Grants Committee and the Australian Institute of Nuclear Science and Engineering for the support of this research.

DEPARTMENT OF PHYSICAL CHEMISTRY
THE UNIVERSITY OF NEW SOUTH WALES
KENSINGTON, N.S.W. 2033, AUSTRALIA
K. P. DAVIS
J. L. GARNETT

RECEIVED JANUARY 18, 1971

Comment on "Ionic Species Formed from Benzene during Radiolysis of Its Solutions in 3-Methylpentane at 77°K" by A. Ekstrom

Publication costs borne completely by The Journal of Physical Chemistry

Sir: The object of this note is to question Ekstrom's assignment of an optical absorption band to the species, $(C_6H_6)_2^-$.[1]

The term "dimer cation" is used for species, M_2^+, where M is a stable neutral molecule such as an aromatic hydrocarbon: as in the similar case of excimers, M_2^*, the interaction between the two partners is believed to be weak, *i.e.*, no rearrangement of bonds occurs. Dimer cations have been clearly identified by their esr spectra; their optical spectra have been studied and they have been detected in mass spectrometers (see ref 1–3 and references therein). Simple explanations of the stability of dimer cations[2-4] suggest that dimer anions, M_2^-, should be equally stable. It is surprising, therefore, that the numerous esr studies of aromatic hydrocarbon anions in solution have not detected such species. (Anion dimers, M_2^{2-}, do exist, *e.g.*, where M is benzoquinone;[5] these species have two bonding electrons instead of one).

The radiolysis of solutions in organic glasses forms a convenient method of preparing ions of the solutes. Anions are produced in ethers (such as methyltetrahydrofuran, MTHF), cations in halides, and both in hydrocarbons.[6] Having studied the formation of dimer cations in butyl chloride–isopentane mixtures,[3] we made a search for dimer anions in MTHF. Only monomer anions could be detected in naphthalene solutions up to 1 *M* and pyrene to 0.5 *M* concentration even on annealing after radiolysis. Comparison with the cation results suggests that the dimer anions are not stable.

Benzene in MTHF glass produces a very broad absorption through the visible region;[3,7] apparently benzene does not produce a well defined anion under these conditions. The spectrum is quite different from that of trapped electrons in MTHF but does not show the narrower band at 435 nm produced by potassium reduction of benzene in dimethoxyethane at $-80°K$.[8] (In the latter case, the ion may be stabilized by the solvent or the counterion.) Stabilization of benzene anions in a nonpolar solvent therefore appears unlikely, but Ekstrom assigns bands at 525 and 930 nm in 3-methylpentane to $C_6H_6^-$ and $(C_6H_6)_2^-$ on the basis of their removal by carbon tetrachloride.[1] However, these wavelengths agree well with ours (550 and 930 nm) obtained in the halide glass and assigned to monomer and dimer cations while Gallivan and Hamill state that the 930-nm band in 3-methylpentane is enhanced by the electron scavengers, carbon tetrachloride and isopropyl chloride, but suppressed by the positive charge scavengers, 2-methylpentene-1, triethylamine, and MTHF.[9]

In solutions containing carbon tetrachloride, Ekstrom observed bands at 320 and 1030 nm which he ascribed to monomer and dimer cations.[1] The 320-nm band cannot be the same transition as our band at 550 nm; (which is consistent with photoelectron spectral data;[10] this band is masked in CCl_4 solutions). It could be a higher transition[8] but it may be due to the radical, $C_6H_7\cdot$.[11] The identity of the species absorbing at 1030 nm is not clear.

I conclude that there is as yet no definite evidence for a dimer anion. Their apparent instability remains puzzling. An explanation given recently for the case of the naphthalene dimer anion[4] is not likely to be generally applicable.

(1) A. Ekstrom, *J. Phys. Chem.*, **74**, 1705 (1970).

(2) B. Badger, B. Brocklehurst, and R. D. Russell, *Chem. Phys. Lett.*, **1**, 122 (1967).

(3) B. Badger and B. Brocklehurst, *Trans. Faraday Soc.*, **65**, 2576, 2582, 2588 (1969).

(4) B. Badger and B. Brocklehurst, *ibid.*, **66**, 2939 (1970).

(5) K. Kimura, H. Yamada, and H. Tsubomura, *J. Chem. Phys.*, **48**, 440 (1968).

(6) W. H. Hamill in "Radical Ions," E. T. Kaiser and L. Kevan, Ed., Interscience, New York, N. Y., 1968, p 321.

(7) T. Shida and W. H. Hamill, *J. Chem. Phys.*, **44**, 4372 (1966).

(8) C. L. Gardner, *ibid.*, **45**, 572 (1966).

(9) J. B. Gallivan and W. H. Hamill, *ibid.*, **44**, 2378 (1966).

(10) D. W. Turner, *Advan. Phys. Org. Chem.*, **4**, 31 (1966).

(11) T. Shida and W. H. Hamill, *J. Amer. Chem. Soc.*, **88**, 3689 (1966); T. Shida and I. Hanazaki, *Bull. Chem. Soc. Jap.*, **43**, 646 (1970).

CHEMISTRY DEPARTMENT
THE UNIVERSITY
SHEFFIELD, S3 7HF, ENGLAND
B. BROCKLEHURST

RECEIVED SEPTEMBER 8, 1970

Reply to "Comment on 'Ionic Species Formed from Benzene during Radiolysis of Its Solutions in 3-Methylpentane at 77°K' "

Publication costs assisted by A. Ekstrom

Sir: In reply to Brocklehurst's comments we would like to draw attention to the following.

1. Brocklehurst suggests that the 320-nm band, which we attribute to the benzene monomer cation, may be due to the cyclohexadienyl radical. However, the spectrum of the cyclohexadienyl radical shows a very distinct fine structure[1] which is totally absent in the 320-nm band found in 3MP–C_6H_6–CCl_4 mixtures.

2. We observe that the yield of the species absorbing at 320 nm is increased by the addition of CCl_4. This behavior is commonly accepted as evidence of a cationic species.[2,3] If the 320-nm band were attributed to a cyclohexadienyl radical, it is difficult to arrive at a plausible mechanism for the enhancement of its yield in the presence of CCl_4.

3. As pointed out above, the cyclohexadienyl radical is readily observed in methanol solutions containing benzene which were irradiated at 77°K.[1] It is believed to be formed by the reactions

$$C_6H_6 + e^- \longrightarrow C_6H_6^- \quad (1)$$

$$C_6H_6^- + ROH \longrightarrow C_6H_7 + RO^- \quad (2)$$

Thus in the alcohols the benzene anion and its dimer are not stable. However, in solvents which are not able to react with $C_6H_6^-$ by a reaction analogous to eq 2, the benzene anion and its dimer would be expected to be observed. It is therefore not possible to make general statements regarding the stability of the benzene anion and its dimer in a variety of solvents which have greatly different polarities.

4. Brocklehurst has not offered any explanation for the unusual concentration dependency of the 525-, 930-, 320-, and 1030-nm bands which we have observed. While it is quite possible that our assignments may be in error, the alternatives offered by Brocklehurst do not appear to satisfy the observed results.

(1) T. Shida and W. H. Hamill, *J. Amer. Chem. Soc.*, **88**, 3689 (1966).
(2) D. W. Skelly and W. H. Hamill, *J. Phys. Chem.*, **70**, 1630 (1966).
(3) B. Wiseall and J. E. Willard, *J. Chem. Phys.*, **46**, 4387 (1967).

CHEMISTRY DIVISION A. EKSTROM
AUSTRALIAN ATOMIC ENERGY COMMISSION
LUCAS HEIGHTS, SYDNEY, AUSTRALIA

RECEIVED NOVEMBER 5, 1970

Platinum Group Metals and Compounds

ADVANCES IN CHEMISTRY SERIES
NO. 98

Eleven papers from a symposium by the Division of Inorganic Chemistry of the American Chemical Society chaired by U. V. Rao.

What new complexes of the platinum group metals have been synthesized? Here is a collection of papers presenting data on chalcogenides, oxides, nitrido and hydrido complexes, as well as the catalytic properties of these metals and their alloys. Information is included on

- synthesis
- structure
- magnetic susceptibility
- double bond migration

The platinum group metals are considered from the viewpoints of both industry and research. Their magnetic and thermodynamic properties are explored, as well as recent chemistry of σ- and π-bonded complexes. Crystal structure is discussed by several authors, with data presented in the form of

- x-ray scattering data
- absorption spectra
- crystal spectra
- infrared spectra
- Mossbauer spectra
- vibrational spectra

165 pages with index. Cloth bound (1971) $9.00
Postpaid in U.S. and Canada; plus 35 cents elsewhere.
Set of L. C. cards with library orders upon request.

Other books in the ADVANCES IN CHEMISTRY SERIES of interest to inorganic chemists include:

No. 89 Isotope Effects in Chemical Processes
278 pages Cloth bound (1969) $13.00

No. 82 Radiation Chemistry — II
558 pages Cloth bound (1968) $16.00

No. 81 Radiation Chemistry — I
616 pages Cloth bound (1968) $16.00

No. 81 and No. 82 ordered together $30.00

No. 78 Literature of Chemical Technology
732 pages Cloth bound (1968) $17.50

No. 73 Trace Inorganics in Water
396 pages Cloth bound (1968) $12.50

No. 72 Mass Spectrometry in Inorganic Chemistry
329 pages Cloth bound (1968) $12.00

Order from:
Special Issues Sales
American Chemical Society
1155 16th St., N. W.
Washington, D. C. 20036